NASA Technical Memorandum 101578, Part Two

WORKSHOP on COMPUTATIONAL ASPECTS in the CONTROL of FLEXIBLE SYSTEMS

Held at the Royce Hotel in Williamsburg, Virginia
July 12-14, *1988*
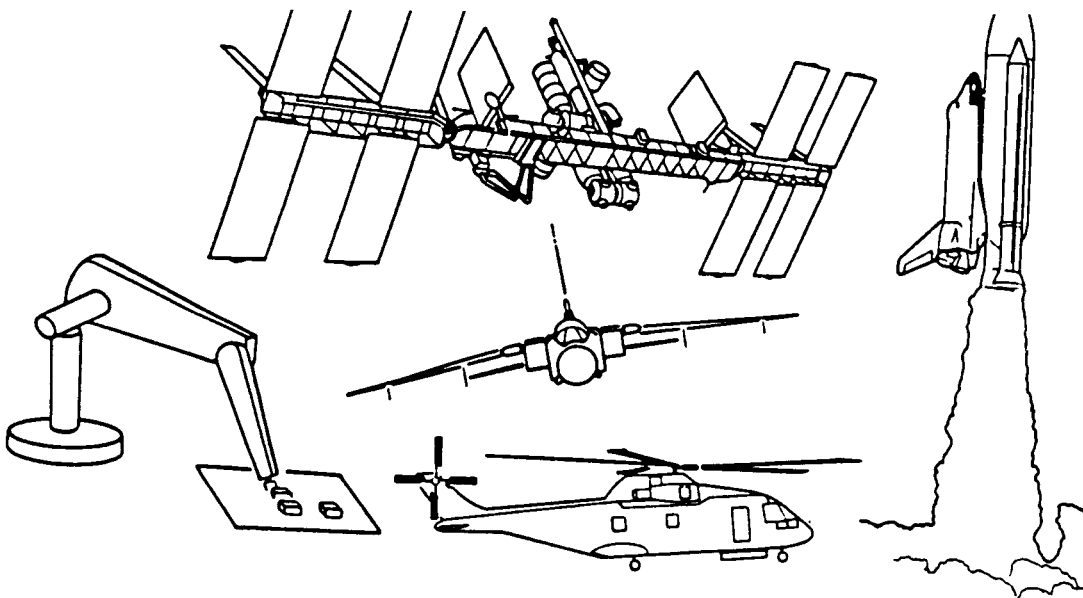
Sponsored by the NASA Langley Research Center

Proceedings Compiled by Larry Taylor

Table of Contents

******* PART ONE *******

Computational Efficiency and Capability

####### PART TWO #######

Modeling and Parameter Estimation

Control Synthesis and Optimization Software

SESSION IV - MODELING AND PARAMETER ESTIMATION

FLEXIBLE ROBOT CONTROL: MODELING AND EXPERIMENTS

By

Irving J. Oppenheim
Carnegie-Mellon University
Pittsburgh, Pennsylvania

and

Isao Shimoyama
University of Tokyo
Tokyo, JAPAN

ABSTRACT

A dynamic model fills several roles in the development of flexible manipulators and their control structures. A proper dynamic model permits identification of the proper state variables for control, completes the mathematical model used in design studies and in simulation, and provides the forward transform needed in model-based control. While there exist many proven analytical approaches, and although numerous models have been constructed and tested, there remains a need for *simple* models which capture all the important behavior while otherwise suppressing modeling complexities and computational demands. Such simple models are necessary for online applications because of their computational compactness, and are advantageous for design and simulation studies because of their accessibility by users. For manipulator control applications, an *ideal* (simple) model might contain independent variables no greater in number than the state variables required for acceptable control. This paper describes such a model and its use in experimental studies of flexible manipulators.

The analytical model developed in this research uses the equivalent of Rayleigh's method to approximate the displaced shape of a flexible link as the static elastic displacement which would occur under end rotations as applied at the joints. The generalized coordinates are thereby expressly compatible with joint motions and rotations in serial link manipulators, because the amplitude variables are simply the end rotations between the flexible link and the chord connecting the end points. The equations for the system dynamics are quite simple and can readily be formulated for the multi-link, three-dimensional case. When the flexible links possess mass and (polar moment of) inertia which are small compared to the concentrated mass and inertia at the joints, the analytical model is exact and displays the additional advantage of reduction in system dimension for the governing equations.

Four series of pilot tests have been completed. Studies on a planar single-link system were conducted at Carnegie-Mellon University, and tests conducted at Toshiba Corporation on a planar two-link system were then incorporated into the study. A single link system under three-dimensional motion, displaying biaxial flexure, was then tested at Carnegie-Mellon. The most recent tests, also conducted at Carnegie-Mellon, studied a three-dimensional system in which coupled (biaxial) flexural-torsional vibrations were present. In every test series effective control of the flexible system was accomplished; performance of the proposed model was studied and confirmed.

FLEXIBLE ROBOT CONTROL: MODELLING AND EXPERIMENTS

Irving J. Oppenheim, Carnegie-Mellon University

Isao Shimoyama, University of Tokyo

Describing a simple dynamic model:
- Useful for rapid prototyping and control system development
- Useful during manipulator design
- Applicable for real-time computation

Describing experimental results:
- Single-link 2-D
- Single-link 3-D
- Two-link 2-D
- Two-link 3-D

550

Modelling Link Flexibility Effects

Problems:

- Manipulators are non-linear by their configuration

- All models for flexible dynamics must approximate the solutions to PDE's

- Generalized co-ordinates (mode shapes) are often utilized

- Truncated mode shape models: OK, but not fully consistent with manipulator control

Demands:

- Generalizable to M-DOF manipulators

- Simple to formulate and use in simulation

- Computable in real-time

551

Intended Users

Laboratory research in flexible manipulator control

These restrictions are common:
- Single-link distributed mass systems
- Direct drive motors
- Planar systems
- Modelling based on truncated mode shapes

Our experimental target:
- General multi-link, 3-D system
- Mechanical actuation, with friction, backlash, etc.
- Possibly joint-dominated in mass

Experimental Apparatus at Carnegie-Mellon

Reconfigurable manipulator; modular design, up to 6DOF

- **Mechanical**
    - Each joint: DC-motor/harmonic drive/ potentiometer
    - Reconfiguration and link changeout using tubing and NPT hardware

- **Computational:**
    - Motorola VMEbus System 1000: 68010, VersaDOS, Pascal
    - Smalltalk-80 (One concurrent implementation under VersaDOS, a second Unix implementation on Sun-3)

- **Sensing:**
    - Position (rotation) sensing on joints
    - Strain sensing on links
    - Vision end-point sensing (not used for control)

553
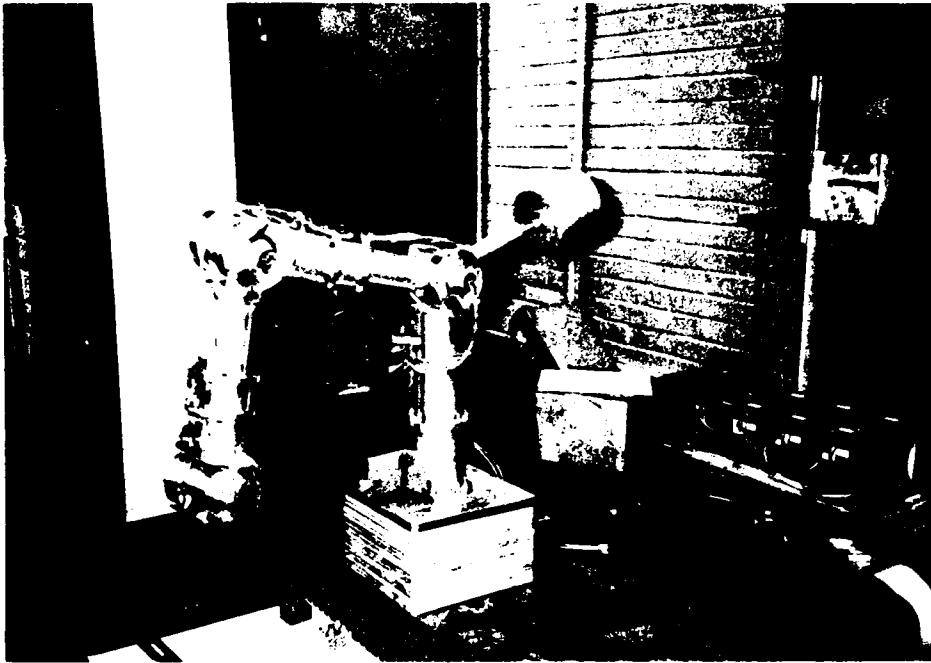
MANIPULATOR IN A 6-DOF TWO LINK CONFIGURATION (BOTH LINKS RIGID)

MANIPULATOR IN A 3-DOF TWO LINK CONFIGURATION (ONE RIGID, ONE FLEXIBLE)

554
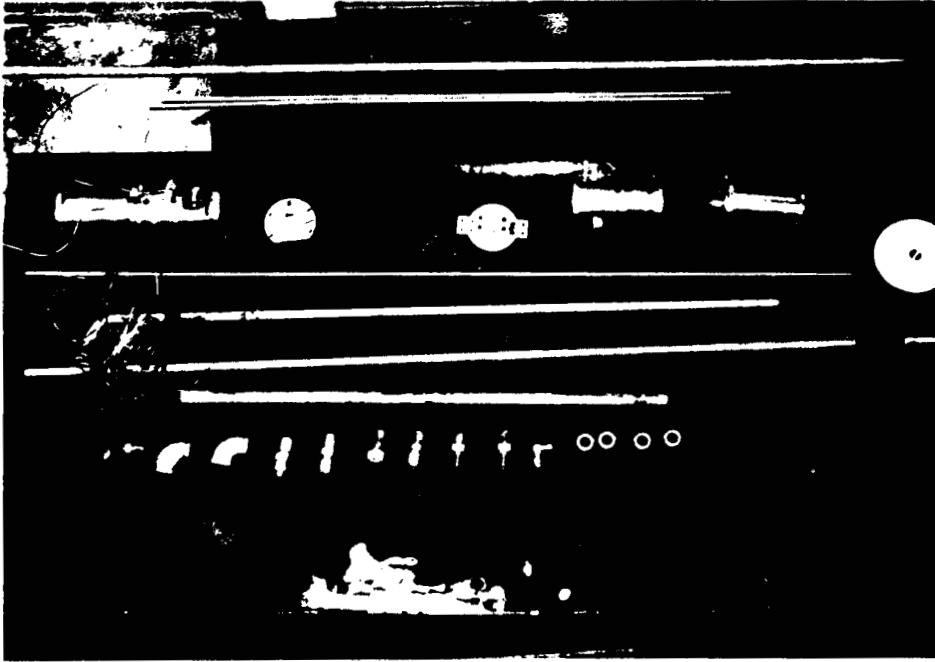
HARDWARE FOR TUBING (SWAGELOK), NPT, AND LINK CHANGEOUT
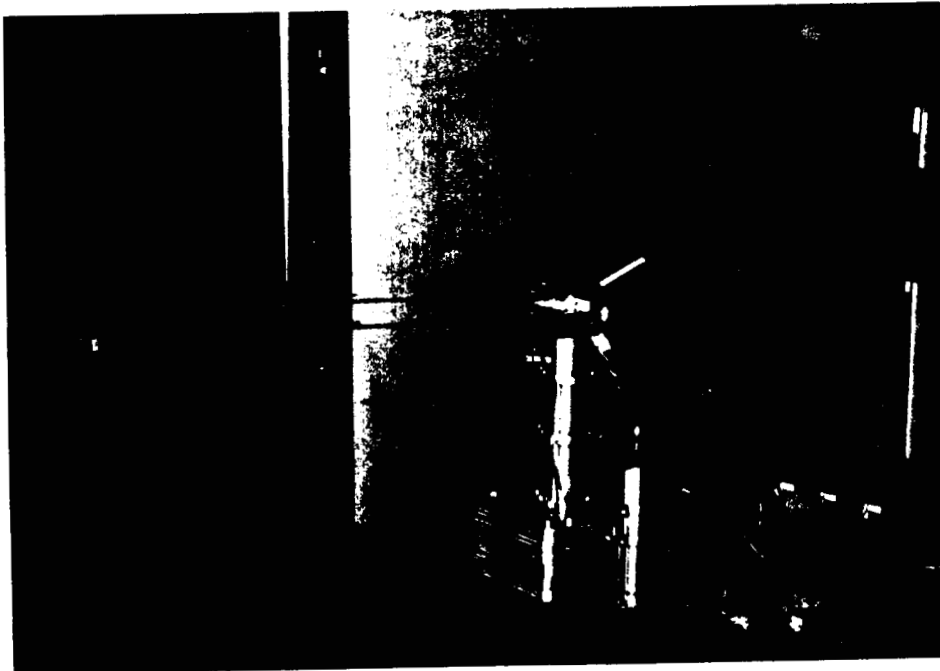
MANIPULATOR IN A SINGLE LINK 3-D CONFIGURATION

555
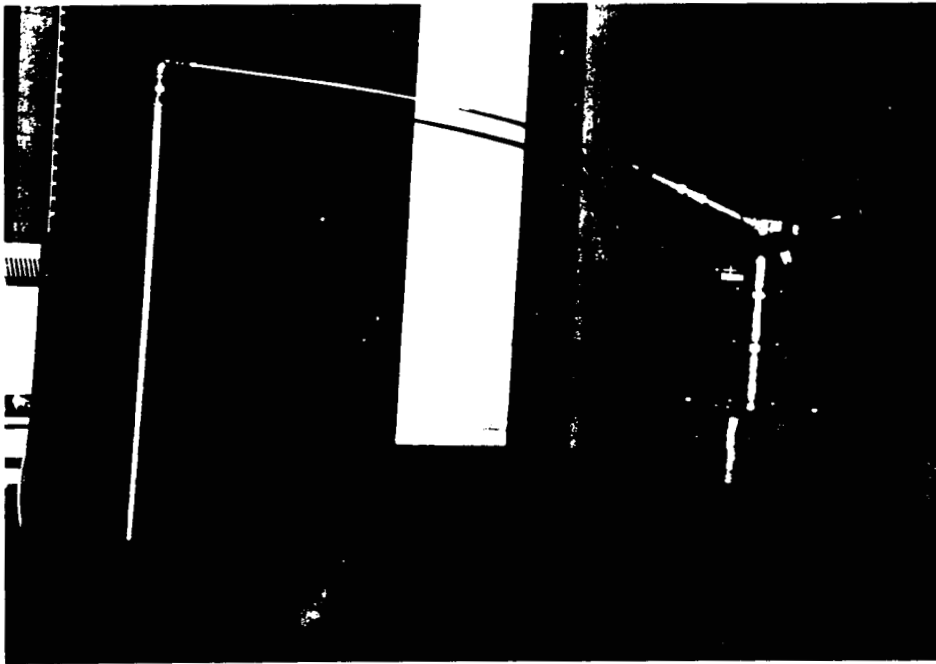
MANIPULATOR IN A 3-DOF TWO LINK CONFIGURATION

MANIPULATOR IN A 4-DOF TWO LINK CONFIGURATION FOR FORCE COGNITIVE EXCAVATION

556

A Simple Model for a General Flexible Link

Starting points to consider:

- Link motion results from concatenation to other links; the non-linear configuration problem, present in rigid manipulators as well.

- The link itself deforms as a result of the end-forces and the inertial forces acting on it.

- Which quantities can be observed or sensed?

- Which quantities can be controlled?

- How is the (approximate) solution to the PDE for link deformation to be contained within the dynamics equation? (What are the amplitude variables for the generalized co-ordinates chosen?)

First step in the approach: View first the motion of the *chord* connecting the end points, and then refer the (elastic) deformations to that chord.
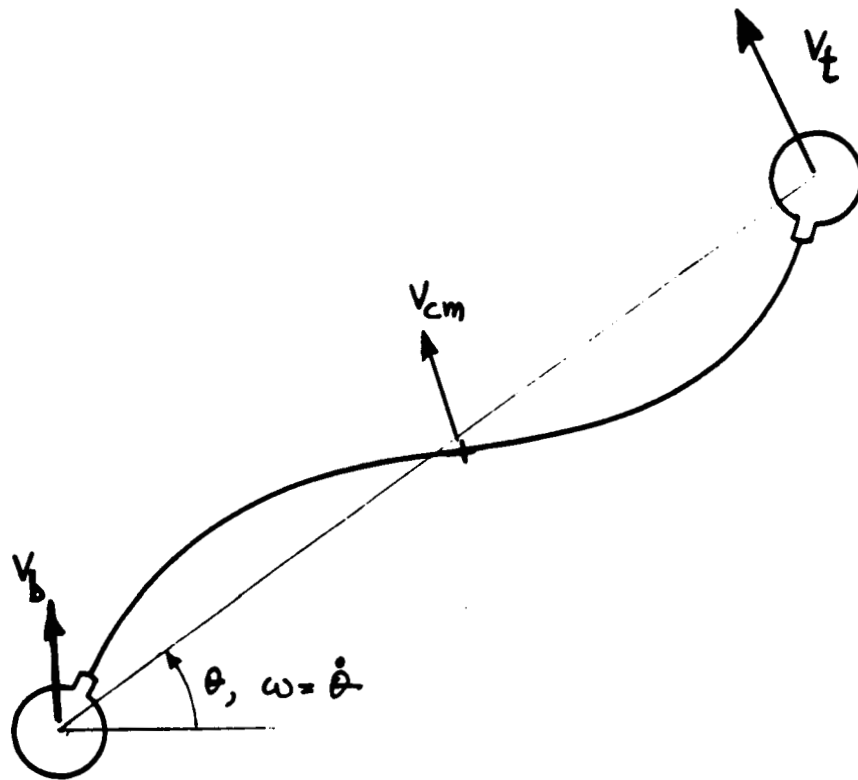
A FLEXIBLE LINK (SHOW IN 2-D) IN MOTION

NOTE "CHORD" ACTS AS A "RIGID BODY"
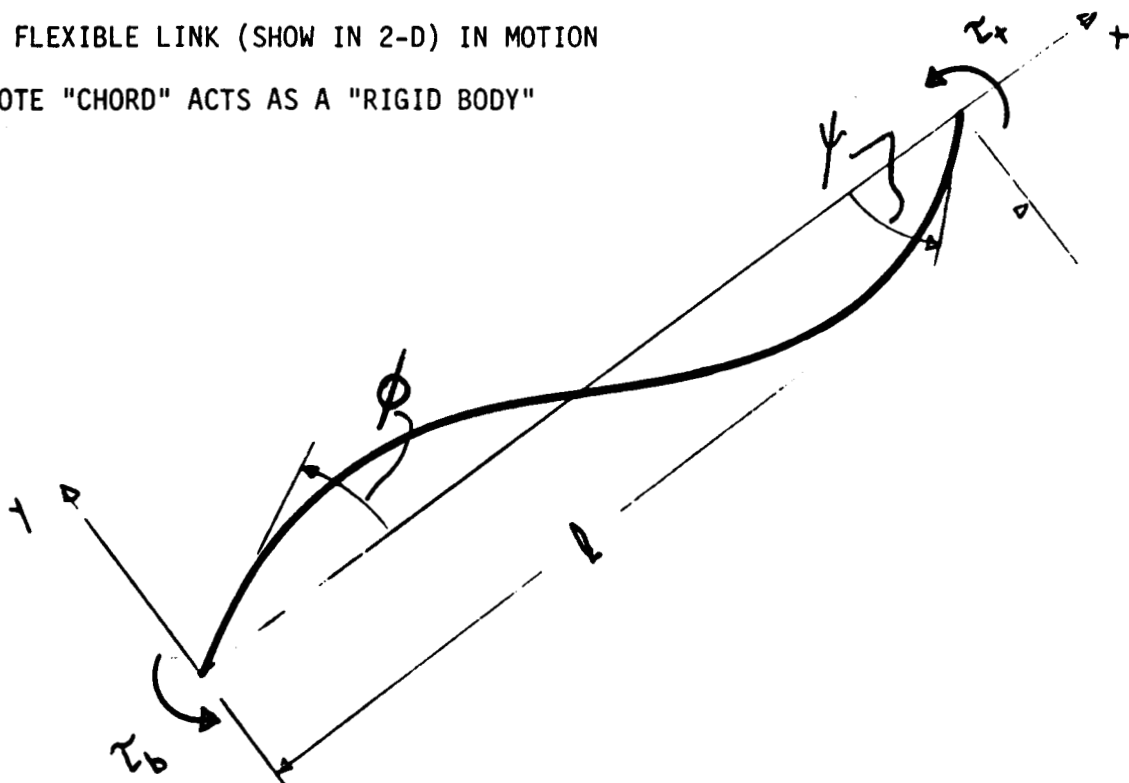
ELASTIC DEFORMATIONS REFERENCED TO THE CHORD

558

Kinematics/Mechanics of the Simple Model

Chord motion:

- Denote rotation by θ, equivalent to a rigid-link formulation.

- Include dynamic effects of concentrated masses and inertias at joints.

- *Assume* that inertial effects of the link are modelled (from θ and ω) by the translation and rotation of the (c.m. of) the chord.

Deformations (displacements) of the flexible link:

- Displacements $y(x)$ are referenced to the chord.

- *Assume* that the displacements equal those resulting from static application of end-rotations ϕ and ψ.

- Displacement and potential energy:

$$y(x) = x(x-\ell)\left[(\phi + \psi)x - \phi\ell\right]/\ell^2$$

$$U = 2EI\left[\phi^2 + 2\phi\psi + \psi^2\right]/\ell$$

559
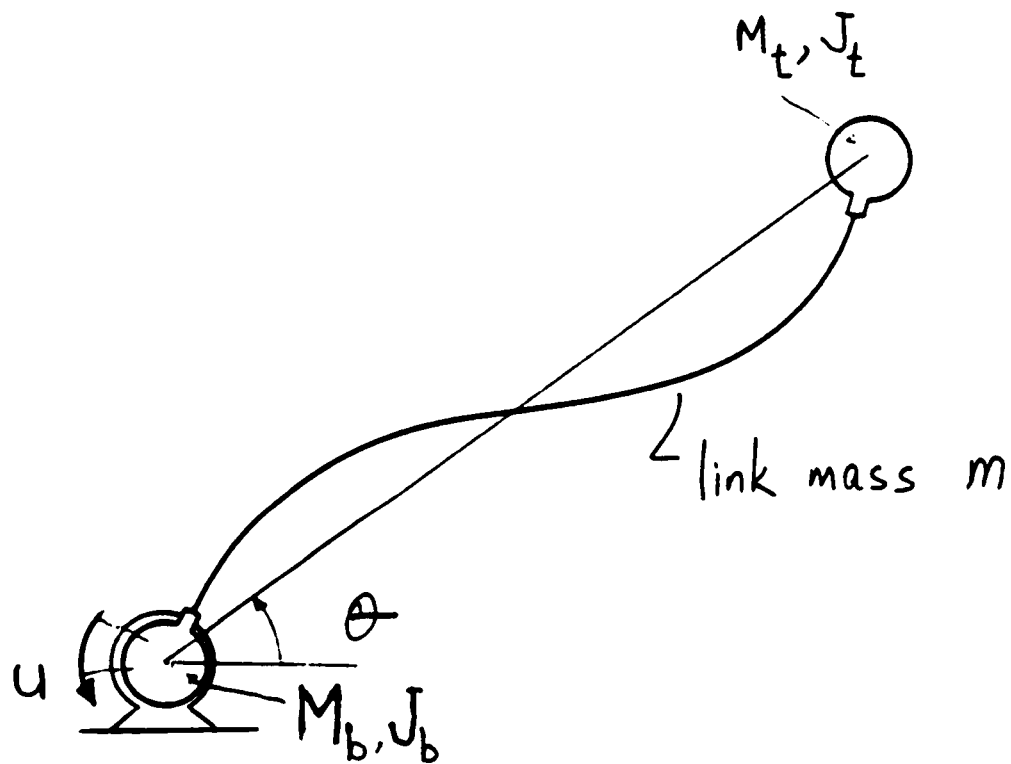
$$
\begin{bmatrix}
\left(J_b + J_t + \frac{1}{3}m\ell^2 + M_t\ell^2\right) & J_b & J_t \\
J_b & J_b & 0 \\
J_t & 0 & J_t
\end{bmatrix}
\begin{Bmatrix}
\ddot{\theta} \\
\ddot{\phi} \\
\ddot{\gamma}
\end{Bmatrix}
+ \frac{EI}{\ell}
\begin{bmatrix}
0 & 0 & 0 \\
0 & 4 & 2 \\
0 & 2 & 4
\end{bmatrix}
\begin{Bmatrix}
\theta \\
\phi \\
\gamma
\end{Bmatrix}
=
\begin{Bmatrix}
u \\
u \\
0
\end{Bmatrix}
$$

A SINGLE LINK SYSTEM; EQUATIONS OF MOTION FROM APPLICATION OF THE SIMPLE MODEL

560
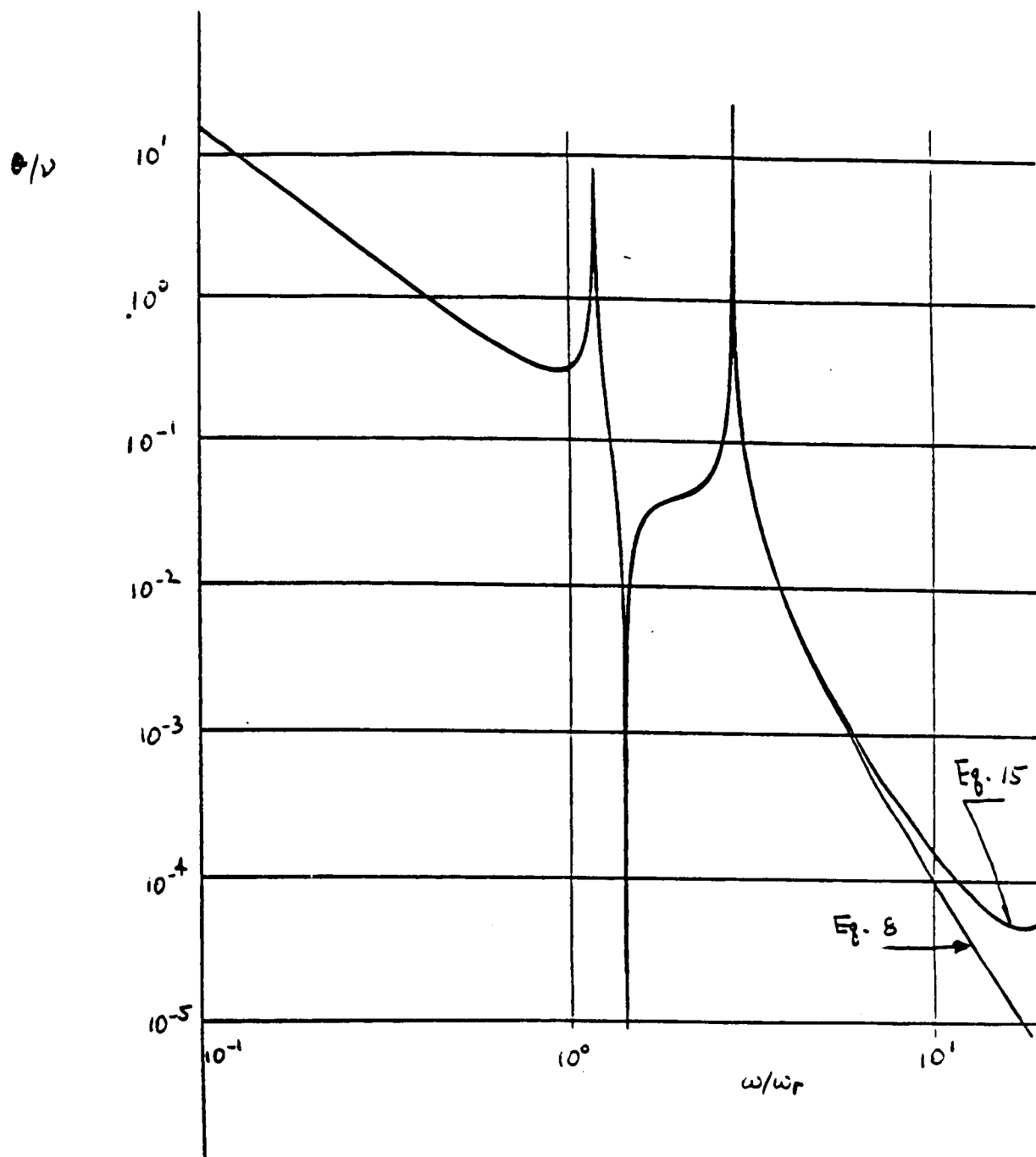
COMPARISON OF TRANSFER FUNCTIONS, SIMPLE MODEL VS. EXACT MODEL

561

Properties of the Simple Model

The model is equivalent to Rayleigh's method, using an assumed shape with two *amplitude variables*, ϕ and ψ.

- Inertial effects of the joints are properly modelled, and are consistent with the mathematical formulation. (Functions in θ)

- The model is also a lumped mass assumption of m acting on the *chord*. (If this is the dominant link inertial effect, then the error is small.)

- The assumed shape has only 2 "dof," and can only approximate the real shape.

- Some higher order effects are plainly "missed," as they would be for a truncated mode solution.

- The formulation would be useful for control, because the variables θ, ϕ and ψ can be measured and actuated.

- For joint-dominant systems the model should be very accurate, and if joint inertias are small the equations reduce in order.

562

7

Applications to Manipulator Control

Equations of motion can be used as follows:

- To confirm the number and the identity of *state variables* for control.

- To perform simulation studies.

- To set gains from classical control theory. (In principle)

- To compute variable gains for a non-linear system. (In principle)

- To accomplish model-based (shaped) control.

- To accomplish model-based feedforward control; requires real-time performance.

563

Single Link Systems

1. Planar (2-D) motion

   - Actuator was a direct drive DC motor.

   - The simple model produces 3x3 equations of motion.

   - Tip has mass but low inertia; system order reduces to 2; state variables are identified as θ and ϕ.

   - Sensing of rotation ($\theta+\phi$) and strain ($\sim\phi$).

   - Perform experiments; set gains by trial and error.

   - Discussion of friction effects.

2. Spherical (3-D) motion

   - Actuation using two joints of the modular manipulator.

   - See videotaped results.

   - Controllable despite friction and backlash.

564

9
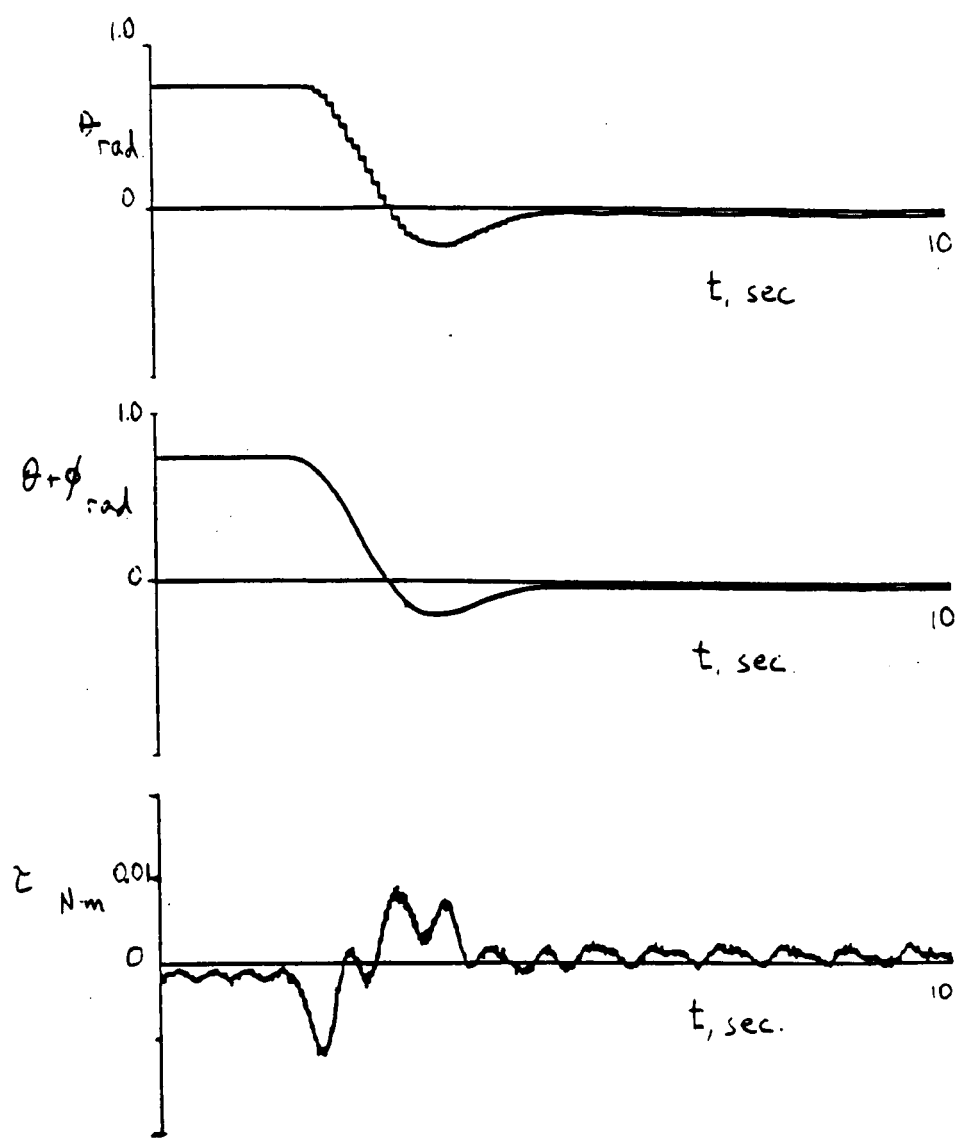
EXPERIMENTAL RESULTS, PLANAR SINGLE LINK SYSTEM

565
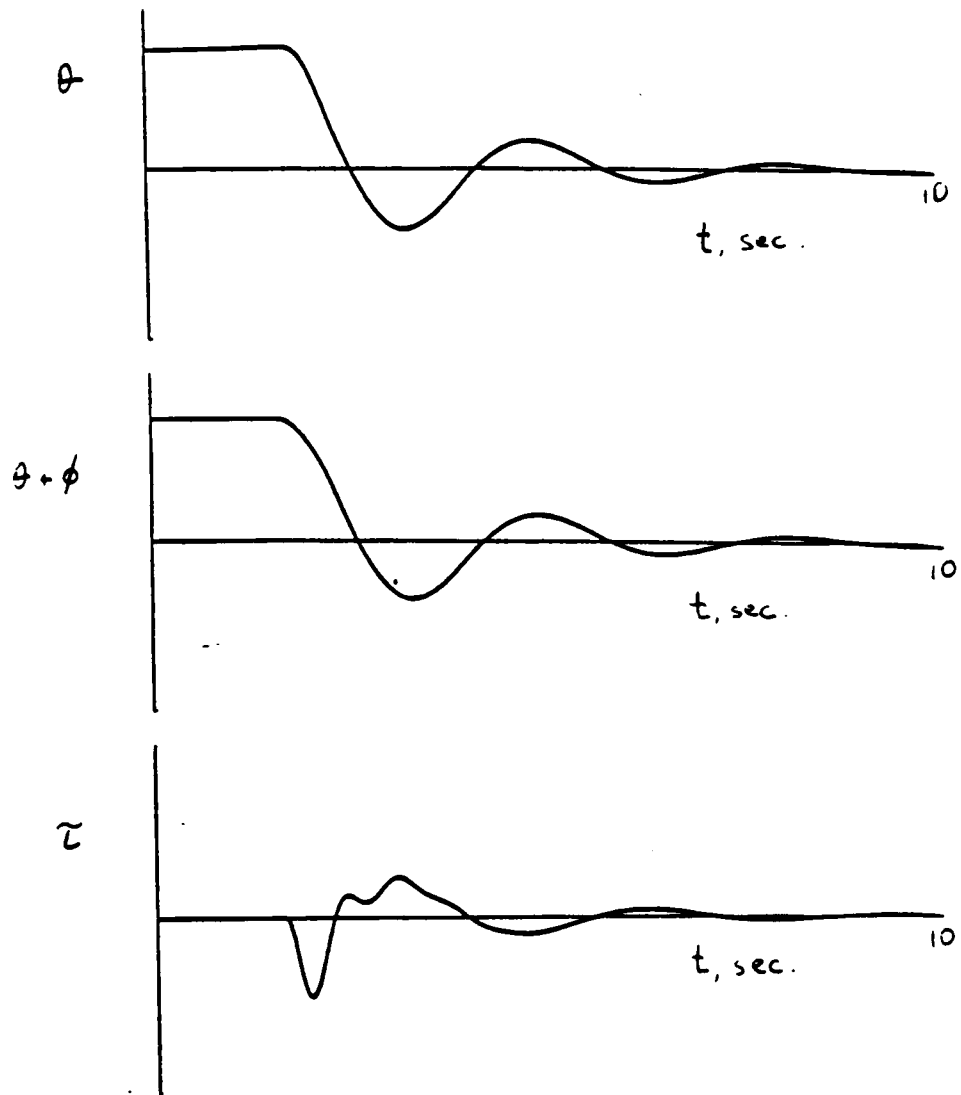
SIMULATION RESULTS, PLANAR SINGLE LINK SYSTEM

566
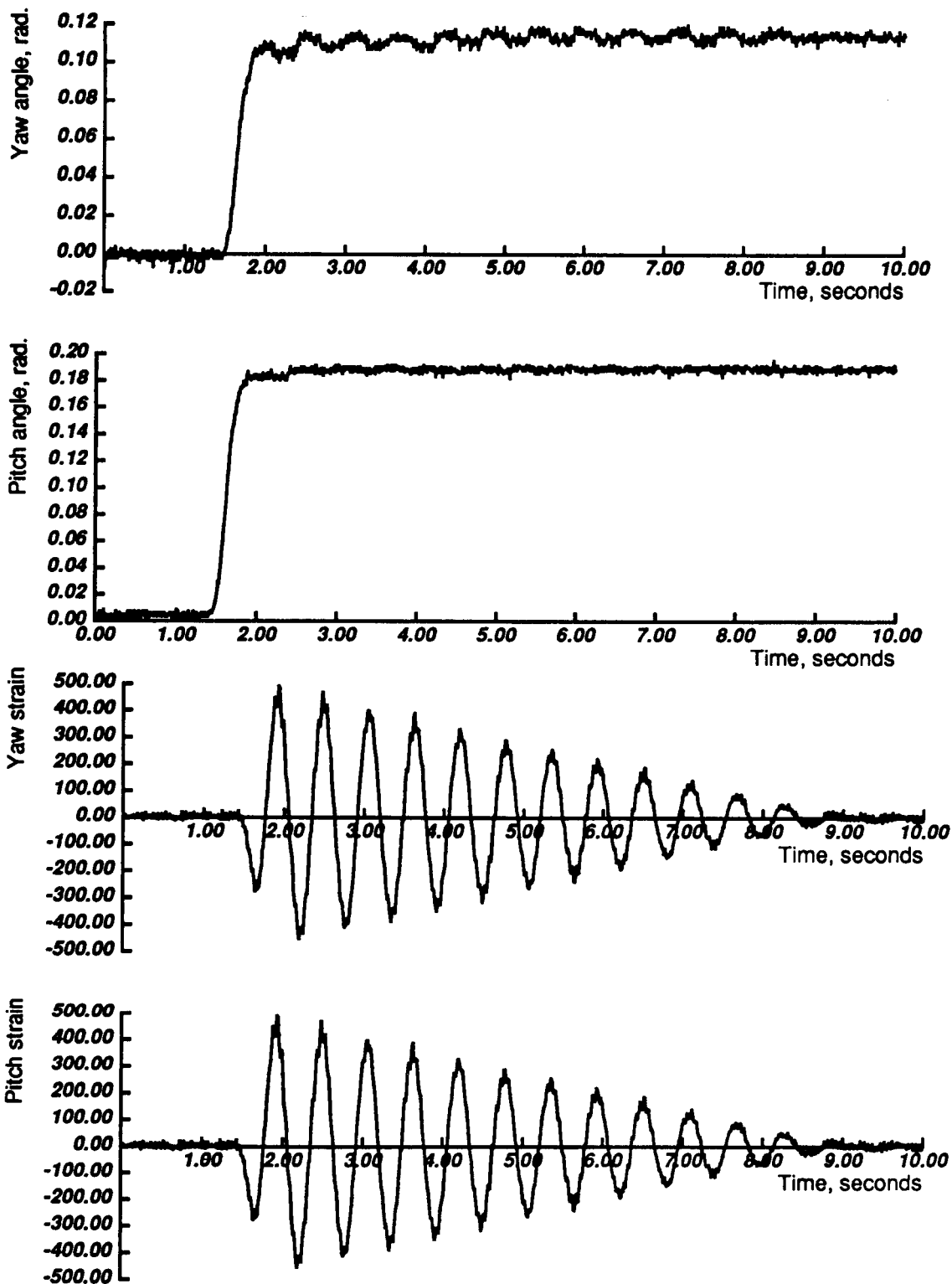
Figure 1: Feedback on Position (Rotation) Only

SINGLE LINK SYSTEM, 3-D (SPHERICAL) MOTION
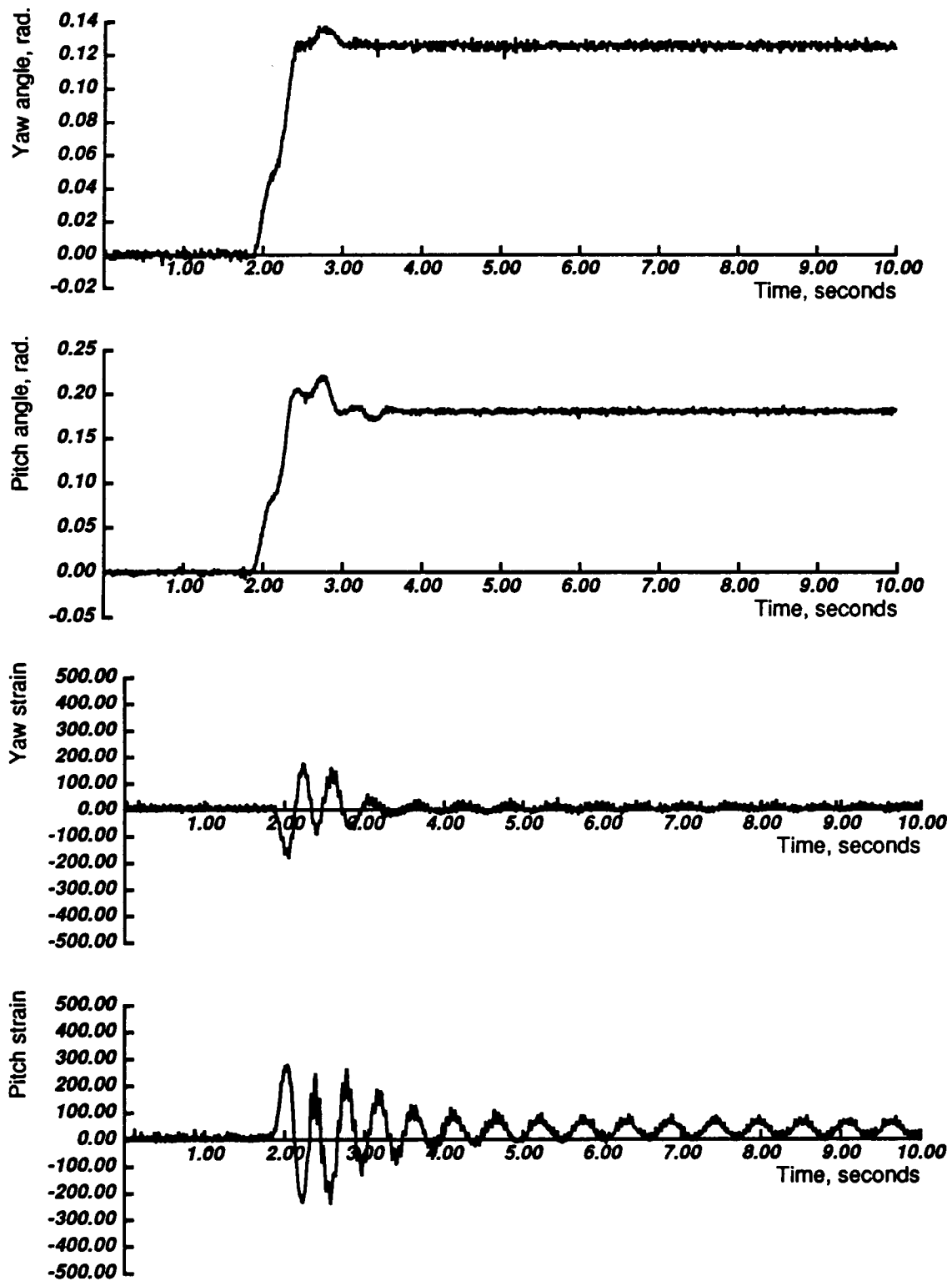
Figure 1: Feedback on Position (Rotations) and Strains

SINGLE LINK SYSTEM, 3-D (SPHERICAL) MOTION

568

Planar Two Link System

- Experiments performed at Toshiba.

- Air table, 2-D manipulator.

- Four state variables: θ's and ϕ's.

- Compare experimental and simulation results.

- Friction in actuators causes vibration.

- Feedforward control is attempted, inclusive of friction effects.

- Model based feedforward control limits vibration.

569

M_{t1}, J_{t1}

M_{b2}, J_{b2}

$(-) \theta_2$

u_2

link 1

link 2

M_{t2}, J_{t2}

M_{b1}, J_{b1}

θ_1

u_1
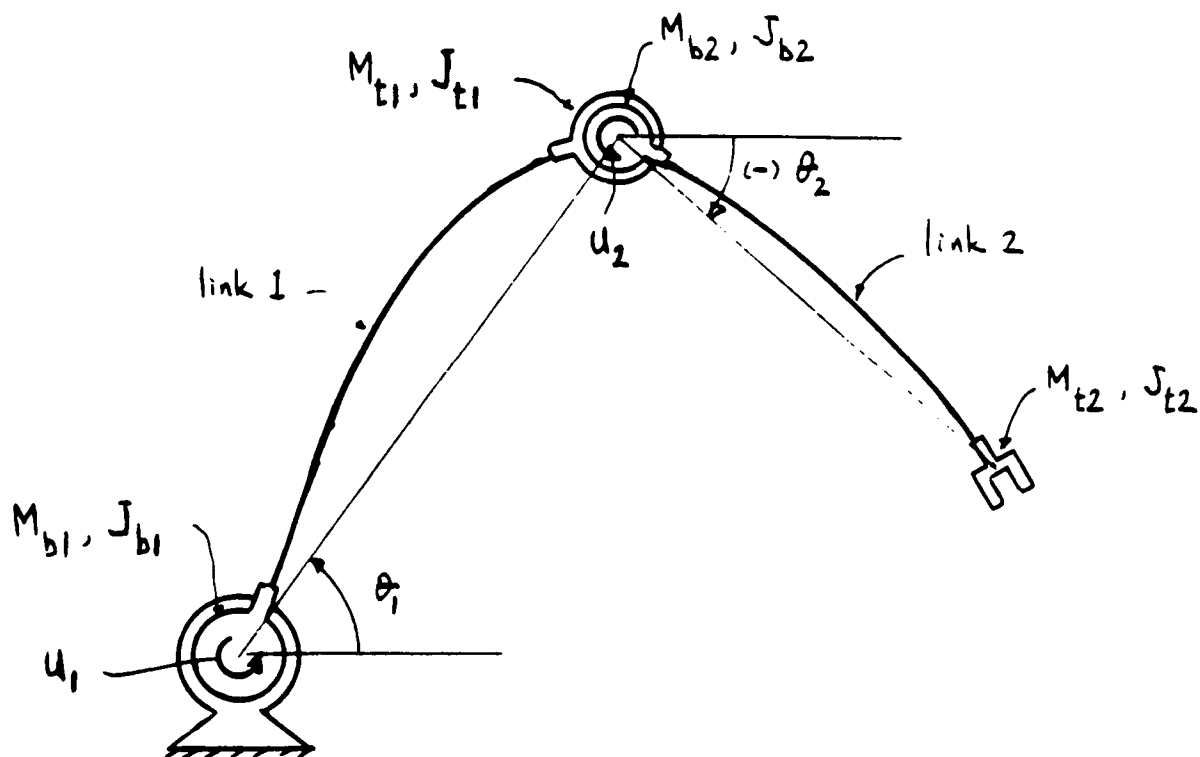
2-DOF TWO LINK PLANAR SYSTEM (AIR TABLE, HORIZONTAL PLANE)
(EXPERIMENTS CONDUCTED AT TOSHIBA)

570
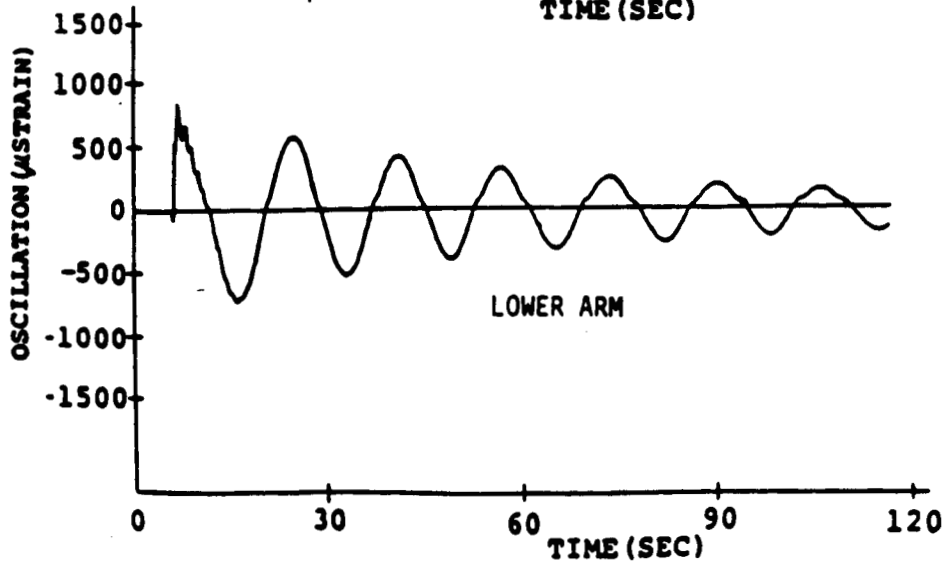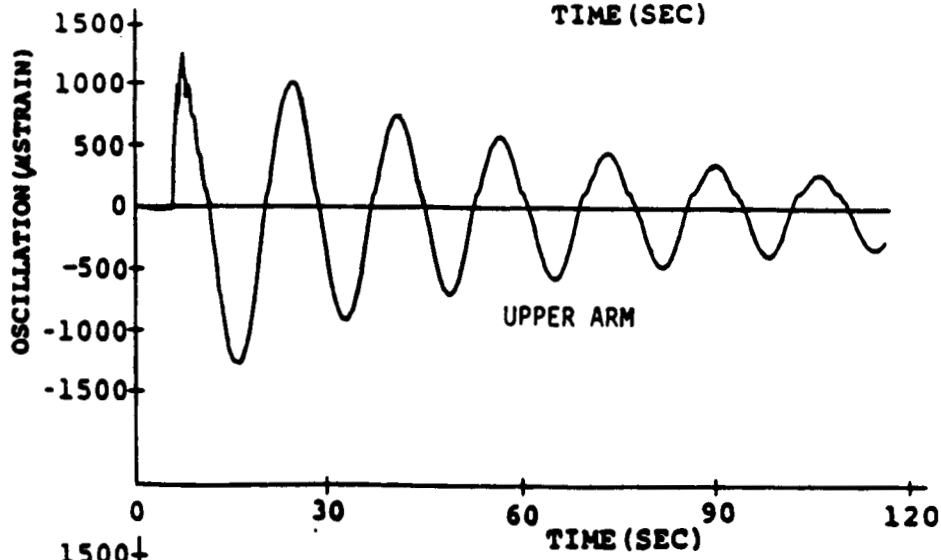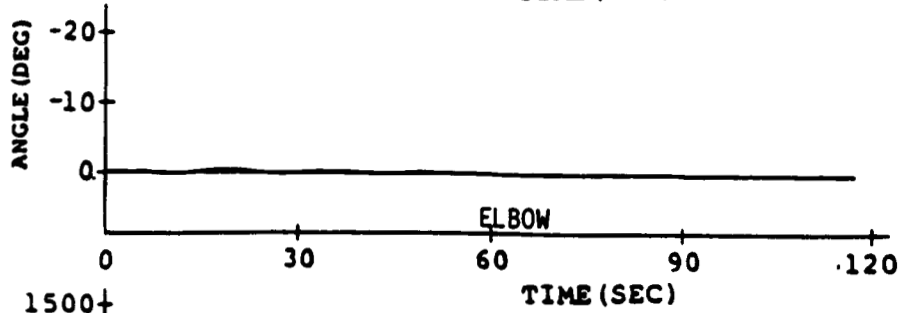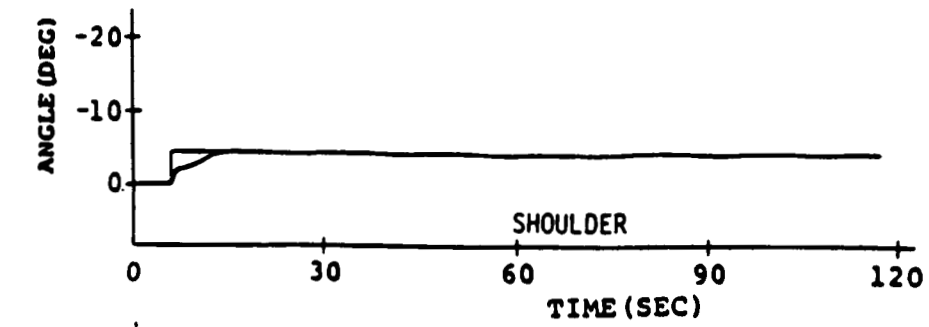
PLANAR TWO-LINK MANIPULATOR: EXPERIMENTAL RESULTS

571
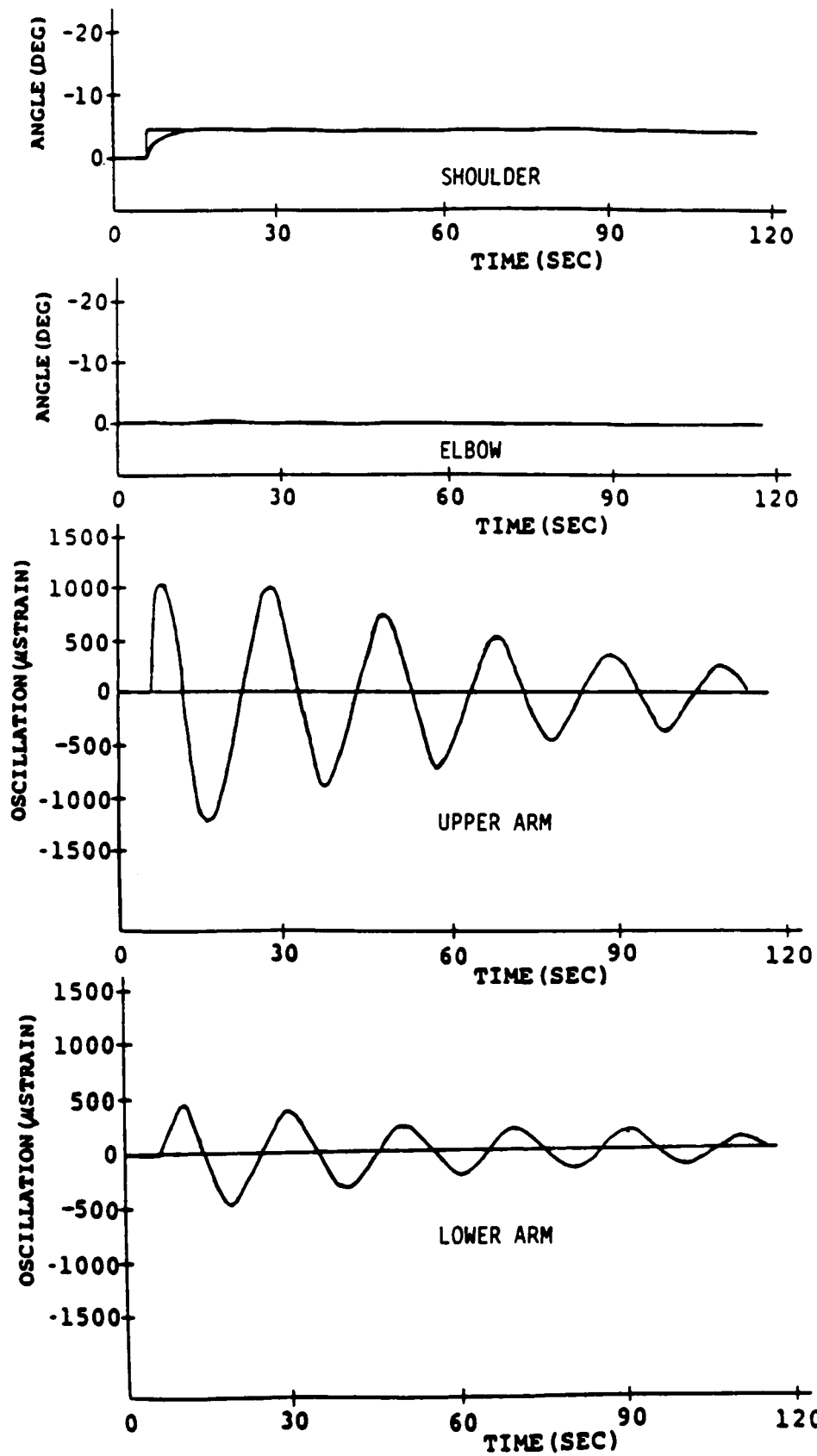
PLANAR TWO-LINK MANIPULATOR: SIMULATION RESULTS

Fig. 6a

572
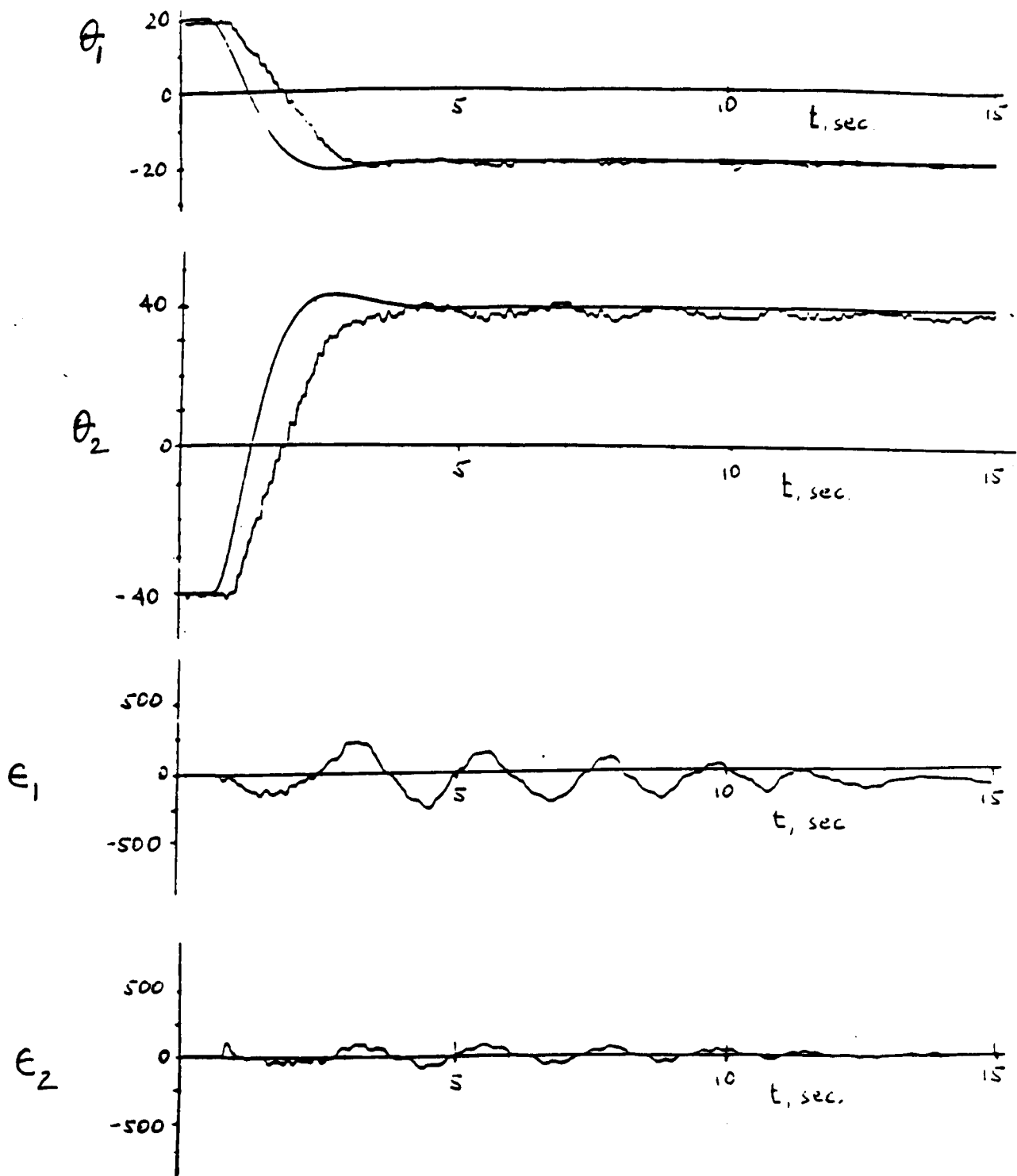
EXPERIMENTAL RESULTS, FEEDBACK CONTROL: NOTE VIBRATION EFFECT, FROM FRICTION

573
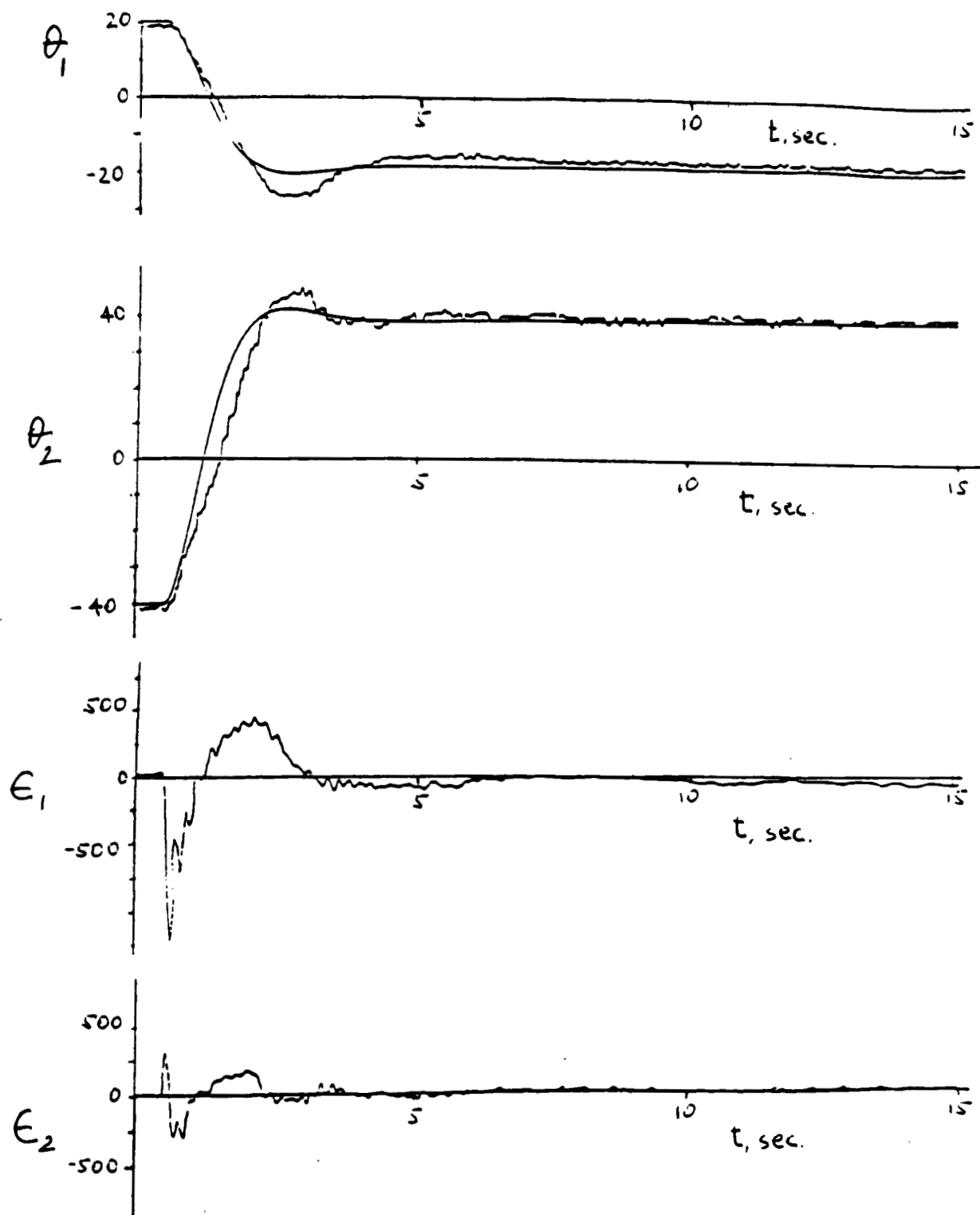
EXPERIMENTAL RESULTS, FEEDFORWARD CONTROL: NOTE ELIMINATION OF VIBRATION

574

Combined Flexural-Torsional (3-D) Motion

Experiments performed April 1988:

- Three actuated DOF (yaw, pitch, roll).

- Two links; one flexible, one rigid.

- Linear feedback control; gains by trial and error.

- Coupled flexural and torsional vibrations.

- See videotape; see experimental results.

- Actuator properties by system identification (in process).

- Analtyical model used in simulation studies (in process).

- Next phase: distal link made flexible, 4 (or 5) actuated DOF.
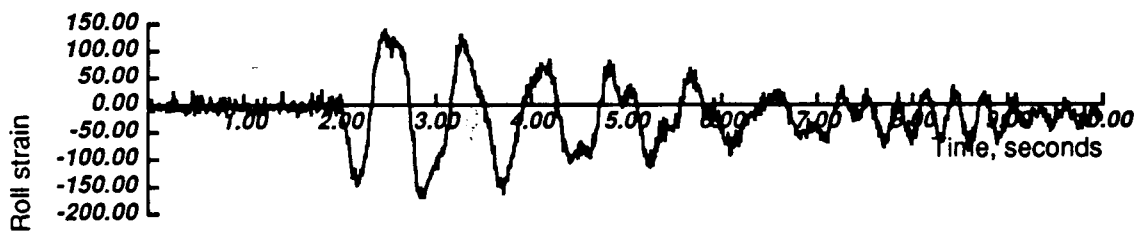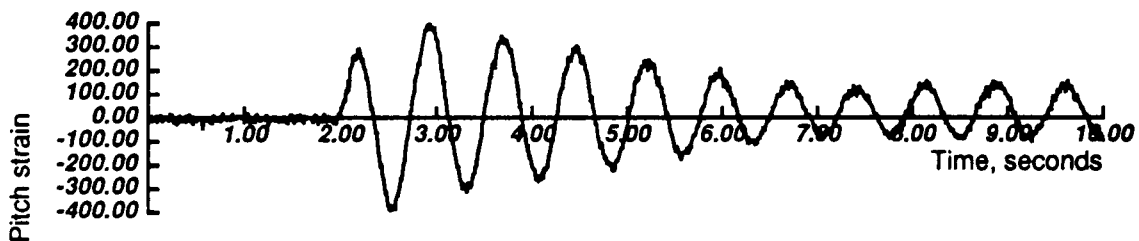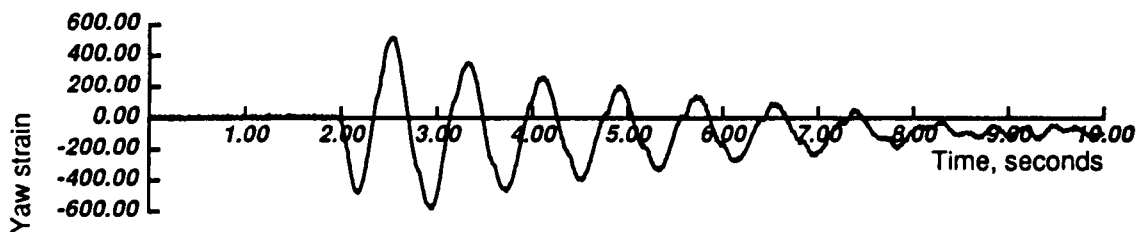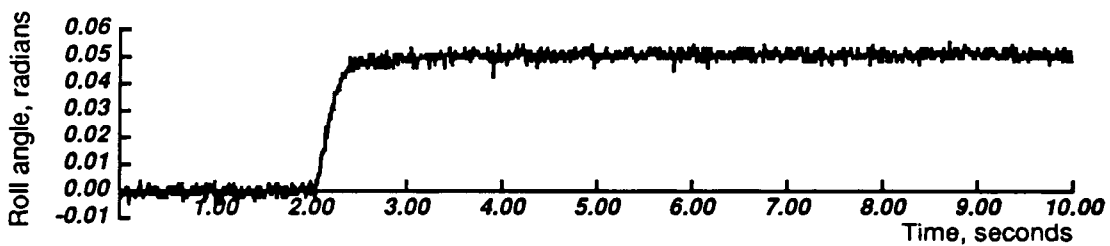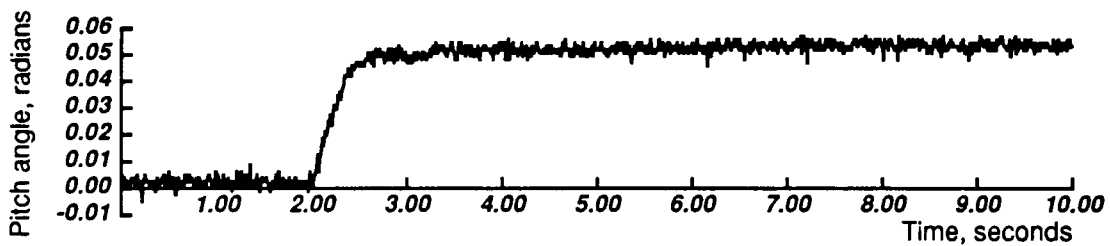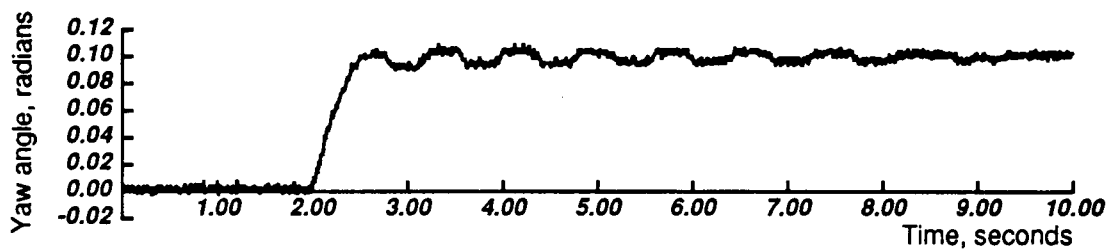
COUPLED FLEXURAL-TORSIONAL MOTIONS ROTATIONS AND STRAINS

FEEDBACK CONTROL ON POSITION; NO FEEDBACK ON STRAIN
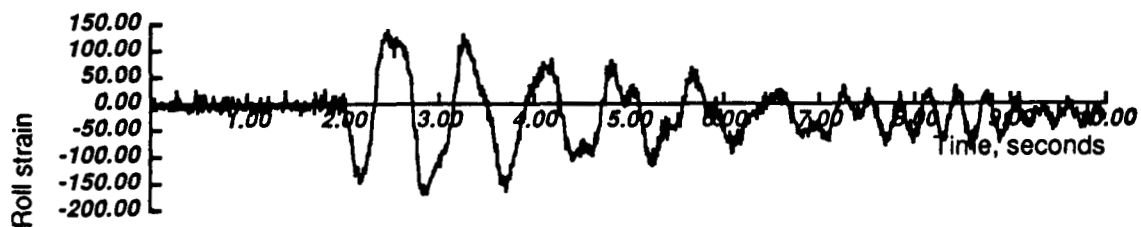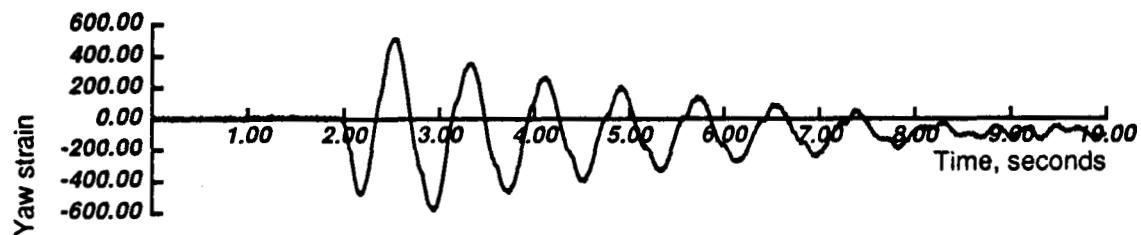
576

COUPLED FLEXURAL-TORSIONAL MOTION: STRAINS

FEEDBACK CONTROL ON POSITION; NO FEEDBACK ON STRAIN

577
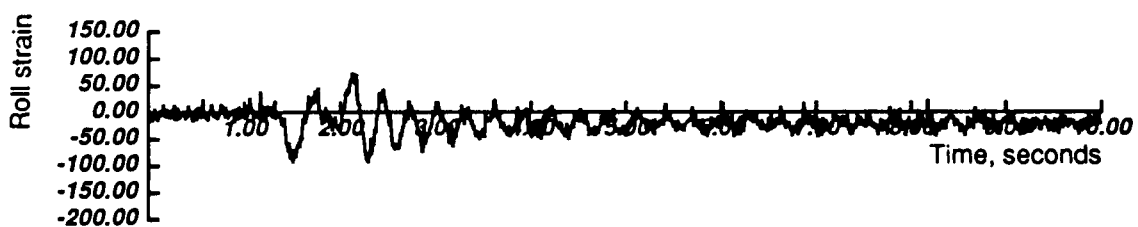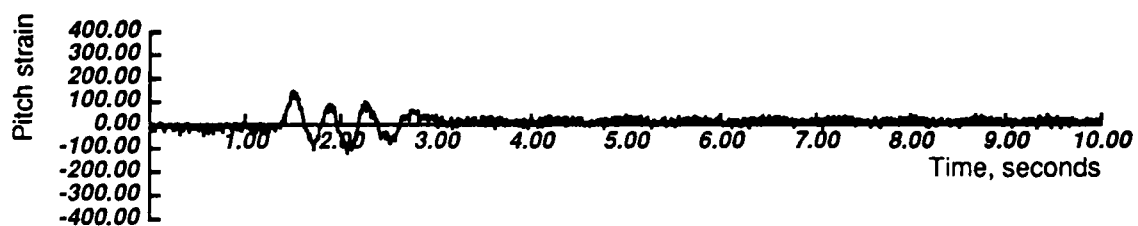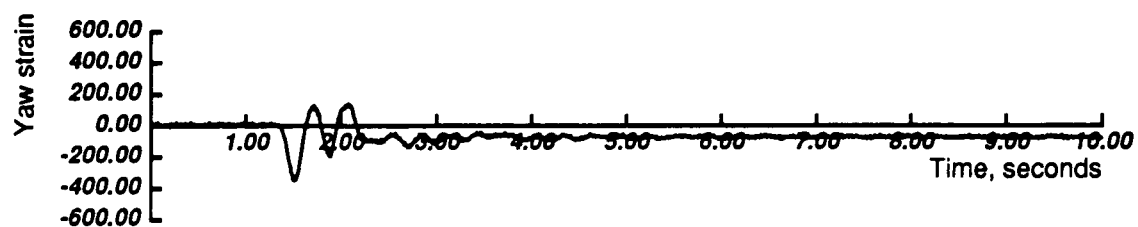
COUPLED FLEXURAL-TORSIONAL MOTION: STRAINS

FEEDBACK CONTROL ON POSITION AND ON STRAIN

578

Discussion and Conclusions

- The model may be well suited for serial link manipulators, including joint-dominated systems.

- Accuracy for MDOF systems, non-linear in configuration, remains to be examined.

- Control experiments must be extended beyond linearized regions.

- The major application is model-based control, still to be studied in depth.

- Effects of friction, backlash, deadband should be included.

- Friction or torque ripple can excite higher modes.

- Frequencies of unmodelled (higher) modes can be adjusted by inserting "redundant" actuators.

579

MINIMUM-VARIANCE REDUCED-ORDER ESTIMATION ALGORITHMS FROM PONTRYGIN'S MINIMUM PRINCIPLE

By

Yaghoob S. Ebrahimi
Boeing Commercial Airplanes
Seattle, Washington

ABSTRACT

It has become apparent with the introduction of modern control and estimation theory that the entire knowledge of a system cannot be included in the system design for most practical applications. Such mechanization of a total system usually results in a model exceeding the capacity of a real-time processor, thus requiring a reduction in the state size. In addition, linear filtering and smoothing problems have been extensively investigated for a case wherein the filter or smoother is of the same state dimension as the dimension of the "best state" model available.

This paper presents a uniform derivation of minimum-variance reduced-order (MVRO) filter-smoother algorithms from Pontrygin's Minimum Principle. An appropriate performance index for a general class of reduced order estimation problem is formulated herein to yield optimal results over the entire time interval of estimation. These results provide quantitative criteria for measuring the performance of certain classes of heuristically designed, suboptimal reduced-order estimators as well as explicit guidance to the suboptimal filter design process with both continuous and discrete filter-smoother algorithms being considered.

By the duality principle, the algorithms of reduced-order estimation can be easily extended to the deterministic problems of optimal control (i.e., the regulator and linear tracking problem).

581

MODIFYING HIGH-ORDER AEROELASTIC MATH MODEL OF A JET TRANSPORT USING MAXIMUM LIKELIHOOD ESTIMATION

By

Amir A. Anissipour and Russell A. Benson
The Boeing Company
Seattle, Washington

ABSTRACT

The design of control laws to damp flexible structural modes requires accurate math models. Unlike the design of control laws for rigid body motion (e.g., where robust control is used to compensate for modeling inaccuracies), structural mode damping usually employs narrow band notch filters. In order to obtain the required accuracy in the math model, maximum likelihood estimation technique is employed to improve the accuracy of the math model using flight data. This paper presents all phases of this methodology: (1) pre-flight analysis (i.e., optimal input signal design for flight test, sensor location determination, model reduction technique, etc.), (2) data collection and preprocessing, and (3) post-flight analysis (i.e., estimation technique and model verification). In addition, a discussion is presented herein of the software tools used for this study and the need for future study in this field.

PRECEDING PAGE BLANK NOT FILMED.

Modifying High-Order Aeroelastic Math Model of a Jet Transport Using Maximum Likelihood Estimation

Amir A. Anissipour
Russell A. Benson

The Boeing Company
Boeing Commercial Airplanes
P.O. Box 3707   M/S 9W-38
Seattle ,Wa. 98124

ABSTRACT

The design of control laws to damp flexible structure modes requires accurate math models of the dynamic system. To obtain the required accuracy of a math model, the parameter estimation technique using maximum likelihood estimation is employed to improve the accuracy of the model based on flight data. This paper presents all phases of this methodology: pre-flight analysis (i.e., optimal input signal design for flight test, sensor location determination, model reduction technique, etc.), data collection and preprocessing, and post-flight analysis (i.e., estimation technique and model verification). The results of this study indicate that the parameter estimation technique (i.e., maximum likelihood estimation) is an effective and powerful technique in modifing high-order aeroelastic aircraft models. However, the accuracy of the results depends upon the fidelity of the theoretical model with regards to the correct number of dominant modes for the desired frequency bandwith in the model (i.e., model order). If the number of modes in the model are not representative, then an identification problem can occure in the parameter estimation technique. Nevertheless, this problem can be overcome using the system identification technique.

584

INTRODUCTION

Having an accurate mathematical representation is fundamental to any aircraft control system design. In general, aircraft models are developed from a theoretical basis and modified by analyzing the experimental data (i.e., wind-tunnel data for aerodynamic models or ground shake test data for structural models). Although present techniques provide very good dynamic models for the design stages of an aircraft, often these models do not match the actual dynamic flight response. This problem has generated a need for advanced system identifiaction and parameter estimation techniques in upgrading dynamic models of an aircraft based on flight test data. This modeling problem is more apparent with high-order aeroelastic models with which our experince with modeling techniques is limited.

Low-frequency structural modes are easily excited for a jet transport with a long fuselage. This excitation causes a lateral ride discomfort in certain flight conditions. In order to design a yaw damper to dampen Dutch roll response and suppress the undesirable low-frequency structure modes by means of active control, an accurate aeroelastic model of the aircraft must be available. In this study, parameter estimation technique is applied to upgrade the high-order aeroelstic math model of a jet transport. The following is a summary of the parameter estimation technique using maximum likelihood estimation.

Maximum Likelihhood Estimation

Suppose the actual system is described by (Reference 1):

$$\dot{x}(t) = A\,x(t) + B\,u(t) + S\,s(t) + F\,n(t)$$
$$z(t_i) = C\,x(t_i) + D\,u(t_i) + H\,s(t_i) + G\,m(t_i) \tag{1}$$

where

$x(t)$	state vector
$u(t)$	control vector
$z(t_i)$	measurement vector
$s(t)$	bias vector
$n(t)$	process noise
$m(t_i)$	measurement noise
t_i	time sample
A, B, C, D, S, H, F, G	system matrices with unknown parameters
$n(t)$ and $m(t)$	are zero mean, Gaussian and independent noise

Assume k is the vector of unknowns that contains elements of the system matrices A, B, C, D, S, H, F and G. The objective is to maximize the probability distribution of unknowns (i.e., k) when the measurements z are available. Therefore, maximizing P(k/z), where P is the probability distribution function of k given z.

By Bayes' rule:

$$P(k/z) \; P(z) \;=\; P(k,z) \;=\; P(z/k) \; P(k) \tag{2}$$

or

$$P(k/z) \;=\; P(z/k) \; \frac{P(k)}{P(z)} \tag{3}$$

Since in these equations z is given, so P(z) becomes a constant. Assume there is no a priori preference for k, so P(k) becomes a constant. Therefore, P(z/k) differs from P(k/z) only by a constant. In other words equation (3) becomes:

$$P(k/z) \;=\; P(z/k) \;\cdot\; \text{constant} \tag{4}$$

Equation (4) indicates that P(z/k) may be maximized instead of P(k/z). Therefore, using Gaussian assumption, the likelihood ratio may be written as:

$$P(z/k) = \left[(2\pi)^L \left| GG^* \right| \right]^{-\frac{1}{2}N} \exp\left\{ -\frac{1}{2} \sum_{i=1}^{N} \left[z_k(t_i) - z(t_i) \right]^* (GG^*)^{-1} \left[z_k(t_i) - z(t_i) \right] \right\} \tag{5}$$

where
$z_k(t_i)$	predicted estimate at time t_i
GG^*	measurement noise covariance matrix
L	number of measurements

If the logarithm of equation (5) is taken, the consatnt terms are eliminated by the maximization, and the equation is multiplied by -1 to do minimization rather than maximization, then equation (6) will be obtained as:

$$J(k) = \frac{1}{2} \sum_{i=1}^{N} \left\{ \left[z_k(t_i) - z(t_i) \right]^* (GG^*)^{-1} \left[z_k(t_i) - z(t_i) \right] \right\}$$

(6)

where J(k) is the cost function to be minimized. Two steps are taken to obtain $z_k(t_i)$. Prediction step:

$$x_k(t_{i+1}) = \Phi \, x_k(t_i) + \Psi \, u(t_{i+1/2})$$
$$z_k(t_{i+1}) = C \, x_k(t_{i+1}) + D \, u(t_{i+1})$$

(7)

where

$$\Phi = e^{A \, \Delta t} \qquad \text{and} \qquad \Psi = \int_0^t e^{A \, s} \, ds$$

and the correction step:

$$x_k(t_{i+1}) = x_k(t_{i+1}) + K \left[z(t_{i+1}) - z_k(t_{i+1}) \right]$$

(8)

K in equation (8) is the Kalman filter gain matrix given by:

$$K = P \, C^* (GG^*)^{-1}$$

(9)

where P is the solution to the discrete time Riccati equation:

$$A P + P A^* - \frac{1}{\Delta t} P C^* (GG^*)^{-1} C P + F F^* = 0$$

(10)

After obtaining the cost function J(k), the Newton-Raphson algorithm is used iteratively to minimize the cost function by revising the unknowns parameters.

$$k_{i+1} = k_i - \left\{ \nabla_k^2 J(k_i) \right\}^{-1} \left\{ \nabla_k^* J(k_i) \right\}$$

(11)

587

This algorithm requires an intial estimate for the vector of unknowns (k_0). A priori estimate is available for each unknown parameter through the analytical model.

The MMLE software tool developed by NASA Dryden is a parameter estimation program supporting this estimation technique. This software has been modified by Boeing to accept and handle higher order models. A comprehensive description of this software tool is described in Reference 1.

PRE-FLIGHT ANALYSIS

Math Model

A sixtieth order linear aeroelastic math model for a flight condition of Mach .6 speed, 15000 foot altitude, and no turbulance, and cruise configuration of a jet transport was provided in the form of:

$$M \ddot{q} + C \dot{q} + K q = u \tag{12}$$

where   M   mass matrix
          C   damping matrix
          K   stiffness matrix
          q   generalized coordinate
          u   control inputs

The model is defined in the inertial axis system, and the dynamics (q), consist of rigid body and flexible modes. The model is tuned using data from ground shake testing. The system of equations (12) was transformed into state-space form using the following transformation:

$$X_m = \begin{bmatrix} q \\ \dot{q} \end{bmatrix}$$

therefore the system equation (12) becomes:

$$\dot{x} = A_m x_m + B_m u$$
$$y = C_m x_m + D_m u \tag{13}$$

where

$$A_m = \begin{bmatrix} 0 & I \\ -M^{-1}K & -M^{-1}C \end{bmatrix}$$

and

$$B_m = \begin{bmatrix} 0 \\ M^{-1} \end{bmatrix}$$

This transformation always exists because the mass matrix is positive definite. Although this is a well-posed theoretical problem, it is not trivial. The flexible model is usually on the order of one hundred states, thus causing numerical inaccuracies in the inversion of the mass matrix. In our analysis the software package MPAC was used to perform the transformation. (MPAC is a numerically robust modern control and analysis software tool developed by the Boeing Company.)

For the identification process, the system equation (13) was transformed into the conjugate modal form using the following transformation:

$$m = T^{-1} x_m$$

Equation (13) becomes:

$$\dot{m} = \Lambda m + \bar{B} u$$
$$y = \bar{C} m + D u \tag{14}$$

where

$$\Lambda = \text{dia} (\lambda_i) \qquad \lambda_i = i^{th} \text{ eigenvalue}$$

$$\bar{B} = T^{-1} B \qquad \text{controllability} \quad \text{matrix}$$

$$\bar{C} = C\,T \qquad \text{observability} \quad \text{matrix}$$

The advantage of using the modalized form given by equation (14) is that all the modes through Λ matrix, along with the controllability and observability matrices are readily available for an analyst to quickly locate uncontrollable and unobservable modes. In addition, the modes in the Λ matrix are decoupled and may be partitioned into rigid model and elaastic model.

The order of the model was reduced to nineteen by deleting the modes above 6 Hz. Since this model will eventually be used for ride quality study and modal supperasion design, only those modes less than 6 Hz were retained.

The reduced order, modal model (19th order) is represented by:

$$\dot{m}_r = \Lambda_r\, m_r + \bar{B}_r\, u$$
$$y \;\; = \bar{C}_r\, m_r + D_r\, u \tag{15}$$

This model contains one state for heading, one for the spiral mode, two for the Dutch roll mode, one for roll mode, eight for low-damped elastic modes, and six for high-damped elastic modes.

To support this study, a special set of sensors were installed on the aircraft to measure the dynamic response of the jet transport. The locations of these sensors were based on the mode shapes of the aircraft determined by the math model and physical constraints (Table I). (A complete discussion on sensor selection and location placement on the aircraft is omitted herein for proprietary reasons.)

TABLE I: Sensor Type and Locations for High-order Aeroelastic Modeling

SENSOR TYPE	SENSOR LOCATION
Position Transducer	On all control surfaces
Yaw Rate Gyro	Pilot seat, IRU (a station between CG and cockpit below the cabin floor), CG station
Lateral Accelerometer	1 Pilot seat, 1 Cockpit ceiling, 8 on the passanger cabin floor from the cockpit to the aft galley, 1 on the aft galley ceiling, 3 on vertical tail (tip and mid section, front and rear spar), three on each nacelle, 1 IRU station
Vertical Accelerometer	1 on the pilot seat, 1 IRU, 1 aft galley, 8 on each wing, 3 on each horizontal tail, 2 on each nacelle
Roll rate, Yaw rate, Bank angle, Heading,	IRU and CG stations

The sensors selected for the analysis were: body roll angle (Φ), heading angle (Ψ), roll rate (p) and yaw rate (r) at the IRU; body yaw rate at the pilot seat; 9 lateral accelerometers along the fuselage; 2 lateral accelerometers on the nacelle number 2; and 3 lateral accelerometers on the vertical tail.

Input Signal Design

The flight test input-signal design analysis for high-order aeroelastic modeling was performed using the reduced order analytical model (equation 15). Although a number of "optimum" input signals have been proposed for flight testing in conjunction with parameter estimation, none have been found to be appropriate for

high-order aeroelastic modeling. Essentially, all the analytical techniques proposed in designing the optimum input signals are based on the analytical model. This model is the subject of improvement by the identification and estimation techniques. Hence, no "optimum" input signal exists.

A number of different input signals were evaluated for this study. After a comprehensive simulation study, it was determined that a frequency sweep of a linear sine-wave with adequate energy to excite all the modes (rigid and elastic) yeilds the best results. In addition, the linear sine-wave frequency sweep optimizes the most commonly used criterion for input signal design:

$$\mathfrak{R} = -\log \ (\det M) \tag{16}$$

where M is the Fisher information matrix (or sensitivity matrix) defined by:

$$M = \nabla^2_k \ J(k) \tag{17}$$

J is the cost function defined in equation (6). The criterion $\mathfrak{R}$ defined in equation (16) is related to the volume of highest probability density region for the parameters k. An interesting property of the determinant criterion is that it is independent of scaling parameters (Refernce 2).

Fifteen tests were designed for the same flight condition. Five frequency sweeps were designed for each control surface. Each test was repeated for rudder, aileron, and both surfaces in phase. The first frequency sweep covered 0 to 6 Hz to excite all the modes in one test. The other four tests were then designed to excite specifically high-damped modes by sweeping from .25 Hz below to .25 Hz above the frequency of the mode.

The amplitude of the input signals were designed to be constant for practical purposes (i.e., rate limits). The designed input signals were tested in the lab to confirm that the signals did not saturate the servos and actuators of the control surfaces. However, the output of the actuators during flight test generated signals with decaying amplitutes. These decaying amplitudes reduced the energy level initially designed for the test. Figures 1 and 2 show the actual control surface
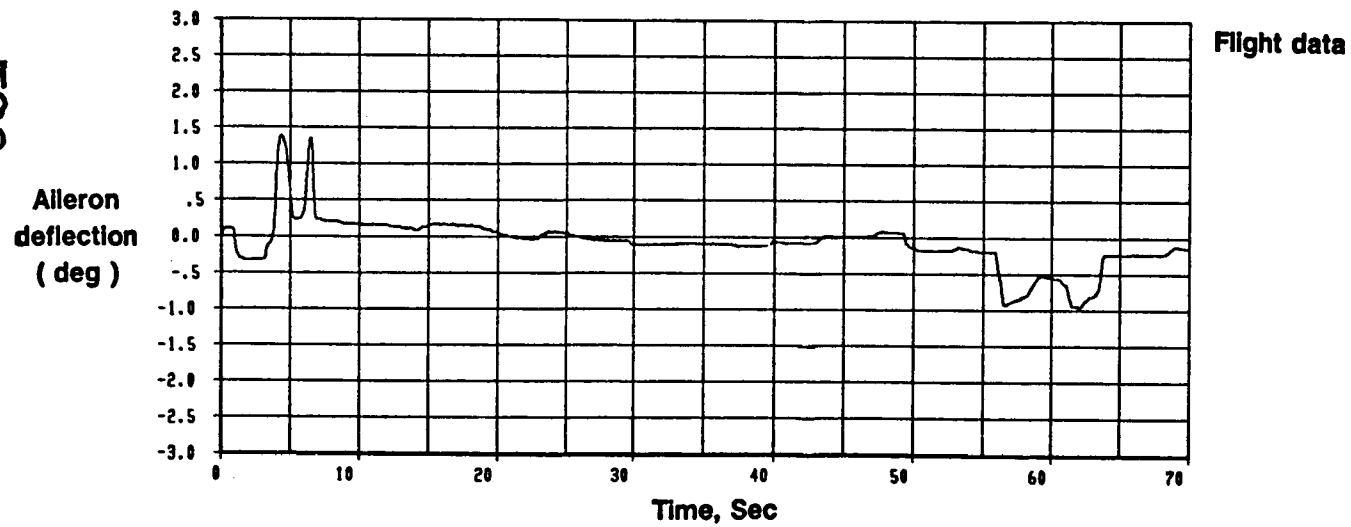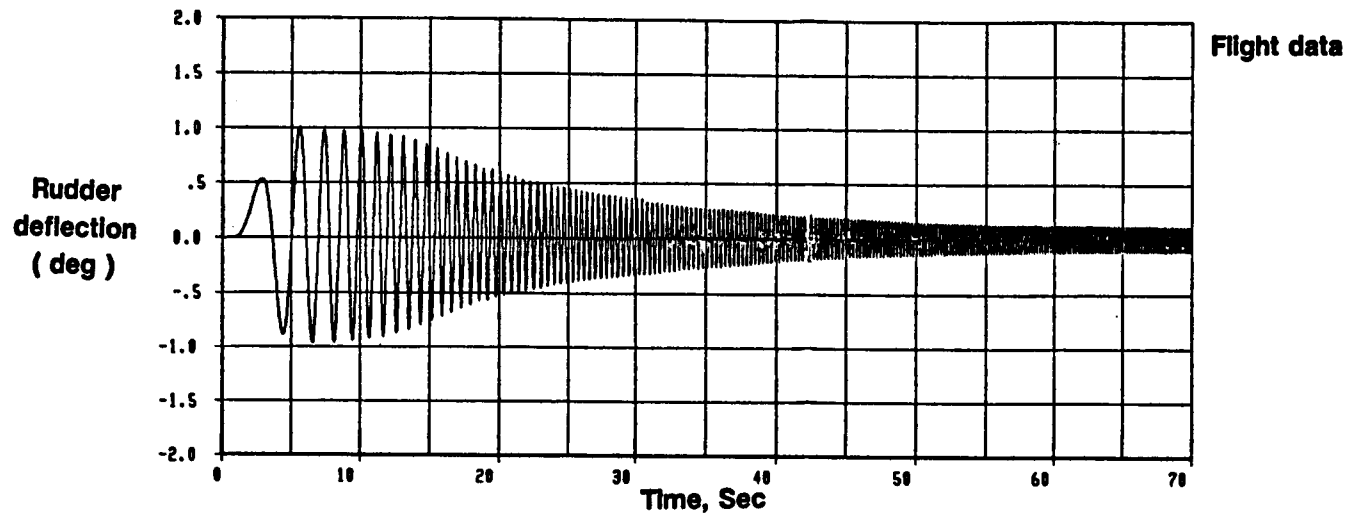
Figure 1. Actual Control Surface Deflections for Flight Condition 21

593
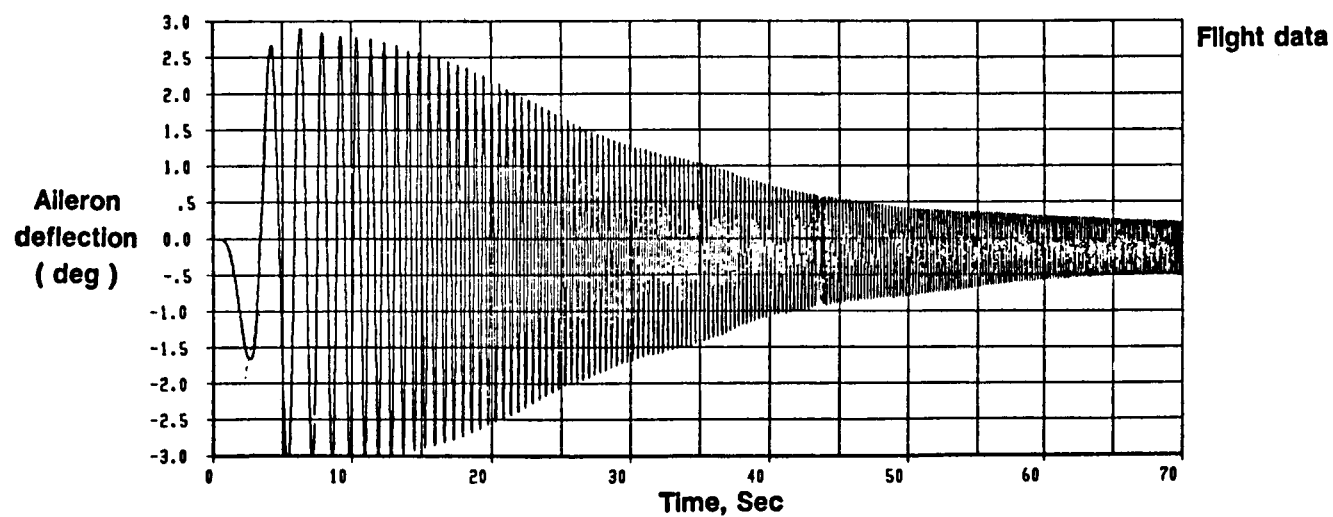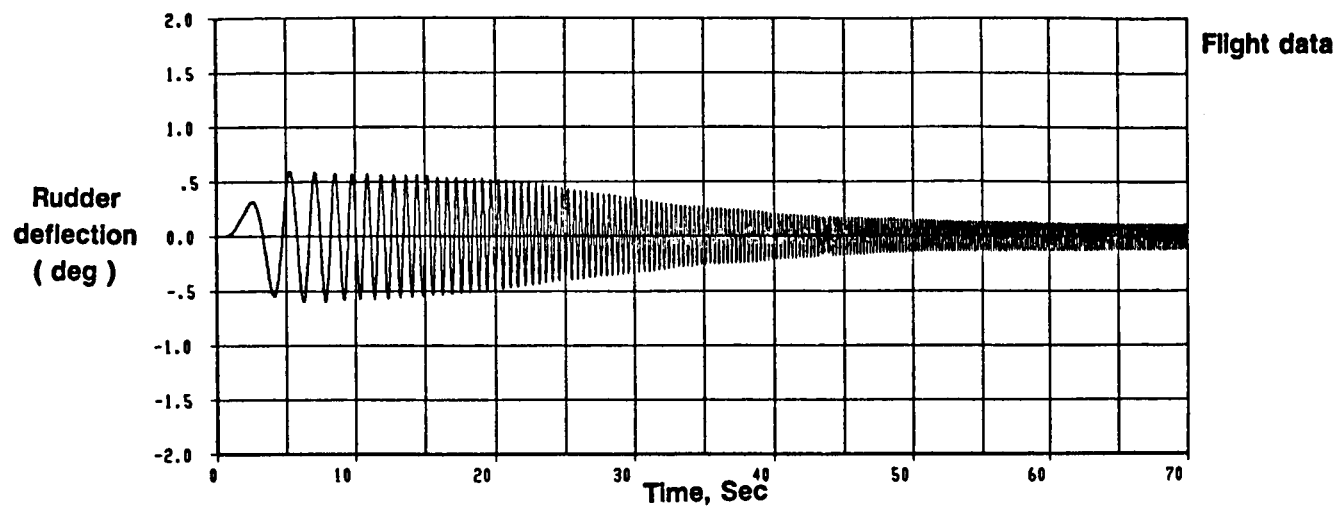
Figure 2. Actual Control Surface Deflections for Flight Condition 41

594

deflections for rudder sweep alone, and for rudder and aileron surfaces simultaneously in phase.

Sampling Frequency

To record the data in flight test, a simulation study was conducted to determine the required sampling frequency. The analytical model (i.e., system equations 15) was assumed to be the true model, and simulated using the designed input signal. A considerable amount of noise was added to the simulation data, and then that data was treated as pseudo-flight data. The acutal model was used for parameter estimation to determine the required sampling frequency. Sampling frequencies of 20, 25, 50, 100, 200 Hz were considered for this study. One mode or group of modes at a time were selected for the estimation process of each sampling frequency. The results indicated that 100 Hz is the best sampling frequency for this study. Figure 3 shows the typical results for identified parameters when different sampling frequencies were used.
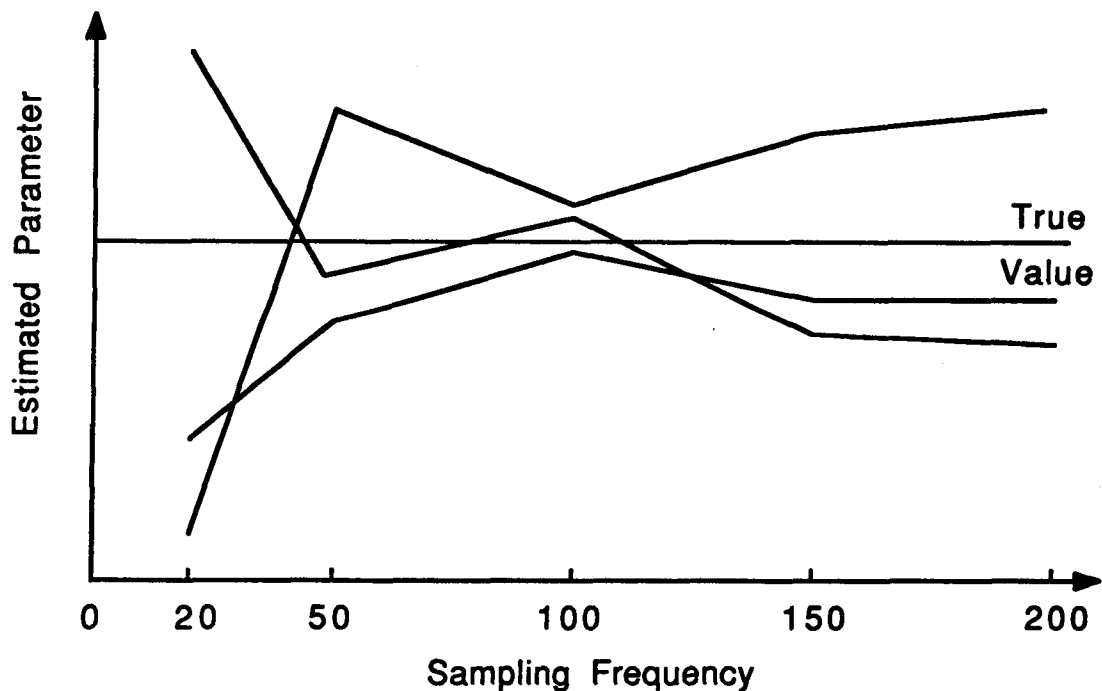
Figure 3.   Typical Results from Estimation with Different Sampling Frequency

FLIGHT TEST

The flight test was performed using designed linear sine-wave frequency sweeps for rudder and aileron. The test conditions were conducted at a speed of Mach .6, an altitude of 15,000 feet, and minimal turbulence. A preprogrammed frequency function generator was used to apply the linear sinusoidal frequency sweeps (0-6 Hz) to the aileron and rudder (through the autopilot servo).

The flight test data were recorded with 100 sample per second, and then filtered using a Graham low-pass filter with the cutoff frequency of 10 Hz and rolloff frequency of 15 Hz. Prior to estimation analysis, the data were cleaned up by removing all the sensor biases and data dropouts.

POST FLIGHT ANALYSIS

The analytical model (system equations 15) was simulated using actual control surface defelection during flight as input signals. The comparison of flight data with the response of the analytical model for flight condition 41, where both rudder and aileron frequency sweeps are used, is presented in the Figures 4-11.

The maximum likelihood estimation software tool (MMLE) developed by NASA Dryden was used to minimize the residuals between flight data and response of the analytical model in Figures 4-11. At the time of analysis, MMLE was hosted on the Cyber mainfram. Due to Cyber having a memory limit, the capability of using process noise was not available for analysis. Hence the results obtained herein, are preliminary results which do not include the effect of process noise. The final results of this study will be reported at the 1989 AIAA Guidance, Navigation and Control conference.

The high-order model was partitioned into two sections: rigid model and elastic model. For rigid model identification, 15 seconds of data were used. First the rigid portion of the control and measurement matrices were upgraded. Then, the Λ matrix was upgraded. Finally, all the parameters in the rigid section of the Λ, $\bar{B}$ and $\bar{C}$ matrices were simultaneously estimated.

596
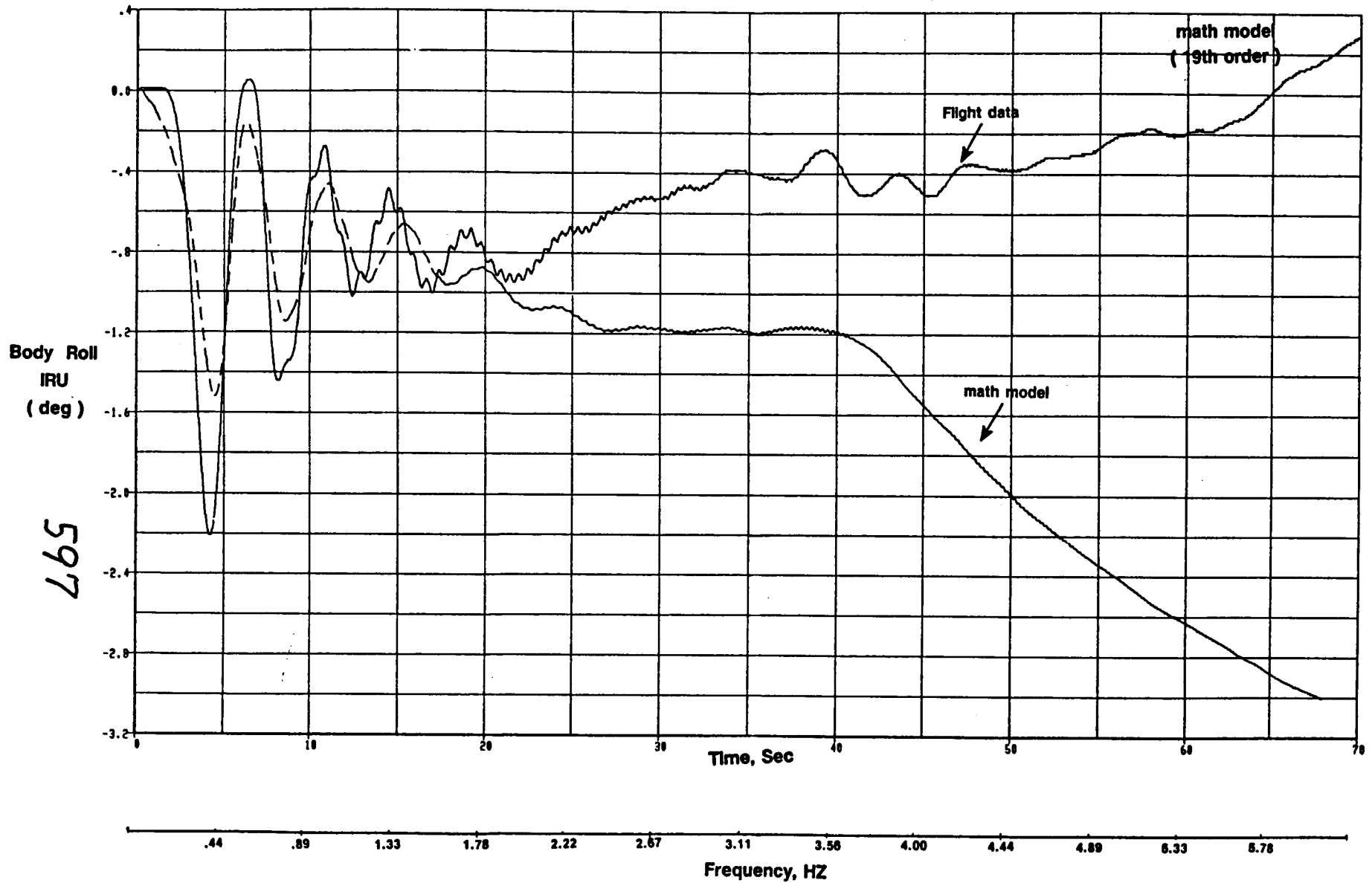
Figure 4. Time Response of Body Roll at IRU Comparing Flight Data with Math Model
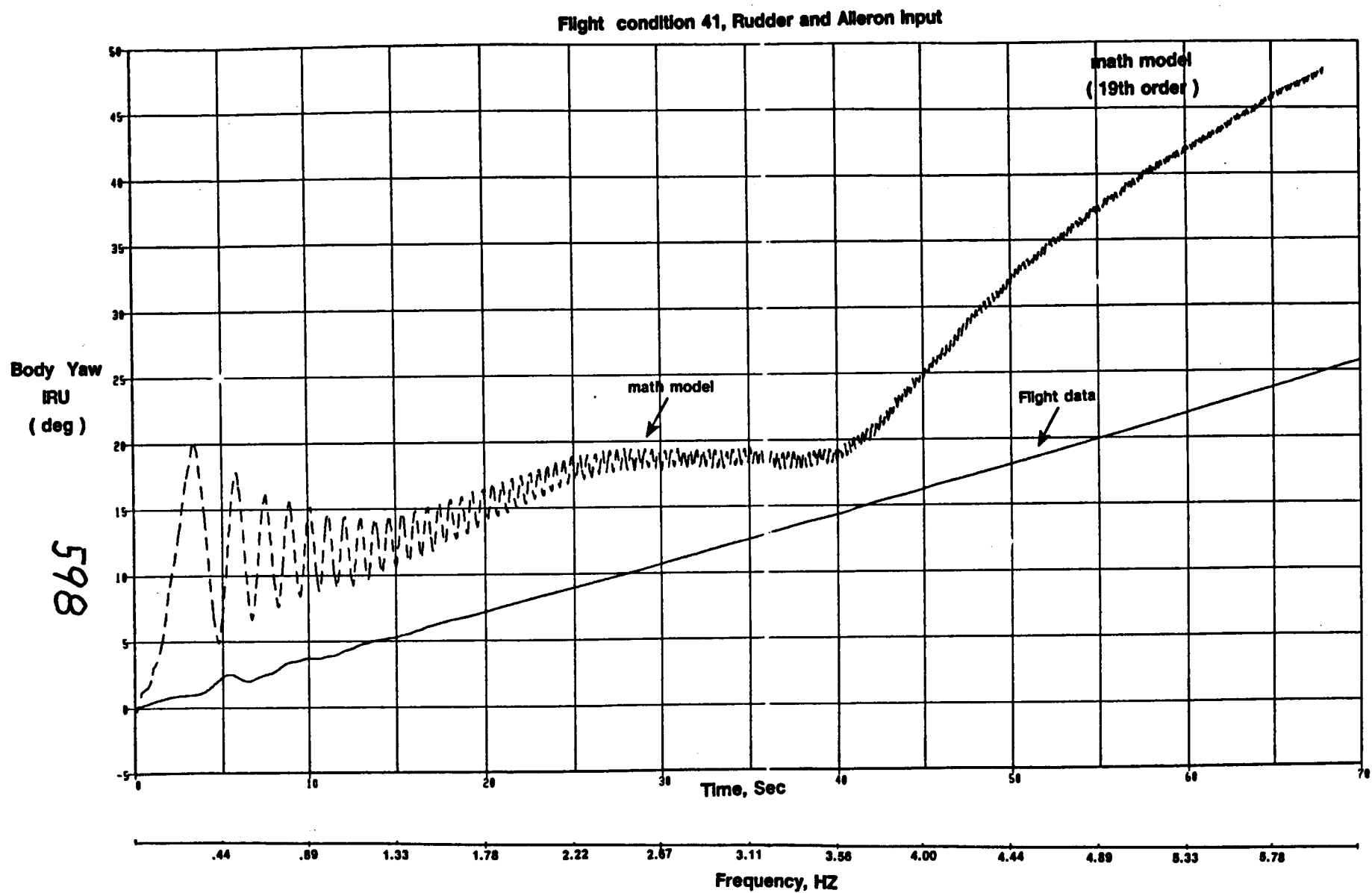
Figure 5. Time Response of Body Yaw at IRU Comparing Flight Data with Math Model

Flight condition 41, Rudder and Aileron input
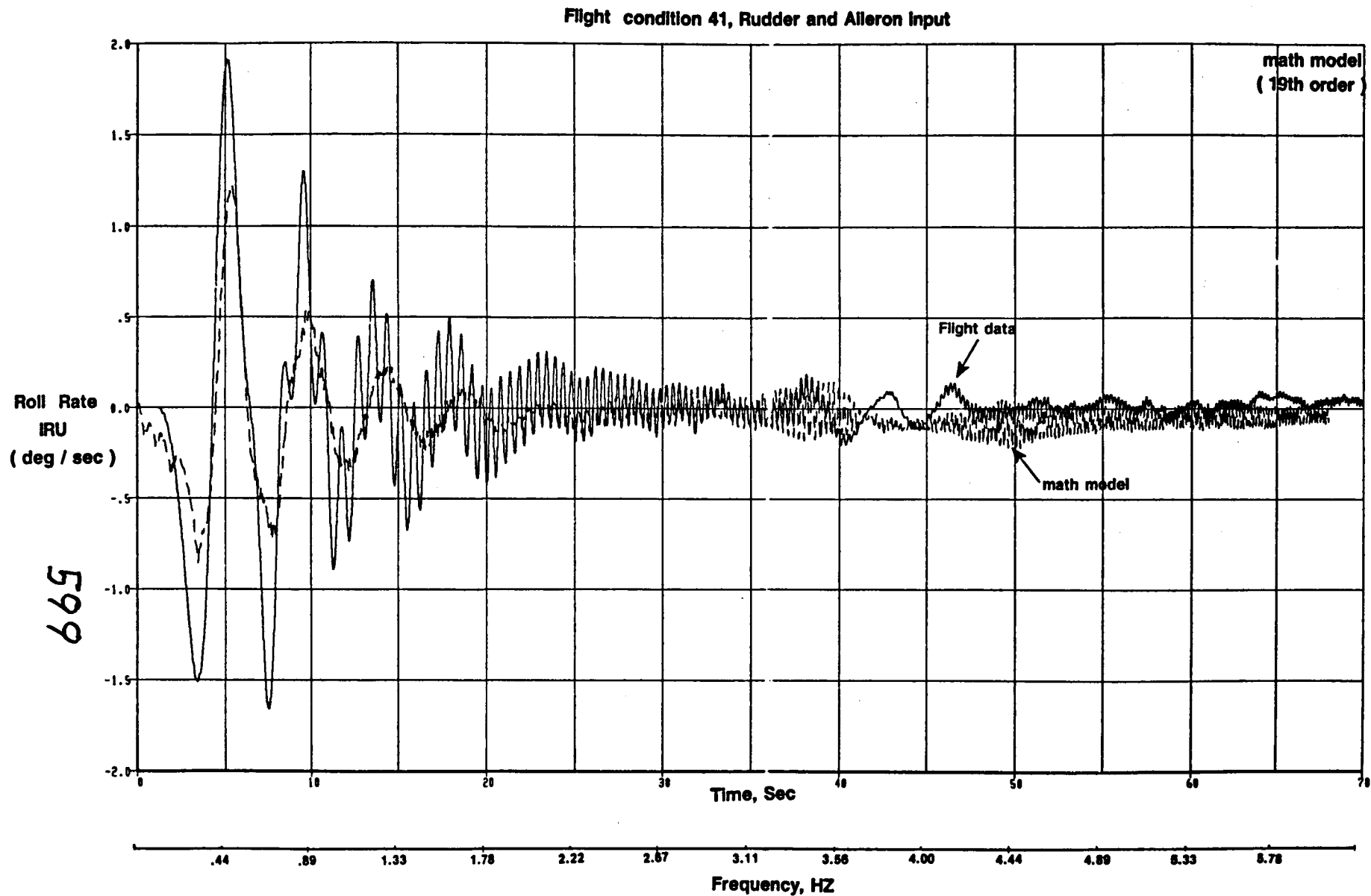
Figure 6.   Time Response of Roll Rate at IRU Comparing Flight Data with Math Model
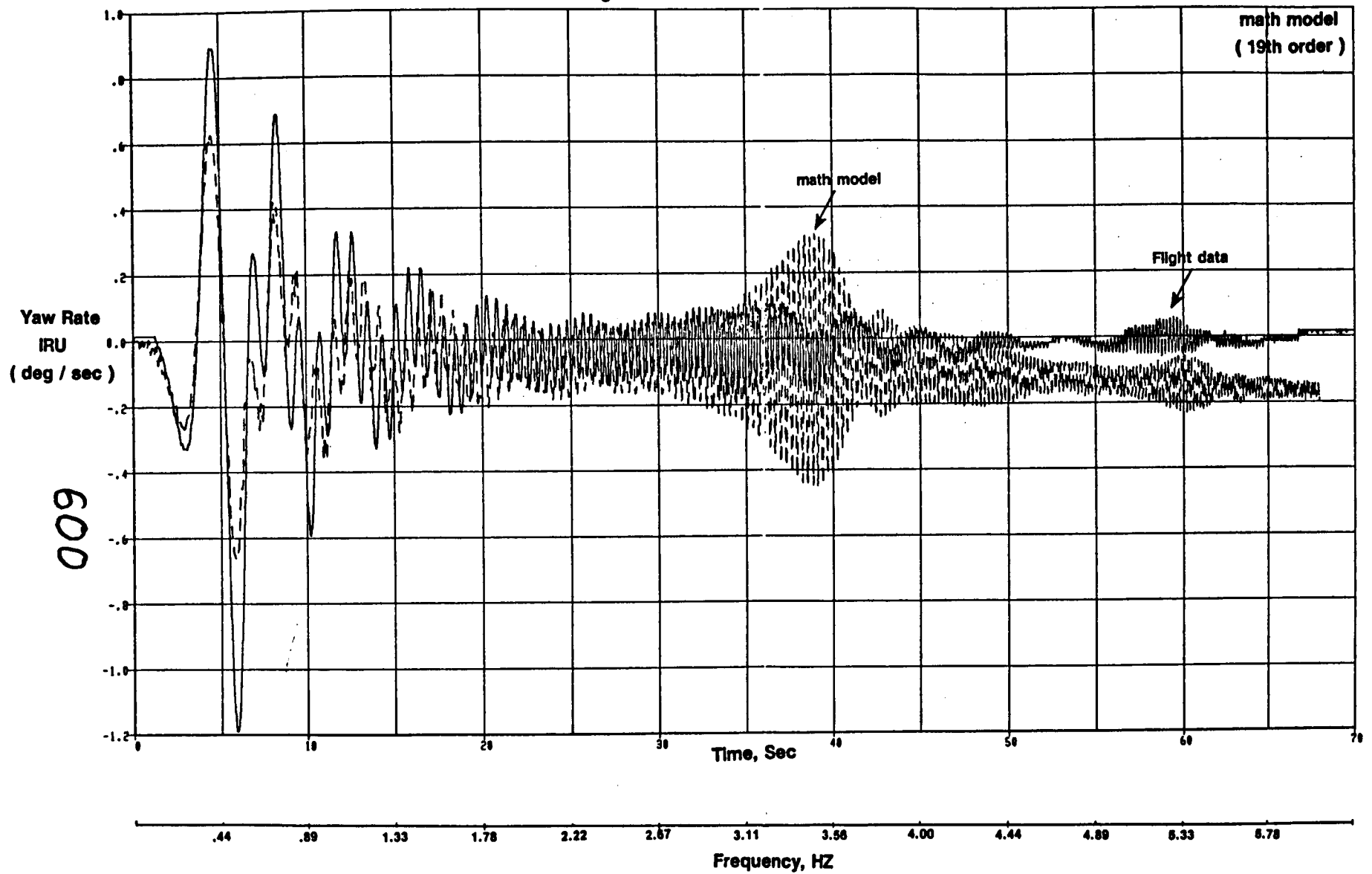
Figure 7. Time Response of Yaw Rate at IRU Comparing Flight Data with Math Model
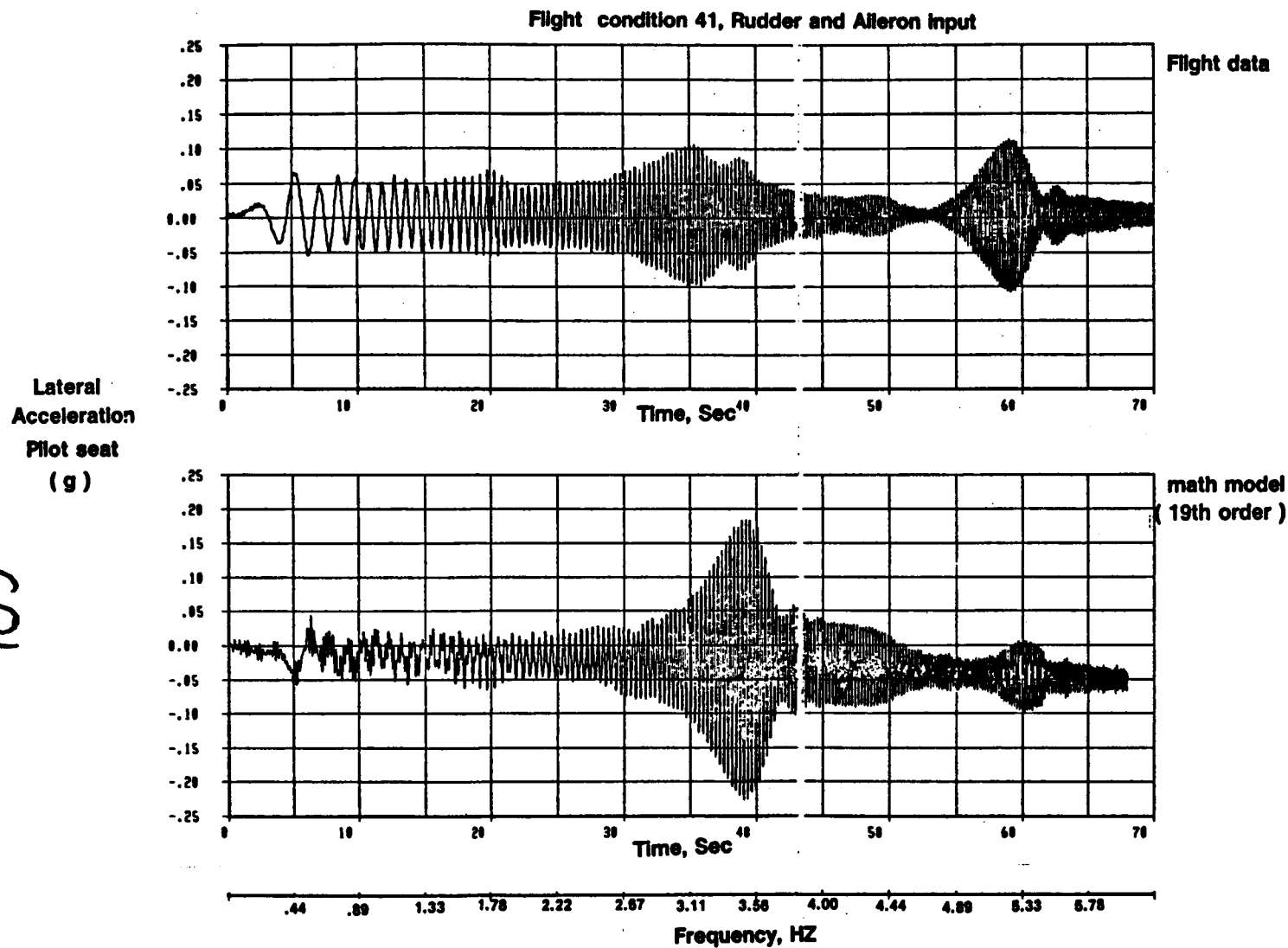
Figure 8. Time Response of Lateral Acceleration at Pilot Seat Comparing Flight Data with Math Model
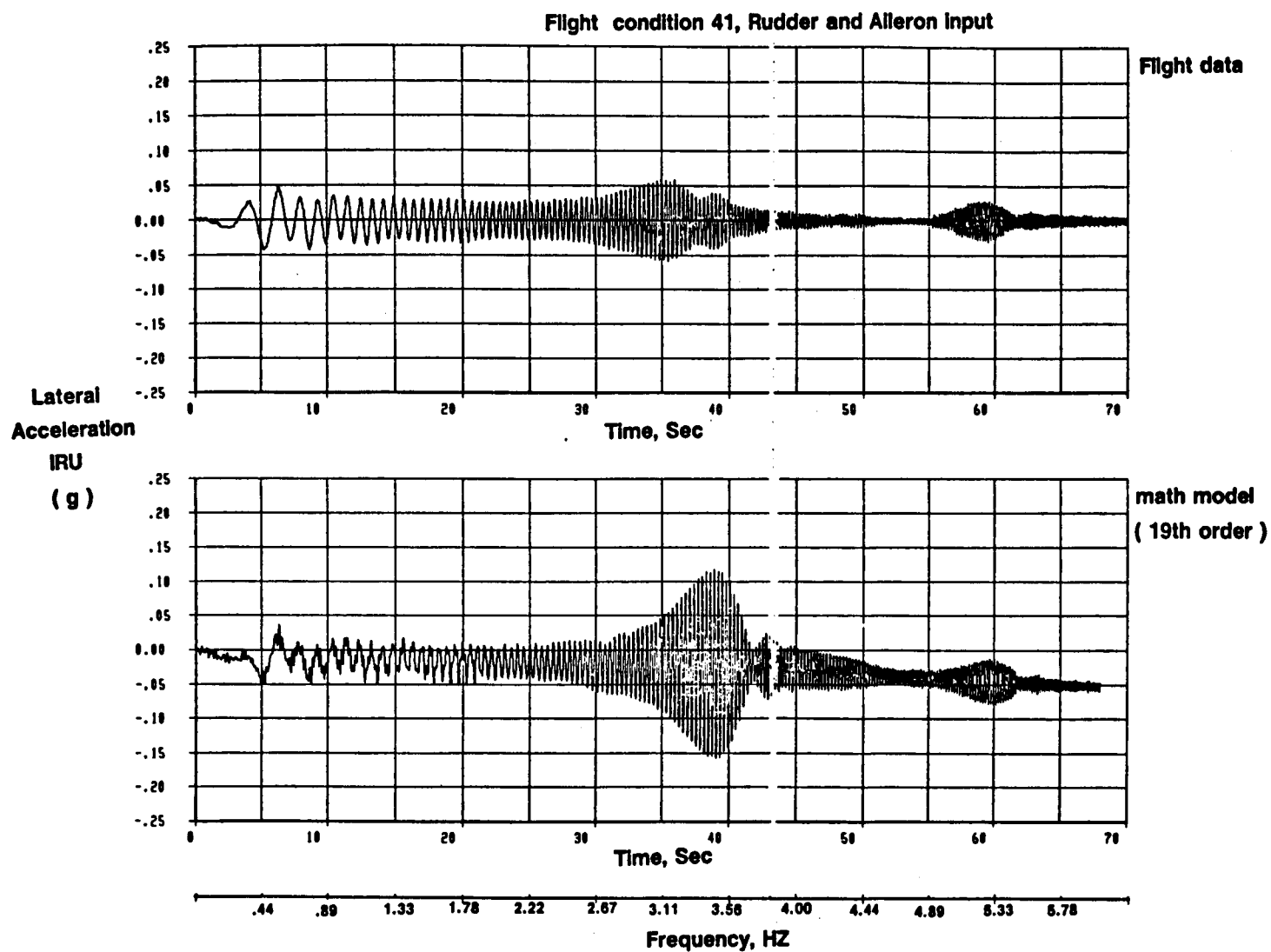
Figure 9.   Time Response of Lateral Acceleration at IRU Comparing Flight Data with Math Model
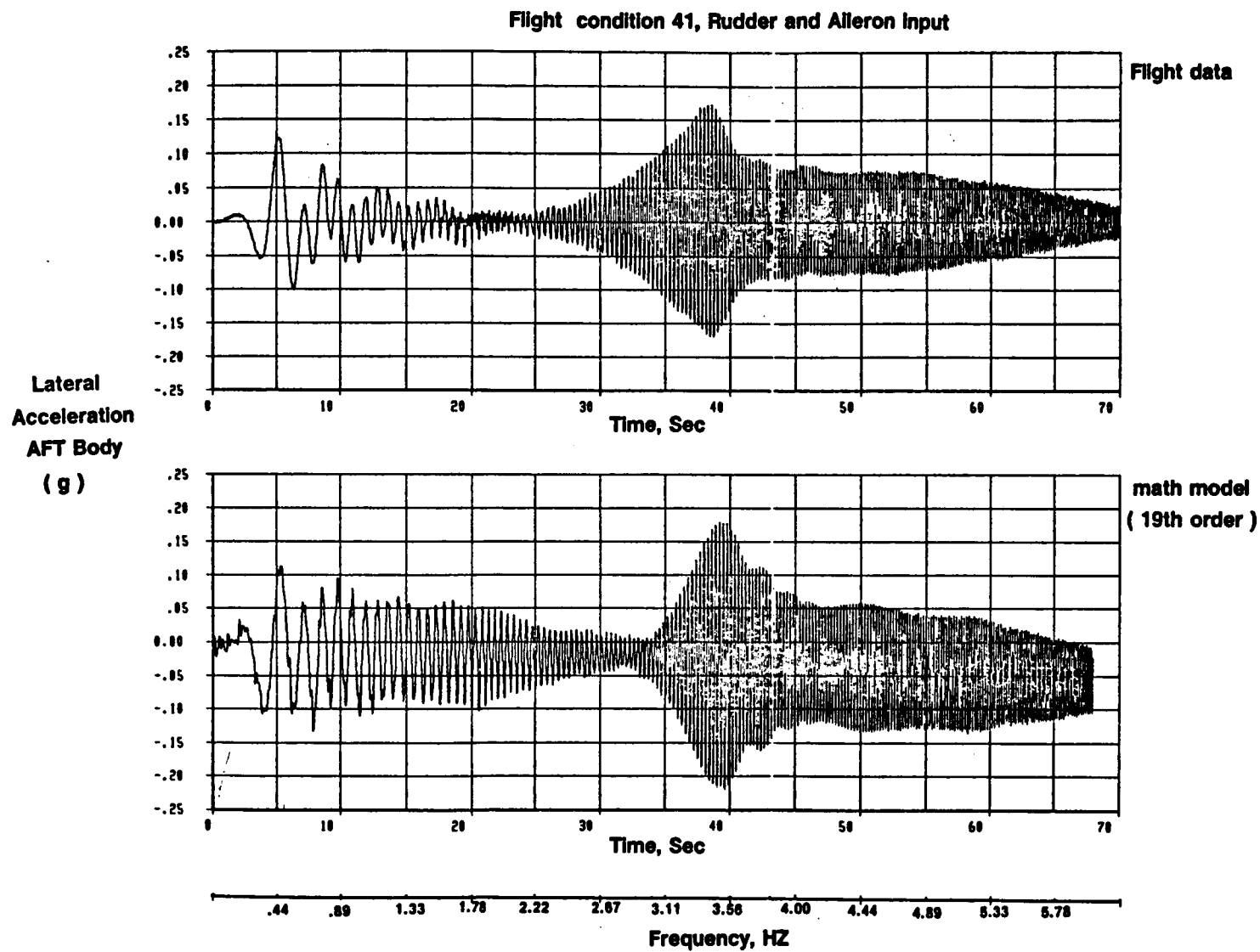
Figure 10. Time Response of Lateral Acceleration at AFT Body Comparing Flight Data with Math Model

603
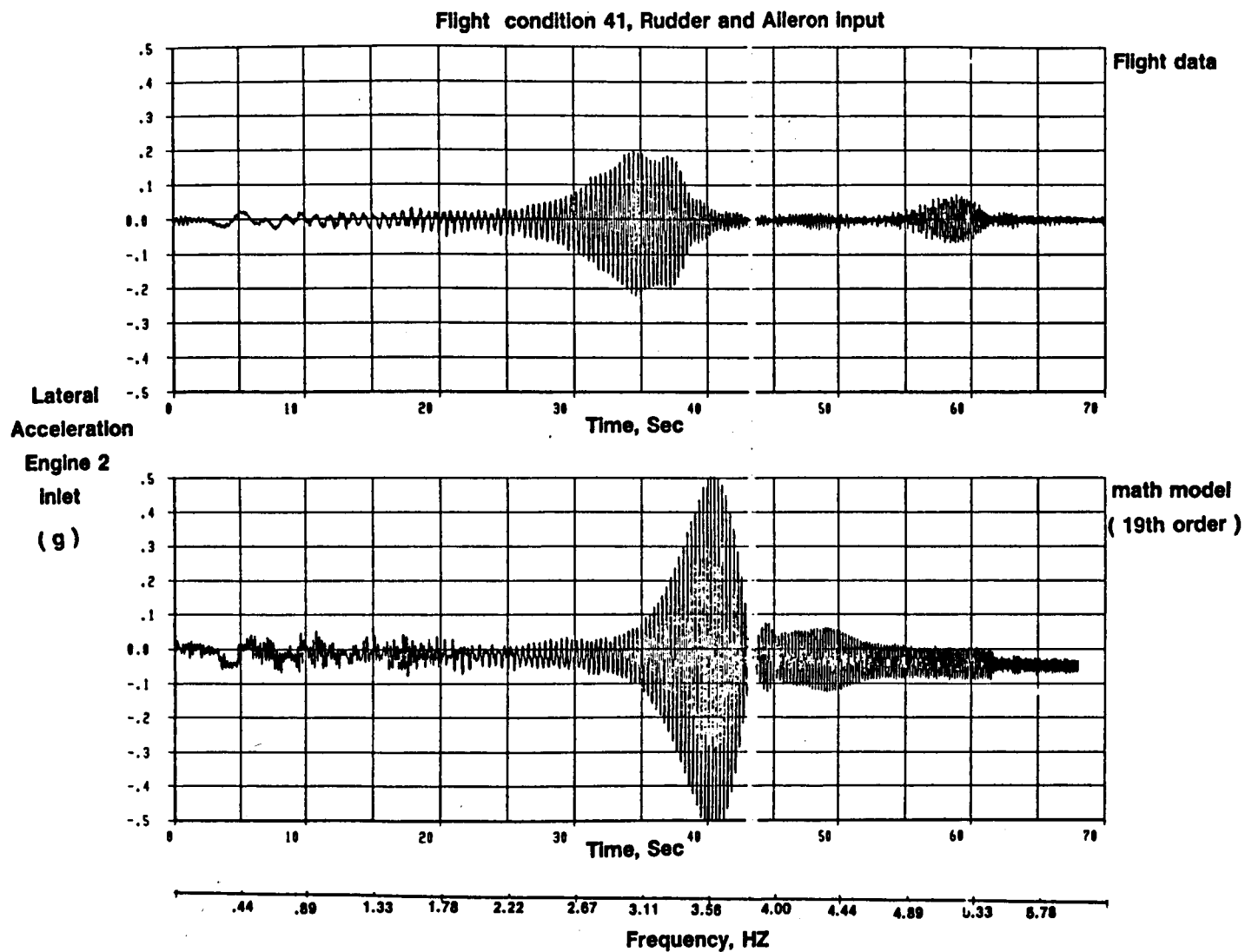
Figure 11. Time Response of Lateral Acceleration at Engine 2 Inlet Comparing Flight Data with Math Model

Two different approches were taken for the elastic model identification. In the first approach, the 19th order model was used for the analysis with all the elements of $\bar{B}$ and $\bar{C}$ being estimated. All 70 seconds of data were used for this estimation approach, . In this process, those parameters in the $\bar{B}$ and $\bar{C}$ that did not contribute to the residuals were identified and kept constant for the remainder of the analysis. Then, the elements of A were added to the estimation process while keeping some of the elements of $\bar{B}$ and $\bar{C}$ constant. The results of this estimation approach are show in Figures 12-19.

The second approach was to add one elastic mode at a time to the rigid model. For this approach, the first elastic mode was added with 28 seconds of data used for the analysis. The corresponding parameters in the $\bar{B}$ and $\bar{C}$ matrices were estimated every time a mode was added to the model. The result of this approach was not satisfactory because several times the algorithem diverged and the residuals were big.

Figures 20-26 show the PSD plots obtained from the analytical model. Figures 27-34 show the PSD plots obtained from the estimated model. The PSD plots obtained from the estimated model, clearly show that the estimation analysis improved the accuracy of the model in terms of its modal representation. However, the estimated parameters in the $\bar{B}$ and $\bar{C}$ matrices are biased. Since an accurate representation of the transfer functions was desired for this study rather than true values of the $\bar{B}$ and $\bar{C}$ matrices, the biased estimates in the $\bar{B}$ and $\bar{C}$ matrices did not create any problem.

Figures 16, 17 and 19 indicate that another mode is present in the flight data which is not modeled in the analytical or estimated model. This problem can not be solved via parameter estimation technique which assumes the structure of the model (i.e., the order of the model) is correct. Hence, it is suggested that the system identification technique developed by V. klein and J. Batterson of NASA LaRC be used to overcome this problem.

Flight condition 41, Rudder and Aileron Input
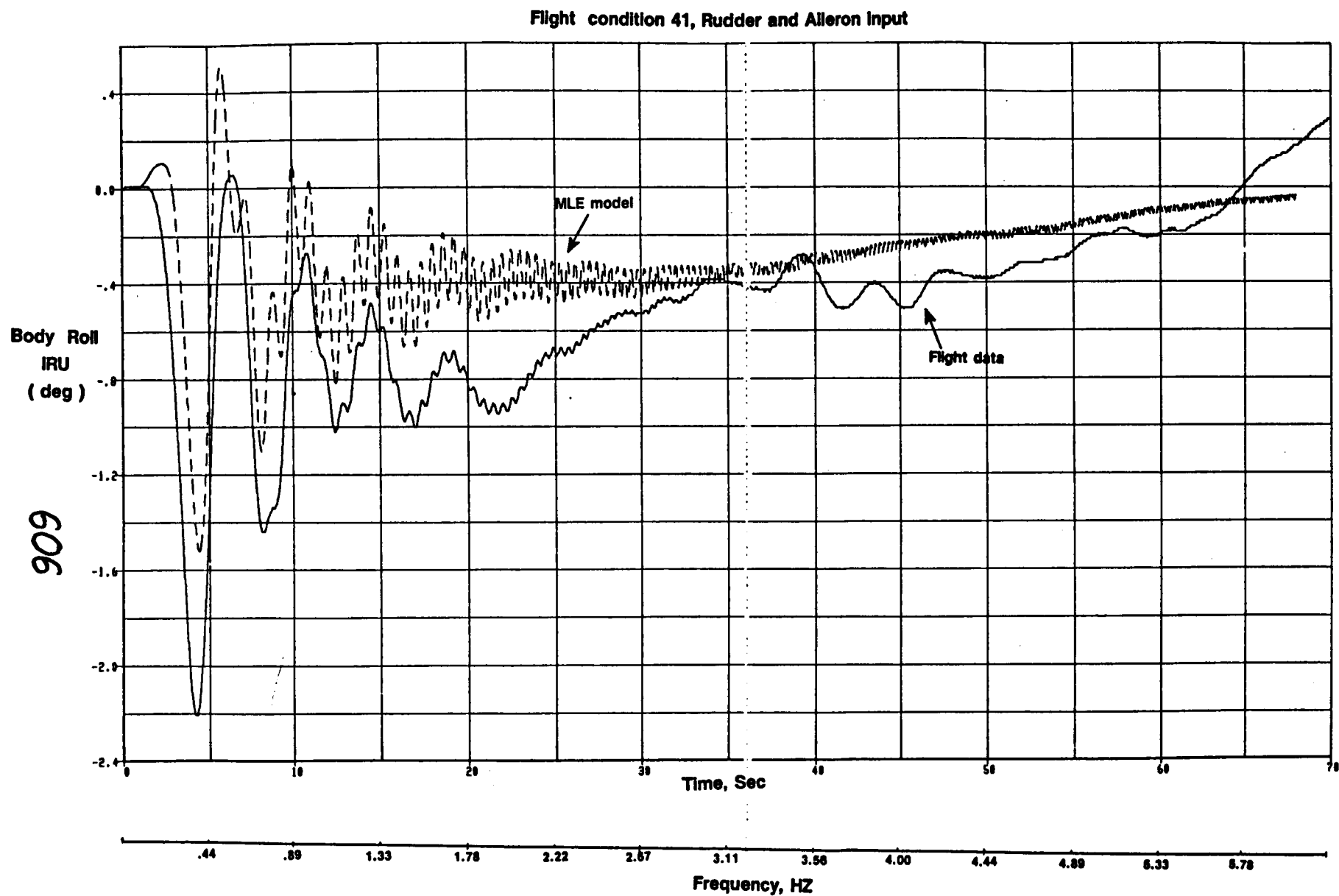
Figure 12. Time Response of Body Roll at IRU Comparing Flight Data with MLE Model
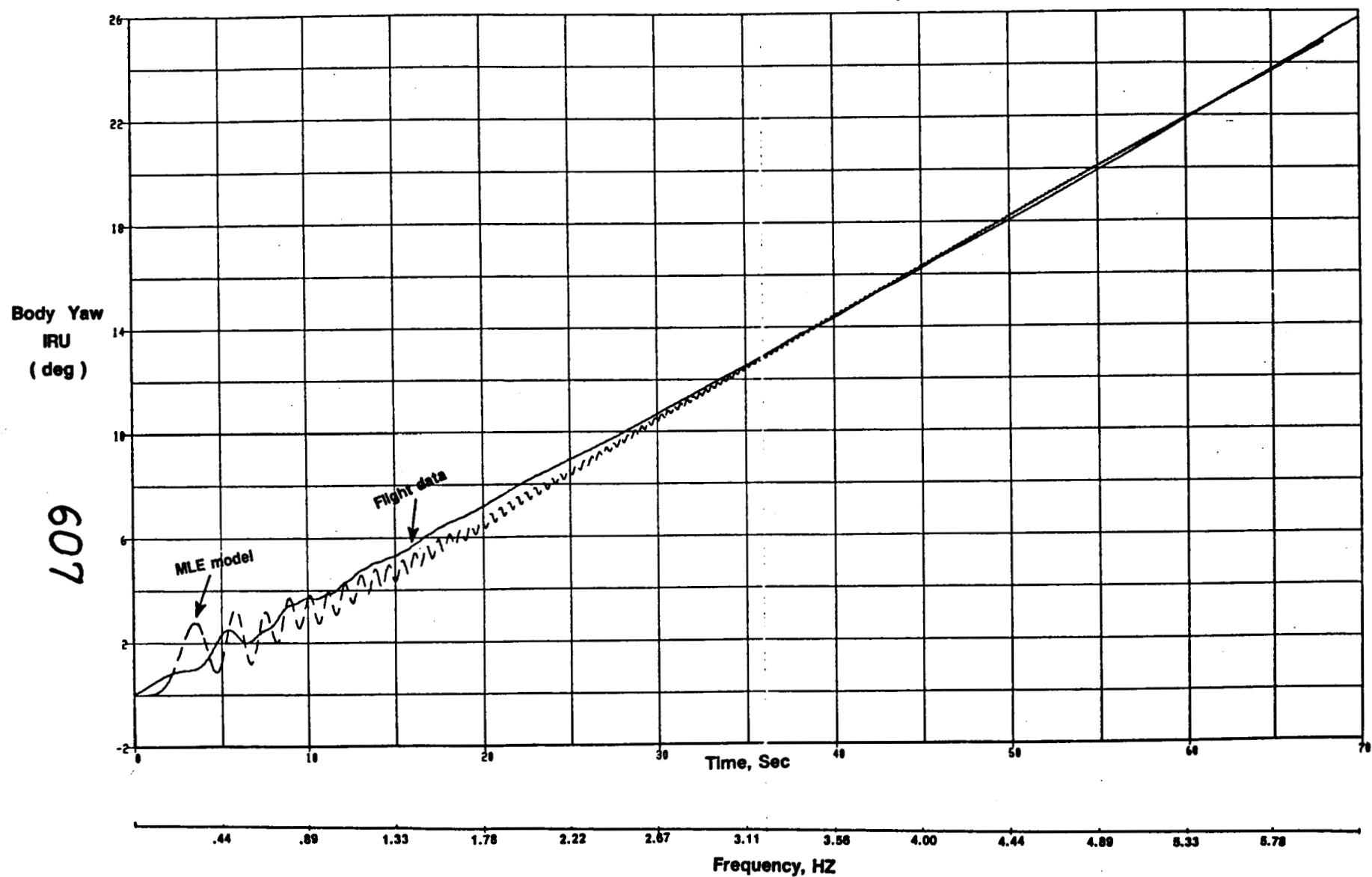
Figure 13. Time Response of Body Yaw at IRU Comparing Flight Data with MLE Model
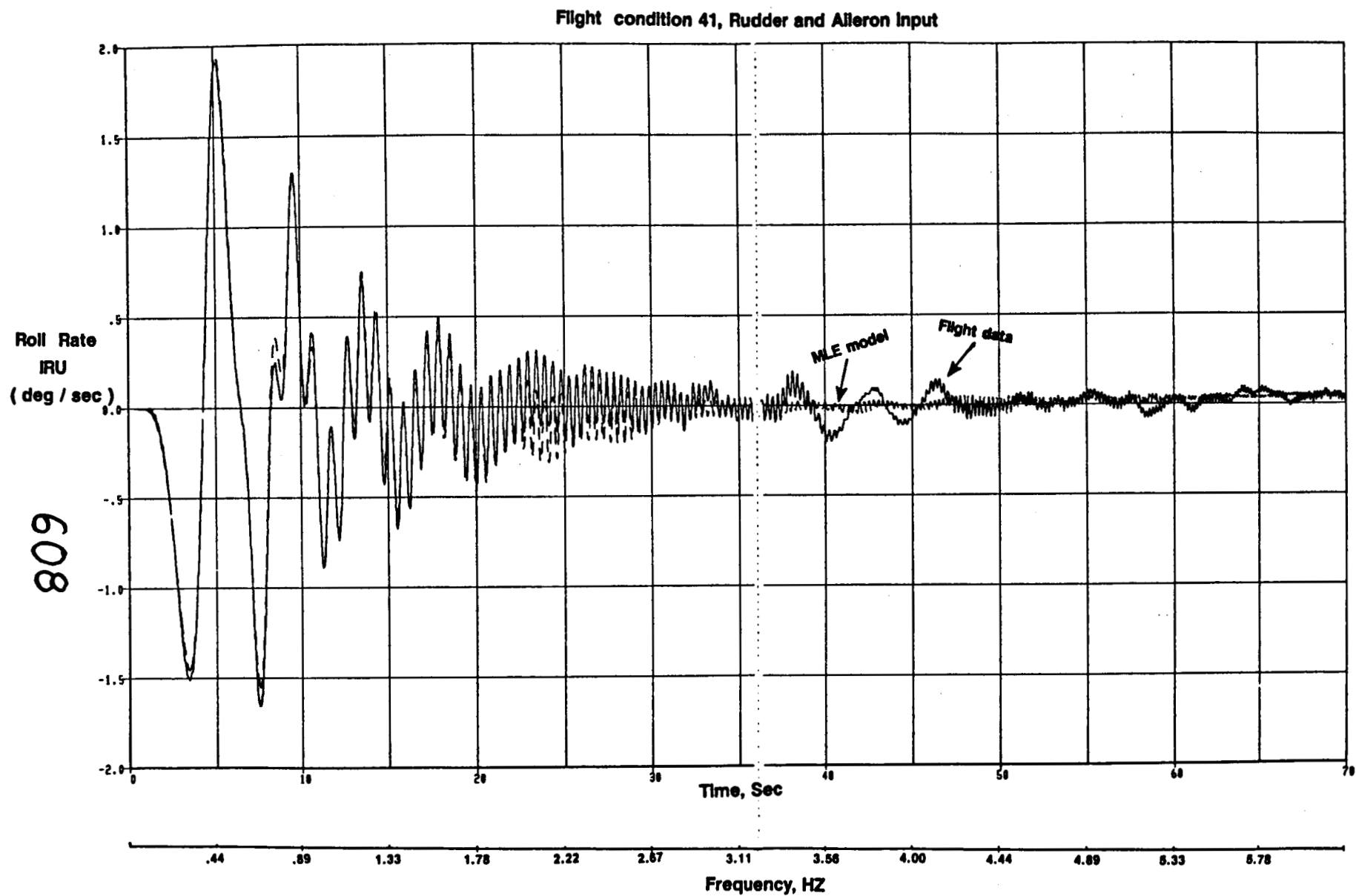
Figure 14. Time Response of Roll Rate at IRU Comparing Flight Data with MLE Model

Flight condition 41, Rudder and Aileron Input

Yaw Rate
IRU
(deg / sec)

609

Flight data

MLE model

Time, Sec

Frequency, HZ

.44   .89   1.33   1.78   2.22   2.67   3.11   3.56   4.00   4.44   4.89   5.33   5.78
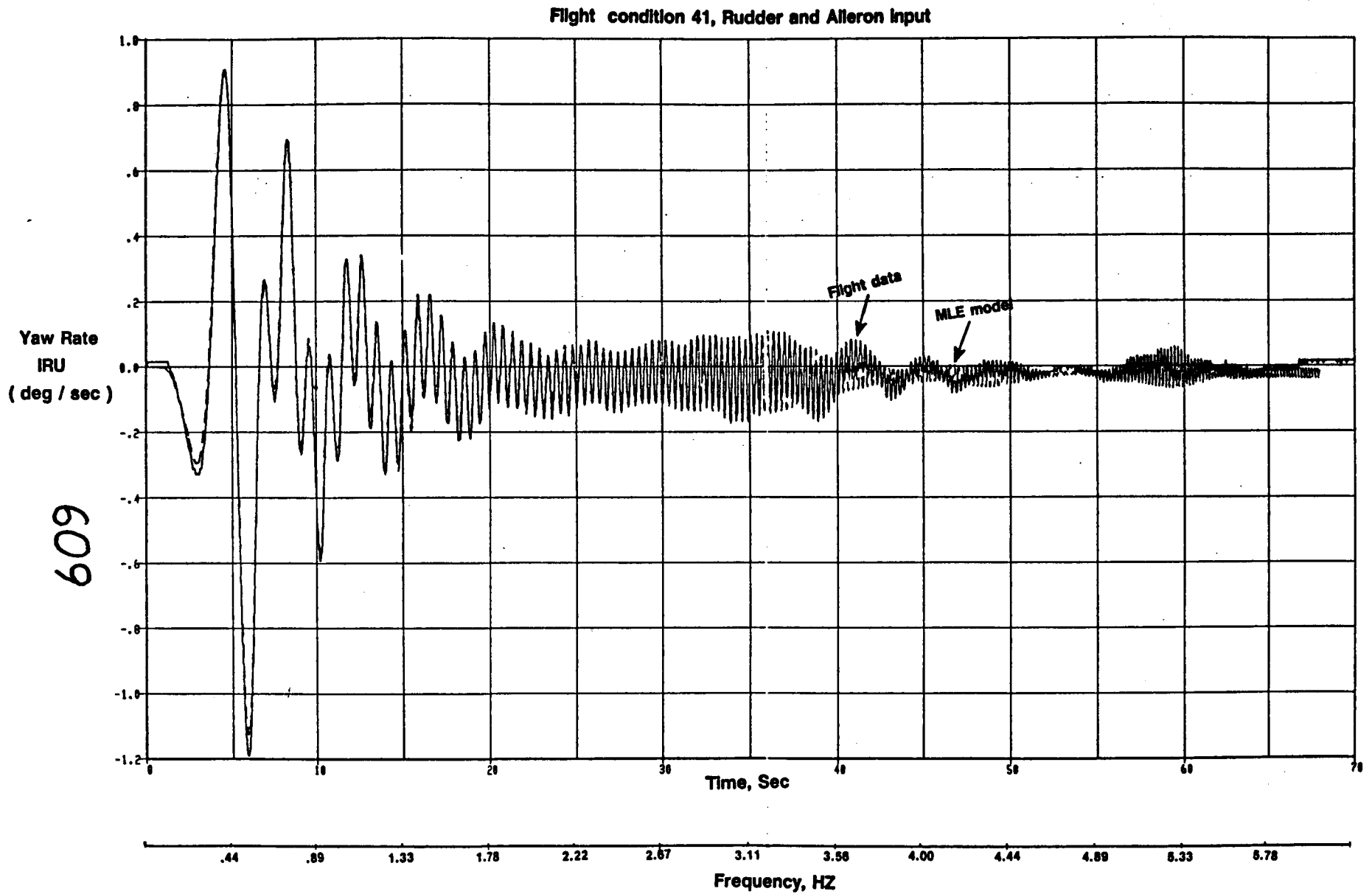
Figure 15.   Time Response of Yaw Rate at IRU Comparing Flight Data with MLE Model
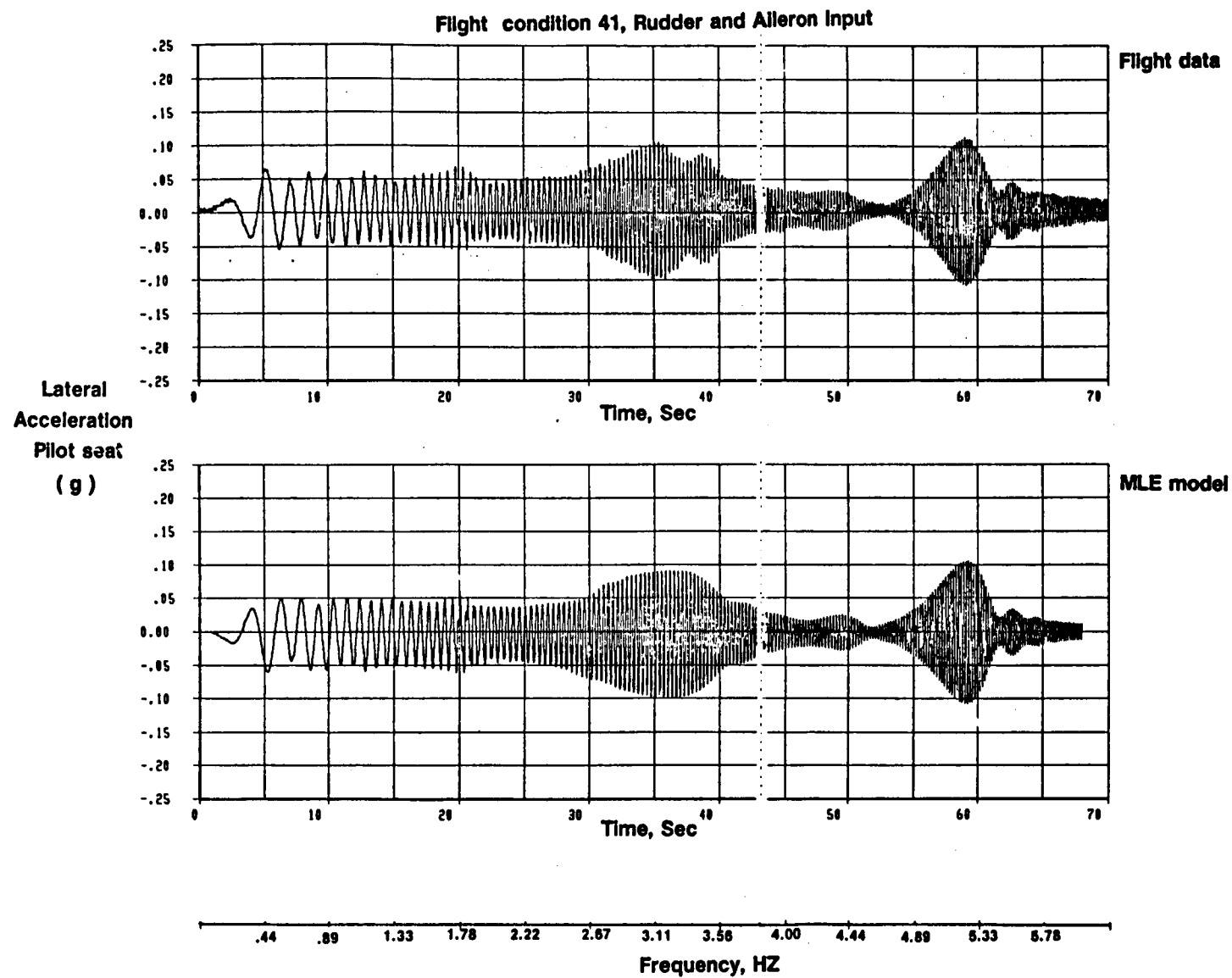
Figure 16. Time Response of Lateral Acceleration at Pilot Seat Comparing Flight Data with MLE Model
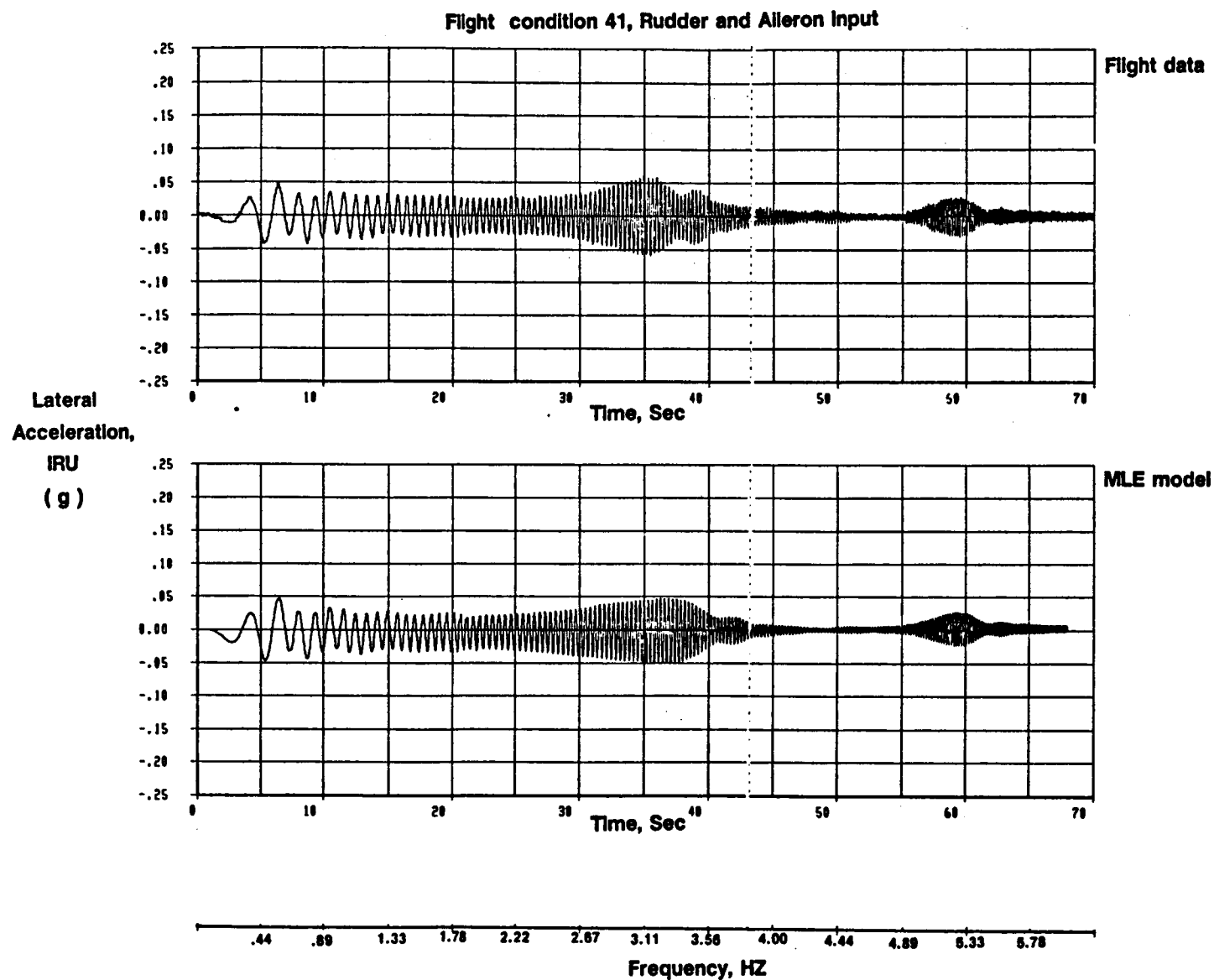
Figure 17. Time Response of Lateral Acceleration at IRU Comparing Flight Data with MLE Model

Flight condition 41, Rudder and Aileron Input

Lateral
Acceleration
AFT Body
(g)

612

Frequency, HZ

.44   .89   1.33   1.78   2.22   2.87   3.11   3.56   4.00   4.44   4.89   5.33   5.78
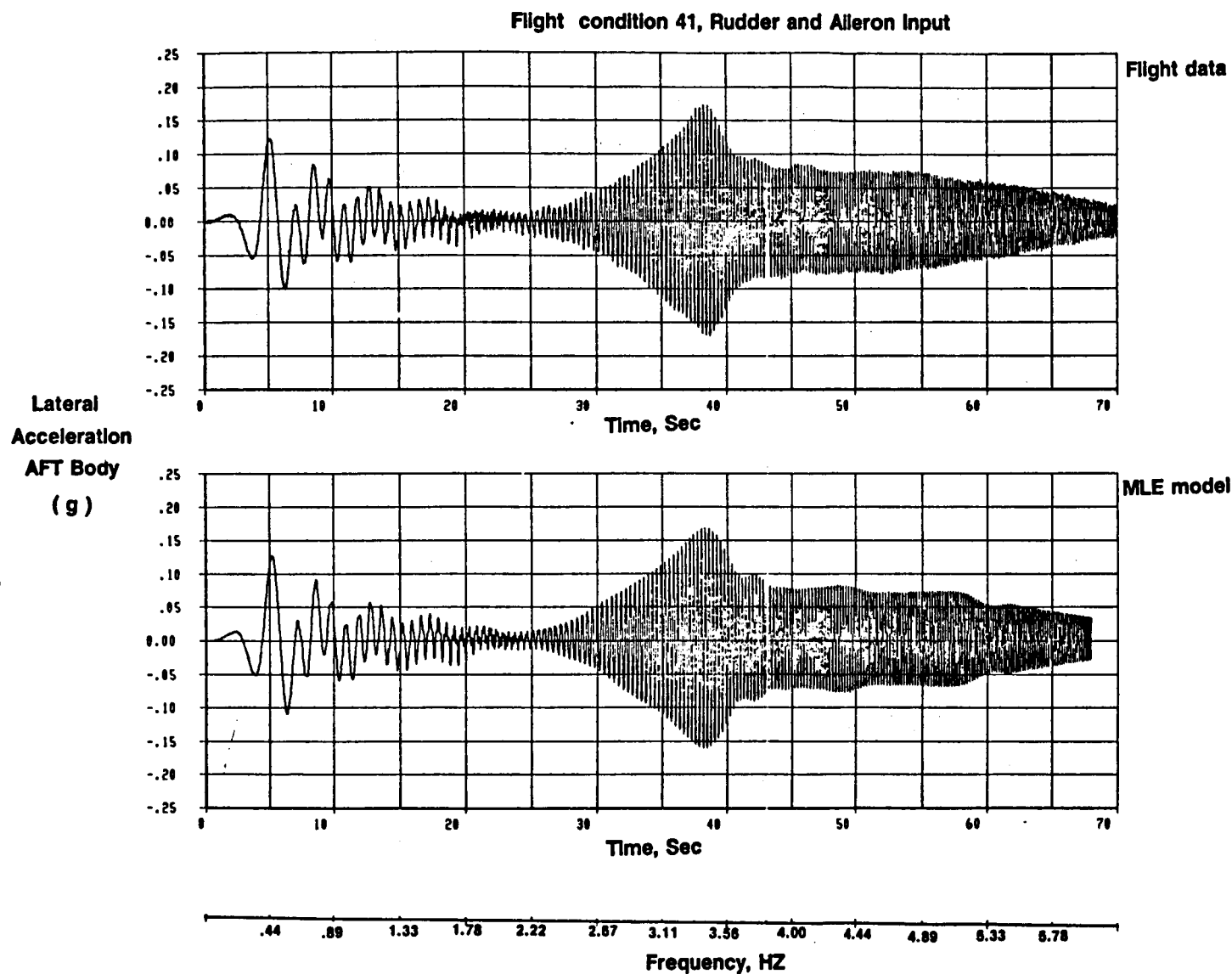
**Figure 18.   Time Response of Lateral Acceleration at AFT Body Comparing Flight Data
with MLE Model**
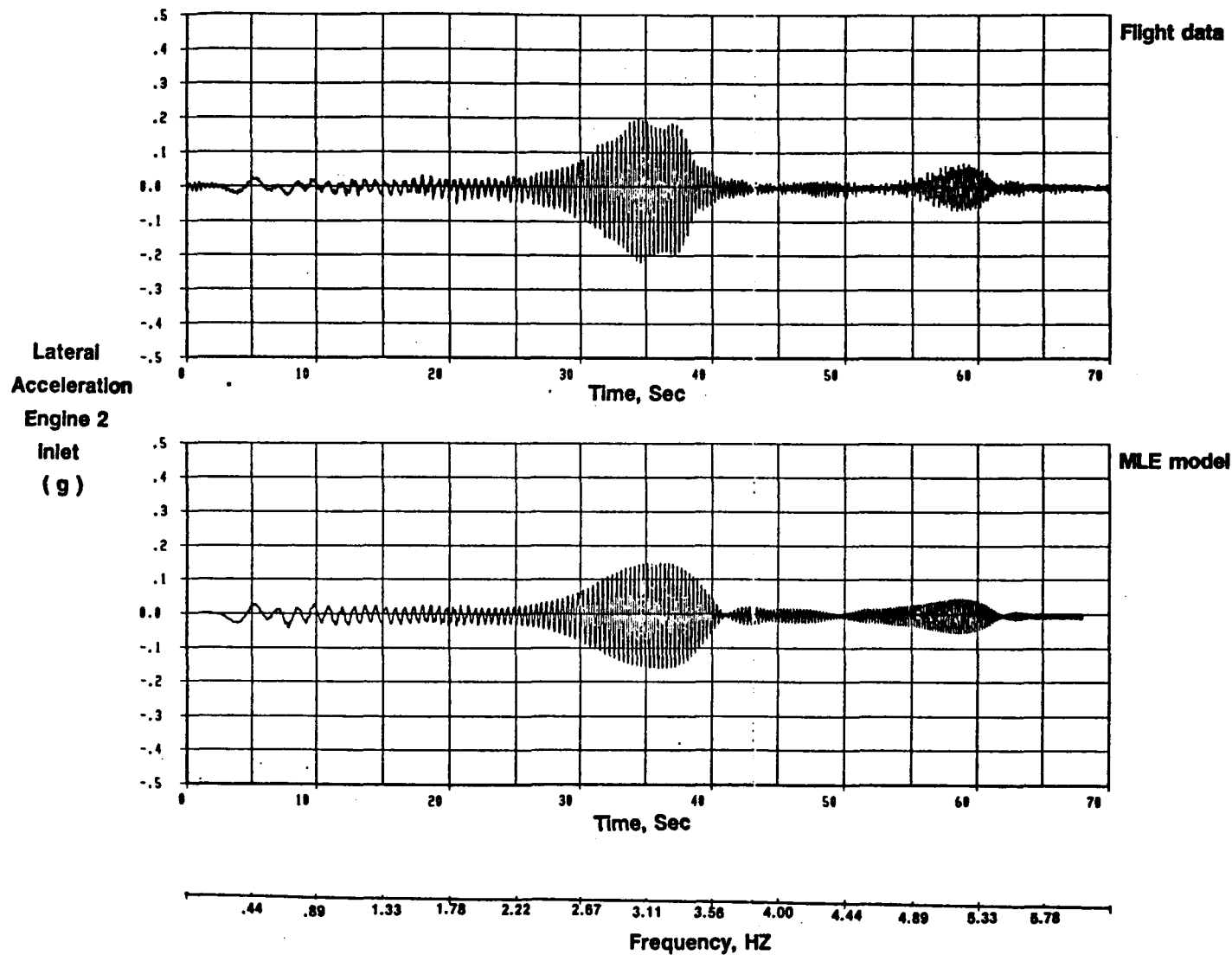
Figure 19. Time Response of Lateral Acceleration at Engine Comparing Flight Data with MLE Model

POWER SPECTRAL DENSITY

Body Roll

IRU

614
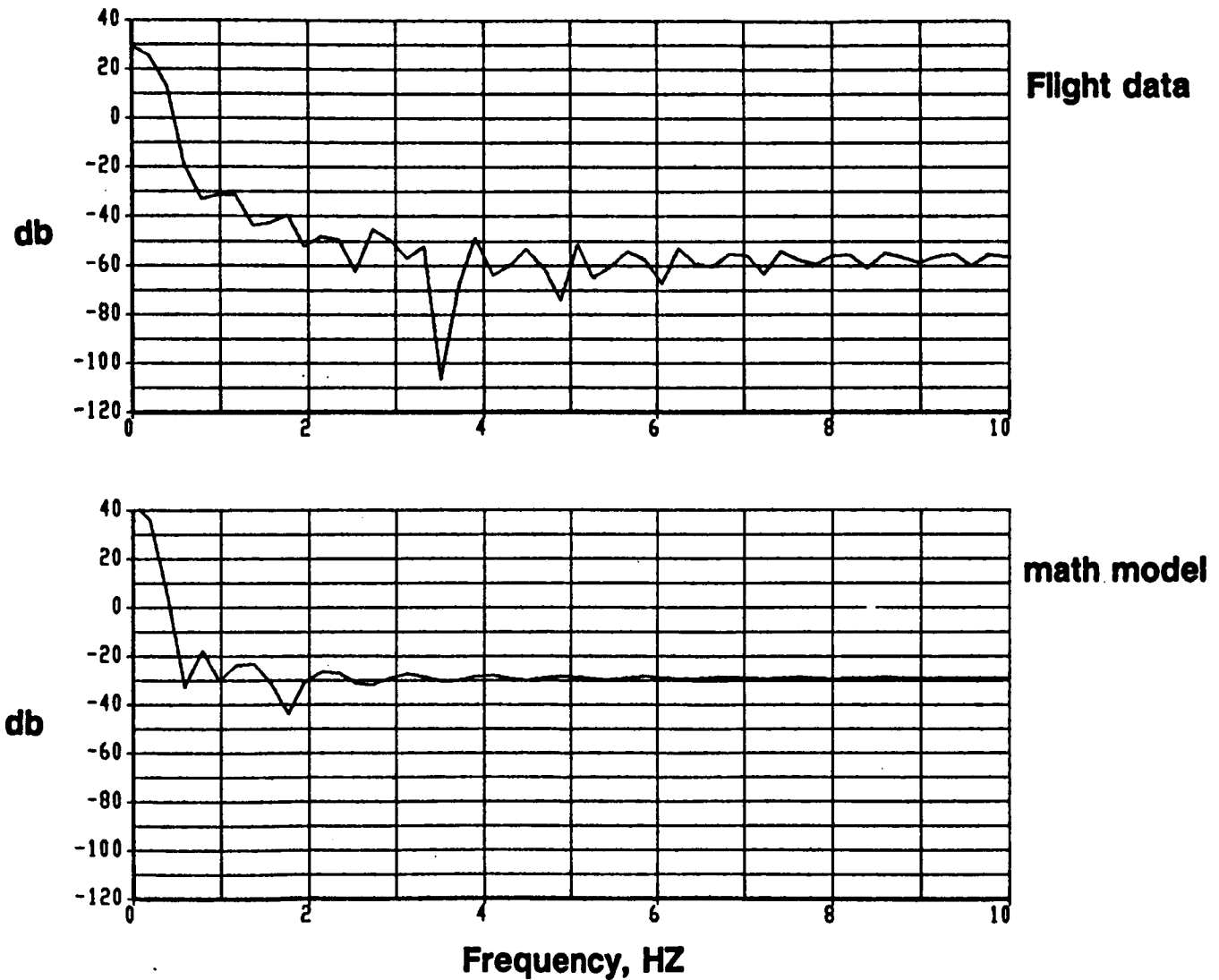
Figure 20. Power Spectral Density Response of Body Roll at IRU Comparing Flight Data with Math Model

POWER SPECTRAL DENSITY

Body Yaw
IRU

615
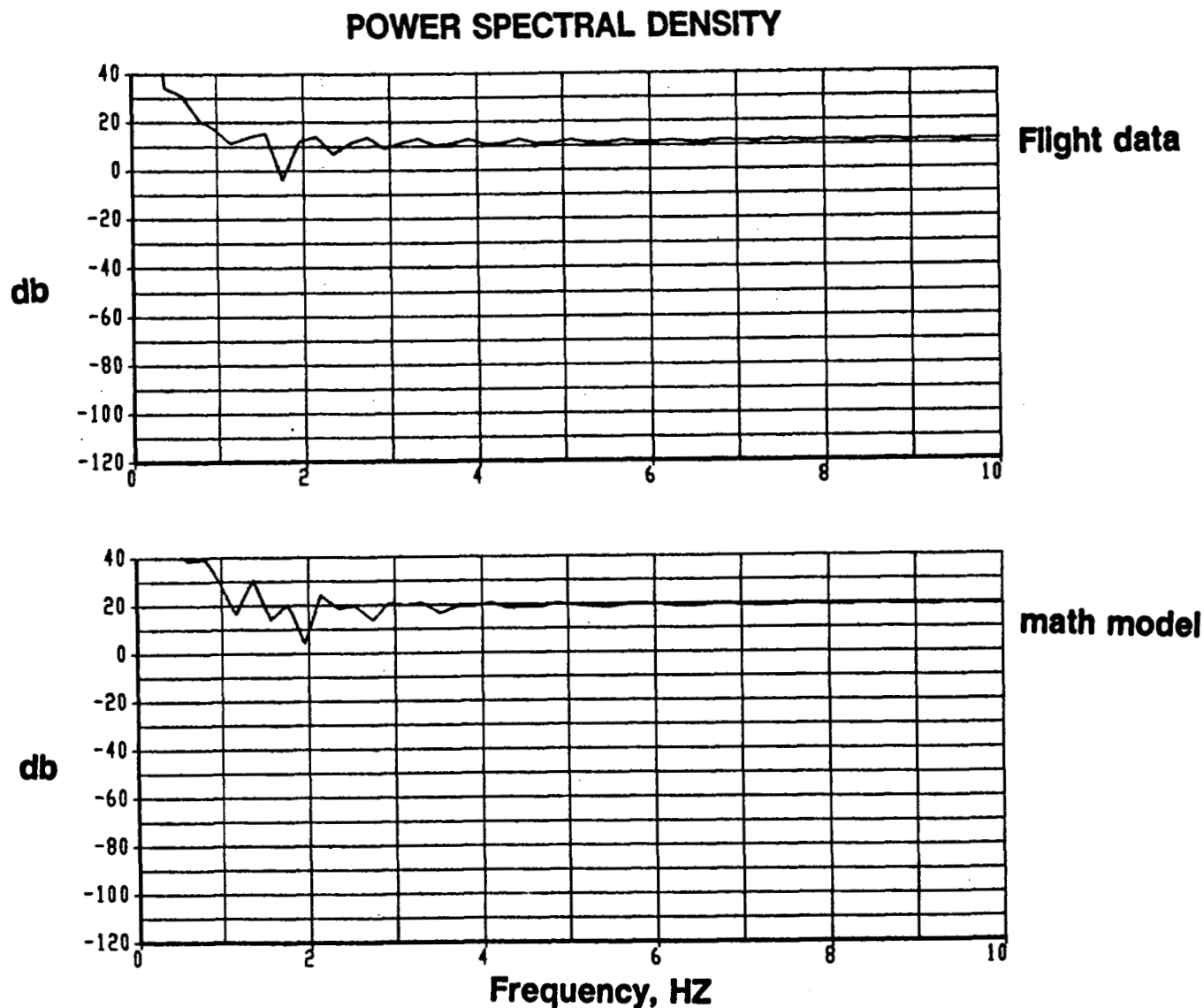
Figure 21.   Power Spectral Density Response of Body Yaw at IRU Comparing Flight Data with Math Model

POWER SPECTRAL DENSITY

Roll Rate

IRU

919
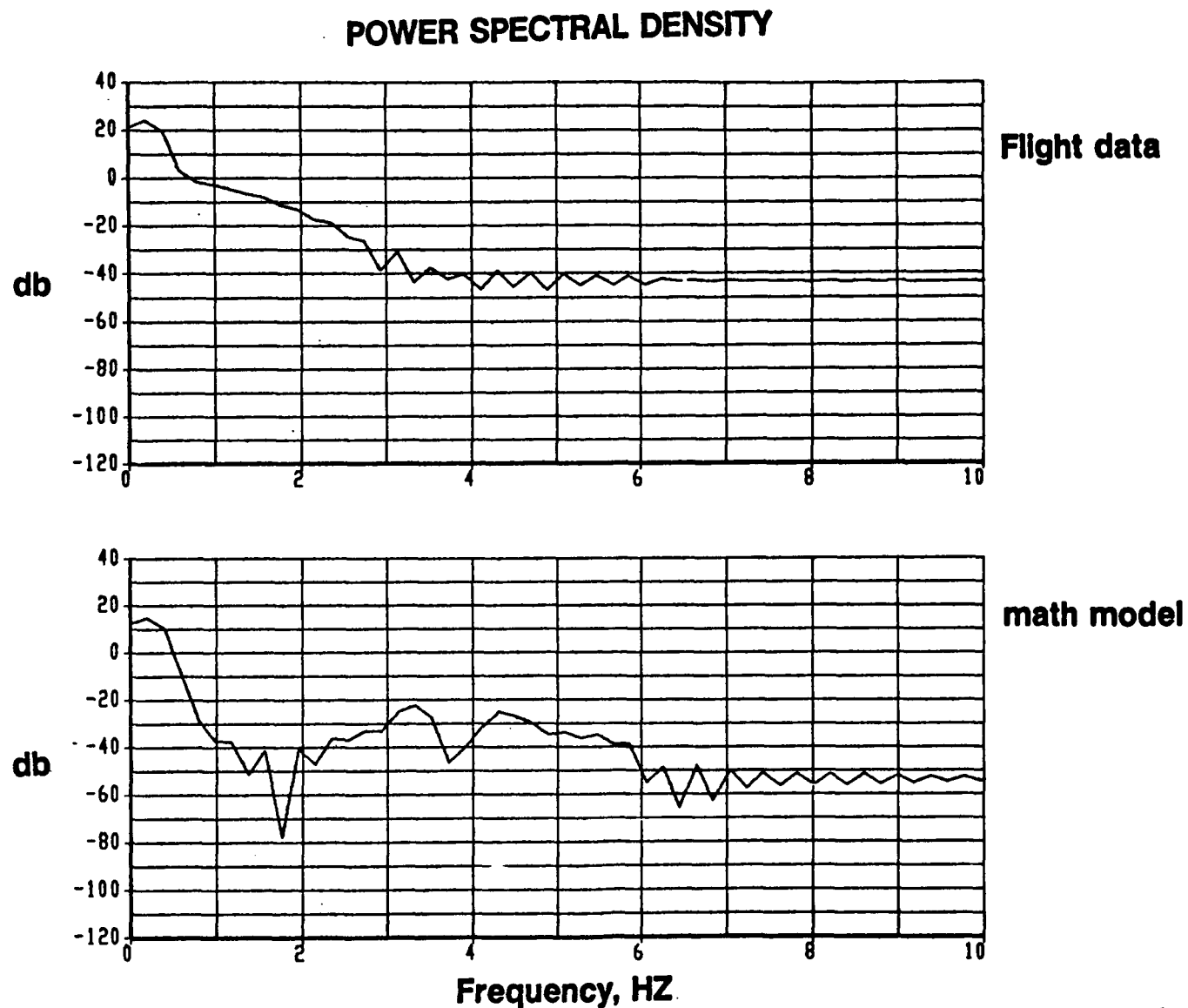
Figure 22.   Power Spectral Density Response of Roll Rate at IRU Comparing Flight Data with Math Model

POWER SPECTRAL DENSITY

Flight data

Yaw Rate

IRU

617

math model

Frequency, HZ
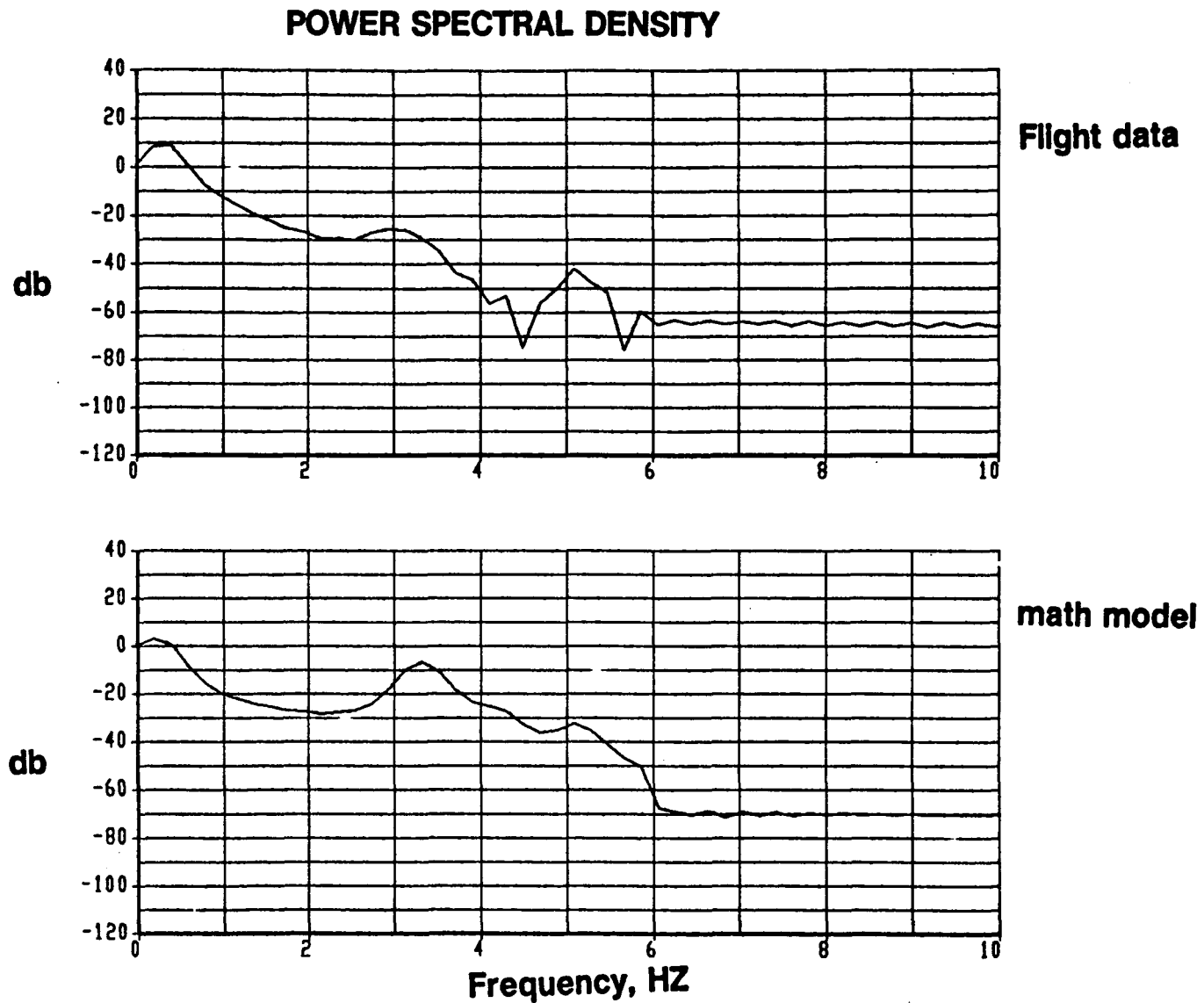
Figure 23. Power Spectral Density Response of Yaw Rate at IRU Comparing Flight Data with Math Model

POWER SPECTRAL DENSITY

Flight data

math model

Lateral Acceleration Pilot seat

819

Frequency, HZ
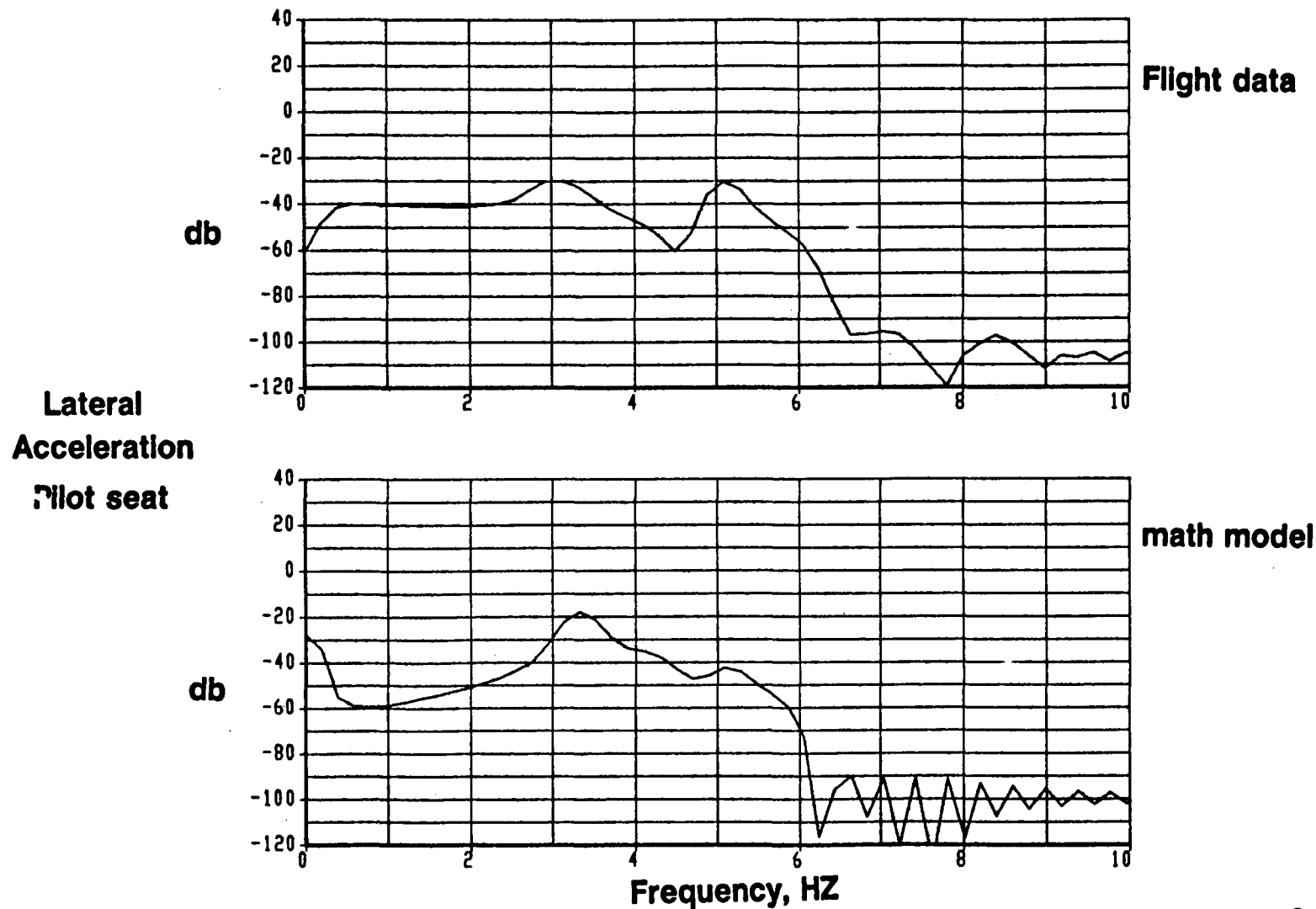
Figure 24. Power Spectral Density Response of Lateral Acceleration at Pilot Seat Comparing Flight Data with Math Model
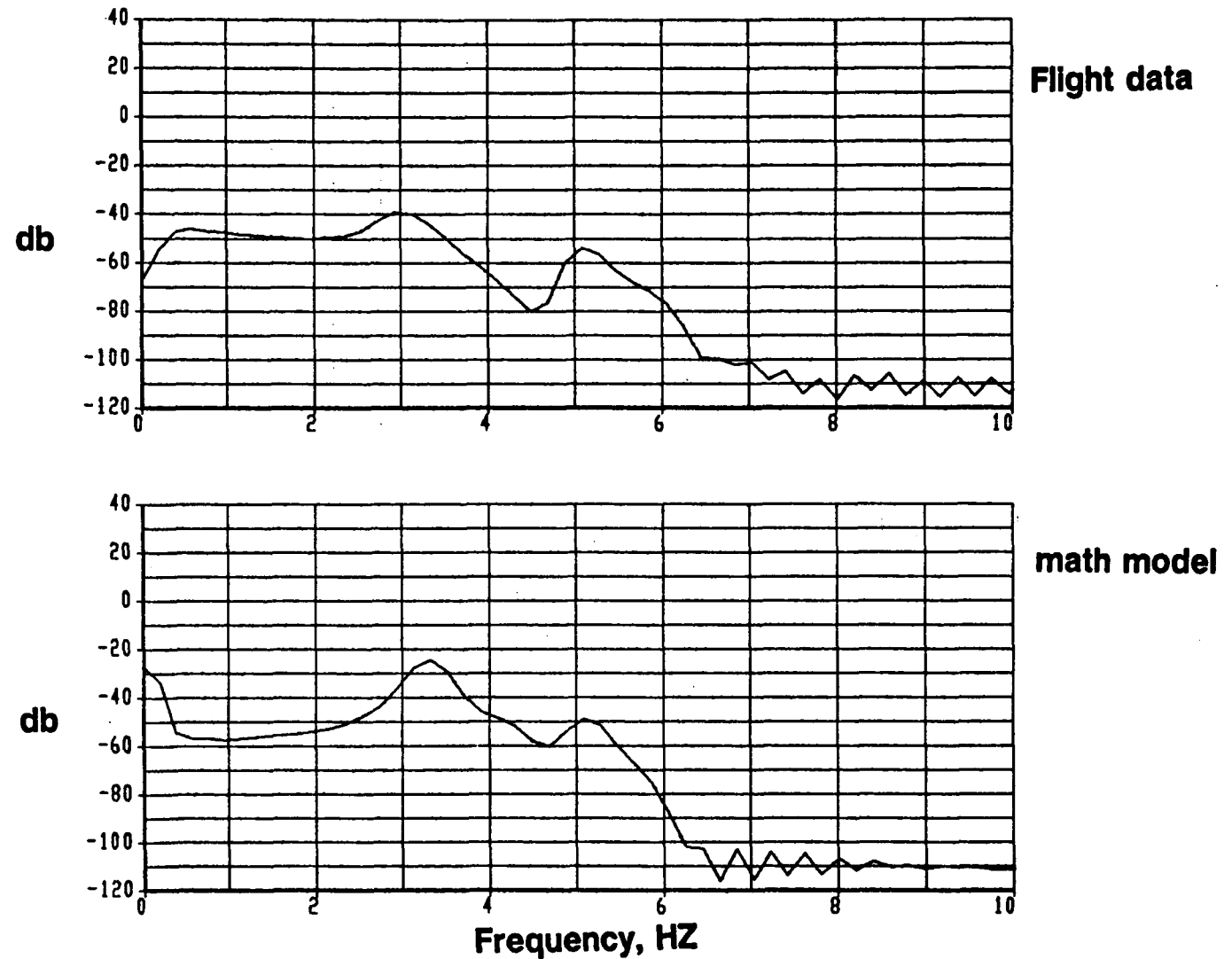
Figure 25. Power Spectral Density Response of Lateral Acceleration at IRU Comparing Flight Data with Math Model

POWER SPECTRAL DENSITY
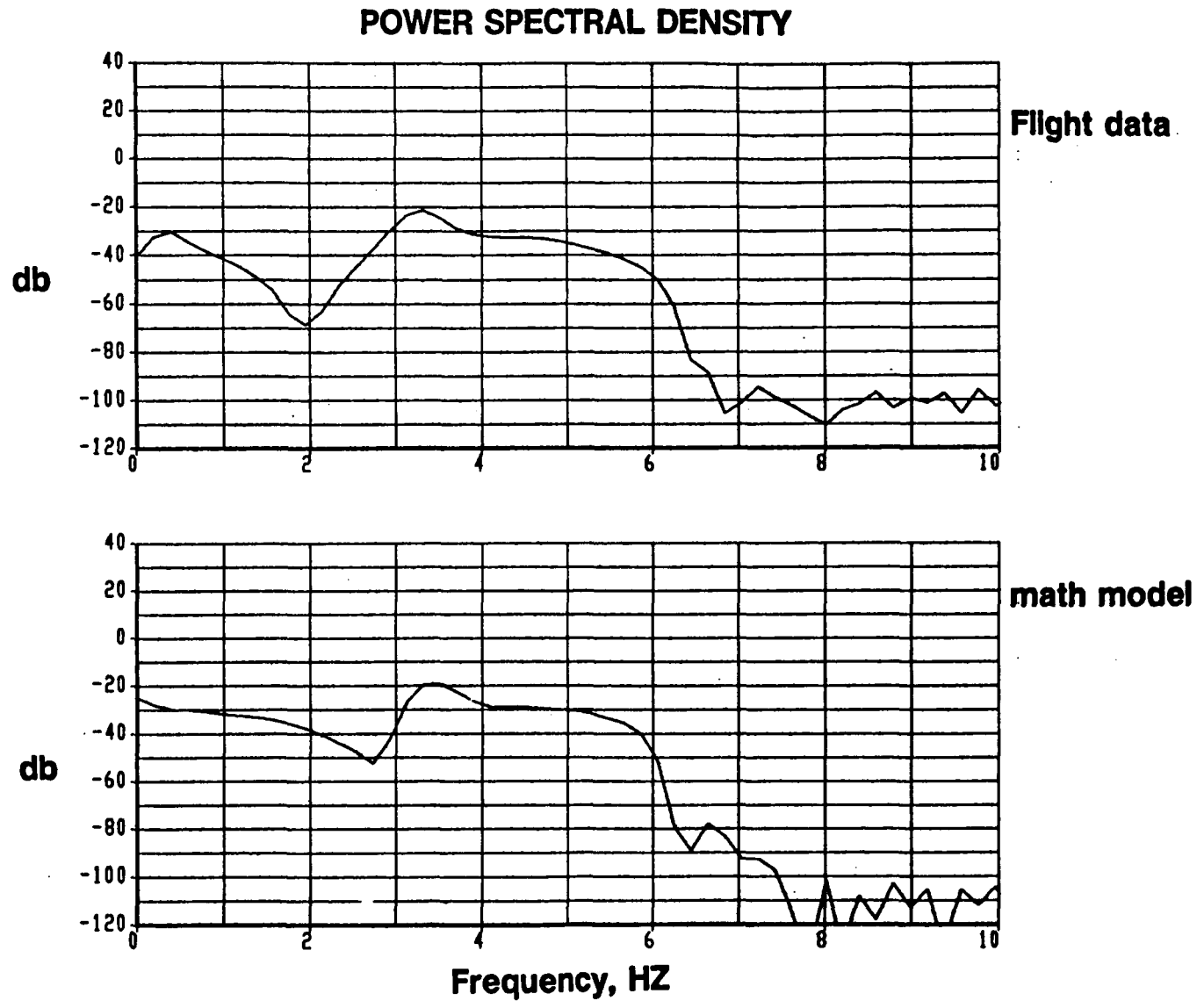
Figure 26. Power Spectral Density Response of Lateral Acceleration at AFT Body Comparing Flight Data with Math Model

POWER SPECTRAL DENSITY

Body Roll
IRU

621

Flight data
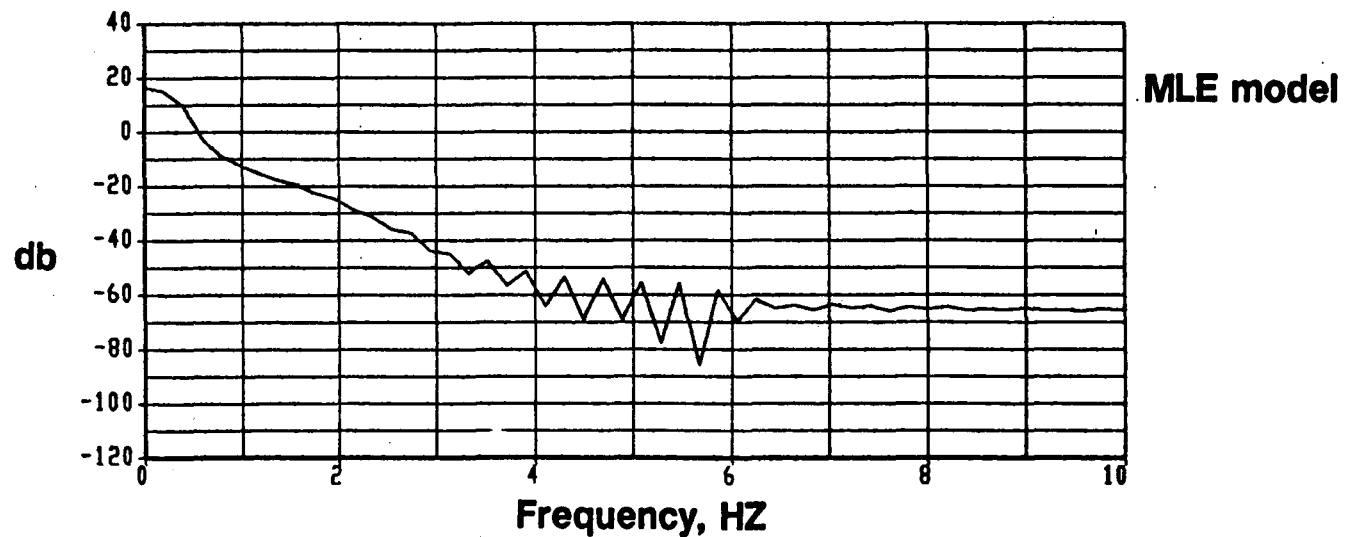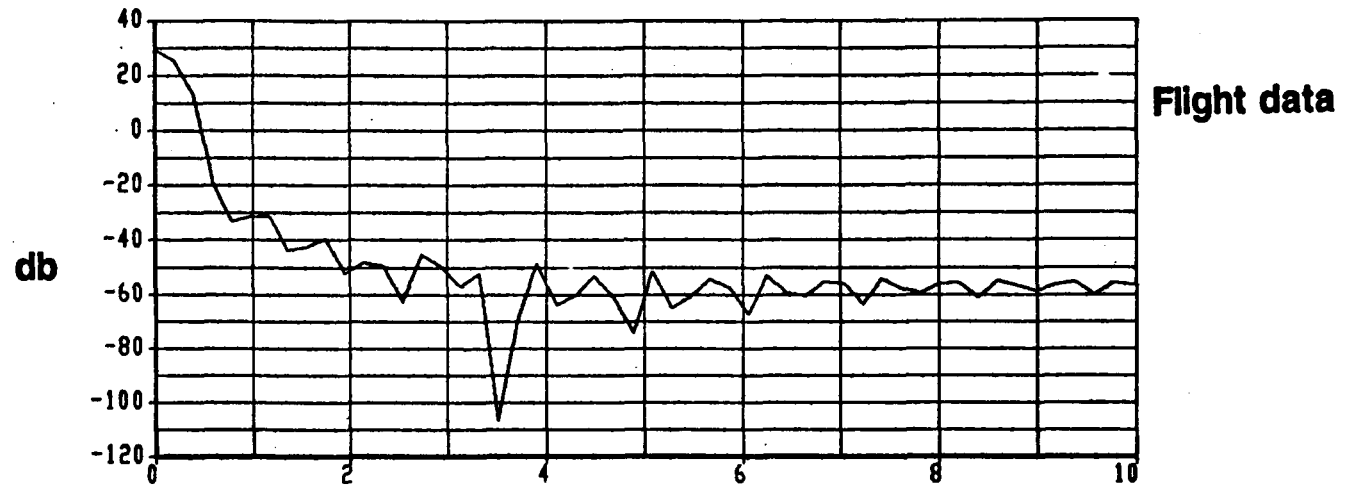
MLE model

Figure 27. Power Spectral Density Response of Body Roll at IRU Comparing Flight Data with MLE Model

POWER SPECTRAL DENSITY

Body Yaw IRU

622
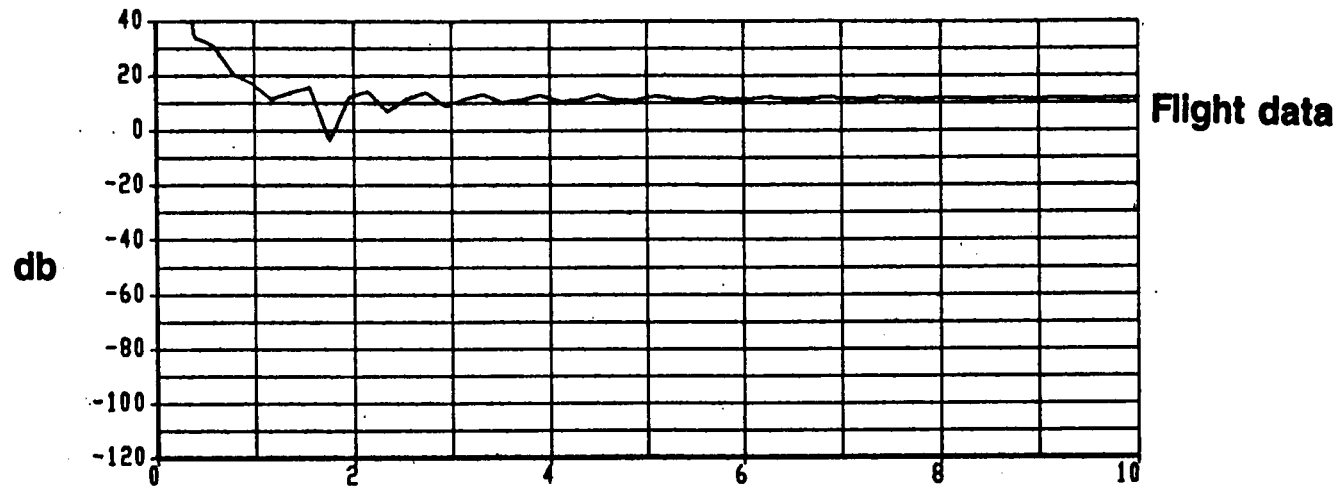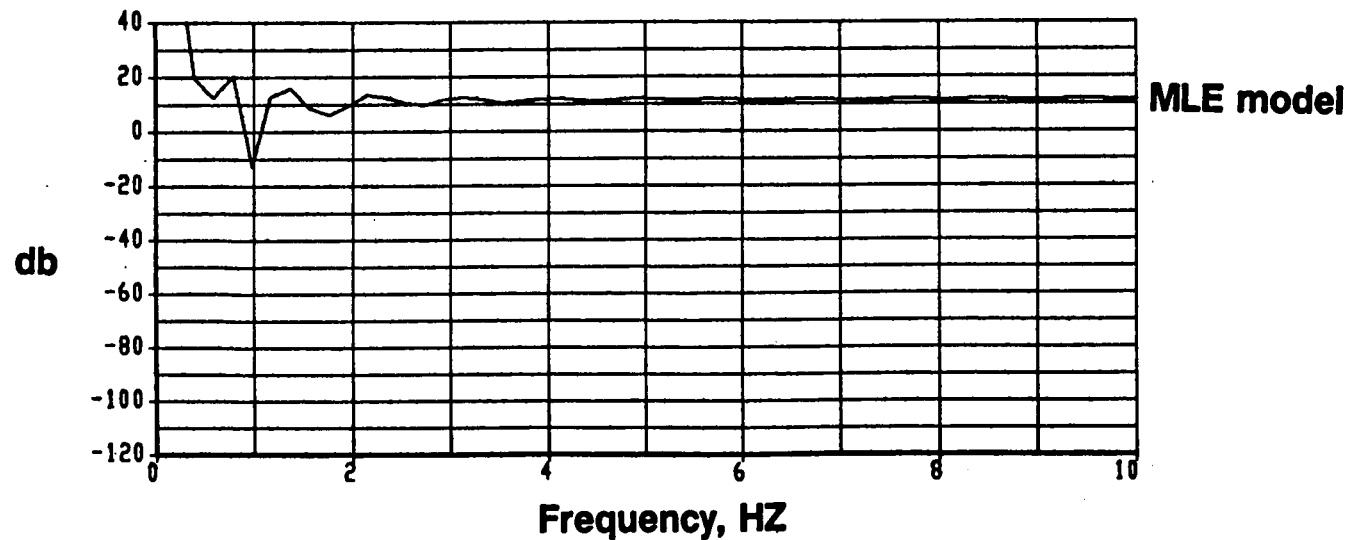
Figure 28. Power Spectral Density Response of Body Yaw at IRU Comparing Flight Data with MLE Model

POWER SPECTRAL DENSITY

Flight data

Roll Rate

IRU

623

MLE model

Frequency, HZ
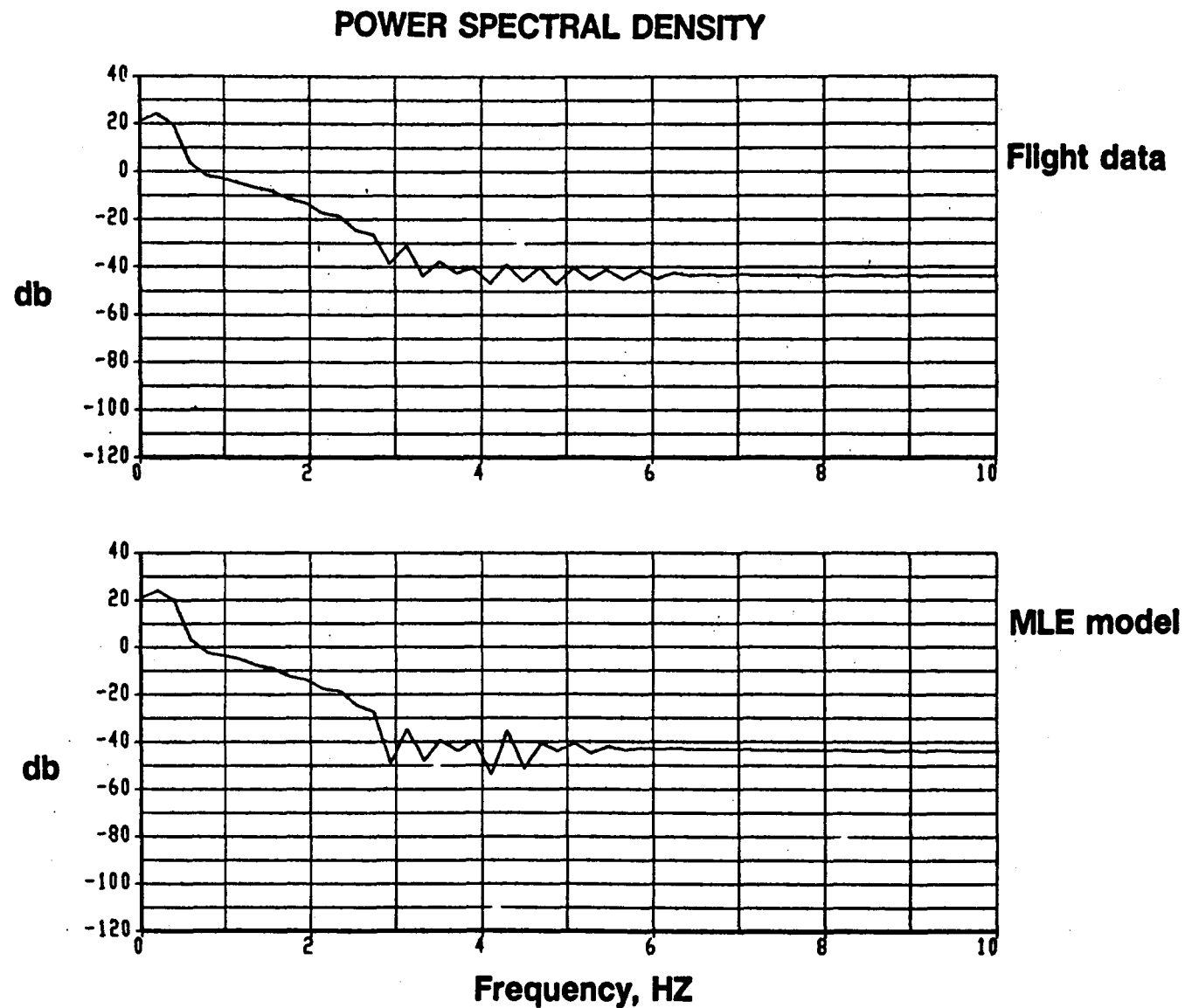
Figure 29. Power Spectral Density Response of Roll Rate at IRU Comparing Flight Data with MLE Model

POWER SPECTRAL DENSITY
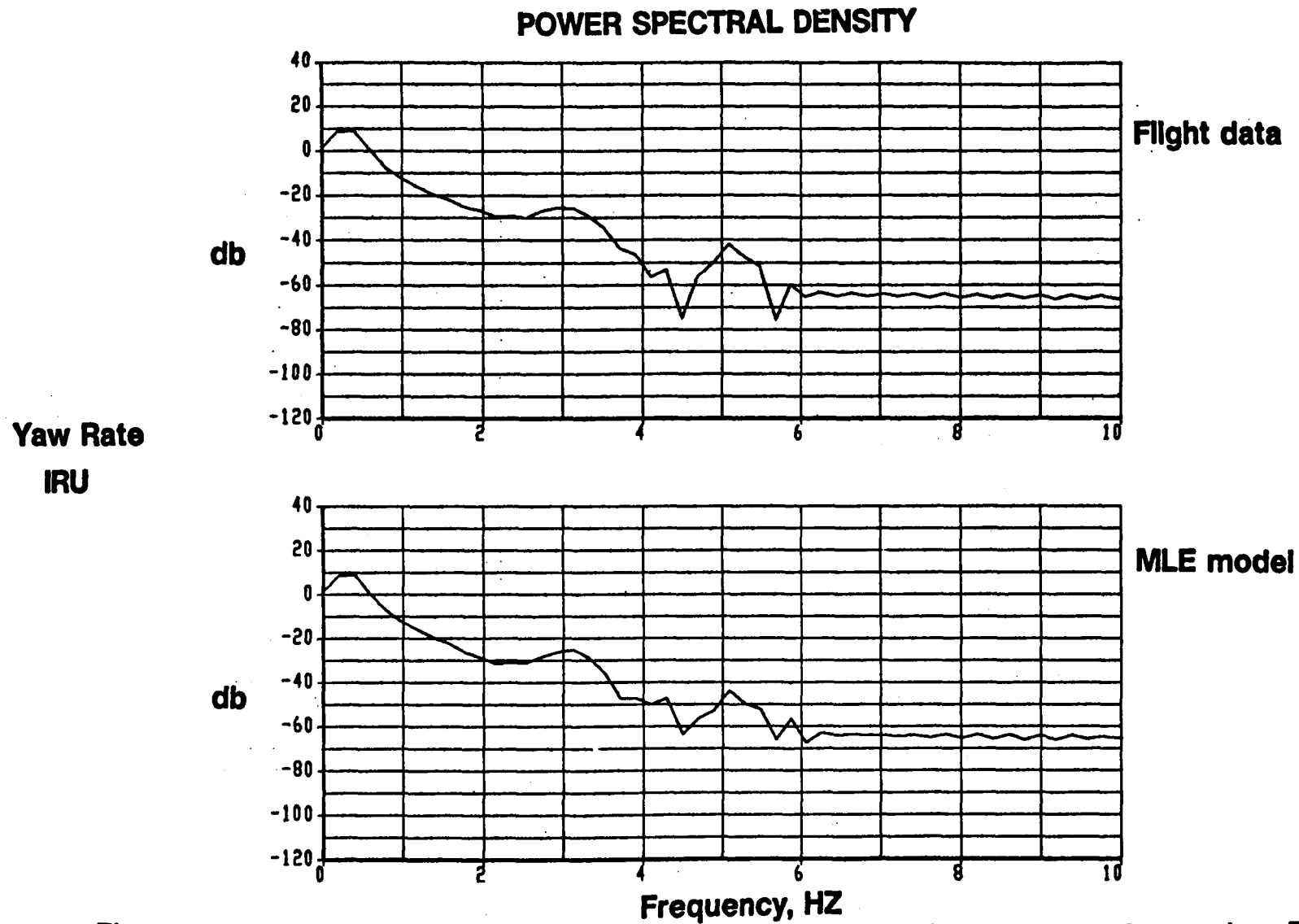
Figure 30. Power Spectral Density Response of Yaw Rate at IRU Comparing Flight Data with MLE Model

POWER SPECTRAL DENSITY

Flight data

MLE model

Lateral Acceleration Pilot seat

625

Frequency, HZ
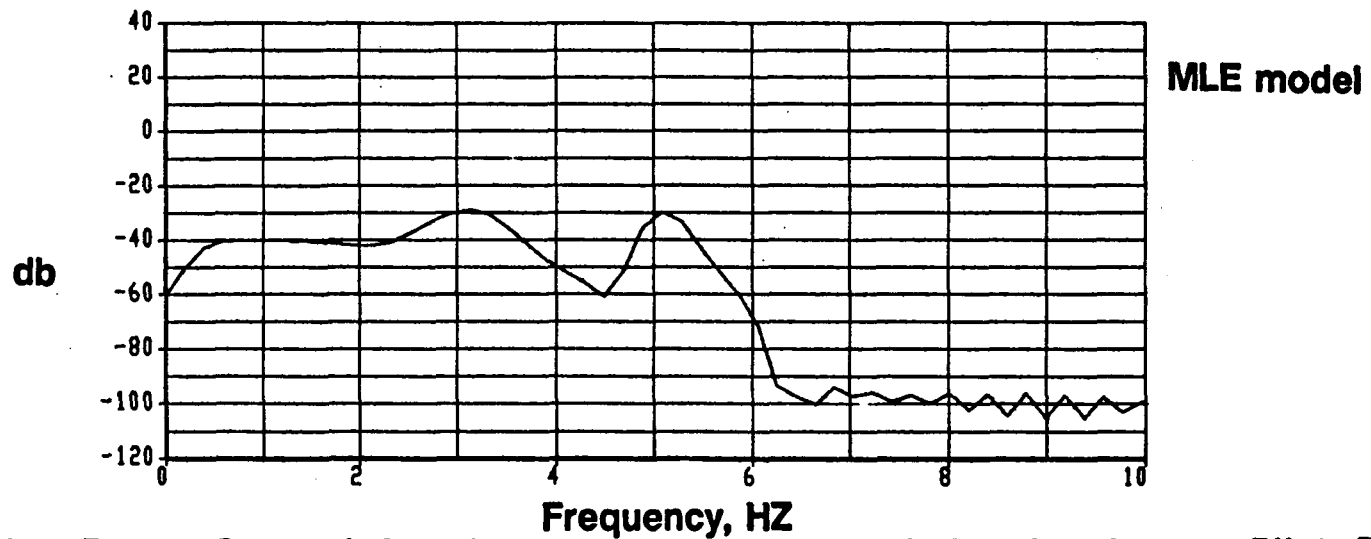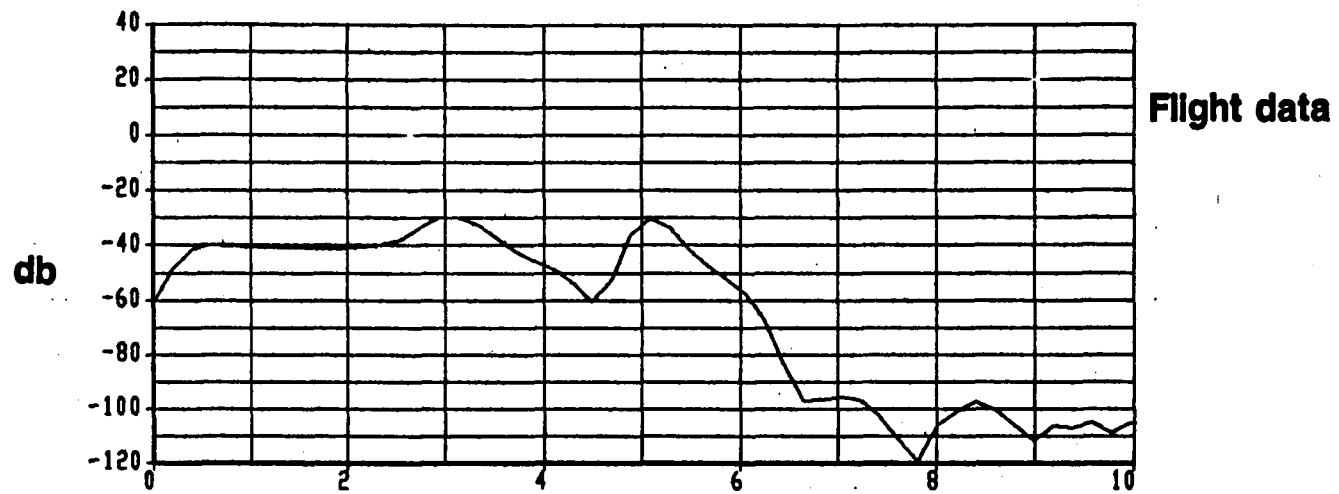
Figure 31. Power Spectral Density Response of Lateral Acceleration at Pilot Seat Comparing Flight Data with MLE Model

POWER SPECTRAL DENSITY
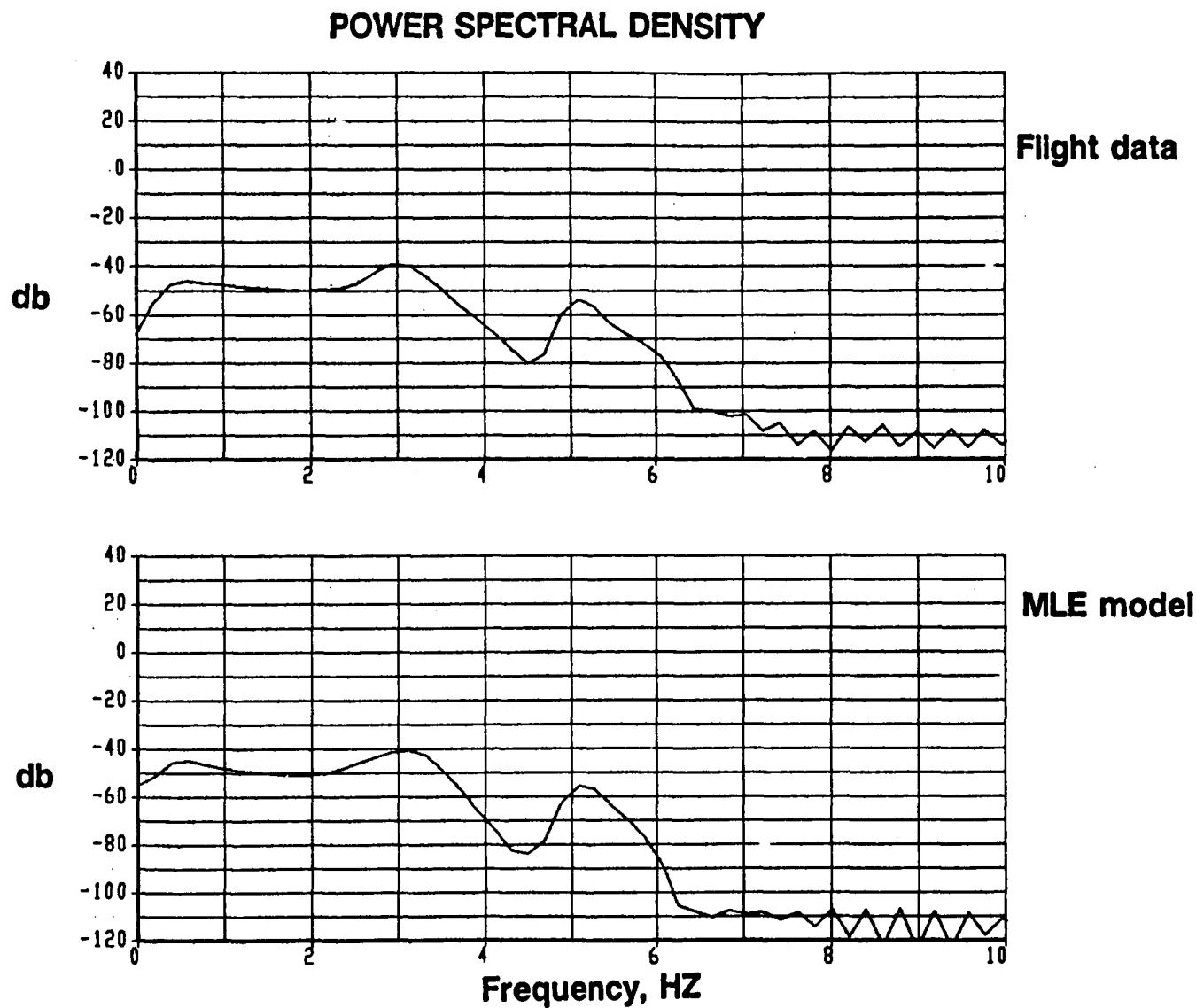
Figure 32. Power Spectral Density Response of Lateral Acceleration at IRU Comparing Flight Data with MLE Model

POWER SPECTRAL DENSITY

Flight data

MLE model

Lateral Acceleration AFT Body

627

Frequency, HZ
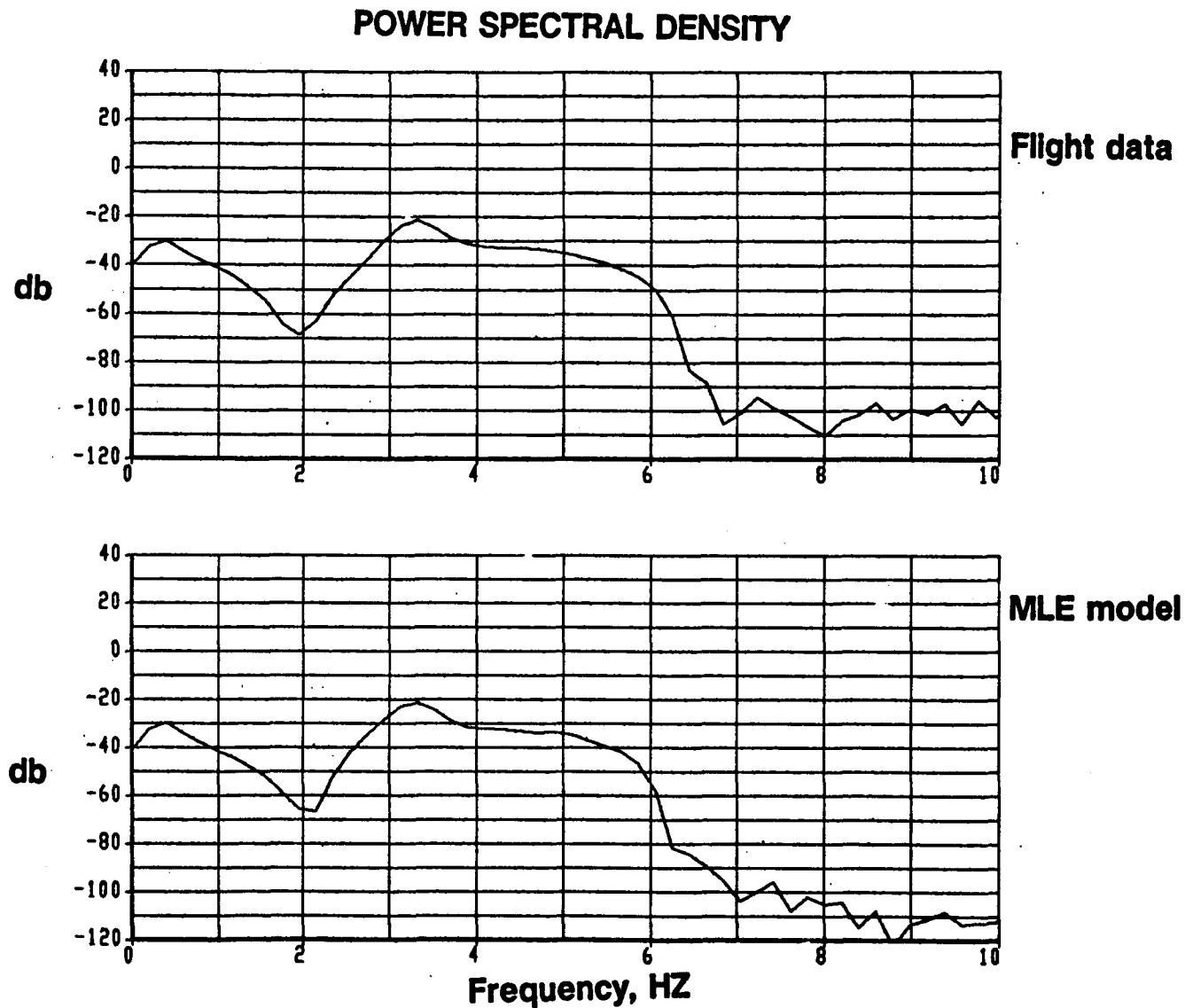
Figure 33. Power Spectral Density Response of Lateral Acceleration at AFT Body Comparing Flight Data with MLE Model

POWER SPECTRAL DENSITY
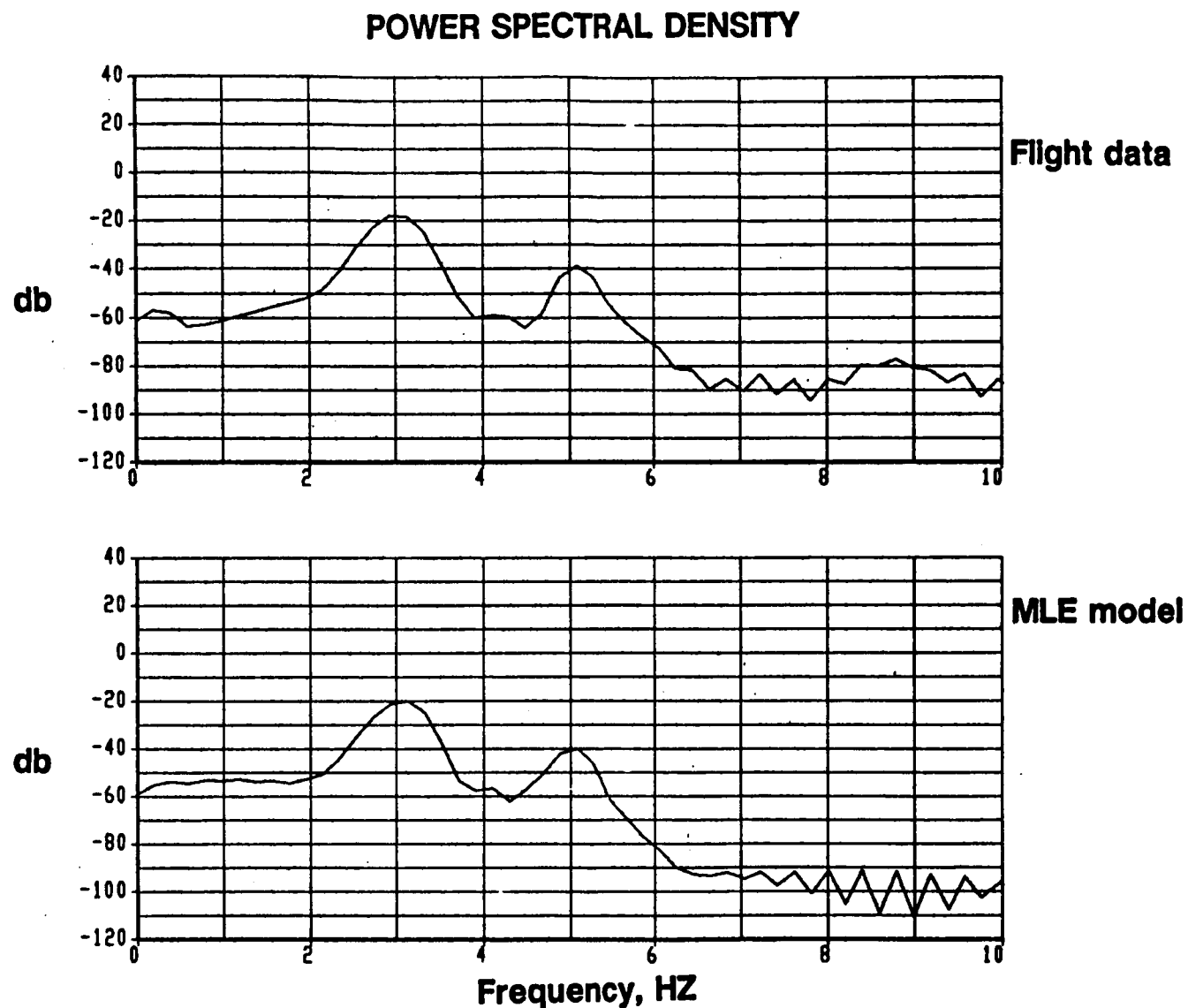
Figure 34.   Power Spectral Density of Lateral Acceleration at Engine 2 Inlet Comparing Flight Data with MLE Model

REFERENCES

1. R.E. Maine and K.W. Iliff, "User's Manual for MMLE, a General FORTRAN Program for Maximum Likelihhood Parameter Estimation", NASA Technical Paper 1563, November 1980.

2. G.C. Goodwin and R.L. Payne, "Dynamic System Identification - Experiment Design and Data Analysis", Academic Press, 1977.

629

AUTOMATED MODEL FORMULATION FOR TIME-VARYING FLEXIBLE STRUCTURES

By

B. J. Glass* and S. Hanagud
Georgia Institute of Technology
Atlanta, Georgia

ABSTRACT

The control of many types of flexible structures, such as robotic manipulators or large space structures, usually requires an accurate analytical model. Once obtained, these models are currently compared with observations of the behavior of the structure and incremental changes can be made by using Kalman filtering techniques or other parameter identification techniques. For time-varying flexible structures, however, such changes may occur in sudden changes to boundary conditions or to the form of the model differential equations. Some of the primary causes for such changes are growth, reconfiguration or damage. This class of changes often requires a reformulation of the analytical model. This paper presents an identification technique that uses the sensor information to choose a new model out of a finite set of discrete model space, in order to follow the observed changes to the given time varying flexible structure. Boundary condition sets or other information on model variations are used to organize the set of possible models laterally into a search tree with levels of abstraction used to order the models vertically within branches. An object-oriented programming approach is used to represent the model set in the search tree. A modified A* best first search algorithm finds the model where the model response best matches the current observations. Several extensions to this methodology will be discussed. Methods of possible integration of rules with the current search algorithm will be considered to give weight to interpreted trends that may be found in a series of observations. This capability might lead, for instance, to identifying a model that incorporates a progressive damage rather than with incorrect parameters such as added mass. Another new direction is to consider the use of noisy time domain sensor feedback rather than frequency domain information in the search algorithm to improve the real-time capability of the developed procedure. The next logical step will be to automatically expand the model space by adding subsets of recognized possible models. This can be accomplished by using developed methods of machine learning. Finally, testing of the currently developed approach with model spaces that are derived from more complex structures will be discussed.

* Dr. Glass is currently with the System Autonomy Demonstration Project Office of the NASA Ames Research Center, Moffett Field, California 94035

NUMERICALLY EFFICIENT ALGORITHM FOR MODEL DEVELOPMENT OF HIGH-ORDER SYSTEMS

By

L. O. Parada
Calspan Advanced Technology Center
Buffalo, New York

ABSTRACT

Frequency domain parameter identification techniques provide a straightforward approach to transfer function estimation. However, for high-order systems, numerical difficulties may be encountered during the estimation process. Inaccuracies may result because of the large variation of the transfer function polynomial coefficients for high-order systems. The lack of numerical precision to represent this variation may cause the estimation process to break down.

This paper presents a technique for estimating transfer functions in partial fraction expansion form from frequency response data for a high-order system. The problem formulation avoids many of the numerical difficulties associated with high-order polynomials and has the advantage of having the option to fix the damping and frequency of a mode, if known, during the estimation process. The resulting transfer function(s) may be converted to Jordan-Form time domain equations directly.

During the implementation of this technique, a frequency and amplitude normalizing window was developed that maximized the efficiency of the optimization algorithm. The combination of estimating the transfer function in factored form, the ability to fix previously determined parameters and the effectiveness of the normalizing window led to a progressive approach to synthesizing transfer functions from frequency response data for high-order systems.

Abstract

Numerically Efficient Algorithm for Model Development of High Order Systems

L. O. Parada
Calspan Advanced Technology Center
P.O. Box 400
Buffalo, NY 14225
(716) 632-7500

for presentation at the

NASA Langley Research Center Workshop on
Computational Aspects in the Control of Flexible Structures

Frequency domain parameter identification techniques provide a straightforward approach to transfer function estimation. However, for high order systems, numerical difficulties may be encountered during the estimation process. Inaccuracies may result because of the large variation of the transfer function polynomial coefficients for high order systems. The lack of numerical precision to represent this variation may cause the estimation process to break down.

This paper presents a technique for estimating transfer functions in partial fraction expansion form from frequency response data for a high order system. The problem formulation avoids many of the numerical difficulties associated with high order polynomials and has the advantage of having the option to fix the damping and frequency of a mode, if known, during the estimation process. The resulting transfer function(s) may be converted to Jordan-Form time domain equations directly.

During the implementation of this technique, a frequency and amplitude normalizing window was developed that maximized the efficiency of the optimization algorithm. The combination of estimating the transfer function in factored form, the ability to fix previously determined parameters and the effectiveness of the normalizing window led to a progressive approach to synthesizing transfer functions from frequency response data for high order systems.

635

NUMERICALLY EFFICIENT ALGORITHM FOR MODEL DEVELOPMENT OF HIGH ORDER SYSTEMS

Statement of Problem

Development of Mathematical Models:

Time Domain – Difficult to implement
– Instrumentation Complement
– Input Design
– Noise
– Computational Load

Freq Domain – Simplified Implementation
– Fewer parameters per computation cycle
– Statistical methods applicable

PREVIOUS WORK

Frequency domain parameter identification requires

    Determination of characteristic equation
        (nonlinear or iterative techniques)

    Estimation of numerator polynomials

    Factor characteristic equation

    Estimate zeros or residues

Inaccuracies (for high order systems) due to:

    Variation of transfer function polynomial coefficients

    Transformation errors

    Sensitivity of polynomial roots to variations in polynomial coefficients

SUMMARY OF CONTRIBUTIONS

Development of technique to estimate transfer functions in partial fraction expansion form from frequency response (amplitude and phase) data

Elimination of numerical difficulties associated with high order polynomials

Incorporation of a priori knowledge of system modes (frequency and damping) directly into the estimation process

Development of frequency and amplitude normalizing window that maximizes effectiveness of the optimization algorithm and eliminates the initial guess problem

Stepwise approach for synthesizing transfer functions where order of system is high and unknown

FACTORED FORM ESTIMATION

Classical Nonlinear Regression Problem

Estimate parameters from measured amplitude and phase data

Error Function:

Square of distance between measured and estimated frequency responses summed over all discrete frequency points

$$\epsilon = \sum_{i=1}^{M} \left[F(j\omega_i) - G(j\omega_i) \right]^2$$

where: M = # frequency points

$F(j\omega)$ = measured frequency response

$G(j\omega)$ = estimated frequency response

Estimated Transfer Function – $G(j\omega)$

Sum of 1st and 2nd order terms

$$G(j\omega) = \frac{a_N}{b_N} + \sum_{k=1}^{Q} \frac{n_{1_k}(j\omega) + N_{0_k}}{(j\omega)^2 + d_{1_k}(j\omega) + d_{0_k}} + \sum_{\ell=1}^{N-2Q} \frac{a_\ell}{(j\omega) + b_\ell}$$

where: N = order of system
Q = # of second order terms

Express measured and estimated frequency responses in terms of real and imaginary components

$$F(j\omega) = R(\omega) + j\,I(\omega)$$

$$G(j\omega) = \frac{a_N}{b_N} + \sum_{k=1}^{Q} \frac{N_{0_k}(d_{0_k} - \omega^2) + N_{1_k} d_{1_k}^2}{(d_{0_k} - \omega^2)^2 + d_{1_k}^2 \omega^2} + \sum_{\ell=1}^{N-2Q} \frac{a_\ell b_\ell}{b_\ell^2 + \omega^2}$$

$$+ j\left[\sum_{k=1}^{Q} \frac{N_{1_k}\omega(d_{0_k} - \omega^2) - N_{0_k} d_{1_k}\omega}{(d_{0_k} - \omega^2)^2 + d_{1_k}^2 \omega^2} - \sum_{\ell=1}^{N-2Q} \frac{a_\ell \omega}{b_\ell^2 + \omega^2} \right]$$

Substitue for F (j ω) & G (j ω) into ε

$$\epsilon = \sum_{i=1}^{M} \left[R(\omega_i) - \frac{a_N}{b_N} - \sum_{k=1}^{Q} \frac{N_{0_k}(d_{0_k} - \omega_i^2) + N_{1_k} d_{1_k} \omega_i^2}{(d_{0_k} - \omega_i^2)^2 + d_{1_k}^2 \omega_i^2} + \sum_{\ell=1}^{N-2Q} \frac{a_\ell b_\ell}{b_\ell^2 + \omega_i^2} \right]$$

$$+ \left[I(\omega_i) + \sum_{k=1}^{Q} \frac{N_{0_k} d_{1_k}\omega_i - N_{1_k}\omega_i(d_{0_k} - \omega_i^2)}{(d_{0_k} - \omega_i^2)^2 + d_{1_k}^2 \omega_i^2} + \sum_{\ell=1}^{N-2Q} \frac{a_\ell \omega_i}{b_\ell^2 + \omega_i^2} \right]$$

Solve for unknown parameters
Set partial derivatives equal to zero
Solve using nonlinear optimization technique

640

Fifth Order Single Precision Example

Simulate parameter identification of high order system

Modes distributed over wide frequency range

Single precision: Scale down problem
Reduce number of variables

5th Order Transfer Function:

Cascade form

$$\frac{(s + 5 \times 10^{-3})\ (s + 5 \times 10^{-1})\ (s + 5 \times 10^{+1})\ (s + 5 \times 10^{+3})}{(s^2 + 2 \times 10^{-3}s + 10^{-4})\ (s + 1)\ (s^2 + 1 \times 10^{+4}s + 10^{+8})}$$

Parallel form

$$\frac{1.253955 \times 10^{-3}s + 6.122844 \times 10^{-6}}{s^2 + 2 \times 10^{-3}\,s + 1 \times 10^{-4}} + \frac{1.221073 \times 10^{-3}}{s + 1} + \frac{9.975250 \times 10^{-1}s + 5.024754 \times 10^{+3}}{s^2 + 1 \times 10^{+4}\,s + 10^{+8}}$$

Frequency Range: 1×10^{-4} to $1 \times 10^{+5}$ Hz.

Points/Decade = 30

DENOMINATOR COEFFICIENTS

Term	Exact Coefficient	Additive Components
s^5	$\boxed{1.000000}$	1.0
s^4	$\boxed{10001.00}2$	$1.002 + 1.0 \times 10^{+4}$
s^3	$\boxed{1000100}2.0021$	$2.1 \times 10^{-3} + 1.002 \times 10^{+4} + 10^{+8}$
s^2	$\boxed{1002002}1.0001$	$1 \times 10^{-4} + 2.1 \times 10^{+1} + 1.002 \times 10^{+8}$
s^1	$\boxed{210001.0}$	$1.0 + 2.1 \times 10^{+5}$
s^0	$\boxed{100004.0}$	$1.0 \times 10^{+4}$

$\boxed{}$ = Single Precision Variable Representation

642

LINEARIZED APPROACH

Initial Error Function:

$$E_k = F(j\omega_k) - \frac{P(j\omega_k)}{Q(j\omega_k)}$$

where: $F(j\omega_k)$ = measured frequency response at ω_k

$P(j\omega_k)$ = estimated numerator polynomial at ω_k

$Q(j\omega_k)$ = estimated denominator polynomial at ω_k

Weighted Error Function:

$$E_k' = E_k Q(j\omega_k) = F(j\omega_k) Q(j\omega_k) - P(j\omega_k)$$

Iterative Error Function:

$$E_k'' = \frac{E_k Q(j\omega_k)_L}{Q(j\omega_k)_{L-1}} = \frac{F(j\omega_k) Q(j\omega_k)_L}{Q(j\omega_k)_{L-1}} - \frac{P(j\omega_k)_L}{Q(j\omega_k)_{L-1}}$$

where: L = iteration #

Minimize E_k'' by taking partial derivatives of E_k'' with respect to each parameter x_i

$$\frac{\partial E_k''}{\partial x_i} = 0$$

Rearrange equations to formulate problem as a set of linear simultaneous algebraic equations:

$$[A][X] = [B]$$

Solve for parameter vector [x]

Iterations converge to minimization of $|E_k|^2$

5th Order example: Polynomial Results

Exact Transfer Function

$$\frac{(s + 5 \times 10^{-3}) \quad (s + 5 \times 10^{-1}) \quad (s + 5 \times 10^{+1}) \quad (s + 5 \times 10^{+3})}{(s^2 + 2 \times 10^{-3}s + 10^{-4})(s + 1)(s^2 + 1 \times 10^{+4}s + 10^{+8})}$$

Linear Results

$$\frac{(s + 5 \times 10^{-3})(s + 5 \times 10^{-1})(s + 4.24 \times 10^{+1})(s - 7.17 \times 10^{+3})}{(s^2 + 2 \times 10^{-3}s + 10^{-4})(s + 9.98 \times 10^{-1})(s - 7.17 \times 10^{+3})(s + 1.72s \, 10^{+4})}$$

Cost Function

$$2.37 \times 10^{-10}$$

+ + + = measured

FREQ-RAD/SEC

FREQ-RAD/SEC

644
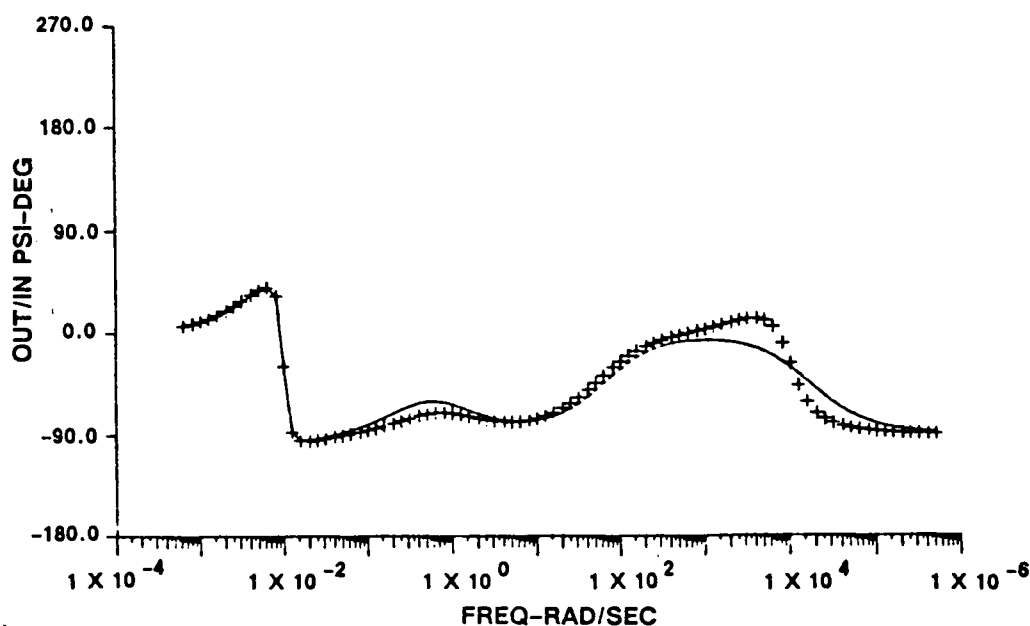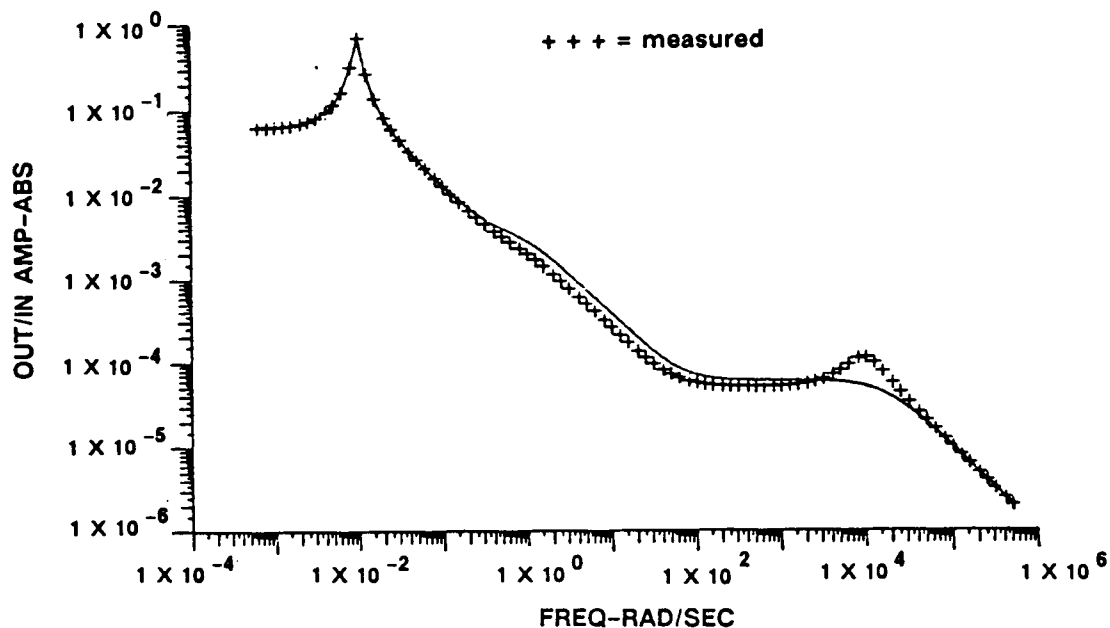
FACTORED FORM APPROACH

Nonlinear method of solution – strong initial guess required

Initial Guess – Examine bode plots to approximate frequency and damping of modes

Problem – Error function relatively insensitive to perturbations in parameters of high frequency modes

– Gradient expressions small compared to those of the lower frequency parameters

Solution – Normalizing window

Scale Data Such That:

– Frequency is centered around 1 rad.

Amplitude is centered around 1 (abs. units)

Benefits – Need for strong initial guess eliminated effectiveness of optimization algorithm maximized

645

STEPWISE   FACTORED   FORM   TECHNIQUE

Plot Amplitude
& Phase Data

Section Amplitude Plot into J
1st & 4th Order Sections

I = 1

Initialize Parameter
Vector Elements to 1

Scale Frequency Data
around 1 radian

Scale Amplitude Data
around 1 (abs.)

Identify
Parameters

I > 1   Y   Improve   Y   Parameter = Estimated
                     Parameters   Vector   Values
  N   ?

I = I+1   N

I > J   Y   Run Nth Order Case
                      over entire frequency
  N   range using estimated
                      values as initial
                      Parameter Vector

STOP

646

5th Order Example: Factored Form Approach

OUT/IN AMP-ABS

FREQ-RAD/SEC

SCALING:
FREQ = 1 X 10^{-2}
AMP = 1 X 10^{-1}

SCALING:
FREQ = 1.0
AMP = 1 X 10^{-3}

SCALING:
FREQ = 1 X 10^{+4}
AMP = 1 X 10^{-5}

647

5th Order Example: Factored Form Results

Exact
Transfer
Function
$$\frac{1.25 \times 10^{-3}s + 6.12 \times 10^{-6}}{s^2 + 2 \times 10^{-3} s + 10^{-4}} + \frac{1.22 \times 10^{-3}}{s + 1} + \frac{9.98 \times 10^{-1}s + 5.02 \times 10^{+3}}{s^2 + 1 \times 10^{+4} s + 10^{+8}}$$

Factored
Form
Results
$$\frac{1.25 \times 10^{-3}s + 6.12 \times 10^{-6}}{s^2 + 2.00 \times 10^{-3} s + 10^{-4}} + \frac{1.23 \times 10^{-3}}{s + 1.01} + \frac{9.79 \times 10^{-1}s + 5.21 \times 10^{+3}}{s^2 + 9.95 \times 10^{+3} s + 1.03 \times 10^{+8}}$$

Cost
Function
$$1.90 \times 10^{-12}$$

648
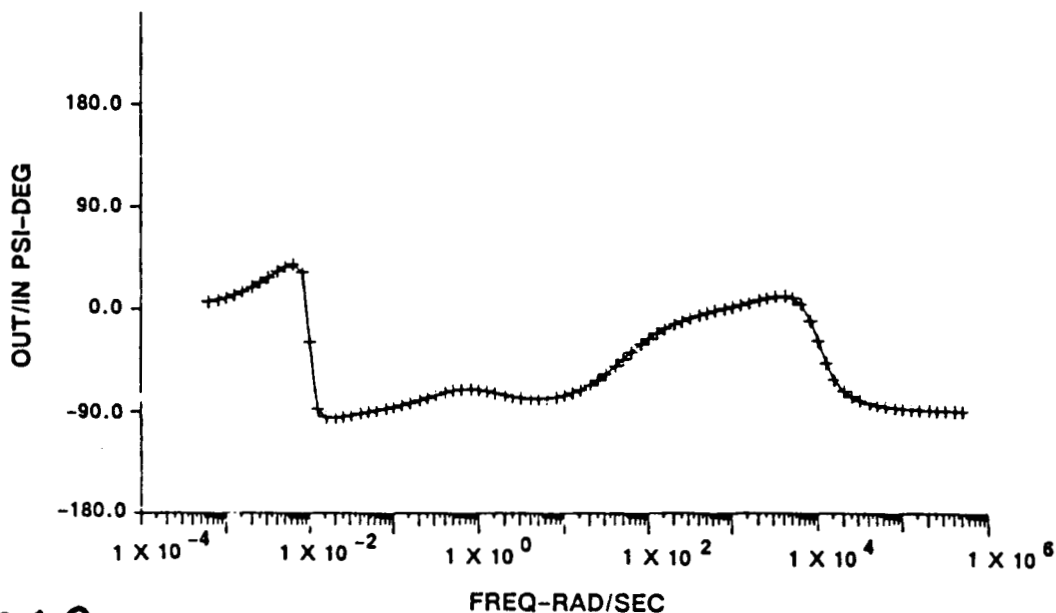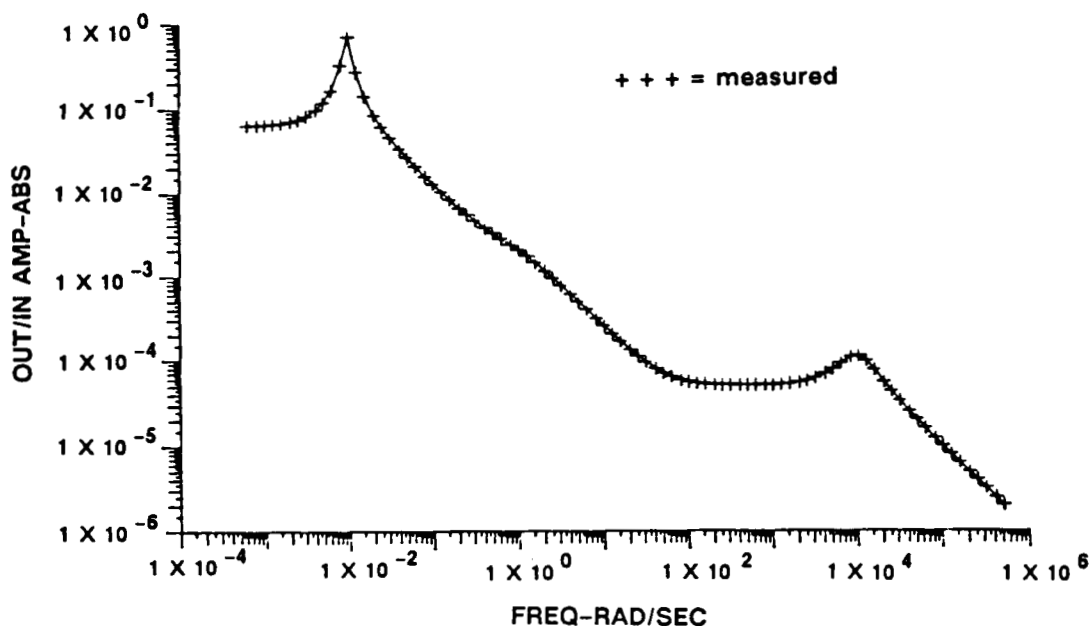
16th Order Transfer Function Estimation

Pcg/Vg: Roll Rate Measured at C.G. of Aircraft

vs.

Unit Gust Along Y-Body Axis

Cost Function: 4.5 x 10^{-12}

649
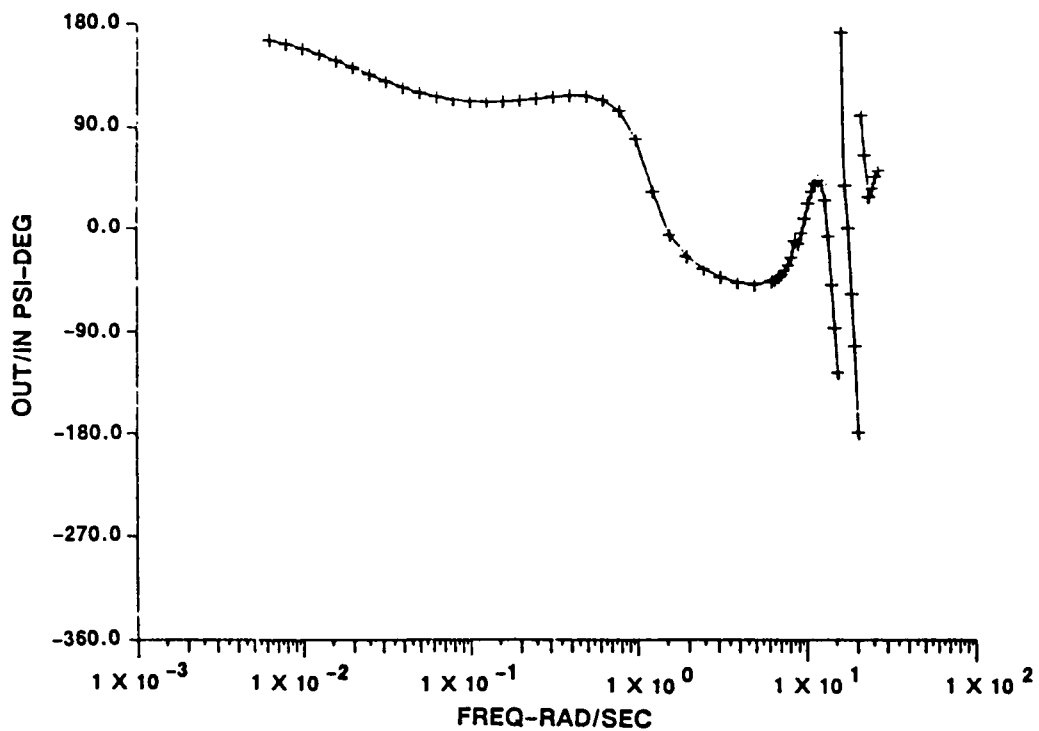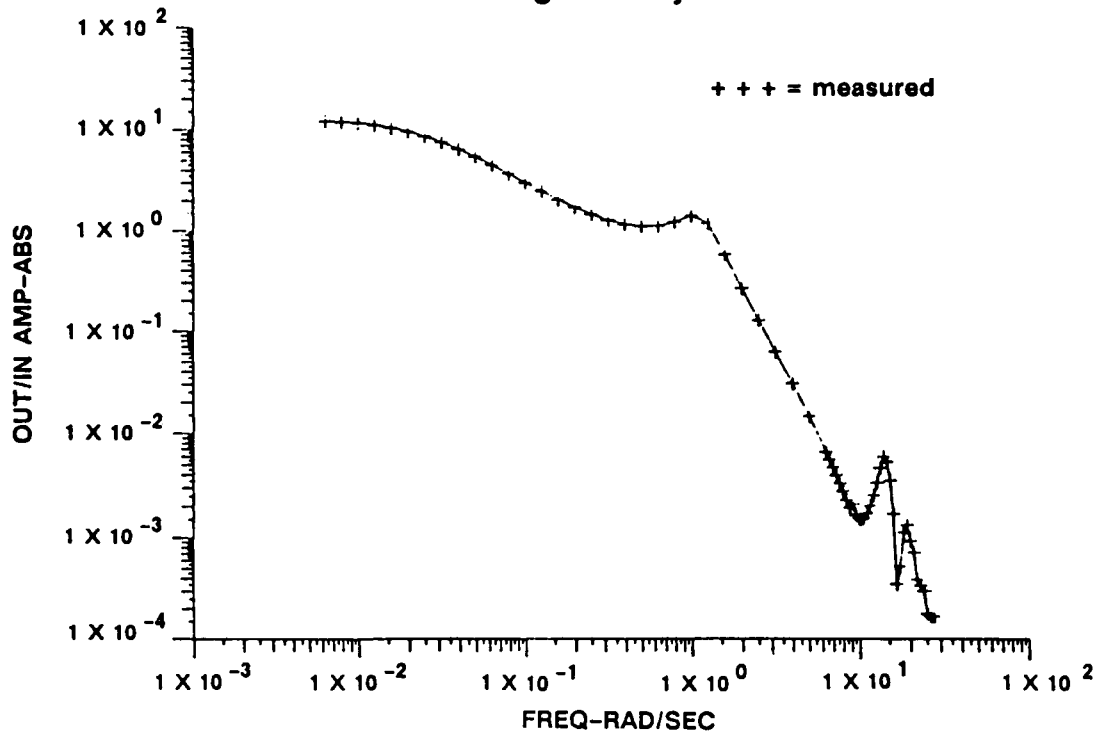
CONCLUSIONS

Development of technique to estimate transfer functions directly in factored form

Advantages:

    Ability to fix damping and frequency of a mode, if known, during the estimation process

    Avoidance of numerical difficulties associated with high order polynomials

    Ability to obtain Jordan–form time domain equations directly

Progressive approach to transfer function estimation through use of a frequency and amplitude normalizing window

Development of frequency and amplitude normalizing window that eliminates the initial guess problem and maximizes the effectiveness of the optimization algorithm

ON MODELLING NONLINEAR DAMPING IN DISTRIBUTED PARAMETER SYSTEMS

A. V. Balakrishnan
UCLA
Los Angeles, California

12 July 1988

SCOLE DAMPING

Amplitude

652

0 100 200 300 400 500 60

Number of Cycles
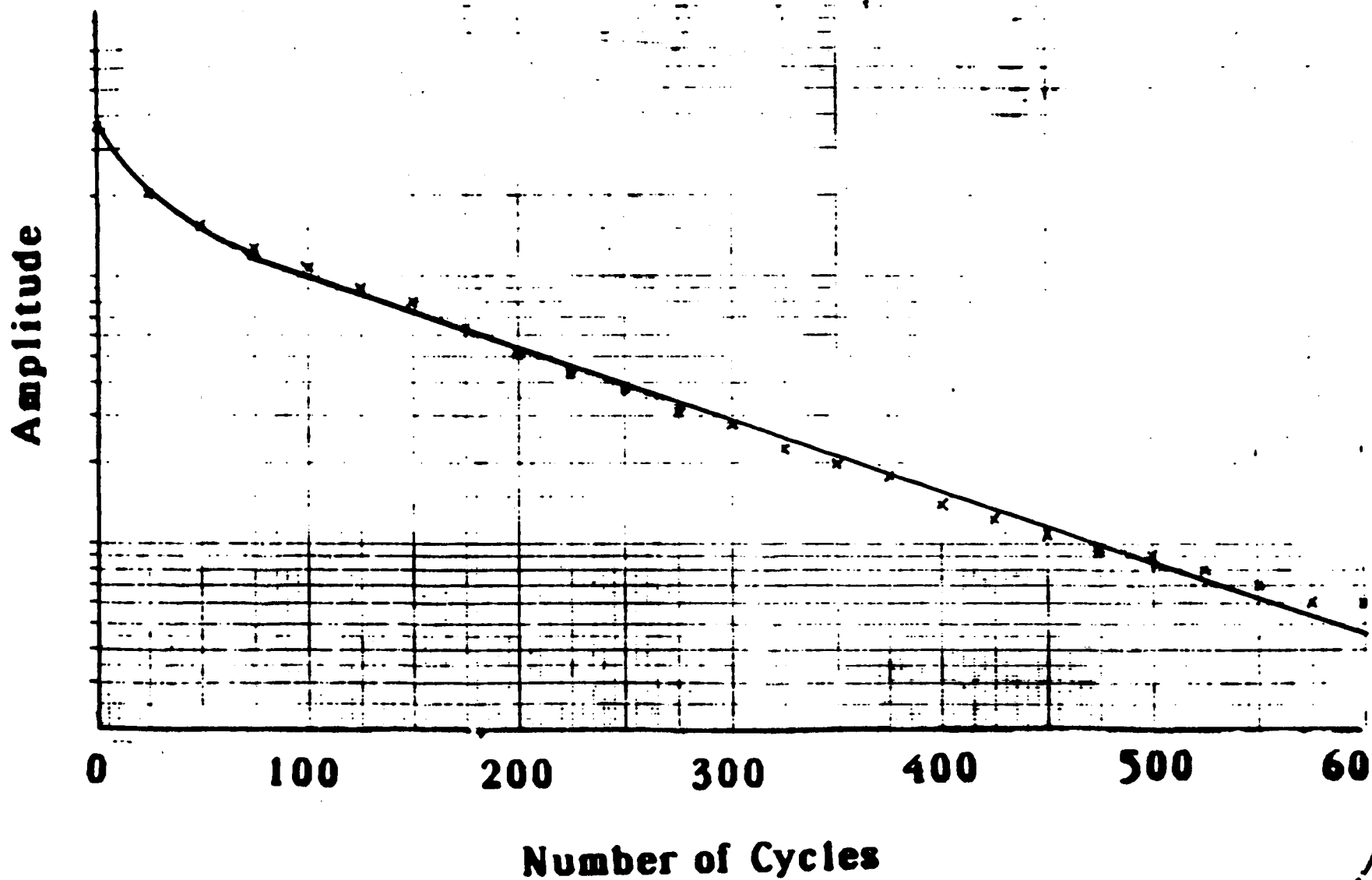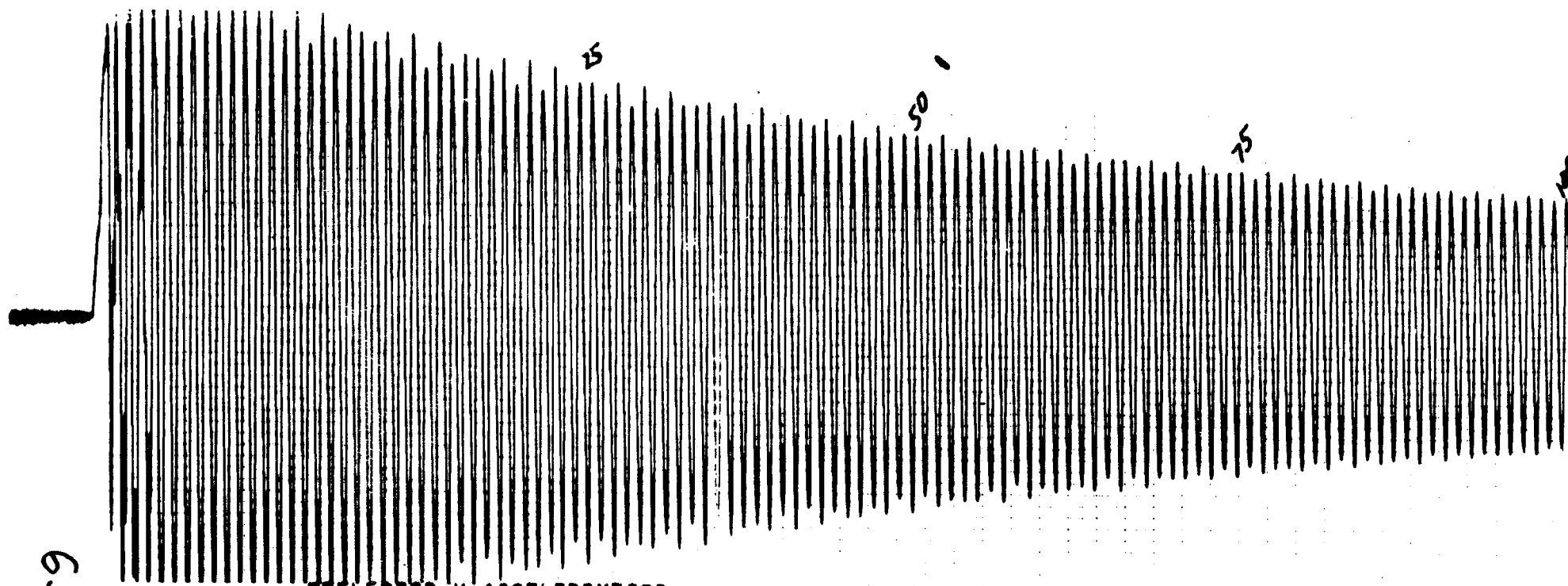
653

REFLECTOR X ACCELEROMETER

$U = \pm 12''$

—⟶ ⊢— 5 SECONDS

25   50   75   100

TIME ⟶

with out mass

with mass

654
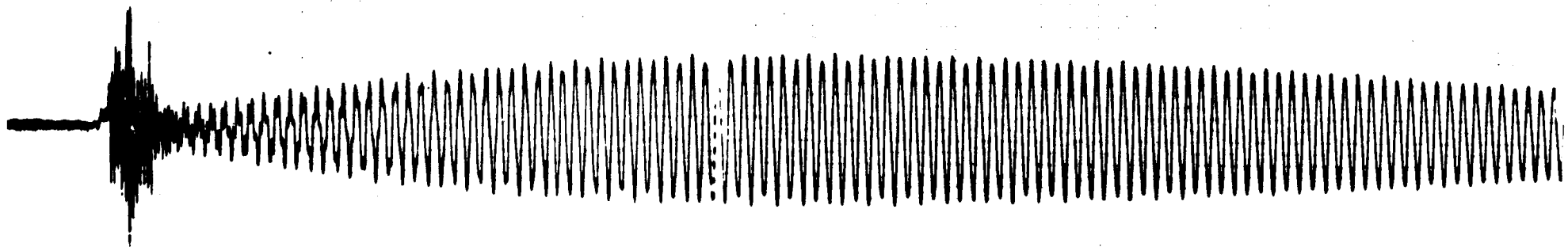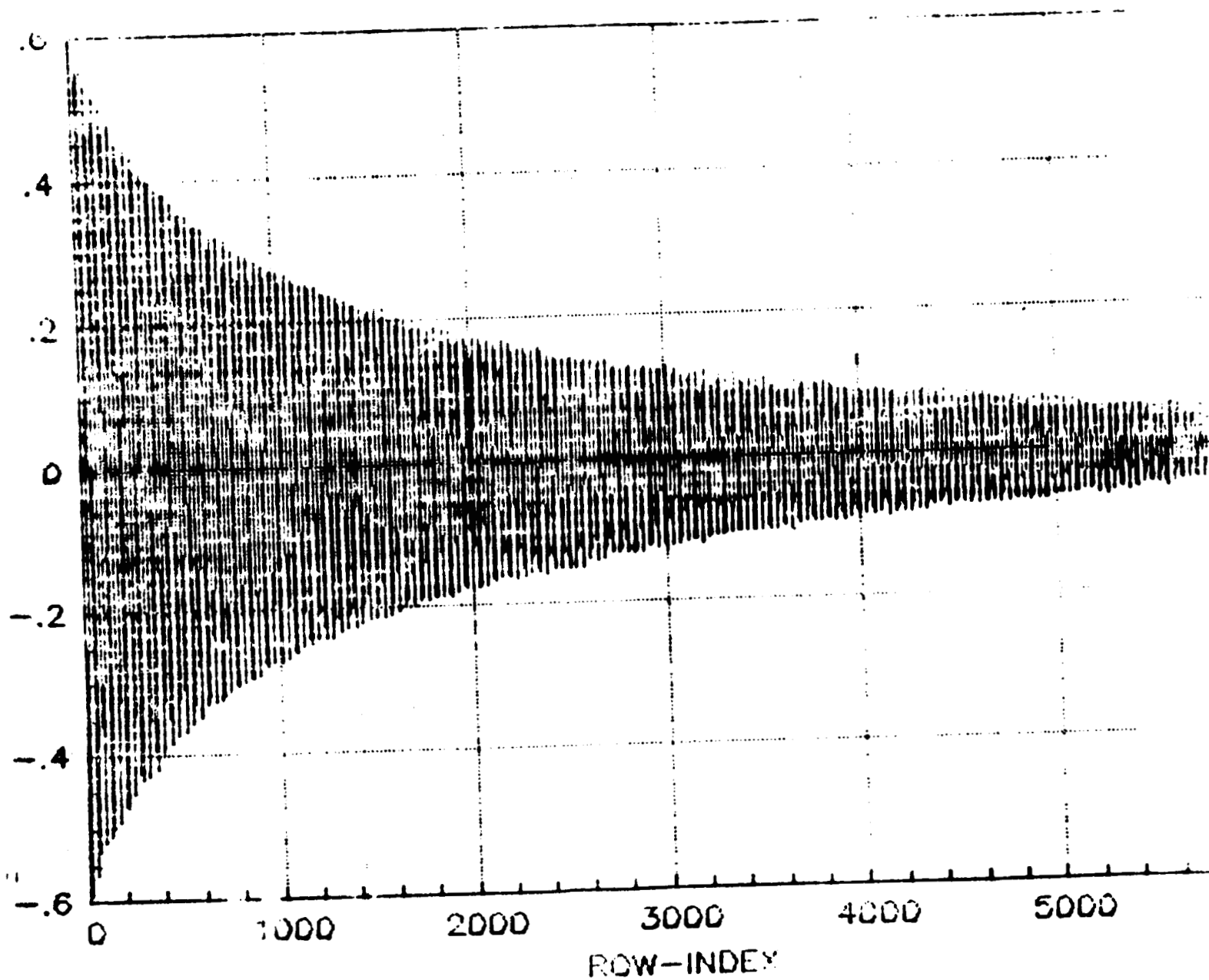
In One Dimension

Without hysteresis

$$\ddot{x}(t) \; + \; \omega^2 x(t) \; + \; 2\omega\zeta\dot{x}(t)$$

$$+ \; \gamma x(t)^{2m} \, |x(t)|^{\alpha} \, \dot{x}(t)^{2n+1} \, |\dot{x}(t)|^{\beta}$$

$$+ \; Bu(t) \; + \; FN(t)$$

$$= \; 0$$

$$0 \leq \alpha, \beta \leq 1 \; .$$

NONLINEAR DAMPING
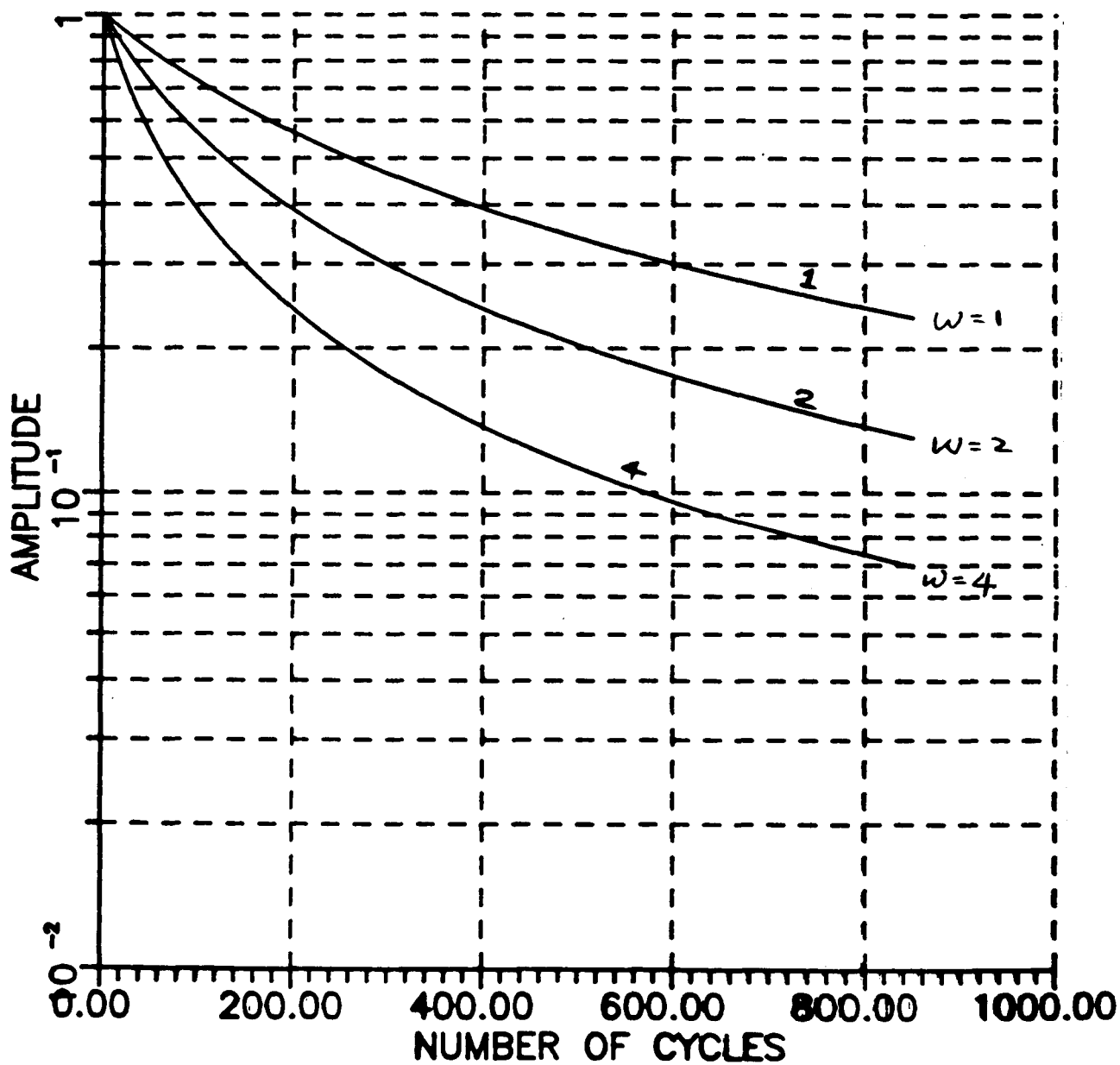
Plot of AMPLITUDE vs NUMBER OF CYCLES showing three curves labeled $\omega = 1$, $\omega = 2$, $\omega = 4$. Y-axis AMPLITUDE ranges from 10^{-2} to 1. X-axis NUMBER OF CYCLES from 0.00 to 1000.00. Label d_{n+1} at upper right.

656

NONLINEAR DAMPING: $\zeta = 0$

657

Beam Model

$$\ddot{u}(s,\ t)\ +\ \lambda u''''(s,\ t)\ -\ 2\zeta\sqrt{\lambda}\ \dot{u}''(s,\ t)$$

$$-\ \gamma\left(\int_0^L u'(s,t)\dot{u}'(s,t)\ ds\right)^{2(n+\beta)+1} u''(s,\ t)$$

$$=\ 0\ ,$$

$$0 < s < L;\ \ 0 < t$$

n: zero or positive integer

$$0 \leq \beta < \frac{1}{2}$$

ζ: Linear Damping Ratio

Prime represents space derivative

Dot represents time derivative

$$A \sim \frac{d^4}{ds^4} : \text{ clamped beam}$$

$$A\phi_k = \omega_k^2 \phi_k$$

$$\sqrt{A}\, \phi_k = \omega_k \phi_k$$

$$\sqrt{A} \sim (-1)\frac{d^2}{ds^2}$$

$$\int_0^L u'(s, t)\, \dot{u}'(s, t)\, ds$$

$$= \left. {}^L_0 [u(s, t)\, \dot{u}'(s, t)] \right.$$

$$- \int_0^L u(s, t)\, \dot{u}''(s, t)\, ds$$

$$x(t) = u(\cdot, t)$$

$$\rightarrow \quad \approx [x(t), \sqrt{A}\,\dot{x}(t)]$$

$$F(x, D\dot{x}) = \gamma([x, \sqrt{A}\,\dot{x}])^{2(n+\beta)+1} \sqrt{A}\,x$$

$$\ddot{x}(t) + \lambda A x(t) + D\dot{x}(t)$$

$$+ F(x(t), D\dot{x}(t)) + Bu(t)$$

$$= 0$$

$$D = 2\zeta\sqrt{\lambda}\,\sqrt{A}$$

$$x(t) = u(\cdot, t)$$

$$M\ddot{x}(t) + \lambda Ax(t) + D\dot{x}(t)$$
$$+ F(x(t), D\dot{x}(t)) + Bu(t) = 0$$

Energy

$$E(t) = \frac{1}{2}\{[\dot{x}(t), \dot{x}(t)] + \lambda[Ax(t), x(t)]\}$$

$$\frac{d}{dt}E(t) = [\ddot{x} + \lambda Ax, \dot{x}]$$

$$= -[D\dot{x}(t), \dot{x}(t)] - [F(x(t), D\dot{x}(t)), \dot{x}(t)]$$

$$[F(x, D\dot{x}), \dot{x}(t)] = ([x, \sqrt{A}\,\dot{x}])^{2(n+\beta)+2}$$

$$\geq 0$$

$$\Rightarrow \frac{dE(t)}{dt} \leq 0$$

661

$$x = a_k(t)\phi_k$$

$$F(x, D\dot{x})$$

$$= \gamma(a_k(t) \quad \omega_k \dot{a}_k(t))^{2(n+\beta)+1} \omega_k a_k(t)\phi_k$$

$$= \gamma a_k(t)^{2(n+\beta)+2} \omega_k^{2(n+\beta)+2} \dot{a}_k(t)^{2(n+\beta)+1} \phi_k$$

$$\alpha = \beta; \quad m = n$$

$$x(t) \; = \; a_k(t)\phi_k$$

$$\ddot{a}_k(t) \; + \; \lambda\omega_k^2 a_k(t) \; + \; 2\zeta\sqrt{\lambda}\,\omega_k\dot{a}_k(t)$$

$$+ \; \gamma(a_k(t)\dot{a}_k(t)\omega_k)^{2(n+\beta+1)}\,\omega_k a_k(t)$$

$$= \; 0$$

$$\gamma a_k(t)^{2m}\,|a_k(t)|^{\alpha}\,|\dot{a}_k(t)|^{\beta}\,\dot{a}_k(t)^{2n+1}$$

$$\sim \; m \; = \; n\,;$$

$$\alpha \; = \; \beta$$

Alternate Form

$$u(s, t) + \lambda u''''(s, t) - 2\zeta\sqrt{\lambda}\, \dot{u}''(s, t)$$

$$+ \gamma\left[\int_0^L u(s,t)\dot{u}''(s,t)\, ds\right]^{2(n+\beta)+1} u''(s, t)$$

$$= 0,$$

$$0 < s < L;\ \ 0 < t$$

n: zero or positive integer

$$0 \le \beta < \frac{1}{2}$$

ζ: Linear Damping Ratio

Prime represents space derivative

Dot represents time derivative

USE OF THE QUASILINEARIZATION ALGORITHM
FOR THE SIMULATION OF LSS SLEWING

By

Feiyue Li and P. M. Bainum
Howard University
Washington, DC 20059

ABSTRACT

The use of the Maximum Principle for the large angle slewing of LSS usually results in the so-called two-point boundary-value problem, in which many requirements (e.g., minimum time, small amplitude, and limited control power, etc.) must be satisfied simultaneously. The successful solution of this problem depends largely on the use of an efficient numerical algorithm. There are many candidate algorithms available for this problem (e.g., quasilinearization, gradient, etc.). Here we discuss only the quasilinearization method which has been used for several cases of large angle slewing of LSS. The basic idea of this algorithm is to make a series of successive approximations of the solution from a particular solvable case (linear or nonlinear) to a more general practical case.

For the rigid spacecraft slewing problem with no constraints on the controls, the solution procedure can be found in the literature. This procedure needs to be modified if a minimum time for the slewing problem is desired with control limits given. Recently, an indirect method for finding the minimum time was developed to meet all these requirements.

For the general mixed (including both rigid and flexible parts) problem, an additional constraint of small vibrational amplitude on the flexible parts is imposed. To solve this problem several steps in which the complexity increases gradually are needed, i.e., from a linearized version to a final nonlinear problem, from a less constrained case for the control to a more constrained one, from a nonminimum-time level to a near-minimum-time slewing in which a trade-off needs to be made between minimum time and small flexural amplitude requirements. Some examples of these algorithms are presented for planar slewing maneuvers of the SCOLE configuration.

USE OF THE QUASILINEARIZATION ALGORITHM
FOR THE SIMULATION OF LSS SLEWING

P. M. BAINUM

PROFESSOR OF AEROSPACE ENGINEERING

FEIYUE LI

GRADUATE RESEARCH ASSISTANT

DEPARTMENT OF MECHANICAL ENGINEERING

HOWARD UNIVERSITY, WASHINGTON, D.C. 20059

WORKSHOP ON COMPUTATIONAL ASPECTS

IN THE CONTROL OF FLEXIBLE SYSTEMS

JULY 12-14, 1988

WILLIAMSBURG, VIRGINIA

667

Use of the Quasilinearization Algorithm

for the Simulation of LSS Slewing

Feiyue Li
Graduate Research Assistant, (202)636-7124
and
P. M. Bainum
Professor of Aerospace Engineering, (202)636-6612
Department of Mechanical Engineering
Howard University, Washington, D.C. 20059

Abstract

The use of the Maximum Principle for the large angle slewing of LSS usually results in the so-called two-point boundary-value problem, in which many requirements (e.g., minimum time, small amplitude, and limited control power, etc) must be satisfied simultaneously. The successful solution of this problem depends largely on the use of an efficient numerical algorithm. There are many candidate algorithms available for this problem (e.g., quasilinearization, gradient, etc.). Here we discuss only the quasilinearization method which has been used for several cases of large angle slewing of LSS. The basic idea of this algorithm is to make a series of successive approximations of the solution from a particular solvable case (linear or nonlinear) to a more general practical case.

For the rigid spacecraft slewing problem with no constraints on the controls, the solution procedure can be found in the literature. This procedure needs to be modified if a minimum time for the slewing problem is desired with control limits given. Recently, an indirect method for finding the minimum time is developed to meet all these requirements.

For the general mixed (including both rigid and flexible parts) problem, an additional constraint of small vibrational amplitude on the flexible parts is imposed. To solve this problem several steps in which the complexity increases gradually are needed, i.e., from a linearized version to a final nonlinear problem, from a less constrained case for the control to a more constrained one, from a non-minimum-time level to a near-minimum-time slewing in which a trade-off needs to be made between minimum time and small flexural amplitude requirements. Some examples of these algorithms are presented for planar slewing maneuvers of the SCOLE configuration.

INTRODUCTION

MAXIMUM PRINCIPLE IS APPLIED TO
THE ATTITUDE MANEUVER AND VIBRATION CONTROL
OF LARGE SPACE STRUCTURES

    (A) PERFORMANCE INDICES

    (B) BOUNDARY CONDITIONS

    (C) CONTROL REQUIREMENTS

THIS LEADS TO THE TWO-POINT BOUNDARY-VALUE PROBLEM
(TPBVP)

ONE OF THE METHODS OF SOLVING TPBVP IS THE
QUASILINEARIZATION ALGORITHM

MAXIMUM PRINCIPLE

STATE EQUATIONS

$$\dot{x} = f(x) + B(x)u, \quad x(0)=x_0, \quad x(t_f)=x_f \tag{1}$$

PERPORMANCE INDICES

$$J_1 = (1/2) \int_0^{t_f} (x^T Q x + u^T R u)\,dt \tag{2}$$

$$J_2 = \int_0^{t_f} (1)\,dt = t_f \qquad |u_i| \le u_{ib}, \quad i=1 \ldots n \tag{3}$$

NECESSARY CONDITIONS

$$H_1 = (1/2)(x^T Q x + u^T R u) + \lambda^T(f(x) + Bu) \tag{4}$$

$$\dot{\lambda} = -(\partial H_1/\partial x), \qquad \lambda(0) \text{ unknown} \tag{5}$$

$$(\partial H_1/\partial u)=0, \qquad Ru = -B^T\lambda \tag{6}$$

$$H_2 = 1 + \lambda^T(f(x) + Bu) \tag{7}$$

$$\dot{\lambda} = -(\partial H_2/\partial x), \qquad \lambda(0) \text{ unknown} \tag{8}$$

$$u_i = -u_{ib}\,\text{sign}(B^T\lambda), \quad i=1 \ldots n \tag{9}$$

TPBVP

$$\dot{z} = g(z), \qquad z=[\,x\,,\,\lambda\,]^T = [\,z_1, z_2\,]^T \tag{10}$$

$z_1(0), z_1(t_f)$ known;

$z_2(0), z_2(t_f)$ unknown.

$z_2(0)$ to be determined.

670

QUASILINEARIZATION ALGORITHM

(A) LINEAR DIFFERENTIAL EQUATION:

Nonhomogeneous: $\dot{z} = Az + B$, $\quad z=[z_1, z_2]^T$. $\qquad$ (11)

$\qquad z_1(0)$, $z_1(t_f)$ known, $z_2(0)$ to be determined

Homogeneous: $\quad \dot{z} = Az$ $\qquad$ (12)

(a) n solns. of (12) + 1 particular soln. of (11)

(b) n +1 particular solns. of (11)

(B) NONLINEAR CASE:

Linearized equation of (10):

$$\dot{z}^{(k+1)} = (\partial g/\partial z)\, z^{(k+1)} + h(\,z^{(k)}\,) \qquad (13)$$

where

$\qquad z^{(k)}$ is the kth approximate solution

$\qquad$ of the nonlinear equation (10),

$\qquad z^{(k+1)} = z^{(k)} + \Delta z^{(k)}$

$\qquad z=[z_1, z_2]^T$,

$\qquad z_1^{(k+1)}(0)$, $z_1^{(k+1)}(t_f)$, known

$\qquad z_2^{(k+1)}(0)$ to be determined

SPACECRAFT CONTROL LAB EXPERIMENT
(SCOLE)
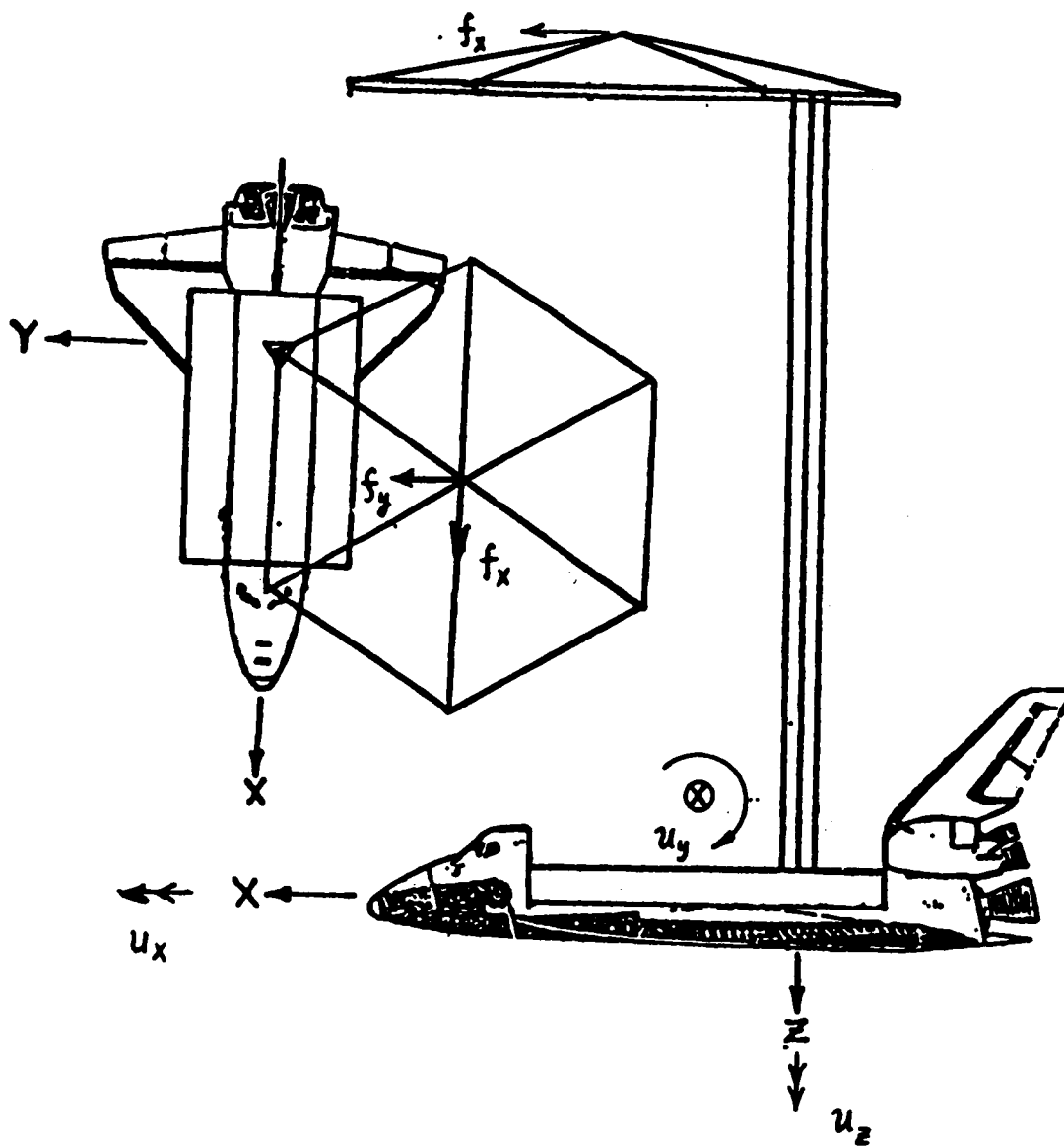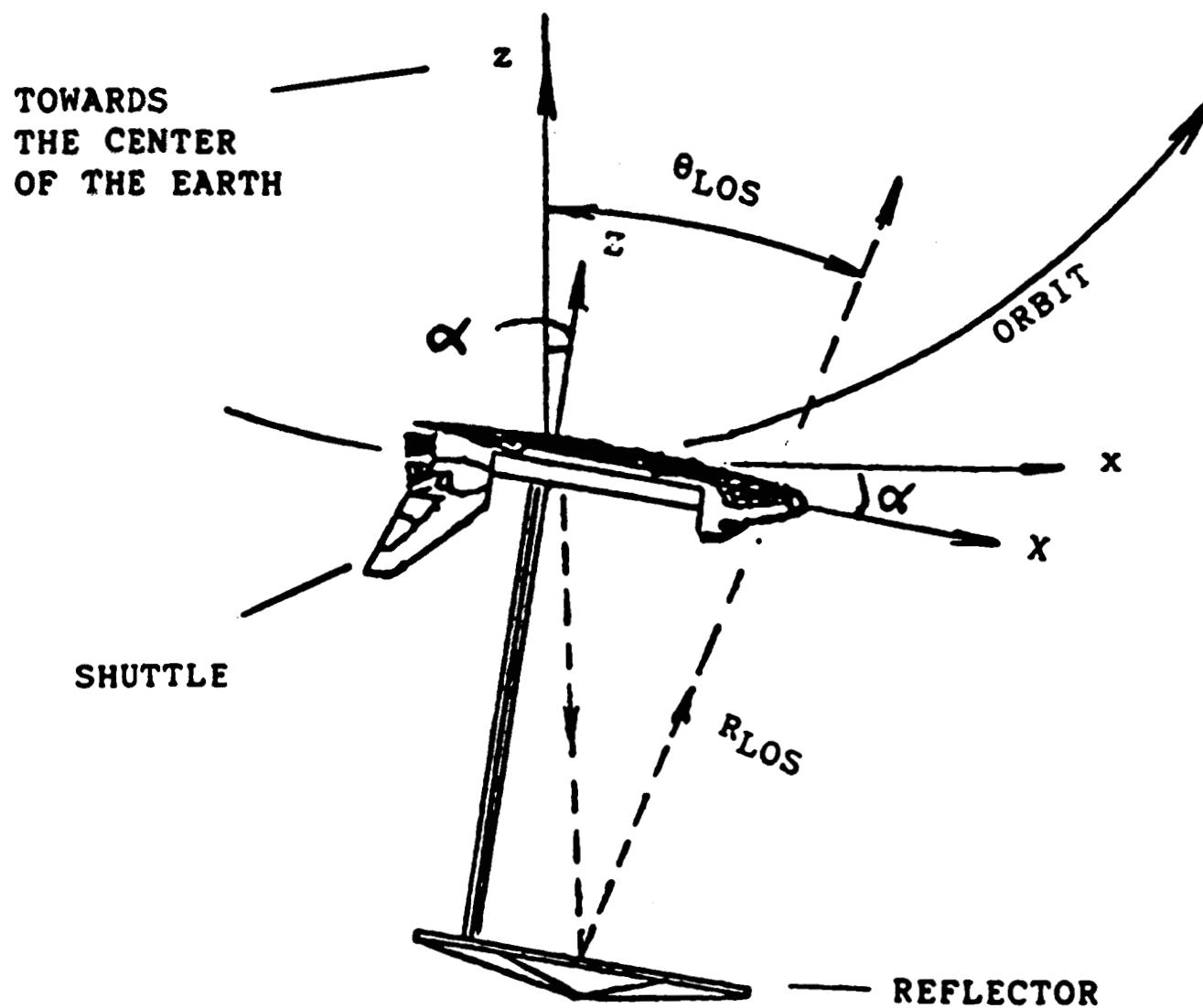
Fig. 1b. Attitude of the SCOLE Showing Antenna Line of Sight

673

TORQUES x 10,000 FT-LB

u_y

u_x

u_z

1.0

0.0

-1.0

0   3   6   9(S)

FORCES x 800 LB

1.0

f_y

f_x

0.0

-1.0

0   3   6   9 (S)

ANGLES (DEG.)

35

θ_{LOS}

θ_x

20

10

0

θ_z θ_y 0

-15

0   3   6   9(S)
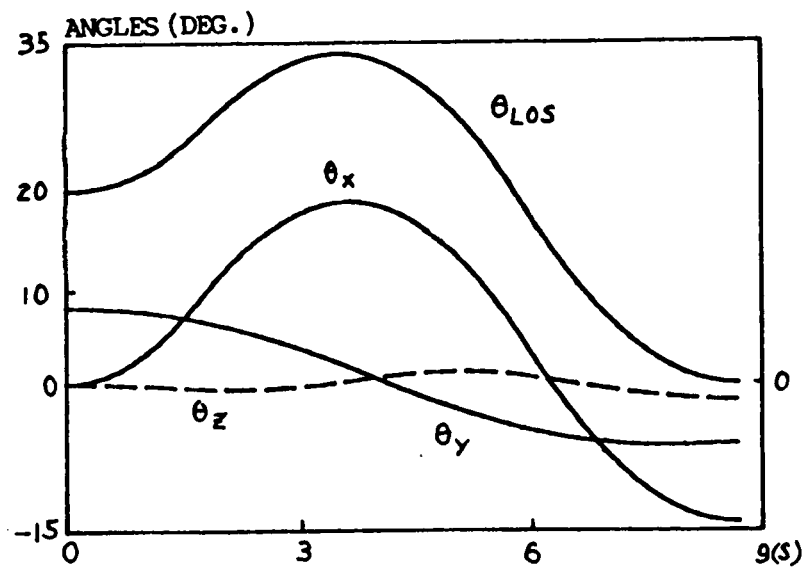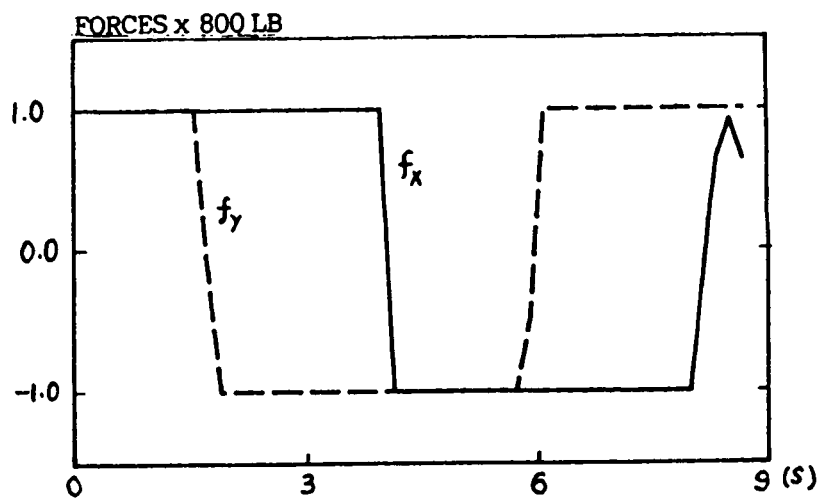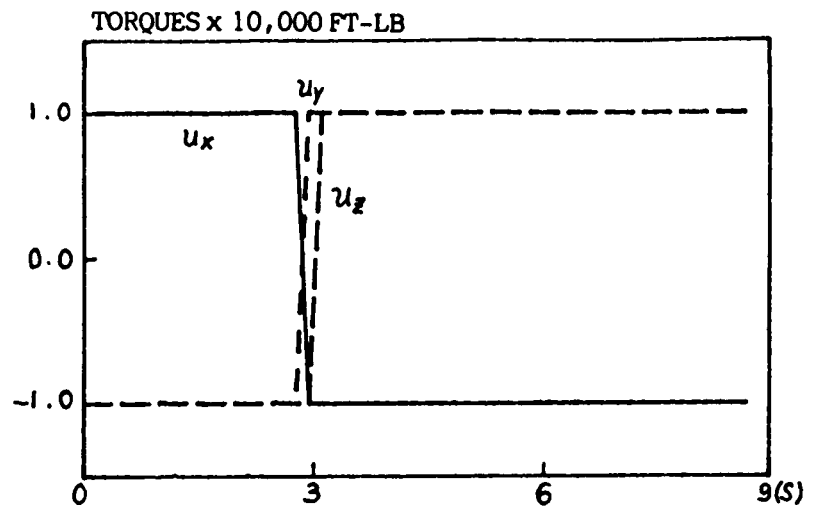
SCOLE (rigid) – Example Slewing,
$t_f = 8.69434$ (s)

674

PLANAR SLEWING OF FLEXIBLE SCOLE

LINEARIZED EQUATION OF MOTION:

$$\begin{bmatrix} 1 & \mathbf{m}^T \\ \\ \mathbf{m} & \mathbf{M} \end{bmatrix} \begin{bmatrix} \ddot{\theta} \\ \\ \ddot{\eta} \end{bmatrix} + \begin{bmatrix} 0 & \underline{0}^T \\ \\ \underline{0} & \mathbf{K} \end{bmatrix} \begin{bmatrix} \theta \\ \\ \eta \end{bmatrix} = \begin{bmatrix} 1 & z_1 & z_2 & L \\ \\ \underline{0} & \phi_1 & \phi_2 & \phi_L \end{bmatrix} \begin{bmatrix} u_s \\ u_1 \\ u_2 \\ u_3 \end{bmatrix}$$

where

θ is the angle of rotation,

$\eta_{n \times 1}$ is the amplitude vector of the flexible modes,

n is the number of mode used,

I is the moment of inertia about the axis of rotation

$\mathbf{m}$, $\mathbf{M}$ are the inertia parameter vector, matrix.

$\mathbf{K}$ is the stiffness matrix,

$\phi(z)$ is the mode shape function vector,

$\phi_i = \phi(z_i)$, z_i is the coordinate along z axis,

L is the length of the beam,

u_s is the control torque on the Shuttle,

u_i are the control actuators on the beam and the reflector.

675

STATE EQUATIONS

$$\dot{s} = As + Bu$$

$$s = \begin{bmatrix} s_1 \\ s_2 \end{bmatrix}, \quad s1 = \begin{bmatrix} \theta \\ \eta \end{bmatrix}, \quad s2 = \begin{bmatrix} \dot{\theta} \\ \dot{\eta} \end{bmatrix}$$

BOUNDARY CONDITIONS FOR s

$$s(0) = \begin{bmatrix} \theta_f \\ 0 \\ -- \\ 0 \\ 0 \end{bmatrix}, \quad s(t_f) = \begin{bmatrix} 0 \\ 0 \\ -- \\ 0 \\ 0 \end{bmatrix} \; 2(n+1) \times 1$$

where n is the number of mode shapes used.

PERFORMANCE INDEX

$$J = (1/2) \int_0^{t_f} (x^T Q x + u^T R u)\, dt \; , \quad x = s$$

TPBVP

$$\dot{z} = Cz, \quad z = [\, s, \lambda \,]^T = [\, z_1, z_2 \,]^T$$

λ is the costate vector,
$z_1(0)$, $z_1(t_f)$ known;
$z_2(0)$ to be determined.

676
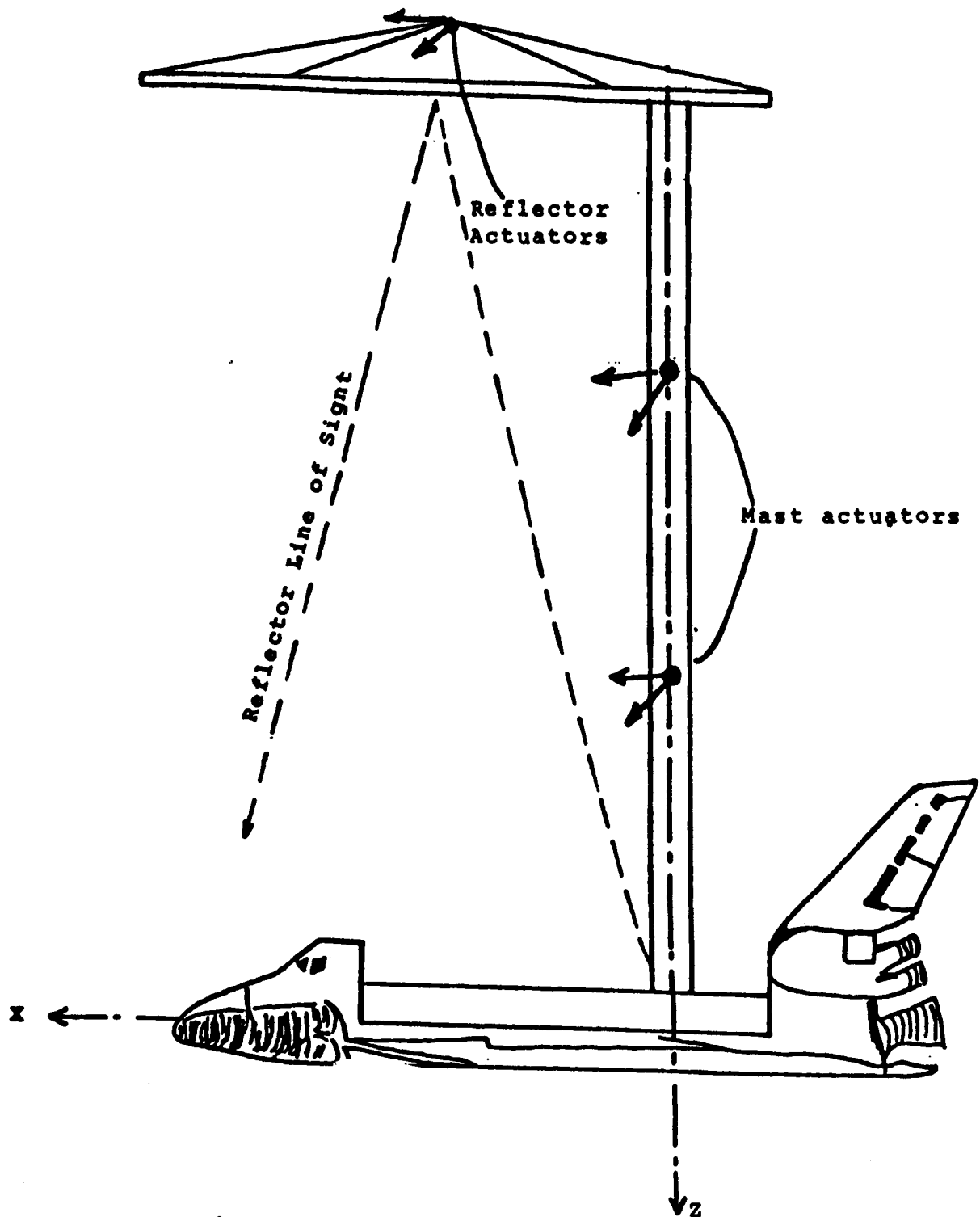
FIGURE I.1: DRAWING OF THE SCOLE CONFIGURATION

67.7

(A) SLEWING ABOUT X-AXIS (ROLL)

Only η_1 (first mode shape) is used.

$$\theta_f = 20 \ (deg) \ , \quad t_f = 40 \ (s)$$

$$J = \frac{1}{2}\int_0^{t_f} (s^T Q s + u^T R u) \, dt \ , \quad s = [\ \theta, \eta_1, \dot{\theta}, \dot{\eta}_1\ ]^T$$

$$R = \begin{bmatrix} 1 & & \\ & 1 & \\ & & 1 \end{bmatrix}$$

CASE 1: u_1 is used,

$$Q_1 = \begin{bmatrix} 0 & & \\ & 0 & \\ & & 0 \\ & & & 0 \end{bmatrix}$$

CASE 2: u_1 is used

$$Q_2 = \begin{bmatrix} 0 & & \\ & 0.001 & \\ & & 0 \\ & & & 0 \end{bmatrix}$$

CASE 3: u_1, u_2 are used

$$Q_3 = \begin{bmatrix} 0 & & \\ & 0.01 & \\ & & 0.01 \\ & & & 0.01 \end{bmatrix}$$

CASE 3: u_1, u_3 are used

$$Q_4 = \begin{bmatrix} 0 & & \\ & 0.01 & \\ & & 0.01 \\ & & & 0.01 \end{bmatrix}$$

CETA-(DEG)

u_1 is used

$$Q_1 = \begin{bmatrix} 0 & & \\ & 0 & \\ & & 0 & \\ & & & 0 \end{bmatrix}, \quad R_1 = \begin{bmatrix} 1 \end{bmatrix}$$

CASE: U1   CONTROLS USED

679
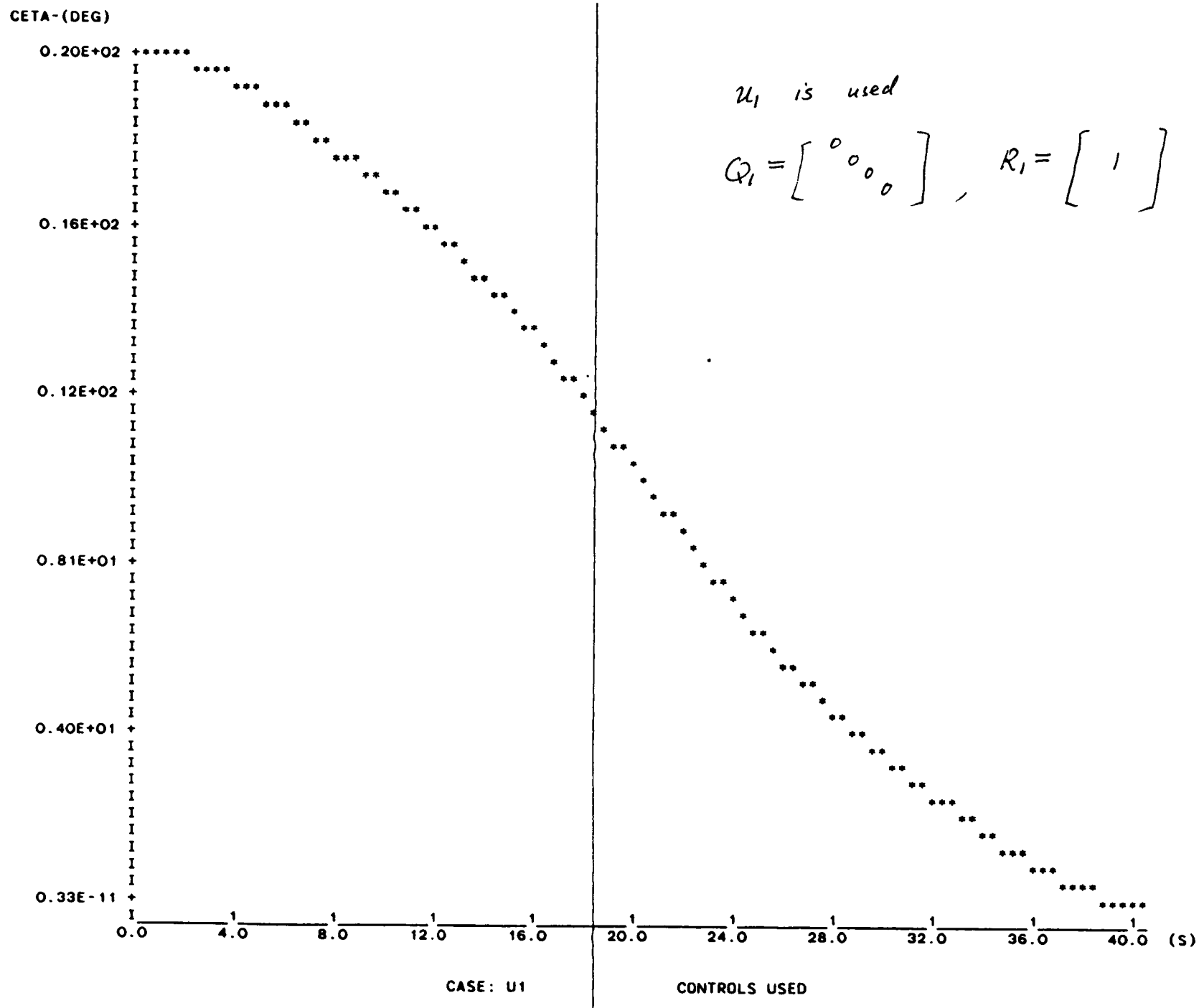
MODE 1-(FT)

0.14E+02 +

0.91E+01 +

0.36E+01 +

-0.24E+01 +

-0.80E+01 +

-0.14E+02 +

0.0   4.0   8.0   12.0   16.0   20.0   24.0   28.0   32.0   36.0   40.0 (S)

CASE: U1   CONTROLS USED

680

U1-X10000(FT-LB)

0.17E+00

0.10E+00

0.37E-01

-0.33E-01

-0.10E+00

-0.17E+00

0.0   4.0   8.0   12.0   16.0   20.0   24.0   28.0   32.0   36.0   40.0   (S)

189

CONTROLS USED

MODE 1-(FT)

0.10E+02 +

0.61E+01 +

0.20E+01 +

-0.20E+01 +

-0.62E+01 +

-0.10E+02 +

682

u_1 is used,

$$Q_2 = \begin{bmatrix} 0 & & \\ & 0.001 & \\ & & 0 \\ & & & 0 \end{bmatrix}, \qquad R = 1$$

0.0   4.0   8.0   12.0   16.0   20.0   24.0   28.0   32.0   36.0   40.0   (S)

U1-X10000(FT-LB)

683
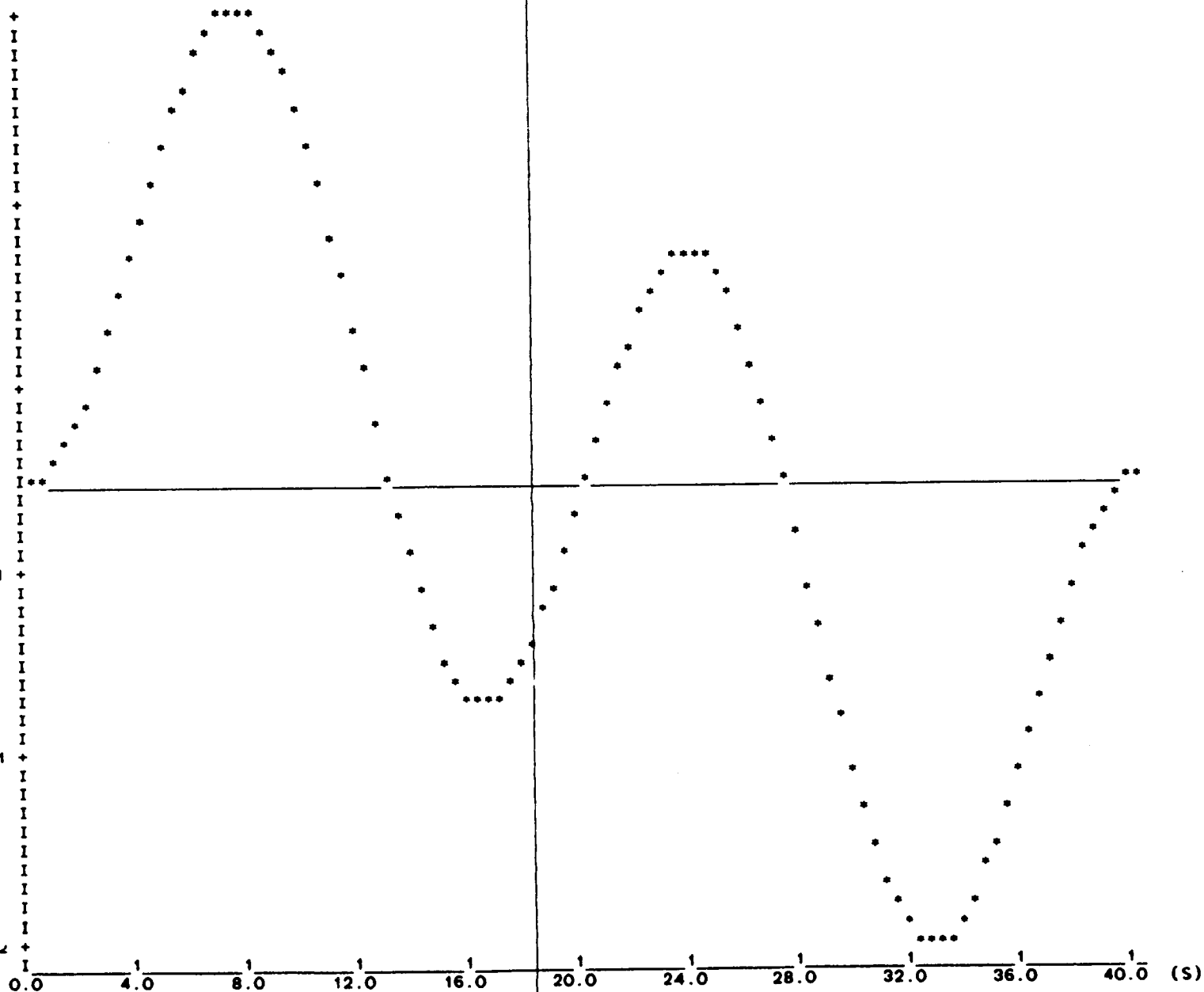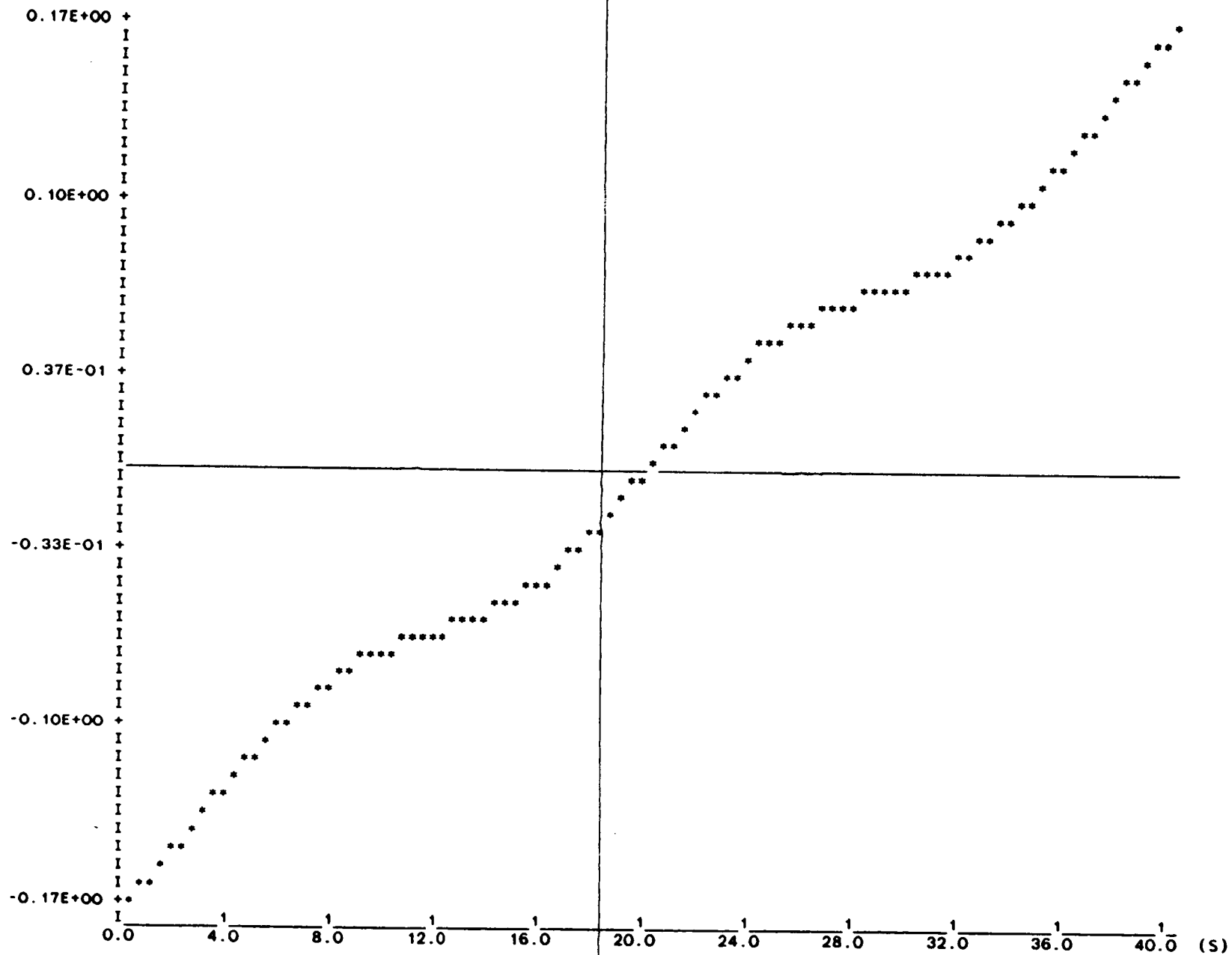
CASE: U=(1 0 0 0), Q=(0.000 0.001 0.000 0.000)

MODE1-(FT)
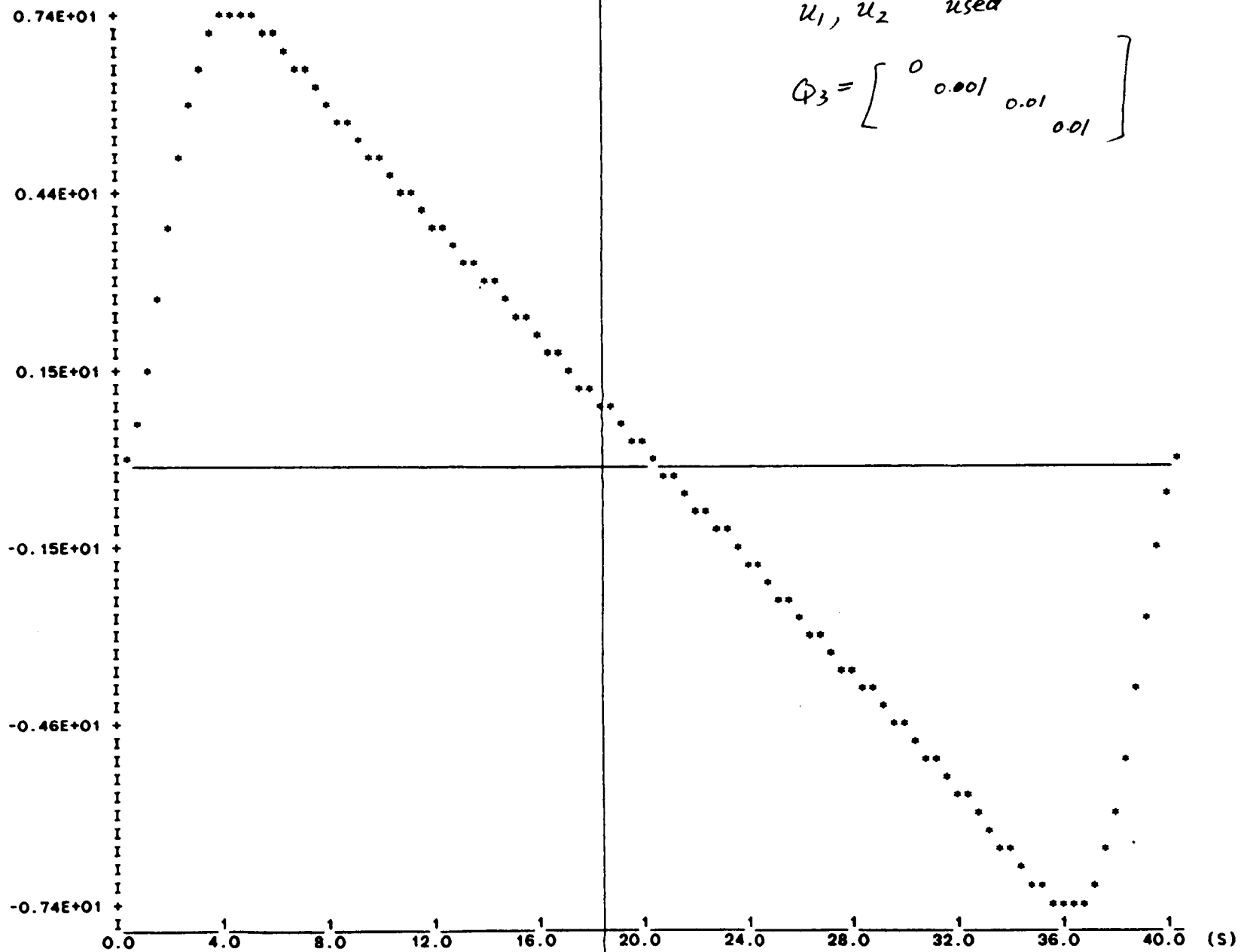
u_1, u_2 used

$$Q_3 = \begin{bmatrix} 0 & 0.001 & 0.01 & 0.01 \end{bmatrix}$$

684

CASE: U=(1 2 0 0), Q=(0.000 0.010 0.010 0.010)

U1-X10000(FT-LB)

685

CASE: U=(1 2 0 0), Q=(0.000 0.010 0.010 0.010)

CASE. U=(1 2 0 0),   Q=(0.000 0.010 0.010 0.010)

MODE1-(FT)

0.22E+01 +

0.13E+01 +

0.45E+00 +

-0.43E+00 +

-0.14E+01 +

-0.22E+01 +

0.0   4.0   8.0   12.0   16.0   20.0   24.0   28.0   32.0   36.0   40.0   (S)

u_1, u_3 used

$$Q_4 = \begin{bmatrix} 0 & & & \\ & 0.01 & & \\ & & 0.01 & \\ & & & 0.01 \end{bmatrix}$$

689

CASE: U=(1 0 3 0), Q=(0.000 0.010 0.010 0.010)

CASE: U=(1 0 3 0), Q=(0.000 0.010 0.010 0.010)

U3-X10(LB)

689
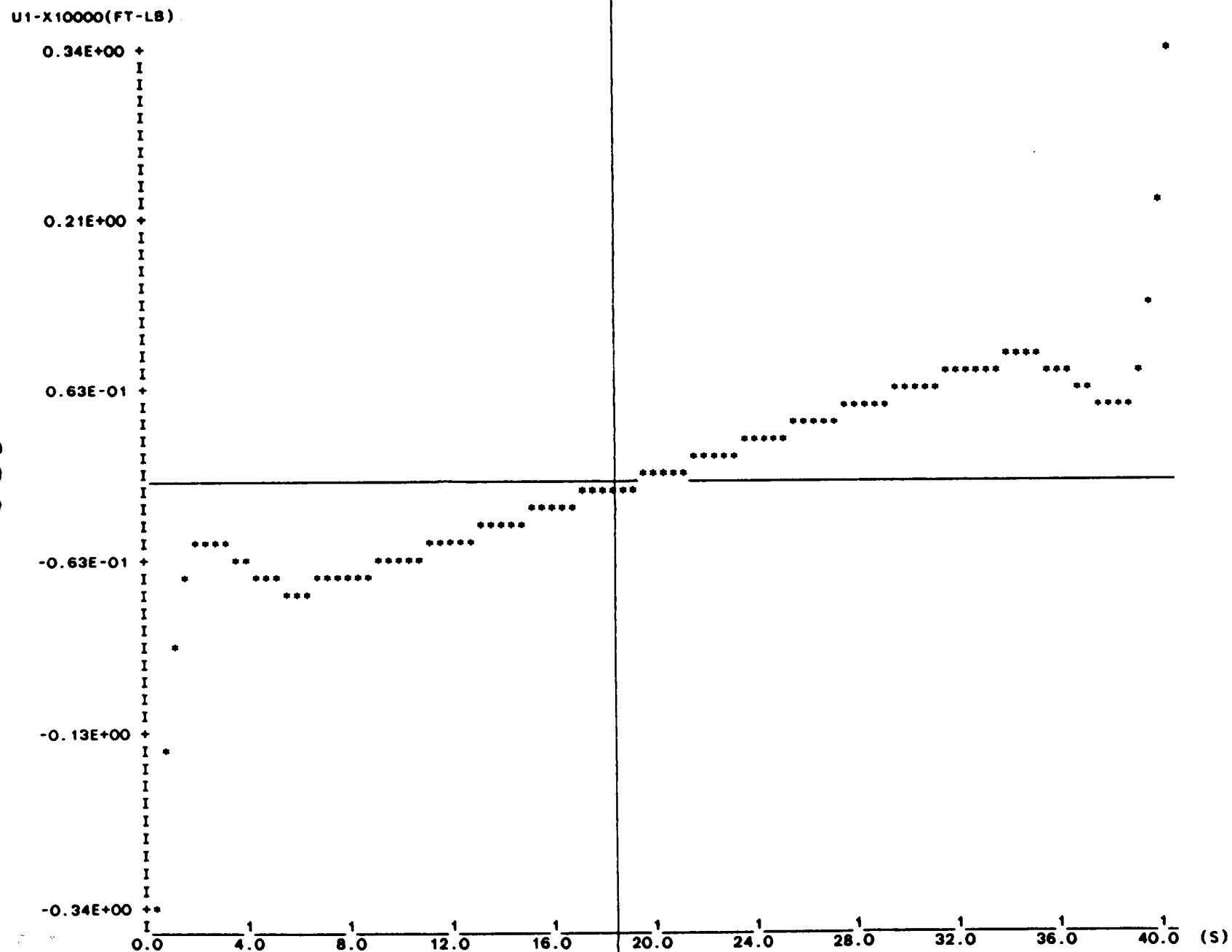
CASE: U=(1 0 3 0), Q=(0.000 0.010 0.010 0.010)

CONCLUDING REMARKS

1) Solution has been obtained for nonlinear rigid spacecraft attitude maneuver (including the rigidized SCOLE).

2) Use of the Maximum Principle can make the states satisfy the boundary conditions very well.

3) Due the fact that the costates must be used in the method, the dimension of equations of the system is doubled, and higher computational ability is needed in this method.

4) Further work on more complicated models (nonlinear differential equation) is needed.

5) Need to consider different cost functions and perform parametric studies.

690

SESSION V - CONTROL SYNTHESIS AND SIMULATION

CONTROL LAW SYNTHESIS AND OPTIMIZATION SOFTWARE FOR LARGE ORDER AEROSERVOELASTIC SYSTEMS

By

V. Mukhopadhyay, A. Pototzky, and T. Noll
NASA Langley Research Center
Hampton, Virginia

ABSTRACT

Motivation: A flexible aircraft or space structure with active control is typically modeled by a large-order state space system of equations in order to accurately represent the rigid and flexible body modes, unsteady aerodynamic forces, actuator dynamics and gust spectra. The control law of this multi-input/multi-output (MIMO) system is expected to satisfy multiple design requirements on the dynamic loads, responses, actuator deflection and rate limitations, as well as maintain certain stability margins, yet should be simple enough to be implemented on an onboard digital microprocessor. This paper describes a software package for performing an analog or digital control law synthesis for such a system, using optimal control theory and constrained optimization techniques.

Software Capabilities: The primary software capability is the optimization of the system by changing the control law design variables to improve stability and performance. A block diagram of the optimization scheme is shown in Fig. 1.

1) The optimization module minimizes a linear quadratic Gaussian (LQG) type cost function, while trying to satisfy a set of constraints on the conflicting design requirements such as design loads, responses and stability margins. Analytical expressions for the gradients of the cost function and the constraints, with respect to the control law design variables, are used for computation. This facilitates rapid convergence of the numerical optimization process. The designer can choose the structure of the control law and the design variables. This enables optimization of a classical control law as well as an estimator-based full or reduced order control law. Selected design responses are incorporated as inequality constraints instead of lumping them into the cost function. This feature is used to modify a control law to meet individual root-mean-square (RMS) response limitations and design requirements.

2) In order to improve the multiloop system stability robustness properties in the frequency domain, the minimum singular value of the return difference matrix at the plant input and output are as additional inequality constraints.

3) Other supporting capabilities include: (a) singular value analysis evaluation and plotting at the plant input and output; (b) linear quadratic optimal control law synthesis; (c) Kalman Filter design, LQG Loop transfer recovery; (d) pole-zero computation; (e) frequency response, Nyquist and Bode Plot; (f) root locus plot; (g) block diagonalization; (h) modal residualization and truncation; (i) transient response to deterministic and white noise input; (j) transfer of quadruple data to and from MATRIX-X and DIGIKON; (k) parameter search to stabilize an unstable control law, and (l) both interactive and batch mode execution using the Cyber NOS system.

Applications: The software has been used in the past for the following applications: (1) flutter suppression control law for the ARW-I wind tunnel wing model; (2) gust load alleviation control law for the ARW-II drone; (3) flutter suppression control law synthesis for ARW-II drone and the DC-10 Derivative wind tunnel wing model; (4) robust Digital gust load alleviation control law synthesis for ARW-II drone; and the (5) Active Flexible Wing (AFW) flutter suppression control law synthesis which is presently being carried out.
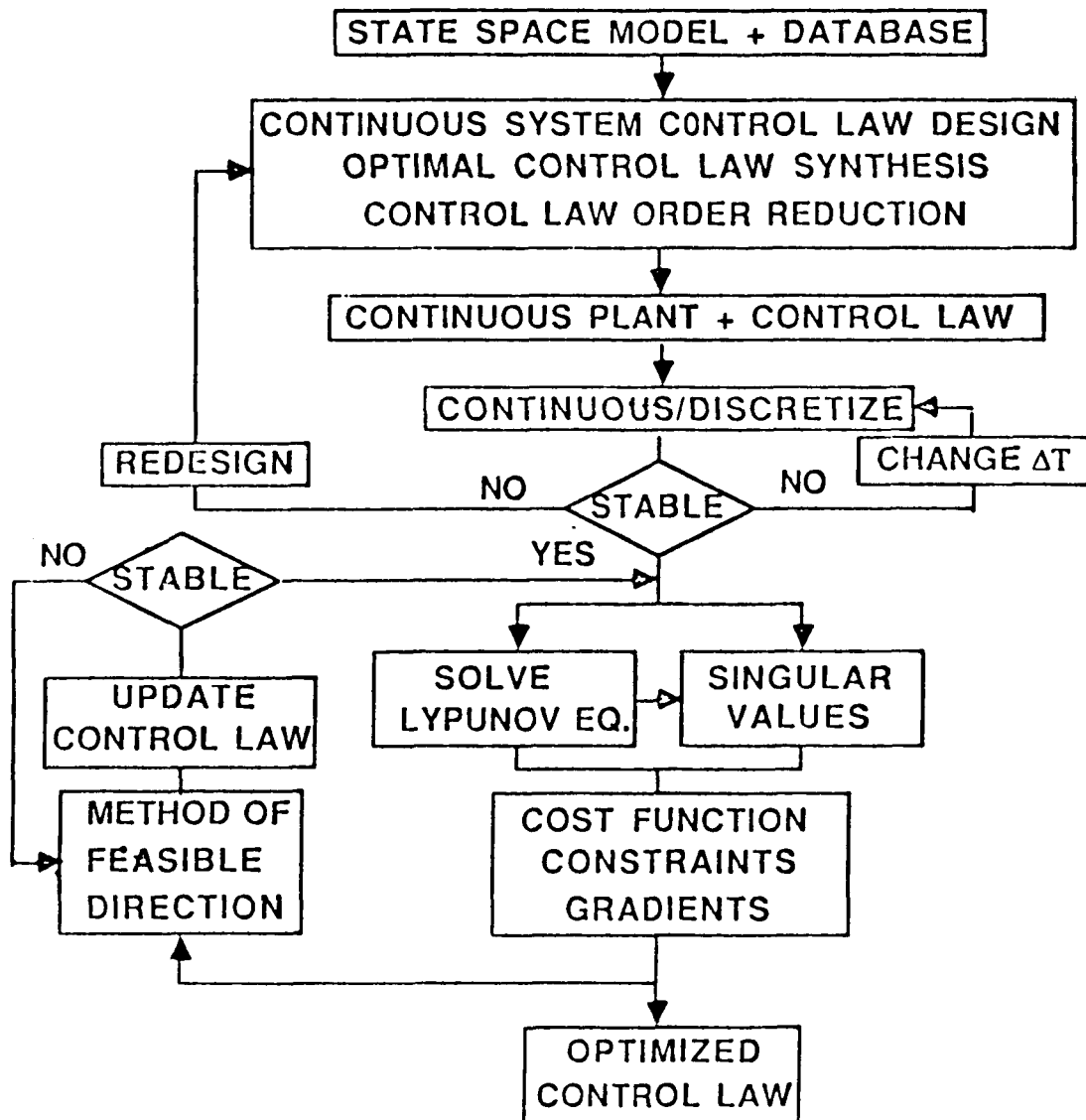
FIG. 1   Optimization scheme block diagram

695

CONTRO LAW SYNTHESIS AND OPTIMIZATION SOFTWARE
FOR LARGE ORDER
AEROSERVOELASTIC SYSTEMS

By

V. Mukhopadhyay, A. Pototzky and T. Noll
Aeroservoelasticity Branch
NASA Langley Research Center
Hampton, VA

696

Abstract

A flexible aircraft or space structure with active control is typically modeled by a large order state space system of equations in order to accurately represent the rigid body and flexible modes, unsteady aerodynamic forces, actuator dynamics and gust spectra. The control law of this multi-input multi-output (MIMO) system is expected to satisfy multiple design requirements on the dynamic loads, root mean square (RMS) responses, actuator deflection and rate limitations as well as maintain certain guaranteed stability margins, yet should be simple enough to be implementable on an onboard digital microprocessor. This paper describes an interactive software named DESIGN for analysis and synthesis of analog and digital control laws for such a system, using optimal control theory and constrained optimization techniques.

large flex. sys

d/a → **dyn model** → a/d

?

dig.comp

697
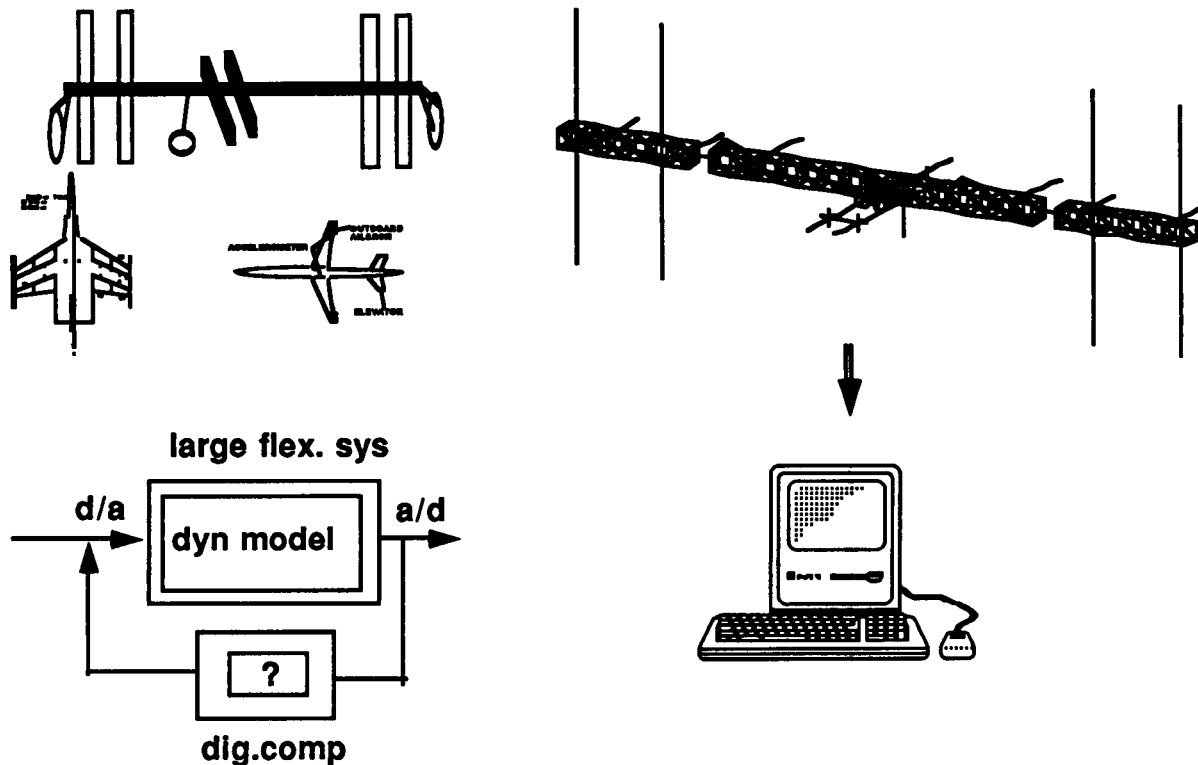
Overview

A multi-input multi-output aeroservoelastic system is typically represented by a large order state-space system of equations in order to accurately represent the rigid body and flexible modes, unsteady aerodynamic forces, actuator dynamics, gust spectra, antialiasing filters, computational delays etc. The active control law is expected to satisfy a set of conflicting design requirements on the performance and stability margins, yet should be simple enough to be implementable on an onboard digital microprocessors. This objective can be achieved using the synthesis software described in this paper. The methodology used are optimal control theory, order reduction techniques, unconstrained and constrained optimization with constraints on the design RMS responses and the minimum singular value of the return difference matrix at the plant input and output. Optimization can be performed for both continuous system and discrete systems. The methodology has been used to synthesize a) Analog and digital gust load alleviation control laws for a remotely controlled drone b) Analog and digital flutter suppression control laws for Active Flexible Wing (AFW) wind tunnel model . Other potential future applications include a) Rapid maneuver load control for AFW d) Vibration suppression for large space structure and control structure interaction study.

OVERVIEW

CONTROL LAW SYNTHESIS AND OPTIMIZATION
SOFTWARE FOR FLEXIBLE STRUCTURE

DESIGN OBJECTIVES
LOW ORDER ROBUST CONTROL LAW FOR A
HIGH ORDER AEROSERVOELASTIC SYSTEM

METHODOLOGY
OPTIMAL CONTROL THEORY
CONTROL LAW ORDER REDUCTION
NUMERICAL OPTIMIZATION

COST FUNCTION	LQG TYPE
CONSTRAINTS	RMS RESPONSES
	SINGULAR VALUES

SYSTEMS
CONTINUOUS   DISCRETE

APPLICATIONS
GUST LOAD ALLEVIATION OF A DRONE
FLUTTER SUPPRESSION OF AFW MODEL
RAPID MANEUVER LOAD CONTROL

698

Optimization Block Diagram

The optimization procedure minimizes a linear quadratic Gaussian (LQG) type cost function, while trying to satisfy a set of constraints on the conflicting design requirements such as dynamic loads, design RMS responses and singular value based stability margins at the plant input and output. The analytical expressions for the gradients of the cost function and the constraints, with respect to the control law design variables are used for computation. This facilitates rapid convergence of the optimization process. The designer can choose the structure of the control law and the design variables. This enables optimization of classical control law as well as an estimator based full or reduced order control law. Selected design responses are incorporated as inequality constraints instead of lumping them into the cost function. This feature is used to modify a control law to meet individual RMS response limitations and design requirements.

DISCRETE SYSTEM

```
                 ┌──────────────────────────────────┐
                 │ STATE SPACE MODEL + DATABASE      │
                 └──────────────────────────────────┘
                                │
         ┌──────────────────────▼──────────────────────┐
         │ CONTINUOUS SYSTEM CONTROL LAW DESIGN         │
         │ OPTIMAL CONTROL LAW SYNTHESIS                │
         │ CONTROL LAW ORDER REDUCTION                  │
         └──────────────────────┬──────────────────────┘
                                │
                 ┌──────────────▼───────────────────┐
                 │ CONTINUOUS PLANT + CONTROL LAW    │
                 └──────────────┬────────────────────┘
                                │
                   ┌────────────▼──────────────┐
                   │ CONTINUOUS/DISCRETIZE      │◄─┐
                   └────────────────────────────┘  │
   ┌──────────┐                                 ┌──────────┐
   │ REDESIGN │        NO    ◇STABLE◇    NO     │ CHANGE ΔT│
   └──────────┘                │YES             └──────────┘
   NO  ◇STABLE◇───────────────┘
         │                              ┌─────────────┐  ┌─────────────┐
   ┌─────▼──────┐                       │ SOLVE       │─▶│ SINGULAR    │
   │ UPDATE     │                       │ LYPUNOV EQ. │  │ VALUES      │
   │ CONTROL LAW│                       └─────────────┘  └─────────────┘
   └─────┬──────┘                       ┌──────────────────┐
   ┌─────▼──────┐                       │ COST FUNCTION    │
   │ METHOD OF  │                       │ CONSTRAINTS      │
   │ FEASIBLE   │                       │ GRADIENTS        │
   │ DIRECTION  │                       └──────────────────┘
   └────────────┘                                │
                                                 ▼
                         OPTIMIZED
```

699
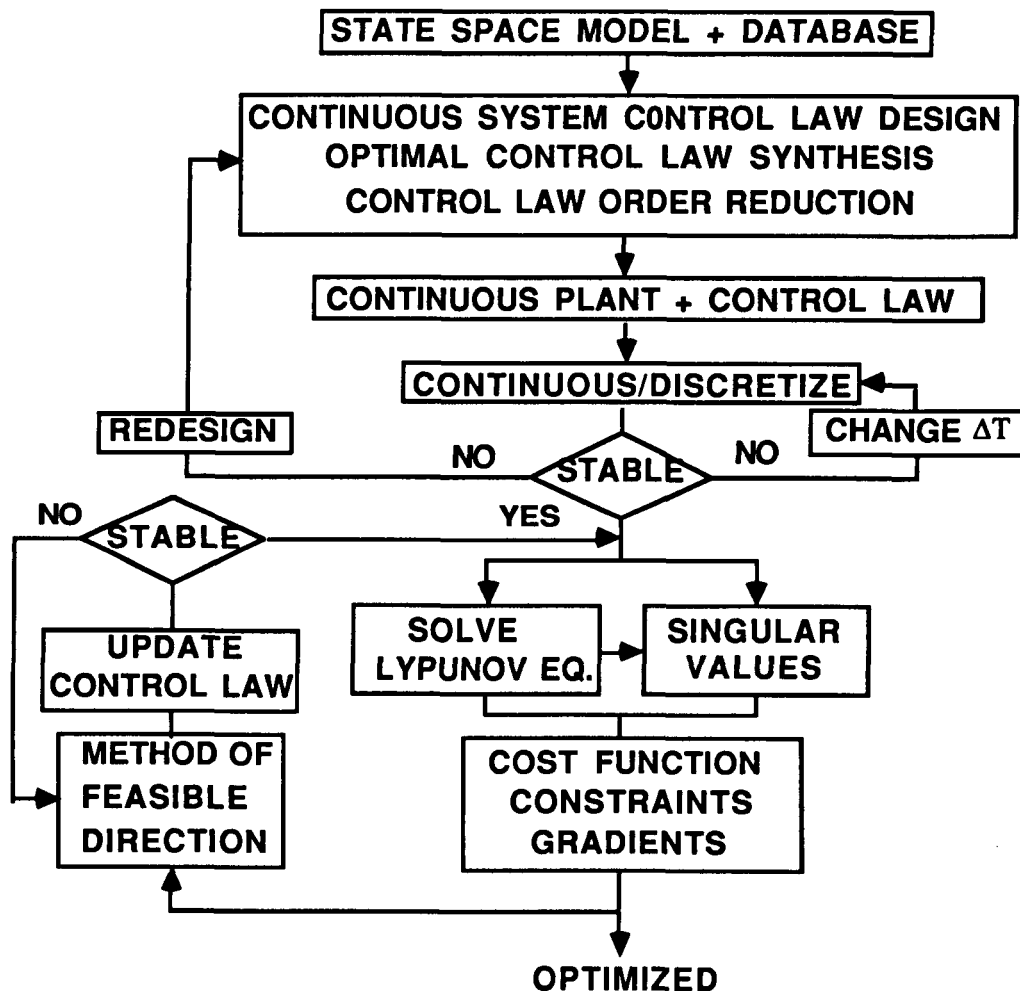
Software Organization

The interactive software DESIGN is organized to interact with several well used softwares such as 1) ISAC (Interaction of Structure, Aerodynamics and Control) for receiving state-space quadruple data, 2) DIGIKON for discretization, interconnection, model generation, digital design, verification and graphics and 3) MATRIX-X for matrix manipulation, interconnection, quadruple data transfer, graphics and design verification. DESIGN can also be run in batch mode on the CYBER/NOS system for large order problems involving systems with more than 120 states with large number of design variables and constraints. This batch version was previously known as PADLOCS (Program for Analysis and Design of Linear Optimal Control Systems).

```
                        ┌─────────────┐
                        │    ISAC     │──────────────┐
                        └─────────────┘              │
                               │                     ▼
┌──────────┐           ┌─────────────┐        ┌───────────┐
│          │◄──────────│   DESIGN    │───────►│  MATRIX   │
│ DIGIKON  │           │ INTERACTIVE │        │     X     │
│          │──────────►│             │◄───────│           │
│          │           │  PADLOCS    │        │           │
│          │           │   BATCH     │        │           │
└──────────┘           └─────────────┘        └───────────┘
```

700
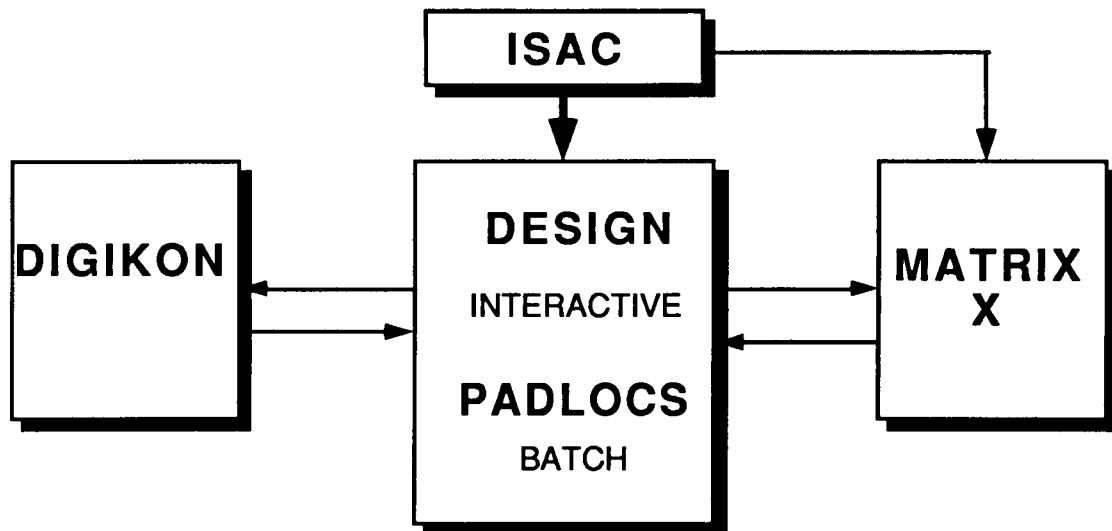
Basic Command Summary

The quadruple data is generated and stored in a sequencial binary file called QDATA. The design starts with the file command

GET, QDATA.
GET, DESIGN.
DESIGN.

The random access files DBASE, and sequencial file PLDATA are used to transport quadruple data to and from DIGIKON and MATRIX-X, while random access file TAPE7 is ued to transfer data from ISAC.using the UTILITY commands. The system parameter and quadruple data are read by the SYSTEM INPUT commands as shown in the figure above. The primary capability of this software is the optimization of the system by changing the control law design variables to improve the stability robustness and performance requirements. The supporting capabilities include a) Linear quadratic optimal control law synthesis; b) Kalman filter design, linear quadratic Gaussian design (LQG) and loop transfer recovery (LTR); c) Singular value analysis , evaluation and plotting at the plant input and output; d) Pole-zero computation; e) Open and closed loop frequency response, Nyquist and Bode plot, and loop breaking test; f) Root locus plot g) Block diagonal transformation; h) Modal residualization and truncation; i) Transient response to deterministic and white noise input; etc.

701
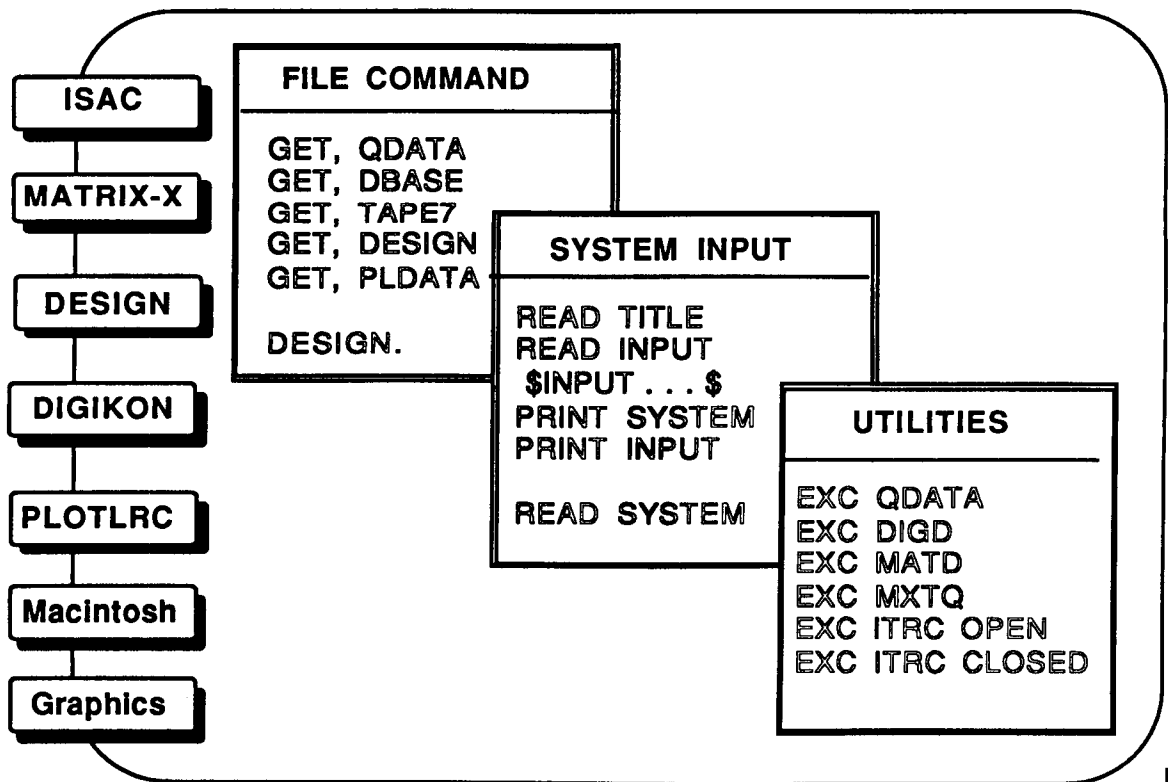
Basic Design Commands

The basic design commands are shown in the figure above. For systems with known stable control laws the optimization procedure can be executed directly using the command EXC OPTM for continuous systems and EXC OPTD for discrete systems. For MIMO systems with no known initial stabilizing control laws, first an Linear Quadratic Gaussian (LQG/LTR) design is performed to obtain a full order robust control law using a set of LQG design commands. The order of the control law is then reduced by truncation, residualization or balanced realization method using DESIGN, DIGIKON or MATRIX-X. The singular value analysis and block diagonal transformation procedure is very helpful in the reduction process. Since this reduced order control law is not optimal and may not satisfy the design requirements, constrained optimization procedure is used to update the reduced order control law. Constraints can be imposed on the design RMS responses and minimum singular values at the plant input and output.

BASIC DESIGN COMMANDS

LQ
LQG/LTR
REDUCE
SING. VAL
OPTIMIZE
CONSTRAIN RMS SV I/O
ANALYSE/REOPTIMIZE

LQG DESIGN
EXC OFSF
EXC KFGM
EXC WRES
EXC COVA
EXC RMSV
EXC OLFR
EXC ZERO

ORDER REDUCTION
EXC DIAG
EXC EIGN
EXC PERM
TRUNCATE
RESIDUALIZE
BALANCE(MX)
EXC ITRC CLO
EXC EIGN
EXC TIME

OPTIMIZATION
EXC OPTM
EXC ITRC CLOSED
EXC SING
EXC OPTD
EXC ITRC OPEN
EXC FREQ
EXC EIGN
EXC SING
EXC TIME
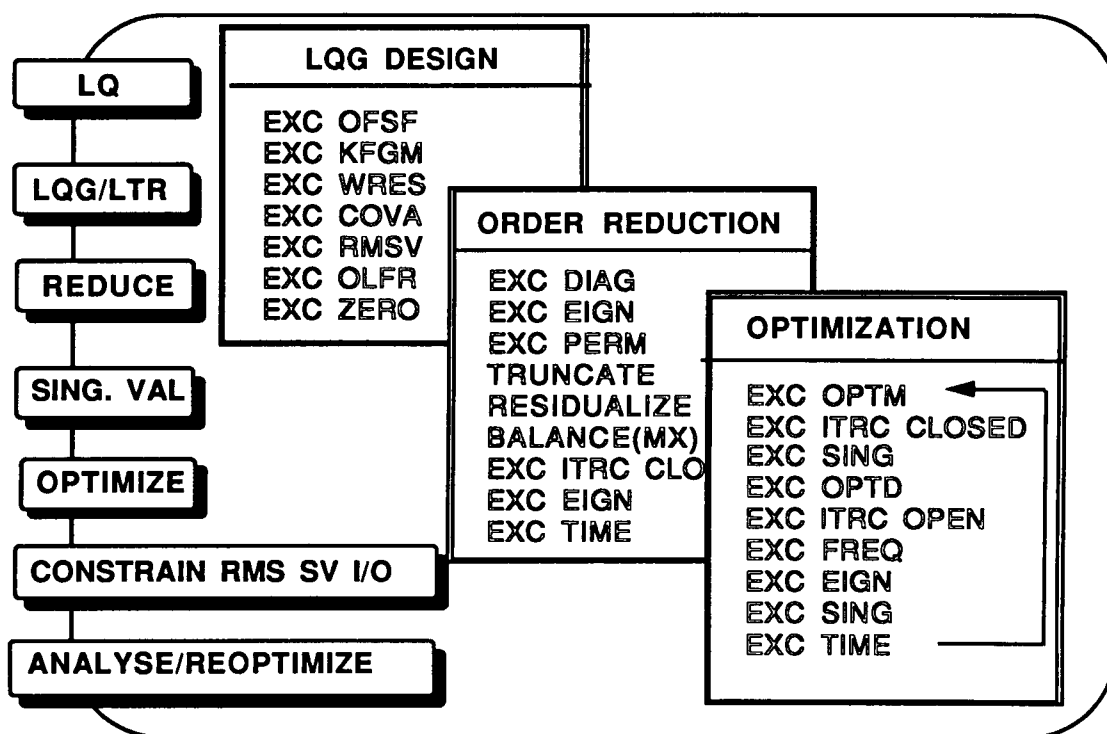
Gust Load Alleviation of A Flexible Drone

The synthesis procedure was applied to the gust load alleviation problem of a flexible drone. The basic control scheme is shown in the figure. In longitudinal motion, the symmetric elevator and outboard aileron deflections are used as the two control inputs. The accelerometer sensors at the outboard aileron and on the fuselage near the center of gravity are used as two measurement outputs. The output signals are filtered through first order antialiasing filters 50/(s+50) before digitization at 100 Hz. The two input two output system was modeled by a 32nd order system flying symmetrically through a Dryden gust.

GUST LOAD ALLEVIATION OF FLEXIBLE DRONE

The objective is to obtain a low order robust digital GLA control law which would reduce the open loop root-mean- square values of the wing root bending moment and shear by 50% without increasing the wing outboard bending moment and torsion The control law should maintain certain guaranteed stability margins based on minimum singular value of 0.6 at both the plant input and output. The control surface deflections and rates should be within the allowable limits. First a full order LQG control law is synthesized to satisfy the design requirements. This 32nd order control law is then reduced to a second order control law and then discretized. This control law does not satisfy the design requirements. After unconstrained optimization most of the requirements are satisfied except the wing outboard bending moment and the singular values. Using constraints on the RMS wing loads and on the minimum singular values of the return difference matrix at the plant input and output, the control law parameters are reoptimized (Ref.1,2).

GUST LOAD ALLEVIATION
DESIGN REQUIREMENTS

Accl. sensors — Aileron

Elevator

32nd order airplane eqns.
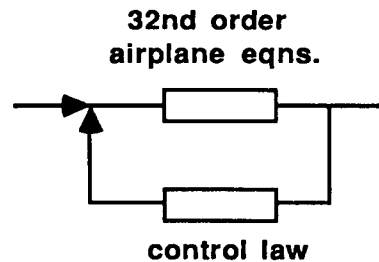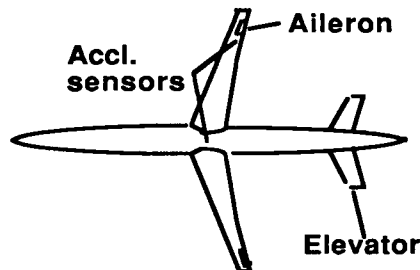
control law

Physical quantities	Design objectives	How we do it
Root bending moment	50% reduction	1. LQG design
Root shear	50% reduction	2. Control law order reduction
Outboard bending mom.	No increase	
Outboard torsion	No increase	3. Discretize
Elevator deflection	Within max limit	4. Optimization
Elevator rate	Within max limit	5. Apply constraints a) on rms loads
Aileron deflection	Within max limit	b) on singular val.
Aileron rate	Within max limit	

704

Symmetric Flutter Suppression System

The software has been used in the past for the following applications: a) Robust flutter suppression control law synthesis for ARW-I wind tunnel wing model; b) Flutter suppression control law synthesis for ARW-II drone and DC-10 derivative wind tunnel wing model and c) s plane summation of forces load model (Ref. 3). A brief survey of the research activities is presented in Ref.4.Digital robust control law synthesis for the Active Flexible Wing (AFW) wind tunnel model is presently being carried out in collaboration with Rockwell International. The basic block diagram for a two input two output symmetric flutter suppression system is shown in the figure for a sting mounted model using leading edge outboard (LEO) and trailing edge outboard (TEO) symmetric actuators and colocated accelerometer sensors.The sampling rate is 200Hz.The design takes into account the effects of actuator dynamics, 4th order 100Hz Butterworth filters and one cycle computational delay at each channel. Full order and reduced order analog and discrete robust control laws were synthesized based on an approximate 38th order system at 300 psf design dynamic pressure. The discrete 8th order control law was able to stabilize the system over the range 300 to 150 psf.The more detailed 80th order model was also stable at 300 and 200 psf. Starting with these preliminary control laws detailed analysis will be carried out using the discrete system optimization procedure EXC OPTD.

SYMMETRIC FLUTTER SUPPRESSION SYSTEM

705
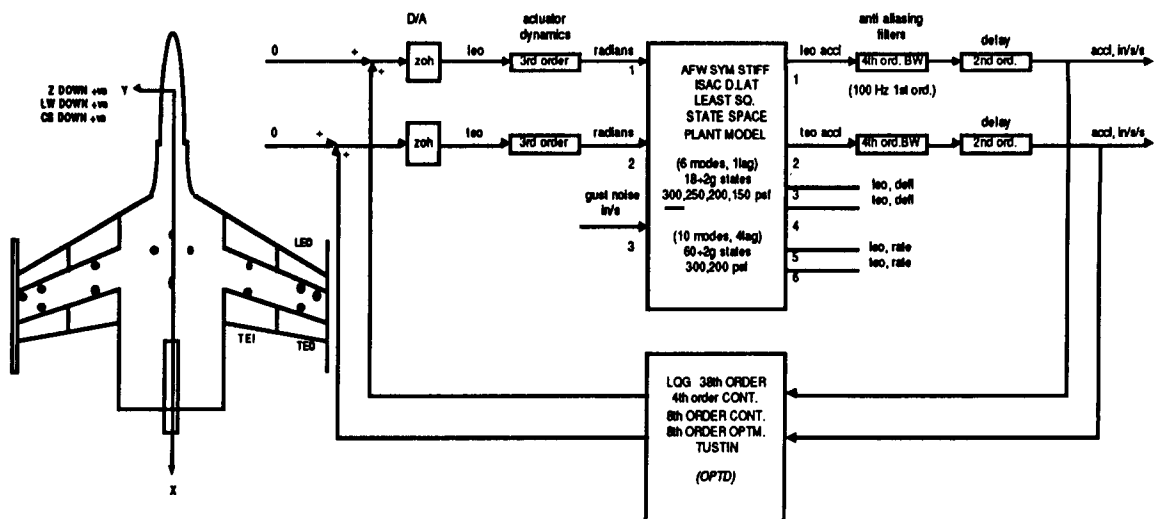
CONCLUDING REMARKS

● Software Improvement

　　　　1. Direct time response constraints
　　　　2. New reduction techniques
　　　　3. H-infinity design
　　　　4. Additional derivative/sensitivity capabilities
　　　　5. User help and online documentation

● Portability improvement

　　　　1. Microvax
　　　　2. NOS VE

● Future Applications

　　　　1. AFW rapid roll maneuver
　　　　2. Large space structure-control interaction

AFW RAPID ROLL CONTROL

Active Flexible Wing Rapid Roll Mechanization
Wind Tunnel Model Digital Control

**LARGE SPACE STRUCTURE
ACTIVE CONTROL**

706
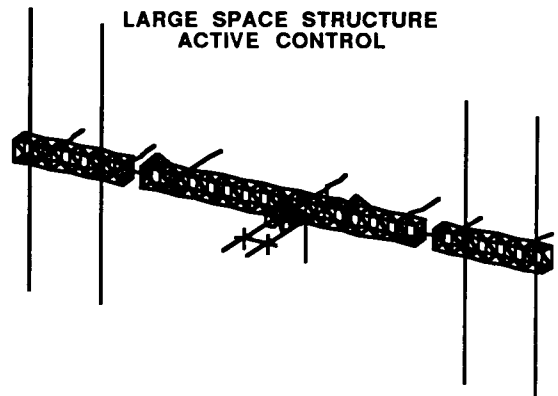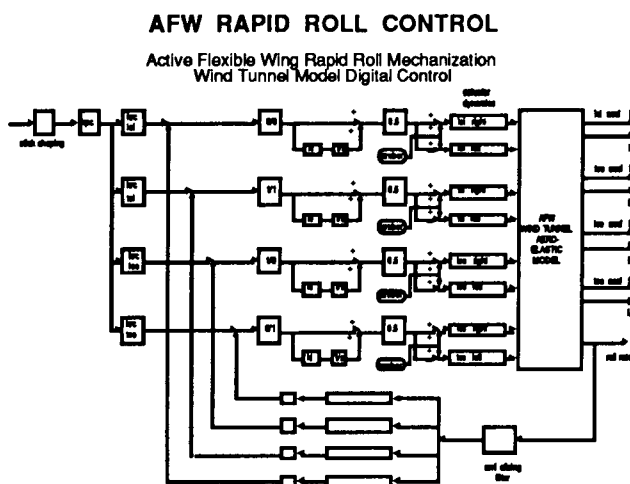
References

1. Mukhopadhyay, V., "Digital Robust Active Control Law Synthesis for Large Order Systems using Constrained Optimization," AIAA Paper 87-2588 CP, Guidance, Navigation and Control Conference, Monterey, CA, 1987.

2. Mukhopadhyay. V., "Digital Robust Control Law Synthesis Using Constrained Optimization," Journal of Guidance Control and Dynamics,1988 (TBP)

3. Pototzsky, A. S. and Perry, III, B.,"New and Existing Techniques for Dynamic Loads Analyses of Flexible Airplanes," Journal of Aircraft, April 1986, pp. 340-347.

4. Abel, I. and Noll, T.E., Research and Applications in Aeroservoelasticity at the NASA Langley Research Center," 16th ICAS Congress, Jerusalem, Israel, August, 1988.

FLEXIBLE AIRCRAFT DYNAMIC MODELING
FOR DYNAMIC ANALYSIS AND CONTROL SYNTHESIS

By

David K. Schmidt
Purdue University
West Lafayette, Indiana

ABSTRACT

The linearization and simplification of a nonlinear, literal model for flexible aircraft is highlighted. Areas of model fidelity that are critical if the model is to be used for control system synthesis are developed and several simplification techniques that can deliver the necessary model fidelity are discussed. These techniques include both numerical and analytical approaches. An analytical approach, based on first-order sensitivity theory is shown to lead not only to excellent numerical results, but also to closed-form analytical expressions for key system dynamic properties such as the pole/zero factors of the vehicle transfer-function matrix. The analytical results are expressed in terms of vehicle mass properties, vibrational characteristics, and rigid-body and aeroelastic stability derivatives, thus leading to the underlying causes for critical dynamic characteristics.

MODELING
FLEXIBLE AIRCRAFT
FOR
DYNAMIC ANALYSIS
AND
CONTROL SYNTHESIS

710

David K. Schmidt

School of Aeronautics and Astronautics

Purdue University

July 1988

TOPICAL OUTLINE

- What Constitutes a Valid Model?
    How Validity Will Be Measured
    What's Important in a Feedback System

- Some Approaches to Obtain (Simple) Valid Models
    Numerical
    Literal

- Physical Causes of Critical Dynamic Characteristics

WHAT VEHICLE DYNAMIC CHARACTERISTICS
ARE CRITICAL IN A FEEDBACK SYSTEM?

They Are Important If They Can:

— Induce Critical Pole/Zero Interactions

— Significantly Affect Frequency Response Near Crossover

— Significantly Affect Time Response

CRITICAL DI-POLE EFFECT
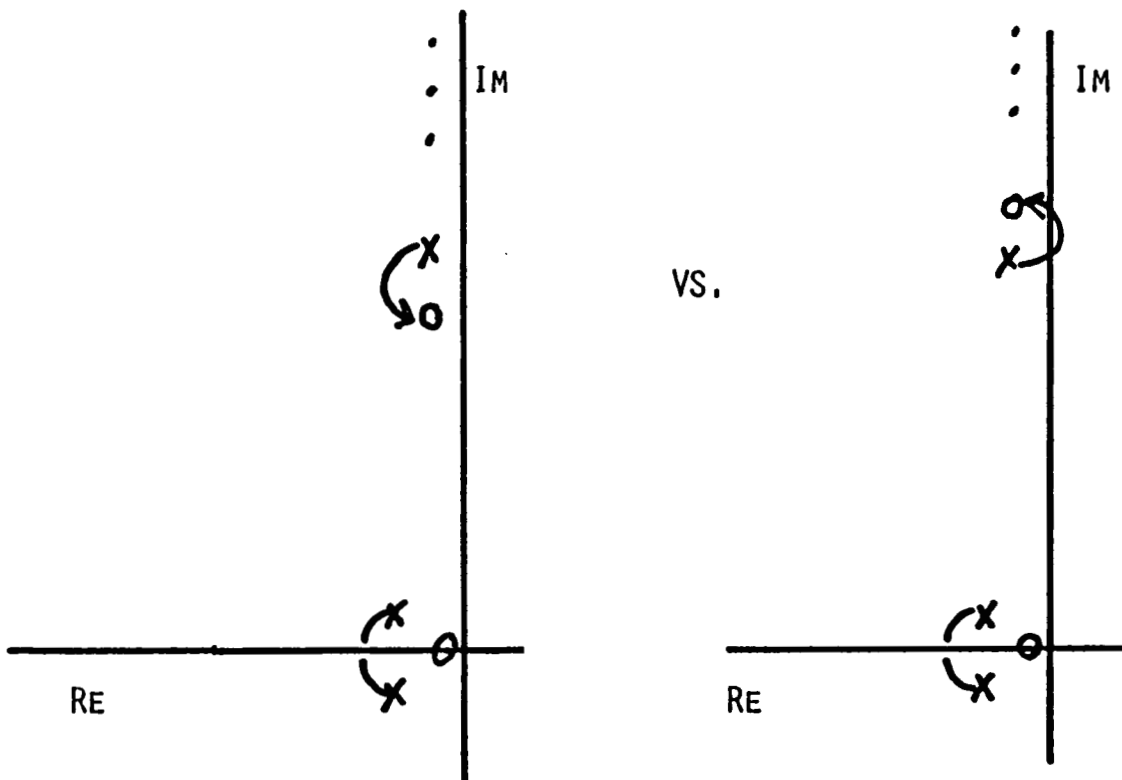
STABILITY IN THE FACE OF UNCERTAINTY

(OR, MODELING ERROR)

NOMINAL LOOP

$\underline{KG^*(j\omega)}$

IM

RE

-1.0

$1 + \underline{KG^*(j\omega)}$

ω

$\underline{K\delta(j\omega)}$

UNCERTAINTY (ERROR) ASSOCIATED WITH $\delta(j\omega)$

$\longrightarrow$ DESIGN MODEL = $\underline{G^*(j\omega)}$

$\longrightarrow$ "TRUE" MODEL = $G^* + \underline{\delta}$

$\longrightarrow$ STABILITY GUARANTEED IF

$$\left| K\delta(j\omega) \right| < \left| 1 + KG^*(j\omega) \right|$$

or if

$$|\varepsilon| < \left| 1 + \left(KG^* \right)^{-1} \right|$$

with $\varepsilon = \left(G^* \right)^{-1} \delta G$

714
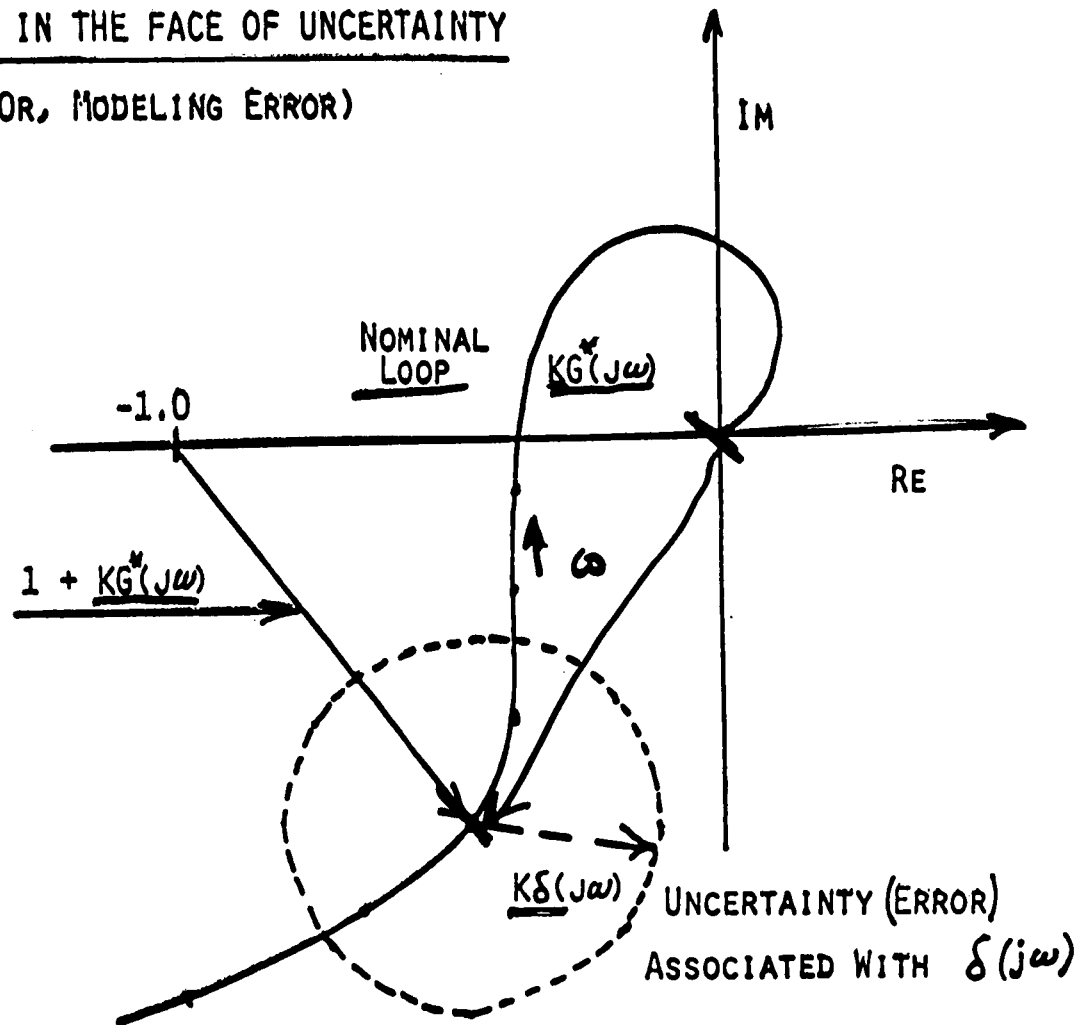
ROBUSTNESS EVALUATION

Slender-Body Configuration

$G^* = $ Rigid Model (M=1.8, S.L.)

$\omega_1 = 9$ rad/sec

$\omega_{sp}^* = 7.2$ rad/sec

715
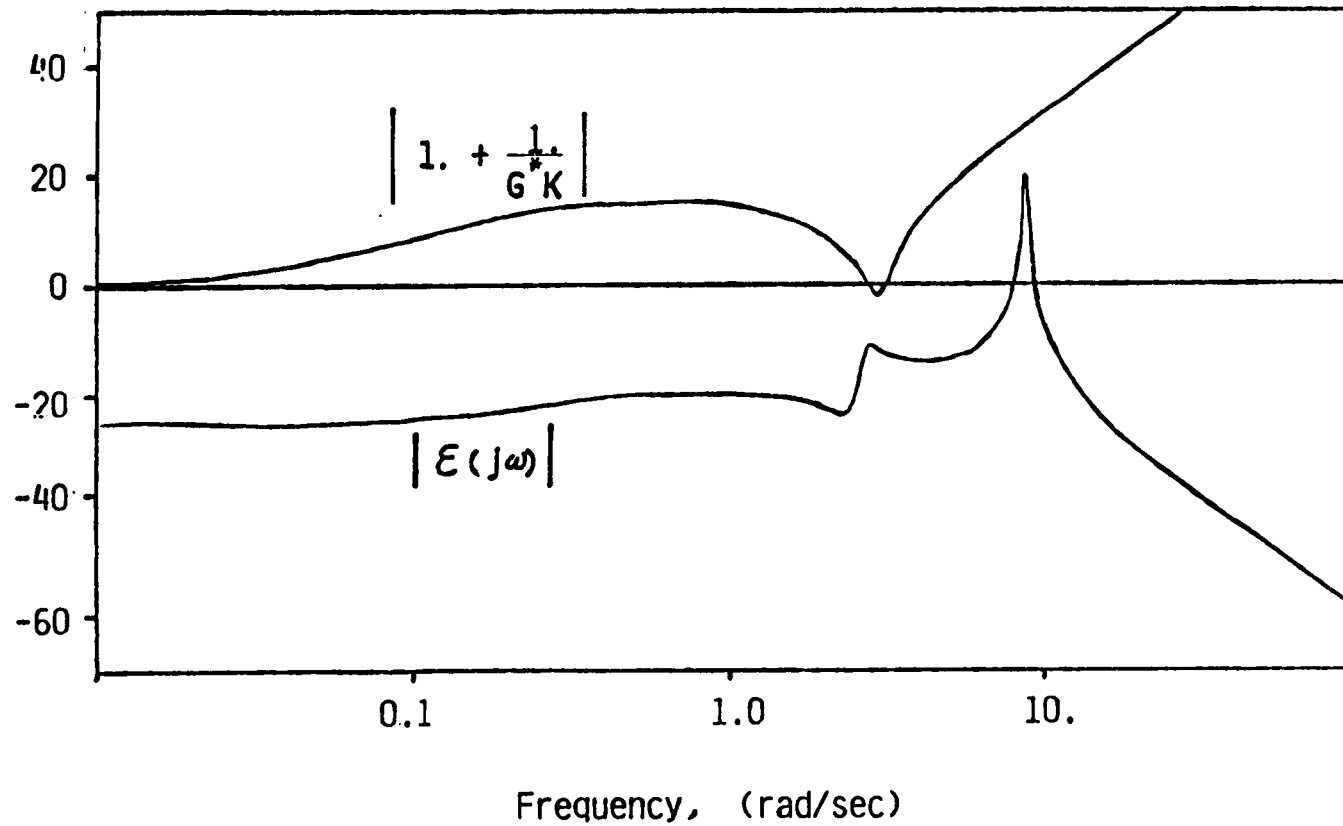
CHARACTERIZING UNCERTAINTY

$$G = G^* + \delta G$$

$$G = G^*(1-\varepsilon)$$
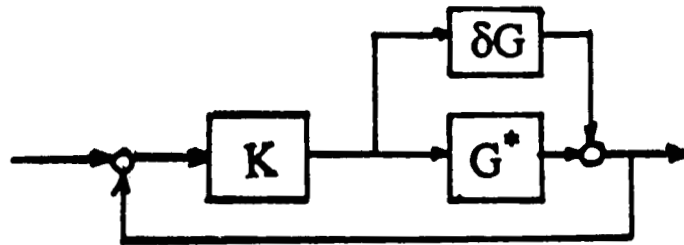
— If N.U.P.(G) = N.U.P(G*)   — If N.U.P.(G) = N.U.P.(G*)

Stability of the Loop
Guaranteed If

Stability of the Loop
Guaranteed If

$$\bar{\sigma}[\delta GK] < \underline{\sigma}[I+GK(j\omega)], \omega > 0$$

$$\bar{\sigma}[\varepsilon] < \underline{\sigma}[I+[GK(j\omega)]^{-1}]$$

Most Critical When $\|GK\| \approx 1$ (crossover)

——→ Let's Look At Potential Sources For δG or $\varepsilon(j\omega)$ ←——

716

A MEANINGFUL METRIC
FOR MODEL VALIDITY

$$\delta G = E(j\omega) = G(j\omega) - G_s(j\omega)$$

$$(\text{or } E(j\omega) = I - G^{-1}G_s)$$

In Crossover
Region

Can Use Singular Values If Desired

$$\bar{\sigma}(E) = \bar{\lambda}^{\frac{1}{2}}(EE^*),$$

A Possible Metric   **A Conservative Metric**

$$\|E(j\omega)\|_{CF} = \frac{\sup \bar{\sigma}(E(j\omega))}{\omega_1 < \omega < \omega_2} \qquad \|E(j\omega)\|_{\infty} = \frac{\sup \bar{\sigma}(E(j\omega))}{0 < \omega < \infty}$$

Or Just look at Bode Plots

CONSIDER THE
SYSTEM IN
POLYNOMIAL - MATRIX FORM

$$\begin{bmatrix} A(s) & c(s) \\ r(s) & m(s) \end{bmatrix} \begin{bmatrix} Z(s) \\ z_r(s) \end{bmatrix} = \begin{bmatrix} B(s) \\ b_r(s) \end{bmatrix} U(s)$$

$$Y(s) = M(s)Z(s) + m_r(s)z_r(s) \quad \Rightarrow \quad Y(s) = [G(s)]U(s)$$

718

$G_{ij}(s)$ — Determined From

$$\frac{Z_i(s)}{U_j(s)} = \frac{m \det [A_i | B_j - cm^{-1}(r_i | b_{r_j})]}{m \det[A - cm^{-1}r]}$$

$$\frac{z_r(s)}{U_j(s)} = \frac{b_{r_j} \det[A - B_j b_{r_j}^{-1} r]}{m \det[A - cm^{-1}r]} \qquad \left(\begin{array}{c} \text{Assumes } z_r(s) \\ \text{Scalar} \end{array} \right)$$

NOW ASSUME

$$c_k r_k \ll m \quad ; \quad k = 1, \cdots, n$$

$$B_{j_k} r_k \ll b_{r_j} \quad ; \quad k = 1, \cdots, n$$

$$c_k (r_i \mid b_{r_j})_k \ll m \quad ; \quad k = 1, \cdots, n$$

Over The Freq. Range Of Interest

In This Case
$$\begin{cases} A_i \mid B_j - cm^{-1}(r_i \mid b_{r_j}) \approx A_i \mid B_j \\[2mm] A - B_j b_{r_j}^{-1} r \approx A \\[2mm] A - cm^{-1} r \approx A \end{cases}$$

And

$$\begin{cases} \dfrac{Z_i(s)}{U_j(s)} \approx \dfrac{\hat{Z}_i(s)}{U_j(s)} = \dfrac{\det [A_i \mid B_j]}{\det [A]} \\[8mm] \\ \dfrac{z_r(s)}{U_j(s)} \approx b_{r_j}/m \end{cases}$$

719

CASE I

If $\dfrac{b_{rj}}{m} \approx 0$ In Freq. of Interest

Truncated Model

$$Y(s) \approx M(s)\hat{Z}(s)$$

$$\frac{\hat{Z}_i(s)}{U_j(s)} = \det[A_i \mid B_j]/\det[A]$$

Adequate Model When Z_r
Corresponds To A Low-Frequency,
Or "Slow" Degree Of Freedom

Special Case — Modal Form

$$\begin{bmatrix} (sI - \Lambda) & 0 \\ 0 & (sI - \Lambda_r) \end{bmatrix} \begin{bmatrix} N(s) \\ N_r(s) \end{bmatrix} = \begin{bmatrix} B \\ B_r \end{bmatrix} U(s)$$

$$Y = M\,N(s) + M_r N_r(s)$$

Here

$$E(s) = G(s) - G_r(s) = M_r(sI - \Lambda_r)^{-1}B_r$$

$$E_{ij}(j\omega) \to 0 \text{ as } |(j\omega - \lambda_r)| \to \infty$$

720

CASE II

If $\dfrac{b_{rj}}{m} \to$ Constant $(\neq 0)$ In Freq. of Interest

Residualized
Model

$$Y(s) \approx M(s)\hat{Z}(s) + m_r(s)\frac{b_r(0)}{k_r}U(s)$$

$$\frac{\hat{Z}_i(s)}{U_j(s)} = \frac{\det[A_i | B_j]}{\det[A]}$$

Adequate Model When Z_r Corresponds to
A (stable) High-Frequency ("Fast")
Degree Of Freedom

Special Case

Modal
Resid.

$$E(s) = M_r(sI - \Lambda_r)^{-1}B_r + M_r(\Lambda_r)^{-1}B_r$$

$$= M_r[s(sI - \Lambda_r)^{-1}\Lambda_r^{-1}]B_r$$

$$|E_{ij}(j\omega)| \to 0 \quad \text{as} \quad |j\omega| \to 0$$

72)

Table 6. Frequency Weighted Internally Balanced Reduction

Given: System state space description A, B, C and weighting filter state space description A_w, B_w, C_w.

Find: r^{th} order system

Step 1: Solve for X and Y

$$\begin{bmatrix} A & BC_w \\ 0 & A_w \end{bmatrix}\begin{bmatrix} X & X_{12} \\ X_{21} & X_{22} \end{bmatrix} + \begin{bmatrix} X & X_{12} \\ X_{21} & X_{22} \end{bmatrix}\begin{bmatrix} A^T & 0 \\ C_w^T B^T & A_w^T \end{bmatrix} + \begin{bmatrix} 0 & 0 \\ 0 & B_w B_w^T \end{bmatrix} = 0$$

$$\begin{bmatrix} A^T & 0 \\ C_w^T B^T & A_w^T \end{bmatrix}\begin{bmatrix} Y & Y_{12} \\ Y_{21} & Y_{22} \end{bmatrix} + \begin{bmatrix} Y & Y_{12} \\ Y_{21} & Y_{22} \end{bmatrix}\begin{bmatrix} A & BC_w \\ 0 & A_w \end{bmatrix} + \begin{bmatrix} CC^T & 0 \\ 0 & 0 \end{bmatrix} = 0$$
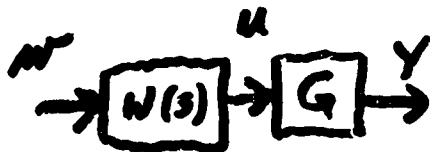
722

Step 2: Find T and Σ where $XY = T\Sigma^2 T^{-1}$, $T = [T_r, T_{n-r}]$, $T^{-T} = [U_r, U_{n-r}]$

$$\Sigma^2 = \begin{bmatrix} \Sigma_r^2 & 0 \\ 0 & \Sigma_{n-r}^2 \end{bmatrix} \qquad \text{where}$$

$$\Sigma_r = \text{diag}(v_{c_i} v_{o_i}) \quad i = 1, ..., r$$

$$\Sigma_{n-r} = \text{diag}(v_{c_i} v_{o_i}) \quad i = r+1, \cdots, n$$

$$v_{c_1} v_{o_1} \geq \cdots \geq v_{c_n} v_{o_n} \geq 0$$

Step 3: r^{th} order system is

$$A_r = U_r^T A T_r$$

$$B_r = U_r^T B$$

$$C_r = C T_r$$

THE SYSTEM IS DESCRIBED BY
(After Linearization)

$$
\begin{bmatrix}
[F_{RB}(s)] & 0 & 0 & \cdots \\
\hline
[0] & s^2+2\xi_1\omega_1 s+\omega_1^2 & 0 & \cdots \\
0 & & \ddots & \\
& & & \ddots \\
& & & & \ddots
\end{bmatrix}
\begin{bmatrix}
\bar{y}_R \\
\hline
\eta_1 \\
\vdots \\
\eta_m
\end{bmatrix}
=
\begin{bmatrix}
M_R \\
\hline
F_1 \\
\vdots \\
F_m
\end{bmatrix}
\bar{\delta}_c(s)
$$

$\underbrace{\qquad\qquad}_{[F(s)]}$ $\underbrace{\qquad}_{[M(s)]}$

$\bar{y}_R \begin{cases} \text{Rigid-Body} \\ \text{D.O.F.} \end{cases}$

$\cdot$ (Elastically Decoupled)

$$
\underline{\text{Aero Coupling}}
\text{(can include}
\text{unsteady effects)}
\left\{
+
\begin{bmatrix}
[A_{RR}(s)] & [A_{RE_1}(s)] & \cdots \\
\hline
[A_{E_1 R}(s)] & A_{E_1}(s) & \cdots \\
\vdots & &
\end{bmatrix}
\begin{bmatrix}
\bar{y}_R \\
\hline
\eta_1 \\
\vdots \\
\eta_m
\end{bmatrix}
\right.
$$

$\underbrace{\qquad\qquad}_{[A(s)]}$

$$
\text{e.g.} \quad A_{E_i}(s) = \frac{N_{E_i}(s)}{D_{E_i}(s)}, \quad (\text{Unsteady})
$$

724

FOR QUASI-STEADY AERODYNAMICS
A STANDARD FORM IS

$$
\overbrace{\phantom{\begin{matrix}(s-Z_w) & -(Z_q+U_0)\end{matrix}}}^{F_{RR}} \quad \overbrace{\phantom{\begin{matrix}-(Z_{\dot\eta_1}s+Z_{\eta_1})\end{matrix}}}^{F_{RE}}
$$

$$
\left[
\begin{array}{cc|ccc}
(s-Z_w) & -(Z_q+U_0) & -(Z_{\dot\eta_1}s+Z_{\eta_1}) & & \cdots \\[4pt]
-M_w & (s-M_q) & -(M_{\dot\eta_1}s+M_{\eta_1}) & & \cdots \\[4pt]
\hline
-F_{1_w} & -F_{1_q} & \{s^2+(2\xi_1\omega_1-F_{1_{\dot\eta_1}})s+(\omega_1^2-F_{1\eta_1})\} & & \\[4pt]
\vdots & & & \ddots &
\end{array}
\right]
\left[
\begin{array}{c}
w \\[4pt]
\dot\theta \\[4pt]
\hline
\eta_1 \\[4pt]
\vdots
\end{array}
\right]
=
\left[
\begin{array}{c}
Z_\delta \\[4pt]
M_\delta \\[4pt]
\hline
F_{1\delta} \\[4pt]
\vdots
\end{array}
\right]
\bar\delta
$$

$$
\underbrace{\phantom{\begin{matrix}-F_{1_w} & -F_{1_q}\end{matrix}}}_{F_{ER}} \quad \underbrace{\phantom{\begin{matrix}\{s^2+(2\xi_1\omega_1-F_{1_{\dot\eta_1}})s+(\omega_1^2-F_{1\eta_1})\}\end{matrix}}}_{F_{EE}}
$$

And, for example

$$
\frac{\dot\theta(s)}{\delta_E(s)} = \frac{C_\theta(s+1/T_\theta)\overset{m}{\Pi}(s^2+2\xi_{\theta_i}\omega_{\theta_i}s+\omega_{\theta_i}^2)}{\underbrace{(s^2+2\xi_{sp}\omega_{sp}s+\omega_{sp}^2)}_{\text{Like Rigid Body}\;\;\text{But Mod}}\underbrace{\overset{m}{\Pi}(s^2+2\xi_{E_i}\omega_{E_i}s+\omega_{E_i}^2)}_{\text{Aero- Elastic Dipoles}}}
$$

725

From Cramer's Rule

Table 4. Elastic Aircraft Linear Longitudinal Equations In Polynomial Matrix Form

$$
\begin{bmatrix}
s-X_u & -X_\alpha & -X_q s - X_\theta & -X_{\dot\eta_1}s - X_{\eta_1} & -X_{\dot\eta_2}s - X_{\eta_2} & \cdots & 0 & 0 \\[2mm]
\dfrac{Z_u}{V_{T_1}} & s - \dfrac{Z_\alpha}{V_{T_1}} & -(1+\dfrac{Z_q}{V_{T_1}})s - \dfrac{Z_\theta}{V_{T_1}} & -\dfrac{Z_{\dot\eta_1}}{V_{T_1}}s - \dfrac{Z_{\eta_1}}{V_{T_1}} & -\dfrac{Z_{\dot\eta_2}}{V_{T_1}}s - \dfrac{Z_{\eta_2}}{V_{T_1}} & & 0 & 0 \\[2mm]
-M_u & -M_\alpha & s^2 - M_q s & -M_{\dot\eta_1}s - M_{\eta_1} & -M_{\dot\eta_2}s - M_{\eta_2} & & 0 & 0 \\[2mm]
-F_{1_u} & -F_{1_\alpha} & -F_{1_q}s & s^2+(2\zeta_1\omega_1 - F_{1_{\dot\eta_1}})s+(\omega_1^2 - F_{1_{\eta_1}}) & -F_{1_{\dot\eta_2}}s - F_{1_{\eta_2}} & & 0 & 0 \\[2mm]
-F_{2_u} & -F_{2_\alpha} & -F_{2_q}s & -F_{2_{\dot\eta_1}}s - F_{2_{\eta_1}} & s^2+(2\zeta_2\omega_2 - F_{2_{\dot\eta_2}})s+(\omega_2^2 - F_{2_{\eta_2}}) & & 0 & 0 \\
\vdots & & & & & & \vdots & \\
-K_u & -K_\alpha & -K_q s & -K_{\dot\eta_1}s - K_{\eta_1} & -K_{\dot\eta_2}s - K_{\eta_2} & & 1 & 0 \\[2mm]
0 & 0 & -s & \dot\phi_1 s & \dot\phi_2 s & \cdots & 0 & 1
\end{bmatrix}
\begin{bmatrix}
u(s) \\ \alpha(s) \\ \theta(s) \\ \eta_1(s) \\ \eta_2(s) \\ \vdots \\ a_z(s) \\ q_p(s)
\end{bmatrix}
=
\begin{bmatrix}
X_{\delta_e} & X_{\delta_c} \\[2mm]
\dfrac{Z_{\delta_e}}{V_{T_1}} & \dfrac{Z_{\delta_c}}{V_{T_1}} \\[2mm]
M_{\delta_e} & M_{\delta_c} \\[2mm]
F_{1_{\delta_e}} & F_{1_{\delta_c}} \\[2mm]
F_{2_{\delta_e}} & F_{2_{\delta_c}} \\
\vdots & \vdots \\
K_{\delta_e} & K_{\delta_c} \\
0 & 0
\end{bmatrix}
\begin{bmatrix} \delta_e \\ \delta_c \end{bmatrix}
$$

where

$$K_u = Z_u - x_p M_u + \sum_{i=1}^{\infty}\phi_i F_{i_u}$$

$$K_\alpha = Z_\alpha - x_p M_\alpha + \sum_{i=1}^{\infty}\phi_i F_{i_\alpha}$$

$$K_q = Z_q - x_p M_q + \sum_{i=1}^{\infty}\phi_i F_{i_q}$$

$$K_{\eta_i} = Z_{\eta_i} - x_p M_{\eta_i} - \phi_i(\omega_i^2 - F_{i_{\eta_i}}) + \sum_{\substack{j=1 \\ j\neq i}}^{\infty}\phi_j F_{i_{\eta_j}}$$

$$K_{\dot\eta_i} = Z_{\dot\eta_i} - x_p M_{\dot\eta_i} - \phi_i(2\zeta_i\omega_i - F_{i_{\dot\eta_i}}) + \sum_{\substack{j=1 \\ j\neq i}}^{\infty}\phi_j F_{i_{\dot\eta_j}}$$

$$K_{\delta_e} = Z_{\delta_e} - x_p M_{\delta_e} + \sum_{i=1}^{\infty}\phi_i F_{i_{\delta_e}}$$

$$K_{\delta_c} = Z_{\delta_c} - x_p M_{\delta_c} + \sum_{i=1}^{\infty}\phi_i F_{i_{\delta_c}}$$

$$u = \begin{Bmatrix} \delta_e \\ \delta_c \end{Bmatrix}$$

$$Y = [G(s)]\, U(s)$$

VEHICLE

CONFIGURATION

δ_c

δ_E

727

a_x, q

$\omega_s/2$ 1-4

MODE 1
$\omega_1 = 6.3$ r/s

MODE 2
$\omega_2 = 7.0$ r/s

Fuselage

Wing

MODE 3
$\omega_3 = 10.6$ r/s

Tail

MODE 4
$\omega_4 = 11.0$ r/s

728
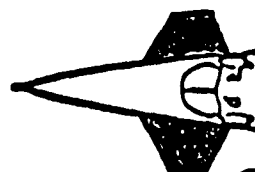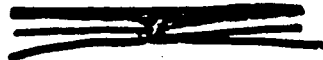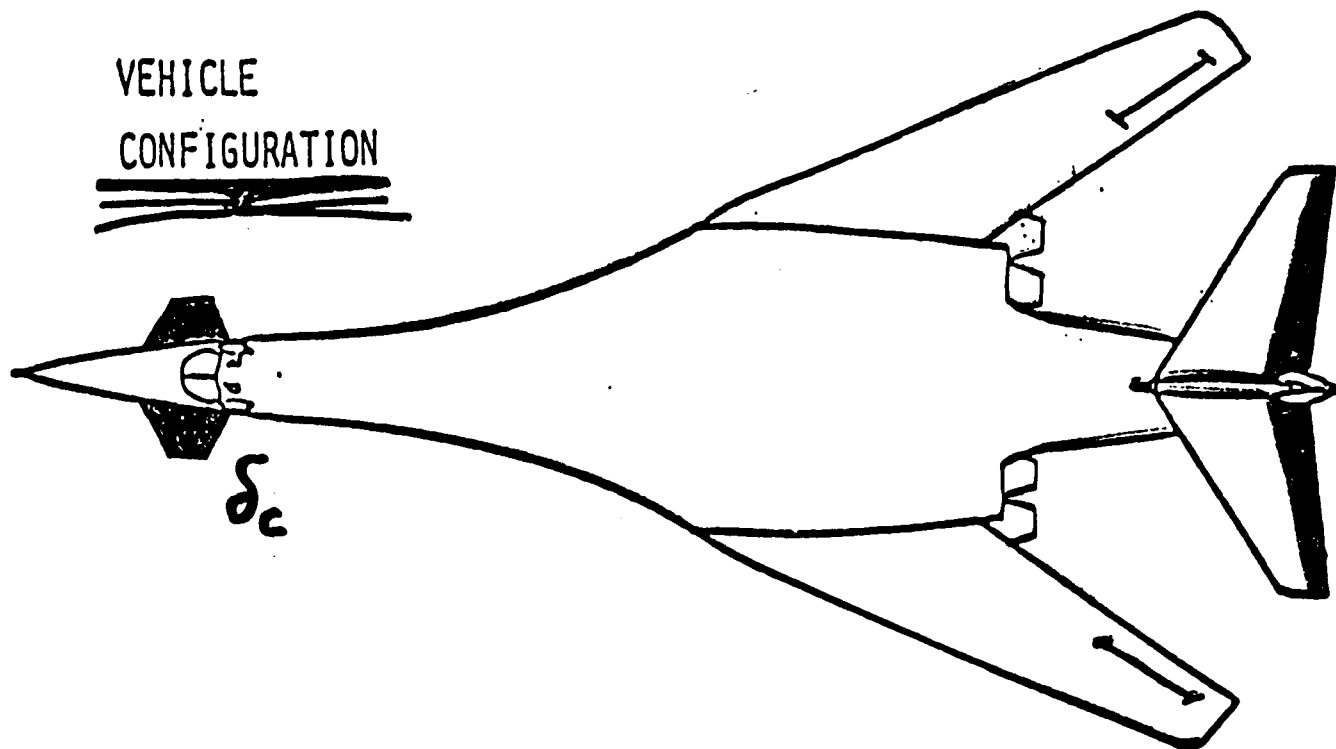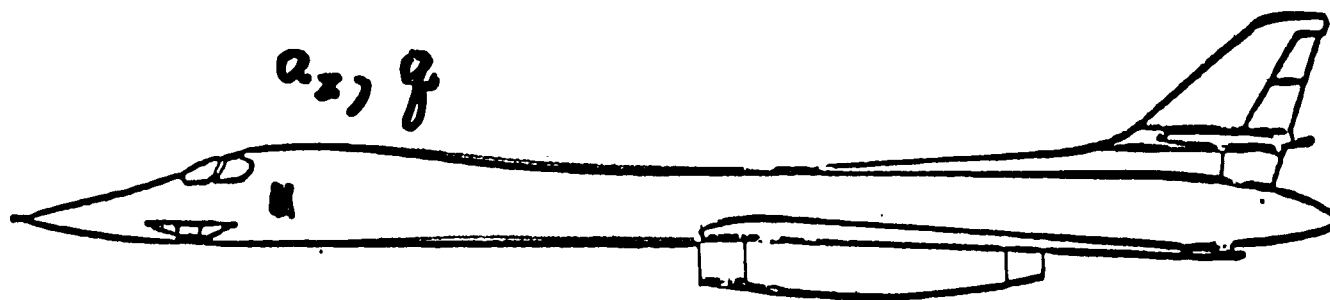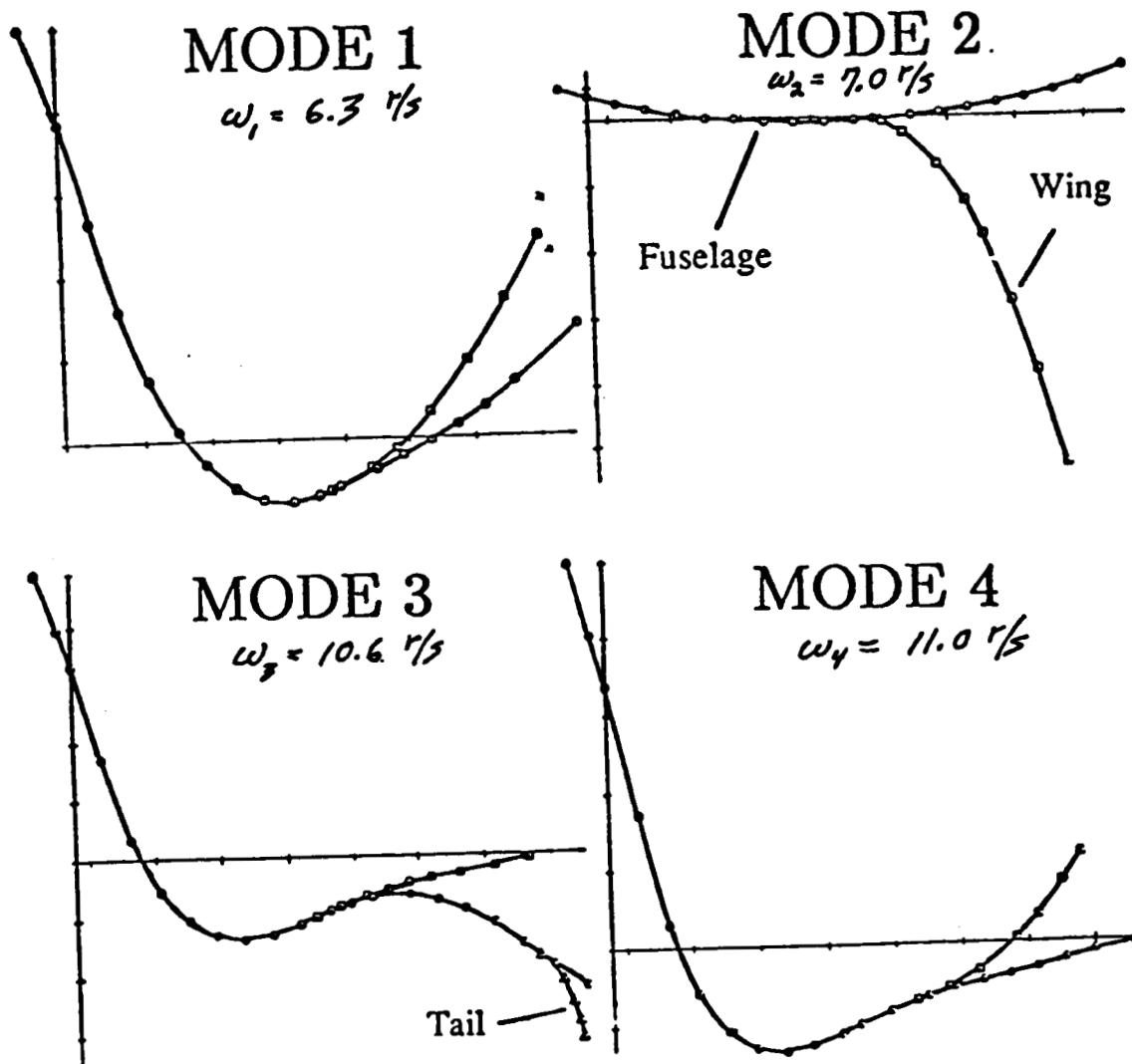
Table 10. Transfer Functions For the True Model

	$G_{a_z}^{\delta_B}$ (ft/s²/deg)	$G_{q_p}^{\delta_B}$ (rad/s/deg)	$G_{a_z}^{\delta_c}$ (ft/s²/deg)	$G_{q_p}^{\delta_c}$ (rad/s/deg)
gains	52.01	8.001	-244.5	15.65
zeros	6.473E-5	0	1.087E-4	0
	-.008887	-.05103	-.008093	-.05541
	$-.01958\pm j1.661$	-.2020	$.1703\pm j1.795$	-.1172
	$-.3610\pm j11.00$	3.642	$-.8996\pm j4.132$	$-.5973\pm j2.912$
	$-1.003\pm j11.13$	-4.020	$-.2252\pm j10.77$	$-.2556\pm j10.68$
	$1.549\pm j11.71$	$-.3610\pm j11.00$	$-.3607\pm j11.00$	$-.3562\pm j10.99$
	$-3.144\pm j14.34$	$-2.838\pm j12.71$	$-2.601\pm j13.06$	$-2.564\pm j13.12$
		$.5735\pm j13.41$		
poles	.03324			
	-.04268			
	$-.4513\pm j1.171$			
	$-.4408\pm j6.010$			
	$-.2240\pm j10.78$			
	$-.3611\pm j11.00$			
	$-2.558\pm j13.05$			

729

Bode Magnitude
$$G_{a_z}^{\delta_E}$$
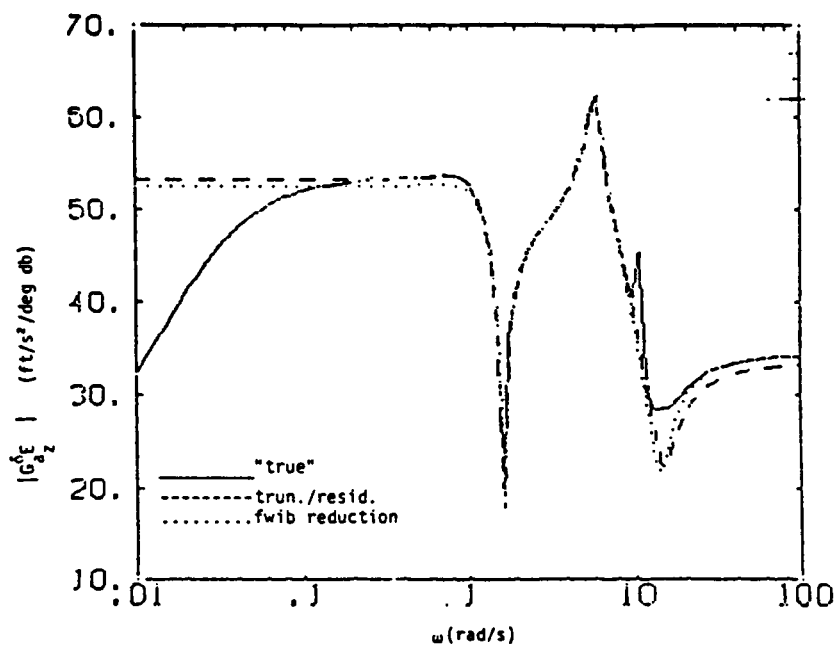
Bode Phase
$$G_{a_z}^{\delta_E}$$
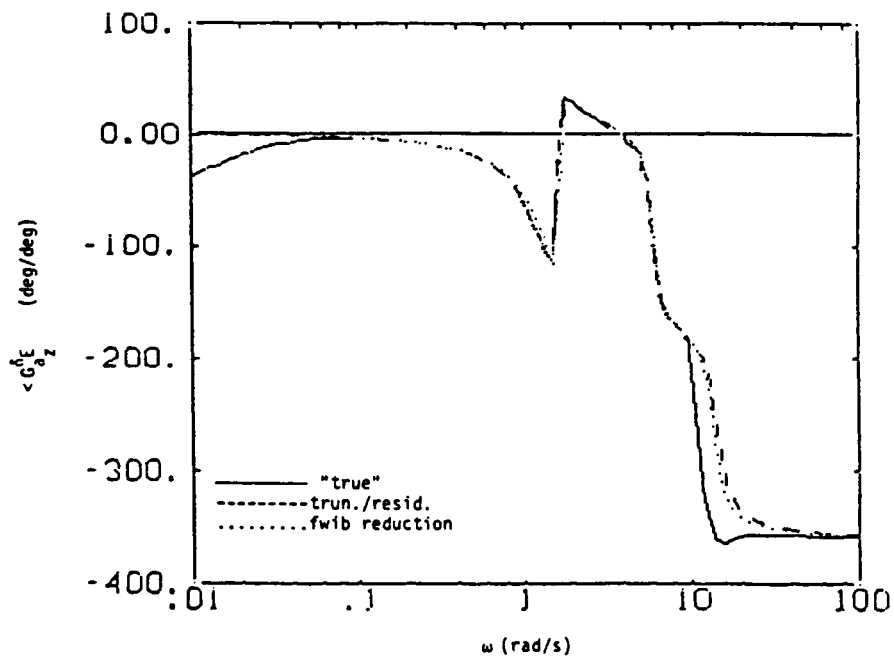
730

Figure 4. $< G_{a_z}^{\delta_E}$ Frequency Response
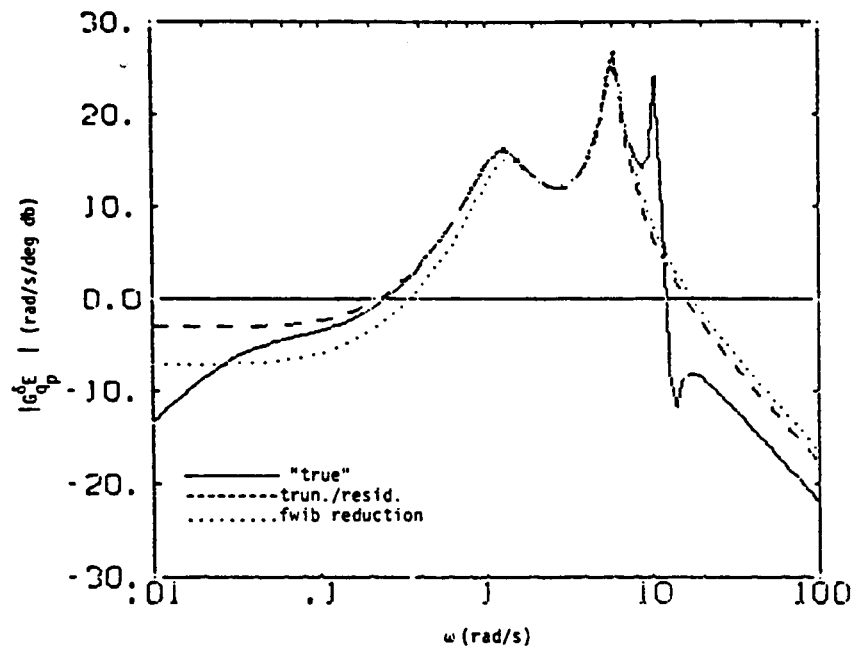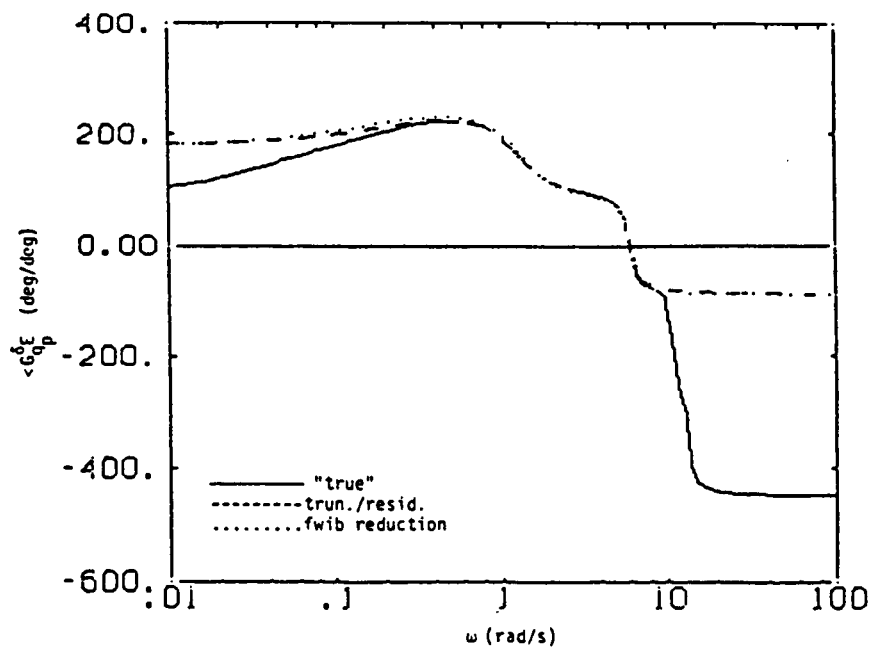
Bode Magnitude

$$G_q^{\delta_E}$$

Bode Phase

$$G_q^{\delta_E}$$

Figure 6. $<G_{q_p}^{\delta_E}$ Frequency Response

731

Bode Magnitude

$$G_{a_z}^{\delta_c}$$
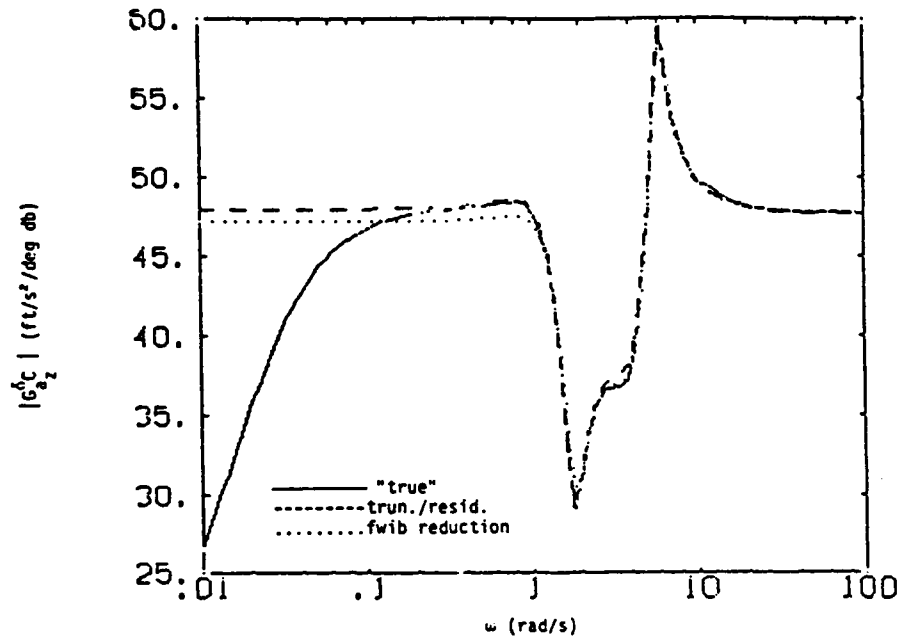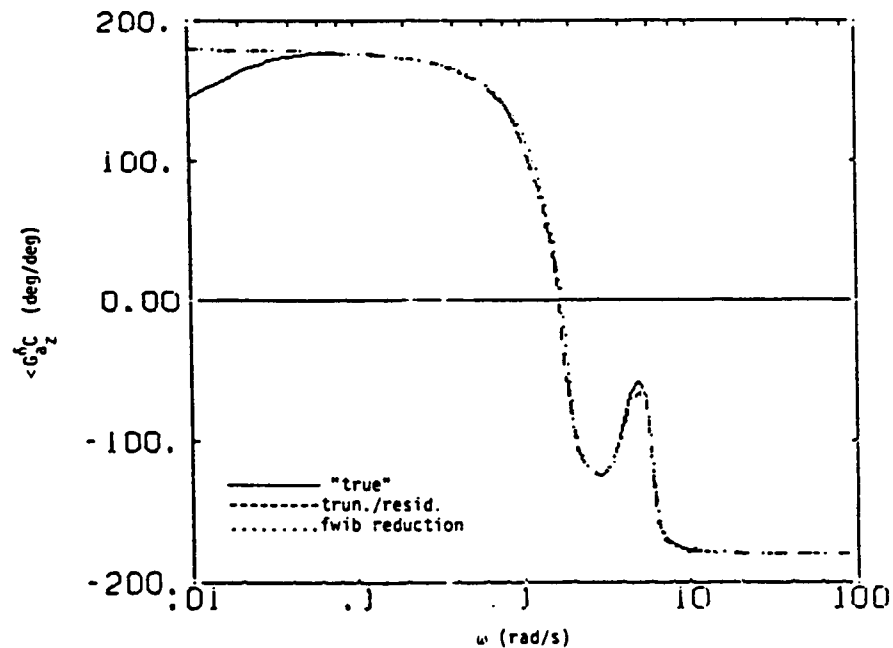
Legend:
- "true"
- trun./resid.
- fwib reduction

Vertical axis: $|G_{a_z}^{\delta_c}|$ (ft/s²/deg db)

Horizontal axis: ω (rad/s)

Bode Phase

$$G_{a_z}^{\delta_c}$$

Legend:
- "true"
- trun./resid.
- fwib reduction

Vertical axis: $<G_{a_z}^{\delta_c}$ (deg/deg)

Horizontal axis: ω (rad/s)

732

Figure 8. $< G_{a_z}^{\delta_c}$ Frequency Response

Bode Magnitude

$$G_q^{\delta_c}$$

Bode Phase

$$G_q^{\delta_c}$$

Figure 10. $< G_{q_p}^{\delta_c}$ Frequency Response

733
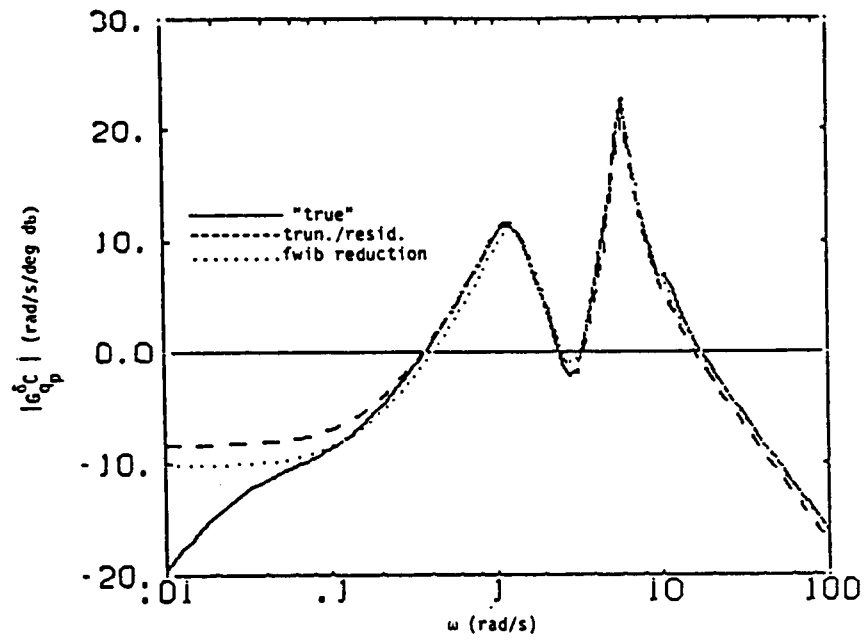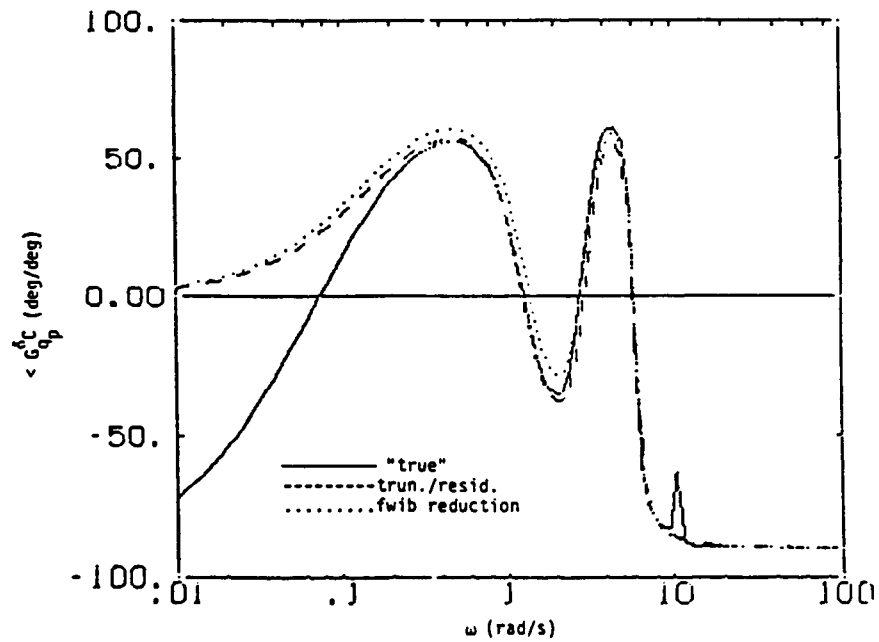
Table 12. Transfer Functions For FWIB Reduction Model

	$G_{a_z}^{\delta_B}$ (ft/s^2/deg)	$G_{q_p}^{\delta_B}$ (rad/s/deg)	$G_{a_z}^{\delta_c}$ (ft/s^2/deg)	$G_{q_p}^{\delta_c}$ (rad/s/deg)
gains	52.01	14.96	-244.5	15.29
zeros	$-.02102 \pm j1.670$ $1.244 \pm j13.51$	$-.1789$ 2.781 -3.732	$.1725 \pm j1.806$ $-.9177 \pm j4.143$	$-.1437$ $-.6806 \pm j2.900$
poles	$-.4679 \pm j1.234$ $-.4413 \pm j6.015$			

734

Table 14. Lower–Order Transfer Function Forms

$$G_{a_z}^{\delta_E}(s) = \frac{K_{a_z}^{\delta_E} s [s^2 + {}_{sp}(2\zeta\omega)_{a_z}^{\delta_E} s + {}_{sp}(\omega^2)_{a_z}^{\delta_E}][s^2 + {}_{f1}(2\zeta\omega)_{a_z}^{\delta_E} s + {}_{f1}(\omega^2)_{a_z}^{\delta_E}]}{D(s)}$$

$$G_{q_P}^{\delta_E}(s) = \frac{K_{q_P}^{\delta_E} s [s + {}_{sp}(\frac{1}{T})_{q_P}^{\delta_E}][s + {}_{f11}(\frac{1}{T})_{q_P}^{\delta_E}][s + {}_{f12}(\frac{1}{T})_{q_P}^{\delta_E}]}{D(s)}$$

$$G_{a_z}^{\delta_c}(s) = \frac{K_{a_z}^{\delta_c} s [s^2 + {}_{sp}(2\zeta\omega)_{a_z}^{\delta_c} s + {}_{sp}(\omega^2)_{a_z}^{\delta_c}][s^2 + {}_{f1}(2\zeta\omega)_{a_z}^{\delta_c} s + {}_{f1}(\omega^2)_{a_z}^{\delta_c}]}{D(s)}$$

$$G_{q_P}^{\delta_c}(s) = \frac{K_{q_P}^{\delta_c} s [s + {}_{sp}(\frac{1}{T})_{q_P}^{\delta_c}][s^2 + {}_{f1}(2\zeta\omega)_{q_P}^{\delta_c} s + {}_{f1}(\omega^2)_{q_P}^{\delta_c}]}{D(s)}$$

where $D(s) = s[s^2 + (2\zeta\omega)_{sp}s + (\omega^2)_{sp}][s^2 + (2\zeta\omega)_{f1}s + (\omega^2)_{f1}]$

735

C-3

Table 7. Truncated/Residulized Model

$$
\begin{bmatrix}
s-\dfrac{Z_\alpha}{V_{T_1}} & -(1+\dfrac{Z_q}{V_{T_1}})s-\dfrac{Z_\theta}{V_{T_1}} & -\dfrac{Z_{\dot\eta_1}}{V_{T_1}}s-\dfrac{Z_{\eta_1}}{V_{T_1}} & 0 & 0 \\[2ex]
-M_\alpha & s^2-M_q s & -M_{\dot\eta_1}s-M_{\eta_1} & 0 & 0 \\[2ex]
-F_{1_\alpha} & -F_{1_q}s & s^2+(2\zeta_1\omega_1-F_{1_{\dot\eta_1}})s+(\omega_1^2-F_{1_{\eta_1}}) & 0 & 0 \\[2ex]
-K_\alpha & -K_q s & -K_{\dot\eta_1}s-K_{\eta_1} & 1 & 0 \\[2ex]
0 & -s & \phi_i's & 0 & 1
\end{bmatrix}
\begin{bmatrix}
\alpha(s) \\[2ex] \theta(s) \\[2ex] \eta_1(s) \\[2ex] a_z(s) \\[2ex] q_p(s)
\end{bmatrix}
=
\begin{bmatrix}
\dfrac{Z_{\delta_E}}{V_{T_1}} & \dfrac{Z_{\delta_C}}{V_{T_1}} \\[2ex]
M_{\delta_E} & M_{\delta_C} \\[2ex]
F_{1_{\delta_E}} & F_{1_{\delta_C}} \\[2ex]
K_{\delta_E} & K_{\delta_C} \\[2ex]
0 & 0
\end{bmatrix}
\begin{bmatrix}
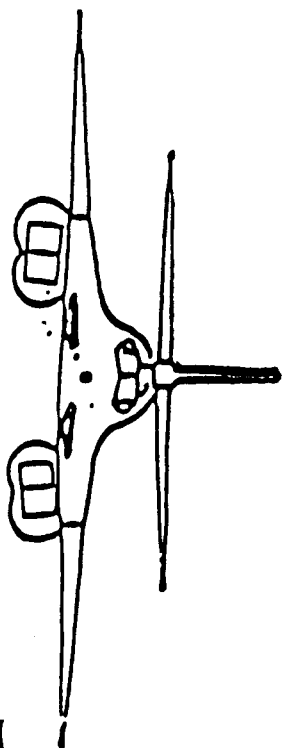\delta_E(s) \\[2ex] \delta_C(s)
\end{bmatrix}
$$

$$D(s) = -(\frac{Z_{\dot{\eta}_1}}{V_{T_1}}s + \frac{Z_{\eta_1}}{V_{T_1}})[M_\alpha F_{1_q}s + F_{1_\alpha}(s^2 - M_q s)]$$

$$- (M_{\dot{\eta}_1}s + M_{\eta_1})[F_{1_q}s(s - \frac{Z_\alpha}{V_{T_1}}) + (1 + \frac{Z_q}{V_{T_1}})F_{1_\alpha}s] \qquad (23)$$

$$+ (s^2 + (2\zeta_1\omega_1 - F_{1_{\dot{\eta}_1}})s + (\omega_1^2 - F_{1_{\eta_1}}))[(s - \frac{Z_\alpha}{V_{T_1}})(s^2 - M_q s) - (1 + \frac{Z_q}{V_{T_1}})M_\alpha s]$$

$$N(s) = \frac{Z_{\delta_B}}{V_{T_1}}\{s[M_\alpha(s^2 + (2\zeta_1\omega_1 - F_{1_{\dot{\eta}_1}})s + (\omega_1^2 - F_{1_{\eta_1}})) + F_{1_\alpha}(M_{\dot{\eta}_1}s + M_{\eta_1})]$$

$$- \phi_1's[M_\alpha F_{1_q}s + F_{1_\alpha}(s^2 - M_q s)]\}$$

$$+ M_{\delta_B}\{s[(s - \frac{Z_\alpha}{V_{T_1}})(s^2 + (2\zeta_1\omega_1 - F_{1_{\dot{\eta}_1}})s + (\omega_1^2 - F_{1_{\eta_1}})) - F_{1_\alpha}(\frac{Z_{\dot{\eta}_1}}{V_{T_1}}s + \frac{Z_{\eta_1}}{V_{T_1}})]$$

$$- \phi_1's[F_{1_q}s(s - \frac{Z_\alpha}{V_{T_1}}) + (1 + \frac{Z_q}{V_{T_1}})F_{1_\alpha}s]\}$$

$$+ F_{1_{\delta_B}}\{s[(s - \frac{Z_\alpha}{V_{T_1}})(M_{\dot{\eta}_1}s + M_{\eta_1}) + M_\alpha(\frac{Z_{\dot{\eta}_1}}{V_{T_1}}s + \frac{Z_{\eta_1}}{V_{T_1}})]$$

$$- \phi_1's[(s - \frac{Z_\alpha}{V_{T_1}})(s^2 - M_q s) - M_\alpha(1 + \frac{Z_q}{V_{T_1}})s]\}$$

737

Table 8. Polynomial Coefficient and Factor Relationships

$$\tilde{d}_1 = (\tilde{\omega}^2)_{sp}\,(\tilde{\omega}^2)_{f1}$$

$$\tilde{d}_2 = (2\zeta\omega)_{sp}(\tilde{\omega}^2)_{f1} + (2\zeta\omega)_{f1}(\tilde{\omega}^2)_{sp}$$

$$\tilde{d}_3 = (\tilde{\omega}^2)_{sp} + (\tilde{\omega}^2)_{f1} + (2\zeta\omega)_{sp}(2\zeta\omega)_{f1}$$

$$\tilde{d}_4 = (2\zeta\omega)_{sp} + (2\zeta\omega)_{f1}$$

$$\tilde{n}_1 = \tilde{K}_{q_p}^{\delta_B}\,_{sp}\left(\frac{1}{\tilde{T}}\right)_{q_p}^{\delta_B}\,_{f11}\left(\frac{1}{\tilde{T}}\right)_{q_p}^{\delta_B}\,_{f12}\left(\frac{1}{\tilde{T}}\right)_{q_p}^{\delta_B}$$

$$\tilde{n}_2 = \tilde{K}_{q_p}^{\delta_B}\left[\,_{sp}\left(\frac{1}{\tilde{T}}\right)_{q_p}^{\delta_B}\,_{f11}\left(\frac{1}{\tilde{T}}\right)_{q_p}^{\delta_B} + \,_{sp}\left(\frac{1}{\tilde{T}}\right)_{q_p}^{\delta_B}\,_{f12}\left(\frac{1}{\tilde{T}}\right)_{q_p}^{\delta_B} + \,_{f11}\left(\frac{1}{\tilde{T}}\right)_{q_p}^{\delta_B}\,_{f12}\left(\frac{1}{\tilde{T}}\right)_{q_p}^{\delta_B}\right]$$

$$\tilde{n}_3 = \tilde{K}_{q_p}^{\delta_B}\left[\,_{sp}\left(\frac{1}{\tilde{T}}\right)_{q_p}^{\delta_B} + \,_{f11}\left(\frac{1}{\tilde{T}}\right)_{q_p}^{\delta_B} + \,_{f12}\left(\frac{1}{\tilde{T}}\right)_{q_p}^{\delta_B}\right]$$

$$\tilde{n}_4 = \tilde{K}_{q_p}^{\delta_B}$$

Table 9. Polynomial Coefficient and Factor Difference Relationships

$$\Delta \tilde{d}_1 = \tilde{\omega}_{sp}^2 \, \Delta(\tilde{\omega}^2)_{f1} + (\tilde{\omega}^2)_{f1} \, \Delta(\tilde{\omega}^2)_{sp}$$

$$\Delta \tilde{d}_2 = (2\zeta\omega)_{sp} \, \Delta(\tilde{\omega}^2)_{f1} + (\tilde{\omega}^2)_{f1} \, \Delta(2\zeta\omega)_{sp} + (2\zeta\omega)_{f1} \, \Delta(\tilde{\omega}^2)_{sp} + (\tilde{\omega}^2)_{sp} \, \Delta(2\zeta\omega)_{f1}$$

$$\Delta \tilde{d}_3 = \Delta(\tilde{\omega}^2)_{sp} + \Delta(\tilde{\omega}^2)_{f1} + (2\zeta\omega)_{sp} \, \Delta(2\zeta\omega)_{f1} + (2\zeta\omega)_{f1} \, \Delta(2\zeta\omega)_{sp}$$

$$\Delta \tilde{d}_4 = \Delta(2\zeta\omega)_{sp} + \Delta(2\zeta\omega)_{f1}$$

$$\Delta \tilde{n}_1 = \tilde{K}_{q_p}^{\delta_B} {}_{sp}(\tfrac{1}{\tilde{T}})_{q_p}^{\delta_B} {}_{f11}(\tfrac{1}{\tilde{T}})_{q_p}^{\delta_B} \Delta {}_{f12}(\tfrac{1}{\tilde{T}})_{q_p}^{\delta_B} + \tilde{K}_{q_p}^{\delta_B} {}_{sp}(\tfrac{1}{\tilde{T}})_{q_p}^{\delta_B} {}_{f12}(\tfrac{1}{\tilde{T}})_{q_p}^{\delta_B} \Delta {}_{f11}(\tfrac{1}{\tilde{T}})_{q_p}^{\delta_B}$$

$$+ \tilde{K}_{q_p}^{\delta_B} {}_{f11}(\tfrac{1}{\tilde{T}})_{q_p}^{\delta_B} {}_{f12}(\tfrac{1}{\tilde{T}})_{q_p}^{\delta_B} \Delta {}_{sp}(\tfrac{1}{\tilde{T}})_{q_p}^{\delta_B} + {}_{sp}(\tfrac{1}{\tilde{T}})_{q_p}^{\delta_B} {}_{f11}(\tfrac{1}{\tilde{T}})_{q_p}^{\delta_B} {}_{f12}(\tfrac{1}{\tilde{T}})_{q_p}^{\delta_B} \Delta \tilde{K}_{q_p}^{\delta_B}$$

$$\Delta \tilde{n}_2 = \tilde{K}_{q_p}^{\delta_B} [\, {}_{sp}(\tfrac{1}{\tilde{T}})_{q_p}^{\delta_B} + {}_{f11}(\tfrac{1}{\tilde{T}})_{q_p}^{\delta_B}] \, \Delta {}_{f12}(\tfrac{1}{\tilde{T}})_{q_p}^{\delta_B} + \tilde{K}_{q_p}^{\delta_B} [\, {}_{sp}(\tfrac{1}{\tilde{T}})_{q_p}^{\delta_B} + {}_{f12}(\tfrac{1}{\tilde{T}})_{q_p}^{\delta_B}] \, \Delta {}_{f11}(\tfrac{1}{\tilde{T}})_{q_p}^{\delta_B}$$

$$+ \tilde{K}_{q_p}^{\delta_B} [\, {}_{f11}(\tfrac{1}{\tilde{T}})_{q_p}^{\delta_B} + {}_{f12}(\tfrac{1}{\tilde{T}})_{q_p}^{\delta_B}] \, \Delta {}_{sp}(\tfrac{1}{\tilde{T}})_{q_p}^{\delta_B} + [\, {}_{sp}(\tfrac{1}{\tilde{T}})_{q_p}^{\delta_B} {}_{f11}(\tfrac{1}{\tilde{T}})_{q_p}^{\delta_B}$$

$$+ {}_{sp}(\tfrac{1}{\tilde{T}})_{q_p}^{\delta_B} {}_{f12}(\tfrac{1}{\tilde{T}})_{q_p}^{\delta_B} + {}_{f11}(\tfrac{1}{\tilde{T}})_{q_p}^{\delta_B} {}_{f12}(\tfrac{1}{\tilde{T}})_{q_p}^{\delta_B}] \Delta \tilde{K}_{q_p}^{\delta_B}$$

$$\Delta \tilde{n}_3 = \tilde{K}_{q_p}^{\delta_B} \Delta {}_{f12}(\tfrac{1}{\tilde{T}})_{q_p}^{\delta_B} + \tilde{K}_{q_p}^{\delta_B} \Delta {}_{f11}(\tfrac{1}{\tilde{T}})_{q_p}^{\delta_B} + \tilde{K}_{q_p}^{\delta_B} \Delta {}_{sp}(\tfrac{1}{\tilde{T}})_{q_p}^{\delta_B} + [\, {}_{sp}(\tfrac{1}{\tilde{T}})_{q_p}^{\delta_B} + {}_{f11}(\tfrac{1}{\tilde{T}})_{q_p}^{\delta_B} + {}_{f12}(\tfrac{1}{\tilde{T}})_{q_p}^{\delta_B}] \Delta \tilde{K}_{q_p}^{\delta_B}$$

$$\Delta \tilde{n}_4 = \Delta \tilde{K}_{q_p}^{\delta_B}$$

Table 14. Transfer Functions from Literal Approximations

	$G_{a_z}^{\delta_B}$ (ft/s²/deg)	$G_{q_p}^{\delta_B}$ (rad/s/deg)	$G_{a_z}^{\delta_c}$ (ft/s²/deg)	$G_{q_p}^{\delta_c}$ (rad/s/deg)
gains	46.43	13.06	-241.5	14.06
zeros	0	0	0	0
	$-.1301 \pm j2.039$	$-.2038$	$.1092 \pm j1.834$	$-.1592$
	$1.854 \pm j14.25$	3.497	$-.7248 \pm j4.006$	$-.7430 \pm j2.825$
		-3.946		
poles	0			
	$-.4497 \pm j1.246$			
	$-.4838 \pm j6.050$			

CLOSED-FORM EXPRESSIONS
FOR THESE TERMS

Specifically, it has been shown that for a slender (low aspect ratio) vehicle

$$\omega_{sp}^{*2} - \omega_{sp}^2 = \frac{(U_o + Z_q) M_{\eta_1} F_{1_w}}{(\omega_1^2 - F_{1_{\eta_1}}) + (U_o + Z_q) M_w}$$

$$\omega_{1_E}^2 - \omega_{\theta_1}^2 = \frac{(U_o + Z_q) M_{\eta_q} F_{1_w}}{(\omega_1^2 - F_{1_{\eta_a}}) + (U_o + Z_q) M_w} - M_{\eta_1} F_{1\delta}/M_\delta$$

$$2\xi_{E_1}\omega_{E_1} = (2\xi_1\omega_1 - F_{1_{\dot{\eta}_1}}) + \frac{Z_{\eta_1} F_{1_w} + M_{\eta_1} F_{1_q}}{(\omega_1^2 - F_{1_{\eta_1}}) + (U_o + Z_q) M_w}$$

74)

FURTHERMORE, IT CAN BE SHOWN

For Example, That

$$M_{\eta_i} = \frac{1}{2}\,\rho V^2 S\bar{c}C_{m_{\eta_i}}$$

$$C_{m_{\eta_i}} = \frac{1}{S\bar{c}}\left\{\int_{-b/2}^{b/2} c_{l_{\alpha_w}}\left(\frac{\Delta x_w}{c_w}\right)\left(\frac{d\phi_i}{dx}\right)_w c_w^2 dy_w + C_{L_{\alpha_c}}\left(\frac{\Delta x_c}{\bar{c}}\right)\left(\frac{d\phi_i}{dx}\right)_c S_c\bar{c}\right\}$$

where

$$c_{l_{\alpha_w}} = \text{wing section lift–curve slope}$$

$$\left(\frac{d\phi_i}{dx}\right)_{(\cdot)} = \text{mode i slope at location } (\cdot)$$

SUMMARY

- Key Issues In Feedback Systems Reviewed

- Physics Of Model Uncertainty Addressed

- Mode Frequencies Near Crossover ⎫
⎬ Purely Elastic
- Mode Shapes And Dipoles ⎭

- With Aeroelastic Coupling, Both Affected

- Closed-Form Expressions Developed To Show Sources Of Interactions

- Sensitivity To Uncertainty In These Parameter May Be Further Explored

743

EXPERIMENTAL VALIDATION OF FLEXIBLE ROBOT ARM MODELING AND CONTROL

OUTLINE

- **INTRODUCTION**
  Motivation
  Background

- **MODEL EVALUATION**
  Formulation
  Results

- **CONTROLLER EVALUATION**
  Formulation
  Results

- **SUMMARY AND CONCLUSIONS**

M A. Galip Ulsoy

Mechanical Engineering and Applied Mechanics
College of Engineering
University of Michigan

INTRODUCTION

- Flexibility is important for high speed, high precision operation of lightweight manipulators.
- Accurate dynamic modeling of flexible robot arms is needed. Previous work has mostly been based on linear elasticity with prescribed rigid body motions (i.e., no effect of flexible motion on rigid body motion).
- Little or no experimental validation of dynamic models for flexible arms is available. Experimental results are also limited for flexible arm control.
- We include the effects of prismatic as well as revolute joints.
- We investigate the effect of full coupling between the rigid and flexible motions, and of axial shortening.
- We also consider the control of flexible arms using only additional sensors.

746

BACKGROUND

Research since 1970's
   (e.g., [Book, Maizzo-Neto, Whitney 75])

Modeling of flexible mechanisms and structures
   (e.g., Elasto-Kineto Dynamics, Floating
   Frames, 70's)

Approaches to control
   Trajectory planning [Meckl, Seering 83,85]
   Open loop (none)
   Closed loop with micromanipulator
      [Cannon et al, Book et al]
   Closed loop with additional sensors only (none)

Experimental work
   [Zalucky and Hardt 84]
   [Cannon et al 83, 84]

Theoretical control studies
   [Book et al, Cannon et al, etc, early 1980's]
   Various control strategies proposed typically
   assuming all states available, no spillover, simple
   models, no implementation considerations.

MODELING AND SIMULATION OF FLEXIBLE ROBOTS WITH PRISMATIC JOINTS

- Robots with both rigid and flexible links attached with revolute and/or prismatic joints can be modeled and analyzed.
- The equations of motion are derived using Lagrange's equations. The prescribed motion, and prescribed torque/force cases can both be handled.
- Flexible elements are represented as Euler-Bernoulli beams, and the axial shortening effect is also included.
- Finite element analysis is used for the discretization of the resulting hybrid equations of motion.
- Constraints are handled using Lagrange multipliers.
- The resulting algebraic-differential equations are solved numerically using constraint stabilization methods.
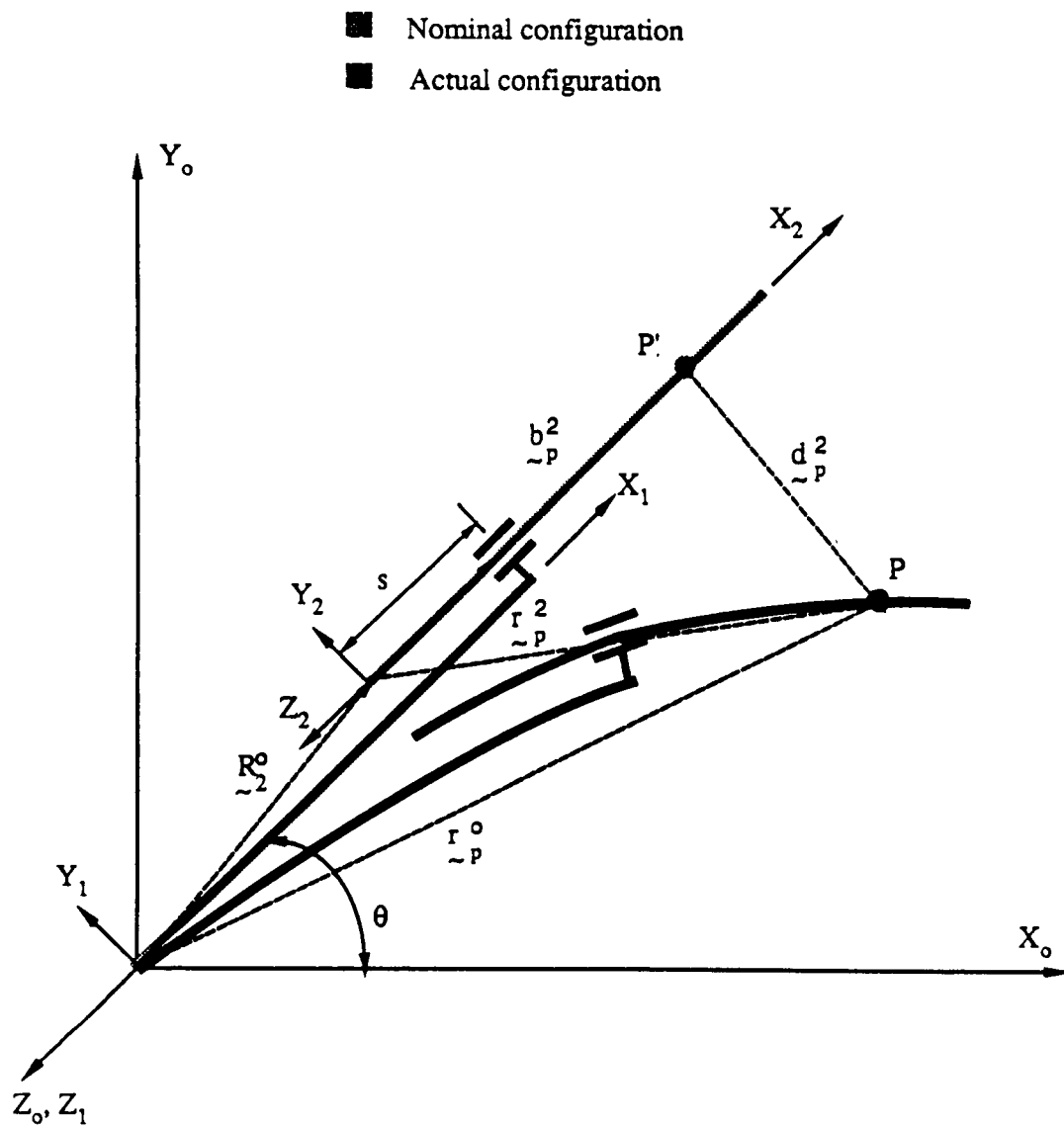
Schematic of a two-link robot.

749
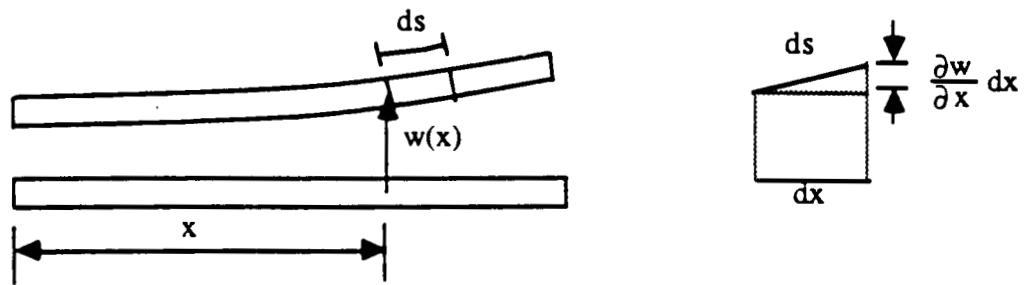
Axial shortening of a beam under plane transverse deflection.
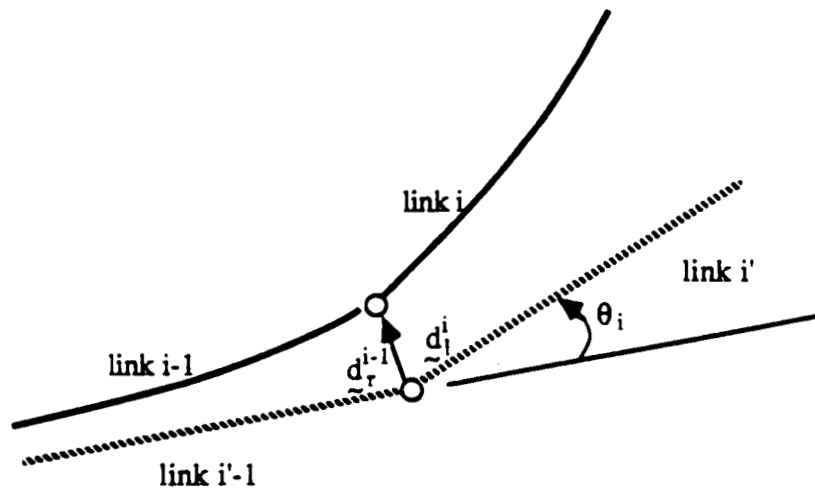
Schematic of revolute joint i.

750
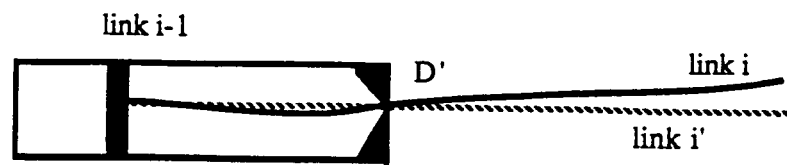
Schematic of prismatic joint i.

Schematic of prismatic joint i.

751
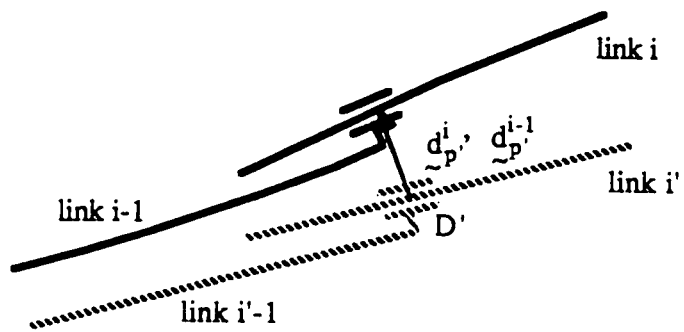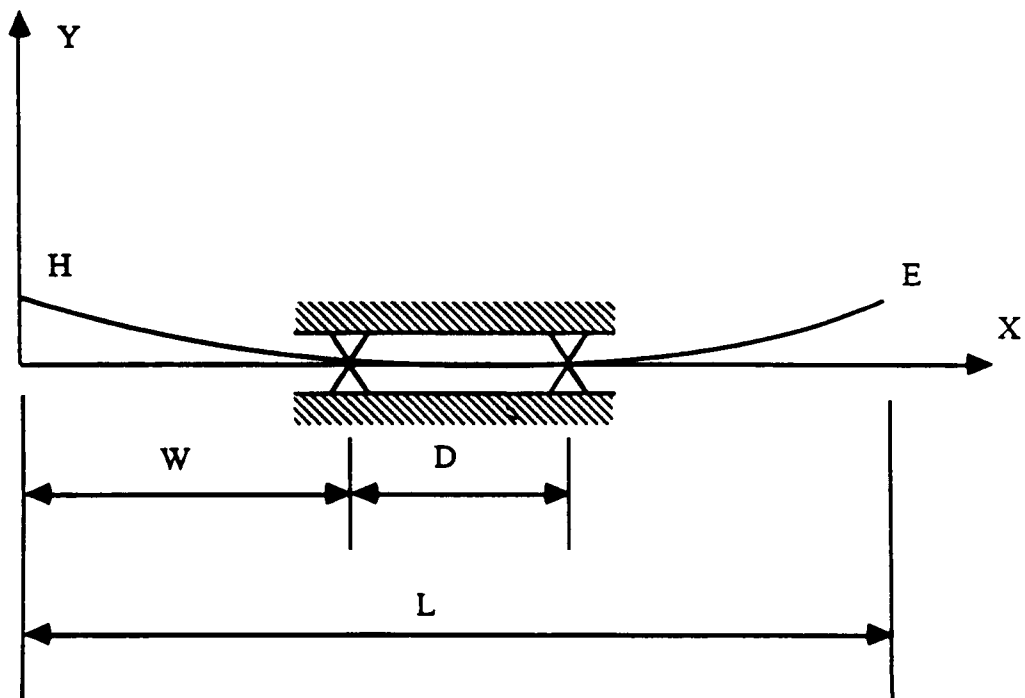
Beam moving over bilateral supports.
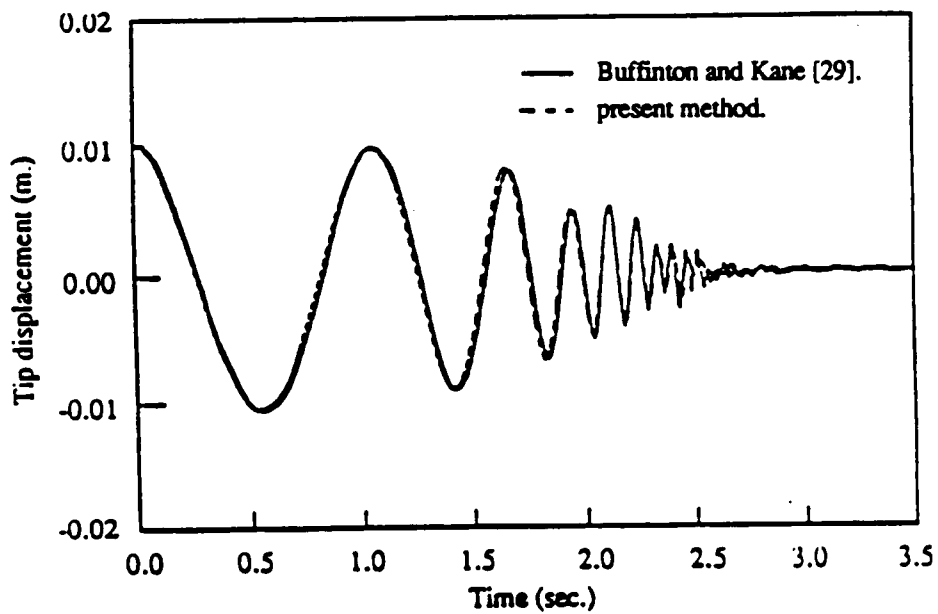
Tip displacement in "slow push" case with
$C_1 = 0.725$ m, $C_2 = 0.7$ m and T = 3.5 sec.

752
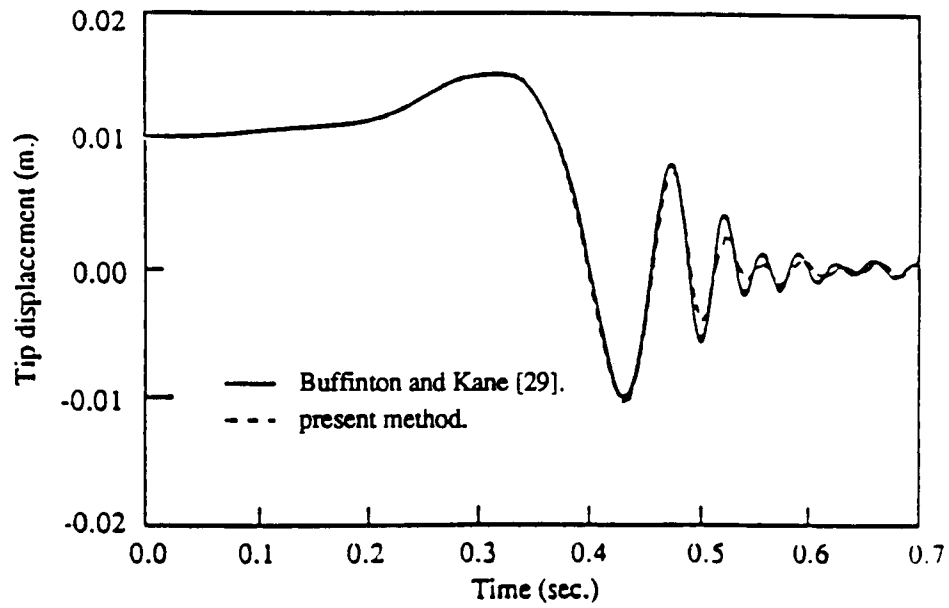
Tip displacement in "fast push" case with
$C_1 = 0.725$ m, $C_2 = 0.7$ m and T = 0.7 sec.
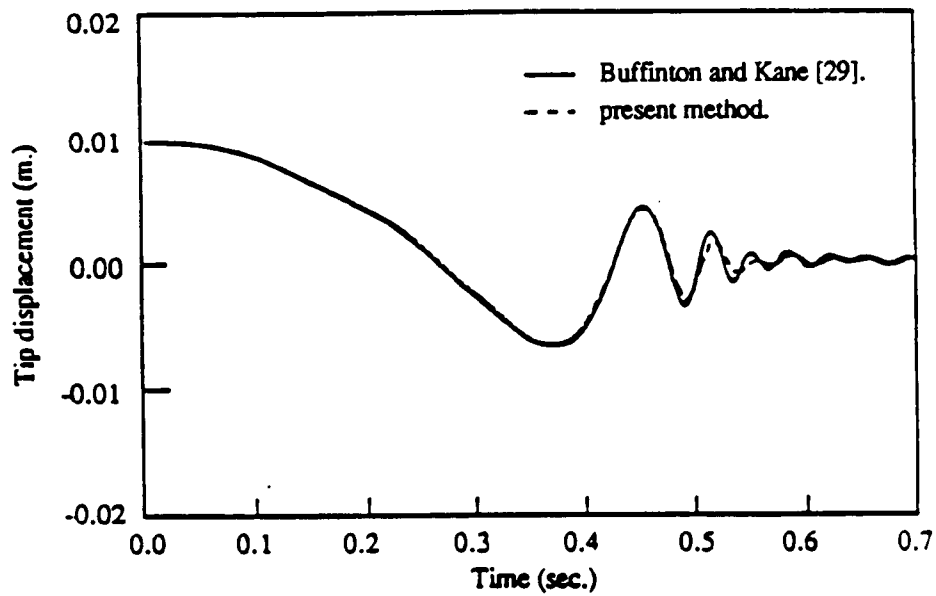
Tip displacement in "fast pull" case with
$C_1 = 0.025$ m, $C_2 = -0.7$ m and T = 0.7 sec.

753

LABORATORY ROBOT

Small table top spherical coordinate robot with 3 DOF

Designed and built at UM

Interfaced to an IBM PC/XT

Convienent test bed experimental research work

r and θ axes are dc motor driven through leadscrews

ϕ axis is dc motor driven driven through a gear train

all axes have tachometers and optical incremental
   encoders with counter circuits

last link is intentionally designed to be flexible

accelerometers (in two orthogonal directions)
   measure end of arm accelerations which are
   integrated to get velocities and positions

754
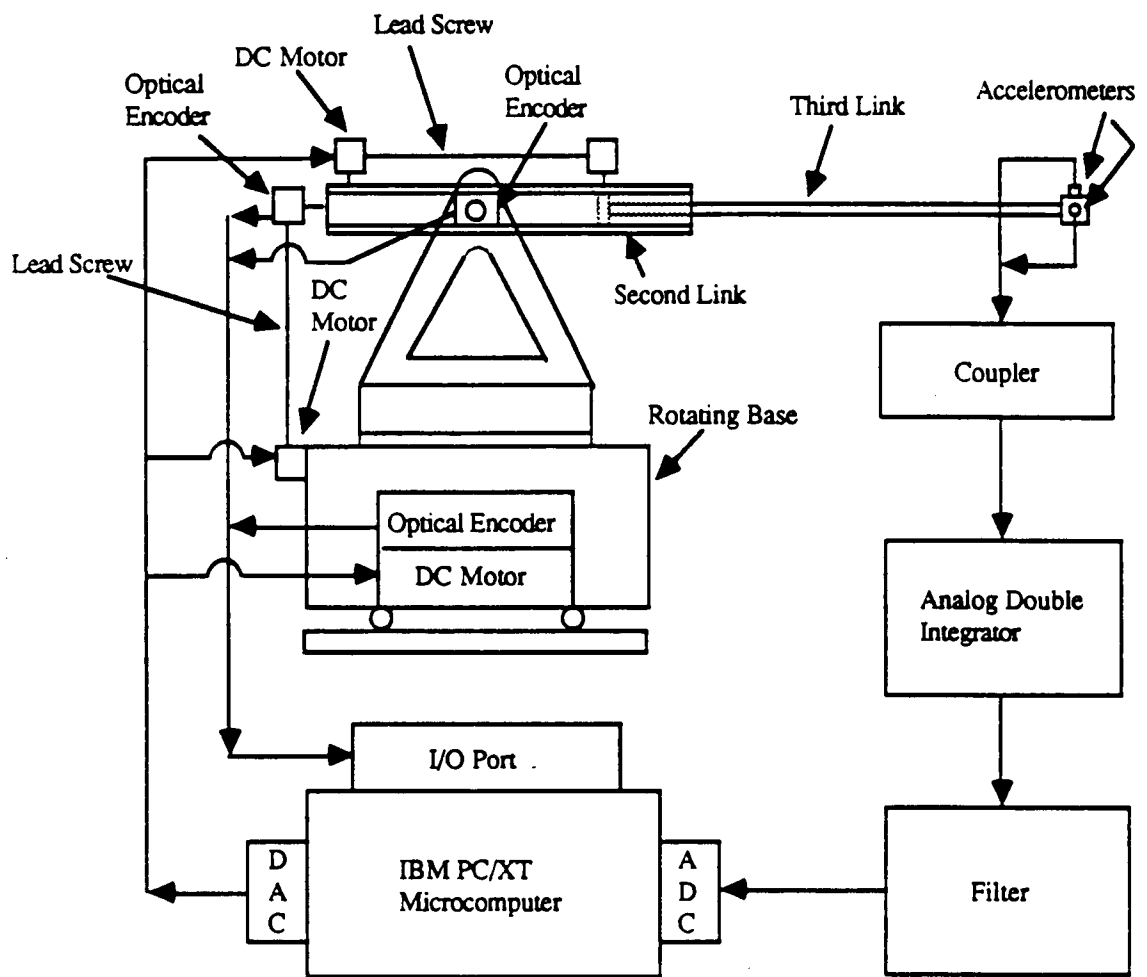
Schematic of the experimental setup.

755
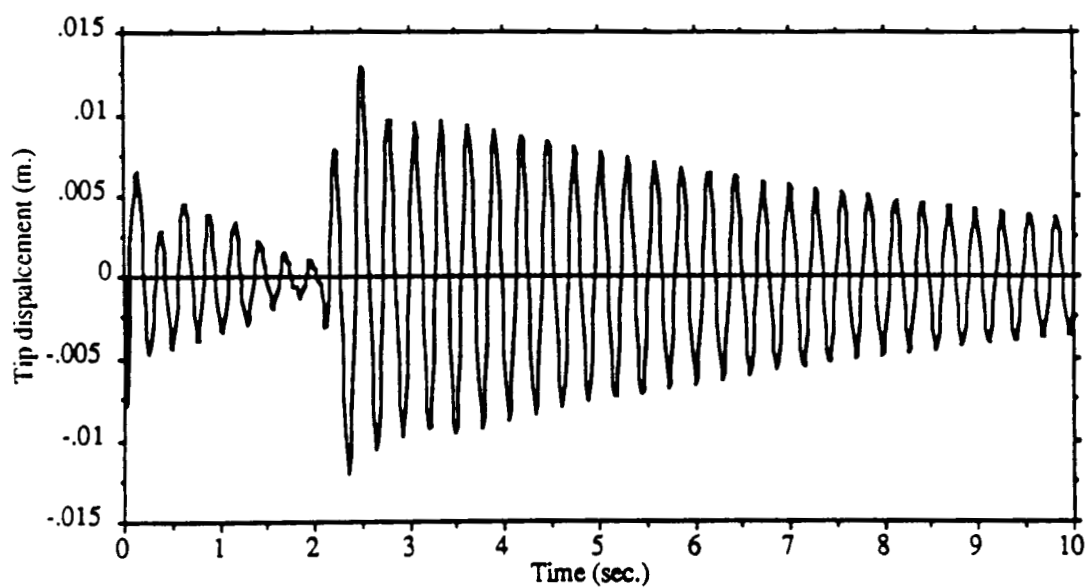
Elastic tip displacement obtained by numerical simulation after filtering.
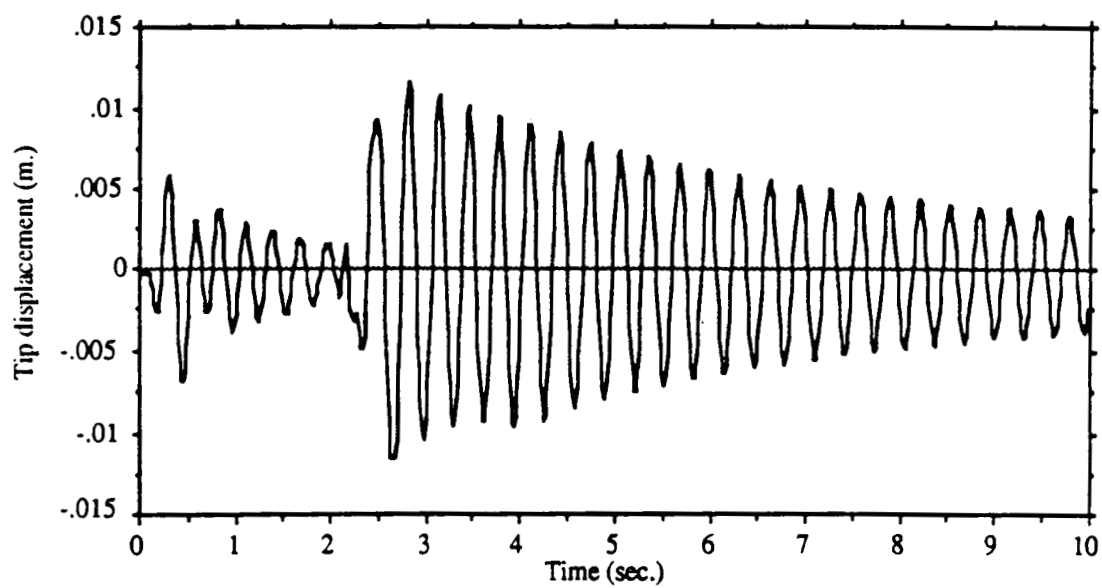
Vertical elastic tip displacement of the last link in the two-dimensional maneuver.

756
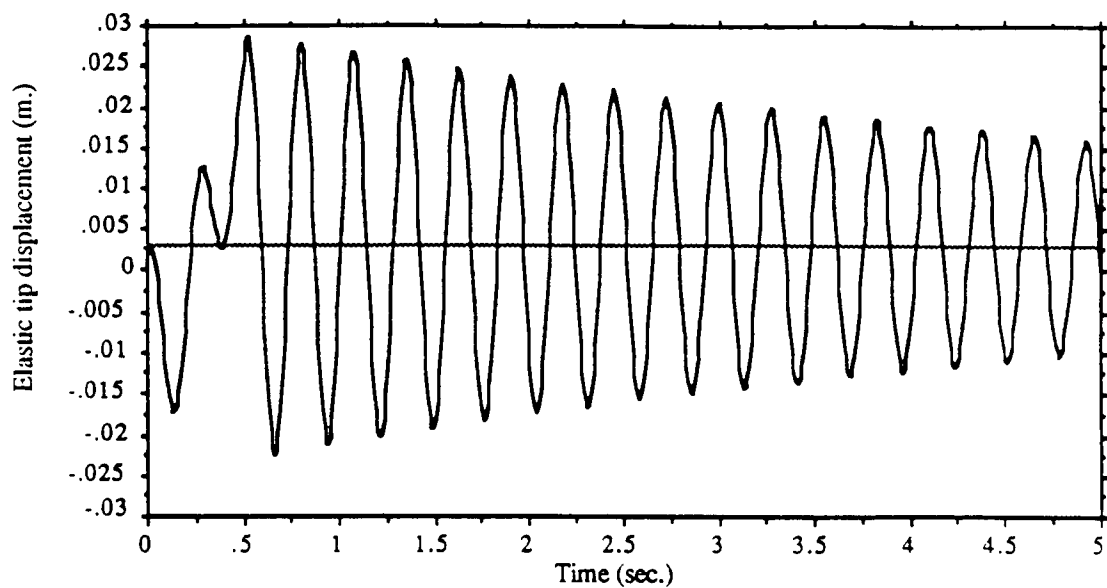
The elastic tip displacement obtained from the equations of motion with prescribed motions.
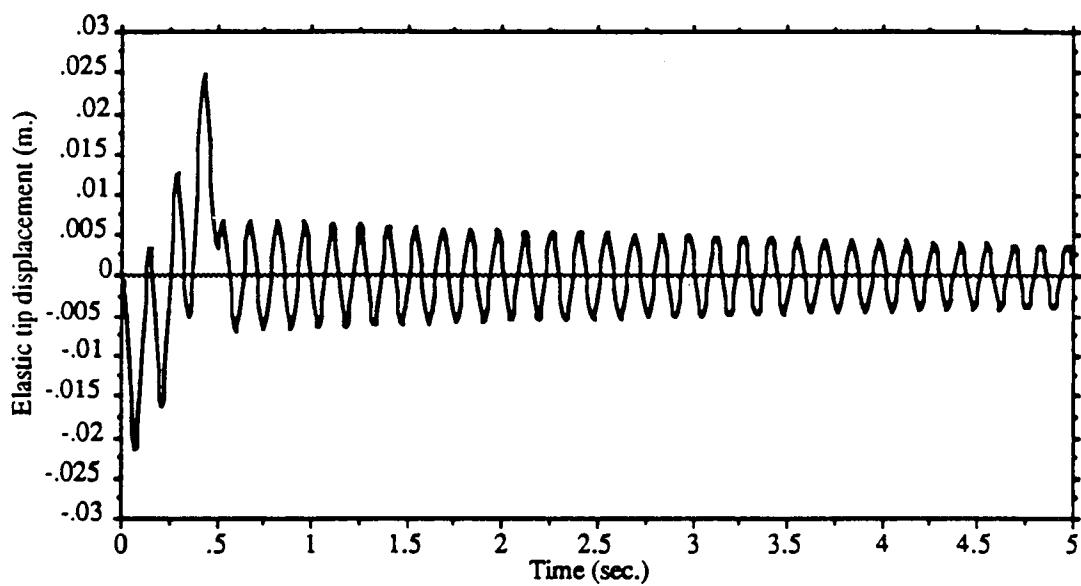
Elastic tip displacement obtained from the equations of motion

with prescribed torque/force.
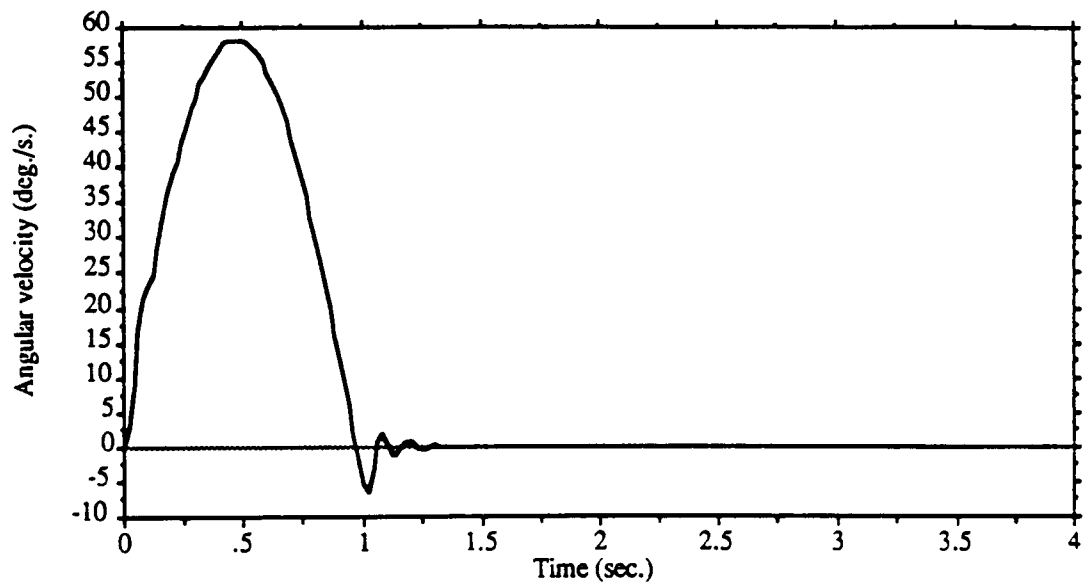
Angular velocity of the first joint of the rigid manipulator
with controller.
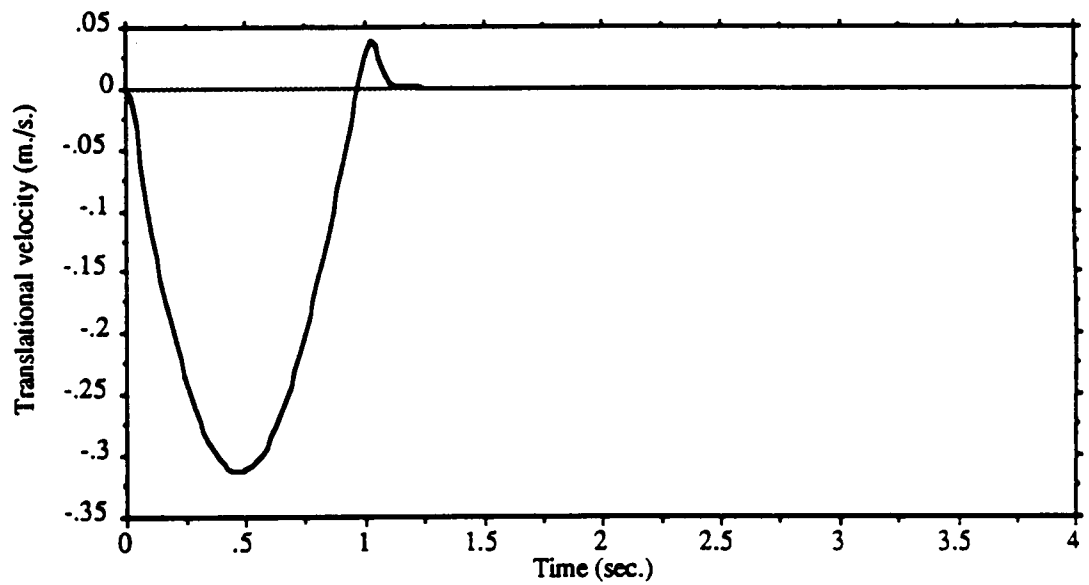
Translational velocity of the third joint of the rigid manipulator
with controller.

758
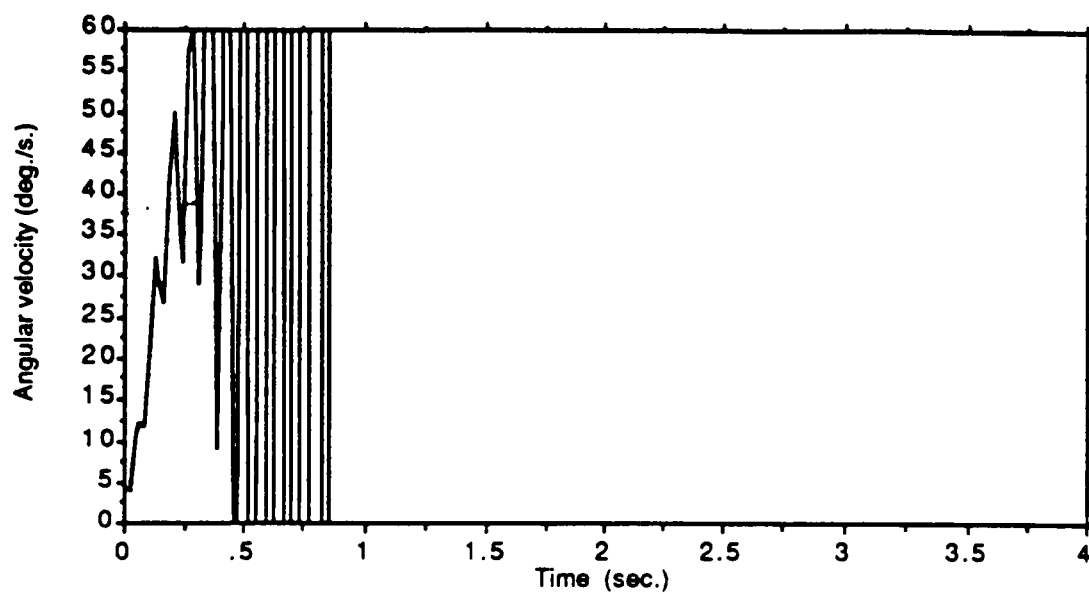
Angular velocity of the first joint of the flexible manipulator
with controller.
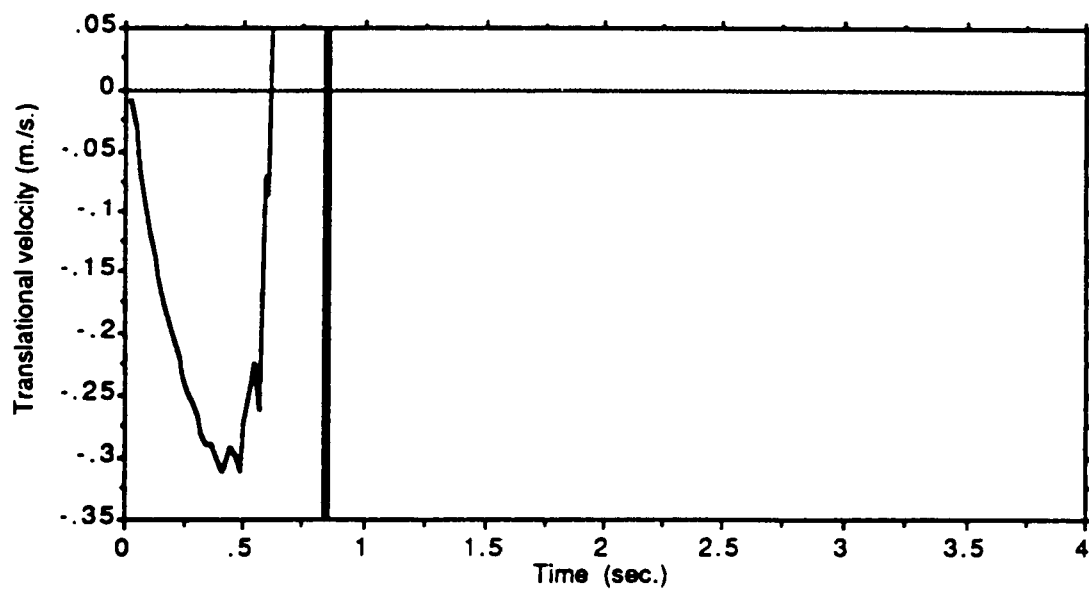
Translational velocity of the third joint of the flexible manipulator
with controller.

759
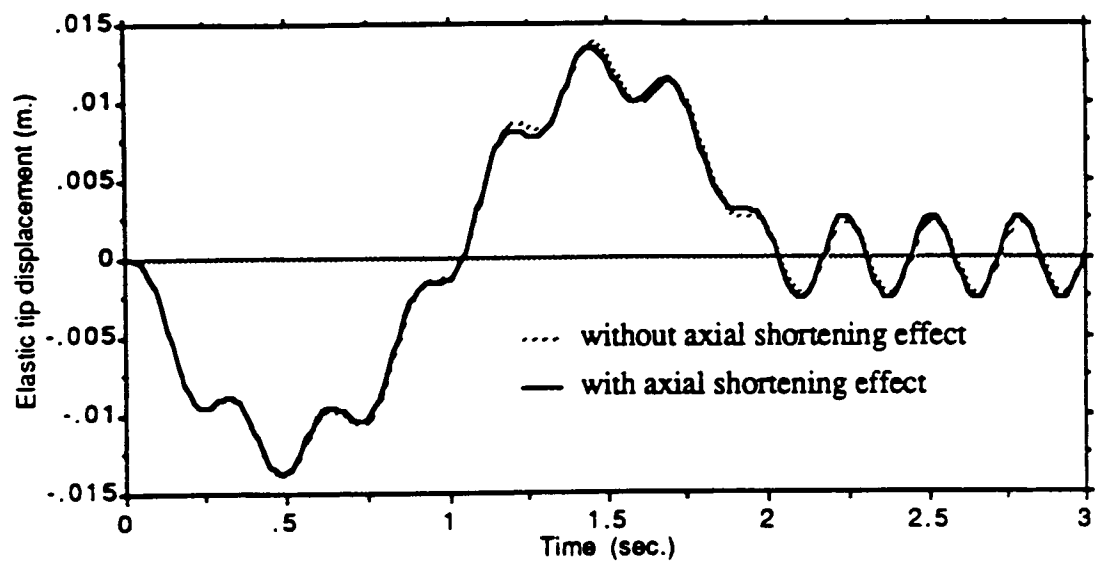
Elastic tip displacements in the case with T = 2 sec.
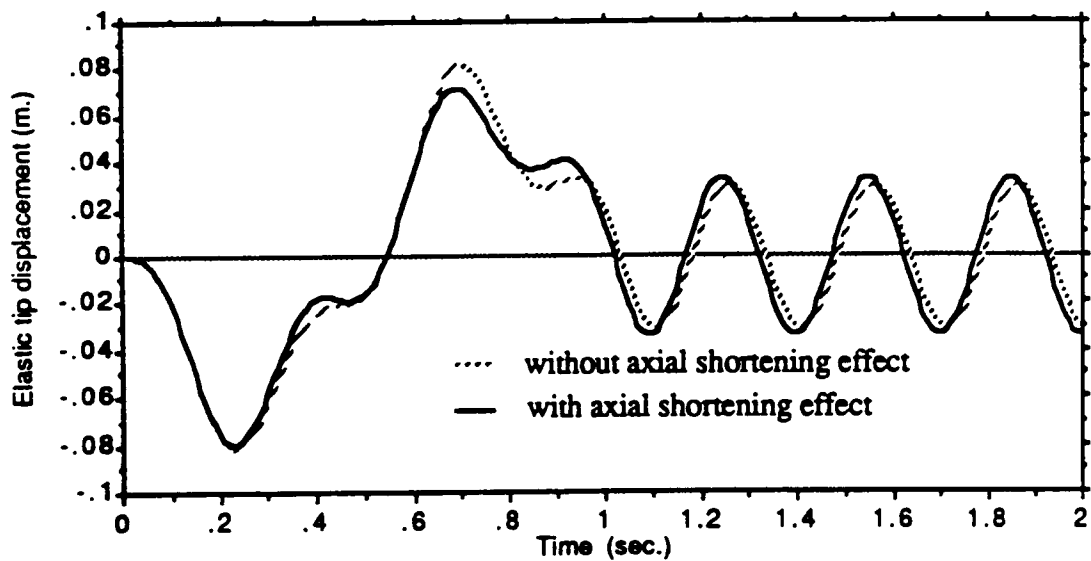
Elastic tip displacement in the case with T = 1 sec.

760

SUMMARY AND CONCLUSIONS

- A general modeling procedure for robot arms consisting of rigid and flexible links connected by revolute and/or prismatic joints has been developed and experimentally validated.
- The significance of full coupling (effect of flexible motion on rigid body motion) has been demonstrated.
- The axial shortening effect is shown to be significant for high speed operation of lightweight manipulators.

CONTROL OF A LEADSCREW DRIVEN FLEXIBLE ROBOT ARM

• The laboratory robot is used to compare the performance of a rigid body motion controller with that of a rigid and flexible motion controller.

• The rigid body motion controller uses only the joint motion measurements and joint actuators. The rigid and flexible motion controller also uses the end of arm motion measurements, but no additional actuators.

• The leadscrew transmission characteristics as well as observation and control spillover are considered.

• The numerical and experimental results show good agreement, and indicate that significant reductions in arm vibration are possible through use of the rigid and flexible motion controller.
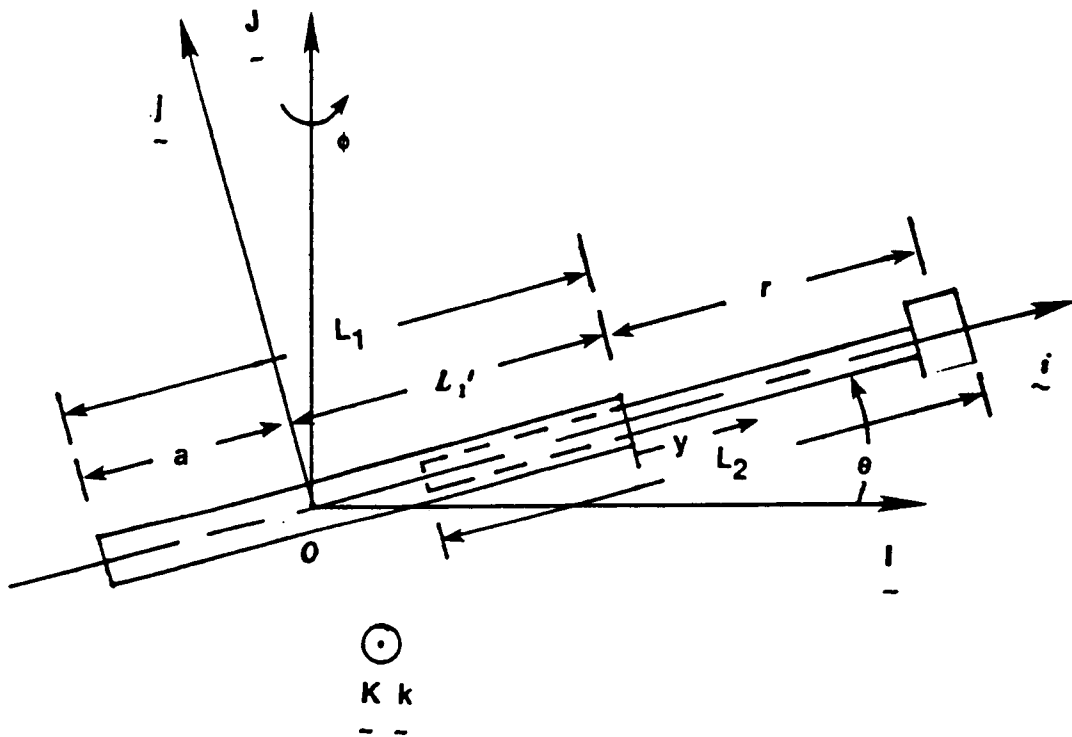
Arm geometry and coordinates.

763

PHYSICAL CONSTRAINTS

The physical constraints that are considered in this work are the ones imposed by the leadscrews only.

. Condition for self locking assumption to be valid is:

$$\mu > \tan(\psi_1)$$

where

μ is the thread coefficient of friction.

ψ_1 is the thread helix angle.

. Effect of the self locking condition.

. Effect of coulomb friction.

764

CONTROLLER DESIGN

Equations of motion:

$$\underline{M}(\underline{x})\,\ddot{\underline{x}} + \underline{F}(\underline{x},\dot{\underline{x}}) = \underline{F}'(\underline{T})$$

$$\underline{x}^T = [\, r,\, \theta,\, \phi,\, g_{11},\, g_{12},\, g_{21},\, g_{22}\,]$$

$$\underline{T}^T = [\, T_1,\, T_2,\, T_3\,]$$

Linearized equations:

$$\dot{\underline{y}} = \underline{A}\,\underline{y} + \underline{B}\,\underline{u}$$

$$\underline{y}^T = [\, \delta\underline{x}^T \quad \delta\dot{\underline{x}}^T\,] \quad ; \quad \underline{u} = \delta\underline{T}$$

$$\delta\underline{x}^T = [\, \delta r,\, \delta\theta,\, \delta\phi,\, \delta g_{11},\, \delta g_{21}\,]$$

Integral plus state feedback controller:

$$y_{11} = \int_0^t (y_1 - R_1)\,dt \;\; ; \;\; y_{12} = \int_0^t (y_2 - R_2)\,dt \;\; ; \;\; y_{13} = \int_0^t (y_3 - R_3)\,dt$$

$$\underline{u} = -\underline{K}^F\,\underline{y}$$

$$\dot{\underline{y}} = (\underline{A} - \underline{B}\underline{K}^F)\,\underline{y}$$

765
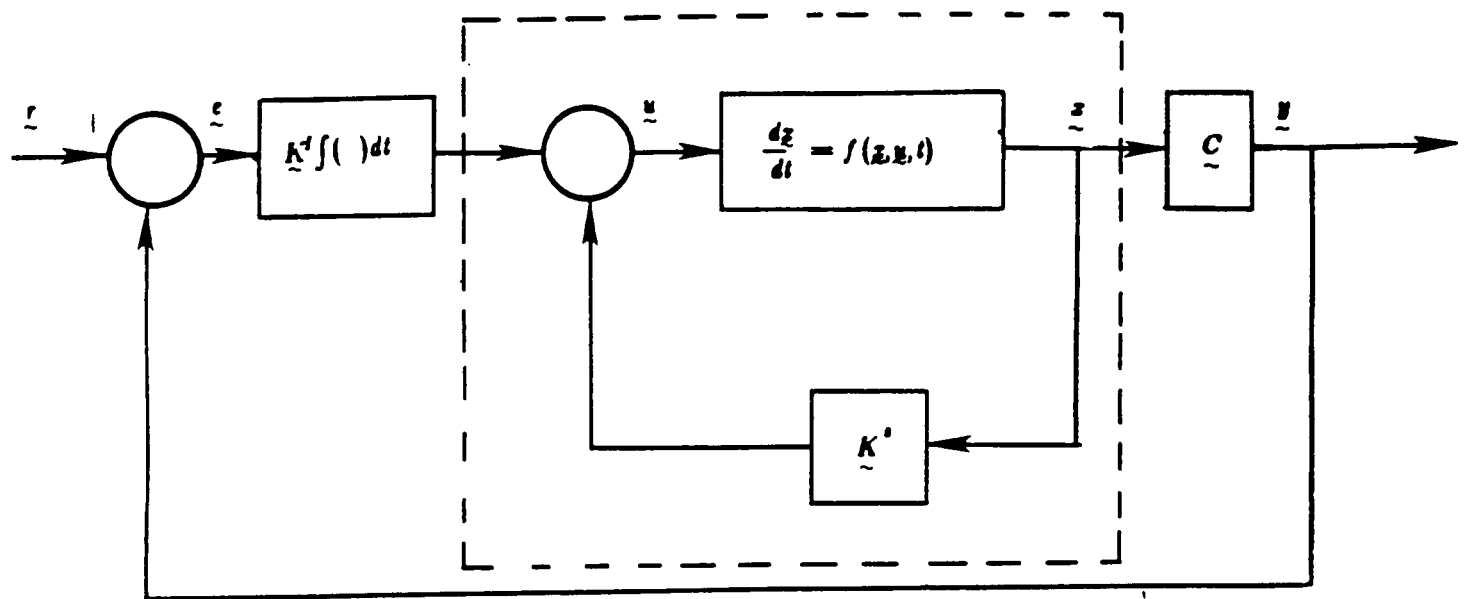
Block diagram of the integral plus state feedback controller.

Figure 3. Flexible motion coordinate, $q_{11}(t)$, in response to the rigid and flexible motion controller in the reduced order model case.

Figure 4. Flexible motion coordinate, $q_{21}(t)$, in response to the rigid and flexible motion controller in the reduced order model case.

767

Displacement
$q_{11}(t)$ (meter)
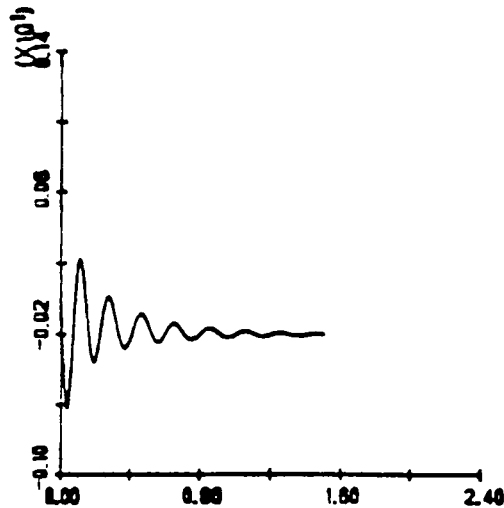
Time, t (second)

Figure 5.   Flexible motion coordinate, $q_{11}(t)$, in response to the rigid and flexible motion controller in the control spillover case.

Displacement
(meter)
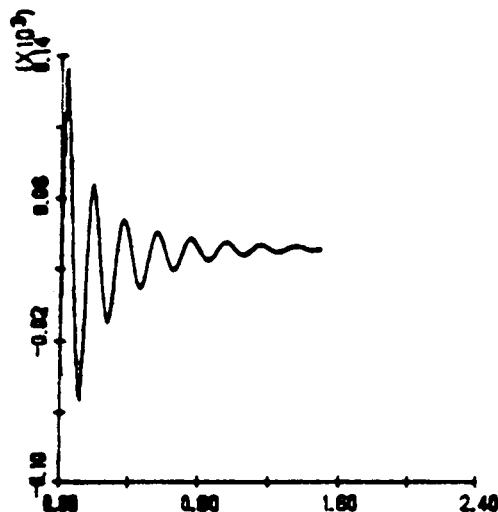
Time, t (second)

Figure 6.   Flexible motion coordinate, $q_{12}(t)$, in response to the rigid and flexible motion controller in the control spillover case.

768
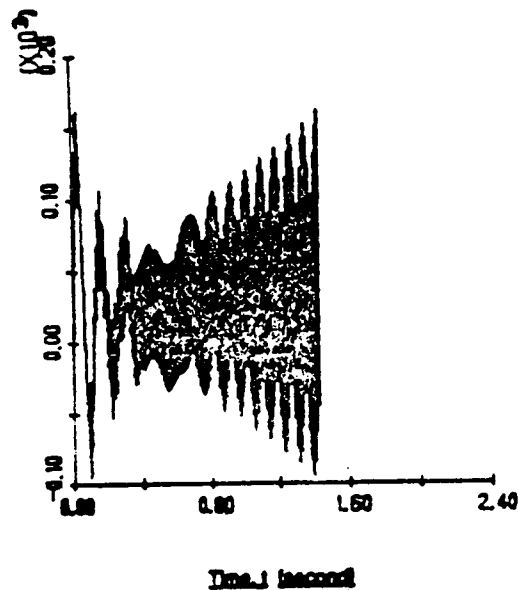
Figure 7. Flexible motion coordinate, $q_{12}(t)$, in response to the rigid and flexible motion controller in the control and observation spillover case.
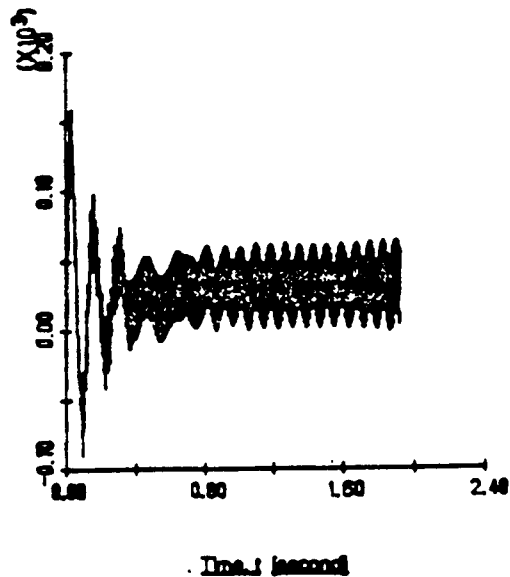
Figure 8. Flexible motion coordinate, $q_{12}(t)$, in response to the rigid and flexible motion controller in the control and observation spillover with structural damping included.

769

Standard Set of Physical System Parameters	VALUE
Mass of the first beam (m_1)	0.454 Kg
Mass of the second beam (m_2)	0.816 Kg
Mass of the Payload (m_p)	0.07 Kg
Cross sectional area of the second beam (A_2)	0.000151 m^2
Length of the first beam (L_1)	0.233 m
Length of the second beam (L_2)	2 m
Gravitational acceleration (g)	9.81 m/sec^2
Aluminum density (ρ)	2707 Kg/m^3
Flexural rigidity (EI)	770.87 Pa
Reference position for r	1.85 m
Reference position for θ	0 rad
Reference position for ϕ	0 rad
Desired reference position for r	2m
Desired reference position for θ	0.5 rad
Desired reference position for ϕ	0.5 rad
Servo natural frequency for r (ω_{nr})	4 rad/sec
Servo natural frequency for θ ($\omega_{n\theta}$)	4 rad/sec
Servo natural frequency for ϕ ($\omega_{n\phi}$)	8 rad/sec
Flexible motion gain, K^f_{19}	-0.000178
Flexible motion gain, K^f_{29}	-0.084
Flexible motion gain, $K^f_{4,10}$	1.568

TABLE 1

	settling time (seconds)	maximum deflection (peak to peak)
rigid body controller	11.0	7.5mm
rigid and flexible motion controller	3.0	2.7mm

Table 2.

770
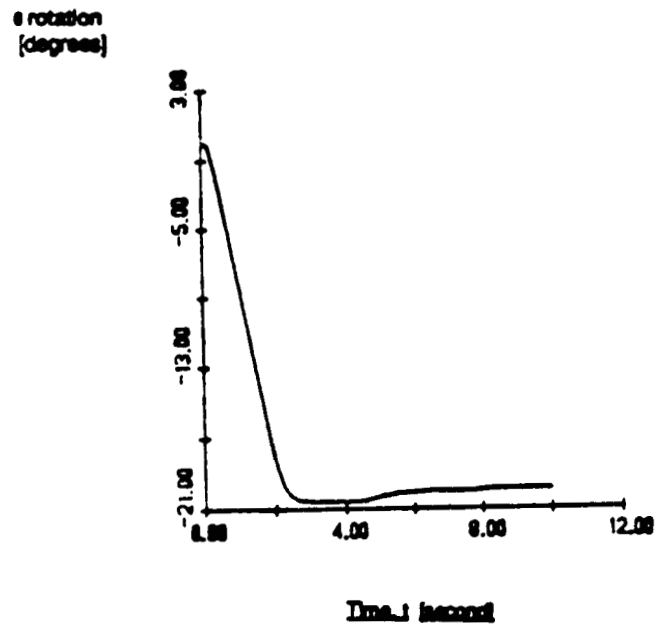
Figure 10. θ response obtained from the rigid body controller in the experimental work.
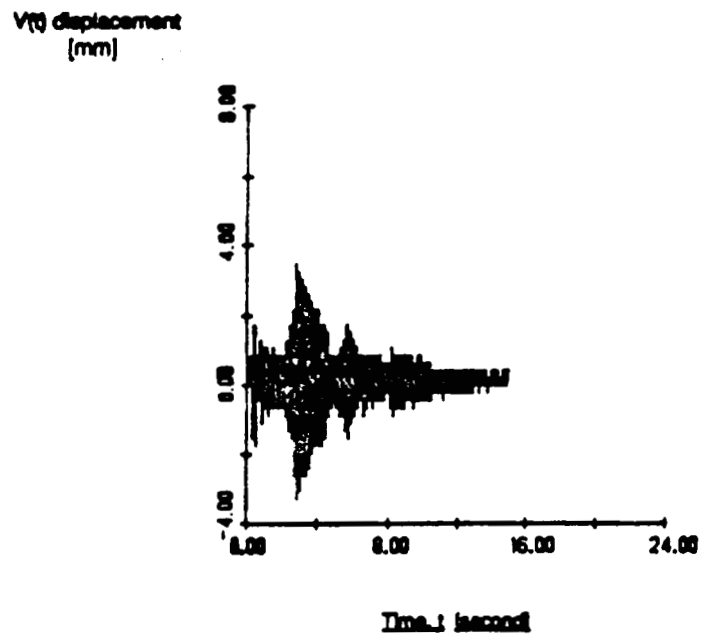
Figure 11. Total vertical deflection in response to the rigid body controller in the experimental work.
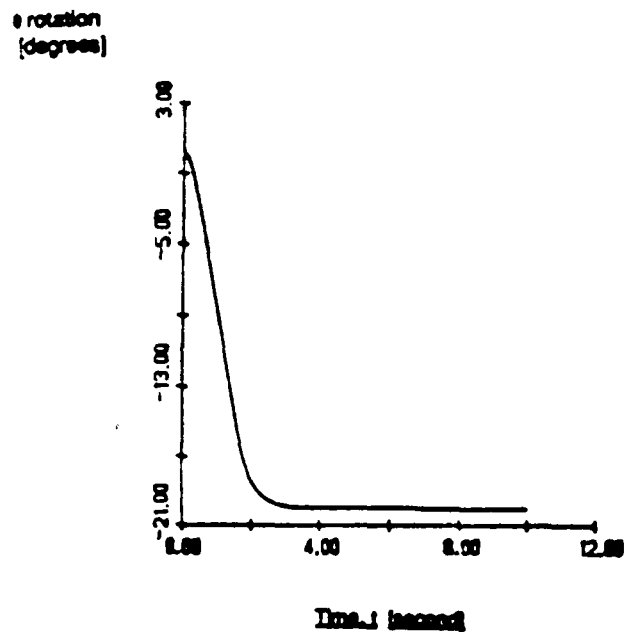
Figure 12. θ response obtained from the rigid and flexible motion controller in the experimental work.
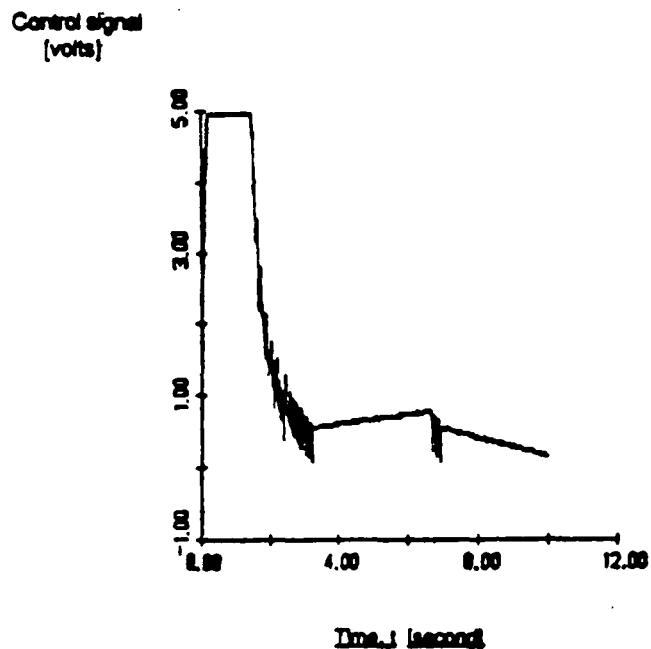
Figure 13. Control signal for the second joint obtained from the rigid and flexible motion controller in the experimental work.
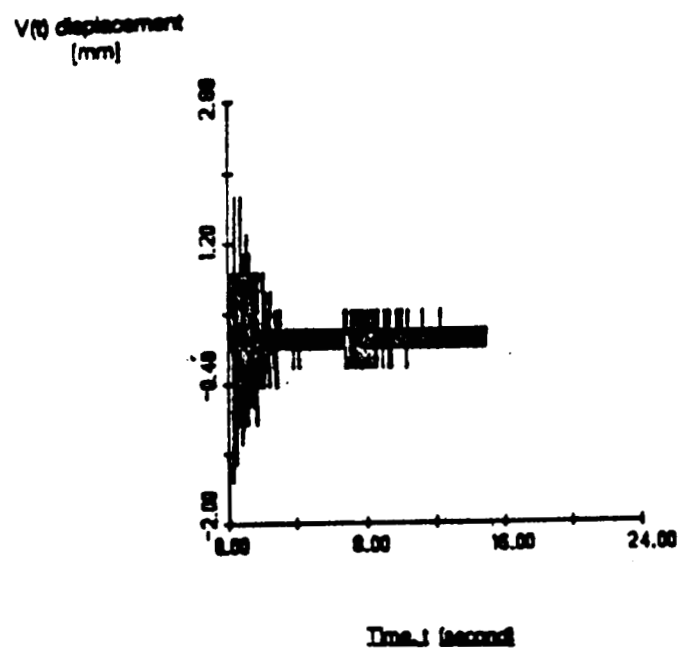
Figure 14. Total vertical deflection in response to the rigid and
flexible motion controller in the experimental work.

RIGID BODY CONTROLLER VERSUS
RIGID AND FLEXIBLE MOTION CONTROLLER

Simulation results:

* Control spillover effect can be observed, but does not cause significant deterioration.

* Control and observation spillover can destabilize the residual mode. However, a small amount of damping (0.0145) eliminates the problem.

* Settling time is reduced from 3.5 to 1.07 seconds, and maximum vibration amplitude is reduced by 50%.

Experimental results:

* With low pass filtering and light structural damping, no detrimental spillover effects were observed.

* Settling time is reduced from 11 to 3 seconds, and maximum vibration amplitude is reduced by 75%.

SUMMARY AND CONCLUSIONS

1. A dynamic model of a spherical coordinate robot arm, whose last link is flexible, is developed. The constraints imposed by the leadscrew transmission mechanisms are also considered.

2. The interrelationships between the robot arm structural flexibility and the controller design are investigated using a rigid body controller.

3. The rigid and flexible motion controller, which employs additional sensors only, has led to an approximate 50% reduction in the magnitude of the flexible motion even in the presence of the observation and control spillover.

4. The experimental results of the rigid and flexible motion controller show good agreement with those of the digital simulation.

SUMMARY AND CONCLUSIONS

- A general modeling method for robot arms with flexible and rigid links connected by prosmatic and revolute joints has been presented and experimentally validated.

- A flexible arm controller which uses end of arm motion meaurements, but only joint actuators has been numerically and experimentally studied and found to give good rigid body control with significant reduction in end of arm vibrations.

M

A. Galip Ulsoy

Mechanical Engineering and Applied Mechanics
College of Engineering
University of Michigan

REFERENCES
(available upon request from A.G. Ulsoy)

- *Dynamics of Flexible Mechanisms with Prismatic Joints*, Ye-Chen Pan, Ph.D. Dissertation, Mechanical Engineering and Applied Mechanics, University of Michigan, Ann Arbor, Michigan, April 1988.
- "Dynamic Modeling and Simulation of Flexible Robots with Prismatic Joints, Part I: Modeling and Solution Method," Y.C. Pan, R.A. Scott, and A.G. Ulsoy, (in preparation).
- "Dynamic Modeling and Simulation of Flexible Robots with Prismatic Joints, Part II: Experimental Validation and Numerical results," Y.C. Pan, A.G. Ulsoy, and R.A. Scott, (in preparation).
- *Control of a Leadscrew Driven Flexible Robot Arm*, Nabil G. Chalhoub, Ph.D. Dissertation, Mechanical Engineering and Applied Mechanics, University of Michigan, Ann Arbor, Michigan, June 1986.
- "Dynamic Simulation of a Leadscrew Driven Flexible Robot Arm and Controller," N.G. Chalhoub and A.G. Ulsoy, *ASME Journal of Dynamic Systems, Measurement and Control*, Vol. 108, No. 2, June 1986, pp 119-126.
- "Control of a Flexible Robot Arm: Experimental and Theoretical Results", N.G. Chalhoub, and A.G. Ulsoy, *ASME Journal of Dynamic Systems, Measurement, and Control*, Vol. 109, No. 4, December 1987, pp 299-309.
- "Dynamic Modeling of a Self-Locking Leadscrew and Its Implications in Robotics," N.G. Chalhoub and A.G. Ulsoy, *ASME Journal of Dynamic Systems, Measurement and Control* (submitted).

CONTROLLING FLEXIBLE STRUCTURES - A SURVEY OF METHODS

By

A. A. Anissipour, R. A. Benson, and E. E. Coleman
The Boeing Company
Seattle, Washington

ABSTRACT

In response to the demand for higher fuel efficiency, new jet transport designs are using composites to reduce weight. Since these composites have less inherent damping than the materials they are replacing, flexible body dynamics are becoming more significant. Low frequency structural modes that in the past had sufficient open loop damping to avoid stability and ride performance problems now require compensation. Control law design can no longer be concerned solely with rigid-body dynamics.

Control systems design techniques which have proven effective for rigid dynamics may no longer be applicable when including flexible modes. This paper studies the different control strategies and their application to systems including flexible dynamics. The control law design goal with respect to flexible modes is twofold. First, the modal damping must be increased to some minimum acceptable level. Second, the rigid body modes must be controlled while minimizing excitation of the flexible modes. A necessary, and often nontrivial first step is identification of the flexible modes (both mode frequency and shape). The following addresses these issues with respect to a particular control law design technique.

1) Off-line Modeling/Off-line Controller Design

The off-line modeling controller design technique has been used historically as the standard for airplane control system design. This technique consists of building up a model on mathematical prediction, wind tunnel analysis, and flight test data. Controllers are then designed off-line based on the model. Controller implementation may include scheduling based on flight condition, but with no on-line modifications made to the controller.

2) Off-line Modeling/On-line Controller Design

The same type of model used for the previous technique is developed using the off-line modeling/on-line controller design with the primary difference being that the controller structure is defined off-line, while the controller gains are adapted on-line to minimize certain performance criteria. With this technique no attempt is made to model the open loop system on-line, and all controller gain changes are made solely in response to performance criteria.

779

3) On-line Modeling/Off-line Design

On-line modeling/off-line design technique defines the controller in terms of a general open loop system model for a specified structure. With this technique each controller gain is defined as a function of model parameter values. Implementation is executed by building an on-line adaptive open loop estimator. The controller gains are then set based on the model estimate values per the definitions developed off-line.

4) Off-line Modeling/Off-line Controller/On-line Adjustment

The control law is designed using the off-line modeling/off-line controller to stabilize the nominal plant. With this technique an adaptive loop is placed around the system, creating an adaptive system that tunes the control input to improve the off-nominal performance. This adaptive loop is designed to never destabilize the nominal plant and when the plant is at nominal, the adaptive control signal is zero.

CONTROLLING FLEXIBLE STRUCTURES - A SURVEY OF METHODS

RUSSELL A. BENSON
EDWARD E. COLEMAN

The Boeing Company
Boeing Commercial Airplanes
P. O. Box 3707
Seattle, Washington 98124-2207

ABSTRACT

Most of the presently available control system design techniques applicable to flexible structure problems were developed to design controllers for rigid body systems. Although many of these design methods can be applied to flexible dynamics problems, recently developed techniques may be more suitable for flexible structure controller design. The purpose of this presentation is to examine briefly the peculiarities of the dynamics of flexible structures and to stimulate discussion about top level controller design approaches when designing controllers for flexible structures.

This presentation contains a suggestion of a set of categories of design methods for designing controllers for flexible structures as well as a discussion of the advantages and disadvantages of each category. No attempt has been made herein to select one category of design techniques as the best for flexible structure controller design. Instead, it is hoped that the structure suggested by these categories will facilitate further discussion on the merits of particular methods that will eventually point to those design techniques suitable for further development.

CHARACTERISTICS OF FLEXIBLE STRUCTURE DYNAMICS

Flexible structure dynamics tend to differ from rigid body dynamics in several important ways. First, flexible dynamics are higher order than rigid body dynamics. By definition, rigid body dynamics involve six degrees of freedom. Since each degree of freedom results in two states, the full set of dynamics for a rigid body system will involve only twelve states. (Additionally, servo, actuator, sensor, and controller compensation states must be added.) By comparison, a flexible structure model may have 100 or more states. This increase in the number of states derives an increase in the complexity of the control problem. Hence, those design techniques which work well for tenth order systems may have difficulties handling systems with ten times that many states.

A second important difference between rigid body and flexible dynamics is flexible dynamics tend to be more difficult to predict than rigid body dynamics. It is the

structure of a system which derives its flexible dynamics. Parameters such as mass distribution, material stiffness and damping, and unsteady aerodynamics become influential. Often mathematical models developed to predict the flexible dynamics differ with the physical system representation. As a result, the controller design based on these prediction models must be made robust to withstand the discrepancies between the model and physical system.

A third difference between these dynamics is that rigid body dynamics can often be treated as decoupled, whereas flexible body dynamics are most often highly coupled. As a result, control problems that can often be treated as a single input / single output (SISO) or as a series of SISO problems when dealing with rigid body systems, become multiple input / multiple output (MIMO) problems when dealing with flexible systems. SISO methods appropriate for decoupled rigid body system controller design may be unsuitable for flexible system controller design.

A fourth difference between these dynamics is the goal of the systems designed to control them. Rigid body control usually involves commanding the rigid degrees of freedom to follow desired trajectories. For an airplane these might be altitude, heading, and airspeed. By contrast, the goal of most flexible structure controllers is either to perform the desired rigid body control without exciting flexible modes, or to provide active damping for structural modes that are excited. In almost all applications the objective is to keep flexible structure dynamic responses at the lowest possible levels. The difference between the goals for rigid body control and flexible structure control may require different controller design approachs.

CONTROLLER DESIGN METHOD CATEGORIES

Four categories of controllers are detailed in the following paragraphs with a discussion on the advantages and disadvantages of each category with respect to the design of controllers for flexible structure systems. It is not the author's intent to favor any category of controller design techniques over another. The divisions herein are made simply to facilitate comparison of different top level strategies for the design of controllers for flexible structures. The categories are deliniated by the types of models each use for controller synthesis, and whether the controller is designed off-line, on-line, or both.

1)   Off-line Modeling / Off-line Controller Design

Off-line modeling / off-line controller design techniques have been historically used as the standard for control system design. This technique consists of building up a model using mathematical prediction, wind tunnel analysis, and flight test data. Controllers are then designed off-line based on the model. Although separate controllers may be designed for different flight conditions (i.e., requiring gain scheduling based on flight condition), only these on-line modifications defined previous to flight are made to the controller.

782

This category of controller design techniques has the advantage of all controller synthesis work being completed ahead of time off-line. As a result, the on-line computational load is kept to a minimum. In addition, since the controller is well defined for each flight condition, rigorous analysis is possible for predicting performance and robustness characteristics.

A disadvantage of this controller design approach is that discrepancies between the model and the physical system itself must be handled solely by controller robustness. The controller is unable to tune itself to account for modeling errors or changes in the dynamics as a result of different flight conditions or weight distributions. Hence, this design approach requires development of an accurate system model. Whenever possible, the off-line model is updated to concur with the obtained test data using the physical system to be controlled. In those cases where test data is not available, analysis must be done to show that the controller will function in an acceptable manner for the set of anticipated dicrepancies between the model and the physical system.

2) Off-line Modeling / On-line Controller Design

The same type of model used for the previous category of controller is used for off-line modeling / on-line controller design techniques. However, the primary difference with this category is that while the controller structure is defined off-line, the controller gains are adapted on-line to minimize certain performance criteria. With this technique no attempt is made to model the open-loop system on-line, and all controller gain changes are made solely in response to performance criteria.

This approach has the advantage of the controller being able to tune itself to account for parameter variations between the model and the physical system. The off-line system model does not have to be as precise for this type of controller as for those described in category 1. The off-line model is used to note the structure of the system and the general trend of the dynamics. Furthermore, a related advantage is that since the controller is able to tune itself, gain scheduling does not have to be as detailed as for a controller that is designed completely off-line.

A disadvantage of this approach is that the controller must be tuned on-line, thus requiring more computation power. Another disadvantage is that while the controller is able to tune itself to account for parameter variations, its structure is fixed. If the structure of the flexible system changes or there are wide swings in its general dynamics, the controller may not be able to tune itself sufficiently to provide the necessary control. A third disadvantage is that while the controller is continuously tuning itself, it is impossible to predict the gains for any given flight condition. As a result, it is impossible to obtain the level of performance and robustness analysis possible with each flight condition assigned a fixed set of controller gains.

3) On-line Modeling / Off-line Design

On-line modeling / off-line design techniques define the controller in terms of a general open-loop system model of a specified structure. With these techniques each controller gain is defined as a function of model parameter values. Implementation consists of building an on-line adaptive estimator to estimate the model parameters. The controller gains are then set based on the model estimate values per the definitions developed off-line.

An advantage of this approach is that the controller gain definitions can be chosen to give the desired performance and robustness properties regardless of the model parameters. (It is assumed that sufficient controllability and observability exist for all variations of the model parameters.) Gain scheduling is not an issue since the controller gain definitions automatically give appropriate gains for any given operating condition.

A disadvantage of this approach is that the controller gains must be defined symbolically rather than numerically. Controller synthesis requires solution of symbolic rather than numeric equations. Fortunately this task is done off-line and will not require real-time computing resources, but it is still a formidable task nonetheless. Another disadvantage is that on line estimation of the model parameters is required along with computation of the controller gains. Evaluation of the equations defining the controller gains may be quite expensive to compute. An additional disadvantage is that the controller gain definitions may include singular points within the region of possible model parameter sets. A method to avoid singularity is needed.

4) Off-line Modeling / Off-line Controller / On-line Adjustment

The final controller design approach category involves off-line modeling, off-line nominal controller design, and on-line controller adjustment. The nominal controller is designed to stabilize the nominal system. With this technique an adaptive loop is placed around the system to tune the control input for improving the off-nominal performance. This adaptive loop is designed to consistantly stabilize the nominal system. Furthermore, when the system is at nominal, the adaptive control signal is zero.

An advantage of this system is that while the controller is able to tune itself to account for modeling errors, the tuning is restricted so that the closed-loop system remains stable. This method can be thought of as a compromise between a fixed gain controller and fully adaptive controller. The nominal controller gains are fixed while the adaptive algorithm is free to vary the gains within a range about nominal.

A disadvantage of this system is that if the physical system varies greatly from the nominal given by the off-line model, there is no longer a guarantee of stability.

784

Hence on the one hand, the adaptive tuning is restricted to keep from destabilizing the nominal system. On the other hand, this restriction may lead to a situation where the actual system is driven unstable and the limitations on the adaptive tuning are such that the controller is unable to tune itself sufficiently to provide closed-loop stability.

SUMMARY

Rather than point to a single design approach as the best for designing controllers for flexible structures, the goal of this presentation is to simulate thought and discussion. Most likely a single approach is not well suited for all problems. The key is to realize that there are fundemental differences between rigid body and flexible structure dynamics and that these differences may require different approaches to controller design.

CONTROLLING FLEXIBLE STRUCTURES:

A SURVEY OF METHODS

Russell A. Benson
Edward E. Coleman

The Boeing Company
Boeing Commercial Airplanes
P.O. Box 3707
Seattle, Washington 98124-2207

786

Goal of Presentation:

Stimulate discussion of merits and

maturity of different top level approaches

to controller design for flexible structures

787

BOEING COMMERCIAL AIRPLANES
GUIDANCE AND CONTROL RESEARCH

Outline of Presentation:

o Characteristics of Flexible Structure Dynamics

o Four Categories of Controller Design Approaches

o Open Discussion on Merits and Maturity of Design Approaches

Characteristics of Flexible Structure Dynamics

o High order (100 or more states)

o Difficult to predict

o Coupled dynamics

789

Four Categories of Controller Design Approaches:

1) Off-line Modeling / Off-line Controller Design

2) Off-line Modeling / On-line Controller Design

3) On-line Modeling / Off-line Design

4) Off-line Modeling / Off-line Controller Design /
   On-line Adjustment

790

BOEING COMMERCIAL AIRPLANES
GUIDANCE AND CONTROL RESEARCH

1) Off-line Modeling / Off-line Controller Design

o Model developed off-line using mathematical predictions, wind tunnel data, and/or flight test data

o Controller designed based on model

o Controller structure and gains may vary from condition to condition but controller is fixed for a given operating point

Advantages:

o Low on-line computation requirement

o Well defined controller allows for rigorous analysis

Disadvantages:

o Controller cannot react to modeling errors

o Model must match physical system closely

o Controller must have significant robustness

BOEING COMMERCIAL AIRPLANES
GUIDANCE AND CONTROL RESEARCH

2) Off-line Modeling / On-line Controller Design

o Model developed off-line using mathematical predictions, wind tunnel data, and/or flight test data.

o Controller structure chosen based on off-line model

o Criteria outputs specified to drive controller adaptation

o Controller gains adapted on-line in effort to minimize criteria outputs

BOEING COMMERCIAL AIRPLANES
GUIDANCE AND CONTROL RESEARCH

Advantages:

    o Controller can tune itself to overcome modeling errors

    o Model must represent structure and general trend of
       the dynamics, but need not be exact

Disadvantages:

    o On-line gain tuning requires greater computational power

    o Gains may diverge resulting in an instability

    o Because gains are not fixed for a given flight condition,
       rigorous closed loop analysis is not possible

794

3) On-line Modeling / Off-line Controller Design

- o System model adapted on-line to fit a specified structure

- o Controller gains defined as functions of model parameters

- o Controller gain equations developed off-line as functions of generalized model parameters

795

BOEING COMMERCIAL AIRPLANES
GUIDANCE AND CONTROL RESEARCH

Advantages:

o Controller gain equations give explicitly the desired performance and robustness characteristics

o Controller gain equations developed off-line and must be computed only once

Disadvantages:

o Controller gain equations must be solved symbolically rather than numerically

o On-line model estimation is computationally expensive

796

BOEING COMMERCIAL AIRPLANES
GUIDANCE AND CONTROL RESEARCH

4) Off-line Modeling / Off-line Controller Design / On-line Controller Adjustment

797

o Model developed off-line using mathematical predictions, wind tunnel data, and/or flight test data

o Controller structure defined based on off-line model

o Nominal controller gains chosen based on off-line model

o Controller gains allowed to adapt on line in such a way that the nominal plant (as defined by the model) is never driven unstable

BOEING COMMERCIAL AIRPLANES
GUIDANCE AND CONTROL RESEARCH

Advantages:

o Controller can tune itself to adjust to modeling errors

o Controller self tuning is restricted to maintain stability
   of nominal plant as defined be the model

Disadvantages:

o Controller may not be able to tune itself sufficiently

o Analytical analysis difficult because controller not fixed
   for a given flight condition

Discussion of Merits and Maturity

of Top Level Approaches to Controller

Design for Flexible Structures

799

AIRCRAFT MODAL SUPRESSION SYSTEM: EXISTING DESIGN APPROACH AND ITS SHORTCOMINGS

By

J. K. Ho, T. J. Goslin,and C. B. Tran
The Boeing Company
Seattle, Washington

ABSTRACT

The bending of flexible body aircraft may degrade the ride comfort of passengers. This is especially noticeable towards the aft end of the aircraft (due to the relatively large tail surfaces) which may easily be excited when flying through turbulence. In addition, some aircraft may experience a front body bending mode which can be annoying to the cabin crew and first class passengers. Normally, this dominant body bending mode falls between 1-5 Hz. This range is easily perceived by the human body. Also, in some situations, the rigid body control law may be out of phase with the mode and aggravate the vibration. Hence, an active modal suppression system is desirable for improving the ride quality of the airplane.

The size of the mathematical model, which has both the airplane rigid body and flexible characteristics, could easily exceed 100 states. This paper addresses the computational burden and fidelity of this large structural model. Later, the design methodology of the control law, which could be categorized into three steps:--(1) sensor selection, (2) modal phase determination and (3) modal suppression filter design--will be discussed. Each of these steps will be discussed in detail. Then we will present the theoretical results and compare them with flight test results. Here we will highlight the shortcomings of this design approach and briefly discuss what can be done in light of these deficiencies. Finally, we will include a brief description of the software tools.

AIRCRAFT MODAL SUPPRESSION SYSTEM:

EXISTING DESIGN APPROACH AND ITS SHORTCOMINGS

BY

J. HO, T. GOSLIN, AND C. TRAN

BOEING COMMERCIAL AIRPLANES

SEATTLE, WASHINGTON

OBJECTIVES OF MODAL SUPPRESSION YAW DAMPER

o CONTROL DUTCH ROLL RESPONSE

o PROVIDE GOOD TURN COORDINATION

o IMPROVE LATERAL RIDE COMFORT BY SUPPRESSING FLEXIBLE BODY MODES

803

DESIGN PROCESS

o MODEL GENERATION
o BASIC YAW DAMPER DESIGN
o MODAL SUPPRESSION SYSTEM DESIGN

   o SELECTION OF SENSOR LOCATION, CONTROL SURFACE
   o ESTABLISHMENT OF MODAL PHASE RELATIONSHIP
   o MODAL SUPPRESSION FILTER DESIGN

o FLIGHT TEST
o ITERATE IF NEEDED

804

STRUCTURAL MODEL

o ORDER OF STRUCTURAL MODEL EXCEEDS 60 STATES

o WITH ANTI-ALIASING FILTER, TRANSPORT DELAY, SAMPLE AND HOLD, CONTROL
  LAW, RUDDER PCU, ORDER OF MODEL EXCEEDS 100 STATES

o MAIN FRAME COMPUTER REQUIRED FOR REASONABLE TURNAROUND TIME

805

Design Requirements

The damping ratio for the closed loop airplane should be 0.4 or greater for the Dutch roll mode. Phase and gain margin requirements are:

Mode frequency (fM)	Gain Margin	Phase Margin
Hz	dB	degs
————————	————————	————————
fM <= 0.06	> ±3	> ±20
.06 <= fM <= 1st aeroelastic mode	> ±4.5	> ±30
fM > 1st aeroelastic mode	> ±6	> ±45
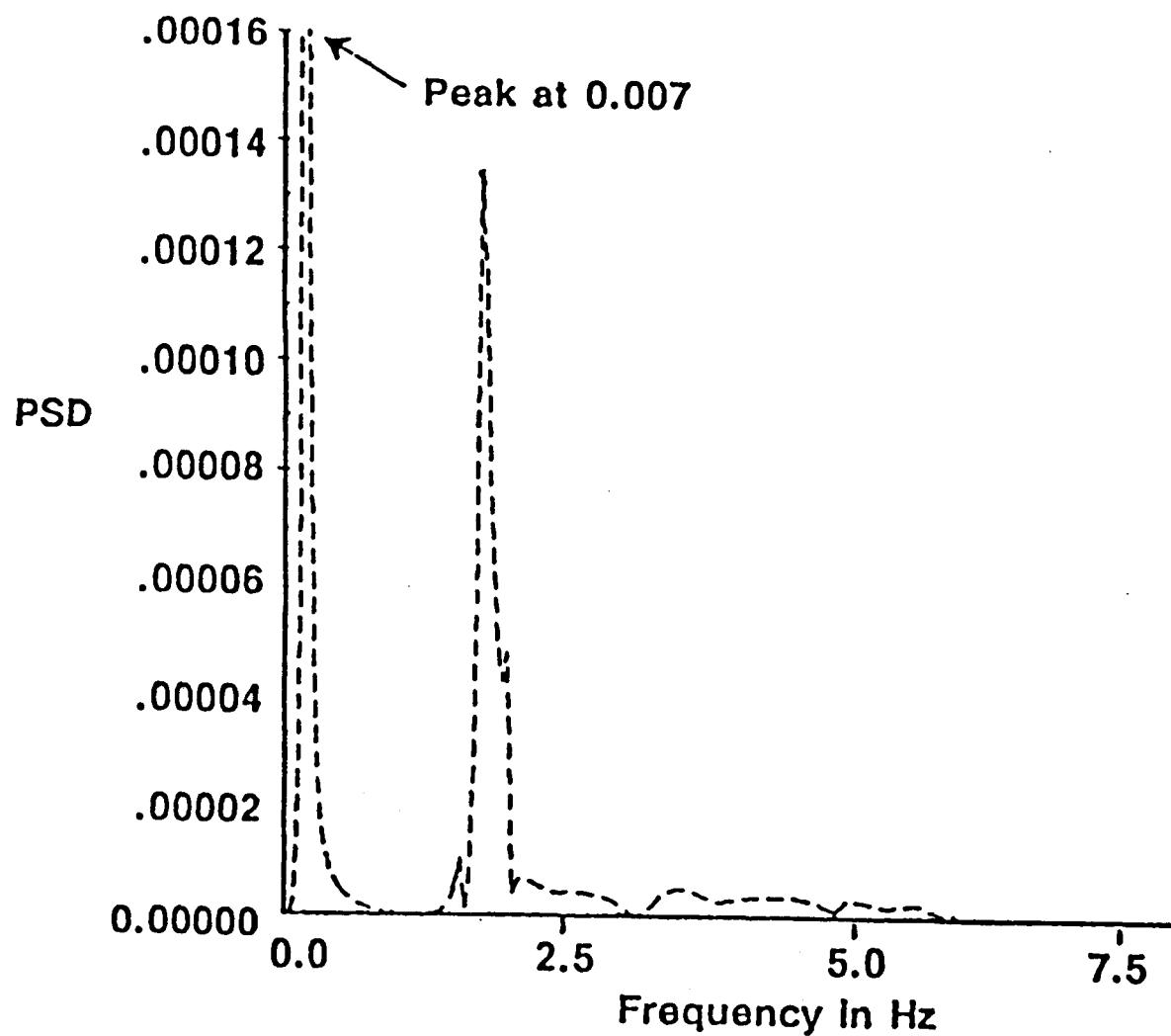
908

PSD Level of the Lateral Acceleration at the Aft Galley

PSD Level of the Lateral Acceleration at the Pilot Station
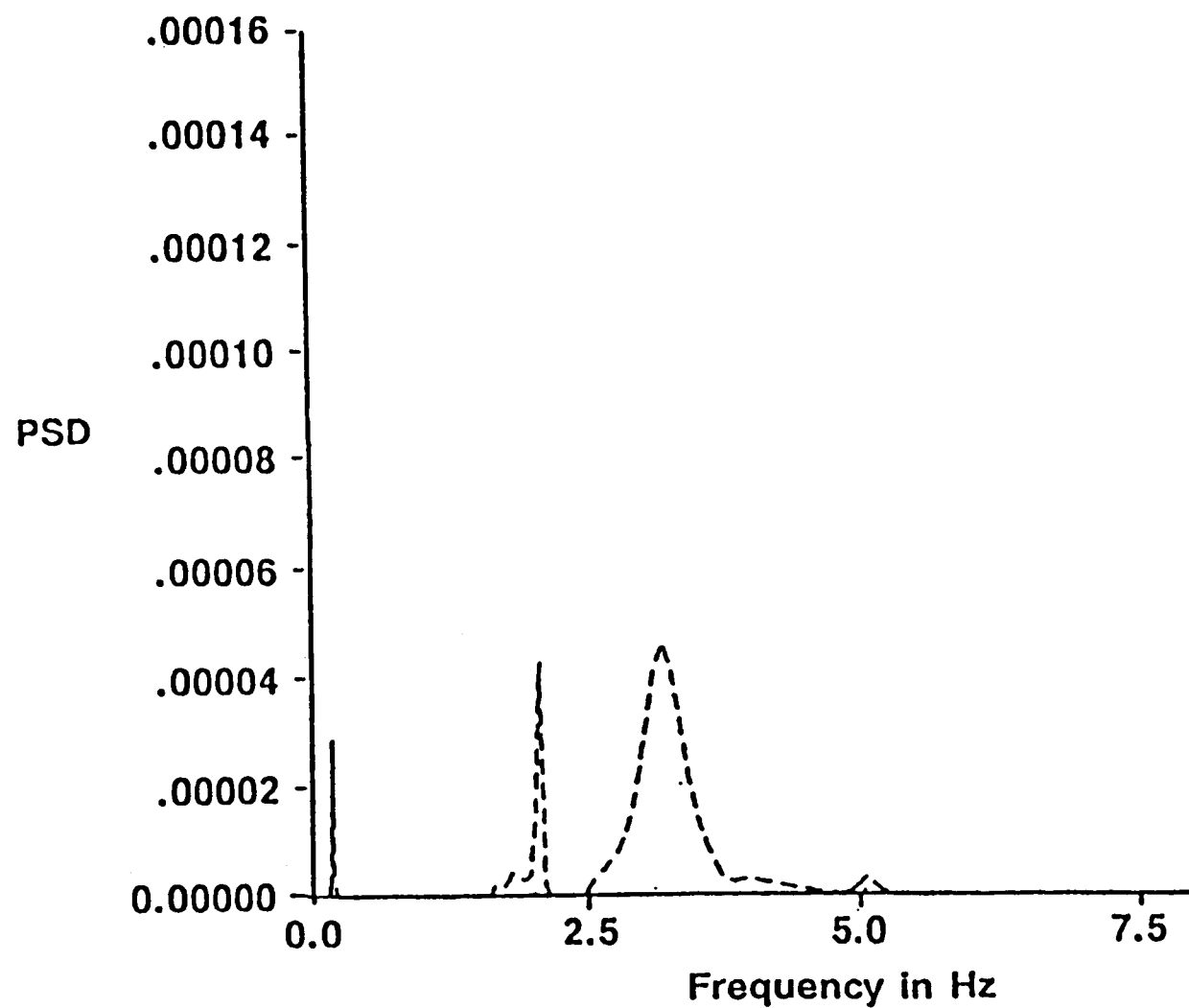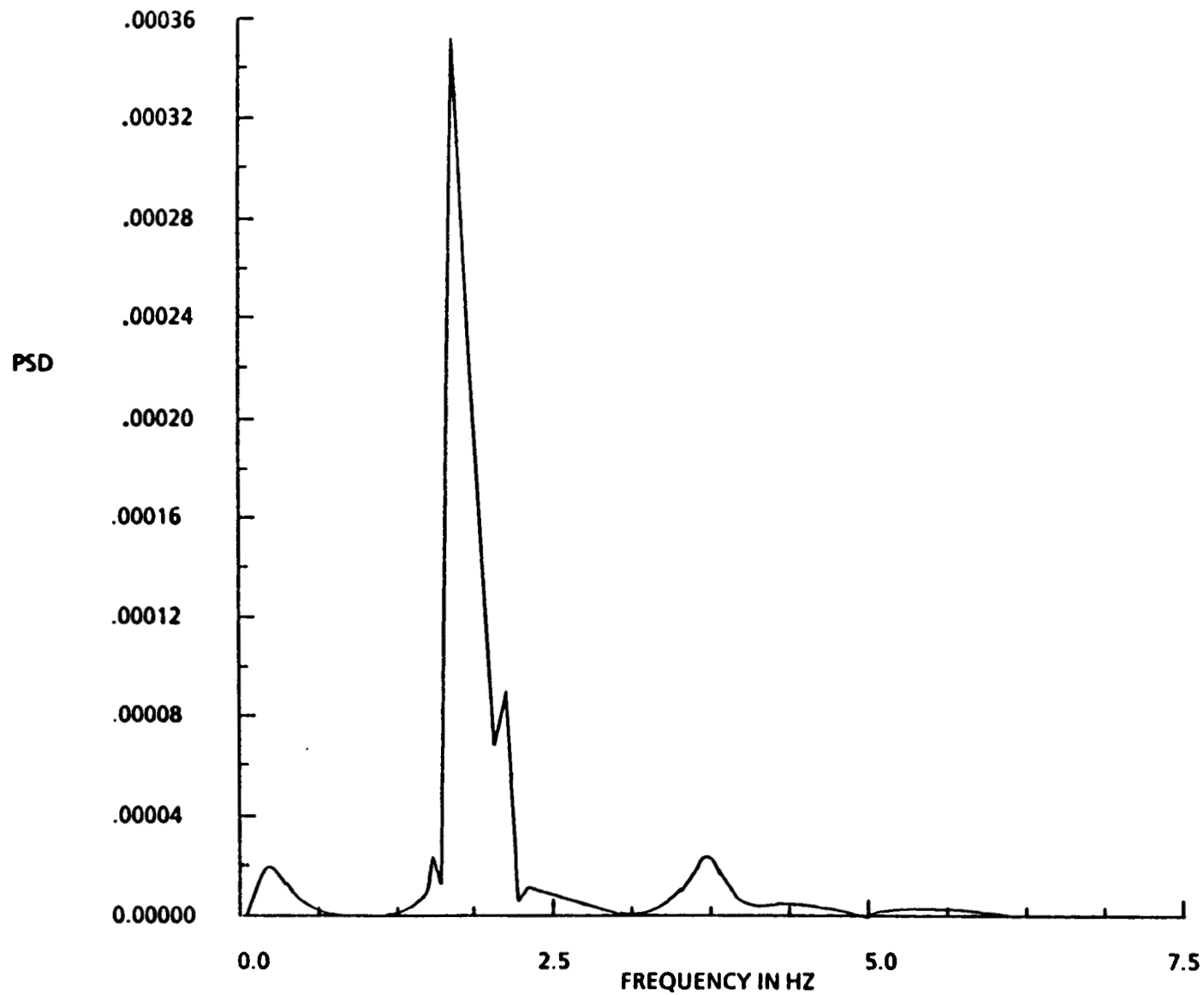
YAW DAMPER CLOSED LOOP AIRPLANE
PSD OF THE LATERAL ACCELERATION AT THE AFT STATION

608
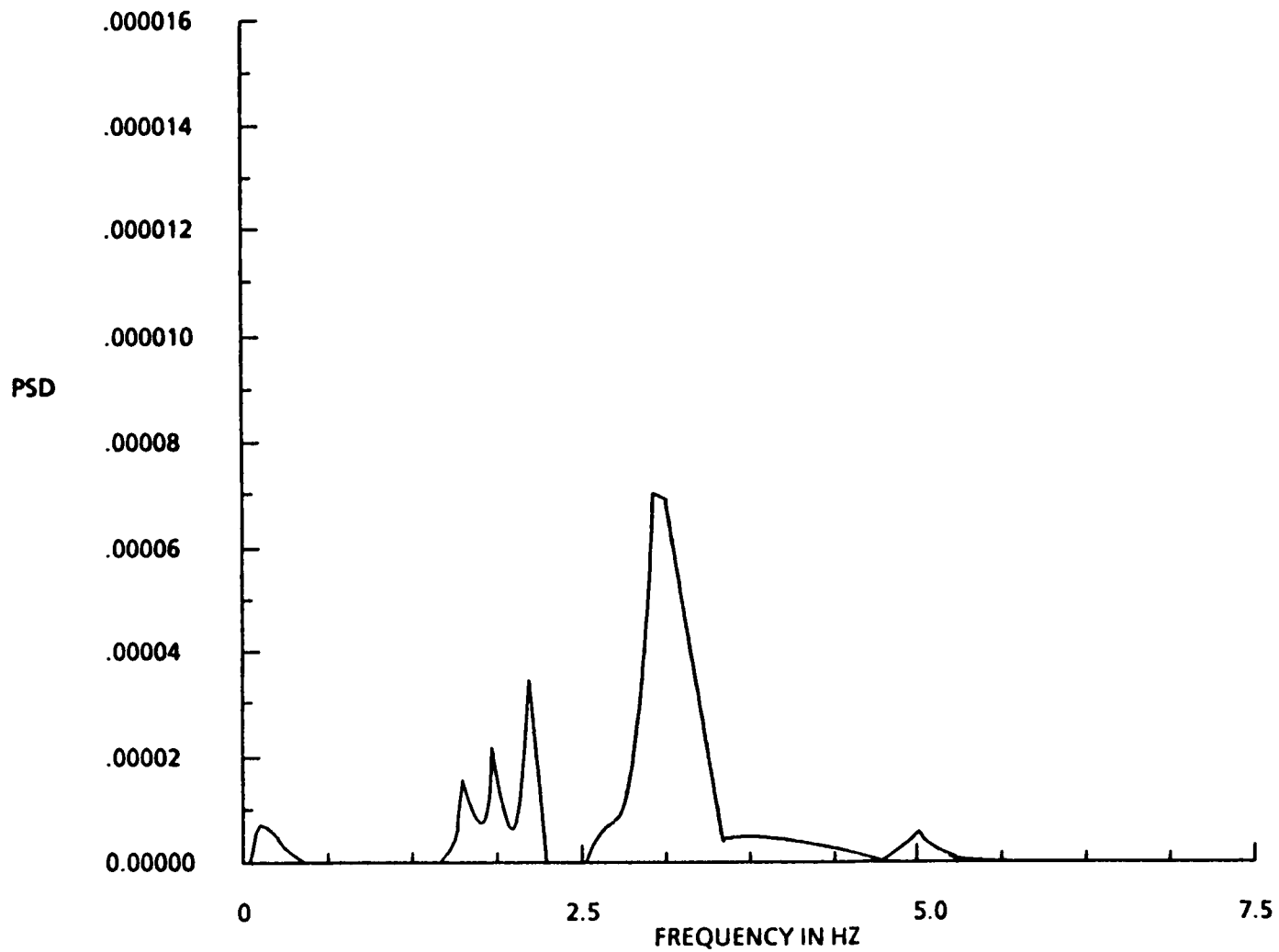
YAW DAMPER CLOSED LOOP AIRPLANE
PSD OF THE LATERAL ACCELERATION AT THE PILOT STATION

o WITH BASIC YAW DAMPER LOOP CLOSED, USE MPAC TO COMPUTE OBSERVABILITY
  AND CONTROLLABILITY

o PICK $\left\{ \begin{array}{l} \text{LATERAL ACCEL AT PILOT STATION} \\ \text{LATERAL ACCEL AT AFT GALLEY} \end{array} \right\}$ AS SENSORS

  PICK RUDDER AS CONTROL SURFACE

o DESIGN AFT FILTER FIRST BY DETERMINING ITS MODAL PHASE RELATIONSHIP
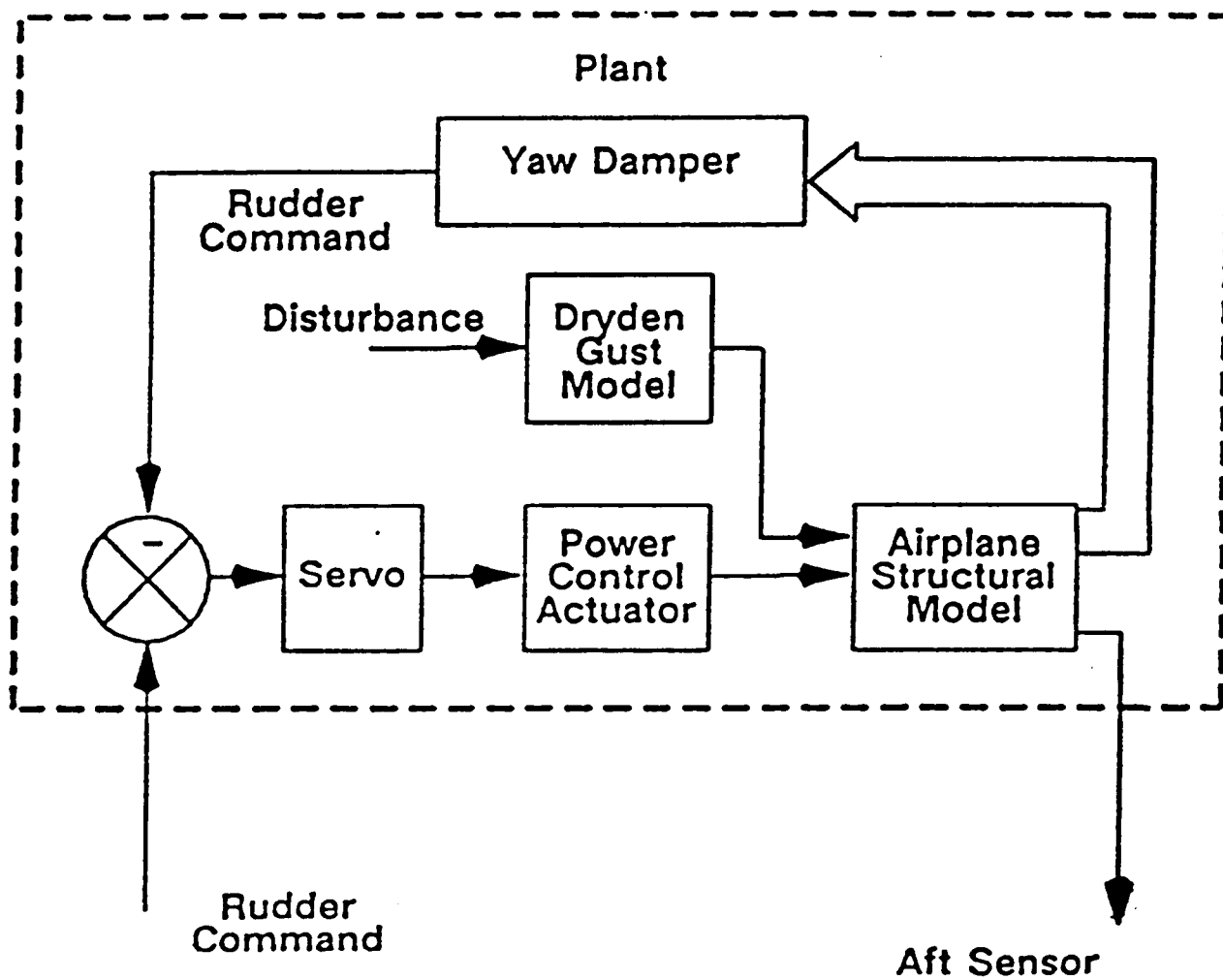
Plant Model for Aft Filter Design

812
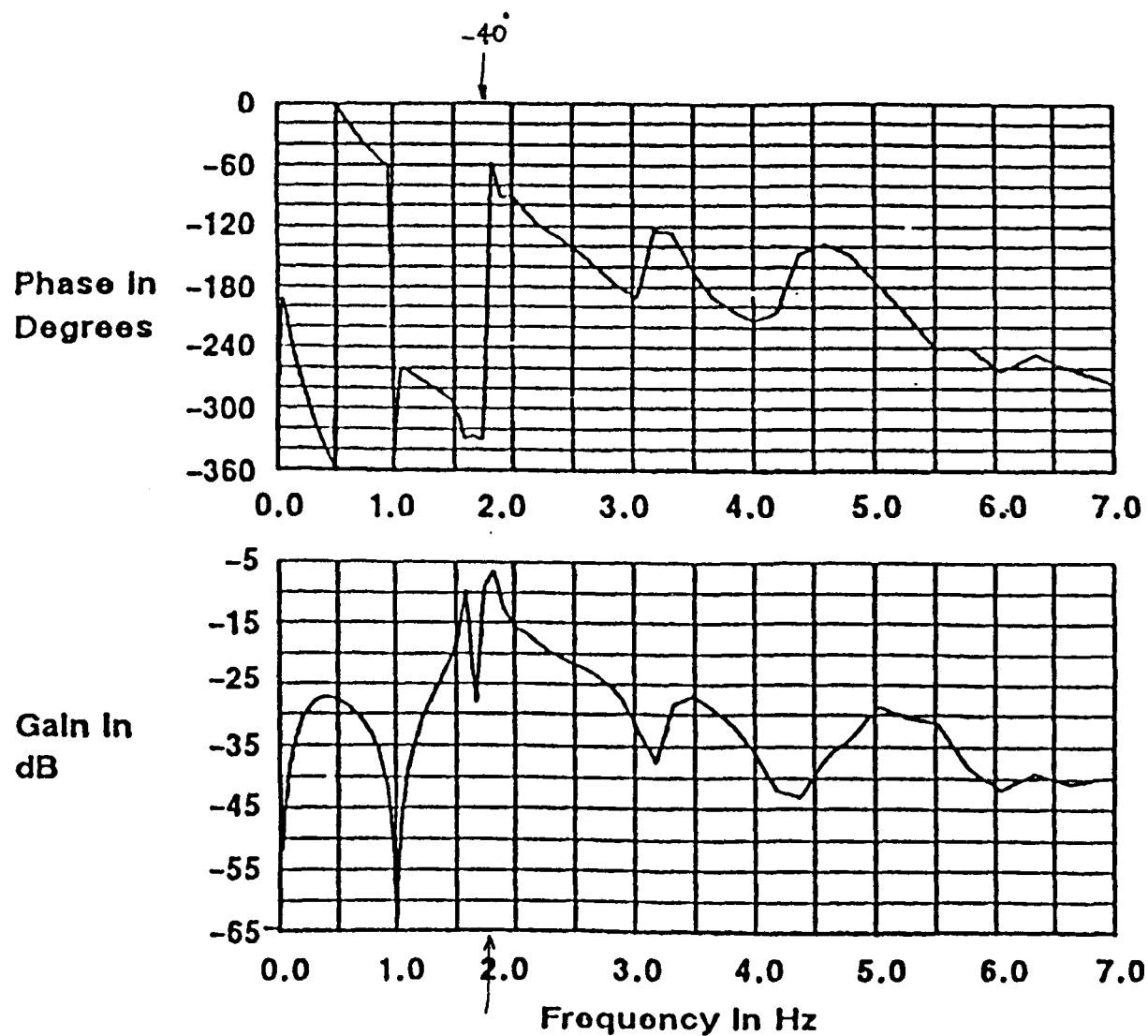
Bode Plot of the Transfer Function From Rudder Command to Aft Galley Sensor

813

Phase In Degrees

Gain In dB

40°

Frequency In Hz

8/4
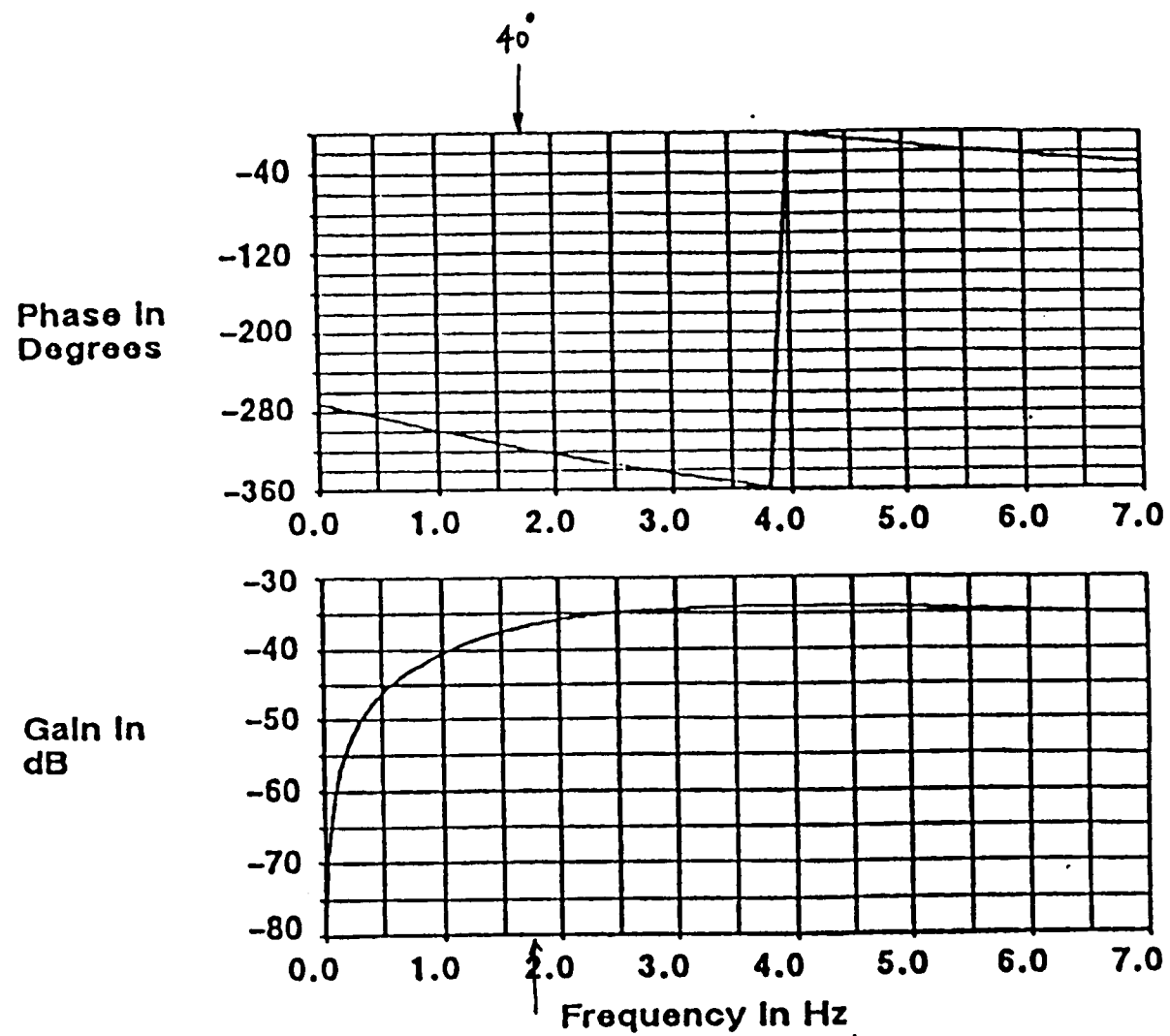
Bode Plot of the Aft Filter
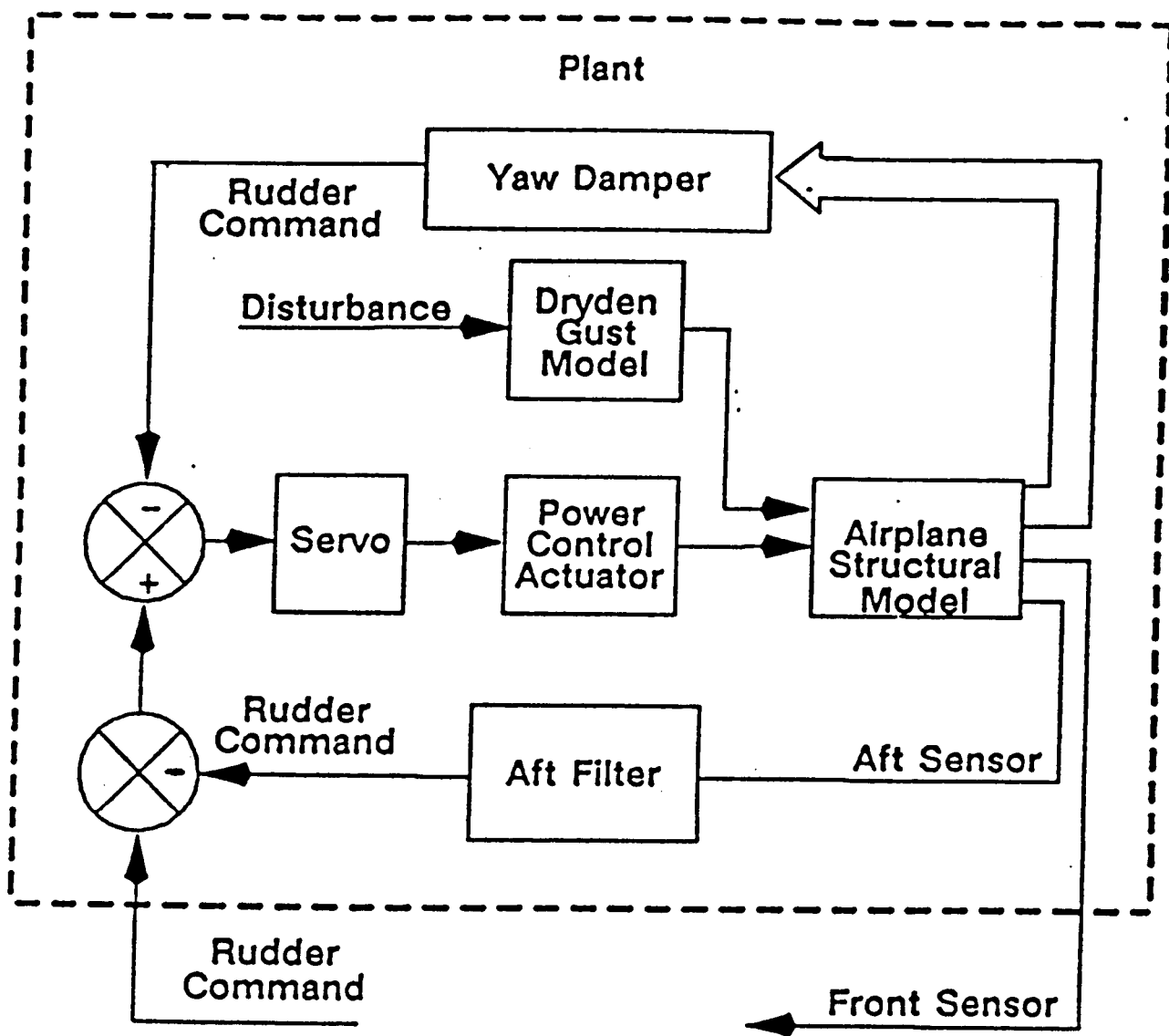
Plant Model for Pilot Station Filter Design

815
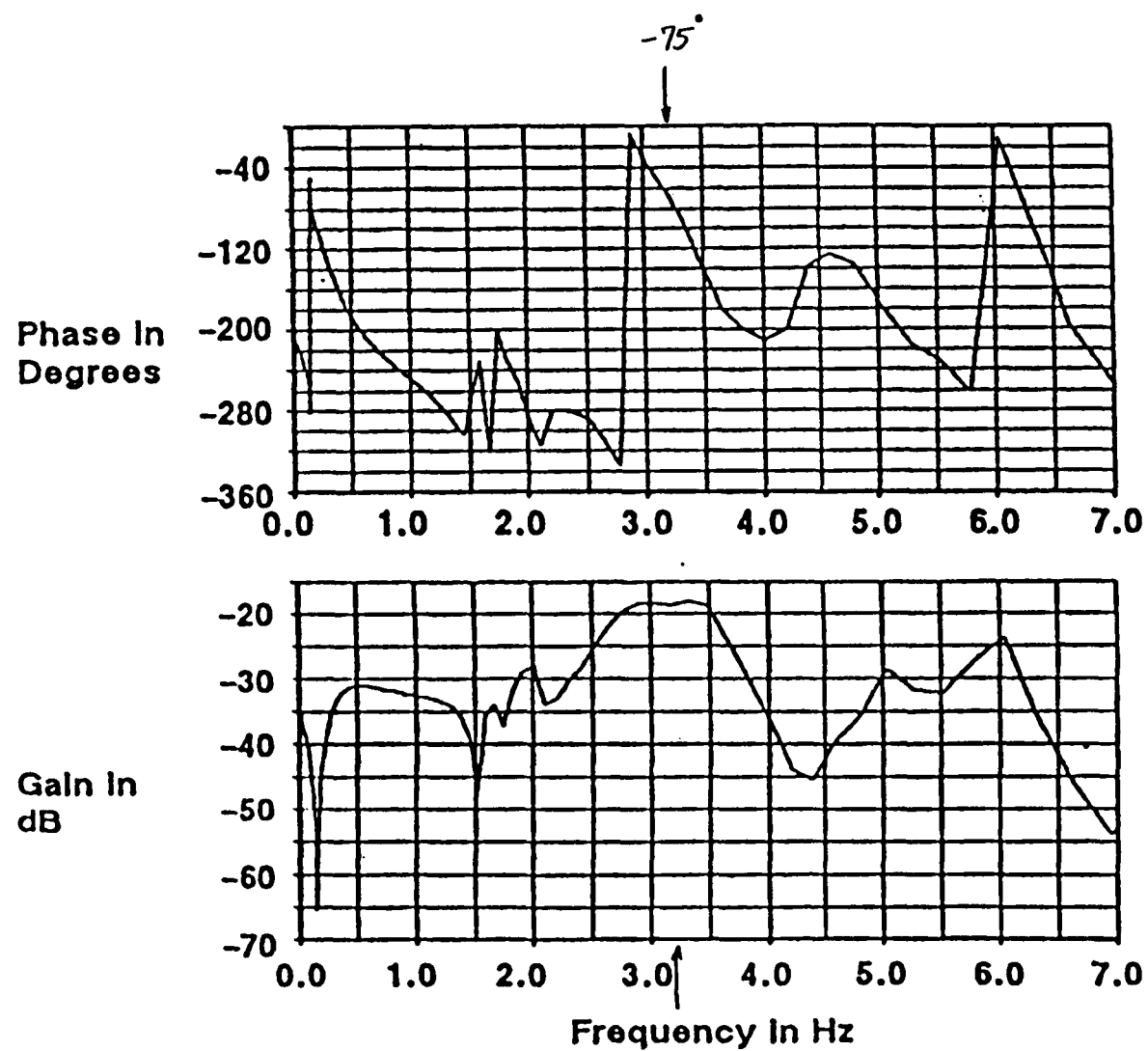
Bode Plot of the Transfer Function From Rudder Command to Pilot Station Sensor

80°

Phase in Degrees

-40
-120
-200
-280
-360

0.0 1.0 2.0 3.0 4.0 5.0 6.0 7.0

Gain in dB

-40
-50
-60
-70
-80

0.0 1.0 2.0 3.0 4.0 5.0 6.0 7.0

Frequency in Hz

817
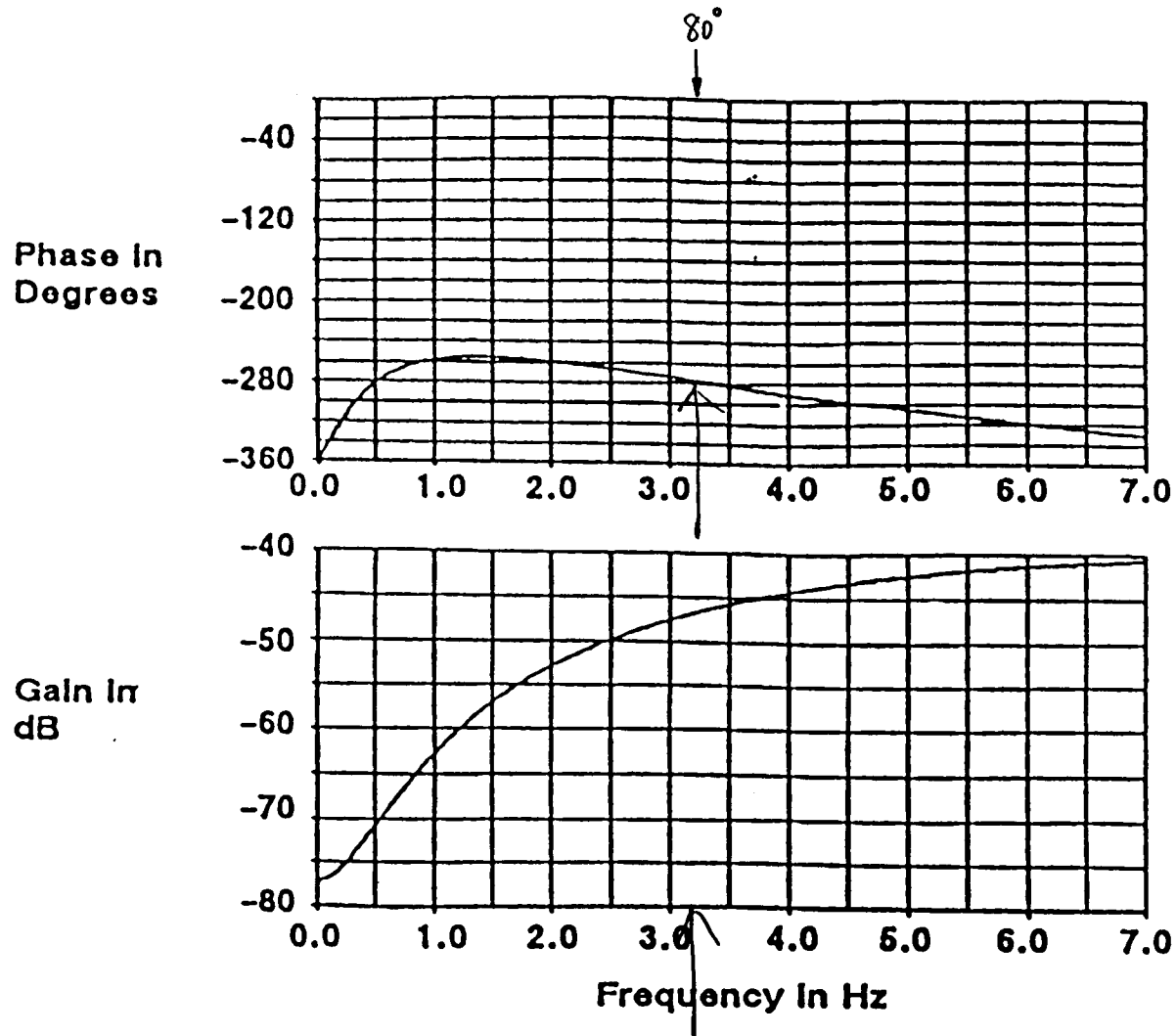
Bode Plot of Pilot Station Filter
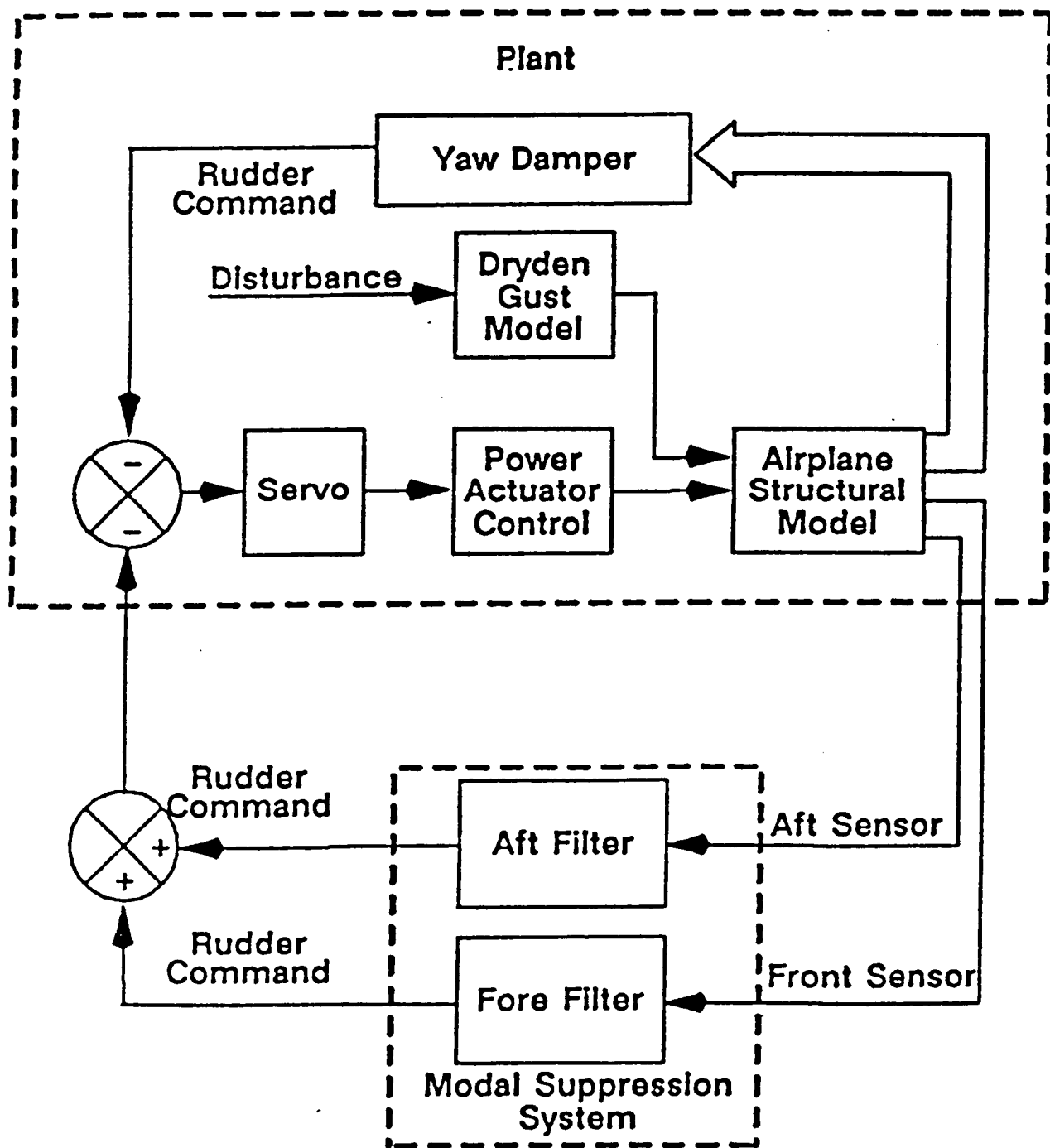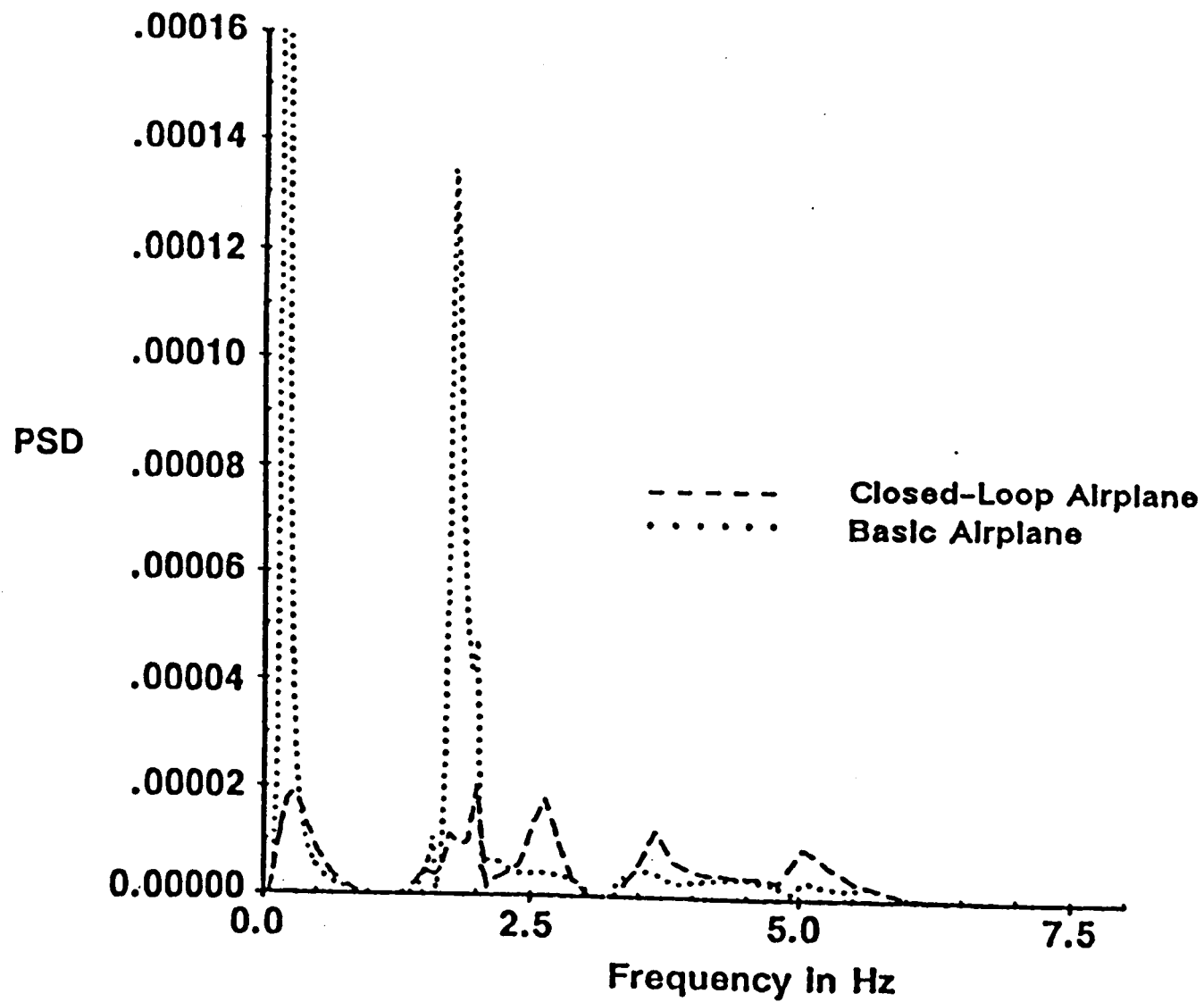
Plant

Rudder
Command — Yaw Damper

Disturbance → Dryden Gust Model

— (−, −) → Servo → Power Actuator Control → Airplane Structural Model

Rudder Command

Aft Filter ← Aft Sensor

Rudder Command

Fore Filter ← Front Sensor

Modal Suppression System

Closed-Loop System

818

PSD of the Lateral Acceleration at the Aft Galley

PSD of the Lateral Acceleration at Pilot Station

FLIGHT TEST RESULTS

(Graph) X-axis: FREQUENCY HZ, from 0.0 to 5.0. Y-axis: LAT ACCEL PILOTS SEAT PSD, from 0.0000 to .0026.
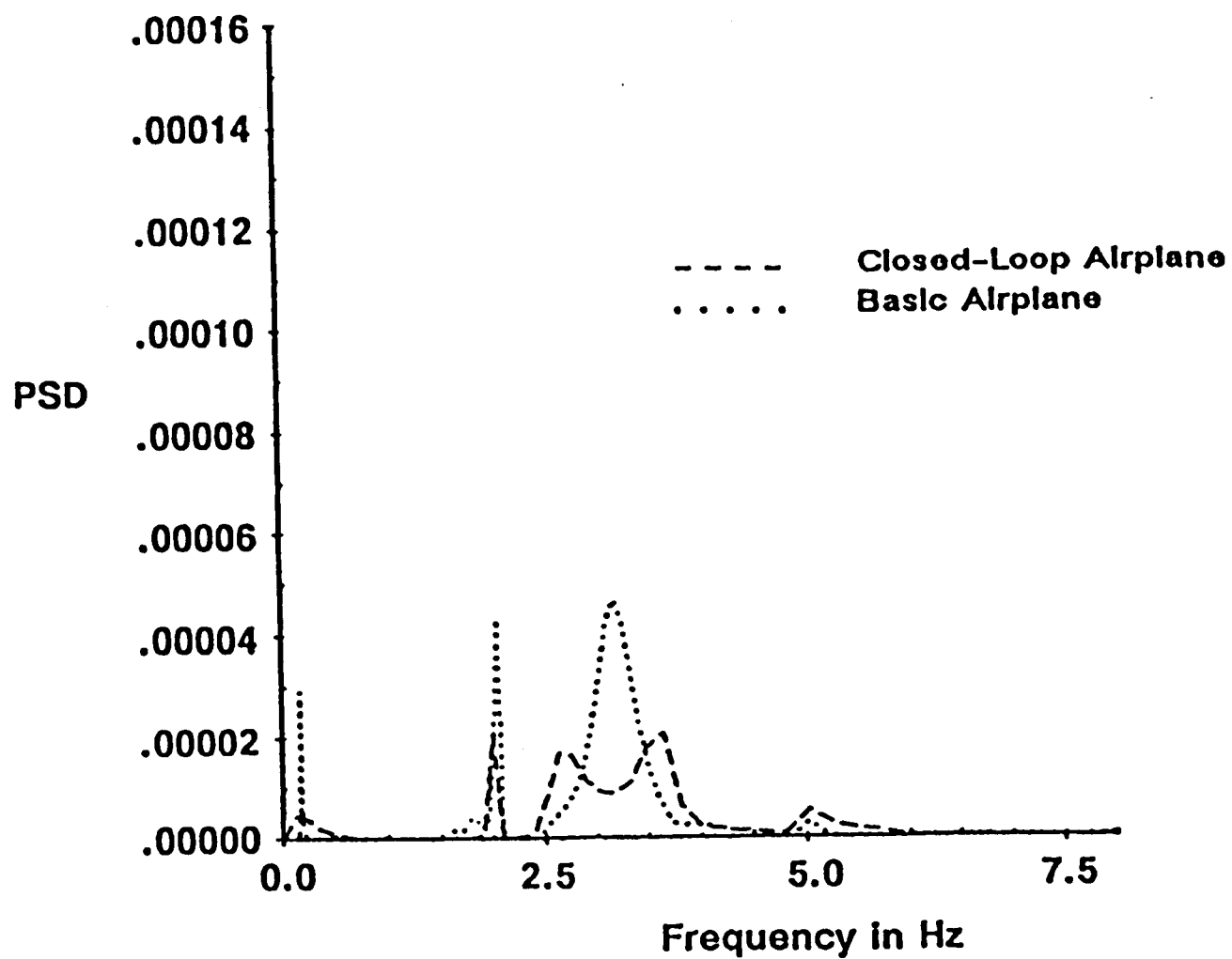
Legend:
- – – – MSS OFF
- ——— MSS ON

821
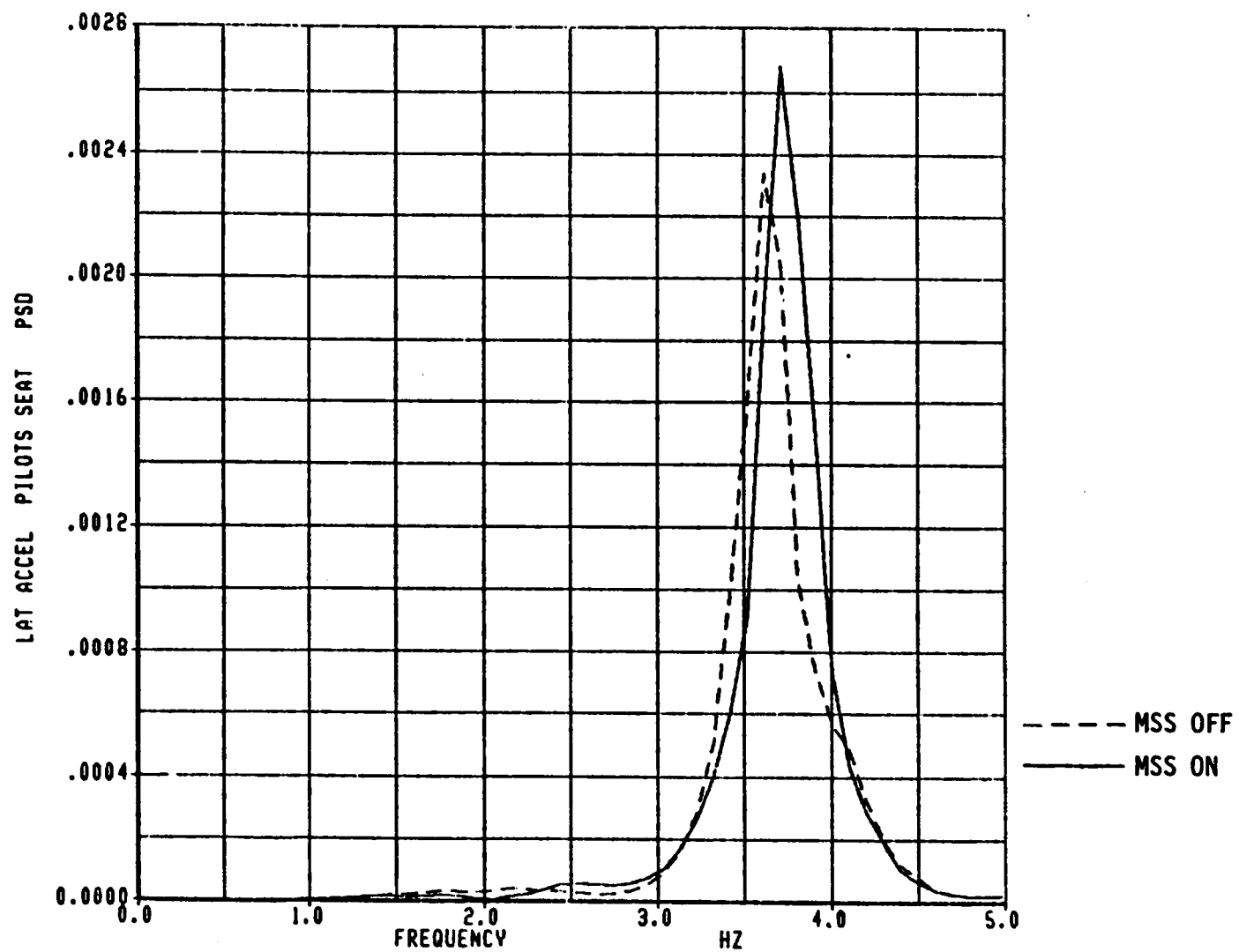
FLIGHT TEST RESULTS
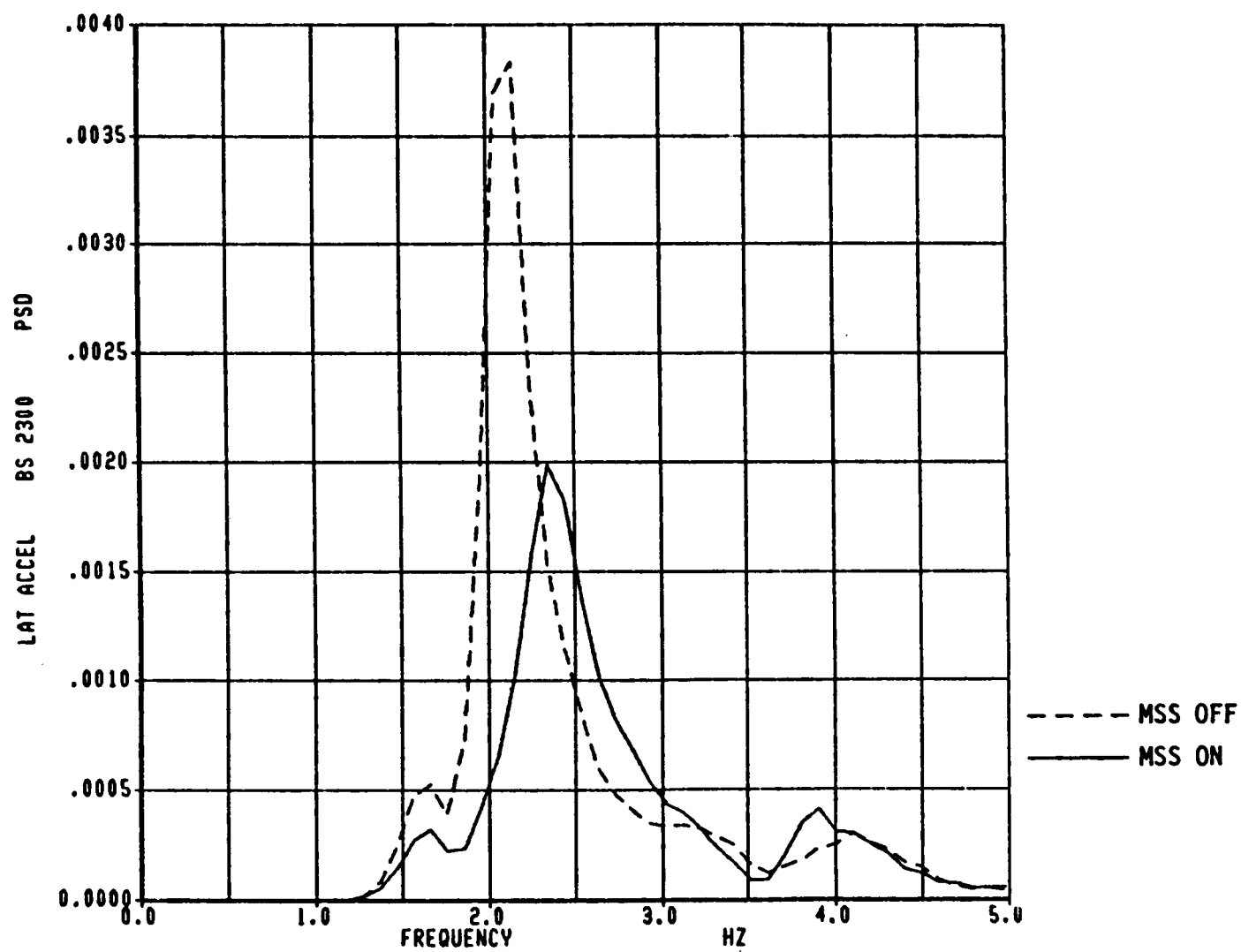
MODELLING DIFFICULTIES

o LACK OF ACCURACY IN STRUCTURAL MODEL

o RUDDER ACTUATION SYSTEM INCLUDES NON-LINEAR ELEMENTS:

   RATE SATURATION, POSITION LIMITER, HYSTERESIS, DEADZONE, VARIABLE
   GAIN

o USE OF TRANSFER FUNCTIONS RESULT IN LOSS OF ACCURACY IN FREQUENCY
   DOMAIN

823

STRUCTURAL STABILITY AUGMENTATION SYSTEM DESIGN USING BODEDIRECT: A QUICK AND ACCURATE APPROACH

By

T. J. Goslin and J. K. Ho
Boeing Commercial Airplane Company
Seattle, Washington

ABSTRACT

Both aft and forward sections of long slender aircraft suffer from lateral accelerations in turbulence. Some of these accelerations can be attributed to flexible body bending of the airplane in the 1-6 Hz region. Given an accurate flexible body model of the aircraft, a control law can be employed using lateral acceleration feedback loop augmented with the basic dutch roll yaw damper system to actively damp out these modes.

In this paper a methodology will be presented for a modal suppression control law design using flight test data instead of mathematical models to obtain the required gain and phase information about the flexible airplane. This approach will be referred to as BODEDIRECT. The purpose of the BODEDIRECT program is to provide a method of analyzing the modal phase relationships measured directly from the airplane. These measurements can be achieved with a frequency sweep at the control surface input while measuring the outputs of interest. The measured "Bode-models" can be used directly for analysis in the frequency domain, and for control law design. Besides providing a more accurate representation for the system inputs and outputs of interest, this method is quick and relatively inexpensive.

To date, the BODEDIRECT program has been tested and verified for computational integrity. Its capabilities include calculation of series, parallel and loop closure connections between Bode-model representations. System PSD, together with gain and phase margins of stability may be calculated for successive loop closures of multi-input/multi-output systems. Current plans include extensive flight testing to obtain a Bode model representation of a commercial aircraft for design of a structural stability augmentation system.

In addition to the BODEDIRECT approach, an indirect approach using flight test data to derive a mathematical mode for analysis using a Transfer Function Matching Routine will be presented along with the strengths and weaknesses of each approach.

STRUCTURAL STABILITY AUGMENTATION SYSTEM

DESIGN using BODEDIRECT; A QUICK and ACCURATE APPROACH

By

T. J. GOSLIN and J. K. HO

BOEING COMMERCIAL AIRPLANES

826

THE RIDE QUALITY PROBLEM

1   Rigid Body Airplane

   a)   Roll
   b)   Pitch
   c) * Yaw
   d) * Lateral Motion
   e)   Vertical Motion
   f)   Longitudinal Motion

2   Structural Airplane (Long Slender Bodies)

   a) * Body Bending Modes
   b)   Tortional Modes
   c)   Wing and Empennage Modes

827

THE MODES WHICH MUST BE ACTIVELY CONTROLLED INCLUDE

BASIC YAW DAMPER :

The Dutch Roll Mode

Spiral Mode for turn coordination

MODAL SUPPRESSION SYSTEM :

1st and 2nd Body Bending Modes

All other modes must be passively controlled or have sufficient gain and phase margins.

Note : This discussion is limited to the sysnthesis of a modal suppression system using the BODEDIRECT program. It is assumed that a good basic yaw damper already exists.

TRADITIONAL METHOD

THEORETICAL ANALYSIS

WIND TUNNEL AERODYNAMIC DATA

FLIGHT TEST DATA

LARGE STATE - SPACE STRUCTURAL MODELS

NUMBER CRUNCHING

BODE PLOTS AND PSD

CONTROL LAW DESIGN

FIGURE 1A

BODEDIRECT

FLIGHT TEST DATA

BODE PLOTS AND PSD

CONTROL LAW DESIGN

FIGURE 1B

829

Mathematical Models	BODEDIRECT
Advantages :	**Disadvantages :**
1) No prototype is necessary	1) A prototype must exist
2) Analysis in both time and frequency domain	2) Analysis in frequency domain only
3) Observability/controllability directly available	3) Observability/controllability not directly available
4) Eigenvalues & damping ratios directly available	4) Eigenvalues/damping ratios not directly available
Disadvantages :	**Advantages :**
1) Require large computing budgets (main frame computer)	1) Quick and inexpensive (work station environment)
2) Lack required precision	2) Accurate

830

BODE - MODEL GENERATION

FREQUENCY SWEEP

RUDDER ACTUATOR

BASIC

AIRPLANE

Outputs
(Used in BYD and
MSS control laws)

1 - 10 HZ

30-60 SECONDS

831

Bode-models are measured for all inputs and
outputs of interest for the free-airplane

MODAL SUPPRESSION SYSTEM
CONTROL LAW DESIGN
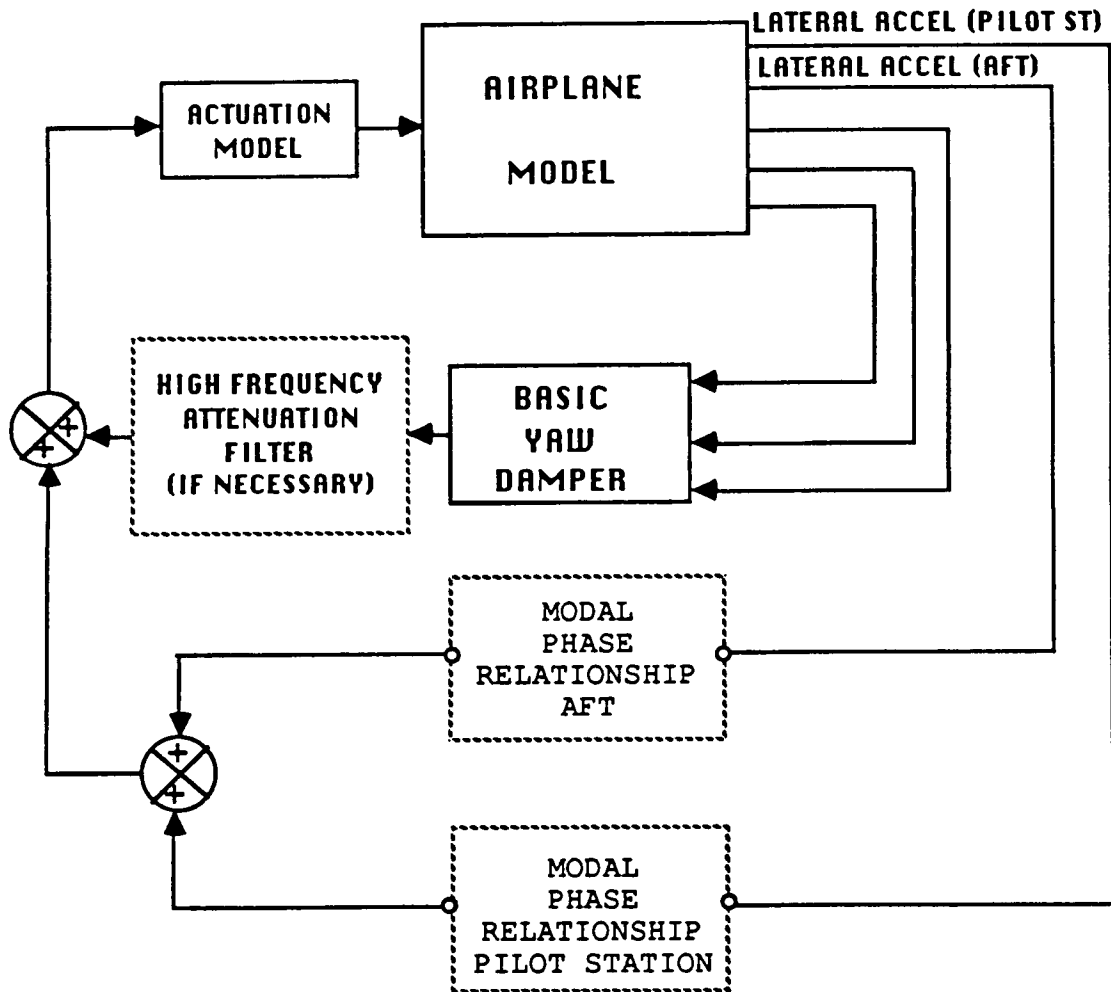
For control law design, we determine the
modal phase relationship in the feedback
loop such that a compensator can be synthesized
to bring the feedback signal into phase with
the desired mode(s).

832

c-4

DATA PRE-PROCESSING

Each bode-model requires magnitude and phase at each frequency point. With the current program version,

Up to 500 frequency points may be stored for the frequency range. The frequency vector may be loaded from a file or generated.

Example:

*LOAD FREQUENCY POINTS
201

↖ Number of frequency points   (from file)

*GENERATE FREQUENCY POINTS
LOG
0.1,10.0,201

Number of frequency points

Starting point   Ending point

Frequency points may be loaded or generated in log or linear scale.

Similarly bode-models may either be loaded from a file in terms of magnitude and phase or generated from a transfer function.

Example:

*LOAD 'modelname'

*GENERATE 'modelname'

transfer
function
coefficients {

In addition, a bode-model may be extrapolated from a previous bode-model or a set of lab test data using the command:

*CREATE BODE-MODEL 'modelname'

data
points to
extrapolate {

This allows quick bode-model generation from a few test data points.

834
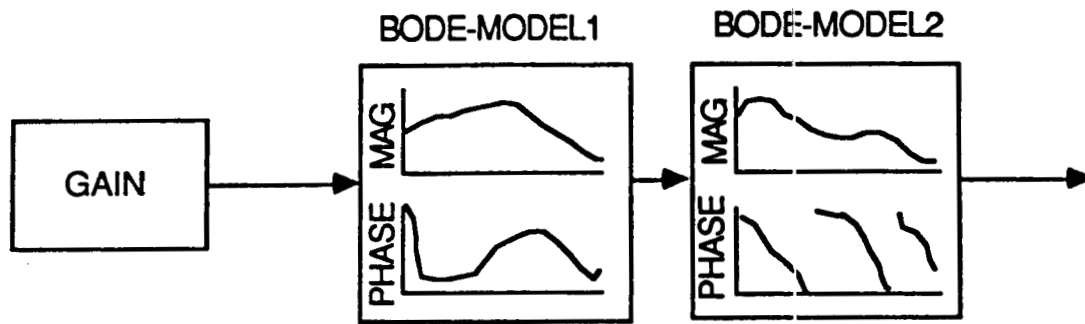
*CONNECT IN SERIES :

MAG = GAIN * MAG1 * MAG2

PHASE = PHASE1 + PHASE2

IF(GAIN .LT. 0) PHASE = PHASE + 180°

*CONNECT IN PARALELL

$$MAG = \sqrt{XCOM^2 + YCOM^2}$$

$$PHASE = TAN^{-1}(YCOM/XCOM)$$

where

XCOM = GAIN1 * MAG1 * COS (PHASE1)

+ GAIN2 * MAG2 * COS (PHASE2)

YCOM = GAIN1 * MAG1 * SIN (PHASE1)

+ GAIN2 * MAG2 * SIN (PHASE2)

835

*RESOLVE FEEDBACK JUNCTION

$$MAG_{FBAC} = 1/\sqrt{XCOM^2 + YCOM^2}$$

$$PHASE_{FBAC} = -TAN^{-1}(YCOM/XCOM)$$
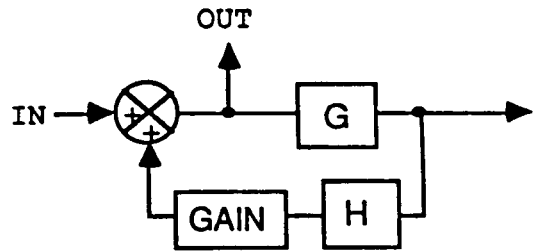
where

XCOM = 1.0 - MAG (G*H) * COS (PHAS (G*H)) * GAIN

YCOM = -MAG (G*H) * SIN (PHAS (G*H))* GAIN

*RESOLVE CLOSED-LOOP SYSTEM

CLOSED-LOOP = FBAC * G   (SERIES CONNECTION)

*COMPUTE BODE-LOCUS

(This routine computes a locus of bode-plots for a range
of specified closed-loop gains. The user provides G,H, and
the range of gain values.)

*COMPUTE GAIN AND PHASE MARGINS

(The gain and phase margins are determined from the broken loop
system bode plot. For good stability the gain should be -6 db or
less at the $\pm 180^o$ crossings. Additionally, the phase should be $\pm 45^o$
away from $\pm 180^o$ at the 0 db crossing. For clarity, all phase
values are scaled between 0 and -360 in all bode-model plots.
Uncertainty values for gain(db) and phase(deg) may be declared by
the user. The program will warn of near 0 db or 180 deg crossings
based on these uncertainties.)

836

EXAMPLE USING SIMPLE (YAW RATE ONLY) BASIC YAW DAMPER
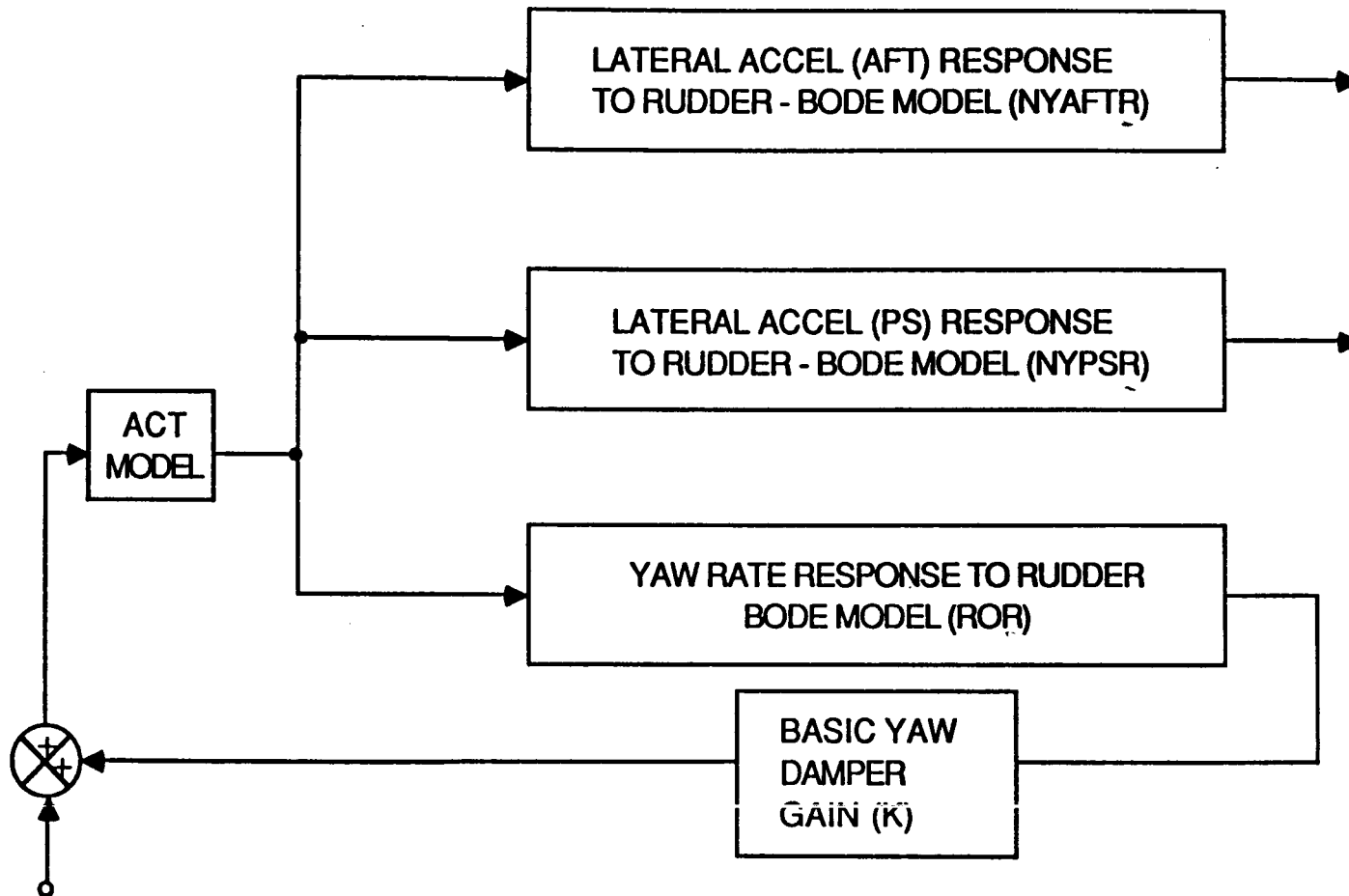
$$MPR_{AFT} = \frac{G}{1 + GH} * NYAFTR$$

where G = act model

$$MPR_{PS} = \frac{G}{1 + GH} * NYPSR$$

and H = ROR * K

12

*RESOLVE OPEN-LOOP SYSTEM

   THIS ROUTINE WILL RESOLVE THE OPEN LOOP BODE-MODELS
(G1, G2, G3...) FOR A MULTILOOP SYSTEM IF THE CLOSED-LOOP AND
FEEDBACK BODE-MODELS ARE KNOWN. A GAUSS-JORDON
SOLUTION IS REPEATED FOR EACH FREQUENCY POINT TO SOLVE
THE SET OF SIMULTANEOUS EQUATIONS.
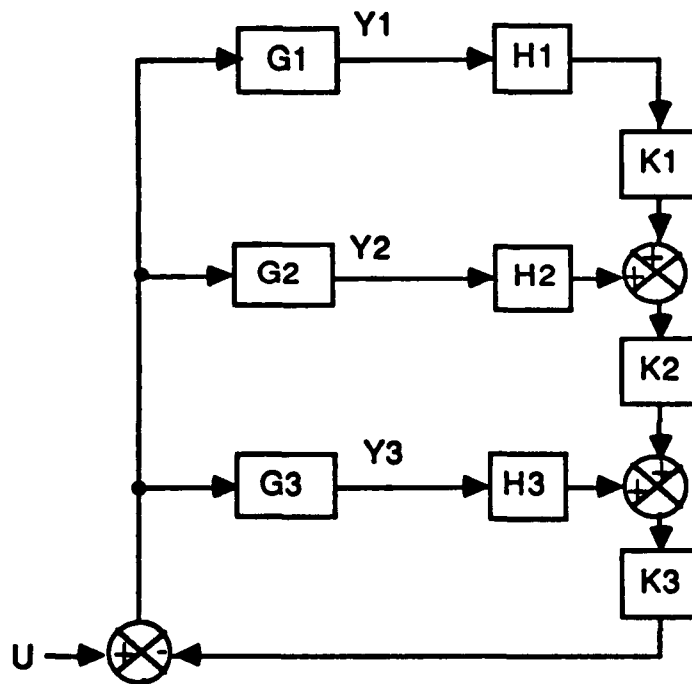
   THIS ROUTINE MAY BE USEFUL WHEN THE FLIGHT TEST DATA IS
OBTAINED WITH THE BASIC YAW DAMPER ON AND THE EFFECTS OF
THE YAW DAMPER ON STRUCTURAL MODES ARE THE DESIRED
INFORMATION.

BODEDIRECT INCLUDES NONLINEAR CAPABILITIES

which incorporates a describing function (DF) analysis

for the following :

a) hysteresis

b) rate or position limits

c) deadzones

d) variable gain

common nonlinearities

in control actuation

(rudder) systems

Using this analysis, different bode-models may be

generated as a function of input amplitude. Using

polar plots for the describing function a prediction

can be made if limit cycling will occur and at what

frequency and amplitude. Notice that BODEDIRECT

may use actual lab test data for the rudder system

if desired over the theoretical model.

CRUISE CONDITION
SQUARE WAVE SWEEP DATA
LATERAL ACCELERATION AT PILOT STATION
BODEDIRECT PERFORMANCE PREDICTION

POWER
SPECTRUM
(G^2)

◇ MSS ON
+ MSS OFF

HZ

840

CRUISE CONDITION
SQUARE WAVE SWEEP DATA
LATERAL ACCELERATION AT AFT STATION
BODEDIRECT PERFORMANCE PREDICTION

84)

CRUISE CONDITION
SINE WAVE SWEEP DATA
LATERAL ACCELERATION AT AFT STATION
BODEDIRECT PERFORMANCE PREDICTION

842

CRUISE CONDITION
SINE WAVE SWEEP DATA
LATERAL ACCELERATION AT PILOT STATION
BODEDIRECT PERFORMANCE PREDICTION

843
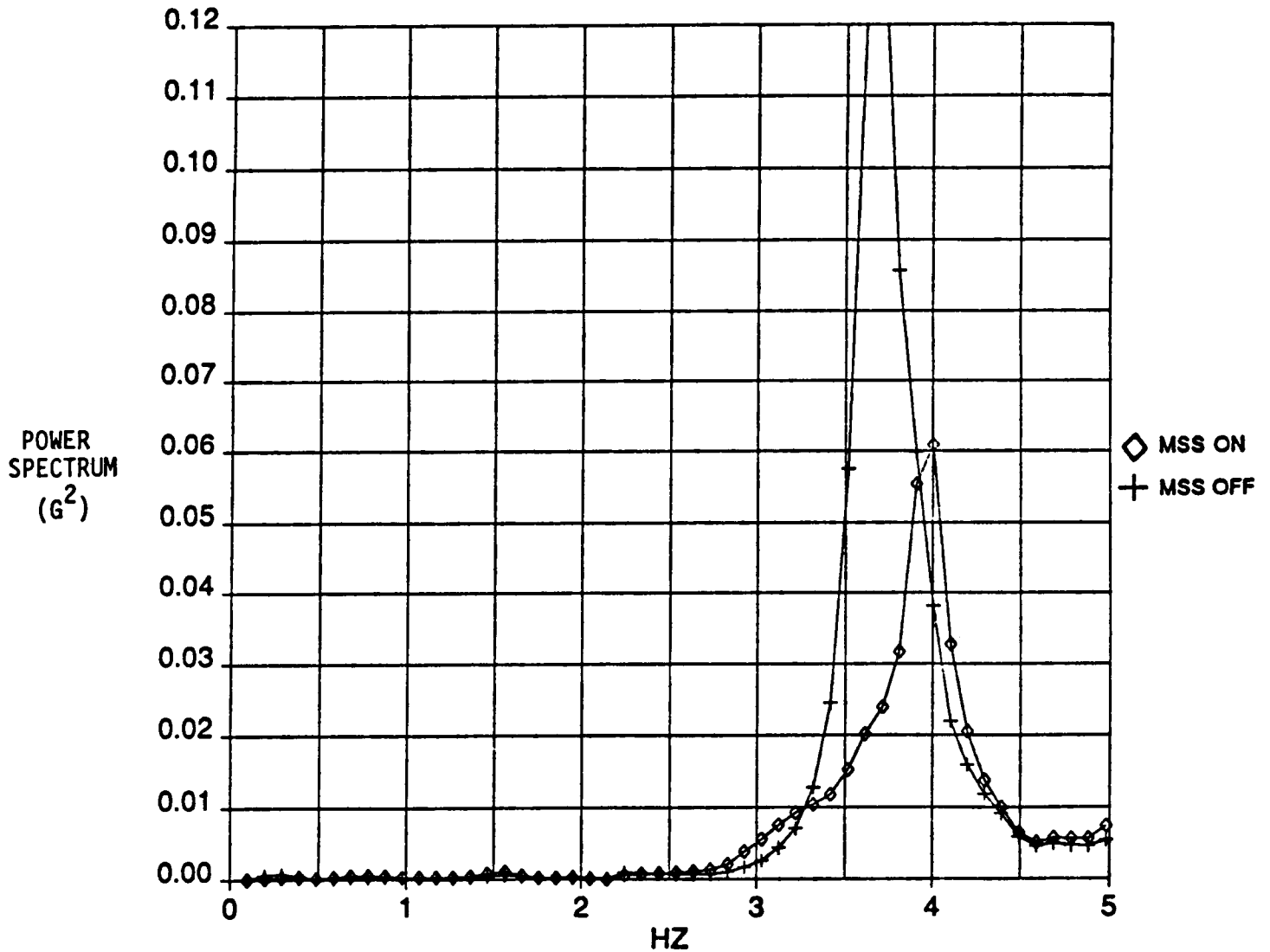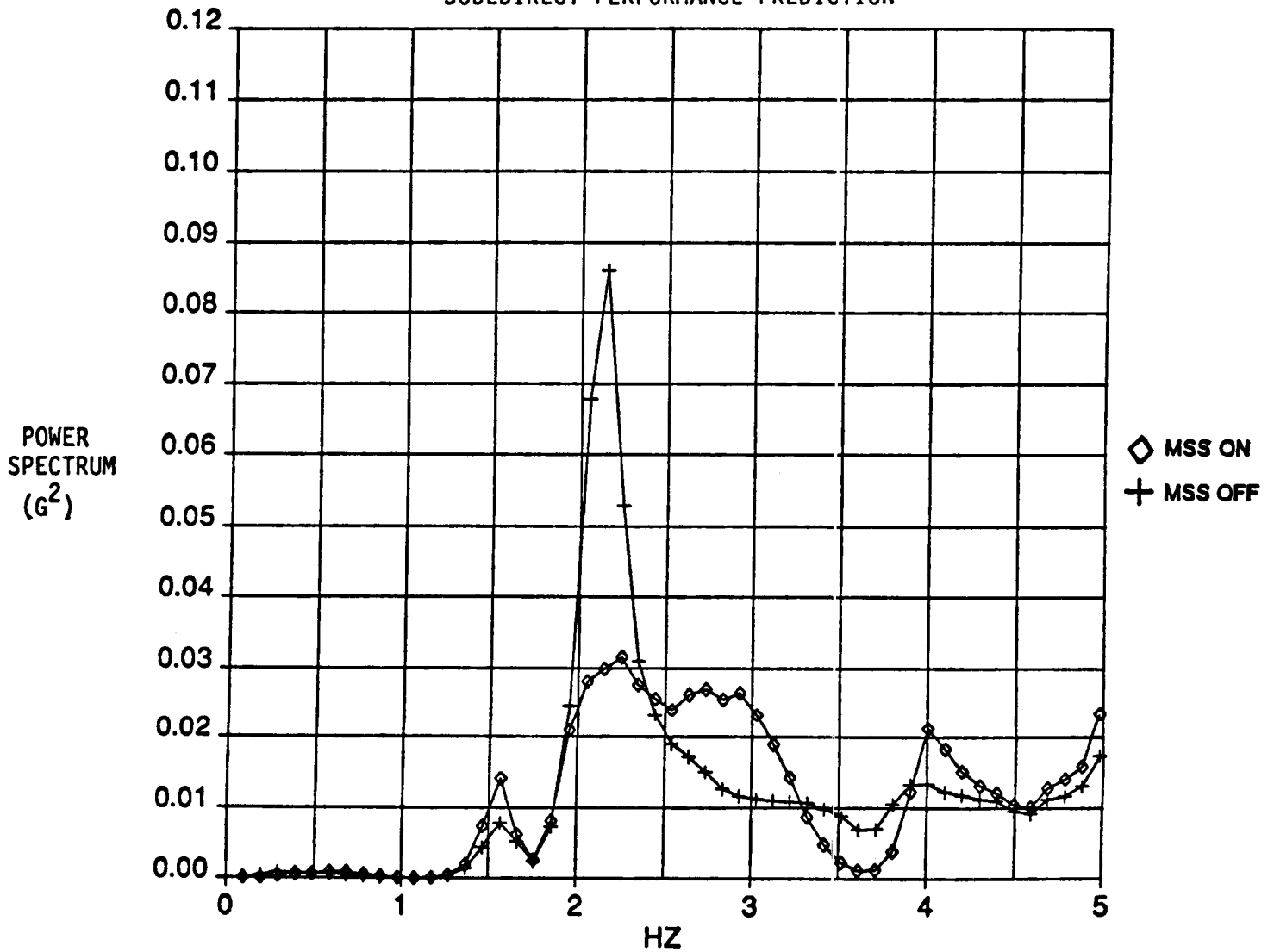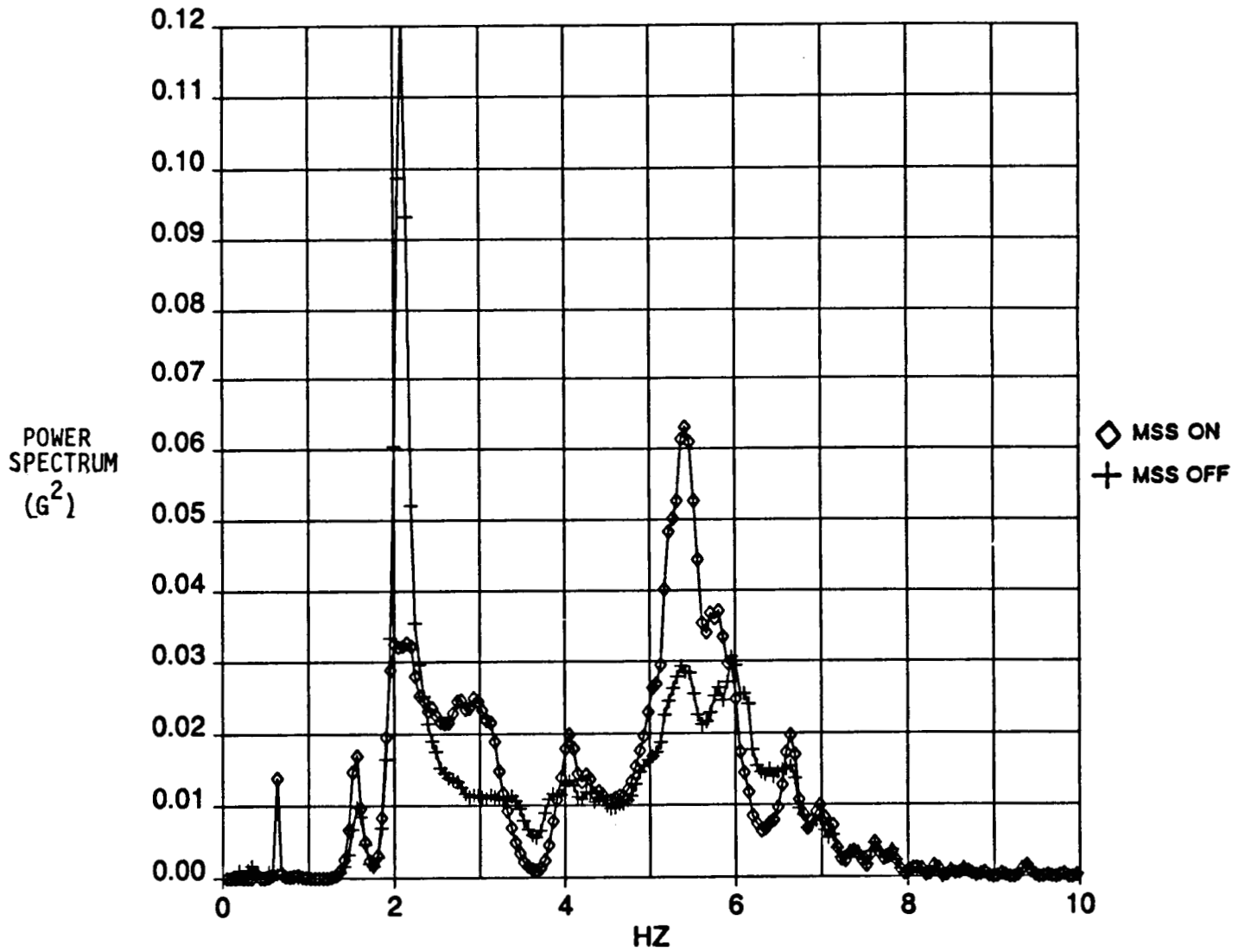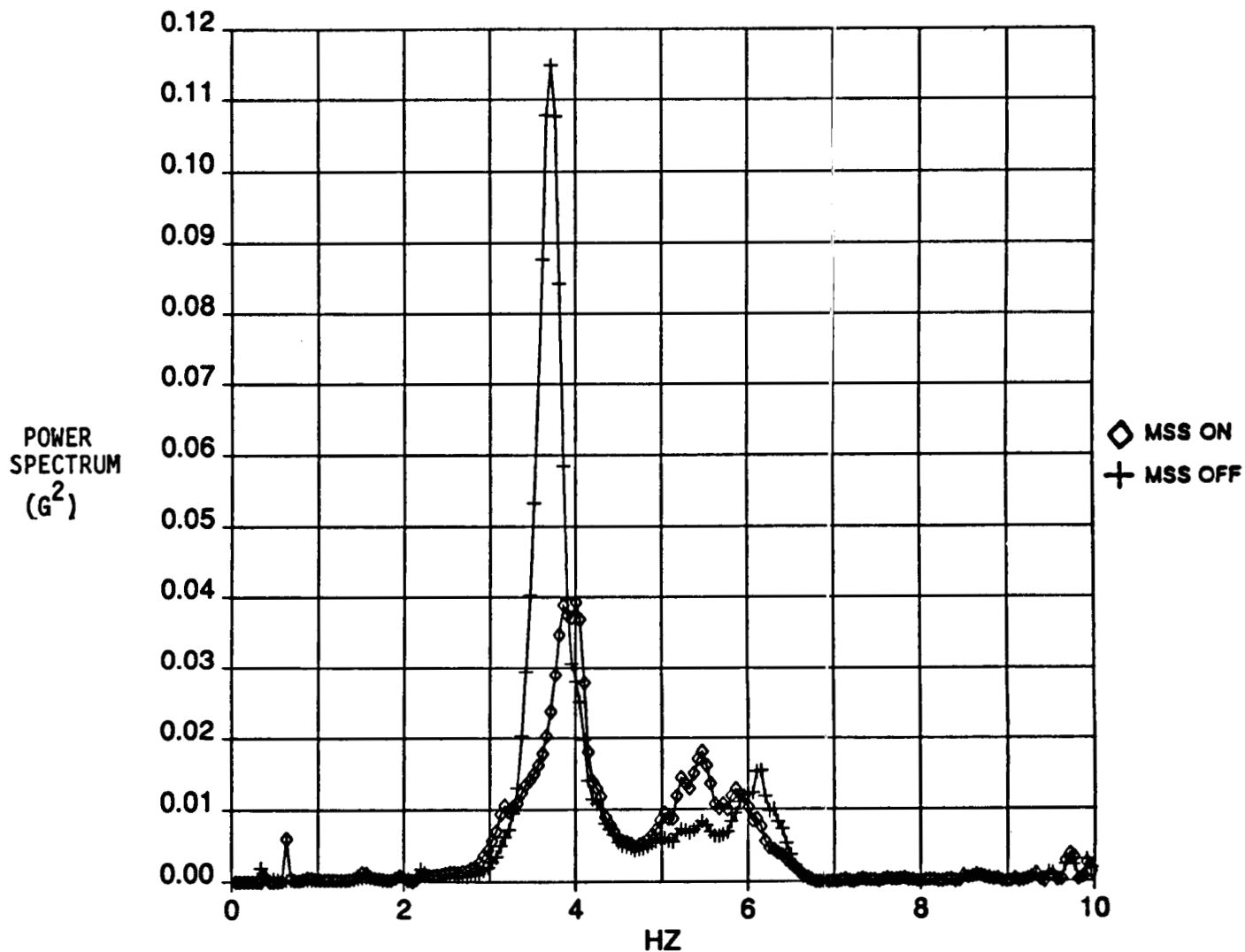
FLIGHT TEST RESULTS - CRUISE CONDITION

844

845

FLIGHT TEST RESULTS (TURBULENCE)
---- MSS OFF
—— MSS ON

8000 ft

.5 M

FLIGHT TEST RESULTS (TURBULENCE)
----- MSS OFF
——— MSS ON
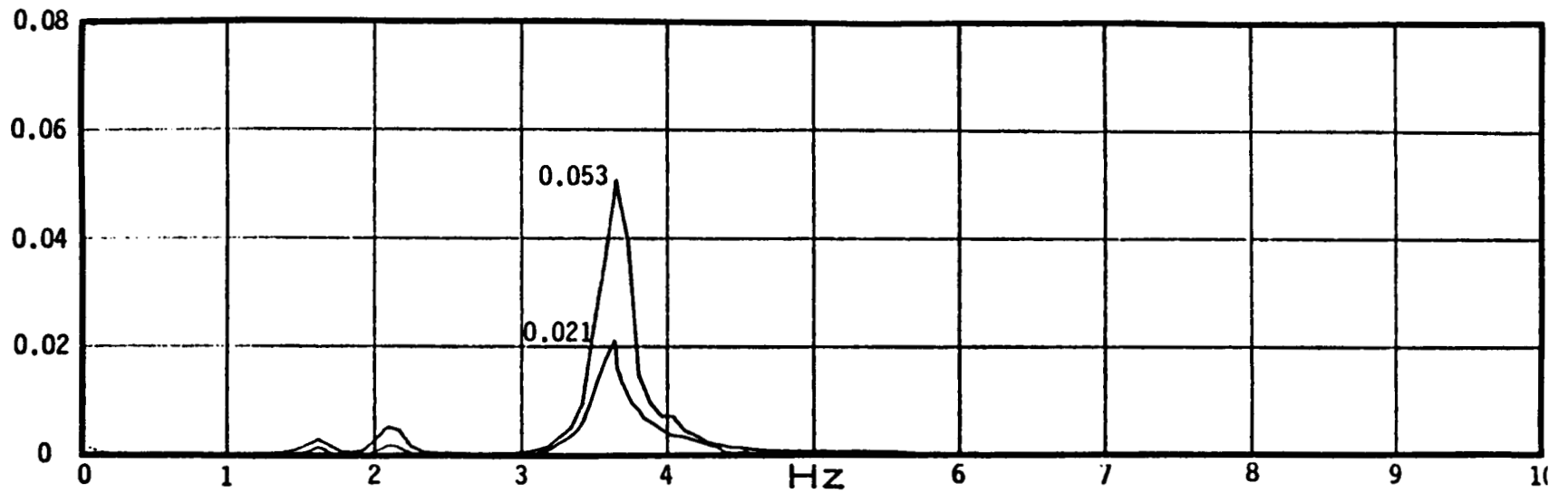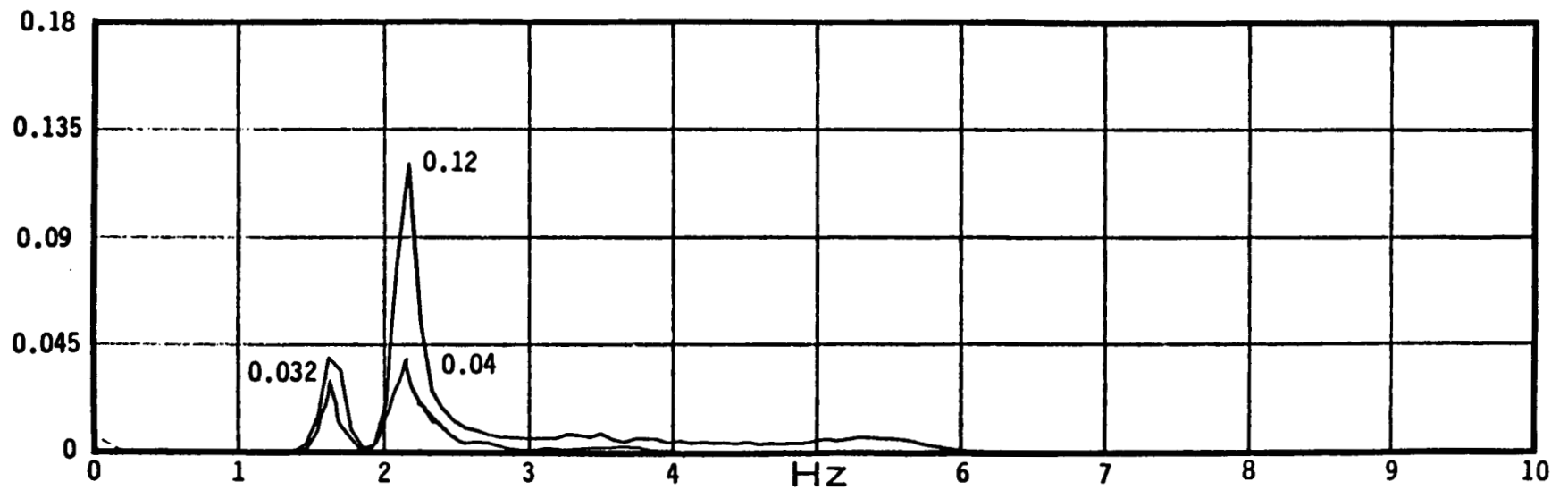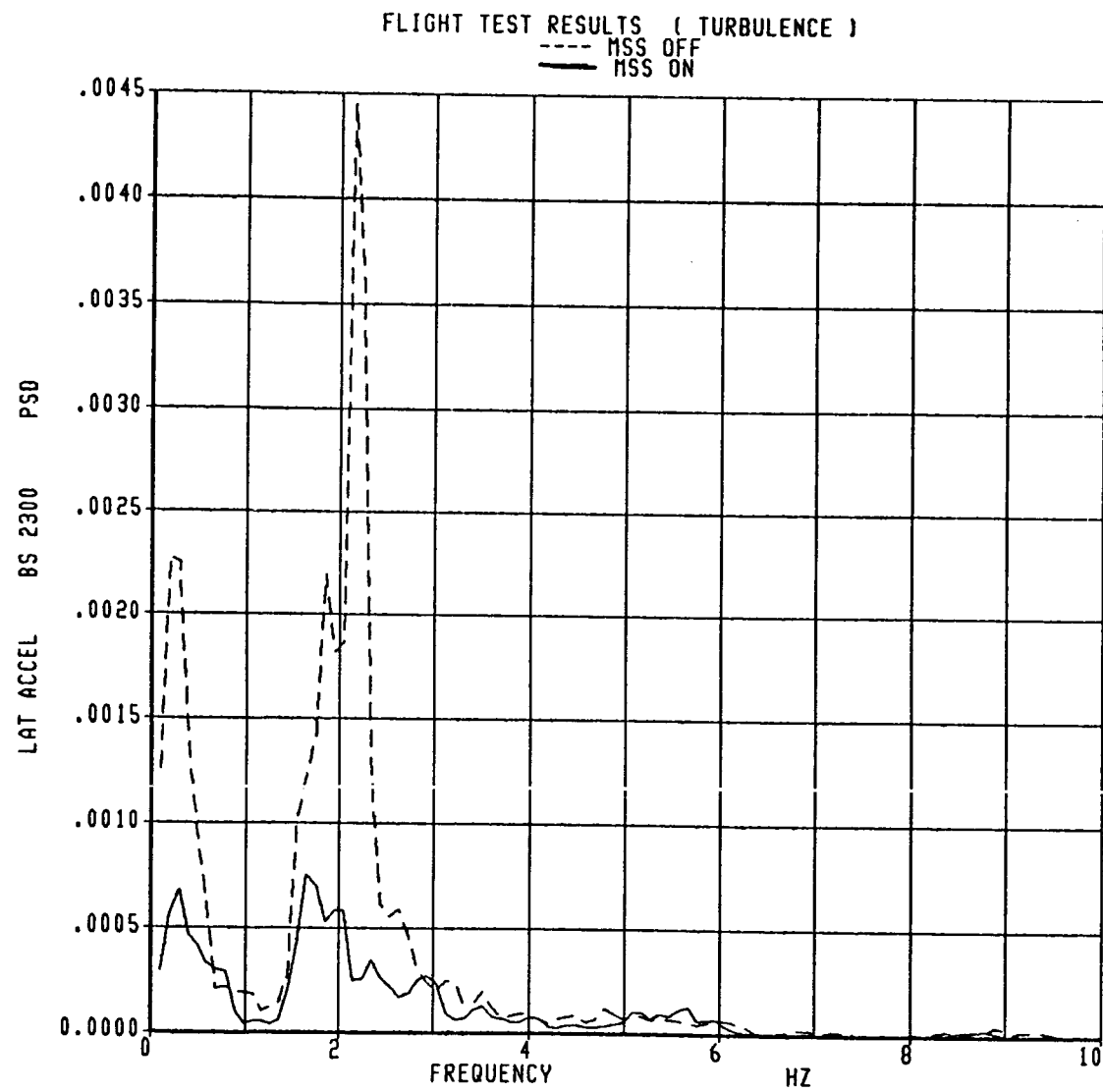
846
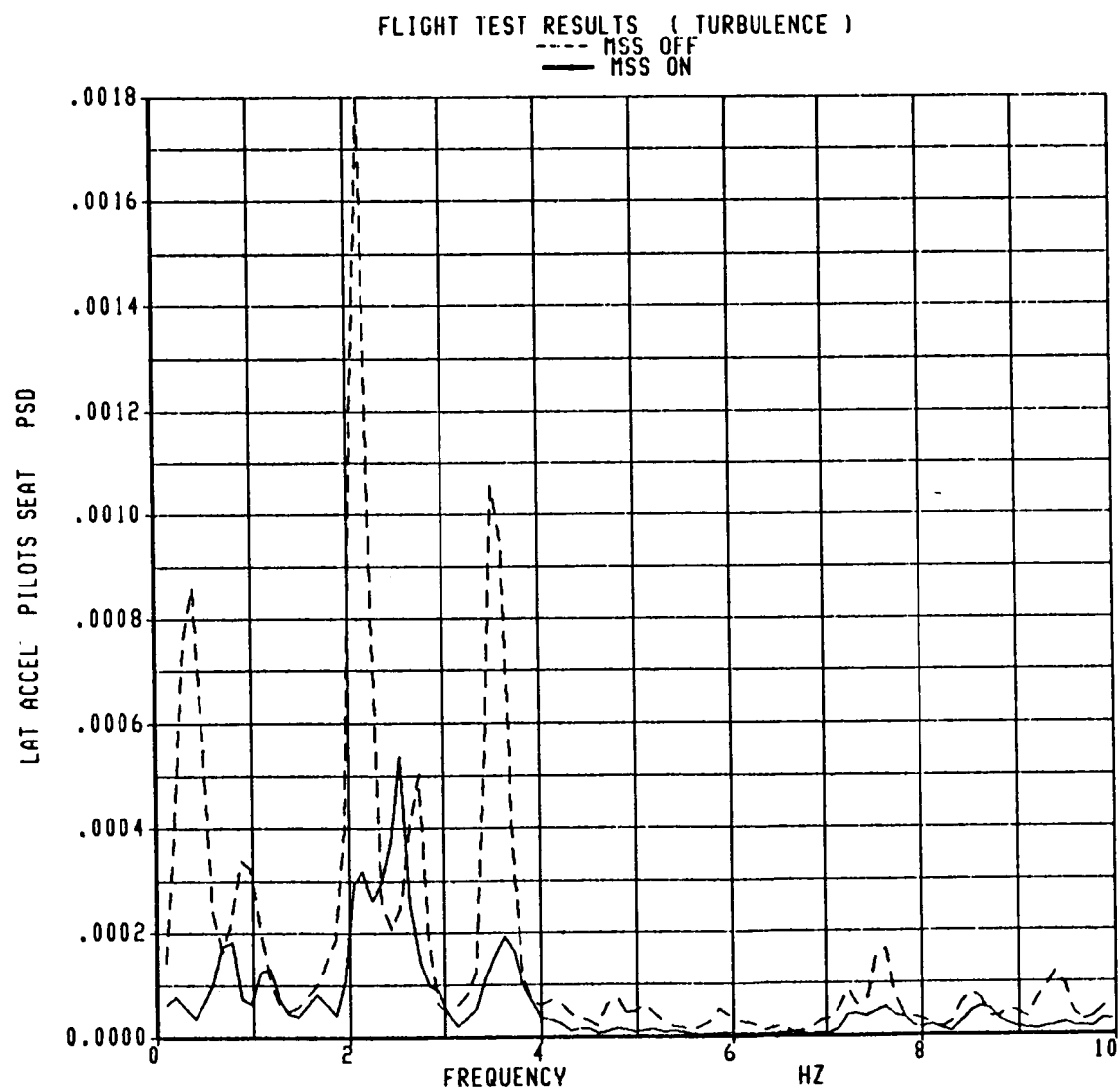
8000 ft

.5 M

## Mathematical Models	## BODEDIRECT
Advantages :	**Disadvantages :**
1) No prototype is necessary	1) A prototype must exist
2) Analysis in both time and frequency domain	2) Analysis in frequency domain only
3) Observability/controllability directly available	3) Observability/controllability not directly available
4) Eigenvalues & damping ratios directly available	4) Eigenvalues/damping ratios not directly available
Disadvantages :	**Advantages :**
1) Require large computing budgets (main frame computer)	1) Quick and inexpensive (work station environment)
2) Lack required precision	2) Accurate

847

DESCENT CONDITION
SQUARE WAVE SWEEP DATA
LATERAL ACCELERATION AT PILOT STATION
BODEDIRECT PERFORMANCE PREDICTION

848

DESCENT CONDITION
SQUARE WAVE SWEEP DATA
LATERAL ACCELERATION AT AFT STATION
BODEDIRECT PERFORMANCE PREDICTION

849

DESCENT CONDITION
SINE WAVE SWEEP DATA
LATERAL ACCELERATION AT PILOT STATION
BODEDIRECT PERFORMANCE PREDICTION

850

DESCENT CONDITION
SINE WAVE SWEEP DATA
LATERAL ACCELERATION AT AFT STATION
BODEDIRECT PERFORMANCE PREDICTION

851

OPTIMAL Q-MARKOV COVER FOR FINITE PRESICION IMPLEMENTATION

By

Darrell Williamson
Australian National University Canberra
ACT 2601, Australia

and

Robert E. Skelton
Purdue University
West Lafayette, Indiana

ABSTRACT

The existing q-Markov COVER realization theory does not take into account the problems of arithmetic errors due to both the quantization of states and coefficients of the reduced order model. All q-Markov COVERs allow some freedom in the choice of parameters. In this talk, we exploit this freedom in the existing theory to optimize the models with respect to these finite wordlength effects.

PRECEDING PAGE BLANK NOT FILMED

Optimal q-Markov Cover for
Finite Precision Implementation

Darrell Williamson* and Robert E. Skelton**

Abstract

The existing q-Markov COVER realization theory does not take into account the problems of arithmetic errors due to both the quantization of states and coefficients of the reduced order model. All q-Markov COVERs allow some freedom in the choice of parameters. In this paper we exploit this freedom in the existing theory to optimize the models with respect to these finite wordlength effects.

*Dept. of Systems Engineering, Research School of Physical Sciences, Australian National University Canberra, ACT 2601, Australia

**School of Aeronautics and Astronautics, Purdue University, West Lafayette, IN 47907, U.S.A.

855

Introduction

An asymptotically stable system can be characterized in terms of its impulse response sequence (Markov parameters) and its output covariance sequence (covariance parameters) due to a zero mean white noise input process. A general approach has been developed [3] for realizing a system which matches q Markov parameters and q covariance parameters. Such a system is referred to as a q-Markov COVER, and q-Markov COVERs may be generated from output data [3,4] or from higher order models [5,6]. The Markov and covariance parameters are not independent and consequently the q-Markov COVER is not unique. In particular, all q-Markov COVERs are not related by state space similarity transformations [4]. In this paper we shall exploit the remaining degrees of freedom to optimize the q-Markov COVER realization with respect to an aspect of its finite wordlength realization.

Specifically, when digital controllers are to be implemented, both the controller coefficients and the controller states must be represented in finite wordlength precision. This finite wordlength (FWL) representation (or quantization) causes inaccuracies in the response when compared to the ideal (i.e. infinite precision) behaviour. Effects of quantization on the controller are increased noise at the output due to internal state quantization, and errors in time and frequency response characteristics due to coefficient errors.

In digital filter design, the FWL effects are known to be most significant when the poles of the filter are very close to the unit circle [12]. In particular, narrow band filters have all these poles near $z = 1\pm\text{jo}$. For digital control, the zero-order-hold equivalent of a continuous time model (or controller) with a pole at λ will have a discrete pole at $\exp(\lambda T)$. Hence for fast sampling and/or low damping of the continuous models, the discrete model will behave like a narrow band filter. The synthesis of optimal digital controllers with respect to arithemetic quantization noise is an important consideration in design especially for continuous time systems operating under a fast sampling rate [9,10]. The effects of quantization depend highly on the structure of the controller. This paper seeks to reduce these errors in the synthesis of q-Markov COVERs.

1. Discrete q-Markov COVER

Consider the asymptotically stable nominal discrete system

$$x(k+1) = Ax(k) + Bu(k) ; \quad x(k)\epsilon R^{n_x}, u(k)\epsilon R^{n_u}$$
$$y(k) = Cx(k) \qquad ; \quad y(k)\epsilon R^{n_y} \tag{1.1}$$

where $\{u(k)\}$ is a zero mean process with unit intensity $E\{u(k)u^*(j)\} = I\delta_{ij}$ and $E\{x(k)u^*(j)\} = 0$ for $k \geq j$. The Markov parameters M_i and covariance parameters R_j of (1.1) are defined by

$$M_i \triangleq CA^iB ; \quad R_j \triangleq CA^jXC^*, \ j \geq 0, \ R_j \triangleq CXA^{*j}C^*, \ j \leq 0 \tag{1.2}$$

where the state covariance matrix X satisfies the Lyapunov Equation

$$X = AXA^* + BB^*. \tag{1.3}$$

These parameters M_i and R_j appear as coefficients in the expansion of the transfer function H(z) and power spectral density $H(z)H^*(z^{-1})$; that is

$$H(z) = C(zI-A)^{-1}B = \sum_{i=0}^{\infty} M_i z^{-(i+1)}; \quad H(z)H^*(z) = \sum_{j=-\infty}^{\infty} R_j z^{-j}$$

We suppose that as data we are given the first q-Markov and first q-covariance parameters $\{M_i, R_i; \ i = 0, 1, ..., q-1\}$ of an asymptotically stable system from which we construct the two data matrices

$$D_q \triangleq R_q - M_q M_q^* \ \epsilon \ R^{n_y q \times n_y q}$$

$$\overline{D}_q \triangleq R_q - \overline{M}_q \overline{M}_q^* \ \epsilon \ R^{n_y q \times n_y q} \tag{1.4a}$$

where R_q, M_q and $\overline{M}_q$ are the Toeplitz matrices of the data as defined by

$$R_q \triangleq \begin{bmatrix} R_0 & R_1^* & ... & R_{q-1}^* \\ R_1 & R_0 & ... & R_{q-2}^* \\ \vdots & \vdots & & \vdots \\ R_{q-2} & ... & & \\ R_{q-1} & R_{q-2} & ... & R_0 \end{bmatrix} \tag{1.4b}$$

$$M_q \triangleq \begin{bmatrix} 0 & 0 & ... & 0 & 0 \\ M_0 & 0 & ... & 0 & 0 \\ M_1 & M_0 & ... & & \\ \vdots & \vdots & & \vdots & ... \\ M_{q-2} & M_{q-3} & ... & M_0 & 0 \end{bmatrix}, \overline{M}_q \triangleq \begin{bmatrix} M_0 & 0 & ... & 0 \\ M_1 & M_0 & ... & 0 \\ \vdots & \vdots & \vdots & \vdots \\ M_{q-2} & & & 0 \\ M_{q-1} & M_{q-2} & ... & M_0 \end{bmatrix}$$

The first data matrix D_q in (1.4a) is Hermitian and it is shown in [3-4] to be

positive semidefinite. Hence we can obtain a (nonunique) full rank factorization

$$D_q = P_q P_q^*; \quad P_q \varepsilon R^{n_y q \times r_q}, \tag{1.5a}$$

where

$$r_q \stackrel{\Delta}{=} \text{rank}(D_q) = \text{rank}(P_q) \leq n_y q \tag{1.5b}$$

If we partition P_q according to

$$P_q^* = [E_q^* \; F_q^*]; \quad E_q \varepsilon R^{n_y \times r_q}, \; F_q \varepsilon R^{(q-1)n_y \times r_q} \tag{1.6}$$

then it follows that the second data matrix $\bar{D}_q$ can be factored as

$$\bar{D}_q = \bar{P}_q \bar{P}_q^*; \quad \bar{P}_q \varepsilon R^{n_y q \times r_q} \tag{1.7}$$

where

$$\bar{P}_q^* = [F_q^* \; G_q^*]; \quad G_q \varepsilon R^{n_y \times r_q} \tag{1.8}$$

for some G_q (to be determined). The following result has been established.

Theorem 1.1 [3]

Given the q Markov parameters $\{M_i; i = 0, 1, ..., q-1\}$ and the q covariance parameters $\{R_i; i = 0, 1, ..., q-1\}$ and a matrix G_q in (1.8) such that (1.7) is satisfied, then the realization $\{A_q, B_q, C_q\}$ of order r_q defined by

$$A_q = P_q^+ \bar{P}_q; \quad B_q = P_q^+ [M_0^* \; \cdots \; M_{q-1}^*]^*; \quad C_q = E_q \tag{1.9}$$

where P_q^+ denotes the Moore-Penrose inverse of P is a q-Markov COVER. The corresponding controllability grammian X_q is given by

$$X_q = I \tag{1.10}$$

Furthermore

$$P_q = [C_q^* \; A_q^* C_q^* \; \cdots \; (A_q^{q-1})^* C_q^*]^* \tag{1.11}$$

□□□

This theorem describes a large but *not* complete class C_q of q-Markov COVERs parameterized by $\{G_q\}$ such that for some E_q, F_q the data matrices $D_q, \bar{D}_q$ satisfy (1.5)-(1.8). Each matrix G_q will (generally) result in a q-Markov COVER having a different transfer function. In order to compute the set of all such G_q, observe in (1.5)-(1.8) that

$$D_q = \begin{bmatrix} E_q \\ F_q \end{bmatrix} [E_q^* \; F_q^*] \; . \tag{1.12a}$$

Then

$$\overline{D}_q = \begin{bmatrix} \overline{D}_{q-1} & \overline{d}_q \\ \overline{d}_q^* & \overline{d}_{qq} \end{bmatrix} = \begin{bmatrix} F_q \\ G_q \end{bmatrix} [F_q^* \; G_q^*] \tag{1.12b}$$

$$\overline{d}_{qq} \in R^{n_y \times n_y}$$

implies

$$E_q E_q^* = R_o \; , \quad F_q F_q^* = \overline{D}_{q-1}, \quad F_q G_q^* = \overline{d}_q, \quad G_q G_q^* = \overline{d}_{qq} \tag{1.13}$$

Now expand D_q in terms of its singular value decomposition

$$D_q = (U_1 \; U_2) \begin{bmatrix} \Sigma_1 & 0 \\ 0 & 0 \end{bmatrix} \begin{bmatrix} U_1^* \\ U_2^* \end{bmatrix} \; ; \quad \Sigma_1 \in R^{r_q \times r_q} \; . \tag{1.14}$$

Then from (1.12a)

$$(E_q^* \; F_q^*) = \Sigma_1^{1/2} U_1^* \tag{1.15}$$

so that $E_q = C_q$ is defined by the first n_y rows and F_q by the last $(q-1)n_y$ rows of $U_1 \Sigma_1^{1/2}$. Define

$$\rho_q \overset{\Delta}{=} \text{rank} (F_q) \; . \tag{1.16a}$$

Then from (1.15)

$$\rho_q \leq \min (r_q, (q-1)n_y) \; . \tag{1.16b}$$

Next, expand F_q in (1.13) in terms of its singular value decomposition. If strict inequality occurs in (1.16b) we have

$$F_q = [U_\alpha \; U_\beta] \begin{bmatrix} \Sigma_q & 0 \\ 0 & 0 \end{bmatrix} \begin{bmatrix} V_\alpha^* \\ V_\beta^* \end{bmatrix} \; ; \quad \Sigma_q \in R^{\rho_q \times \rho_q} \tag{1.17}$$

The Moore-Penrose inverse F_q^+ of F_q is then given by

$$F_q^+ = V_\alpha \Sigma_q^{-1} U_\alpha^* \tag{1.18}$$

Corollary 1.1

859

Define

$$\text{(i)} \quad G_{q1} \triangleq (F_q^+ \bar{d}_q)^* \in R^{n_y \times r_q} \tag{1.19}$$

$$\text{(ii)} \quad G_{q2} \in R^{n_y \times s_q} \text{ such that } G_{q2} G_{q2}^* \triangleq \bar{d}_{qq} - \bar{d}_q^* \bar{D}_{q-1}^+ \bar{d}_q \tag{}$$

where

$$s_q \triangleq \text{rank} \, [\bar{d}_{qq} - \bar{d}_q^* \bar{D}_{q-1}^+ \bar{d}_q] \tag{1.20}$$

and

$$\text{(iii)} \quad G_{q3} \triangleq V_\beta^* \in R^{(r_q - \rho_q) \times r_q}. \tag{1.21}$$

Then if strict inequality occurs in (1.16b) the set of all G_q which satisfy (1.13) are given by

$$G_q = G_{q1} + G_{q2} U_q G_{q3} \tag{1.22a}$$

where

$$U_q \in R^{s_q \times (r_q - \rho_q)}; \quad s_q \leq r_q - \rho_q \leq n_y \tag{1.22b}$$

is an arbitrary row unitary matrix (i.e. $U_q U_q^* = I$). Furthermore, if the Moore-Penrose P_q^+ of

$$P_q = [E_q^* \ F_q^*]^* \tag{1.23}$$

is expressed as

$$P_q^+ = [\tilde{L}_{11} \ L_{12}]; \quad \tilde{L}_{11} \in R^{r_q \times (q-1) n_y}, \ L_{12} \in R^{r_q \times n_y} \tag{1.24}$$

then the corresponding state space representation $\{A_q, B_q, C_q\}$ of the q-Markov COVER is given by

$$A_q = L_{11} + L_{12} G_q; \quad L_{11} = \tilde{L}_{11} F_q \in R^{r_q \times r_q}$$

$$B_q = P_q^+ [M_0^* M_1^* \cdots M_{q-1}^*]^*; \quad C_q = E_q. \tag{1.25}$$

If $r_q = \rho_q$, then $G_q = G_{q1}$ is unique.

Proof: The expression for $F_q G_q^*$ in (1.13) implies G_q^* is of the form

$$G_q^* = F_q^+ \bar{d}_q + G_{q3}^* M^*; \quad M \in R^{n_y \times (r_q - \rho_q)}$$

for some M. Then expanding $G_q G_q^*$ using (1.13) we have

$$\overline{d}_{qq} = \overline{d}_q^*(F_q^+)^* F_q^+ \overline{d}_q + \overline{d}_q^*(F_q^+)^* G_{q3}^* M^* + M G_{q3} F_q^+ \overline{d}_q - M G_{q3} G_{q3}^* M^*$$

Also from (1.13) and (1.21)

$$(F_q^+)^* F_q^+ = \overline{D}_{q-1}^+, \quad G_{q3} G_{q3}^* = I; \quad (F_q^+)^* G_{q3}^* = 0 \tag{1.26}$$

so that

$$MM^* = \overline{d}_{qq} - \overline{d}_q^*(F_q^+)^* F_q^+ \overline{d}_q$$

Since MM^* has rank s_q,

$$s_q = \text{rank}(G_{q2} G_{q2}^*) \le r_q - \rho_q$$

2. Optimal Finite Wordlength q-Markov COVER

A fixed point finite wordlength realization of the ideal (i.e. infinite precision) q-Markov COVER (1.1) shall be referred to as a q-FWL Markov COVER and is described by

$$\hat{x}(k+1) = \hat{A} Q[\hat{x}(k)] + \hat{B} \hat{u}(k)$$

$$\hat{y}(k) = \hat{C} Q[\hat{x}(k)] \tag{2.1}$$

$$Q[\hat{x}(k)] = \hat{x}(k) - e(k)$$

where $e(k)$ is the error in computing $\hat{x}(k)$. The components of the matrices $\hat{A}$, $\hat{B}$, $\hat{C}$ are assumed to have a W_0 bit fractional representation obtained by quantization of the components of A, B, C in (1.1). The components of $\hat{x}(k)$ have a $W+W_0$ bit fractional part while components of $Q[\hat{x}(k)]$ and $\hat{u}(k)$ all have a W bit fractional part. The components of the state residue vector $e(k)$ has a $W+W_0$ bit fractional representation in which the most significant W bits are zero. The LHS and RHS of (2.1) are therefore consistent with respect to their fractional wordlength representation. The number of bits required to represent the integer parts of $\hat{A}$, $\hat{B}$ and $\hat{C}$ depend on the dynamic range of the coefficients. State space structures in which all coefficients are less than unity are therefore advantageous in this regard. The required integer representation of $Q[\hat{x}(k)]$ will depend on the dynamic range of the input signal $\hat{u}(k)$. Inadequate dynamic range will result in arithmetic overflow. The accuracy in the computation of $\hat{x}(k)$ is determined by its fractional wordlength W.

Define the state error vector $\varepsilon_x(k)$ and output error vector $\varepsilon_y(k)$ by

$$\varepsilon_x(k) \triangleq \hat{x}(k) - x(k); \quad \varepsilon_y(k) \triangleq \hat{y}(k) - y(k) \tag{2.2}$$

Then from (1.1), (2.1) and (2.2)

$$\varepsilon_x(k+1) = A\varepsilon_x(k) - Ae(k) + \Delta A Q[\hat{x}(k)] + \Delta B u(k) + B\Delta u(k) \tag{2.3}$$

$$\varepsilon_y(k) = C\varepsilon_x(k) - Ce(k) + \Delta C Q[\hat{x}(k)]$$

where

$$\Delta A = \hat{A} - A; \quad \Delta B = \hat{B} - B; \quad \Delta C = \hat{C} - C$$

$$\Delta u(k) = \hat{u}(k) - u(k)$$

There are five terms which contribute to the output error (i) internal arithmetic errors $e(k)$ due to state quantization (ii) coefficient errors due to errors ΔA in A (iii) ΔB in B (iv) ΔC in C, and (v) input quantization errors $\Delta u(k)$. Under weak 'sufficiently exciting' conditions on the input $\{u(k)\}$ it can be shown [6] that if $Q[\cdot]$ in (2.1) denotes 'roundoff' quantization, then $\{e(k)\}$ is a zero mean uniform white process with covariance

$$E\{e(k)e^*(k)\} = \gamma^2 I; \quad \gamma^2 = \frac{1}{12} 2^{-2W}. \tag{2.4}$$

Similarly $\{\Delta u(k)\}$ is assumed to be a zero mean white uniform process with

$$E\{\Delta u(k)\Delta^* u(k)\} = \gamma^2 I \tag{2.5}$$

We assume that the quantized coefficients $\hat{A}$, $\hat{B}$, $\hat{C}$ are obtained by rounding A, B, C to W_0 bit fractions. Consequently, all components Δp of the error matrices ΔA, ΔB, ΔC satisfy

$$|\Delta p| < \gamma_0; \quad \gamma_0 = \frac{1}{2} 2^{-W_0}. \tag{2.6}$$

For simplicity we normalize the error matrices and define δA, δB, δC by

$$\delta A \triangleq \frac{1}{\gamma_0} \Delta A; \quad \delta B \triangleq \frac{1}{\gamma_0} \Delta B; \quad \delta C \triangleq \frac{1}{\gamma_0} \Delta C \tag{2.7}$$

so that all components δp of δA, δB and δC satisfy

$$|\delta p| < 1. \tag{2.8}$$

The steady state output error covariance Y of $\{\varepsilon_y(k)\}$ is then given by (we assume independence of $\varepsilon(k)$, $e(k)$ and $\hat{x}(k)$).

$$Y = CPC^* + \gamma^2 CC^* + \gamma_0^2(\delta C)(\hat{X}+\gamma^2 I)(\delta C)^* + \gamma_0\gamma^2[C(\delta C)^* + (\delta C)C^*] , \quad (2.9)$$

where

$$P = E\{\varepsilon_x(k)\varepsilon_x^*(k)\}$$

$$= APA^* + \gamma^2 AA^* + \gamma_0^2(\delta A)(\hat{X}+\gamma^2 I)(\delta A)^* + \gamma_0^2(\delta B)(\delta B)^* + \gamma^2 BB^*$$

and

$$\hat{X} = E\{\hat{x}(k)\hat{x}^*(k)\} = \hat{A}\hat{X}(\hat{A})^* + \gamma^2\hat{A}(\hat{A})^* + (1+\gamma^2)\hat{B}\hat{B}^*$$

For the remainder of this section we assume no coefficient errors (i.e. $\gamma_0 = 0$ in (2.9)) and consider only the effects due to *finite state wordlength* (FSWL). The issue of coefficient error shall be resumed in Section 4.

Theorem 2.1

Define the output noise measure

$$J \triangleq tr[Y] .$$

Then for $\gamma_0 = 0$

$$J = \gamma^2\{tr[K] + tr[B^*KB]\} \quad (2.10)$$

where

$$K = A^*KA + C^*C . \quad (2.11)$$

Proof: From (2.9)

$$Y = C\bar{P}C^*; \quad \bar{P} = A\bar{P}A^* + \gamma^2 Z = P + \gamma^2 I$$

where

$$Z = I + BB^*;$$

Now

$$\bar{P} = \gamma^2 \sum_{k=0}^{\infty} A^k Z(A^k)^*$$

and

$$K = \sum_{k=0}^{\infty} (A^k)^*C^*CA^k$$

so that

$$\text{tr}[\bar{C}PC^*] = \gamma^2 \text{tr}(ZK).$$

□□□

A *fixed point q-FSWL Markov COVER* corresponding to the (ideal) q-Markov COVER (1.1) is therefore described by

$$\hat{x}(k+1) = AQ[\hat{x}(k)] + B\hat{u}(k)$$

$$\hat{y}(k) = CQ[\hat{x}(k)] \tag{2.12}$$

$$Q[\hat{x}(k)] = \hat{x}(k) - e(k)$$

The *output noise gain* (η_x) *due to state quantization* and the *output noise gain* (η_u) *due to input quantization* are defined by

$$\eta_x \triangleq \text{tr}[K]; \quad \eta_u \triangleq \text{tr}[B^*KB] \tag{2.13}$$

The noise gain η_x generally varies with state space representation whereas η_u is independent of the coordinate basis. Specifically, consider the q-FSWL Markov COVER

$$\hat{z}(k+1) = A\,Q[\hat{z}(k)] + B\,\hat{u}(k)$$

$$y(k) = C\,Q[\hat{z}(k)] \tag{2.14a}$$

$$Q[\hat{z}(k)] = \hat{z}(k) - f(k)$$

where

$$A = T^{-1}AT, \quad B = T^{-1}B, \quad C = CT \tag{2.14b}$$

and $Q[\hat{z}(k)]$ has a W bit fractional representation. Assuming 'sufficient excitation' by $\hat{u}(k)$, the state residue sequence $\{f(k)\}$ in (2.14a) due to roundoff quantization will again be a zero mean white uniform process with covariance $\gamma^2 I$ as in (2.5). The corresponding output quantization noise gains η_z and $\tilde{\eta}_u$ due respectively to state and input quantization are given by

$$\eta_z = \text{tr}[K_z]; \quad \tilde{\eta}_u = \text{tr}[B^*K_zB] \tag{2.15}$$

where B is given by (2.14b) and

$$K_z = A\,K_zA^* + C^*C. \tag{2.16}$$

But from (2.11), $K_z = T^*KT$, so that

$$\eta_z = tr[T^*KT]; \quad \tilde{\eta}_u = tr[B^*KB] \qquad (2.17)$$

Notice from (2.13) that the noise gain η_u due to input quantization errors is *unaffected* by a similarity transformation. Conversely the noise gain η_x due to state quantization generally changes with co-ordinate bases. There is no change if T is unitary. The q-FSWL Markov COVER (2.14) is superior to the q-FSWL Markov COVER (2.12) if

$$\eta_z < \eta_x . \qquad (2.18)$$

However the comparison in (2.18) must be made under the assumption of *identical scaling* of the states $\hat{x}(k)$ and $\hat{z}(k)$. Specifically, equal l_2-scaling of gain α from a zero mean unit intensity white noise input $\hat{u}(k)$ to the state components $\hat{x}_j(k)$ of $\hat{x}(k)$ requires

$$X_{jj} = \alpha \text{ for all } j \qquad (2.19)$$

where X_{jj} denotes the jth diagonal component of the state covariance matrix X given by (1.3). Equal l_2-scaling of gain α of components of $\hat{z}(k)$ in (2.14) requires

$$Z_{jj} = \alpha; \quad Z = AZA^* + BB^* \qquad (2.20)$$

Equality in l_2-scaling of representations (2.12) and (2.14) is equivalent to equality in the state dynamic range (i.e. number of bits in the integer representation of states) for a given probability of overflow. We now state a result which is important for establishing l_2-scaling.

Lemma 2.1 [8,9] Suppose $M = M^* > 0$ is an nxn matrix. Then a necessary and sufficient condition for the existence of a unitary matrix V such that

$$VMV_{jj}^* = \alpha \text{ for all } j$$

is

$$tr[M] = n\alpha$$

□□□

We have shown in Lemma 1.1 that different similarity transformations of an ideal q-Markov COVER corresponds to different factorization of the first data matrix D_q in (1.5a). Our aim is to optimize this factorization.

Definition 2.1

The *Optimal q-FSWL Markov COVER* minimizes the output quantization noise gain η due to state quantization errors; that is

$$\eta_{opt} = \min_{T, G_q} tr[T^*K_qT]; \quad T^*T = \Lambda^{-1} \tag{2.21}$$

subject to the l_2-scaling constraint:

$$\Lambda_{jj} = \alpha \text{ for all } j \tag{2.22}$$

where the observability grammian K_q satisfies

$$K_q = A_q^*K_qA_q + C_q^*C_q \tag{2.23}$$

with $\{A_q, B_q, C_q\}$ defined by (1.22)-(1.25).

◻◻◻

In corollary 1.1 we have shown that all the degrees of freedom available to select G_q are confined to an arbitrary row unitary matrix U_q. We now show how to optimize U_q.

Theorem 2.1

a. The optimal q-FSWL Markov COVER (1.25) is defined by

$$\eta_{opt} = r_q^{-1} \min_{U_q} (tr[K_q^{\frac{1}{2}}])^2 \tag{2.24}$$

where $U_q \in R^{s_q \times (r_q - p_q)}$ is an arbitrary row unitary matrix and K_q satisfies (2.23).

b. The transfer function of the optimal q-FSWL Markov COVER has Hankel singular values given by the eigenvalues of K_q defined by the minimizing U_q.

c. Suppose $U_q = U_{qo}$ is the minimizing solution corresponding to the optimal $G_q = G_{qo}$ in (1.22a). Let $\{A_{qo}, B_{qo}, C_{qo}\}$ be the corresponding state space realization in (1.24). Then the optimal q-FSWL Markov COVER has a (nonunique) state space representation $\{T_o^{-1}A_{qo}T_o, T_o^{-1}B_{qo}, C_{qo}T_o\}$ where

$$T_o = U_o\pi_oV_o^* \tag{2.25}$$

such that

(i) the unitary matrix U_o is defined by

866

$$U_o^* K_{qo} U_o = \Sigma_o^2 \tag{2.26a}$$

where

$$K_{qo} = A_{qo} K_{qo} A_{qo}^* + C_{qo}^* C_{qo} \; ; \; \Sigma_o^2 = \text{diag}\{\sigma_{1o}^2, \sigma_{2o}^2, ..., \sigma_{r_qo}^2\} \tag{2.26b}$$

in which $\{\sigma_{jo}^2\}$ are the optimal Hankel singular values (eigenvalues of K_{qo}).
(ii)

$$\pi_o^2 = \frac{1}{\alpha^2 r_q} (\sum_{k=1}^{r_q} \sigma_{ko}) \Sigma_o^{-1} \tag{2.27}$$

and (iii) V_o is unitary such that

$$(V_o \Sigma_o V_o^*)_{jj} = \frac{\sum_{k=1}^{r_q} \sigma_{ko}}{r_q} \quad \text{for all } j \tag{2.28}$$

$$\eta_{opt} \triangleq \eta_q \text{ (optimal)} = \frac{1}{\alpha^2 r_q} (\sum_{k=1}^{r_q} \sigma_{ko})^2 \tag{2.29}$$

Proof: By corollary 1.1 we have for G_q defined by (1.22) for any row unitary matrix U_q (of appropriately specified dimensions) that G_q defines a q-Markov COVER. The corresponding realization $\{A_q, B_q, C_q\}$ for each such U_q has identity controllability grammian and observability grammian K_q defined by (2.23). Now given a particular U_q, apply a similarity transformation

$$T = U_o \pi_o V_o^*$$

to the given q-Markov COVER. Then

$$\text{tr}(T^* K_q T) = \text{tr}(\pi_o^2 U_o^* K_q U_o)$$

and

$$(T^* T)^{-1} = V_o \pi_o^{-2} V_o^*$$

By lemma 2.1, the l_2-scaling constant can be satisfied for some V_o provided $\text{tr}(\pi_o^{-2}) = n\alpha$. Following Williamson [1, Theorem 4.1] (with a minor modification of the l_2-scaling constraint), the optimal performance is given by

$$\eta_{qopt} = \frac{(\sum\limits_{\alpha=1}^{r_q} \sigma_j)^2}{\alpha^2 r_q}$$

where $\{\sigma_j^2\}$ are the eigenvalues of K_q. That is,

$$tr(K_q^{\frac{1}{2}}) = \sum\limits_{j=1}^{r_q} \sigma_j$$

The *optimal* q-FSWL Markov COVER therefore achieves the minimum in (2.24). The structure of U_o, π_o, V_o in (2.25)-(2.29) follow directly from Williamson [1] (see proof of Theorem 4.1 with $U = I$).

3. Computation of the Optimal FSWL Markov COVER

Necessary conditions for the optimal solution in Theorem 2.1 can be obtained using the method of Lagrange multipliers. Specifically, let

$$J = (tr[K_q^{\frac{1}{4}}])^2 + tr[\Lambda(-K_q + A_q^* K_q A_q + C_q^* C_q)] + tr[\Omega(I - U_q U_q^*)] \qquad (3.1a)$$

where

$$K_q = K_q^{\frac{1}{2}} K_1^{\frac{1}{2}^*} \quad \Lambda = \Lambda^* \in R^{r_q \times r_q}; \quad \Omega = \Omega^* \in R^{s_q \times s_q} \qquad (3.1b)$$

are symmetric Lagrange multipliers. After taking derivatives of J using (1.22) and (1.25)

$$\frac{\partial J}{\partial \Lambda} = -K_q + A_q^* K_q A_q + C_q^* C_q$$

$$\frac{\partial J}{\partial \Omega} = I - U_q U_q^*$$

$$\frac{\partial J}{\partial K_q^{\frac{1}{2}}} = 2I - 2\Lambda K_q^{\frac{1}{2}} + 2A_q \Lambda A_q^* K_q^{\frac{1}{2}} \qquad (3.2)$$

$$\frac{\partial J}{\partial U_q} = 2G_{q2}^* L_{12}^* K_q A_q \Lambda G_{q3}^* - 2\Omega U_q$$

By setting these derivatives to zero we obtain the following result.

Lemma 3.1 Necessary conditions for the derivation of the optimal q-FSWL Markov COVER are given by

$$K_q = A_q^* K_q A_q + C_q^* C_q$$

$$\Lambda = A_q \Lambda A_q^* + K_q^{-\frac{1}{2}}; \quad \Lambda = \Lambda^* \in R^{r_q \times r_q}$$

$$U_q U_q^* = I \qquad ; \quad U_q \in R^{s_q \times (r_q - p_q)} \tag{3.3}$$

$$\Omega U_q - P_q U_q Q_q = R_q \quad ; \quad \Omega = \Omega^* \in R^{s_q \times s_q}$$

where

$$P_q = P_q^* = G_{q2}^* L_{12}^* K_q L_{12} G_{q2} \in R^{s_q \times s_q}$$

$$Q_q = Q_q^* = G_{q3} \Lambda G_{q3}^* \in R^{(r_q - p_q) \times (r_q - p_q)} \tag{3.4}$$

$$R_q = G_{q2}^* L_{12}^* K_q (L_{11} + L_{12} G_{q1}) \Lambda G_{q3}^* \in R^{s_q \times (r_q - p_q)}$$

and A_q, G_{qj}, L_{ij} are defined by (1.20)-(1.24)

□□□

These necessary conditions cannot be solved explicitly for the optimal row unitary matrix U_q and so an iterative procedure is required. One possible algorithm is now described.

Recursive Algorithm for Optimal q-FSWL Markov COVER:

(0) Set $j = 0$ and choose any row unitary $U_q(0)$ in (1.21a)

(1) Form $A_q(j)$ from

$$A_q(j) = (L_{11} + L_{12} G_{q1}) + L_{12} G_{q2} U_q(j) G_{q3} \tag{3.5a}$$

(2) Compute $K_q(j)$: $K_1(j) = A_q^*(j) K_q(j) A_q(j) + C_q^* C_q \tag{3.5b}$

(3) Compute $\Lambda(j)$: $\Lambda(j) = A_q(j) \Lambda(j) A_q^*(j) + K_q^{-\frac{1}{2}}(j)$; $\Lambda(j) = \Lambda^*(j) \tag{3.5c}$

(4) Compute $P_q(j)$, $Q_q(j)$ $R_q(j)$:

$$P_q(j) = G_{q2}^* L_{12}^* K_q(j) L_{12} G_{q2}; \quad Q_q(j) = G_{q3} \Lambda(j) G_{q3}^*;$$

$$R_q(j) = G_{q2}^* L_{12}^* K_q(j) (L_{11} + L_{12} G_{q1}) \Lambda(j) G_{q3}^* \tag{3.5d}$$

(5) Update $U_q(j)$ by solving the nonlinear algebra problem:

$$\Omega(j)U_q(j+1) - P_q(j)U_q(j+1)Q_q(j) = R_q(j); \quad \Omega(j) = \Omega^*(j) \qquad (3.5e)$$

$$U_q(j+1)U_q^*(j+1) = I$$

The most difficult step at each stage of the algorithm is to solve (3.5e) for a row unitary $U_q(j+1)$ and symmetric $\Omega(j)$. There is generally no explicit solution except for the following special cases.

Lemma 3.2 Consider the equation

$$\Omega U_q - P_q U_q Q_q = R_q; \quad \Omega \in R^{s_q \times s_q} \qquad (3.6)$$

where

$$P_q = P_q^* \in R^{s_q \times s_q}; \quad Q_q = Q_q^* \in R^{(r_q - p_q) \times (r_q - p_q)}; \quad R_q \in R^{s_q \times (r_q - p_q)} \qquad (3.7)$$

are given. Then there exists an analytical solution (Ω, U_q) with Ω *symmetric* and U_q *row unitary* when $s_q = 1$ or $Q_q = \beta I$. (β scalar)

a. When $s_q = 1$, Ω and P_q are scalars and R_q is a row vector. Then U_q is arbitrary for $R_q = 0$ while for $R_q \neq 0$

$$U_q = R_q(\Omega I - P_q Q_q)^{-1}; \quad \|U_q\| = 1 \qquad (3.8)$$

b. When $Q_q = \beta I$, let $R_q R_q^*$ have the singular value decomposition

$$R_q R_q^* = (V_1 \ V_2) \begin{bmatrix} \Sigma_{q1} & 0 \\ 0 & 0 \end{bmatrix} \begin{bmatrix} V_1^* \\ V_2^* \end{bmatrix}$$

where Σ_{q1} is invertible. Then

$$U_q = (V_1^*)^+ \Sigma_{q1}^{-\frac{1}{2}} V_1^* R_q; \quad \Omega = \beta P_q + V_1 \Sigma_{q1}^{\frac{1}{2}} V_1^* \qquad (3.9)$$

In particular, when $R_q R_q^*$ has full rank,

$$U_q = (R_q R_q^*)^{-\frac{1}{2}} R_q \qquad (3.10)$$

Proof: For case (a)

$$U_q(\Omega I - P_q Q_q) = R_q; \quad \Omega \text{ scalar}$$

so that (3.8) follows by the row unitary property $U_q U_q^* = I$. In case (b)

$$(\Omega - \beta P_q)U_q = R_q$$

and using the row unitary property of U_q

$$(\Omega - \beta P_q)^2 = R_q R_q^*$$

Hence using the SVD of $R_q R_q^*$

$$V_1 \Sigma_{q1}^{\frac{1}{2}} V_1^* U_q = R_q$$

But $V_1^* V_1 = I$ and V_1^* has full row rank which gives (3.9).

□□□

Strictly speaking, (3.8) is not an analytical solution since the scalar Ω must still be chosen so that $\|U_q\| = 1$. Note that by Corollary 1.1, $G_{q3}G_{q3}^* = I$ so that $Q_q(j) = I$ in (3.5b) if $\Lambda(j) = I$. The necessary condition (3.5e) is equivalent to assuming $K_q(j)$, $\Lambda(j)$, $P_q(j)$, $Q_q(j)$ and $R_q(j)$ are known and optimizing over row unitary $U_q(j+1)$. That is, after dropping the index j and $j+1$ in (3.5e) we have the following result.

Lemma 3.3 Suppose P_q, Q_q and R_q in (3.7) are known. Then a necessary condition for a row unitary matrix U_q to achieve optimally for the problem:

$$\min_{U_q} \text{tr}[Q_q U_q^* P_q U_q + 2R_q U_q]; \quad U_q \in R^{s_q \times (r_q - p_q)} \tag{3.11}$$

is that there exists a symmetric matrix Ω such that (3.6) is satisfied.

Furthermore, the optimization in (3.11) is equivalent to

$$\min_{U} J(U); \quad U \in R^{(r_q - p_q) \times (r_q - p_q)} \tag{3.12a}$$

where

$$J(U) = \text{tr}[QU^* PU + 2RU] \tag{3.12b}$$

over unitary matrices $U^* = [U_q^* \quad V_q^*]$ where $Q = Q_q$ and

$$P = P^* = \begin{bmatrix} P_q & 0 \\ 0 & 0 \end{bmatrix} \in R^{(r_q - p_q) \times (r_q - p_q)}$$

$$R = [R_q \quad 0] \in R^{(r_q - p_q) \times (r_q - p_q)}$$

□□□

The advantage of the point of view (3.12) is that U can be treated as a *square*

matrix. The solution to (3.12) when U is a 2x2 unitary matrix is provided in the following lemma. The result can be derived by directly substituting into (3.12).

Lemma 3.4 Suppose $P = P^* = [p_{ij}]$, $Q = Q^* = [q_{ij}]$ and $R = [r_{ij}]$ are 2x2 matrices. Then the minimum in (3.12) over 2x2 unitary matrices U is achieved by either

(i) $U = \text{diag}\{u_1, u_2\}$ where $u_1^2 = 1$, $u_2^2 = 1$ minimize

$$J_1 = r_{11}u_1 + r_{22}u_2 + 2q_{12}p_{12}u_1u_2 \qquad (3.13)$$

or (ii)

$$U = \begin{bmatrix} x & \sqrt{1-x^2} \\ -\sqrt{1-x^2} & x \end{bmatrix}$$

where $|x| \leq 1$ minimizes

$$J_2(x) = ax^2 + 2bx + 2(cx+d)\sqrt{1-x^2} \qquad (3.14)$$

$$a = (p_{11}-p_{22})(q_{11}-q_{22}), \quad b = r_{11}+r_{22}$$

$$c = q_{12}(p_{11}-p_{22}) + p_{12}(q_{22}-q_{11}), \quad d = r_{21} - r_{12}$$

□□□

Note that we must optimize over the disjoint sets of 2x2 unitary matrices consisting of *signature matrices* (as in (3.13)) and *rotations* (as in (3.14)). The optimal solution of (3.13) can be obtained by inspection of the magnitudes of the coefficients in u_j. For example, suppose

$$|r_{11}| \geq |q_{12}p_{12}| \geq |r_{22}|$$

Then

$$u_1 = -\text{sgn}(r_{11}); \quad u_1u_2 = -\text{sgn}(q_{12}p_{12})$$

However the optimization in (3.14) requires numerical solution.

A general nxn unitary matrix U is either a *signature matrix* (i.e. a diagonal matrix Σ such that $\Sigma^2 = I$) or a product of 1/2 n(n−1) *rotations* U_{ij} where the components of $U_{ij}(k,l)$ U_{ij} are defined by

$$U_{ij}(i,i) = U_{ij}(j,j) = \cos\theta_{ij} \qquad (3.15a)$$

$$U_{ij}(i,j) = -U_{ij}(j,i) = \sin \theta_{ij}$$

$$U_{ij}(k,k) = 1 \text{ for } k \neq i, \, k \neq j$$

$$U_{ij}(k,l) = 0 \quad \text{otherwise} \tag{3.15b}$$

A particular signature matrix is also defined by (3.15b) where

$$U_{ij}(k,k) = \pm 1 \quad \text{for } k = i,j$$

$$U_{ij}(k,l) = 0 \quad \text{for } k \neq l \tag{3.16}$$

By letting

$$U = \prod_{i,j} U_{ij}$$

The optimization in (3.12) can be reduced to a sequence of one dimensional optimizations over the angles θ_{ij}. To be complete, $J(U)$ should also be evaluated separately for all 2^n ($n = r_q - p_q$) signature matrices. A compromise during the iterative procedure is to include the possibility of components U_{ij} being defined by (3.16) as well as (3.15a). Rather than present the general result we only illustrate by means of an example.

Specifically, suppose we express a 3x3 unitary matrix U as

$$U = U_{12}U_{13}U_{23} \tag{3.17}$$

Then by invoking the trace property, J in (3.12b) can equivalently be expressed as

$$J(U_{ij}) = tr[Q_{ij}U_{ij}^* P_{ij}U_{ij} + 2R_{ij}U_{ij}] \tag{3.18a}$$

where

$$Q_{12} = U_{12}U_{23}QU_{23}^*U_{13}^*; \quad P_{12} = P; \quad R_{12} = U_{23}U_{13}R$$

$$Q_{13} = U_{23}QU_{23}^*; \quad P_{13} = U_{12}^*PU_{12}; \quad R_{13} = U_{23}RU_{12} \tag{3.18b}$$

$$Q_{23} = Q; \quad P_{23} = U_{13}^*U_{12}^*PU_{12}U_{13}; \quad R_{23} = RU_{12}U_{13}$$

With $i = i_0$, and $j = j_0$ fixed in (3.18a), J can be optimization over $U_{i_0 j_0}$. The procedure is recursive. That is, first assume $i = 1, j = 2$ with U_{13} and U_{23} both initialized to (say) the identity. After optimizing over U_{12}, fix U_{12} and U_{13} and optimize over U_{23}, etc. Many cycles may be necessary for convergence.

In order to explicitly demonstrate the formulation for each of the 2x2 optimizations consider the case $i = 1, j = 2$, and express

$$Q_{12} = \begin{bmatrix} \overset{1}{Q_{12}} & \overset{2}{Q_{12}} \\ \overset{2}{Q'_{12}} & \overset{3}{Q_{12}} \end{bmatrix} \quad P_{12} = \begin{bmatrix} \overset{1}{P_{12}} & \overset{2}{P_{12}} \\ \overset{2}{P^*_{12}} & \overset{3}{P_{22}} \end{bmatrix} \quad R_{12} = \begin{bmatrix} \overset{1}{R_{12}} & \overset{2}{R_{12}} \\ \overset{4}{R_{12}} & \overset{3}{R_{22}} \end{bmatrix}$$

where $\overset{1}{Q_{12}}, \overset{1}{P_{12}}, \overset{1}{R_{12}} \in R^{2 \times 2}$. Then from (3.15), (3.16) the optimal θ_{12} which minimizes $J_{12}(U_{12})$ also minimizes

$$\tilde{J}_{12}(\theta_{12}) = tr[\overset{1}{Q_{12}}U_\theta^* \overset{1}{P_{12}}U_\theta + 2(R_{11} + \overset{2}{Q_{12}}\overset{2}{P^*_{12}})U_\theta]$$

where components of the 2x2 unitary matrix U_θ^* is defined by (3.15a) or (3.16) for $i, j, \in \{1,2\}$ The 2x2 optimization of $\tilde{J}_{12}(\theta_{12})$ over θ_{12} is partially solved in lemma 3.4.

Before concluding this section it is important to reiterate that the dimension of the problem for optimizing over the row unitary matrices U_q is generally low. In particular from (1.21b) both the number of rows and columns of U_q is not greater than the number of outputs. For a single output systems, U_q is a scalar and so there are at most two possibilities, and no optimization is necessary. That is, for $\rho_q < r_q$ we merely evaluate the cost in (2.24) for two values of G_q in (1.21a) corresponding to $U_q = \pm 1$, while if $\rho_q = r_q$, then $G_q = G_{q1}$ is unique.

4. Coefficient Errors

Recall that Y in (2.9) is the error in the covariance of the output $\{\hat{y}(k)\}$ due to finite precision implementation of both states and coefficients of the q-Markov COVER. The optimal q-FSWL Markov COVER minimizes the trace of Y when there are *no coefficient errors* (corresponding to $\gamma_o = 0$). Furthermore, when there are no coefficient errors, there are no errors in either the Markov parameters M_i or covariance parameters R_j in (1.2). Once coefficient errors are introduced and all finite wordlength (FWL) errors are considered, there is no longer a clear interpretation of what should constitute the optimal q-FSWL Markov COVER. One possibility is to again attempt to minimize the trace of Y. Alternative performance criteria could be based on the errors ΔM_i and ΔR_j in the Markov and covariance parameters as given by

$$M_i + \Delta M_i = (C + \Delta C)(A + \Delta A)^i(B + \Delta B);$$

$$R + \Delta R_j = (C + \Delta C)(A + \Delta A)^j \overline{X}(C + \Delta C)^* \tag{4.1}$$

where $\overline{X}$ satisfies $\overline{X} = A\overline{X}A^* + BB^*$. For example, one could attempt to minimize

$$C_M \overset{\Delta}{=} \sum_{i=0}^{q} \text{tr}[\Delta M_i (\Delta M_i)^*] \text{ or } C_R \overset{\Delta}{=} \sum_{i=0}^{q} \text{tr}[\Delta R_i] \tag{4.2}$$

However there are no results which directly connect C_M or C_R with errors in time or frequency response of the q-Markov COVERs. Furthermore, the analytical and computational aspects involved in the resulting optimization would be very difficult if not practically impossible.

A convenient approach to parameter optimization is to assume a *statistical model* for parameter errors. A statistical design can be justified along the following lines. Suppose (as is the case in practice) that both the Markov parameters M_i and covariance parameters R_j are known only to be accurate up to a specified wordlength, and any higher precisional representation is regarded as uncorrelated random noise. Then the calculation of all q-Markov COVERs (for a particular row unitary matrix U_q) will also only be accurate to a finite precision beyond which the parameter representation contains uncorrelated random noise.

Lemma 4.1 Suppose $M = M^* > 0$ and $K = K^* > 0$ are given nxn matrices. Let $v_j \in R^n$ be a zero mean random variable uniformly distributed between ± 1 with uncorrelated components which are also uncorrelated with components of v_i. Then we have

$$E\{v_j^* M v_j\} = \frac{1}{3} \text{tr}[M] . \tag{4.3}$$

Furthermore

$$E\{\text{tr}[V^* M V K]\} = \frac{1}{3} \text{tr}[MK] \tag{4.4}$$

where

$$V = [v_1 v_2 \cdots v_n] \varepsilon R^{nxn} .$$

□□□

Unfortunately these results *cannot* be applied directly to (2.9) since X itself is a random variable. However if we approximate $\hat{X}$ by X we can deduce the following result.

Theorem 4.1

Suppose the components of δA, δB and δC are zero mean uncorrelated random variables uniformly distributed between ± 1. Then $E\{J\}$ where $J = \text{tr}[Y]$ is

approximated by $E\{\hat{J}\}$ where

$$E\{\hat{J}\} = \gamma^2 \text{tr}[B^* KB] + (\gamma^2 + \frac{\gamma_o^2}{3})\text{tr}[K] + \frac{\gamma_o^2}{3}(\text{tr}[XK] + \text{tr}[X]) \quad (4.5)$$

where K, X are defined by (2.11) and (1.3).

□□□

Proof: From (2.9) ignoring the linear term in δC

$$J \doteq \gamma^2\{\text{tr}[K] + \text{tr}[B^* KB]\} +$$

$$\gamma_o^2\{\text{tr}[(\delta A)^* X(\delta A)K] + \text{tr}[(\delta B)^* K(\delta B)] + \text{tr}[(\delta C)^* X \delta C]\}$$

The result then follows using Theorem 2.1.

□□□

Under a similarity transformation T, the performance measure (4.5) becomes

$$E\{\hat{J}_T\} \triangleq \gamma^2 \text{tr}[B^* KB] + (\gamma^2 + \frac{\gamma_o^2}{3})\text{tr}[T^* KT] + \frac{\gamma_o^2}{3}(\text{tr}[XK] + \text{tr}[T^{-1}X(T^{-1})^*] \quad (4.6)$$

Note that both $\text{tr}[B^* KB]$ and $\text{tr}[XK]$ are invariant. In fact the invariant eigenvalues $\{\sigma_k^2\}$ of XK are the squares of the Hankel singular values of the system defined by $\{A,B,C\}$. Consequently we need only consider the minimization of

$$(\gamma^2 + \frac{\gamma_o^2}{3})\text{tr}[T^* KT] + \frac{\gamma_o^2}{3}\text{tr}[T^{-1}X(T^{-1})^*] \quad (4.7)$$

over similarity transformations T. We make use of an earlier result [8] to provide the minimum in (4.7).

Theorem 4.2 [8]

Consider a minimal asymptotically stable order system $\{A,B,C\}$ with controllability grammian X and observability grammian K. Let $\tilde{X}$ and $\tilde{K}$ be the transformed grammians as a result of applying a similarity transformation T; that is

$$\tilde{X} = T^{-1}X(T^{-1})^*; \quad \tilde{K} = T^* KT \quad (4.8)$$

Then

$$\text{tr}[\alpha^2\tilde{X}+\tilde{K}] \geq 2\alpha \sum_{k=1}^{n} \sigma_k \tag{4.9}$$

where $\{\sigma_k^2\}$ are the Hankel singular values. Moreover equality is achieved in (4.9) if and only if

$$\tilde{K} = \alpha^2 \tilde{X} \tag{4.10}$$

In particular, in (4.7)

$$\min_{T} E\{\hat{J}_T\} = \gamma^2 \text{tr}[B^*KB] + \frac{\gamma_0^2}{3}(\sum_{k=1}^{r_q} \sigma_k^2 + 2\alpha \sum_{k=1}^{r_q} \sigma_k) \tag{4.11a}$$

where

$$\alpha = \sqrt{1 + 3(\gamma/\gamma_0)^2} \tag{4.11b}$$

The minimum value is achieved in (4.11a) when $\tilde{K}$, $\tilde{X}$ satisfy (4.10) with α given by (4.11b)

□□□

One optimal realization (4.10) is a scaled internally balanced structure; that is

$$\tilde{X}_1 = \alpha^{-1}\text{diag}\{\sigma_1, \sigma_2, ..., \sigma_{r_q}\}; \quad \tilde{K}_1 = \alpha \, \text{diag}\{\sigma_1, \sigma_2, \cdots, \sigma_{r_q}\} \tag{4.12}$$

From the point of view of l_2-scaling, *equal* diagonal components of $\tilde{X}$ guarantee equal dynamic range of the state components. It is evident from (4.10) that any *unitary* transformation $\tilde{U}$ applied to the coordinate basis having $\tilde{X}$ and $\tilde{K}$ as the respective controllability and observability grammians will not alter the optimal performance. Consequently an optimal realization in which all diagonal components of the controllability grammian are *equal* exists with controllability grammian $\tilde{U}^*\tilde{X}_1\tilde{U}$ and observability grammian $\tilde{U}^*\tilde{K}_1\tilde{U}$ such that

$$\tilde{U}^*\tilde{X}_1\tilde{U}_{jj} = \frac{1}{\alpha r_q} \sum_{k=1}^{r_q} \sigma_k \quad \text{for all } j \tag{4.13}$$

where $\tilde{X}_1$, $\tilde{K}_1$ are defined by (4.12) and $\tilde{U}$ unitary. The existence of $\tilde{U}$ is guaranteed by lemma 2.1 and an explicit algorithm for constructing a (nonunique) $\tilde{U}$ is available in [9, Appendix A].

Corollary 4.1

The optimal q-FSWL COVER which minimizes (2.21) subject to the l_2-scaling constraint

$$\Lambda_{jj} = \frac{1}{\alpha r_q} \sum_{k=1}^{r_q} \sigma_k \quad \text{for all } j \tag{4.14}$$

also minimizes $E\{\hat{J}_T\}$ in (4.6)

□□□

This result provides a connection between the optimal q-FSWL COVER structure which minimizes only the effects due to state quantization noise, and the suboptimal q-FWL Markov COVER structure which minimizes $E\{\hat{J}_T\}$ subject to the assumed random parameter error model stated in Theorem 4.1. Once again we note that the result is *suboptimal* in the sense that $\hat{X}$ and X in (2.9) and (4.5) are only approximately equal. The result of Corollary 4.1 is also only of academic value since the l_2-constraint (4.14) is *not* known *until* the design is complete since the Hankel singular values $\{\sigma_j\}$ depend on the optimal row unitary matrix U_p as provided in Theorem 2.1. However a more explicit result can be stated.

Corollary 4.2

The optimal q-FSWL cover subject to the l_2-scaling constraint (2.22) also minimizes $E\{\hat{J}_T\}$ in (4.12) subject to (2.22).

□□□

5. An Example

Consider a 5 mode simply supported beam of length π having 2 inputs u_1, u_2 and 2 outputs y_1, y_2

$$u_1 = F(0.2\pi, t), \quad u_2 = T(\pi, t)$$

$$y_1 = \theta(0, t), \quad y_2 = \mu(0.6\pi, t)$$

where $F(0.2\pi, t)$ denotes a force applied at $.2\pi$ units from the left end of the beam, $T(\pi, t)$ denotes a torque at the right end of the beam, $\theta(0, t)$ denotes angular deflection at the left end, and $\mu(0.6\pi, t)$ denotes rectilinear deflection at 0.6π from the left end of the beam. The equations of motion are assumed to be described by

$$\ddot{\eta}_k + 2\xi_k \omega_k \dot{\eta}_k + \omega_k^2 \eta_k = [\sin(0.2\pi k) \; k\cos(\pi k)] \begin{bmatrix} u_1 \\ u_2 \end{bmatrix}$$

$$\begin{bmatrix} y_1 \\ y_2 \end{bmatrix} = \sum_{k=1}^{5} \begin{bmatrix} k\cos(0\pi k) \\ \sin(0.6\pi k) \end{bmatrix} \eta_k \tag{5.1}$$

where $\omega_k = k^2$ rads/sec. and $\xi = 0.005$. A continuous time 10th order state space model is defined by

$$\dot{x} = Fx + Gu, \quad y = Cx$$

where

$$x = (\eta_1\dot{\eta}_1 \ \eta_2\dot{\eta}_2 \ \cdots \ \eta_5\dot{\eta}_5)^* \tag{5.2}$$

A zero order hold equivalent 10th order discrete model (1.1) is defined by

$$A = e^{FT}; \quad B = \int_0^T e^{F\sigma} d\sigma G$$

For the numerical work, a sampling period $T = 0.025$ sec. was selected which corresponded to approximately 10 samples in the shortest period. The eigenvalues of A are at

$0.996\pm j0.0250$, $0.9985\pm j0.0500$, $0.9968\pm j0.0750$, $0.9945\pm j0.0998$, $0.9916\pm j0.1246$.

Using the algorithm described in Corollary 1.1 the following results were obtained.

q	s_q	r_q	ρ_q	
2	2	4	2	)
3	2	6	4	} U_q is 2x2
4	2	8	6	)
5	2	8	8	)
6	2	9	9	} no freedom
≥7	2	10	10	)

Hence for $q = 2, 3, 4$, U_q in (1.22b) can be an arbitrary 2x2 unitary matrix, while for $q \geq 5$ there is no remaining freedom in the q-COVER.

Optimal q-FSWL COVER designs:

$$U_q = \begin{bmatrix} \cos\theta_q & \sin\theta_q \\ -\sin\theta_q & \cos\theta_q \end{bmatrix}; \quad \begin{matrix} \theta_2 \simeq 40° \\ \theta_3 \simeq 0° \\ \theta_4 \simeq 65° \end{matrix}$$

(other cases $\begin{bmatrix} 1 & 0 \\ 0 & -1 \end{bmatrix}$ and $\begin{bmatrix} -1 & 0 \\ 0 & 1 \end{bmatrix}$ were also checked and neither was optimal).

The cost ranges from (2.29) for $\alpha = 1$ were

$$\eta_{2opt} = 0.3143 \times 10^6 \le \eta_2 \le 0.8478 \times 10^6$$

$$\eta_{3opt} = 0.2570 \times 10^6 \le \eta_3 \le 0.4764 \times 10^6$$

$$\eta_{4opt} = 0.0019 \times 10^8 \le \eta_4 \le 0.1308 \times 10^8$$

The actual FWL output roundoff noise is given by

$$\gamma^2 \eta_q; \quad \gamma^2 = \frac{1}{12} 2^{-2W}$$

where W bits are assigned to the fractional wordlength of the state. Hence a factor of 4 improvement in η_q corresponds to a wordlength saving of 1 bit. There is little savings in this example when q = 2,3. However for q = 4 we have a saving of 4 bits. In practice, for fast sampling and low structural damping, the savings would increase as the dimension of the model increases (e.g. a simply supported beam of 50 modes with q = 8).

References

[1] D. Williamson, "Structural State Space Sensitivity in Linear Systems," *Systems and Control Lett.*, 7, July (1986) pp. 301-307.

[2] D. Williamson, "Roundoff Noise Minimization and Pole-Zero Sensitivity in Fixed Point Digital Filters using Residue Feedback," *IEEE Trans. on Acoustics, Speech and Signal Processing*, Vol. ASSP-34, No. 4, Aug. 1986, pp. 1013-1016.

[3] A.M. King, V.B. Desai and R.E. Skelton, "A generalized approach to q-Markov covariance equivalent realizations for discrete systems," *1987 ACC*, Minneapolis, USA.

[4] R.E. Skelton and B.D.O. Anderson, "q-Markov Equivalent Realizations," *Int. J. Control*, Vol. 44, No. 5, 1986, pp. 1477-1490.

[5] R.E. Skelton and E.G. Collins, "Set of q-Markov covariance equivalent models of discrete systems," *Int. J. Control*, (to appear).

[6] A.B. Stripad and D.L. Snyder, "A necessary and sufficient condition for quantization errors to be uniform and white," *IEEE Trans. Acoust. Speech Signal Process*, Vol. 25, 1977, pp. 442-448.

[7] B.D.O. Anderson and R.E. Skelton, "The generation of all q-Markov covers," *IEEE Trans or Circuits & Systems* (to appear). Also see *IFAC Congress*, Munich, 1987.

[8] S.Y. Hwang, "Minimum uncorrelated unit noise in state space digital filtering," *IEEE Trans. Acoust., Speech, Signal Processing*, vol. ASSP-25, pp. 273-281, Aug. 1977.

[9] C.T. Mullis and R.A. Roberts, "Synthesis of Minimum Roundoff Noise in Fixed Point Digital Filters," *IEEE Circuits and Systems*, CAS-23, Sept. 1976, pp. 256-262.

[10] D. Williamson, "Finite state wordlength compensation in digital Kalman filters," *IEEE Trans. Auto. Control*, Vol. AC-30, No. 10, Oct. 1985, pp. 930-939.

[11] D. Williamson and K. Kadiman, "Finite wordlength linear quadratic Gaussian regulator," Int. Symp. Circuits & Systems, Philadelphia, USA, June 1987.

INPUT-OUTPUT ORIENTED COMPUTATION ALGORITHMS FOR THE CONTROL OF LARGE FLEXIBLE STRUCTURES

By

K. D. Minto
GE Corporate Research and Development Center
Schenectady, New York

ABSTRACT

This presentation will overview work in progress aimed at developing computational algorithms addressing two important aspects in the control of large flexible space structures; namely, the selection and placement of sensors and actuators, and the resulting multivariable control law design problem.

The issue of sensor/actuator set selection is particularly crucial to obtaining a satisfactory control design, as clearly a poor choice will inherently limit the degree to which "good" control can be achieved. Moreover, it is becoming increasingly clear that systematic methods are required for determining prior to the control law design phase whether a particular candidate sensor/actuator set will yield acceptable closed-loop performance, irrespective of the particular control system design methodology used.

With regard to control law design we are driven by concerns stemming from the practical issues associated with eventual implementation of multivariable control laws, such as reliability, limit protection, multimode operation, sampling rate selection, processor throughput, etc. Naturally, the burden imposed by dealing with these aspects of the problem can be reduced by ensuring that the complexity of the compensator is minimized.

Our approach to these problems is based on extensions to input/output oriented techniques that have proven useful in the design of multivariable control systems for aircraft engines. In particular, we are exploring the use of relative gain analysis and the condition number as a means of quantifying the process of sensor/actuator selection and placement for shape control of a large space platform. Complementing this activity is the development of a new multivariable design approach that allows the designer to precisely control the complexity of the resulting compensator. The technique incorporates input-output performance criteria such as the popular singular-value loop-shaping approach, yet without resorting to high-order compensators inherent to observer-based design approaches.

883

INPUT/OUTPUT ORIENTED COMPUTATIONAL ALGORITHMS FOR THE CONTROL OF LARGE FLEXIBLE STRUCTURES

K. Dean Minto
Control Systems Laboatory, GE - CRD
KWD - 207, Schenectady, NY, 12301
(518) 387 - 6760

Ted F. Knaak
GE - Astro-Space Division
Building 100, U4248
King of Prussia, PA, 19406
(215) 354 - 3672

885

OUTLINE

Motivation for research

Approach

   design philosophy

   focus: shape control

Results

   preliminary experiences with key aspect
of design problem: S/A set selection

Motivation

- control of flexible structures recognized as a key emerging technology for GE

- leverage considerable design experience with MIMO design process for medium complexity problems (aircraft engines) to high complexity systems (LFSS, IFPSC)

- a particularly important unresolved issue: decoupling the process of sensor/actuator selection from control law design phase

GOALS:

- Quantitative, systematic approach to problem of decoupling S/A selection from control law design process

- Complexity reduction/management

    - Design process

    - Final product

887

Complexity clearly a major issue ...

(1) countably infinite number of S/A sets

- number

- placement

- types, etc.

(2) large dynamic-order models (many flex. modes)

- order reduction a critical step, due
  primarily to limitations in traditional
  control law design approaches
  (observer-based compensators imply
  high-order)

- model accuracy/fidelity often sacrificied to
  accomodate these inherent computational
  limitations (spillover effects, etc.)

- conflict with S/A selection process, where
  numerical behaviour improves with model
  dynamic order

(3) Shape Control - very large I/O dimensionality

Approach

- traditional F.E.M. /MIMO design approach, based on the following cycle

```
┌─────────────────────┐
│   Performance       │
│   Specifications    │
└──────────┬──────────┘
           ▼
┌─────────────────────┐
│     Modeling        │
└──────────┬──────────┘
           ▼
┌─────────────────────┐
│  Control  Structure │
│      Design         │
└──────────┬──────────┘
           ▼
┌─────────────────────┐
│   Control  Law      │
│      Design         │
└──────────┬──────────┘
           ▼
┌─────────────────────┐
│  Implementation     │
└─────────────────────┘
```
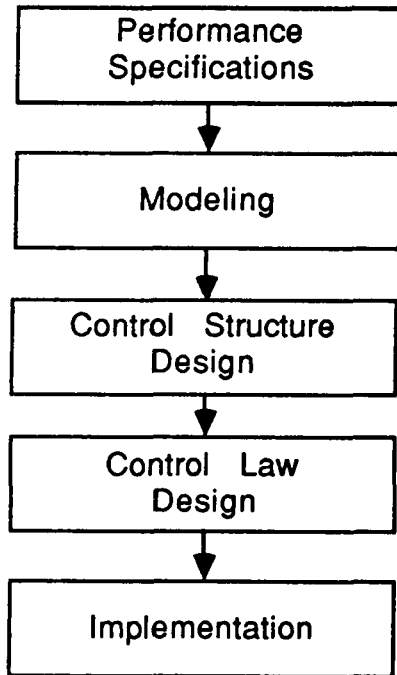
Focus:

(1) Control Structure Design

- selection, pairing

(2) Control Law Design

- **MIMO design w/ fixed order compensators**

(3) Uncertainty Modeling

(4) Computations

- S/A placement

- Frequency-domain control-law design

- Stable Factorization (balancing, order reduction)

- demonstrate via shape control problem for LFSS

Control Structure Design:

" That portion of the control system design process which deals with the selection and pairing of measurement and manipulation variables "

- S.O.A.: typically Ad - hoc, often arbitrarily chosen

    much iteration, involving control law design phase

- probably the most critical step in entire design process (certainly true for shape control via MIMO techniques ...)

(1) Sensor/Actuator Selection

- how many?
- locations?
- types*   (* ignor for the present ...)

colocated   vs.   non-colocated

x = sensor   ◯ = actuator
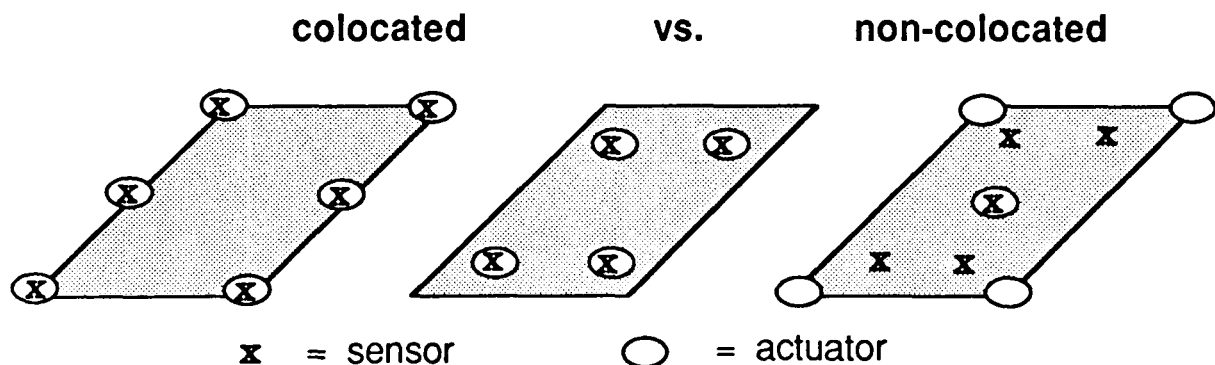
- systematic search for candidates that guarantee "good" closed-loop control

(2)   Pairings   and   Decentralization

- given a S/A set, how do we interconnect for minimal closed-loop interaction?

- assume standard unity-feedback configuration
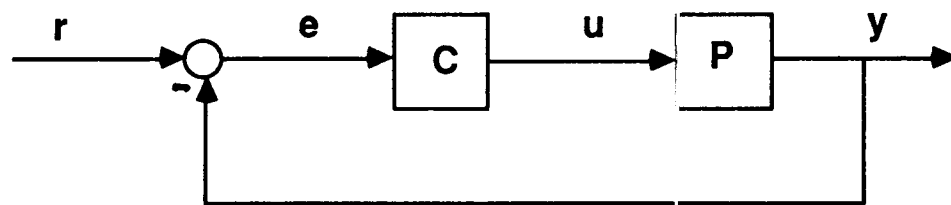
Decentralization: Choose   C   as   follows ...

vs.

vs.
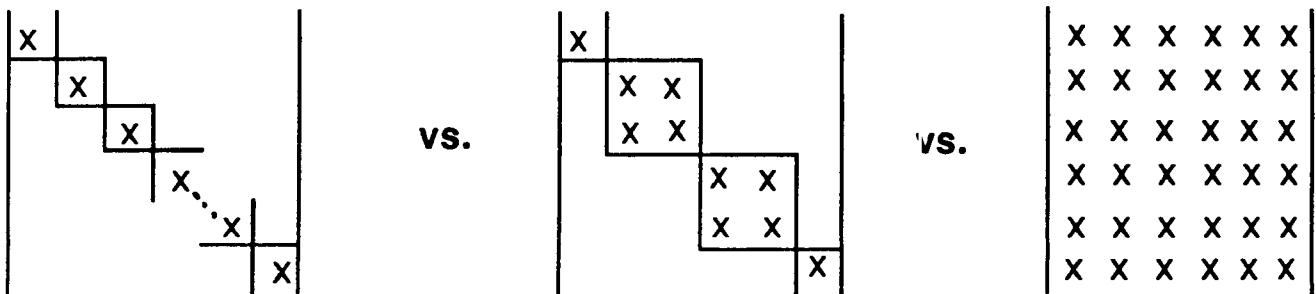
I/O   Pairing:
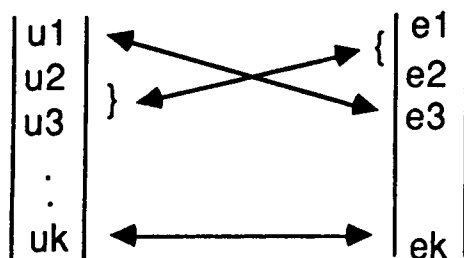
Example:

Colocated, fully decentralized:

ui <--> ei, for all i.

(1) S/A Selection

High level algorithm ...

- determine a large number of candidate
  sensor/actuator sets

- reduce to a manageable number of acceptable
  control structures (design - by - analysis)

Specifics ...

- develop a necessary condition for assessing
  a candidate control structure based on
  stability robustness

- uncertainty characterization: modified additive
  perturbations ...

$$\tilde{G} = G + \Delta G \qquad \frac{\overline{\sigma}(\tilde{G} - G)}{\overline{\sigma}(G)} < \delta$$

- connect control structure design process with
  stability robustness via following accepted fact:
  " plants with low condition number are 'easy'
  to control ... "

- *base selection process on condition number*

- we have the following result ...

Theorem: If C stabilizes P, then necessarily

$$K(P) < \frac{\delta^{-1}}{\underline{\sigma}(\,PC(I+PC)^{-1}\,)} \cong \delta^{-1}, \quad \text{for} \quad \omega < \omega_c$$

- assumes "perfect" control at DC ...

Selection Process:

- compute condition number of candidate structures at DC

- discard those with large condition number ...

Computational Aspects:

- RGA (relative gain array) yields lower bounds on condition number, hence a necessary condition for viable control structures

- computational burden of RGA calculation small, but problem with exponential growth in complexity required to examine all possible combinations

- Example: > 3 x 10D10 ways to choose a 12 x 12 control structure from a set of 20 possible I/O pairs

Heuristic Solution:

- direct selection of inputs/outputs to minimize condition number

- based on SVD of plant DC-gain.

$$\kappa(G) := \frac{\overline{\sigma}(G)}{\underline{\sigma}(G)} \equiv \frac{\max \| G u \|}{\min \| G u \|}$$

- reduce condition number <-> (i) reduce max. sv

(ii) increase min. sv

- DC gain: $G(0) = D + C(-A)^{-1}B$

- SVD: $G(0) = U S V'$

- introduce notion of input/output coupling operators ...
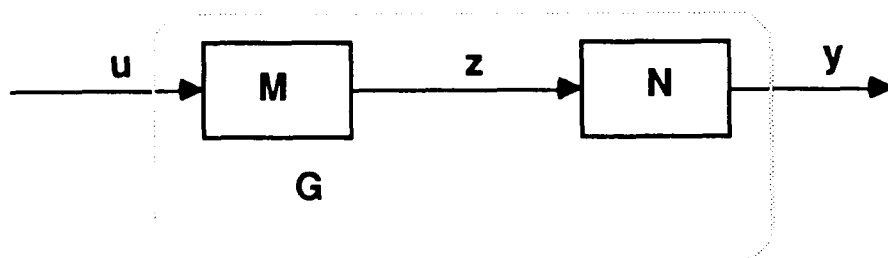
$$M = S^{\frac{1}{2}} V' \qquad N^{-1} = S^{\frac{-1}{2}} U'$$

Note: $z = Mu,$ $z = N^{-1}y$

- express u, y as sums of standard basis vectors, i.e.

$$u = \sum_i \alpha_i e_i, \quad y = \sum_i \beta_i e_i$$

- then we have

$$z = \sum_i \alpha_i M e_i = \sum_i \alpha_i M_i$$

$$z = \sum_i \beta_i N^{-1} e_i = \sum_i \beta_i N_i^{-1}$$

Design   Heuristic:

- drop those inputs (outputs) corresponding to the maximum and minimum gains from u to z (y to z), i.e.

$$\| z \|_2 <= \sum_i | \alpha_i | \cdot \| M_i \|_2$$

- encouraging results for shape control application ...

Coupling Operators: 20 x 20 I/O, 25 flexible modes

INPUT COUPLING OPERATOR

OUTPUT COUPLING OPERATOR
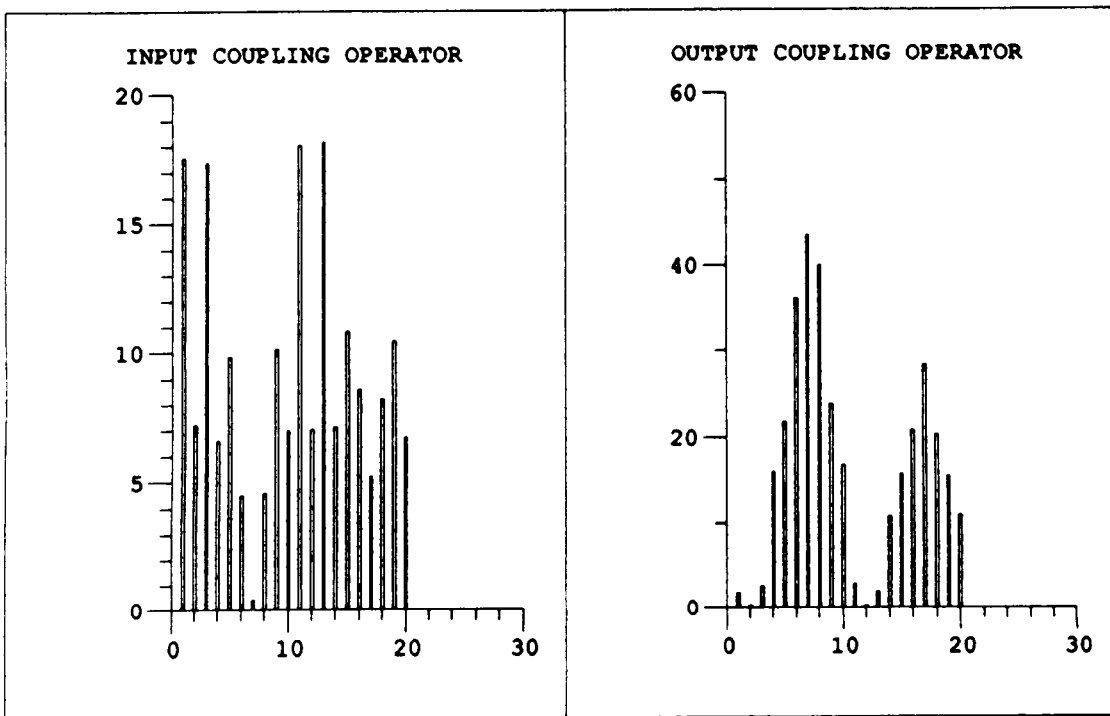
S/A selection: Condition number vs. I/O dimension

R1: I/O - CONDITION NUMBER ANALYSIS

$\times 10^6$

CONDITION NUMBER

R1: K VS. I/O

I/O DIMENSIONALITY

I/O DIMENSIONALITY
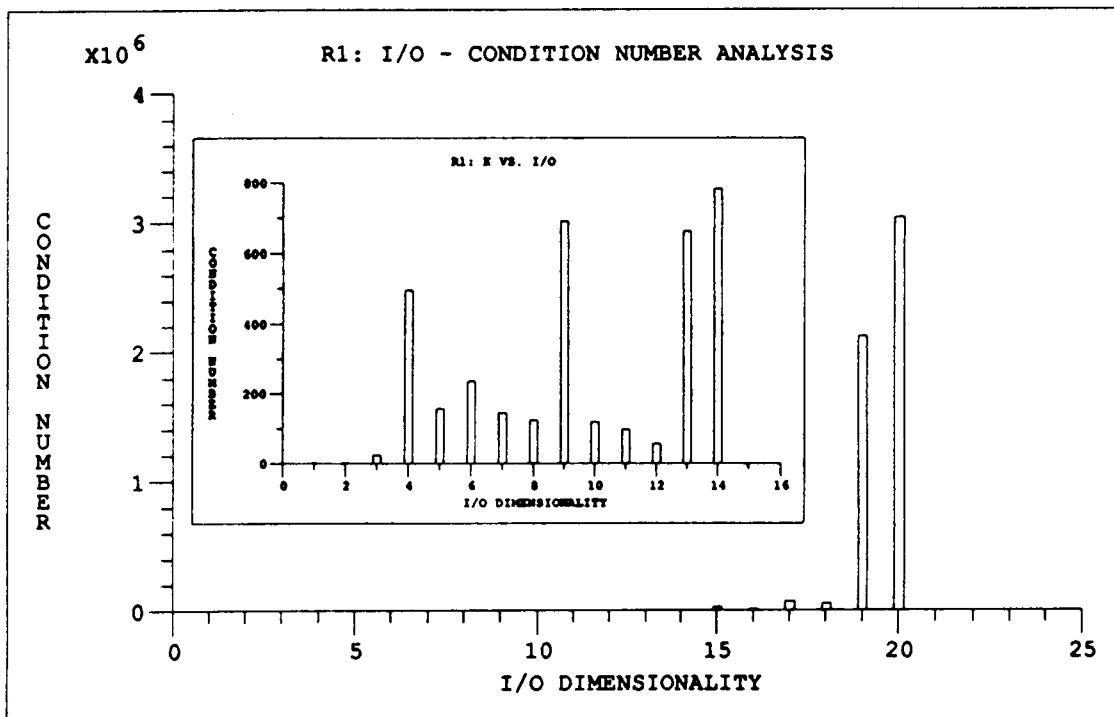
Some Observations :

- systems characterized by large condition numbers
  (in general), and relatively large uncertainty

  - extremely difficult to control

  - severe performance limitations

- tendency towards partially colocated feedback
  structures (as a result of S/A selection process)

- lower condition numbers with non-colocated,
  and in particular, non-square control structures
  (non-square systems a challenge for MIMO
  control law design)

- numerical conditioning improves (generically)
  with increasing information content

  RGA: $G(0)$ = $C(-A)^{-1}B$

         = ▯ ☐ ⊐ = ☐

    Rank($G(0)$) $\leqq$ dim(☐)

  $K(G(0))$ ↓ as dim(A) ↑

         ☐ ☐ ▯ = ☐

    Generically full-rank ...

(2) Pairings/Cross-feed Degradation

Tools:

- RGA, BRG (Bristol, Arkun, Maniousiouthakis)

Usage:

- Assess interactions between various feedback blocks

- Account for cross-feed degradation due to use of decentralized control structure

Preliminary result: 12 x 12 system of previous example ...

□ actuators   ● sensors
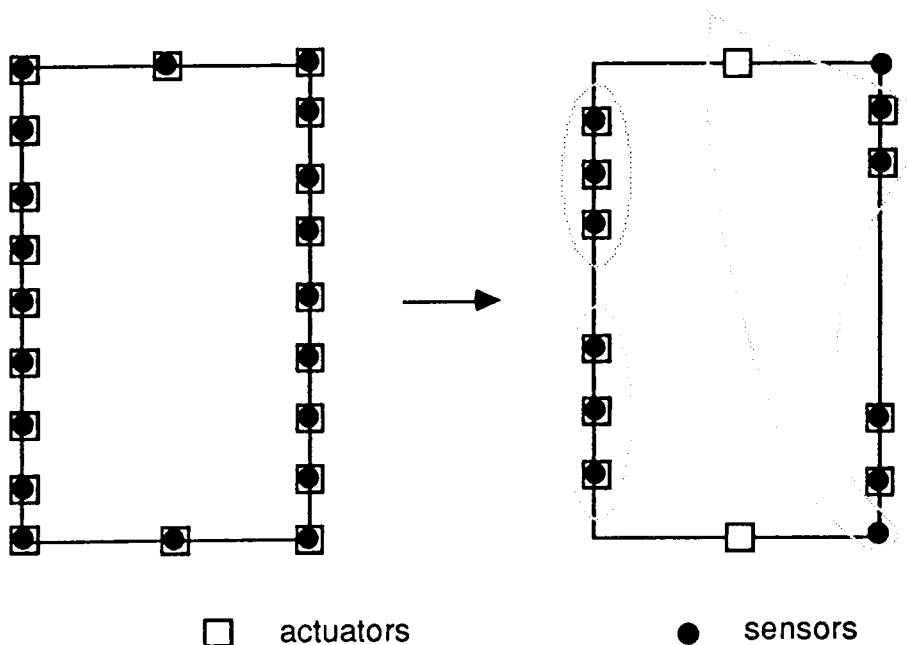
Control Law Design

- loop-shaping design philosophy

- account for practical implementation constraints

  - fault-tolerance and reliability

  - limit-protection and multimode operation

  - digital control aspects

  All severely impacted by complexity of compensator!

- 2 - stage design procedure allowing explicit constraints on compensator complexity

<u>1st Stage:</u>   "Ideal" Compensator computation

- model-matching performance specification
  (sv loop-shaping basis)

- controller parameterization (IMC, SF)

- identify constraints on achievable performance
  (inner-outer factorization)

- compute "ideal" compensator, i.e. K^* such that

  $$\| H - H_D \|_2 = 0$$

2nd Stage: "Low-order" Compensator Computation

- analysis of "ideal" compensator (frequency response) to determine

    (i) approx. required complexity (dynamic order)

    (ii) values of compensator denominator terms, initial values of numerator terms

- parametric optimization to adjust compensator numerator terms (least-square approach) to minimize

$$\| \ H \ - \ H_D \ \|_2 \ = \ 0$$

Features:

- NOT an open-loop order-reduction procedure

- Closed-loop low (fixed) order design procedure, with a flavour of order reduction (Ideal comp. => lower-order parametric design)

- Frequency-domain oriented design, hence complexity proportional to I/O dimension, NOT state dimension

- Reduced emphasis/reliance on explicit order-reduction

Balancing & Order Reduction (SFPACK)

- balancing a popular method for model/controller order reduction

- also useful for avoiding large coefficients in state-space manipulations

Problems: Unstable or marginally stable systems

- decomposition solution: $G = G_+ + G_-$

- balance, reduce components, recombine

- Stable Factorization approach:

    $G = N D^{-1}$, N, D stable, right-coprime

    Form a composite system F, with state-space realization ...

    $$F = \begin{bmatrix} D \\ N \end{bmatrix} \leftrightarrow \left[\begin{array}{c|c} A & B \\ \hline C_1 & E_1 \\ C_2 & E_2 \end{array} \right] \qquad (\text{ as stable as we wish ... })$$

    Order-reduction on F:

    $$\hat{F} \leftrightarrow \left[\begin{array}{c|c} \hat{A} & \hat{B} \\ \hline \hat{C}_1 & E_1 \\ \hat{C}_2 & E_2 \end{array} \right] \leftrightarrow \begin{bmatrix} \hat{D} \\ \hat{N} \end{bmatrix}$$

    $\hat{G} = \hat{N} \hat{D}^{-1}$ - a reduced-order model of G

THE ACTIVE FLEXIBLE WING AEROSERVOELASTIC
WIND-TUNNEL TEST PROGRAM

By

Thomas Noll and Boyd Perry
NASA Langley Research Center
Hampton, Virginia

ABSTRACT

The evolution of advanced, high performance aircraft is requiring that the engineering disciplines of aerodynamics, controls, and structures be integrated into a unified aeroservoelastic technology. To provide for technology maturation, sophisticated analysis and design methodologies must be developed and verified through data correlation with experimental results. The most economical means of obtaining test data that includes the effects of these three disciplines without actually conducting full-scale flight tests is through the use of flexible wind-tunnel models scaled for aeroelastic phenomena. For a specific application of aeroservoelastic technology, Rockwell International Corporation developed a concept known as the Active Flexible Wing (AFW). The concept incorporates multiple active leading- and trailing-edge control surfaces with a very flexible wing such that wing shape is varied in an optimum manner resulting in improved performance and reduced weight. As a result of a cooperative program between the AFWAL's Flight Dynamics Laboratory, Rockwell, and NASA LaRC a scaled aeroelastic wind-tunnel model of an advanced fighter was designed, fabricated, and tested in the NASA LaRC Transonic Dynamics Tunnel (TDT) to validate the AFW concept. Besides conducting the wind-tunnel tests NASA provided a design of an Active Roll Control (ARC) System that was implemented and evaluated during the tests. The ARC system used a concept referred to as Control Law Parameterization which involves maintaining constant performance, robustness, and stability while using different combinations of multiple control surface displacements. Since the ARC system used measured control surface stability derivatives during the design, the predicted performance and stability results correlated very well with test measurements.

The wind-tunnel model described above serves as the basis of a follow-on program to validate LaRC's and Rockwell's aeroservoelastic analysis methodology and multifunction digital control law design capability. This program provides an excellent opportunity for NASA and Rockwell to obtain an experimental database for the subsonic, transonic, and low supersonic speed regimes on an advanced aircraft configuration and to obtain experience with digital control systems and simulation methods. Significant activities to be conducted by NASA LaRC during the next 2 to 3 years to support the program include: (1) the design of multifunction digital control laws for flutter suppression and rolling maneuver load alleviation acting singularly and simultaneously; (2) the design and fabrication of a digital controller and the implementation and coding of advanced control laws; (3) a "hot bench" simulation of a flexible model with unsteady aerodynamics to verify the functionality of the digital controller; and (4) ground vibration, control system functional, and wind-tunnel tests on a model with violent flutter characteristics. Besides providing a multimillion dollar aeroelastic model for the program, Rockwell will design

PRECEDING PAGE BLANK NOT FILMED

and fabricate a wing "tip missile" capable of either inducing flutter within the TDT performance envelope or preventing flutter through a decoupler mechanism, assist in the development of the advanced digital control laws, and participate during the testing and evaluation phases.

Some results from the two previous wind-tunnel entries which describe the ARC system and the Control Law Parameterization concept will be presented during the workshop to establish the background for the more advanced studies now being pursued. In addition, a status report on the follow-on cooperative program will be discussed covering all facets of the effort.

THE ACTIVE FLEXIBLE WING AEROSERVOELASTIC WIND TUNNEL TEST PROGRAM
A STATUS REPORT

/

By

Thomas Noll and Boyd Perry III
Aeroservoelasticity Branch
NASA Langley Research Center
Hampton, Virginia

905

THE ACTIVE FLEXIBLE WING AEROSERVOELASTIC WIND TUNNEL TEST PROGRAM A STATUS REPORT

By

Thomas E. Noll and Boyd Perry III

Aeroservoelasticity Branch

NASA Langley Research Center

Workshop on Computational Aspects in the Control of Flexible Systems

July 12-14, 1988

Williamsburg, Virginia

THE ACTIVE FLEXIBLE WING
AEROSERVOELASTIC WIND TUNNEL TEST PROGRAM

The Active Flexible Wing (AFW) AeroServoElastic (ASE) Wind Tunnel Test Program is a recently-initiated cooperative effort between the NASA LaRC and the Rockwell International Corporation. The objective of this effort is to develop the analysis, design and test methodologies required to apply Active Controls Technology (ACT) for controlling and exploiting the aeroelastic characteristics of a flexible aircraft to improve performance. The approach selected to accomplish the program objectives includes the demonstration of various ACT concepts on a flexible full-span wind tunnel model, and the testing of the model to obtain an experimental data base for validating the analysis and design methodologies associated with ACT. This effort is being directed by the Aeroservoelasticity Branch of the Structural Dynamics Division at LaRC.

OUTLINE

I. Program Objectives

II. Background

III. Current Program/Description of Tasks

     Controller Development

     Design of Tip Missile Concept

     Development of EOM

     Synthesis of RMLA and FSS Control Laws

     "Hot Bench" Simulation

     Wind Tunnel Model Testing

V. Concluding Remarks

808

OUTLINE

This chart shows an outline of the topics to be discussed. Since the effort has only recently begun, today's presentation is a status report on where we are today. I will begin by reviewing the objectives of the program to scope the tasks involved. I will then describe some of the NASA analysis and test results obtained during a previous AFW wind tunnel test program between the Air Force Flight Dynamics Laboratory, the Rockwell International Corporation and the LaRC. This portion of the presentation will demonstrate the requirement to go beyond what had been accomplished, pushing the state-of-the-art into more challenging and rewarding areas for ACT application. Next, a few charts describing each of the major tasks associated with this program will be discussed along with the progress and milestones recently accomplished. Finally, some concluding remarks and projections will end the presentation.

DEMONSTRATION AND VALIDATION
OF ACTIVE AEROELASTIC CONTROL TECHNOLOGY
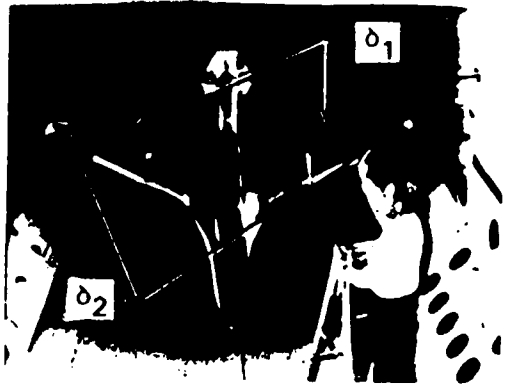
ACTIVE FLEXIBLE WING MODEL
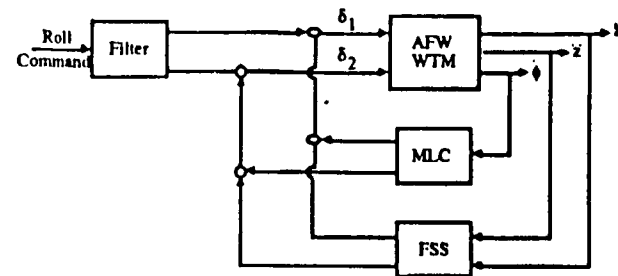
MULTIFUNCTION DIGITAL CONTROL SYSTEM

Objectives:

- Demonstrate Multifunction Control Laws and Validate Analysis Methodologies
- Obtain Experimental Data Base on Advanced Aircraft Configuration
- Obtain Experience with Digital Control Systems and Simulation Methods

NASA Role:

- Design and Fabricate Digital Controller
- Design Advanced Multifunctional Digital Laws and Code Controller
- Perform Real Time Simulation for a Flexible Vehicle Model
- Conduct Ground Vibration, System Functional, and Wind Tunnel Tests

Rockwell Role:

- Provide Flutter Critical AFW Model ($M's) for Technology Demonstration
- Assist in Development of Advanced Control Laws
- Provide Consultation and Participate During Test and Evaluation Phases

DEMONSTRATION AND VALIDATION
OF ACTIVE AEROELASTIC CONTROL TECHNOLOGY

The objective of this effort is to demonstrate the potential of using multifunction active control laws for controlling or exploiting aeroelastic response to improve aircraft performance. In addition, it gives NASA an opportunity to obtain an experimental data base on a flexible high performance advanced fighter configuration for validating analysis and design codes, to develop simulation techniques that include structural flexibility and unsteady aerodynamics, and to gain experience with digital control law implementation procedures. The NASA LaRC team consists of about twelve researchers from three different directorates (Structures, Flight Systems and Electronics). The team as a whole has the multidisciplinary experience required to perform the tasks identified for the AFW Aeroservoelasticity Program. The team will be required to design and fabricate the digital controller, design multifunctional control laws and code the controller, perform simulation studies to verify controller operation and conduct all model ground and wind tunnel tests. Rockwell through a Memorandum of Agreement and a separate support contract will provide the wind tunnel model for use during the program, assist in the development of the active control laws and participate during the wind tunnel tests. This cooperative effort provides an excellent opportunity to directly transfer technology to the aerospace industry.
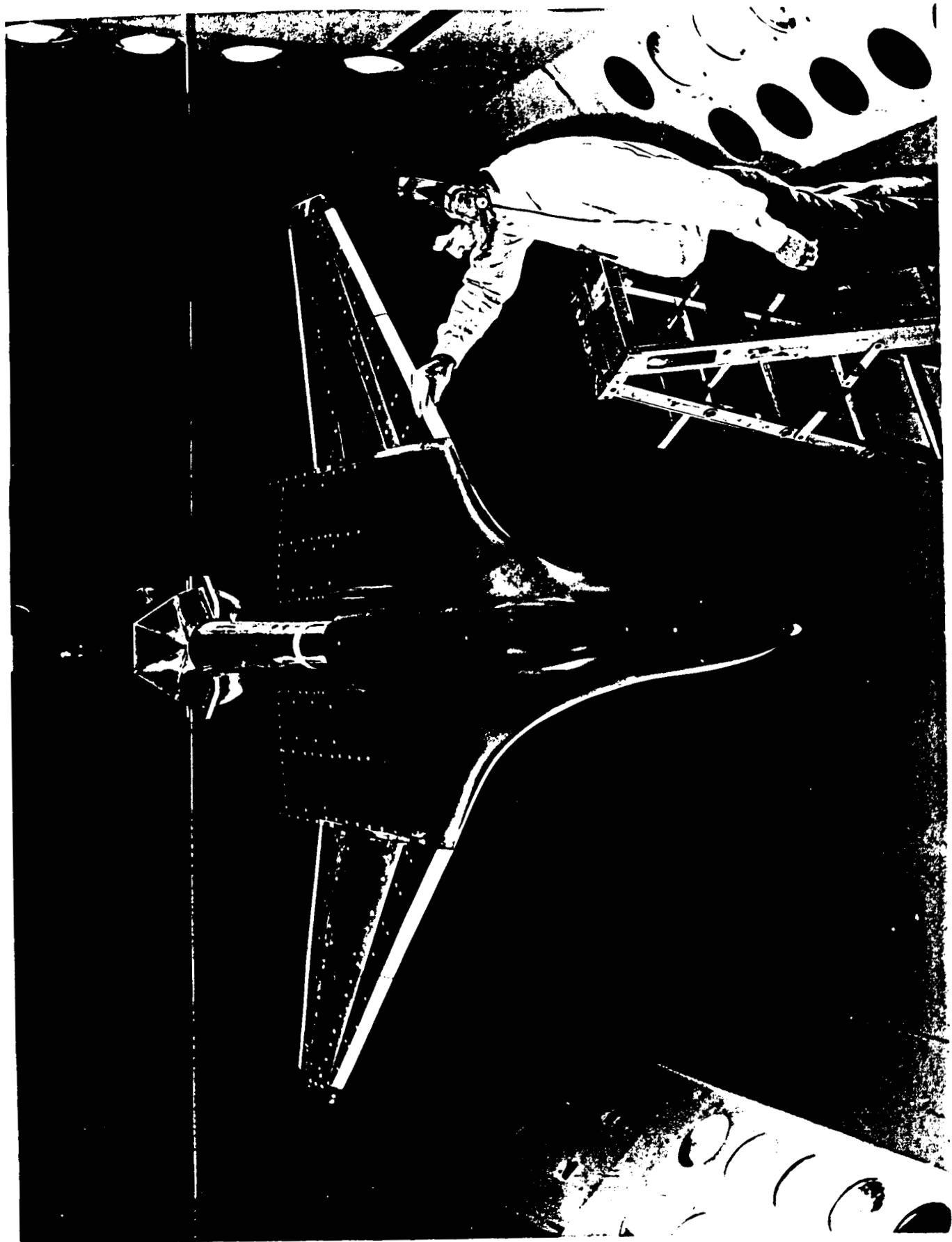
911

ACTIVE FLEXIBLE WING WIND TUNNEL MODEL MOUNTED IN THE 16-FOOT TRANSONIC DYNAMICS TUNNEL

In mid 1985 the Air Force Flight Dynamics Laboratory in cooperation with the NASA LaRC awarded a research contract to Rockwell International to test advanced control concepts on an aeroelastically scaled full-span wind tunnel model representative of an advanced fighter configuration. The model, shown in the photo mounted in the LaRC 16-Foot Transonic Dynamics Tunnel, was designed and fabricated by Rockwell using company funds. To give some perspective to the photo, the wing span from tip-to-tip is about 9 feet. The model consists of a rigid fuselage with scaled inertia characteristics and flexible wings. The wing box contains an aluminum honeycomb core and aeroelastically tailored plies of graphite epoxy. Each wing has two leading edge and two trailing edge control surfaces powered by rotary vane electrohydraulic actuators. The control surfaces have a chord and span of 25 percent of the local chord and 28 percent of the wing semispan, respectively. They can receive constant signals remotely or time varying signals from a computer for active control investigations. Deflection limits are imposed on the various control surfaces to avoid exceeding hinge moment and wing load limitations. The model has the capability to roll about the sting axis or can be held fixed at any roll angle using a roll brake assembly mounted in the sting. In addition, the model can be tested at various pitch angles remotely controlled by an actuator located in the sting. All actuators are powered by an onboard hydraulic system.

913

914
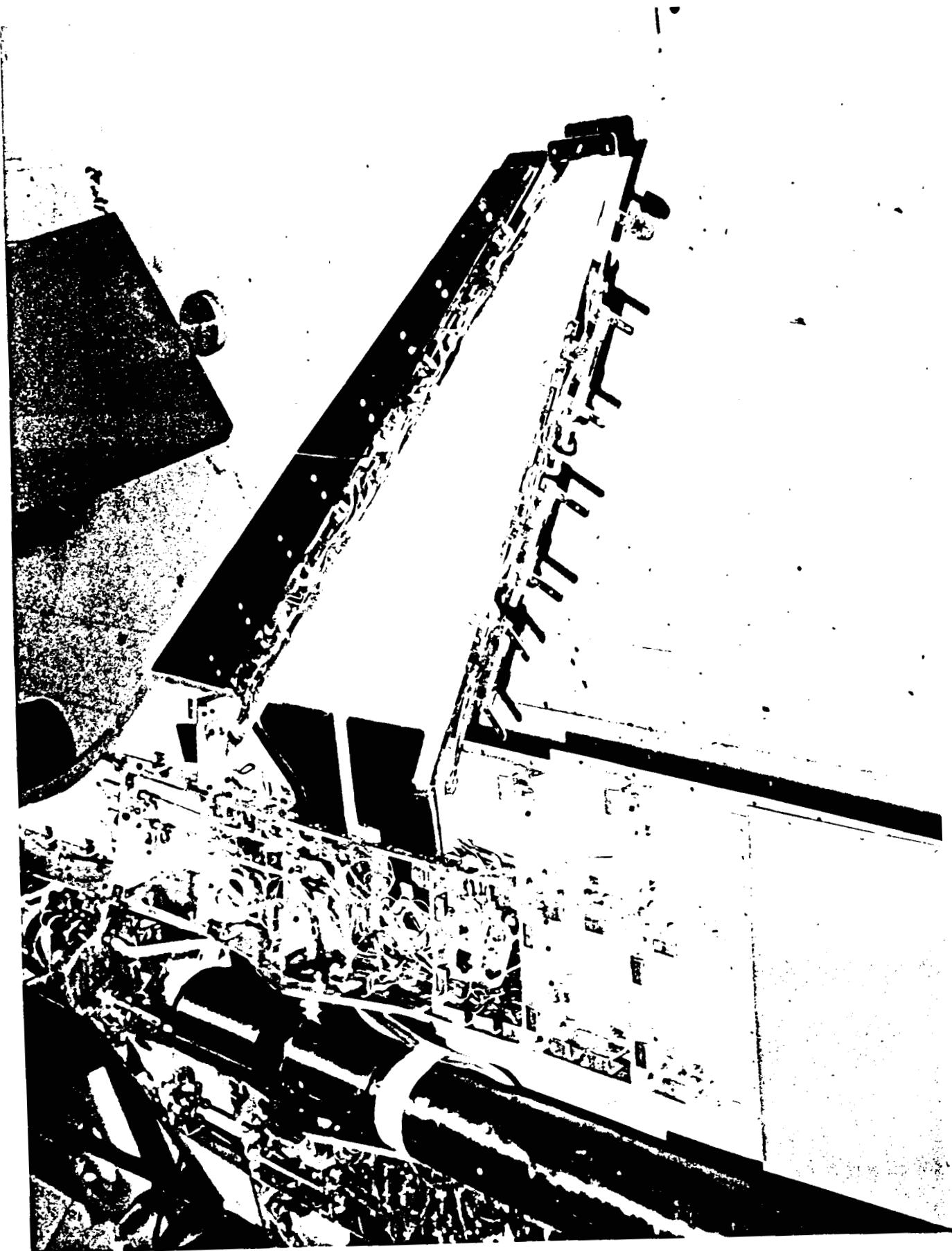
INTERNAL DETAIL OF THE AFW MODEL

This chart shows the wind tunnel model with some of the fuselage and wing panels removed to expose the complex internal detail required for ASE investigations. The outboard trailing edge control surface is driven by one actuator while the other three are driven by two each. Therefore, the control surfaces are powered by 14 actuators all supplied by onboard hydraulics. Eleven accelerometers (five on each wing and one on the fuselage) can be used as sensors for active control systems or for monitoring model response during testing. In addition, the model has sixteen strain gages, nine rotary variable differential transformers (RVDT) to indicate control surface and pitch actuator position, a roll rate gyroscope and 141 static pressure taps on the upper and lower surfaces of the left hand wing along five spanwise stations. A six-degree of freedom force and moment balance is also present.

ACTIVE FLEXIBLE WING WIND TUNNEL TEST PROGRAM

CORRECTED ANALYTICAL DATA
FOR CONTROL LAW DESIGN

- Experiment ~ TDT 3/86
- Analysis ~ uncorrected
- Analysis ~ corrected

C_{l_δ}

Dynamic pressure, psf
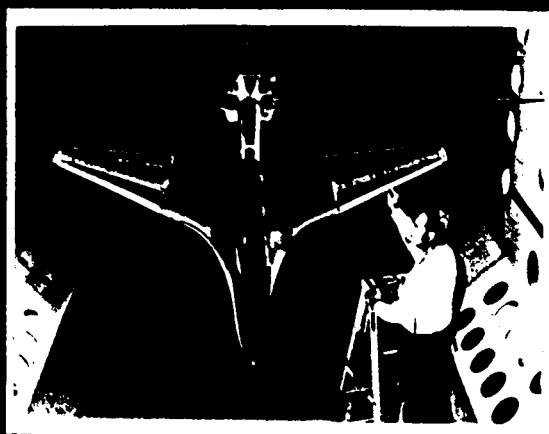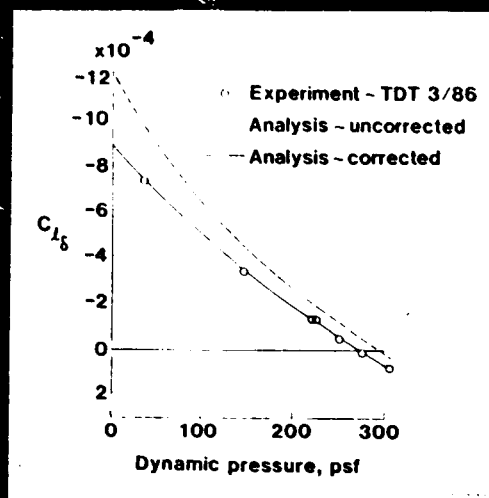
CONTROL LAW DESIGNS

	Q (PSF)	GM (DB)	PM (DEG)	Time to 90 (SEC)
(Goal)	All	6.0	45	.38
	150	9.8	77	.29
	250	11.1	82	.30

ACTIVE FLEXIBLE WING WIND TUNNEL TEST PROGRAM

The AFW concept integrates active controls technology with a flexible structure by using leading and trailing edge control surfaces to deform the wing in an optimum manner to enhance aerodynamic performance and control. Two wind tunnel tests were previously conducted to validate the AFW concept. The purpose of the first test (March and April, 1986) was to measure static aeroelastic and flexiblized stability derivative data as model angle-of-attack and control surface deflections were varied. Some typical comparisons between an experimentally determined stability derivative and the predicted (uncorrected analysis) value as a function of dynamic pressure is shown in the upper right hand corner of the figure. The corrected analysis results were determined by using two separate "correction factors" in the analysis. The first factor was used to match the expected rigid value of the stability derivative (extrapolation of the experimental data to the zero dynamic pressure value). The second factor, which varied with dynamic pressure (flexibility effect), was used to match the experimental values of the stability derivative with dynamic pressure and to match the reversal conditions for each appropriate control surface. These factors were then employed during the design of the active roll control law which was evaluated during the 2nd test period. The predicted performance for the roll control law design is shown in the lower right portion of the figure. For both flight conditions analyzed, the predicted performance exceeded the goals established. In addition to these tests, the model was flutter tested for safety considerations across the planned flight envelop even though the model was designed to be flutter free.

917

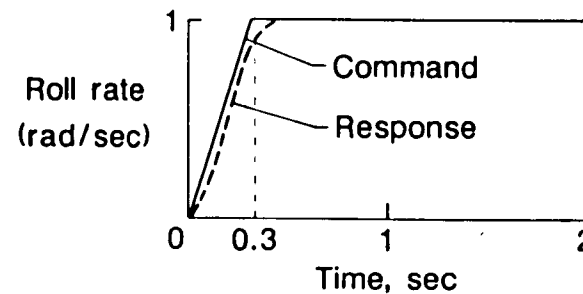# AEROSERVOELASTIC ANALYSIS VALIDATED BY WIND TUNNEL TESTS

Mach = 0.90   Dynamic pressure = 250 psf

Active flexible wing model
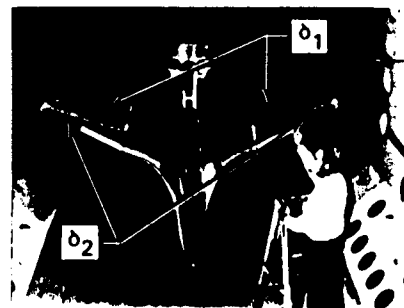
Roll rate performance

Block diagram of active roll control system
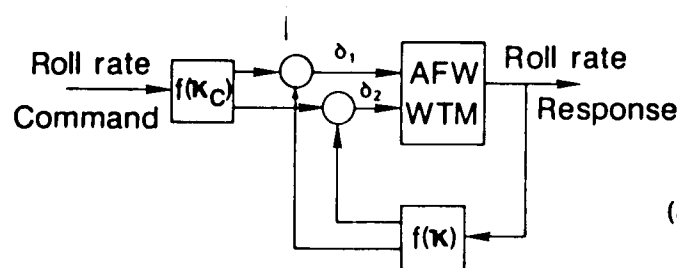
Control law parameterization
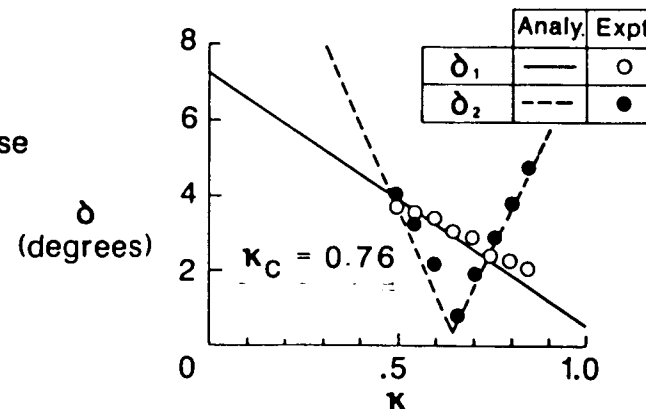
AEROSERVOELASTIC ANALYSES VALIDATED BY WIND TUNNEL TESTS

The 2nd wind tunnel test period was conducted during February and March, 1987 to evaluate Active Roll Control (ARC), Maneuver Load Control and Structural Mode Control Systems developed by Rockwell under Air Force sponsorship. In addition, an ARC system designed by NASA using the aerodynamic corrections factors discussed previously and a "parameterization" procedure was evaluated in the tunnel. This "parameterization" procedure allowed the designer the flexibility of maintaining a fixed closed loop stability and a fixed closed loop roll performance while using different commanded control surface deflections for the active surfaces involved. The consequence of this concept is that the deflections of one pair of control surfaces can be traded-off against the deflections another pair with no loss or gain in aircraft stability or system performance. This idea becomes very important when control surfaces are required to undertake multiple active control functions simultaneously. The chart shows some of the NASA ARC system test results obtained. The lower right hand figure presents a sampling of data to demonstrate the principle of the concept and illustrates the excellent correlation obtained between the test and the calculated data. The figure shows that by changing one control law parameter, stability and performance are maintained while different amounts of leading edge and trailing edge control surface deflections are used.

AFW SCHEDULE FOR FIRST WIND-TUNNEL TEST

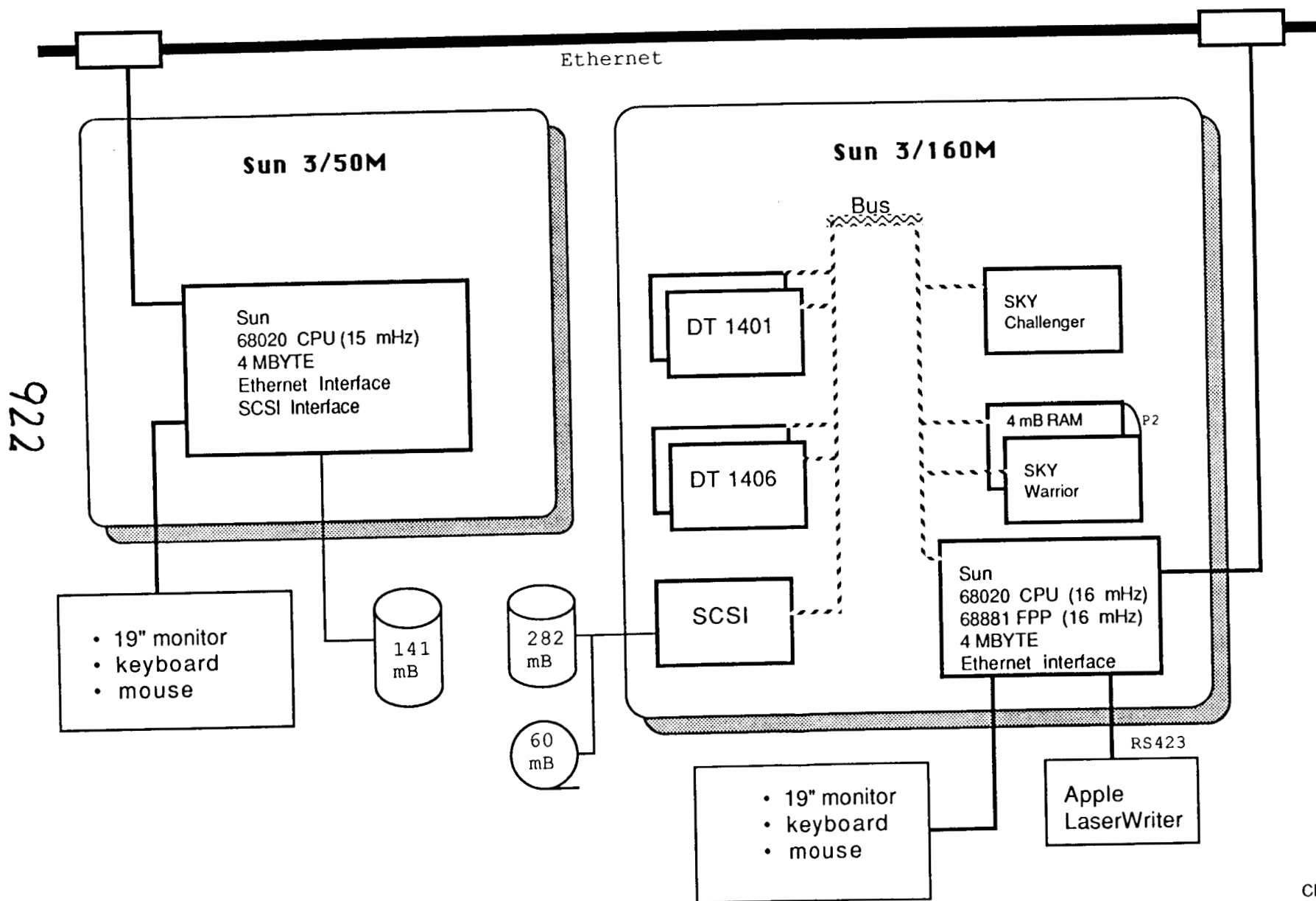|	Oct 87	Jan 88	Apr 88	Jul 88	Oct 88	Jan 89	Apr 89
TASK / QTR	QTR 1	QTR 2	QTR 3	QTR 4	QTR 5	QTR 6	
DIGITAL CONTROLLER	Design	Hardware Acquistion	Checkout	Software Coding		WT Interface	
BALLAST	Analysis		Design & Build				
EQUATIONS OF MOTION	Initial		Final		Update		
CONTROL LAWS		Initial Design		Final Design		Update	
SIMULATION	Selection	Simulation Development			Simulation	Model Check	
WIND-TUNNEL MODEL			Ship	Setup Checkout GVT		Test	

CFS/10

AFW SCHEDULE FOR FIRST WIND-TUNNEL TEST

Two wind tunnel test entries are planned for the current program; the 1st entry is scheduled for April, 1989 and the 2nd test, one year later. During the 1st entry active flutter suppression and rolling maneuver load alleviation systems will be demonstrated separately. A schedule showing the major activities prior to the 1st wind tunnel entry is presented on the chart. These multidiscipline activities include: 1) the model digital controller design, acquisition/fabrication, checkout and software coding; 2) the design and fabrication of a wing tip missile device to cause flutter within the flight envelope of the model and to act as a flutter-stopper for safety purposes; 3) the development of the aeroelastic equations of motion for six different model structural conditions; 4) the synthesis of the RMLA and the FSS active control laws; 5) the "hot bench" simulation of the digital controller and associated software; and 6) the appropriate ground testing of the model to define its structural and dynamic zero-airspeed characteristics. Each of these activities will be discussed separately in the following figures. Although the details involving the 2nd wind tunnel entry will not be discussed here, the goal is to demonstrate active flutter suppression while the model is undergoing rolling maneuvers and alleviating wing loads.

AFW CONTROL LAW DEVELOPMENT SYSTEM

Ethernet

Sun 3/50M

Sun
68020 CPU (15 mHz)
4 MBYTE
Ethernet Interface
SCSI Interface

- 19" monitor
- keyboard
- mouse

141 mB

Sun 3/160M

Bus

DT 1401

DT 1406

SCSI

SKY
Challenger

4 mB RAM   P2

SKY
Warrior

Sun
68020 CPU (16 mHz)
68881 FPP (16 mHz)
4 MBYTE
Ethernet interface

282 mB

60 mB

- 19" monitor
- keyboard
- mouse

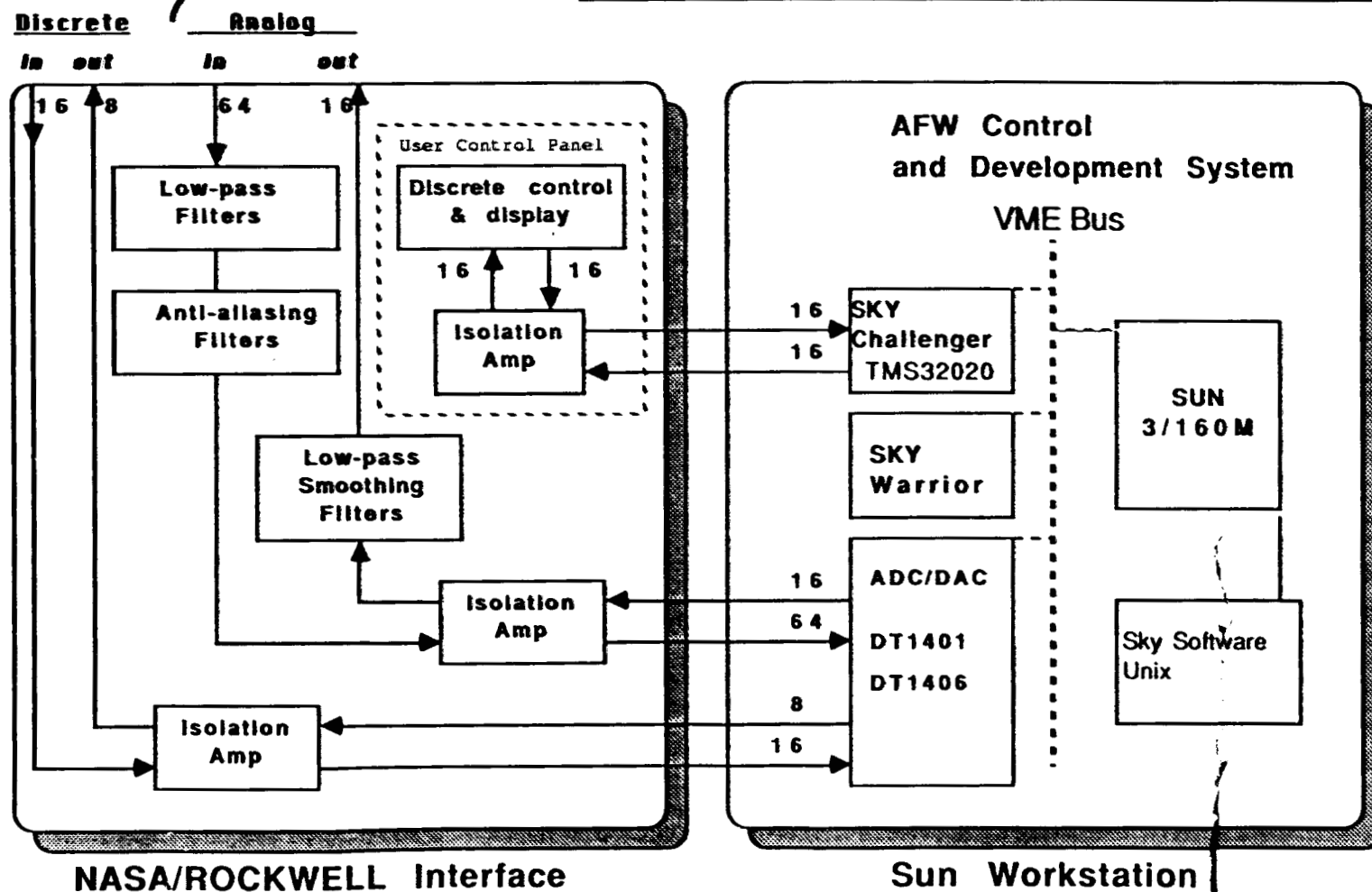RS423

Apple
LaserWriter

922

CFS/11

AFW CONTROL LAW DEVELOPMENT SYSTEM

The control law development system for the AFW wind tunnel model includes a Sun 3/160M and a Sun 3/50M workstation, a 141 megabyte hard disk with a 60 megabyte tape backup and a Apple LaserWriter for printer output. The workstations, driven by the Unix operating system, are connected through a Ethernet line. This network provides an excellent environment for several people to develop software and implement control laws independently. The Sun 3/50M is only used during the control law development, implementation and coding phases of the program. To execute the control laws the Sun 3/160M workstation requires a SKY Challenger processor board and a SKY Warrior processor board to be attached to the VME bus. The SKY Challenger is a VME digital signal processor board that is required to perform the scheduling and interfacing of the control law to the AFW model during simulation and testing phases. The SKY Warrior is a VME array processor board which can be used by either the Sun or the Challenger for performing high speed floating point arithmetic. In addition, two DT 1401 (VME Data Translation Cards) each of which has 32 analog-to-digital converters (ADC) and 2 digital-to-analog converters (DAC), and two DT 1406 each of which has 8 DAC are required to interface the incoming and outgoing model signals. These four boards provide 64 ADC and 20 DAC for use by the control program. A 282 megabyte SCSI is also attached to the bus for the storage of data.

AFW MODEL DIGITAL CONTROLLER

AFW Wind Tunnel Model

AFW Hot Bench Sim (Cyber 175)

Discrete | Analog
In out | In out

16 8 | 64 16

Low-pass Filters

Anti-aliasing Filters

Low-pass Smoothing Filters

Isolation Amp

Isolation Amp

User Control Panel

Discrete control & display

16 | 16

Isolation Amp

AFW Control and Development System

VME Bus

16 | SKY Challenger TMS32020
16

SKY Warrior

16 | ADC/DAC
64 | DT1401
8 | DT1406
16

SUN 3/160M

Sky Software Unix

NASA/ROCKWELL Interface

Sun Workstation

924

CFS/12

AFW MODEL DIGITAL CONTROLLER

This chart contains a schematic drawing of the "interface box" and the AFW Control and Development System the comprise the model digital controller. The interface box processes the signals coming from or going to either the wind tunnel model or the "hot bench" simulation through low-pass filters, anti-aliasing filters and electrical isolation networks. The purpose of the low-pass filters is to reduce the high frequency noise and to limit voltage spikes that might appear on any of the 64 analog input lines. Currently, a 4th order Butterworth filter with a cutoff frequency of 100 Hz is planned to be used during the wind tunnel tests for the anti-aliasing filters. To be compatible with the "hot bench" simulation computers, the cutoff frequency of the anti-aliasing filters will require time scaling. The 16 analog signals returning to the model or to the simulation computer will also be filtered to prevent sharp edge transitions from being sent to the actuators. The Development System consists of several components linked to the Sun Workstation. The SKY Challenger is required to command the SKY Warrior, control the management of the data acquisition system (reads the ADC and writes to the DAC), monitor and update the User Control Panel, check limits and act as the system timekeeper. As described on the previous chart the SKY Warrior performs the required high speed floating point arithmetic.

925

AFW FLUTTER BOUNDARY MODIFIED
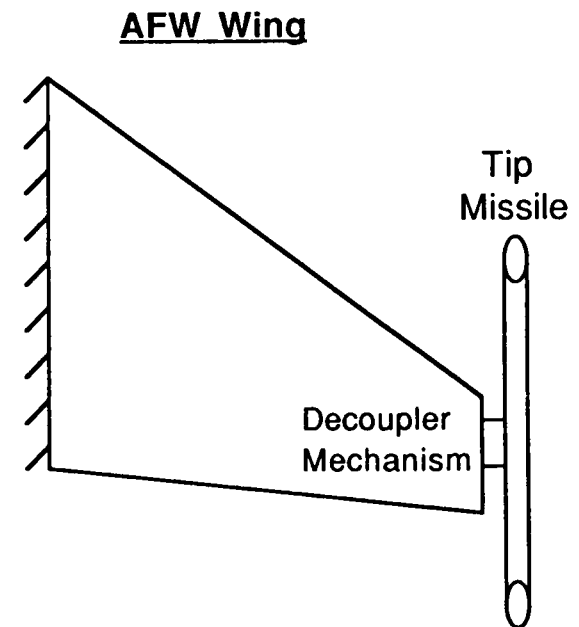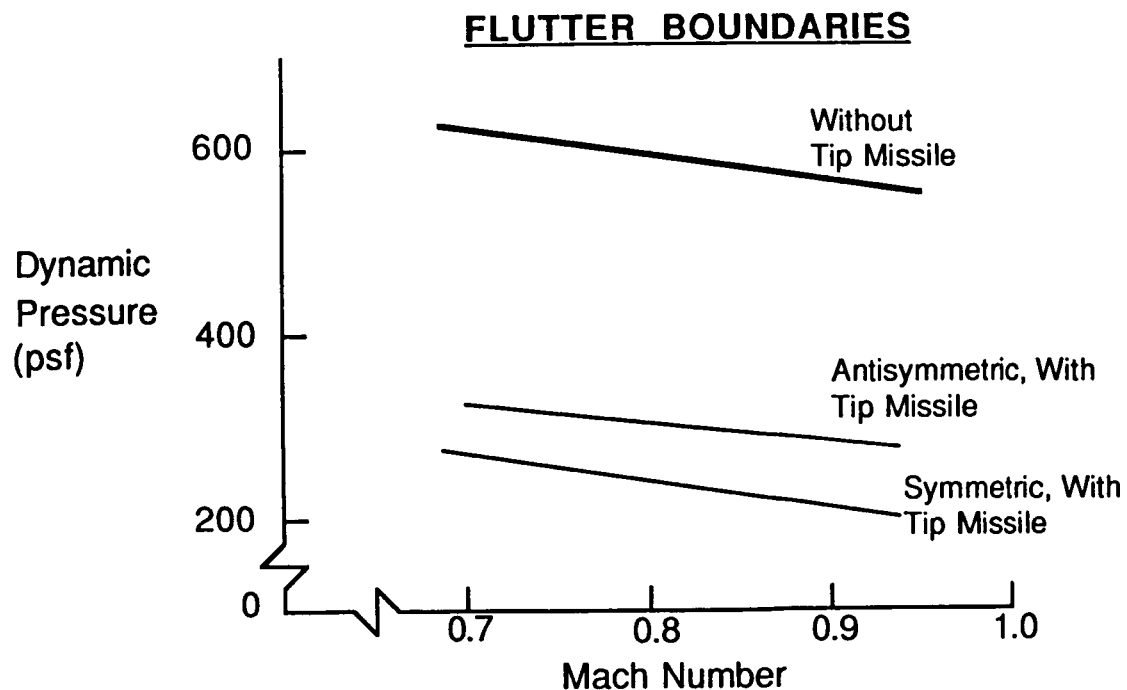# BY THE ADDITION OF A WING TIP MISSILE

Goal: Demonstrate Significant Increase in Flutter Dynamic Pressure Using Digital Active Flutter Suppression System

Problem: Basic AFW Flutter Boundary is Beyond the TDT Tunnel Limits

Solution: Add Wing Tip Missile to Lower Flutter Boundary

Benefit: Tip Missile Designed to be a Flutter Stopper for Safety

FLUTTER BOUNDARIES

AFW Wing

Dynamic Pressure (psf)

600 — Without Tip Missile

400 — Antisymmetric, With Tip Missile

200 — Symmetric, With Tip Missile

0

0.7   0.8   0.9   1.0

Mach Number

Tip Missile

Decoupler Mechanism

976

CFS/13

AFW FLUTTER BOUNDARY MODIFIED
BY THE ADDITION OF A WING TIP MISSILE

Since active flutter suppression is one of the concepts being investigated during the present program, it is necessary to modify the model so that it will have a flutter instability within the operational capabilities of the TDT. In addition, this flutter instability must occur at sufficiently low dynamic pressures such that flutter suppression may be demonstrated experimentally. Several options were considered for lowering the flutter speed of the wind tunnel model; the option most attractive was to add a wing tip missile. The tip missile significantly increases the wing pitch inertia while only slightly changing the wing total mass. This in effect decreases the zero-airspeed 1st wing torsion and 1st bending mode frequencies, and brings the two frequencies closer together. Because of the aerodynamic/structural/inertia interaction, the two modes will coalesce and cause flutter at a significantly lower dynamic pressure than without the tip missile present. The lower left figure on the chart shows typical flutter boundary calculations for the model with and without the tip missile present. Because of the close proximity of a symmetric and an antisymmetric flutter boundary, the active flutter suppression system must be capable of preventing both flutter modes simultaneously if the concept is to be effective. An added benefit of using a tip missile for causing flutter is its ability, with a little ingenuity, of returning the model to a flutter-free and, thus safe condition. This is accomplished by decoupling the missile dynamics from the wing by the use of a soft pitch spring at the wing/missile interface. The decoupling mechanism could be two pins, one stiff and one soft, as shown in the figure to the right. With the two pins installed the model would be flutter critical; with the stiff pin retracted, the wing is decoupled from the missile and becomes flutter free.

927

EQUATIONS OF MOTION

$$[M]\{\ddot{q}(t)\} + [D]\{\dot{q}(t)\} + [K]\{q(t)\} + \tfrac{1}{2}\rho v^2[Q(t)]\{q(t)\} + \tfrac{1}{2}\rho v^2\{Q_G(t)\}\frac{w_g(t)}{v} = \{0\}$$

FREQUENCY DOMAIN:

- Fourier Transform EOM

- $Q(i\omega)$ and $Q_G(i\omega)$ are transcendental tabular functions

LAPLACE DOMAIN:

- Laplace Transform EOM

- $Q(s)$ and $Q_G(s)$ approximated by: $A_0 + A_1\frac{b}{v}s + A_2\left(\frac{b}{v}s\right)^2 + \sum_{m=3}^{6}\dfrac{sA_m}{\left(s + \frac{v}{b}\beta_{m-2}\right)}$
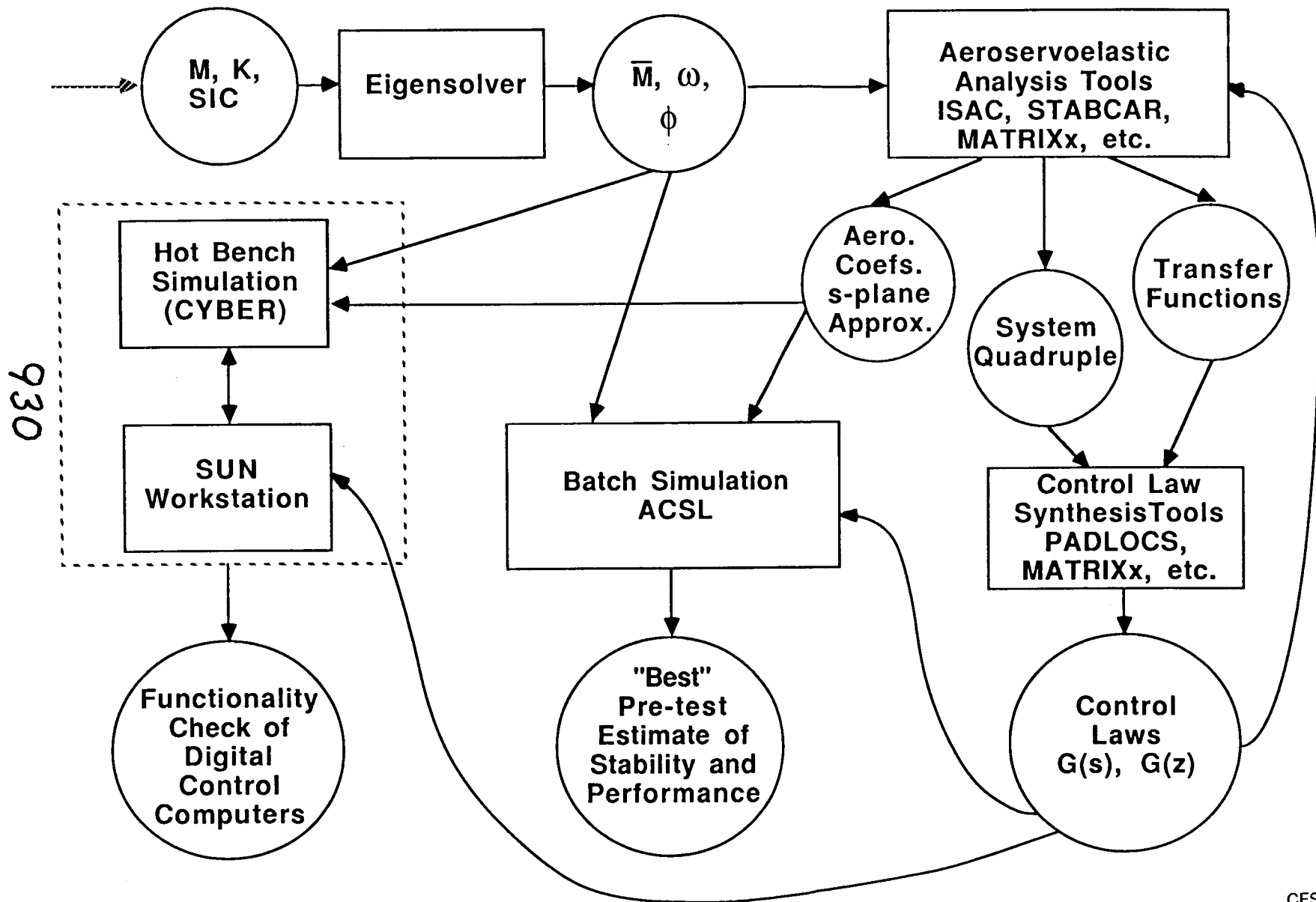
STATE SPACE EOM:

- Inverse Transform Laplace Domain EOM

- Obtain the first order representation: $\dot{x} = Ax + B_c u_c + B_G u_G$

EQUATIONS OF MOTION

One approach to formulating the equations of motion of an elastic aircraft is based on a chosen set of vehicle vibration modes and the Lagrange energy equation. Considering only small perturbations from a level equilibrium flight condition, the aircraft can be represented by a set of linear equations expressed in terms of the generalized coordinates, q(t). An example of such an equation is provided at the top of the slide. This equation represents a summation of forces and includes the inertial, the dissipation and the internal restoring forces, and the aerodynamic forces caused by the aircraft's rigid body, control surface and flexible motions and caused by gusts. To determine the aeroelastic characteristics of the vehicle, these equations are classically transformed into the frequency domain so that state-of-the-art unsteady aerodynamic theories based on simple harmonic motion can be used. These unsteady aerodynamic generalized force coefficients are transcendental tabular functions of several parameters, including frequency. Analyses in the frequency domain are straight forward using common methods. To perform aeroelastic analyses and design studies that include the effects of active feedback control systems, the equations of motion are transformed into the Laplace domain. The transformation of these equations into the Laplace domain is complicated by the transcendental functions of the generalized forces. The use of rational functions to approximate the generalized forces provides one solution to this problem. Several procedures are available for determining the rational function approximations. The equation shown on the slide is one of the more common forms. Here, a least square fit of the aerodynamic data is performed to determine the coefficients of the polynomial for each element of the frequency dependent generalized force matrices. Once the transformed generalized forces are obtained, the equations of motion are then placed into state-space form for design investigations.

929

ANALYSIS FLOW

ANALYSIS FLOW diagram:

M, K, SIC → Eigensolver → $\overline{M}$, ω, ϕ → Aeroservoelastic Analysis Tools ISAC, STABCAR, MATRIXx, etc.

930

Hot Bench Simulation (CYBER) ↔ SUN Workstation → Functionality Check of Digital Control Computers

Aeroservoelastic Analysis Tools → Aero. Coefs. s-plane Approx. / System Quadruple / Transfer Functions

Aero. Coefs. s-plane Approx. → Hot Bench Simulation (CYBER)

Batch Simulation ACSL → "Best" Pre-test Estimate of Stability and Performance

System Quadruple / Transfer Functions → Control Law SynthesisTools PADLOCS, MATRIXx, etc. → Control Laws G(s), G(z)

CFS/15

ANALYSIS FLOW

This chart illustrates the major analyses performed and the flow of data and information between analyses. Circles represent both input to and output from the various analyses; rectangular boxes represent analyses. The starting point, at the upper left, is a circle containing lumped-mass matrices and either stiffness or structural-influence-coefficient matrices. These matrices have come from a structural analysis code (not shown) and go into an eigenvalue/eigenvector analysis yielding in-vacuum frequencies, mode shapes and generalized masses. These quantities then go to three other boxes, the first of which is labelled Aeroservoelastic Analysis. Within this box the open-loop (and, when control laws are available, the closed-loop) aeroelastic equations of motion are generated, various analyses are performed, and intermediate results are passed "downstream" to a Control Law Synthesis box and two Simulation boxes. When generated, control laws are passed back up to the Aeroservoelastic Analysis box for computation of closed-loop frequency responses, closed-loop time responses, closed-loop flutter, etc. Control laws and other data are also passed to the two Simulation boxes which ultimately provide a functionality check of the digital control computers and a "best" pre-test estimate of the stability and performance of the closed-loop wind tunnel model.

C-5

SYMMETRIC FLUTTER ROOT LOCUS

Stiff Tip Missile Spring, M = 0.9

Freq (rad/sec)

Flutter Frequency = 11.1 Hz

Flutter Dynamic Pressure = 213 psf

Real
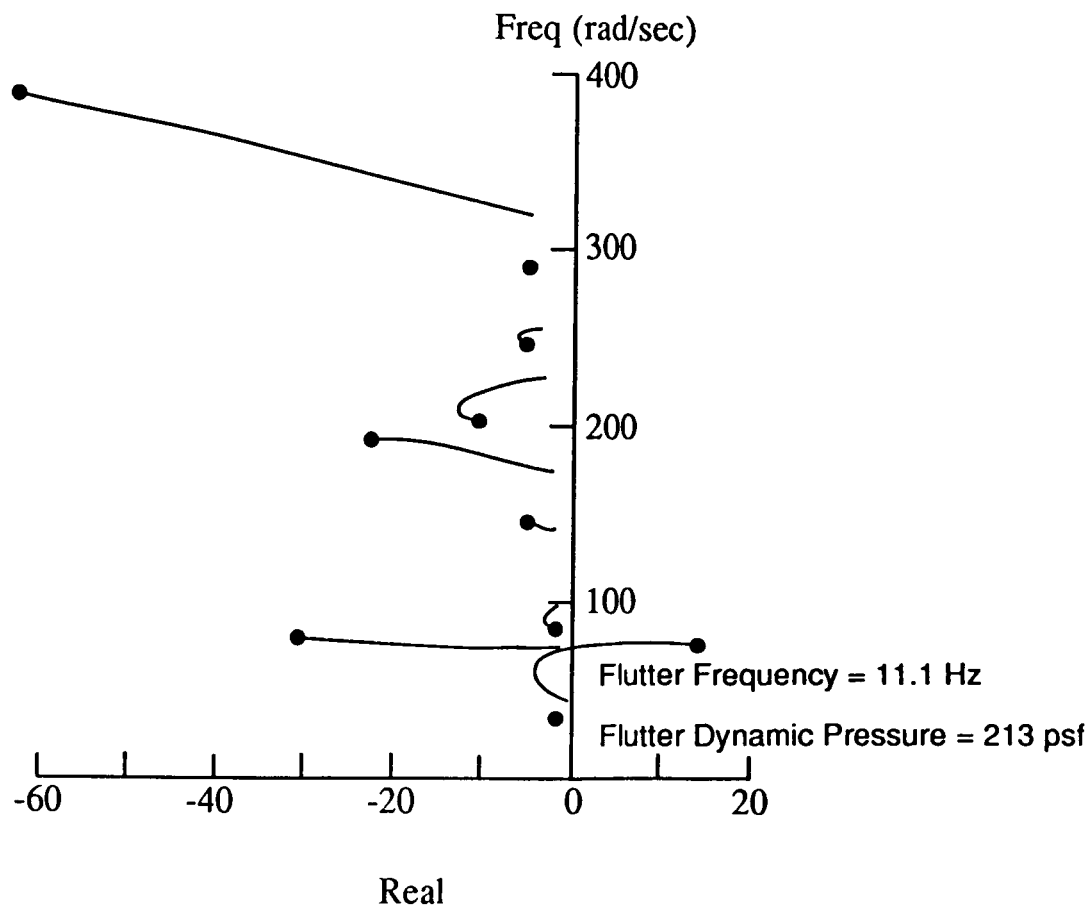
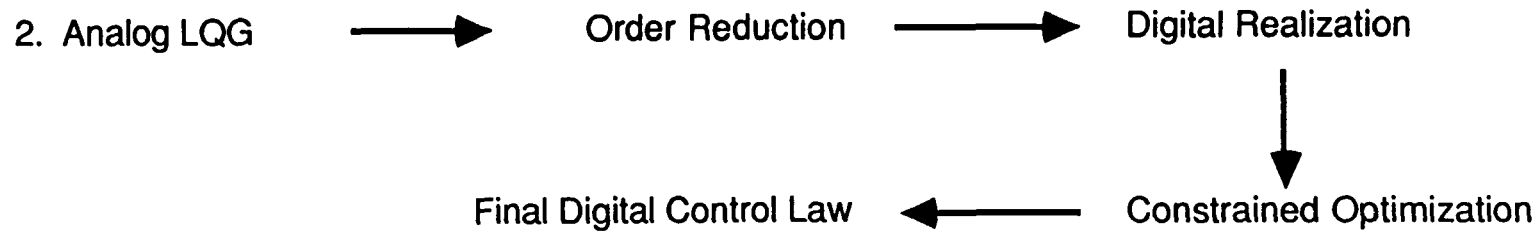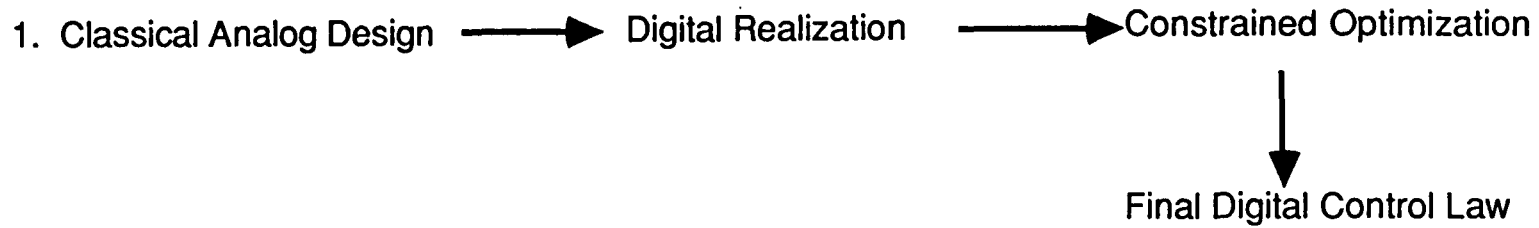## SYMMETRIC FLUTTER ROOT LOCUS

Various analysis procedures can be used to obtain the aeroelastic characteristics of the model. This chart shows typical stability results using a root locus approach. To adequately define the flutter stability for the AFW wind tunnel model it was necessary to develop equations of motion for six different model representations. These included the model undergoing symmetric motion with the tip missile attached to the wing with either the stiff spring or the soft spring as discussed previously, and the model undergoing antisymmetric motion with the tip missile attached to the wing with either the stiff spring or the soft spring with the roll brake on and off. The data shown on the plot represents the AFW model undergoing symmetric motion with the tip missile attached to the wing with a stiff spring. Mach 0.9 doublet lattice unsteady aerodynamics were used for these calculations. Velocity was held constant and the air density was varied so that a matched point solution was obtained. For this analysis, the first ten vehicle elastic modes were used to define the generalized coordinates. The predicted flutter mode involves the coalescence of the 2nd and 3rd elastic modes at a dynamic pressure of 213 psf at a frequency of 11.1 Hz as can be seen when the 2nd elastic mode root moves into the right half plane. The objective of the FSS is to move the unstable root back into the left hand plane of the plot.

933

SYNTHESIS METHODOLOGIES

1. Classical Analog Design ⟶ Digital Realization ⟶ Constrained Optimization

⟶ Final Digital Control Law

2. Analog LQG ⟶ Order Reduction ⟶ Digital Realization

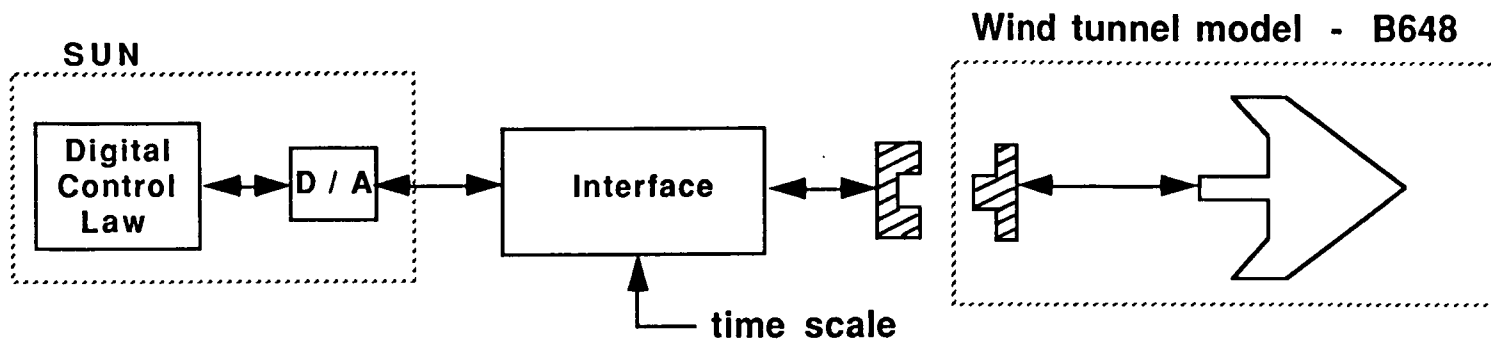⟶ Constrained Optimization ⟶ Final Digital Control Law

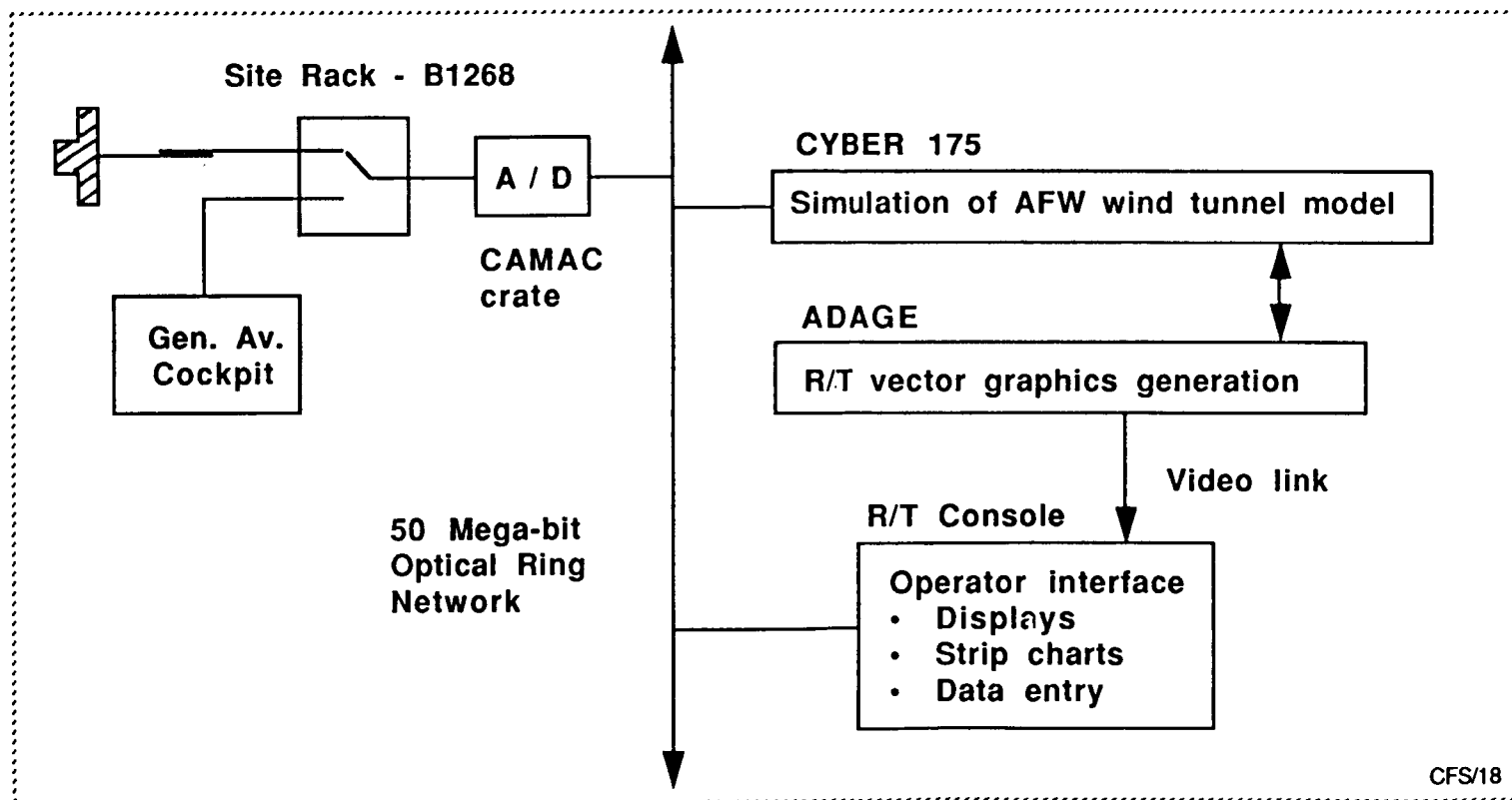3. Direct Digital Design

4. Eigensystem Design Techniques

SYNTHESIS METHODOLOGIES

Several approaches that include classical analog and modern/optimal control techniques are being evaluated for use in designing the digital active flutter suppression system. The classical techniques being considered are based on root locus, Bode (transfer functions) or Nyquist plots and are useful for single-input, single-output systems. Once an analog control law which provides at least minimum stability for the aircraft at a certain design point is found, it is transformed into the z-domain and then optimized based on constraints such as design loads, actuator deflection and rate limits, and stability margins. The optimization task results in improved stability margins and robustness characteristics. The Linear-Quadratic-Gaussian (LQG) method is a systematic approach for designing multi-input, multi-output control laws. The LQG method is based on minimizing a cost performance index consisting of quantities such as control deflection, design loads, accelerations, etc. The control law developed using this technique, however, is the same order as the aircraft being modeled. For flexible aircraft with unsteady aerodynamic forces, the number of states required to represent the vehicle is usually quite large. This order problem is solved through the truncation or residulation of the Kalman Filter. As described above, the LQG reduced-order control law is transformed into the digital domain and further optimized to improve performance and robustness. A third approach being considered involves the direct digital design of the control law. The methodology for the direct synthesis (determination of the coefficients for the z terms) of the digital FSS uses constrained optimization, and will meet multiple design requirements if necessary while maintaining reasonable stability requirements. The last method being evaluated is an eigensystem design technique. The method involves the placement of the closed loop roots to obtain a control law with satisfactory stability, performance and robustness characteristics.

SYSTEM OVERVIEW OF HOT BENCH SIMULATION

Wind tunnel model - B648

SUN

Digital Control Law → D / A → Interface ← time scale

Hot Bench Simulation

Site Rack - B1268

A / D

CAMAC crate

Gen. Av. Cockpit

CYBER 175

Simulation of AFW wind tunnel model

ADAGE

R/T vector graphics generation

Video link

50 Mega-bit Optical Ring Network

R/T Console

Operator interface
- Displays
- Strip charts
- Data entry

936

CFS/18

SYSTEM OVERVIEW OF HOT BENCH SIMULATION

The purpose of the "hot bench" simulation is to provide a comprehensive evaluation of the functionality of the Sun digital controller and the user control software, and to provide a low order, linear check of the flexible/dynamic system coupled with the active control laws. It is planned that this activity will be accomplished by attaching the Sun digital controller to a Cyber 175. The Cyber represents the AFW aeroelastic equations of motion modeled to include a sufficient number of elastic modes and the unsteady aerodynamic forces needed to accurately predict the static and dynamic characteristics of the test article across its expected test envelop. The Cyber will send sensor and other model or test condition information to the Sun for processing by the digital controller and will receive control actuator displacements from the Sun. Issues which can be investigated during the "hot bench" simulation besides the user control software, and control law stability and performance evaluations include:

1) the operation of the flutter stopper,
2) actuator transfer function differences between left and right wings which could cause coupling between symmetric and antisymmetric model characteristics,
3) failed actuators and sensors,
4) control surface displacement and rate limits.

A schematic that demonstrates the procedure to provide the interface between the Sun digital controller with the Cyber 175 during the "hot bench" simulation or to the AFW model during the wind tunnel tests is shown on this chart. On a previous chart, the NASA/Rockwell Interface box was discussed. Recall that this box takes discrete and analog signals from the wind tunnel model or from the Cyber during the "hot bench" simulation studies. Because of the clock step and time step differences between the Sun and the Cyber, it will be necessary to conduct the simulation in synchronized slow time.

937

PRELIMINARY AFW MODEL TEST PLANS

o Ground Vibration Tests

o Control System Functional Tests

   Open Loop Transfer Function Measurements

o Servoelastic Coupling tests

   Closed Loop limit Cycle and Ground Resonance

o Wind Tunnel Tests

   Measure Control Surface Stability Derivatives

   Obtain Static Pressure Distributions at Selected Wing Locations

   Perform Roll Maneuvers with and without Active Load Alleviation

   Define Flutter Free Test Envelop for Decoupled Tip Missile

   Define Passive Flutter Boundary

   Demonstrate Active Flutter Suppression

PRELIMINARY AFW MODEL TEST PLANS

The wind tunnel model will arrive at LaRC during the summer of 1988 for extensive ground testing prior to installing the model into the Transonic Dynamics Tunnel . Initially, the model will be ground vibration tested with the tip missile attached to the wing using both the stiff and soft spring representations separately. Symmetric and antisymmetric elastic mode frequencies, mode shapes and structural damping coefficients will be obtained with the model roll brake on and off. In addition, all sensor signals expected to be used by the active control laws will be measured. During these tests all actuators will be hydraulically powered. Open loop end-to-end tests will be accomplished to obtain transfer functions over a broad frequency range for all control surface/sensor combinations using several different amplitude signals to evaluate the nonlinear effects. The transfer function of selected components, such as the actuators and sensors will also be measured separately. Closed loop tests will also be accomplished for each active control law to be evaluated in the wind tunnel. These tests will include limit cycle tests to measure gain and phase margins at zero airspeed, model stability evaluations following an impulse excitation, and ground vibration tests. The intent of these tests is to obtain measured data for validating math models at zero airspeed (without aerodynamics). The various math models will be corrected and the control system designs updated as appropriate prior to the wind tunnel tests. Finally, the chart shows the expected wind tunnel tests and the order of conducting these tests. Routine force, moment and static pressure data will be measured first. Next the performance of the Rolling Maneuver Load Alleviation System will be evaluated. The higher risk tests which include the passive flutter and the active flutter suppression tests for preventing a high frequency violent flutter mode will be accomplished last.

VALIDATION OF TOOLS
FOR MULTIDISCIPLINARY TECHNOLOGY

MULTIDISCIPLINARY AREAS

Aero   **Servo**

Elasticity

1. Aerodynamics

2. Controls

3. Structures

4. Aeroelasticity

5. Closed-Loop Stability and Control

6. Servoelasticity
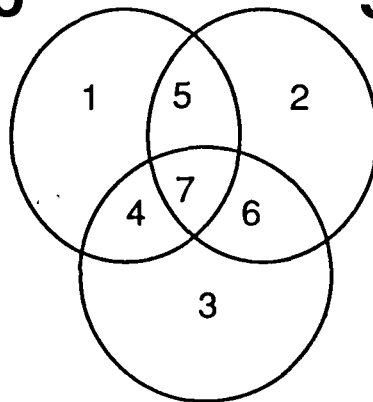
7. Aeroservoelasticity

PLANNED TESTS/VALIDATION

Static Pressure Distributions

Analog and Digital Transfer Functions

Frequencies and Mode Shapes

Control Effectiveness and Flutter

None Planned

Closed-Loop Ground Tests

"Hot Bench" Simulation/RMLA and FSS

940

VALIDATION OF TOOLS FOR MULTIDISCIPLINARY TECHNOLOGY

In summary, aeroservoelasticity is a multidisciplinary technology that involves unsteady aerodynamics, active control systems and flexible structures. This chart illustrates the potential interactions of these three technologies with the aid of three intersecting circles to represent individual technical disciplines. ASE represents that area common to all three circles. To adequately develop analysis and design tools for application to ASE, it is important and critical to validate software within each area of interacting technologies. Recall, that one of the objectives of this program is to obtain test data for evaluating the usefulness and accuracy of our codes involved in the design of flexible vehicles. The approach being followed during this program is to obtain experimental data to validate each of the primary technical disciplines prior to proceeding to levels involving two interacting technologies or three (ASE for this case). In conclusion, the NASA/Rockwell AFW program began in October, 1987 and will continue for about three years. This presentation has been a status report that addressed:

      1) why the program is being pursued,
      2) where we are today, and
      3) what to look forward to in the coming months.

For those interested in pursuing the progress of the program, additional status reports will be presented at various conferences and workshops during the program.

MODELING AND STABILIZATION OF LARGE FLEXIBLE SPACE STATIONS

By

S. S. Lim and N. U. Ahmed
University of Ottawa
Ottawa, CANADA

ABSTRACT

In this paper we present a preliminary formulation of a large space structure. The system consists of a (rigid) massive body, which may play the role of experimental modules located at the center of the space station and a flexible configuration, consisting of several beams, which is rigidly attached to the main body. The equations that govern the motion of the complete system consist of several partial differential equations with boundary conditions describing the vibration of flexible components coupled with six ordinary differential equations that describe the rotational and translational motion of the central body.

In our investigation we consider the problem of (feedback) stabilization of the system mentioned above.

This study is expected to provide an insight into the complexity of design and stabilization of actual space stations. Some numerical results will be presented.

943

Modeling and Stabilization of Space Stations

S. LIM   N. U. Ahmed

University of Ottawa

Ottawa, Ontario

CANADA

945

OUTLINE

MOTIVATION

Modeling of Space Stations

- Motivation
- Reference Coordinate Systems
- Inertia Tensors
- Equations of motion

Stabilization

- Stability by feedback control
- Localized Control
- Other Control (B.B. , D.Z.)

Numerical Simulation

- Finite Difference Method

Future Directions

946

UPPER BOOM
OBSERVATORY

CUSTOMER
PLATFORMS

SERVICING BAY

LABORATORY MODULE

KEEL

ATTACHED P/L MONITORING
& CONTROL FACILITY

PM SERVICING
FACILITY

LOWER BOOM
OBSERVATORY

< NAS19 SPACE STATION >

EXPERIMENT AREA

TDRS
ANTENNA

PHOTOVOLTAIC
ARRAY

OPTIONAL
SATELLITE
SERVICE AREA

OMV. OTV

SOLAR
DYNAMIC
COLLECTOR

THERMAL RADIATOR

REMOTE MANIPULATOR

RCS THRUSTER

OPTIONAL
SATELLITE
SERVICE AREA

EXPERIMENT AREA

Space Station Baseline

947

$$\varphi^1 = (0, \; y_1, \; z_1)',$$

$$\varphi^2 = (0, \; y_2, \; z_2)',$$

$$\varphi^3 = (x_3, \; 0, \; z_3)',$$

$$\tilde{r}_i = R + \underbrace{s_i + \varphi^i}_{r_i}, \qquad i = 1, 2, 3$$

948
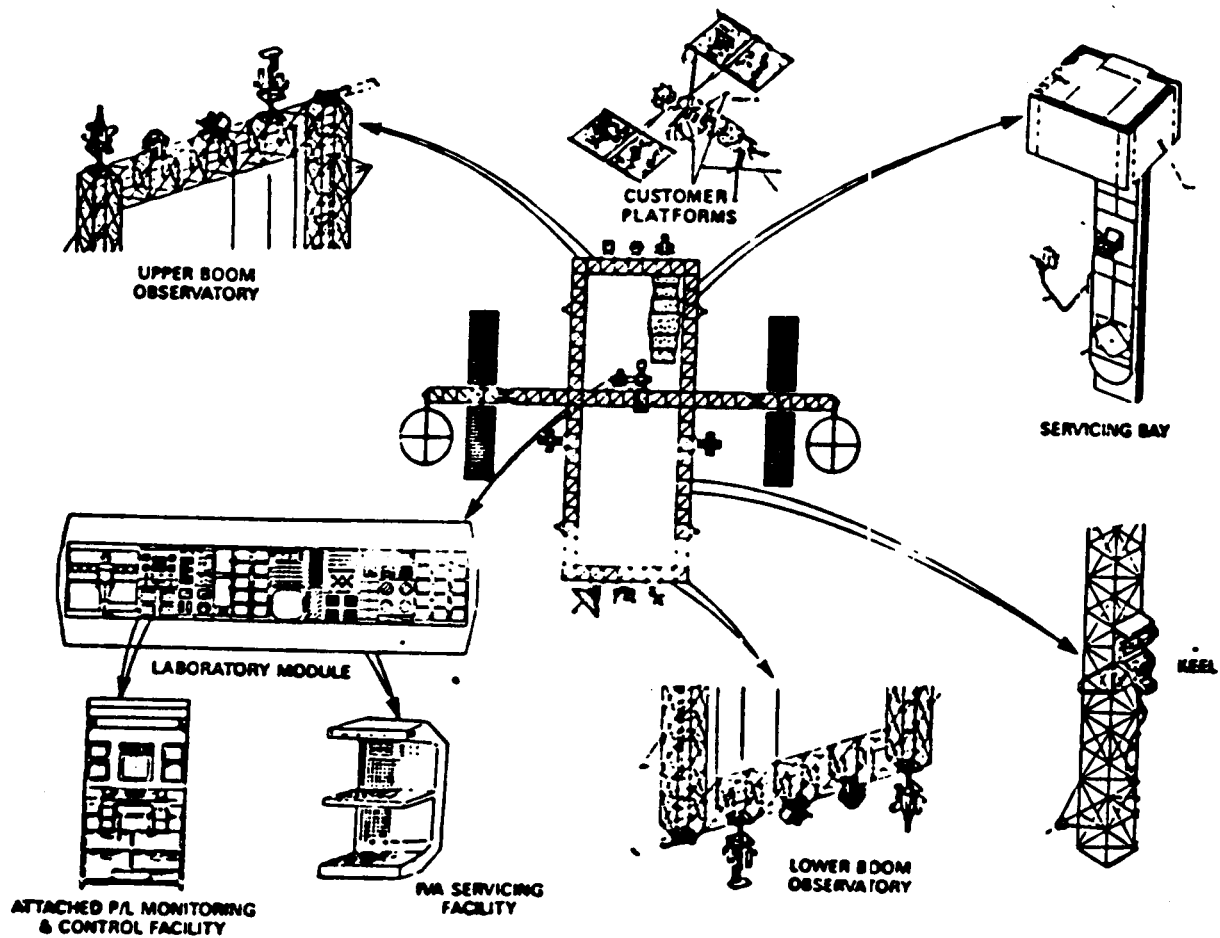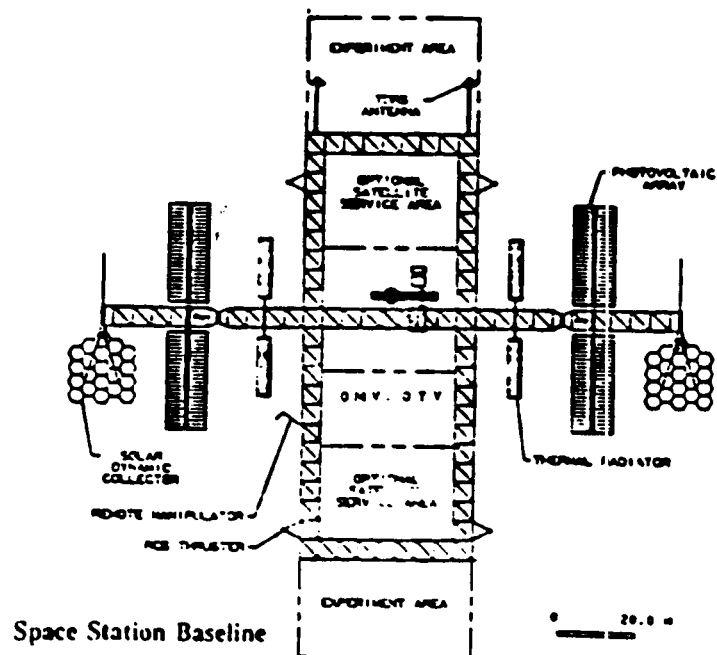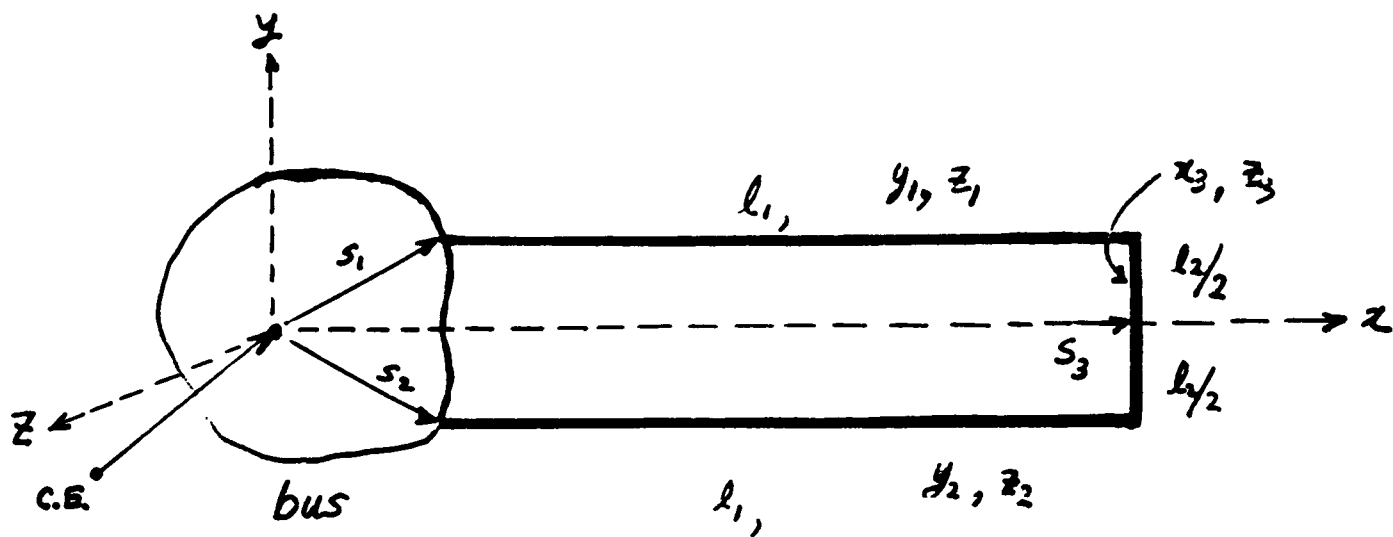
Modeling of Space Station

Three types of motion:

(a) Rigid body translation perturbing the orbit

(b) Rigid body rotation perturbing the orientation

(c) Vibration of elastic members

Reference Coordinate Systems

Body coord.   : (i_b, j_b, k_b)
Orbit Coord. : (i_r, j_r, k_r)
Inertial coord. : (i_I, k_I, k_I)

$\tilde{r} = R + r$
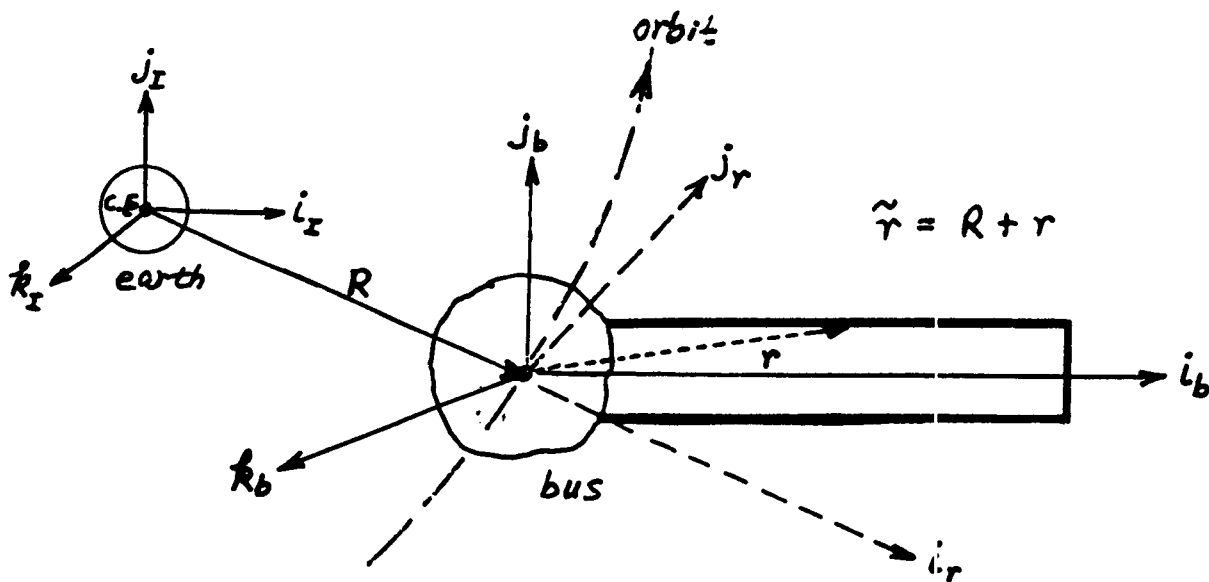
Angular velocities

$$\omega_b = (\omega_x, \omega_y, \omega_z)'$$
$$\omega_r = (\omega_X, \omega_Y, \omega_Z)'$$
$$\omega = \omega_b + \omega_r = (\omega_1, \omega_2, \omega_3)'$$

949

Inertia Tensor

I_S = Inertia tensor of the bus

I_b = Inertia tensor of the elastic members

$$= \begin{pmatrix} I_{xx} & -I_{xy} & -I_{xz} \\ -I_{yx} & I_{yy} & -I_{yz} \\ -I_{zx} & -I_{zy} & I_{zz} \end{pmatrix}$$

where $\quad I_{xx} = \int (y^2 + z^2)\, dm$,

$\qquad I_{yy} = \int (x^2 + z^2)\, dm$,

$\qquad I_{zz} = \int (x^2 + y^2)\, dm$,

$\qquad I_{xy} = \int xy\, dm$,

$\qquad I_{yz} = \int yz\, dm$,

$\qquad I_{zx} = \int zx\, dm$,

$\qquad\qquad r = (x, y, z)'$.

$I_T = I_S + I_b$

Equations of Motion

$$\delta \int_{t_1}^{t_2} (T + W)\, dt = 0$$

where T = Kinetic energy of the system,

W = Total work done by the forces.

$$T = T_s + T_b$$

$$T_s = \frac{1}{2} \int_{bus} \frac{d\tilde{r}}{dt} \cdot \frac{d\tilde{r}}{dt}\, dm, \qquad \tilde{r} = R + r$$

$$T_b = \frac{1}{2} \int_{beam} \frac{d\tilde{r}}{dt} \cdot \frac{d\tilde{r}}{dt}\, dm$$

$$V = V_e + V_g, \qquad \text{Total potential energy;}$$

$$V_e = \frac{1}{2} \int_0^l EI\, \varphi_{\xi\xi} \cdot \varphi_{\xi\xi}\, d\xi$$

$$V_g = - \frac{G\, m_E\, m_T}{|R|}$$

where m_T = Total mass of the system
m_E = Mass of the earth
G = Universal gravitational constant

Notations:

$\frac{d}{dt}(\cdot)$ = time derivative of $(\cdot)$ w.r.t. Inertial frame

$(\dot{\,})$ = time derivative of ( ) w.r.t. body frame

$A \cdot B$ = Scalar product of vectors A and B.
$A \times B$ = vector product of vectors A and B.   951

$$\delta \tilde{r} = \delta R + \delta \theta \times r + \delta r$$

$$\delta \left(\frac{d\tilde{r}}{dt} \right) = \delta \left(\frac{dR}{dt} \right) + \delta w \times r + \delta \theta \times (w \times r + \dot{r}) + \frac{d}{dt}(\delta r)$$

$$\delta \int_{t_1}^{t_2} T_s \, dt = - \int_{t_1}^{t_2} \left\{ m_s \delta R \cdot \frac{d^2 R}{dt^2} + \delta \theta \cdot \frac{d}{dt} \left(I_s w \right) \right\} dt,$$

$$\delta \int_{t_1}^{t_2} T_b \, dt = \delta \sum_{i=1}^{3} \int_{t_1}^{t_2} \int_{\mathcal{L}_i} \frac{1}{2} \frac{d\tilde{r}}{dt} \cdot \frac{d\tilde{r}}{dt} \, dm \, dt$$

$$= - \sum_{i=1}^{3} \int_{t_1}^{t_2} \int_{\mathcal{L}_i} \left\{ \delta R \cdot \frac{d^2 \tilde{r}}{dt^2_i} + \delta \theta \cdot \left(r_i \times \frac{d^2 \tilde{r}_i}{dt^2} \right) \right.$$

$$\left. + \delta r_i \cdot \frac{d^2}{dt^2} \tilde{r}_i \right\} dm \, dt,$$

$$\delta \cdot \int_{t_1}^{t_2} V_e \, dt = - \sum_{i=1}^{3} \delta \int_{t_1}^{t_2} \int_{\mathcal{L}_i} \frac{1}{2} \varphi^i_{\xi\xi} \cdot EI_i \, \varphi^i_{\xi\xi} \, d\xi \, dt$$

$$= \sum_{i=1}^{3} \left\{ \int_{t_1}^{t_2} \delta \varphi^i_\xi \cdot EI_i \, \varphi^i_{\xi\xi} \Big]_{\mathcal{L}_i} dt - \int_{t_1}^{t_2} \delta \varphi^i \cdot (EI_i \, \varphi^i_{\xi\xi})_\xi \Big]_{\mathcal{L}_i} dt \right.$$

$$\left. + \int_{t_1}^{t_2} \int_{\mathcal{L}_i} \delta \varphi^i \cdot \left(EI_i \, \varphi^i_{\xi\xi} \right)_{\xi\xi} \, d\xi \, dt \right\},$$

$$\delta \int_{t_1}^{t_2} V_g \, dt = \int_{t_1}^{t_2} \frac{G m_E m_T}{|R|^2} 1_R \cdot \delta R \, dt, \qquad 1_R = \frac{R}{|R|}$$

$$\delta \int_{t_1}^{t_2} W \, dt = - \int_{t_1}^{t_2} V \, dt + \int_{t_1}^{t_2} \left(\delta R \cdot F_s + \delta \theta \cdot \tau + \sum_{i=1}^{3} \int_{\mathcal{L}_i} \delta r_i \cdot F_i \, d\xi_i \right) dt.$$

$$\delta \int_{t_1}^{t_2} (T + W)\, dt = 0$$

$$\Rightarrow \quad -\int_{t_1}^{t_2} \delta R \cdot \left\{ \underbrace{m_s \frac{d^2 R}{dt^2} + \sum_{i=1}^{3} \int_{\Omega_i} \frac{d^2 \tilde{r}_i}{dt^2}\, dm_i + \frac{G m_E m_T}{|R|^2} 1_R - F_S}_{I} \right\} dt$$

$$-\int_{t_1}^{t_2} \delta \theta \cdot \left\{ \underbrace{\frac{d}{dt}(I_s \cdot \omega) + \sum_{i=1}^{3} \int_{\Omega_i} r_i \times \frac{d^2 \tilde{r}_i}{dt^2}\, dm_i - \tau}_{II} \right\} dt$$

$$-\int_{t_1}^{t_2} \sum_{i=1}^{3} \left\{ \underbrace{\int_{\Omega_i} \delta r_i \cdot \frac{d^2 \tilde{r}_i}{dt^2}\, dm_i + \int_{\Omega_i} \delta \varphi^i \cdot (EI_i\, \varphi^i_{\xi\xi})_{\xi\xi}\, d\xi - \int_{\Omega_i} F_i \cdot \delta r_i\, d\xi}_{III} \right\} dt$$

$$-\int_{t_1}^{t_2} \sum_{i=1}^{3} \left[\underbrace{\delta \varphi^i_\xi \cdot EI_i\, \varphi^i_{\xi\xi} - \delta \varphi^i \cdot (EI_i\, \varphi^i_{\xi\xi})_\xi}_{IV} \right]_{\Omega_i} dt = 0$$

Since δR, $\delta \theta$, δr_i (or $\delta \varphi^i$) are arbitrary, we have

$$I = 0, \quad II = 0, \quad III = 0, \quad IV = 0;$$

$$m_s \frac{d^2}{dt^2} R + \sum_{i=1}^{3} \int_{\Omega_i} \frac{d^2 \tilde{r}_i}{dt^2}\, dm_i + \frac{G m_E m_T}{|R|^2} 1_R = F_S \quad \left(\begin{array}{l} \text{Translational eq.} \\ \text{of the bus} \end{array} \right)$$

$$\frac{d}{dt}(I_s\, \omega) + \sum_{i=1}^{3} \int_{\Omega_i} r_i \times \frac{d^2 \tilde{r}_i}{dt^2}\, dm_i = \tau \quad \left(\begin{array}{l} \text{Rotational eq.} \\ \text{of the bus} \end{array} \right)$$

$$\sum_{i=1}^{3} \int_{\Omega_i} \delta r_i \cdot \frac{d^2 \tilde{r}_i}{dt^2}\, dm_i + \sum_{i=1}^{3} \int_{\Omega_i} \delta \varphi^i \cdot (EI_i\, \varphi^i_{\xi\xi})_{\xi\xi}\, d\xi_i = \sum_{i=1}^{3} \int_{\Omega_i} \delta r_i \cdot F_i\, d\xi_i \quad (\text{Beam eqs.})$$

$$\sum_{i=1}^{3} \left[\delta \varphi^i_\xi \cdot (EI_i\, \varphi^i_{\xi\xi}) - \delta \varphi^i \cdot (EI_i\, \varphi^i_{\xi\xi})_\xi \right]_{\Omega_i} = 0 \quad (\text{Boundary conditions})$$

953

Bus dynamics (Translation)

$$m_T \frac{d^2 R}{dt^2} + \sum_{i=1}^{3} \int_{\Omega_i} \frac{d^2}{dt^2} r_i \, dm_i + \frac{G m_E m_T}{|R|^2} 1_R = F_S$$

Bus dynamics (Rotation)

$$I_T \dot{\omega} + \omega \times (I_T \omega) + \dot{I}_b \omega + \sum_{i=1}^{3} \int_{\Omega_i} \left\{ r_i \times \left(\frac{d^2 R}{dt^2} + \ddot{r}_i \right) + \omega \times (r_i \times \dot{r}_i) \right\} dm_i = \tau$$

Beam dynamics (Vibration)

$$\rho_i \ddot{r}_i + (EI_i \, r_{i\xi\xi})_{\xi\xi} + \rho_i \Big(\underbrace{2\omega \times \dot{r}_i}_{\text{Coriolis Acc.}} + \underbrace{\dot{\omega} \times r_i}_{\text{Euler Acc.}} + \underbrace{\omega \times (\omega \times r_i)}_{\text{Centrifugal Acc.}}$$

$$+ \frac{d^2}{dt^2} R \Big) = F_i, \qquad i = 1, 2, 3$$

Boundary Conditions

$$\delta \varphi'_\xi \cdot \left(EI_1 \, \varphi'_{\xi\xi} \right) \Big]_0^{l_1} - \delta \varphi' \cdot \left(EI_1 \, \varphi'_{\xi\xi} \right)_\xi \Big]_0^{l_1}$$

$$+ \delta \varphi^2_\xi \cdot \left(EI_2 \, \varphi^2_{\xi\xi} \right) \Big]_0^{l_1} - \delta \varphi^2 \cdot \left(EI_2 \, \varphi^2_{\xi\xi} \right)_\xi \Big]_0^{l_1}$$

$$+ \delta \varphi^3_\xi \cdot \left(EI_3 \, \varphi^3_{\xi\xi} \right) \Big]_{-\frac{l_2}{2}}^{\frac{l_2}{2}} - \delta \varphi^3 \cdot \left(EI_3 \, \varphi^3_{\xi\xi} \right)_\xi \Big]_{-\frac{l_2}{2}}^{\frac{l_2}{2}} = 0$$

Boundary Conditions

$$y_1(0,t) = z_1(0,t) = 0,$$
$$y_2(0,t) = z_2(0,t) = 0,$$
$$y_{1,\xi}(0,t) = z_{1,\xi}(0,t) = 0,$$
$$y_{2,\xi}(0,t) = z_{2,\xi}(0,t) = 0,$$

$$x_3(l_2/2, t) = x_3(-l_2/2, t) = 0,$$
$$z_1(l_1, t) = z_3(l_2/2, t),$$
$$z_2(l_1, t) = z_3(-l_2/2, t),$$
$$y_{1,\xi}(l_1,t) = -x_{3,\eta}(l_2/2, t),$$
$$y_{2,\xi}(l_1,t) = -x_{3,\eta}(-l_2/2, t),$$

$$EI_1 \, y_{1,\xi\xi}(l_1,t) = EI_3 \, x_{3,\eta\eta}(l_2/2, t),$$
$$EI_2 \, y_{2,\xi\xi}(l_1,t) = -EI_3 \, x_{3,\eta\eta}(-l_2/2, t),$$
$$EI_1 \, z_{1,\xi\xi\xi}(l_1,t) = -EI_3 \, z_{3,\eta\eta\eta}(l_2/2, t),$$
$$EI_2 \, z_{2,\xi\xi\xi}(l_1,t) = EI_3 \, z_{3,\eta\eta\eta}(-l_2/2, t),$$

$$EI_1 \, y_{1,\xi\xi\xi}(l_1,t) = EI_2 \, y_{2,\xi\xi\xi}(l_1,t) = 0,$$
$$EI_1 \, z_{1,\xi\xi}(l_1,t) = EI_2 \, z_{2,\xi\xi}(l_1,t) = 0,$$
$$EI_3 \, z_{3,\eta\eta}(l_2/2, t) = EI_3 \, z_{3,\eta\eta}(-l_2/2, t) = 0,$$

STABILIZATION

$$\dot{\psi} = \mathcal{A}\psi + F(\psi, \dot{\psi})$$

$$\psi(0) = \psi_0$$

where $\quad \psi = (R, \dot{R}, \omega, \varphi_i, \dot{\varphi}_i)'$

Suppose that the velocity feedback controls are applied and given by

$$\mathcal{F} = \left(-c_1\left[\tfrac{dR}{dt}\right]_i, \ -c_2\left[\tfrac{dR}{dt}\right]_j, \ -c_3\left[\tfrac{dR}{dt}\right]_k\right)', \qquad c_1, c_2, c_3 > 0$$

$$\tau = \left(-c_4\, \omega_1, \ -c_5\, \omega_2, \ -c_6\, \omega_3\right)', \qquad c_4, c_5, c_6 > 0$$

$$F_i = \left(-c_1(\xi)\left[\tfrac{\partial \varphi^i}{\partial t}\right]_1, \ -c_2(\xi)\left[\tfrac{\partial \varphi^i}{\partial t}\right]_2\right)', \qquad \begin{array}{l} i=1,2,3 \\ c_1, c_2 > 0 \end{array}$$

Then the system is stable.

ACTIVE VIBRATION MITIGATION OF DISTRIBUTED PARAMETER, SMART-TYPE STRUCTURES USING PSEUDO-FEEDBACK OPTIMAL CONTROL (PFOC)

By

W. N. Patten, H. H. Robertshaw, D. Pierpont, R. H. Wynn
Virginia Polytechnic Institute and State University
Blacksburg, Virginia

ABSTRACT

A new, near-optimal feedback control technique is introduced that is shown to provide excellent vibration attenuation for those distributed parameter systems that are often encountered in the areas of aeroservoelasticity and large space systems. The technique relies on a novel solution methodology for the classical optimal control problem. Specifically, the quadratic regulator control problem for a flexible vibrating structure is first cast in a weak functional form that admits an approximate solution. The necessary conditions (first-order) are then solved via a time finite-element method. The procedure produces a low dimensional, algebraic parameterization of the optimal control problem that provides a rigorous basis for a discrete controller with a first-order "like" hold output.

Simulation has shown that the algorithm can successfully control a wide variety of plant forms including multi-input/multi-output systems and systems exhibiting significant nonlinearities. In order to firmly establish the efficacy of the algorithm, a laboratory control experiment was implemented to provide planar (bending) vibration attenuation of a highly flexible beam (with a first clamped-free mode of approximately 0.5 Hz). Base actuation for the cantilever was accomplished using a three degree-of-freedom active bay (variable geometry truss) actuator. On-line processing was accomplished with a 14 mhz "AT" type microcomputer with data acquisition capability. The results of the tests corroborate the utility of the method.

957

ACTIVE VIBRATION MITIGATION OF

DISTRIBUTED PARAMETER SYSTEMS

USING

PSEUDO-FEEDBACK OPTIMAL CONTROL

W. PATTEN -- U. IOWA

&

H. ROBERTSHAW, D. PIERPONT, R. WYNN

SMART STRUCTURES LAB, MECH. ENGR. DEPT.

VA TECH

858

ORGANIZATION OF PAPER

- OVERVIEW OF METHOD (PFCA)

- EXPERIMENTAL RESULTS

- DISCUSSION

VARIATIONAL FORMULATION

OPTIMAL CONTROL PROBLEM

$$\text{Min } J_0 [\bar{u}] \equiv C(\bar{x}(T)) + \int_T g(\bar{x}, \bar{u}, t) \, dt$$

$$\dot{\bar{x}} = \bar{f}(\bar{x}, \bar{u}, t) + \bar{\bar{B}}(\bar{x}, t) \bar{u} \qquad \bar{x}(O) = \bar{x}_0$$

$$H = g + \langle \bar{\gamma}, (\bar{f} + \bar{\bar{B}} \bar{u}) \rangle$$

$$J_1 [\bar{u}] = \int_T \{ H - \langle \bar{\gamma}, \dot{\bar{x}} \rangle \} \, dt$$

NECESSARY CONDITIONS

$$0 = \int_{\Upsilon} \{ \langle \bar{e}_1, \delta \bar{x} \rangle + \langle \bar{e}_2, \delta \bar{y} \rangle + \langle \bar{e}_3, \delta \bar{u} \rangle \} \, dt$$

$$0 = \langle (c_{,\bar{x}} - \bar{y}), \delta \bar{x} \rangle \Big|_T$$

$$\bar{0} = \bar{e}_1 = \bar{H}_{,x} + \bar{y}$$

$$\bar{0} = \bar{e}_3 = \bar{H}_{,u}$$

$$\bar{0} = \bar{e}_2 = \bar{H}_{,y} - \bar{x}$$

CLASSICAL SOLUTION TECHNIQUES

- LINEAR SYSTEMS

    CLOSED FORM SOLUTIONS

    RICCATI METHODS

- NONLINEAR SYSTEMS

    GRADIENT METHODS

    SHOOTING METHODS

    QUASILINEARIZATION

WEAK (VARIATIONAL) FORMULATION

WHY?

- TECHNIQUE FAMILIAR TO COMMUNITY

- EASE OF IMPLEMENTATION

    USING FINITE ELEMENT PARADIGMS AND CODES

- PROVIDES AUTOMATED BASIS FOR FEEDBACK CONTROL LAWS

    FOR LINEAR AND NONLINEAR SYSTEMS

963

WHAT IS

PSEUDO

FEEDBACK CONTROL

964

- DRIVER -IN-THE-LOOP CONTROL

  (OHIO STATE --LATE 60'S)

OVERVIEW OF ANALYTICAL DEVELOPMENT

TWO-POINT BOUNDARY VALUE PROBLEM

WEAK FORM OF NECESSARY CONDITIONS

$$\bar{u} = -\bar{\bar{R}}^{-} \cdot \bar{\bar{B}}^{t} \cdot \bar{\gamma}$$

$$0 = \int_{\Upsilon} \cdot \langle \bar{e}_1, \delta \bar{x} \rangle \, dt \qquad\qquad 0 = \int_{\Upsilon} \langle \bar{e}_2, \delta \bar{\gamma} \rangle \, dt$$

DISCRETIZE DOMAIN OF OPERATOR (TIME)

KNOTS

DEPENDENT VECTOR

TIME

996
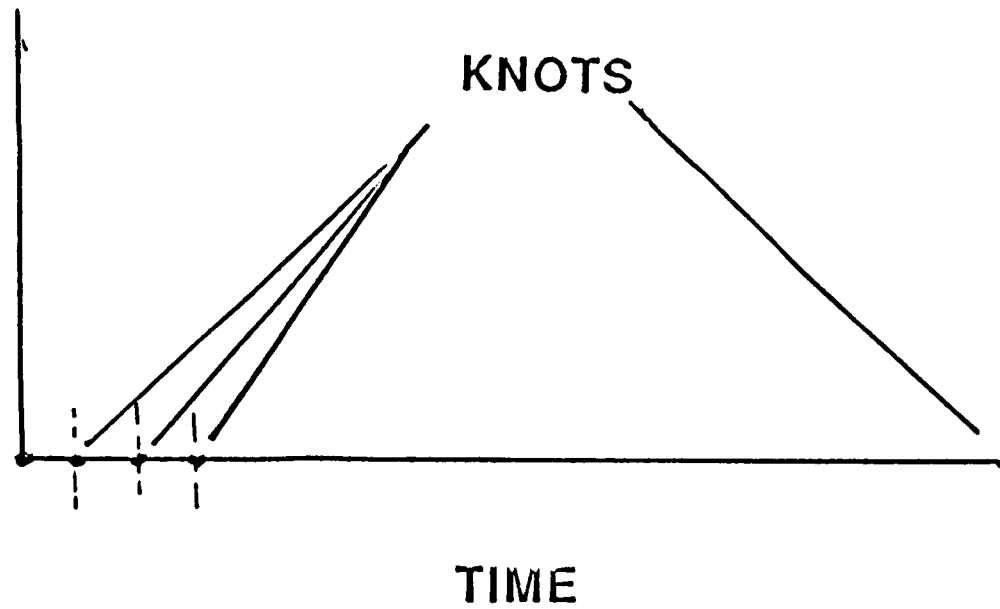
SLIDING INTERVAL CONTROL

CONSTRUCT INTERPOLENTS TO APPROXIMATE

STATE, COSTATE AND CONTROL VECTORS

ON EACH OF THE SUBDOMAINS

$$|| \bar{z} ||_{W_2^1}^2 \equiv \int_{\Upsilon} [\dot{\bar{z}}^t \cdot \dot{\bar{z}} + \bar{z}^t \cdot \bar{z}] \, dt$$

$$\bar{x} \stackrel{\sim}{=} \sum_{e=1}^{n} \bar{x}^e = \sum_{e=1}^{n} \bar{\bar{N}}^e \cdot \bar{q}^e = \sum_{e=1}^{n} \bar{\bar{N}}^e \cdot \bar{\bar{T}}^e \cdot \mathcal{E}_{\bar{q}}$$

$$\bar{\gamma} \stackrel{\sim}{=} \sum_{e=1}^{n} \bar{\gamma}^e = \sum_{e=1}^{n} \bar{\bar{N}}^e \cdot \bar{p}^e = \sum_{e=1}^{n} \bar{\bar{N}}^e \cdot \bar{\bar{T}}^e \cdot \mathcal{E}_{\bar{p}}$$

EXAMPLE

LINEAR SECOND ORDER OSCILLATOR (UNDAMPED)

--------Analytical Solution
————Applied Control
●-----Update

b

--------Analytical Solution
————Actual Response
●----Update

a

968
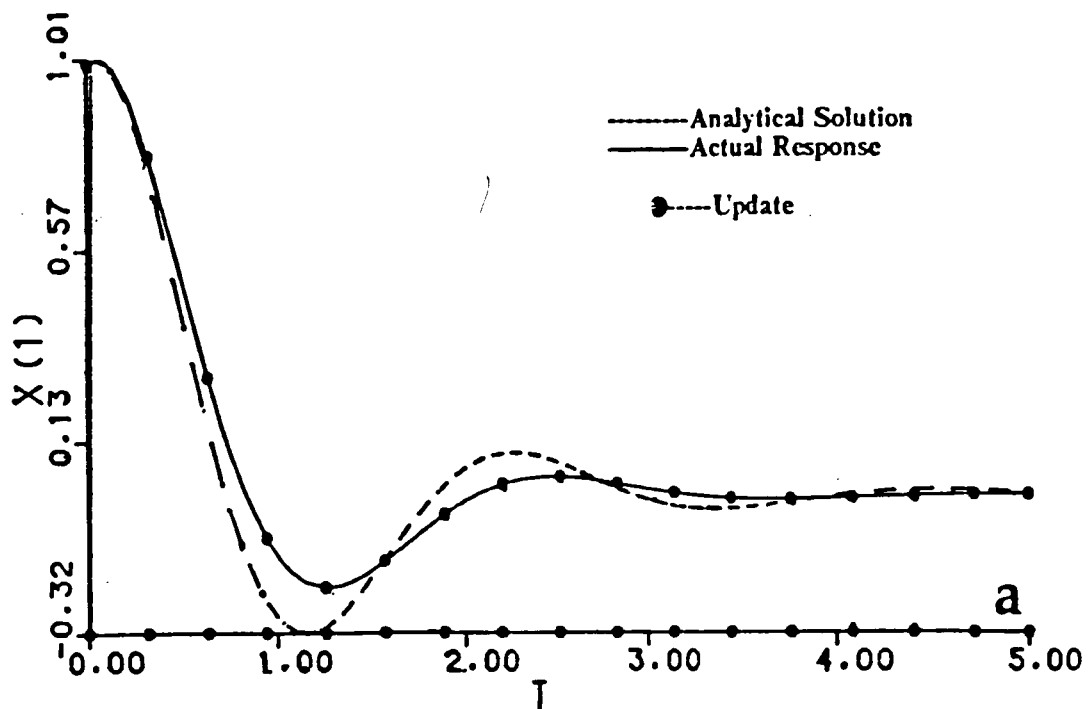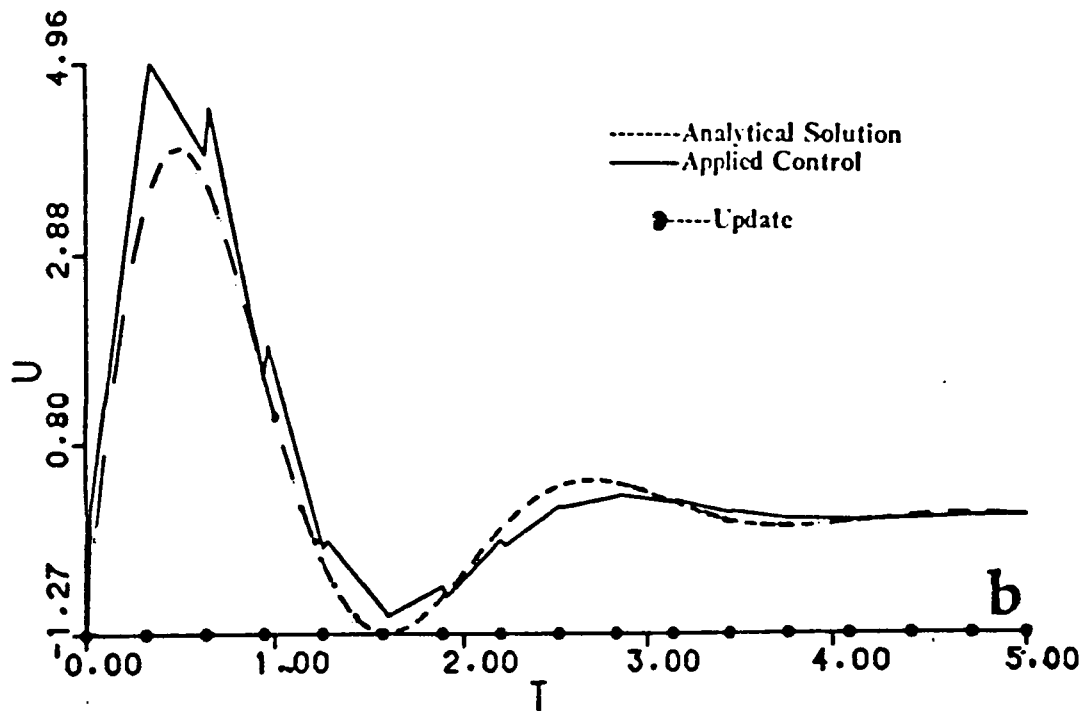
EXAMPLE

NONLINEAR SECOND ORDER MODEL OF

WINGROCK EXHIBITED BY

FREE-TO-ROLL MODEL OF

X-29

EQUATION OF MOTION

$$\ddot{\phi} + \omega^2 \phi = \mu_1 \dot{\phi} + b_1 \phi^3 + \mu_2 \phi^2 \dot{\phi} + b_2 \phi \dot{\phi}^2$$

where

$$\omega^2 = - c_1 a_1$$

$$\mu_1 = c_1 a_2 - c_2$$

$$b_1 = c_1 a_3$$

$$\mu_2 = c_1 a_4$$

$$b_2 = c_1 a_5$$

c_1 - CONSTANT
c_2 - CONSTANT
$a_i - f(\alpha) \qquad i = 1, 5$

CONTROL-U .VS. TIME

Figure 6
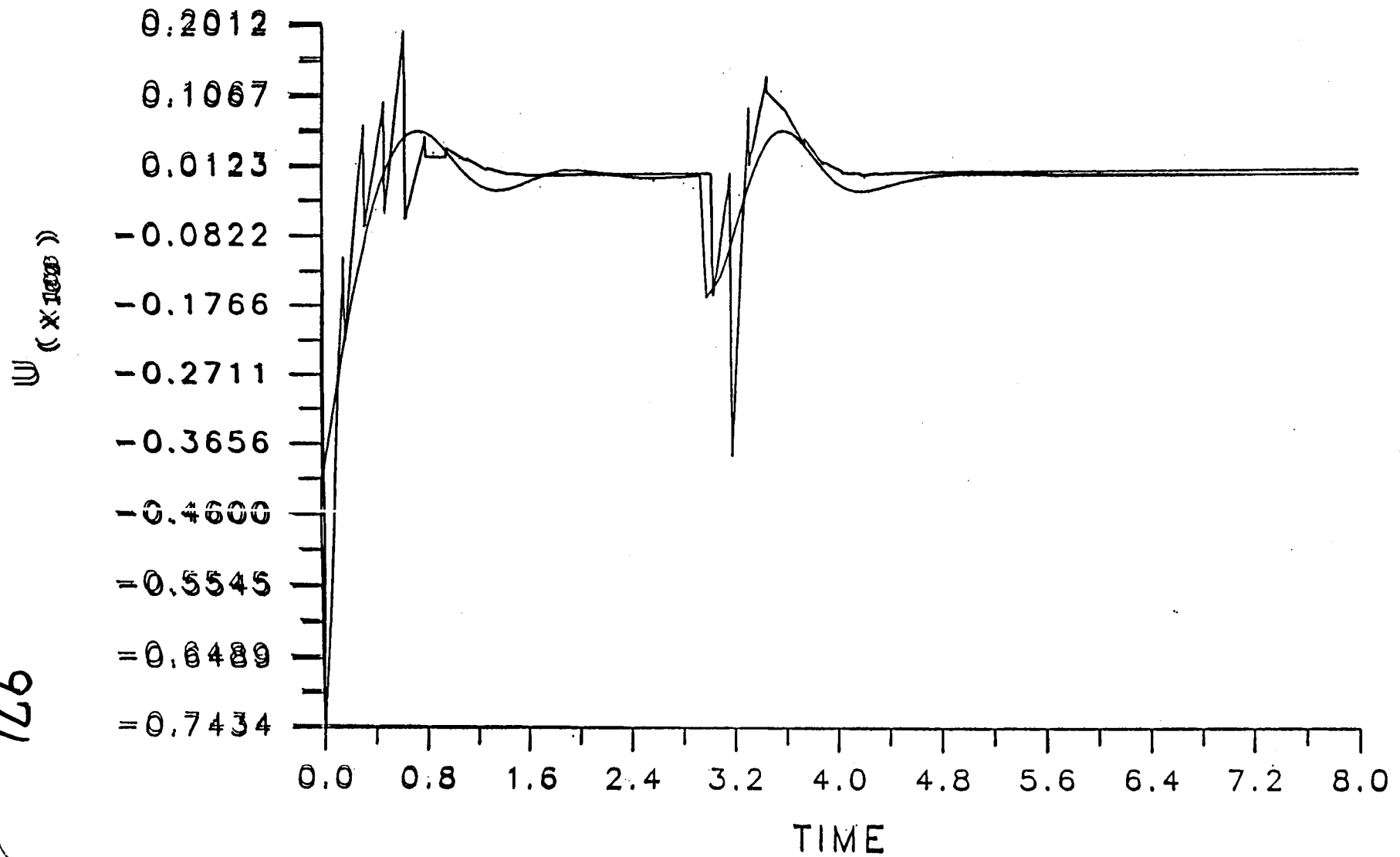
EXPERIMENTAL VALIDATION

OF ALGORITHIM

THE CONTROL OF

A FLEXIBLE BEAM USING

A PLANAR TRUSS ACTUATOR

PLANAR ACTUATOR

MOTOR

VARIABLE LINK LENGTHS

BEAM

$\lambda_0 = .6$ Hz.

$L = 40''$

PROCEDURE

$$\dot{X} = AX + BU$$

$$X = [\text{LINK STATES, BEAM STATES}]$$

APPLY FEM APPROXIMATION

ALGEBRAIC EVOLUTION OPERATOR

$$Z = K Z_0$$

$$Z = [\text{ STATE VECTORS, COSTATE VECTORS}]$$

974

40"

$\lambda_o \simeq .6\, Hz$

$\zeta_o \simeq .02$

$\delta(F_d)$

4"

UNCONTROLLED

1 SEC.

975

CONTROLLED

$\delta(T_o)$
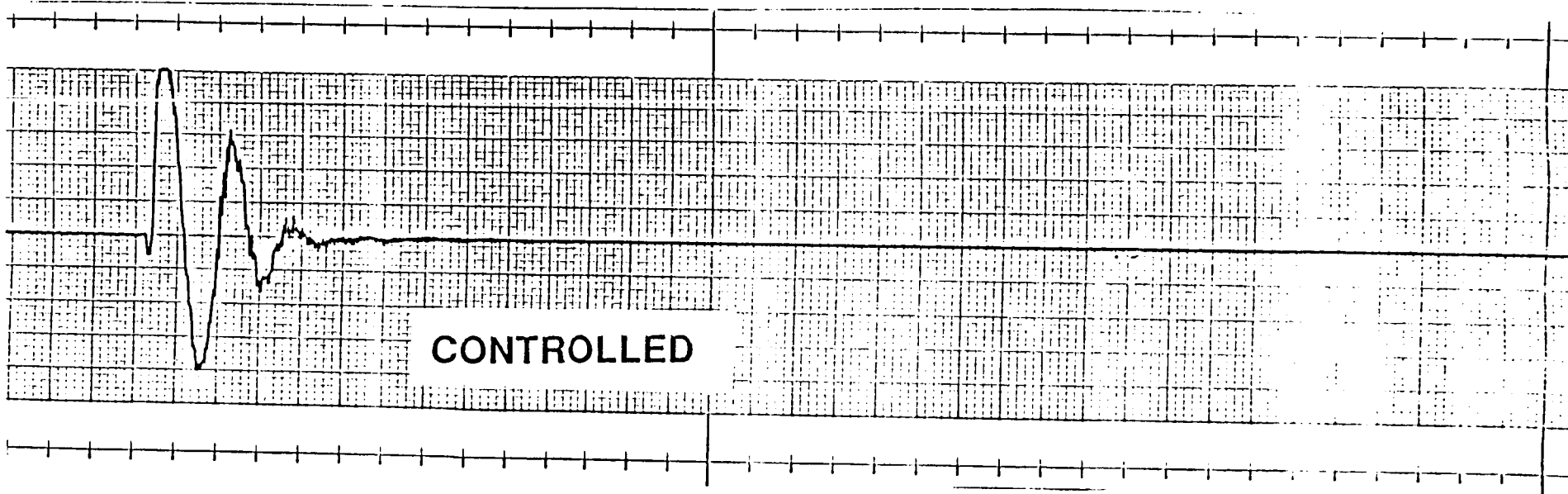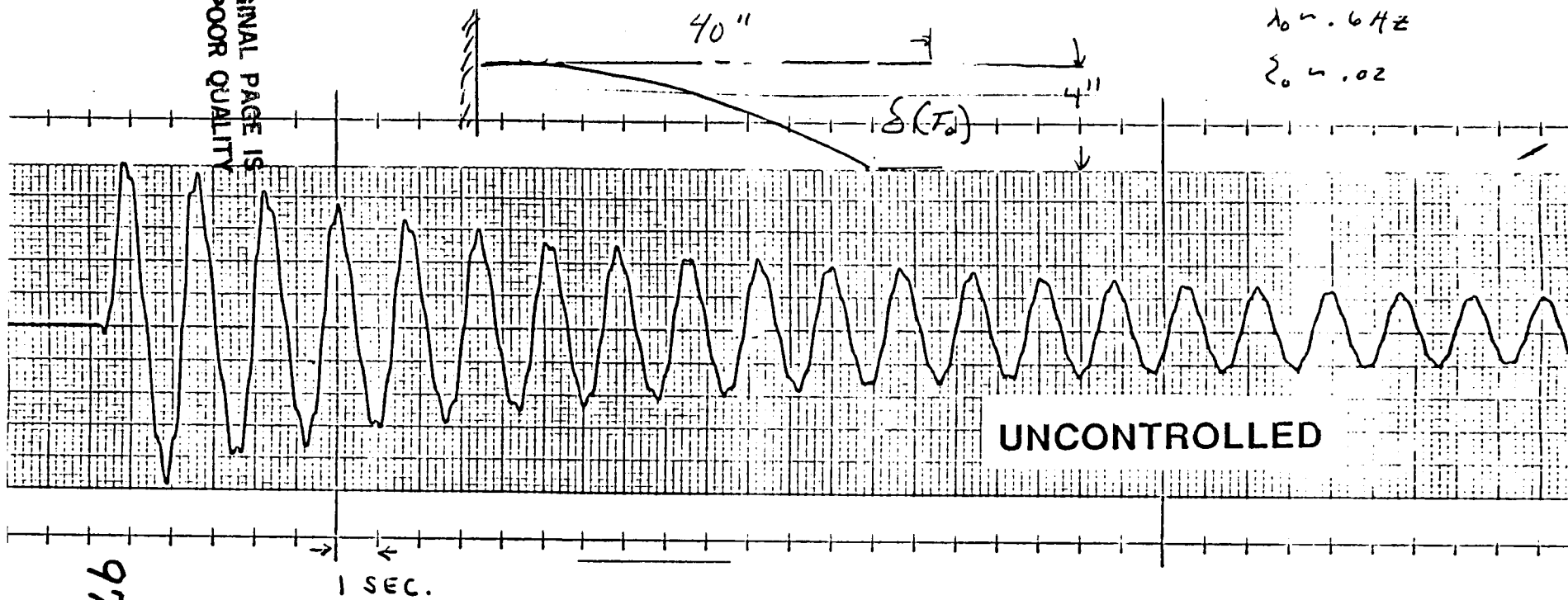
"SECOND MODE LIKE INITIAL CONDITION"

UNCONTROLLED

976

1 SEC.

CONTROLLED

IMPULSE RESPONSE

UNCONTROLLED

1 SEC.

CONTROLLED
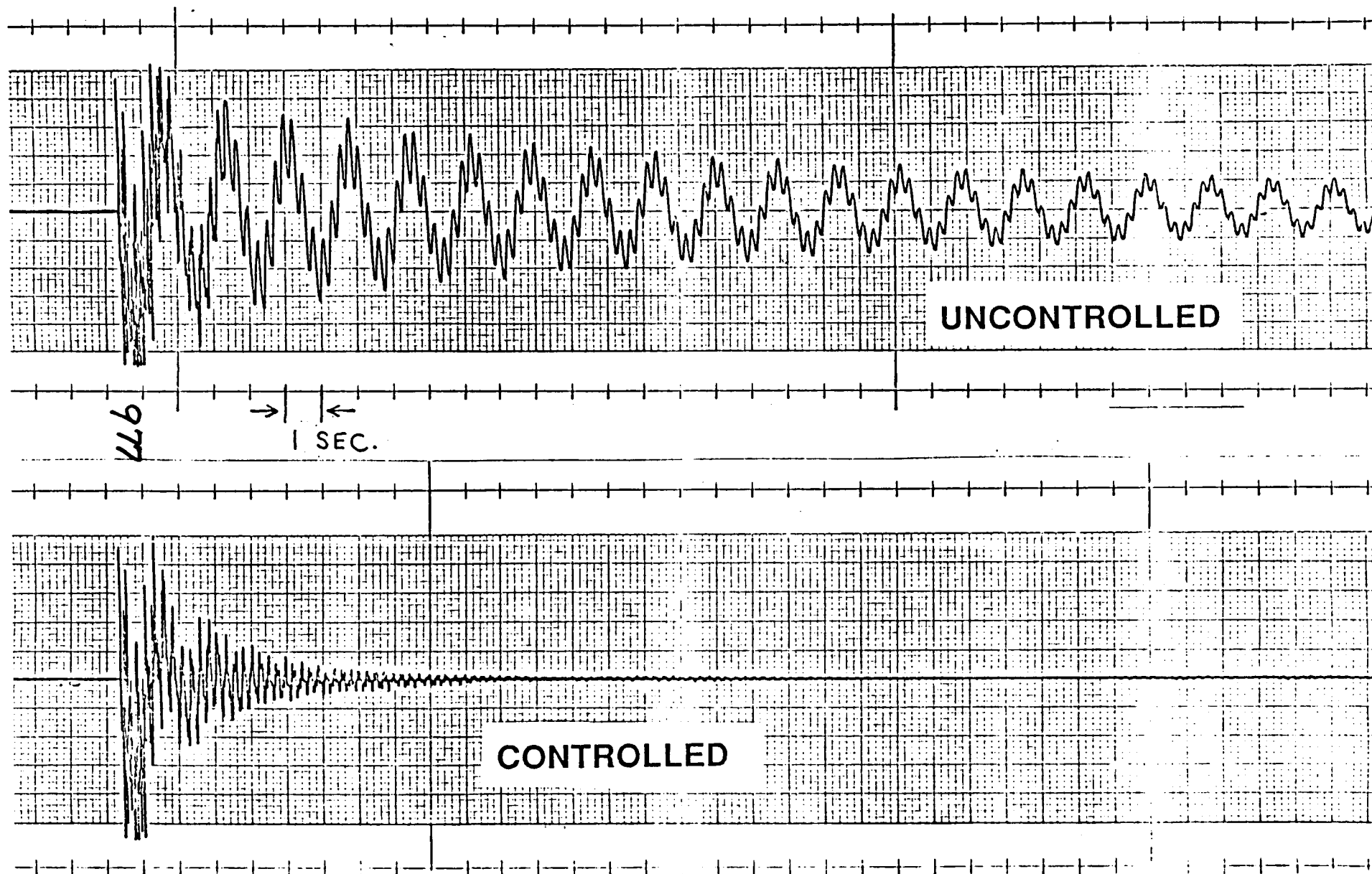
MOTOR # 3

ACCUCHART™   Gould Inc.

Cleveland, Ohio   Printed in U.S.A.

MOTOR # 2

MOTOR # 1

978

ROOT STRAIN
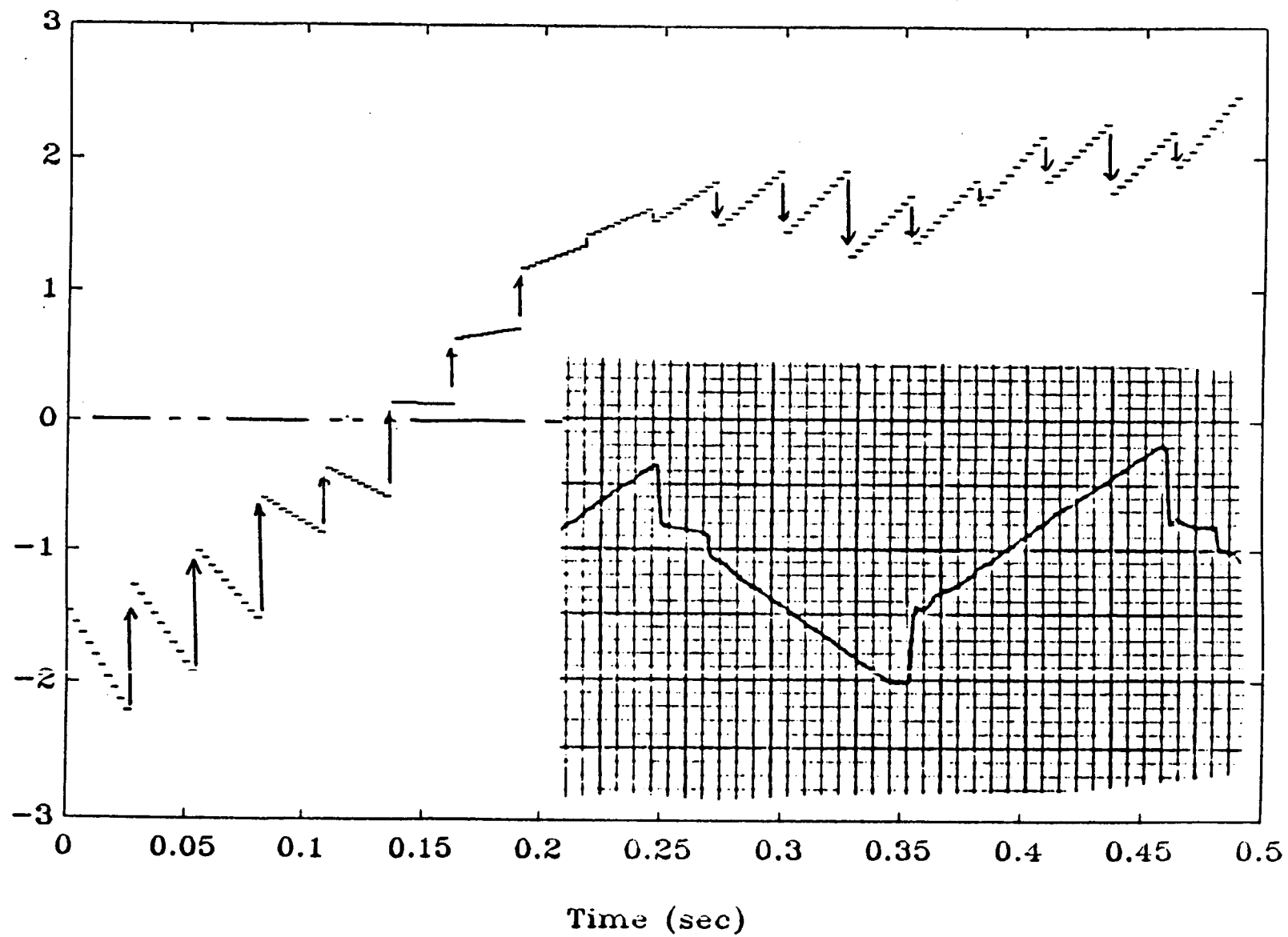
CONCLUSIONS

- ALGORITHIM VALIDATED

- REAL TIME IMPLEMENTATION POSSIBLE
  ON LOW-LEVEL PC ARCHITECTURE
  (80286 WITH 27.5 KHZ D/A)

ACKNOWLEDGEMENTS:

186

SHAPE CONTROL OF HIGH DEGREE-OF-FREEDOM VARIABLE GEOMETRY TRUSSES

By

R. J. Salerno, C. F. Reinholtz, and H. H. Robertshaw
Virginia Polytechnic Institute and State University
Blacksburg, Virginia

ABSTRACT

Common static trusses are constrained to permit no relative motion between truss elements. A Variable Geometry Truss (VGT), however, is a truss which contains some number of variable length links. The extensible links allow the truss to change shape in a precise, controllable manner. These changes can also be used to control the vibrational response of a truss structure or to perform robotic tasks.

Many geometric configurations, both planar and spatial, are possible candidates for VGT manipulators. For this presentation only two geometries will be discussed; the three degree-of-freedom (DOF) spatial octahedral/octahedral truss and the three DOF planar tetrahedral truss. These truss geometries are used as the fundamental element in a repeating chain of trusses. This results in a highly dexterous manipulator with perhaps 30 to 60 degrees of freedom that retains the favorable stiffness properties of a conventional truss. From a fixed base, this type of manipulator could perform shape or vibration control while extending and "snaking" through complex passageways or moving around obstacles to perform robotic tasks.

In order for this new technology to be useful in terms of robotic applications the forward and inverse kinematic solutions must be efficiently solved. The approach taken here is to first concentrate on fully understanding the forward and inverse kinematics of the fundamental elements and then utilizing the insight thus gained to solve the more complex problem of the kinematic chains. The inverse solution of a 30 DOF planar manipulator will be discussed. The discussion will focus on how to specify parameters for an underspecified system by using shape control algorithms.

Shape Control of High Degree-of-Freedom Variable Geometry Trusses

Robert J. Salerno

Babu Padmanabhan

Charles F. Reinholtz

Harry H. Robertshaw

984

Variable Geometry Trusses

Definition

In simple terms a VGT is a statically determinant truss which contains some number of variable length members.

Variable Geometry Trusses

Characteristics

- Composed entirely of
      two force members
  (pure tension/compression)

- Excellent stiffness to
      weight ratio

- Number of DOF is equal
      to the number of
      extensible links

Two Candidate Geometries

Planar(2-D)
Tetrahedral Truss
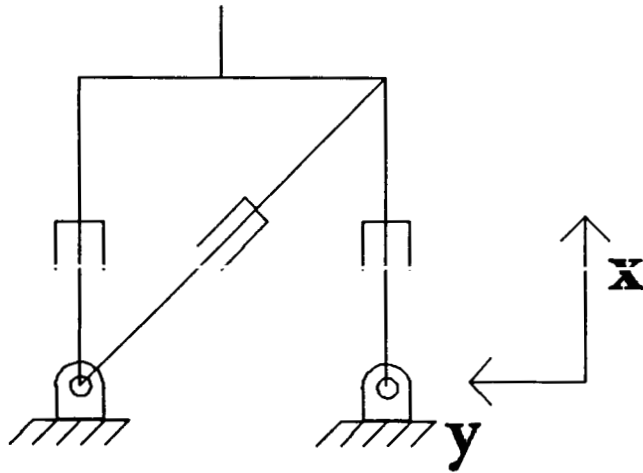
Spatial(3-D)
Octahedral truss
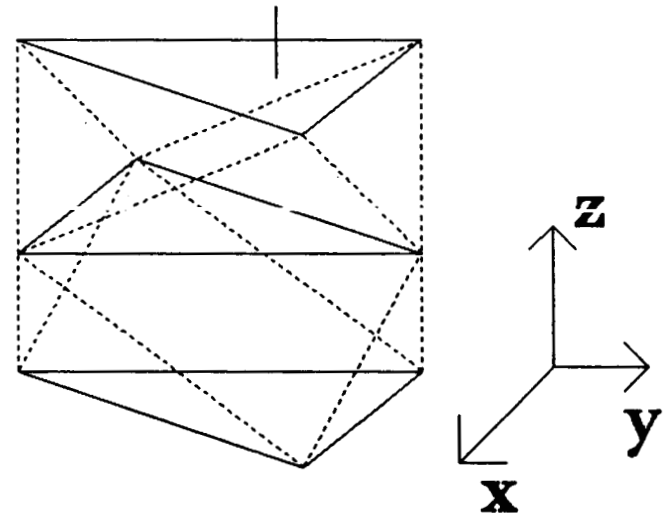
Kinematics

The study of constrained motion of interconnected rigid links.

"Motion" includes position, velocity, acceleration and all higher derivatives.

Planar VGT Manipulator
Kinematics

Forward Kinematics
Given: L_1, L_2, L_3
Find : X, Y, Theta

Inverse Kinematics
Given: X, Y, Theta
Find : L_1, L_2, L_3
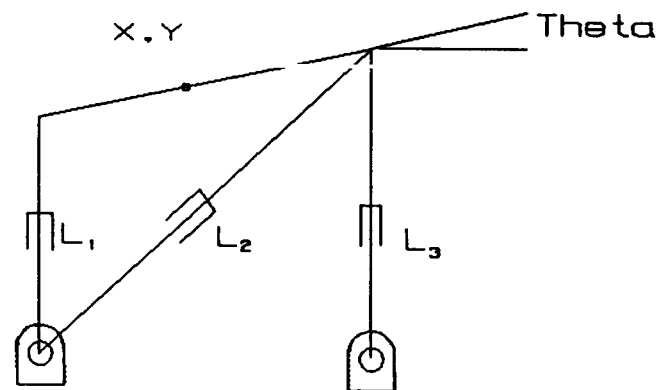
Chaining n-Bays of Planar VGT's Together

- Extended range
- More degrees-of-freedom
            (Dexterity)

- Must specify 3n parameters
            (27 Free choices)
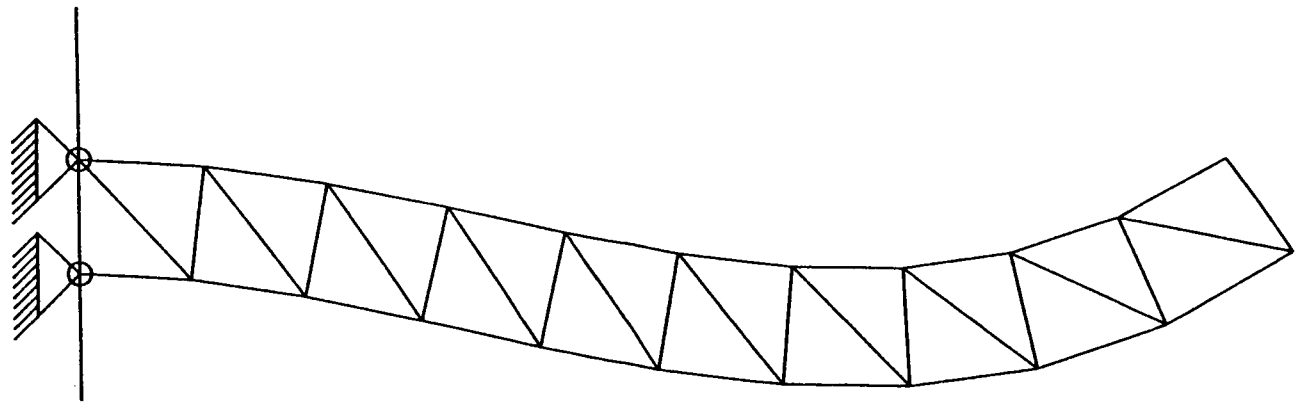
The Position Control Problem
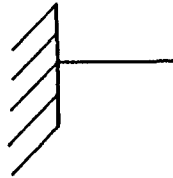
(X, Y, THETA)

How to specify 3(n-1) free choices?

Curve Fitting Approach

Goal

- To specify some minimum number of parameters which determines the truss shape

Input only the three end parameters, X, Y, and Theta, and have an algorithm which assigns the other 27 variables in some systematic manner.

The Position Control Problem

$$F(X) = A_0 + A_1 X + A_2 X^2 + A_3 X^3$$

(XF, YF)

(XO, YO)

How to specify $3(n-1)$ free choices?

Curve Specification by Boundary Conditions

$$f(x_0) = a_0 + a_1 x_0 + a_2 x_0^2 + a_3 x_0^3$$

$$f'(x_0) = a_1 + 2a_2 x_0 + 3a_3 x_0^2$$

$$f(x_f) = a_0 + a_1 x_f + a_2 x_f^2 + a_3 x_f^3$$

$$f'(x_f) = a_1 + 2a_2 x_f + 3a_3 x_f^2$$

Curve Partitioning
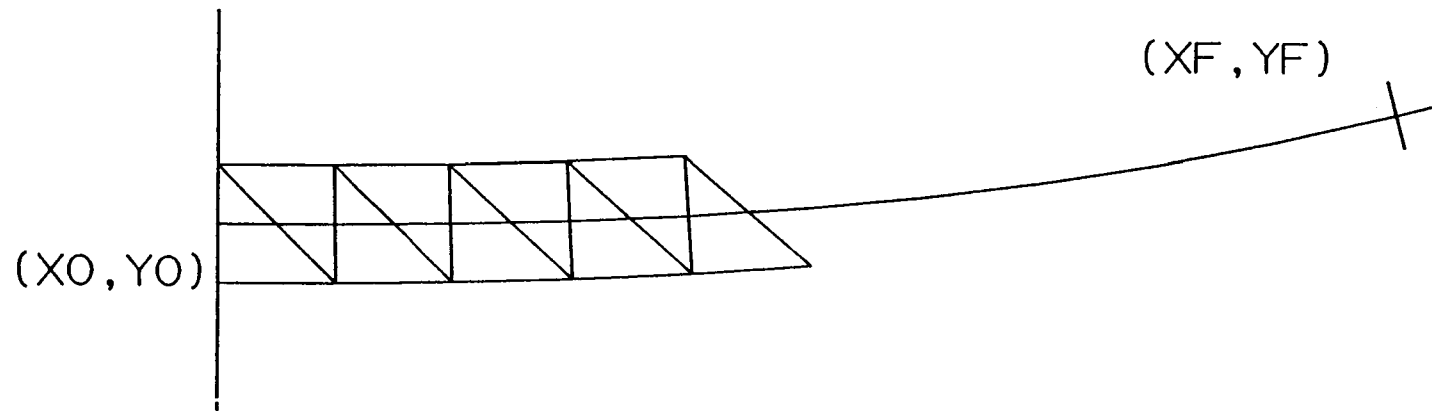
- Regular X spacing
- Regular arc length spacing
- Adaptable spacing

Results
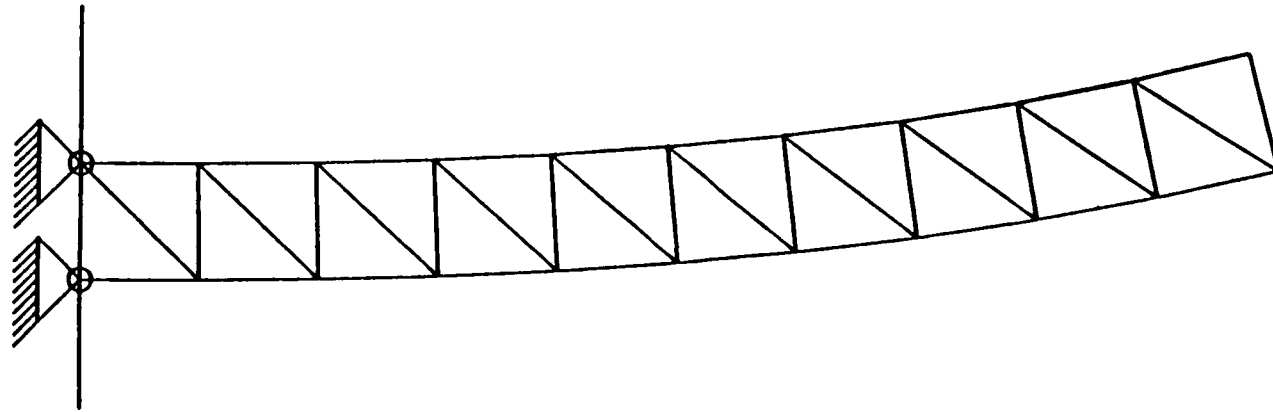
966

- Closed form solution
- Minimum input specification
- Parallel processing potential

Intermediate Shape Control

Specifying an alternative path while still minimizing input requirements.
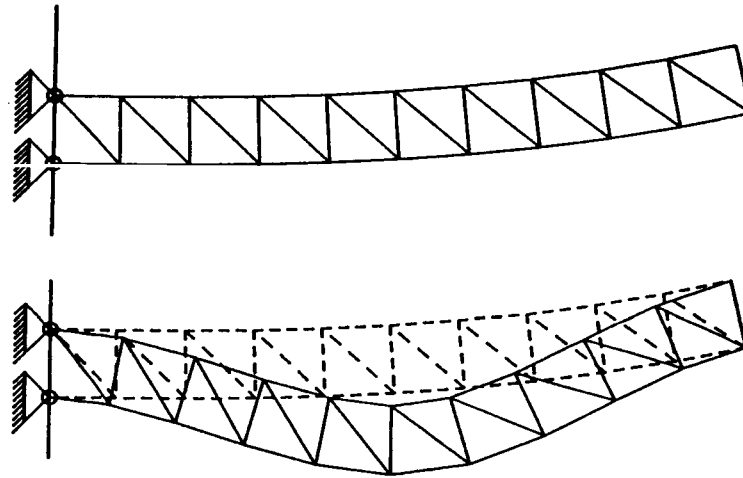
Spatial Octahedral Truss
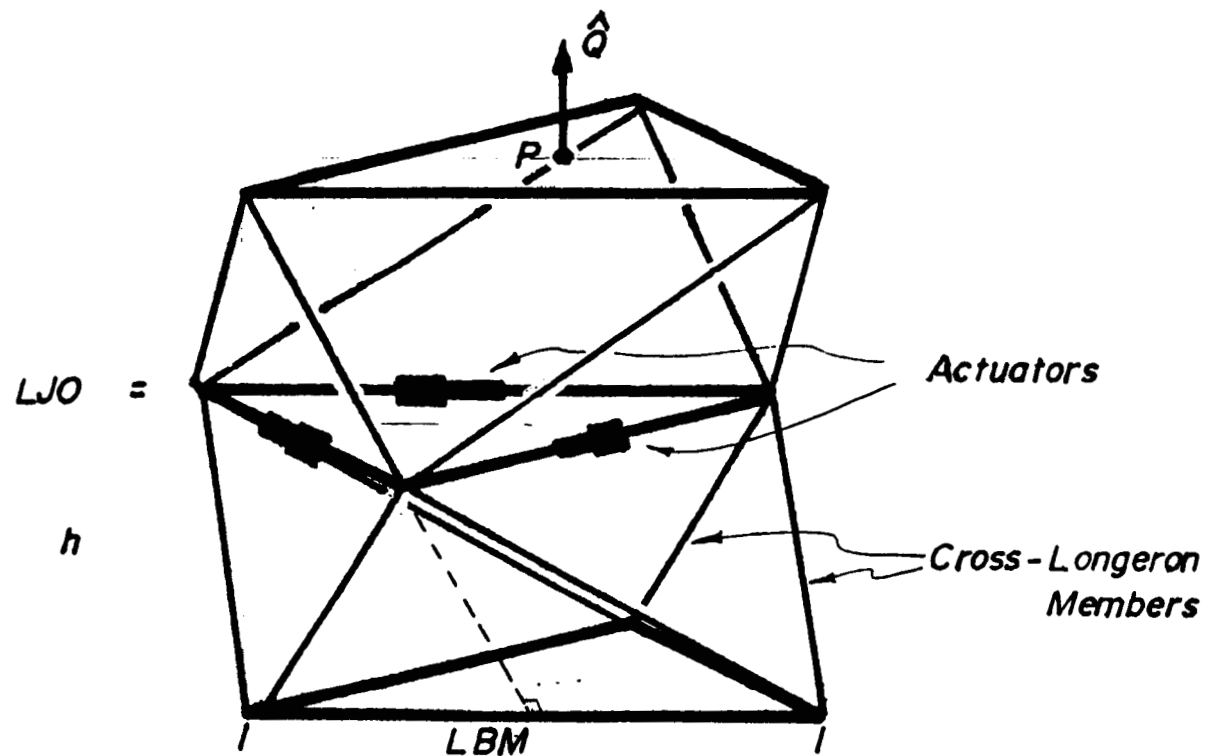
Spatial Truss Forward Kinematics

Employ the concept of kinematically equivalent devices

SPHERIC
JOINT

REVOLUTE
JOINT
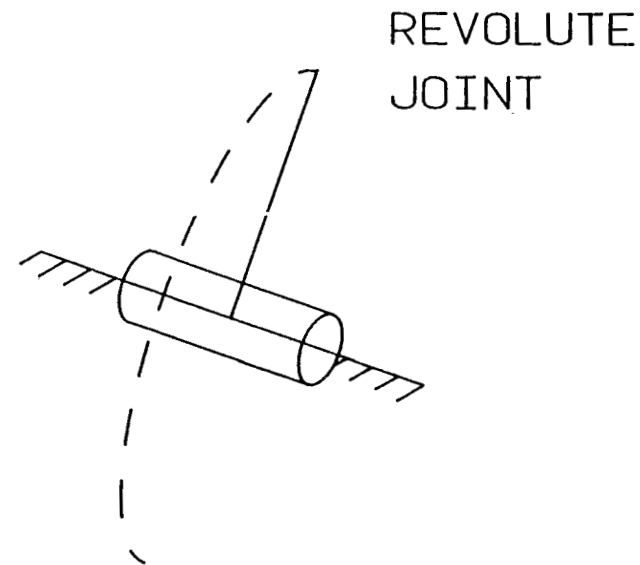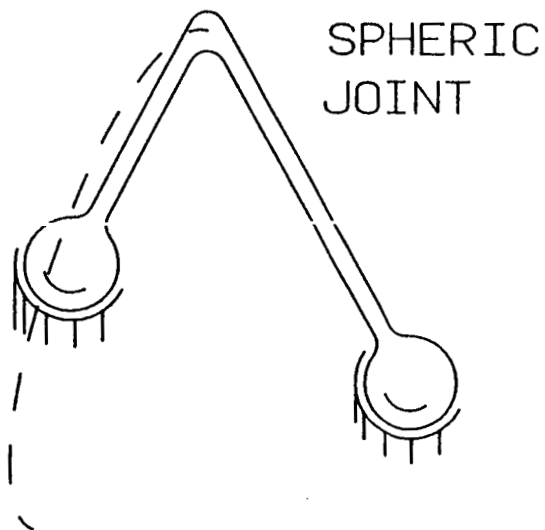
Lower Half of Spatial VGT
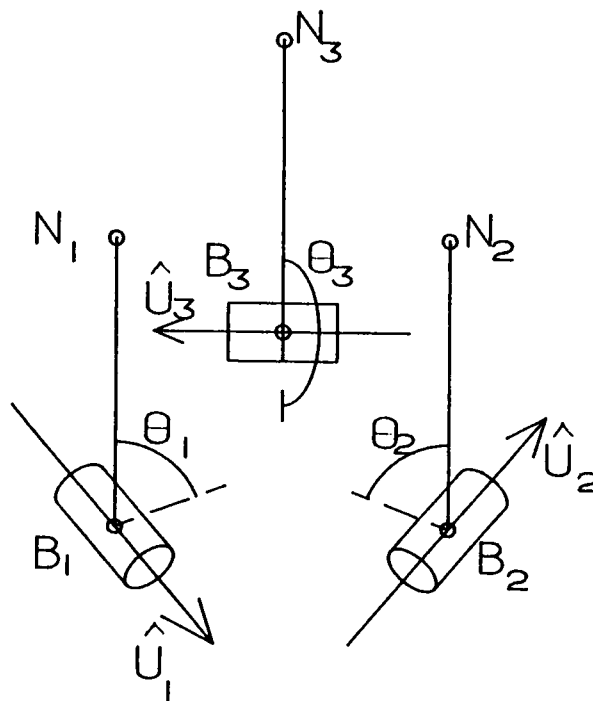
$$\underline{N}_I = \underline{B}_I + (R\theta_I, \hat{\underline{U}}_I)H_I$$

Constraint Equations

$$L_1 = \overline{n_1 n_2} = f(\theta_1, \theta_2)$$

$$L_2 = \overline{n_2 n_3} = f(\theta_2, \theta_3)$$

$$L_3 = \overline{n_3 n_1} = f(\theta_3, \theta_1)$$

$$0 = L - \sqrt{A\cos\theta_1 + A\cos\theta_2 + B\cos\theta_1 \cos\theta_2 - B\sin\theta_1 \sin\theta_2 + C}$$

Continuing Research
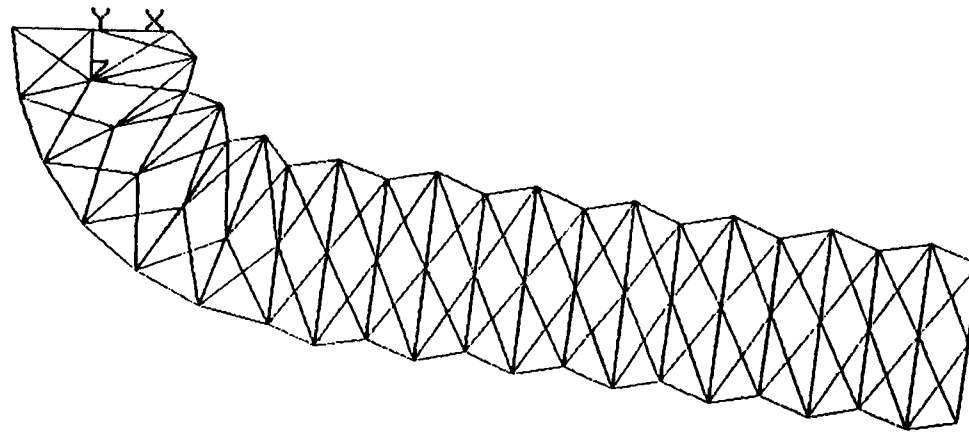
OPTIMAL INTEGRAL CONTROLLER WITH SENSOR FAILURE ACCOMMODATION

By

Dr. T. Alberts
Old Dominion University
Norfolk, Virginia

and

Dr. T. Houlihan
The Jonathan Corporation
Norfolk, Virginia

ABSTRACT

An Optimal Integral Controller that readily accommodates Ser.sor Failure - without resorting to (Kalman) filter or observer generation - has been designed. The system is based on Navy-sponsored research for the control of high performance aircraft.

In conjunction with a NASA developed Numerical Optimization Code, the Integral Feedback Controller will provide optimal system response even in the case of incomplete state feedback. Hence, the need for costly replication of plant sensors is avoided since failure accommodation is effected by system sof.ware reconfiguration.

The control design has been applied to a particularly ill-behaved, third-order system. Dominant-root design in the classical sense produced an almost 100 percent overshoot for the third-order system response. An application of the nevrly-developed Optimal Integral Controller--assuming all state information available--produces a response with NO overshoot. A further application of the controller design--assuming a one-third sensor failure scenario--produced a slight overshoot response that still preserved the steady state time-point of the full-state feedback response.

The control design should have wide application in space systems. The design can be expanded to include gain scheduling that enhances system response to large-scale transients. For this latter instance, using the NASA optimization scheme, the guesswork normally required to determine feedback gains for large transients is eliminated.

Optimal Integral Control

With

Sensor Failure Accommodations

Dr. Thomas Alberts

Old Dominion University

Norfolk, Virginia

Dr. Thomas Houlihan

The Jonathan Corporation

Norfolk, Virginia

1005

Optimal Integral

Control Design

Introduction

Optimal Regulator

Augmented System

(Rates of Change of Input Signals)

Optimal Tracker

Optimal Integral

Control Design

Sensor Failure

Accommodation

Preliminary Results:

Third Order System

1006

Introduction

Optimal Control Designs Compromised By:

Inaccessible States (Sensors)

Noisy Feed back Signals

OC Designs Resort To Use Of

Filter / Estimating Techniques

To Overcome These Obstacles

NAVY Research in 1970s

Leads to Alternative Approach

1007

Optimal Regulator - Classic Design

Tradeoffs Between Accuracy of Control

And Energy Expenditure Reflected

In Weighting Matrices (**Q** and **R**)

Of Performance Index (**J**)

$$J = \int (X^TQX + U^TRU)\, dt$$

Performance Index Formulation

Assumes Unconstrained Inputs.

In Reality, Inputs are Limited.

Futhermore, Rates of Change of

Input Signals Are Limited.

1008
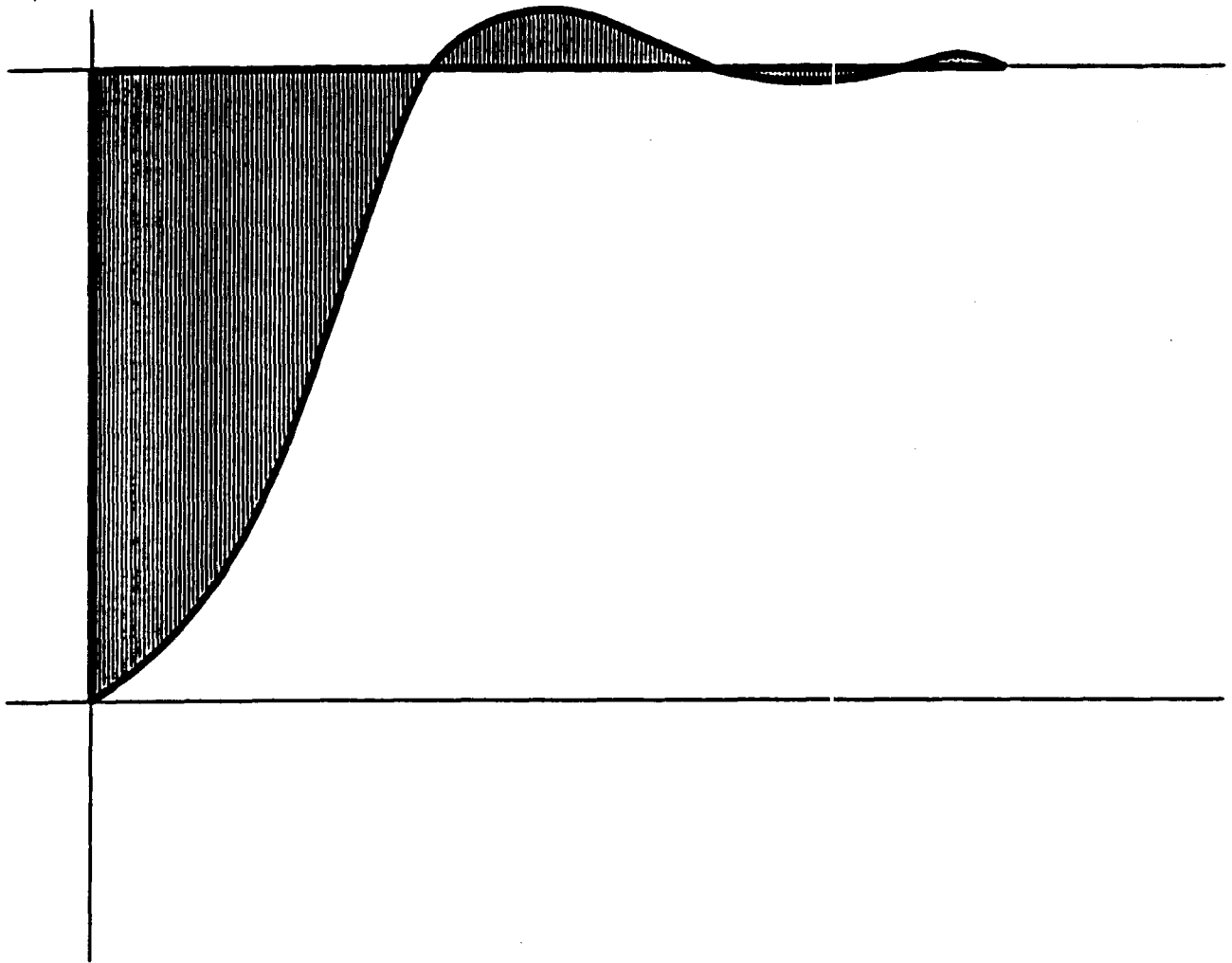
Figure 1.   Typical System Response.

1009
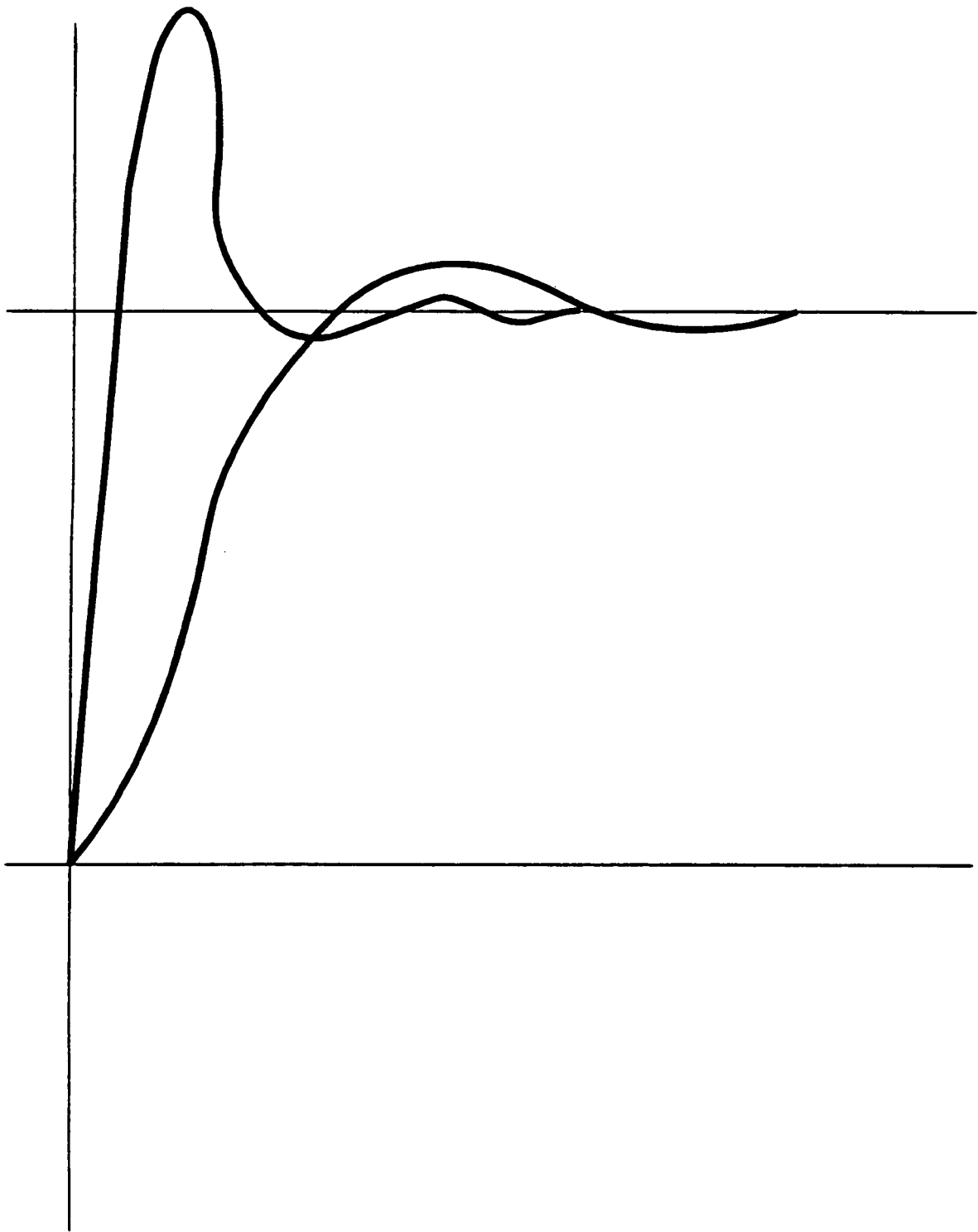
Figure 2.   Comparative Optimal Responses.

1010
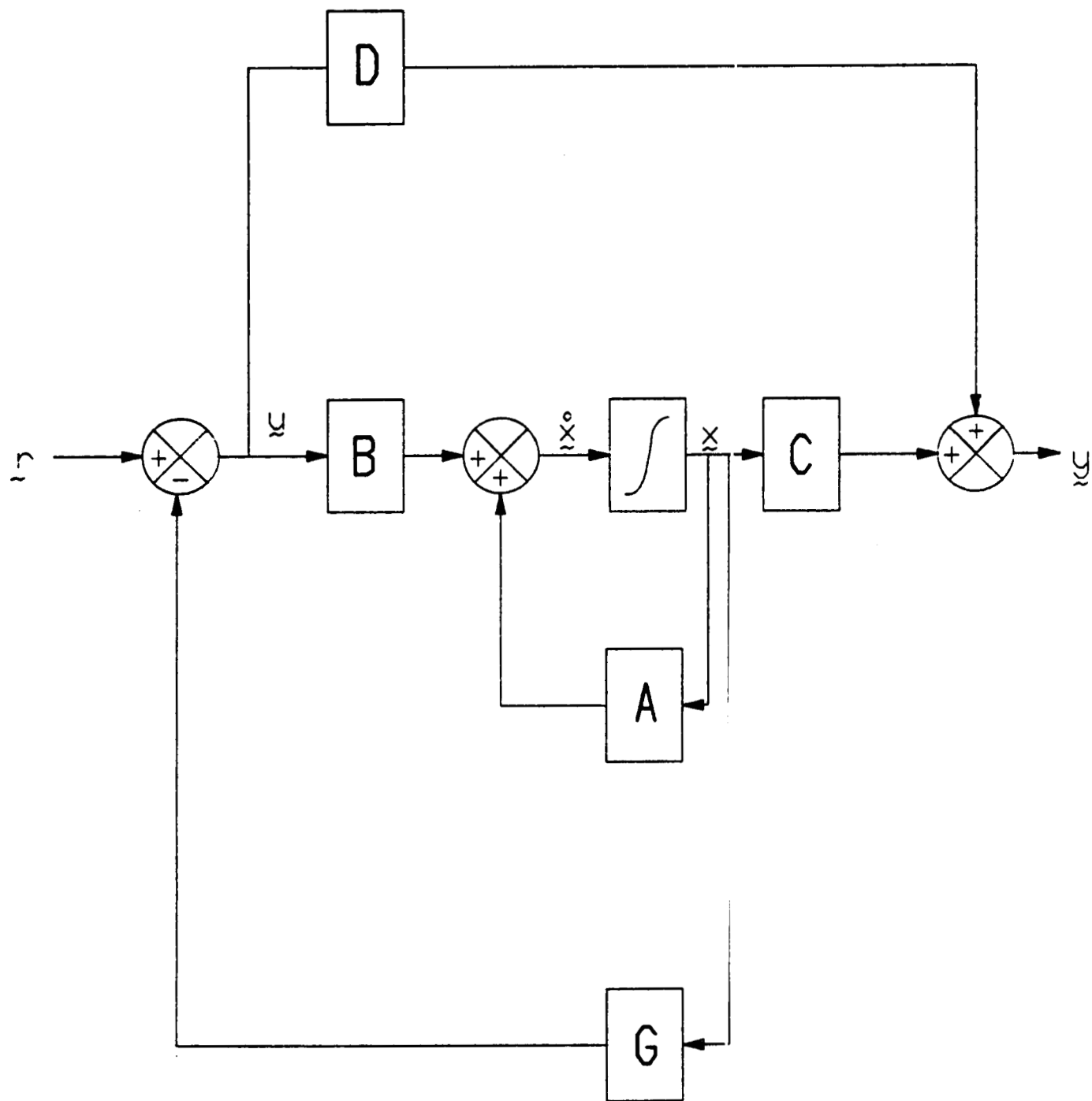
FIGURE 3. OPTIMAL REGULATOR SYSTEM

IDII

Augmented System:

Rates of Change of Input Signals

Can be Considered

New State Vector = Old State Vector
+
Input Signals

Optimal Regulator Solution of

Agumented System:

$$U^* = -G^*X^* \qquad G^* = |G_1\ G_2|$$

Gain Matrix (G*) of Augmented

System Carries Information on System

States (X) and Inputs (U)!

1012
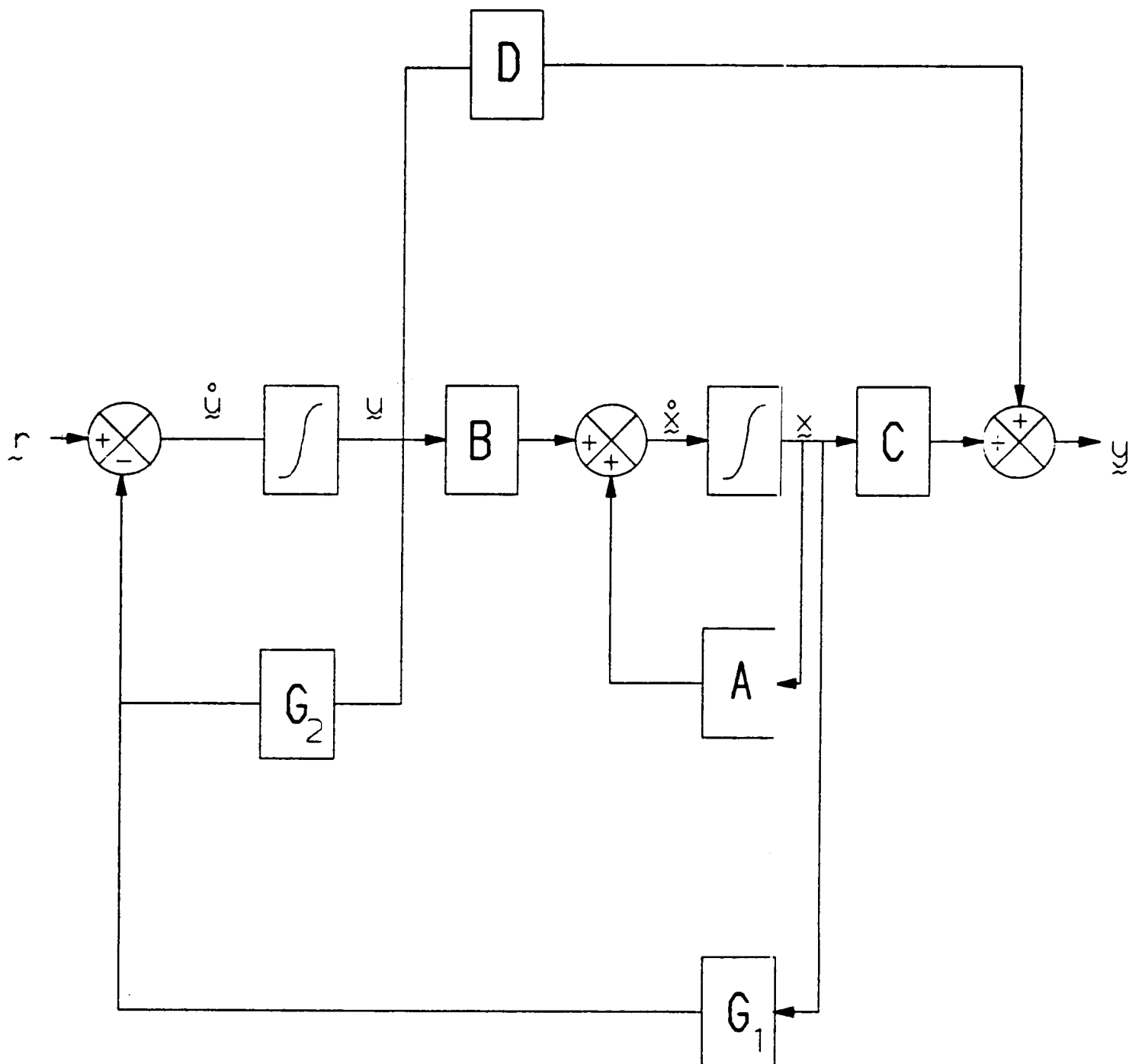
FIGURE 4. OPTIMAL REGULATOR-AUGMENTED SYSTEM

1013

Optimal Tracker:

Add Gain Matrix (M) to

Select Command Inputs

NOTE: Tracker is NOT Integral Controller

Since Control Commands are NOT

Generated by Integral of Error

Between Desired Signals (r)

And Output Signals (z).

NOTE: Solution to Tracker Control

Configuration is KNOWN. It is

Solution of Augmented System.
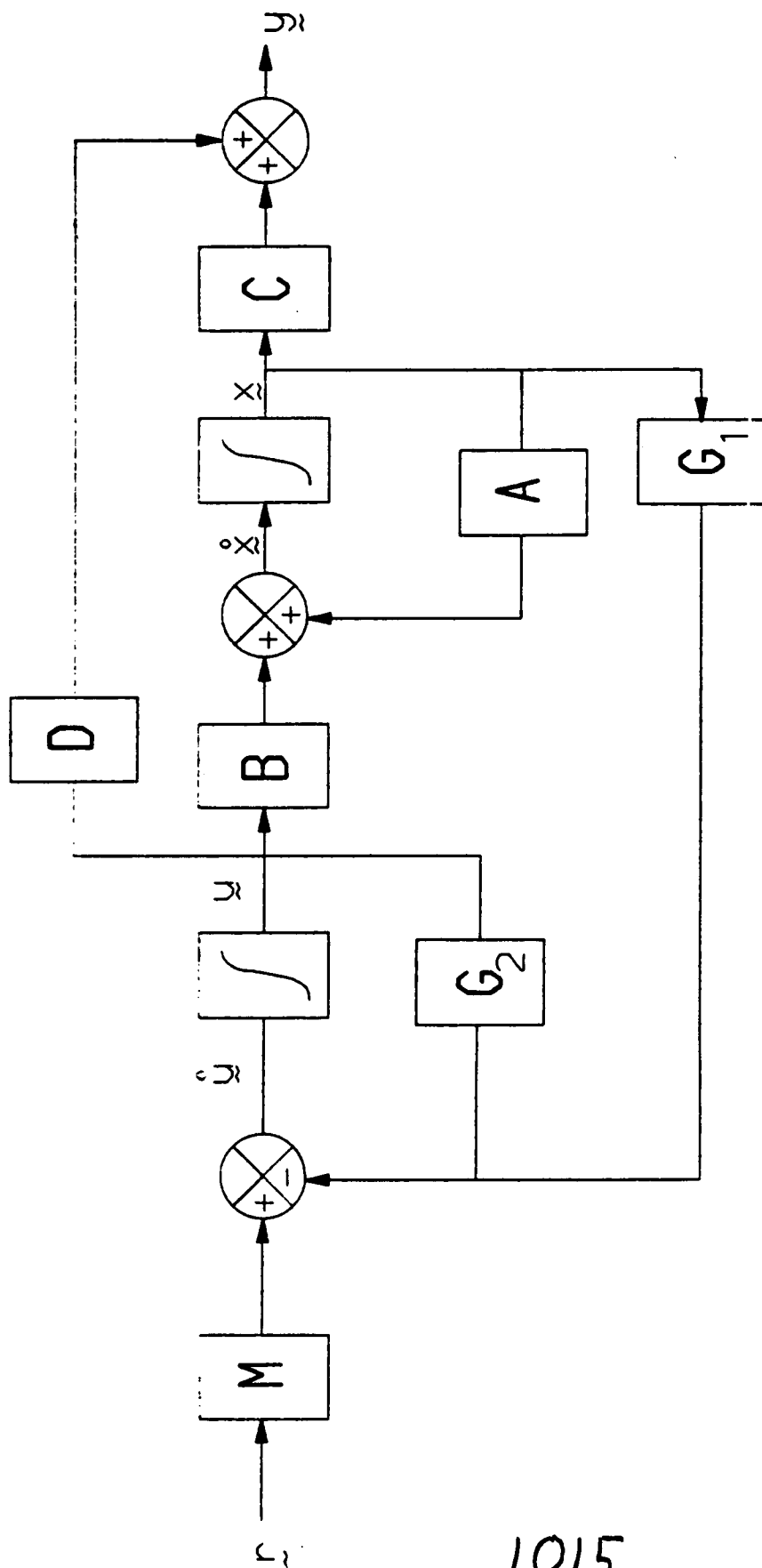
FIGURE 5. OPTIMAL TRACKING SYSTEM

1015

Optimal Integral Control Design

Equality of Optimal Integral Control

Design and Optimal Tracker Design

Effected by Block Diagram Reduction

Techniques (Laplace Domain).

Results:

$$| L H | = | G_1 \ G_2 | \begin{vmatrix} A & B \\ EC & ED \end{vmatrix}^{-1}$$

Knowns:

A, B, C, D, E - Configuration Matrices

G_1, G_2 - Augmented System Solution

Thus:

L and H Matrices are Determinable

1016
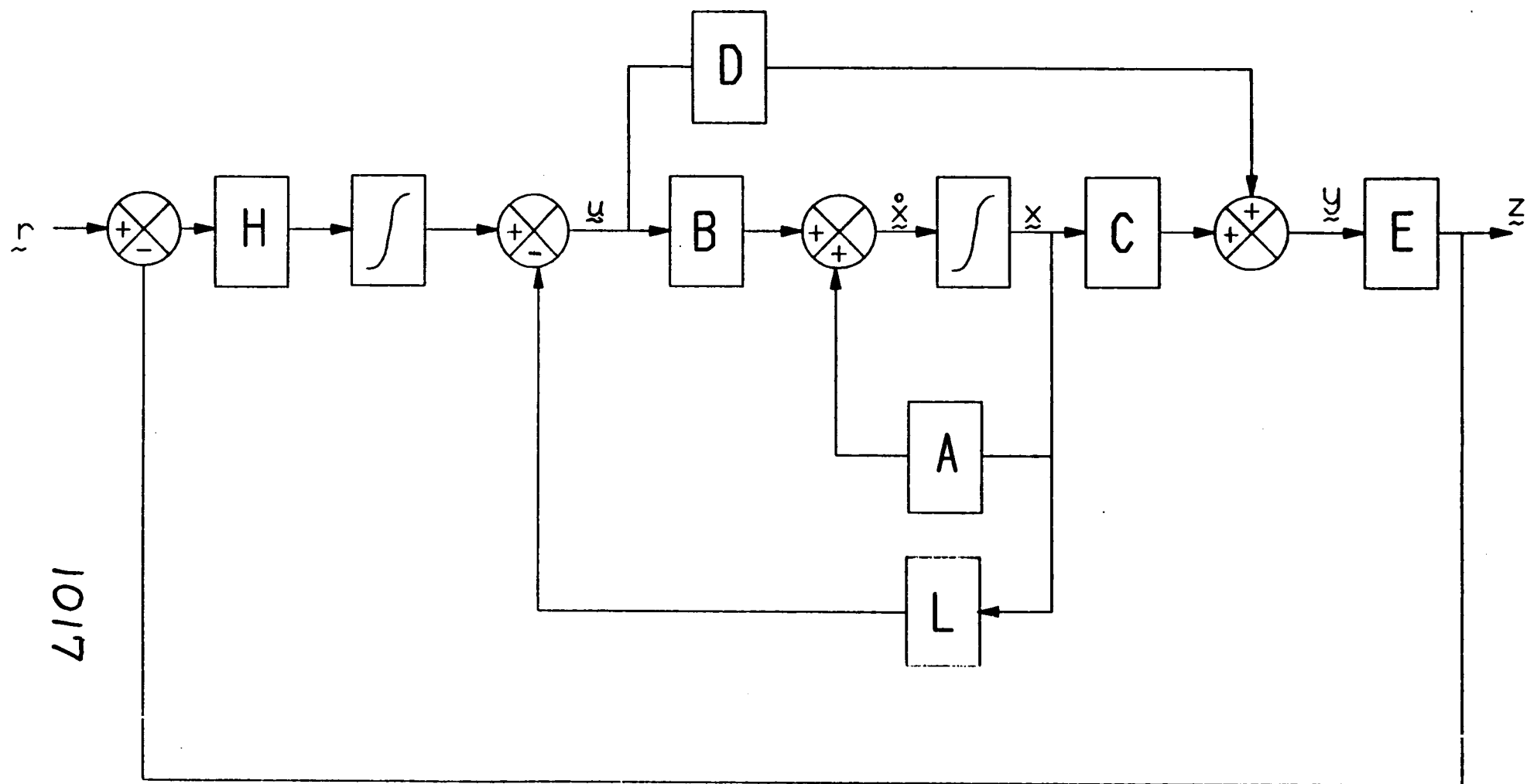
FIGURE 6. OPTIMAL INTEGRAL TRACKING SYSTEM

Sensor Failure Accommodation

Matrices:

H = Error Gain Matrix
L = State Gain Matrix

If State Information Unavailable,

Corresponding Column Elements of L

Matrix Are Zeroed - Suboptimal Control!
From Before

$$| G_1 G_2 | = | L_s H | \begin{vmatrix} A & B \\ EC & ED \end{vmatrix}$$

Hence, New Gain Matrix $| G_s | = | G_{1s} G_{2s} |$

Can be Determined to Effect Control

Preliminary Results are Encouraging
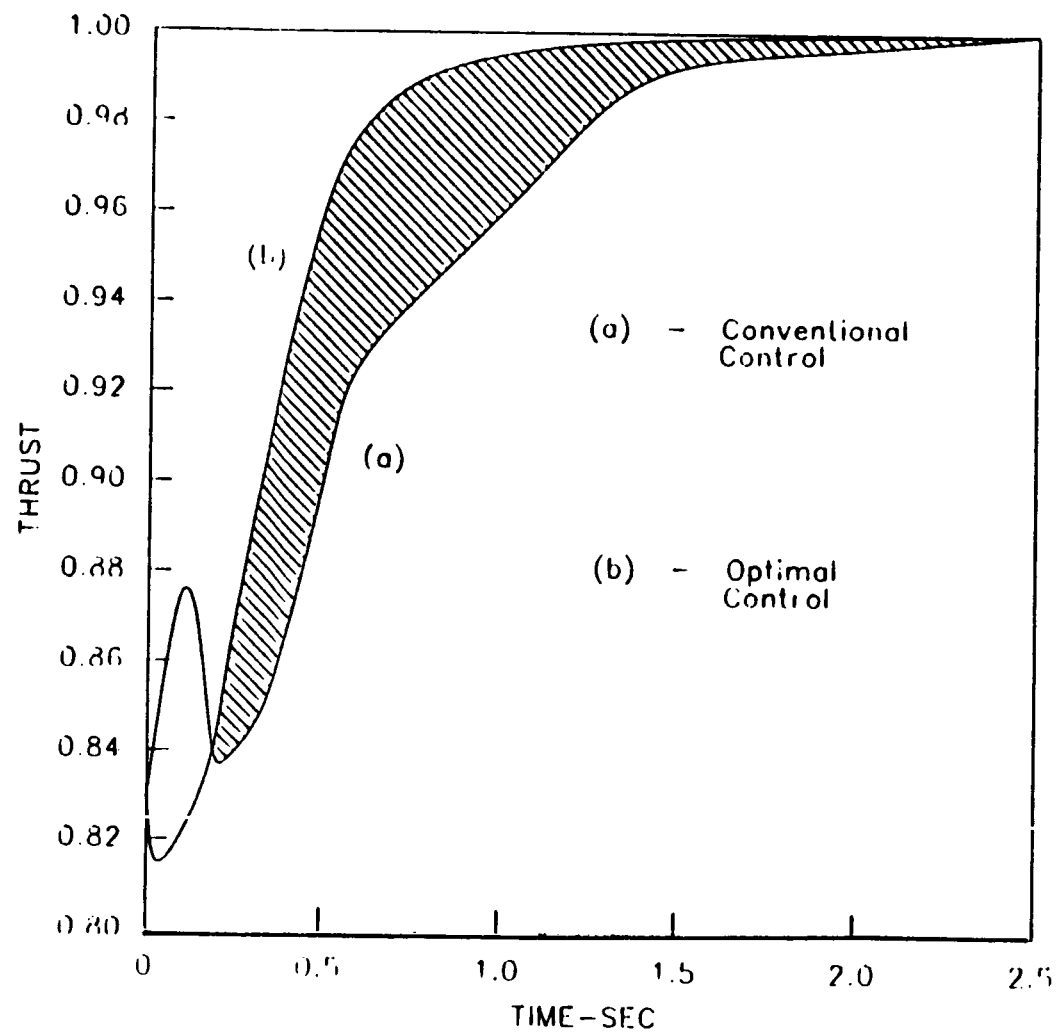
FIG. 7   F-100 THRUST CONTROL

1020
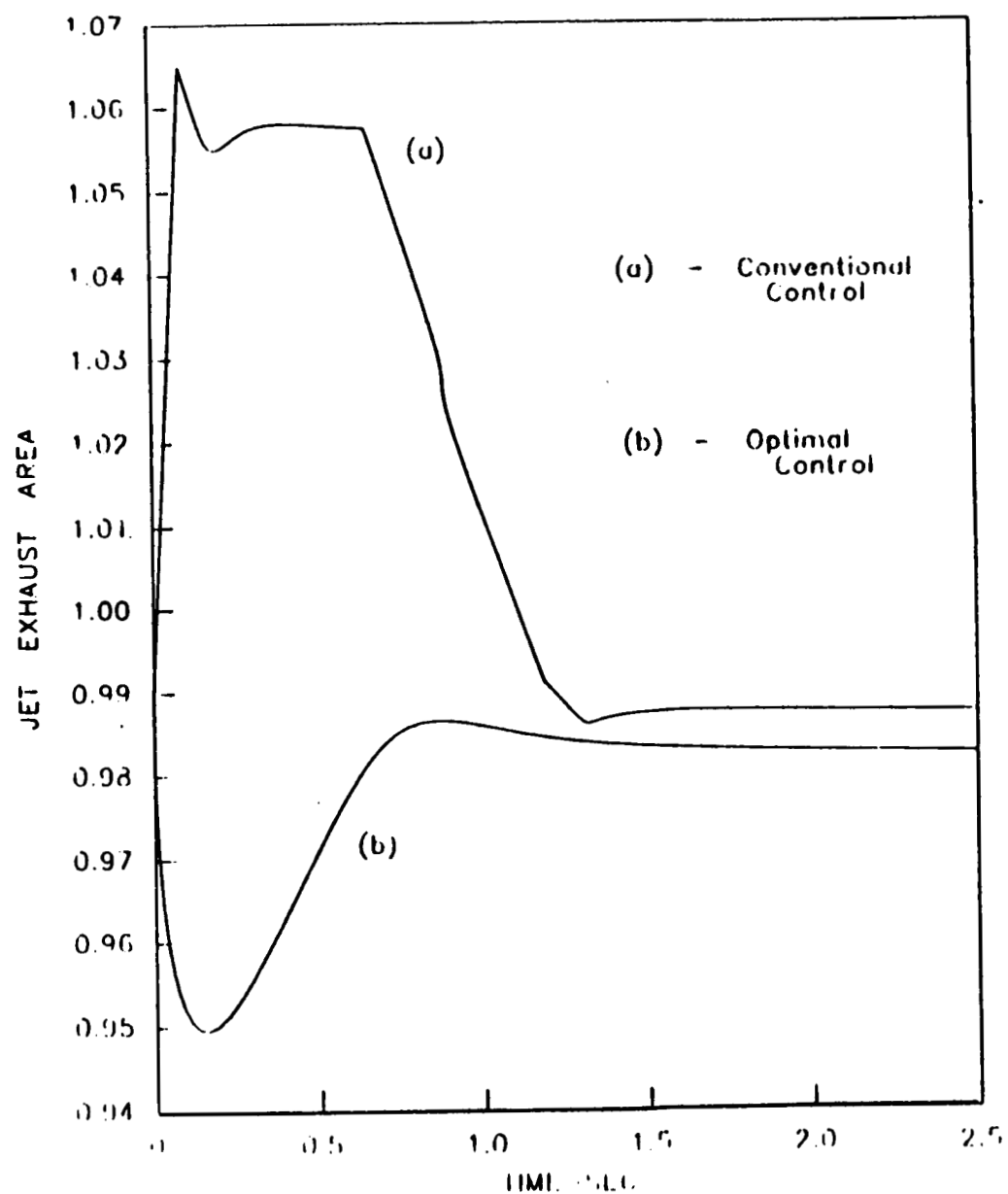
FIG. 8   F-100 AFTERBURNER CONTROL

Fig.9. Third Order System Response Comparison

1022

(b)

(a)

(a) Optimal
     Control

(b) Suboptimal
     Control

AMPLITUDE

TIME
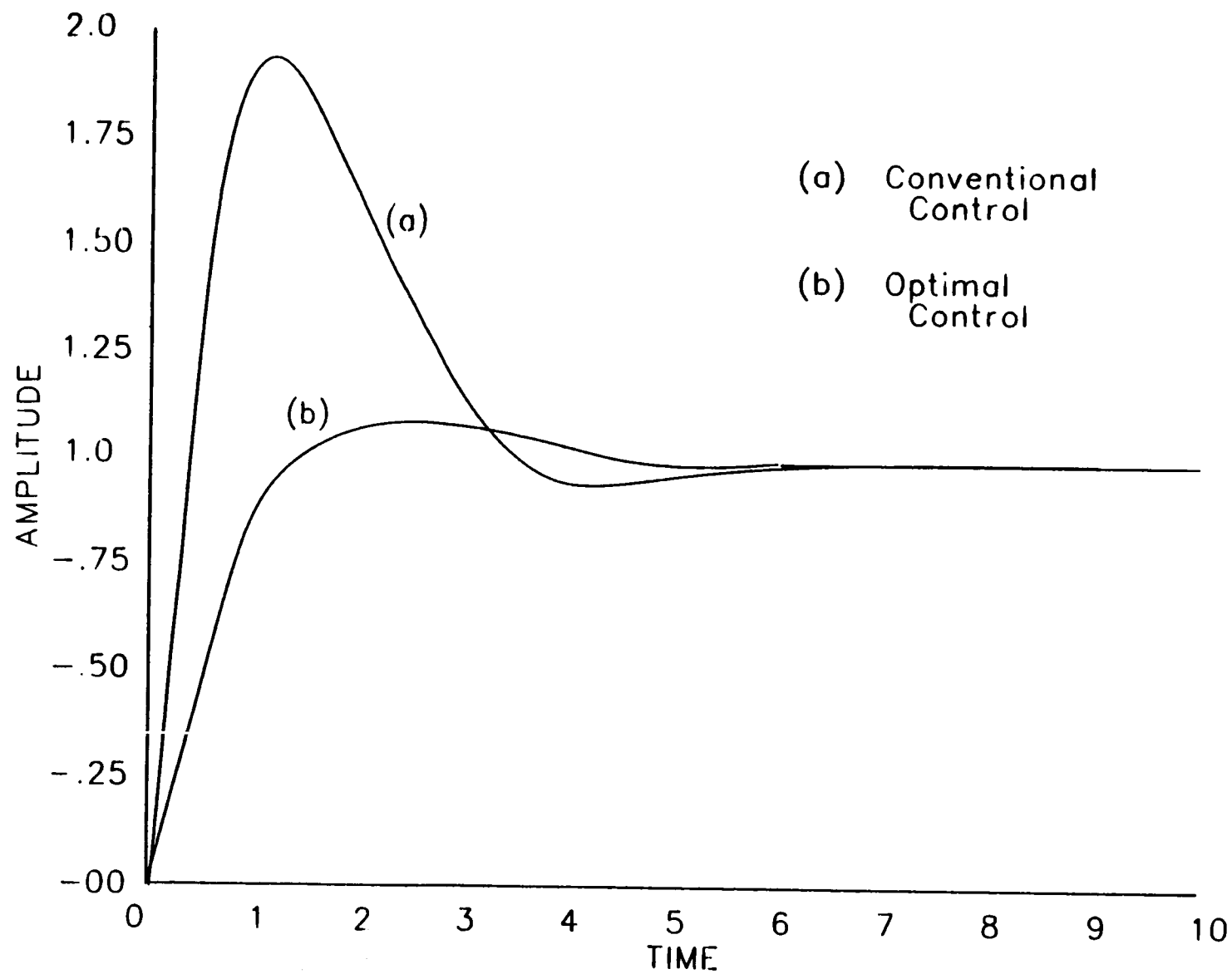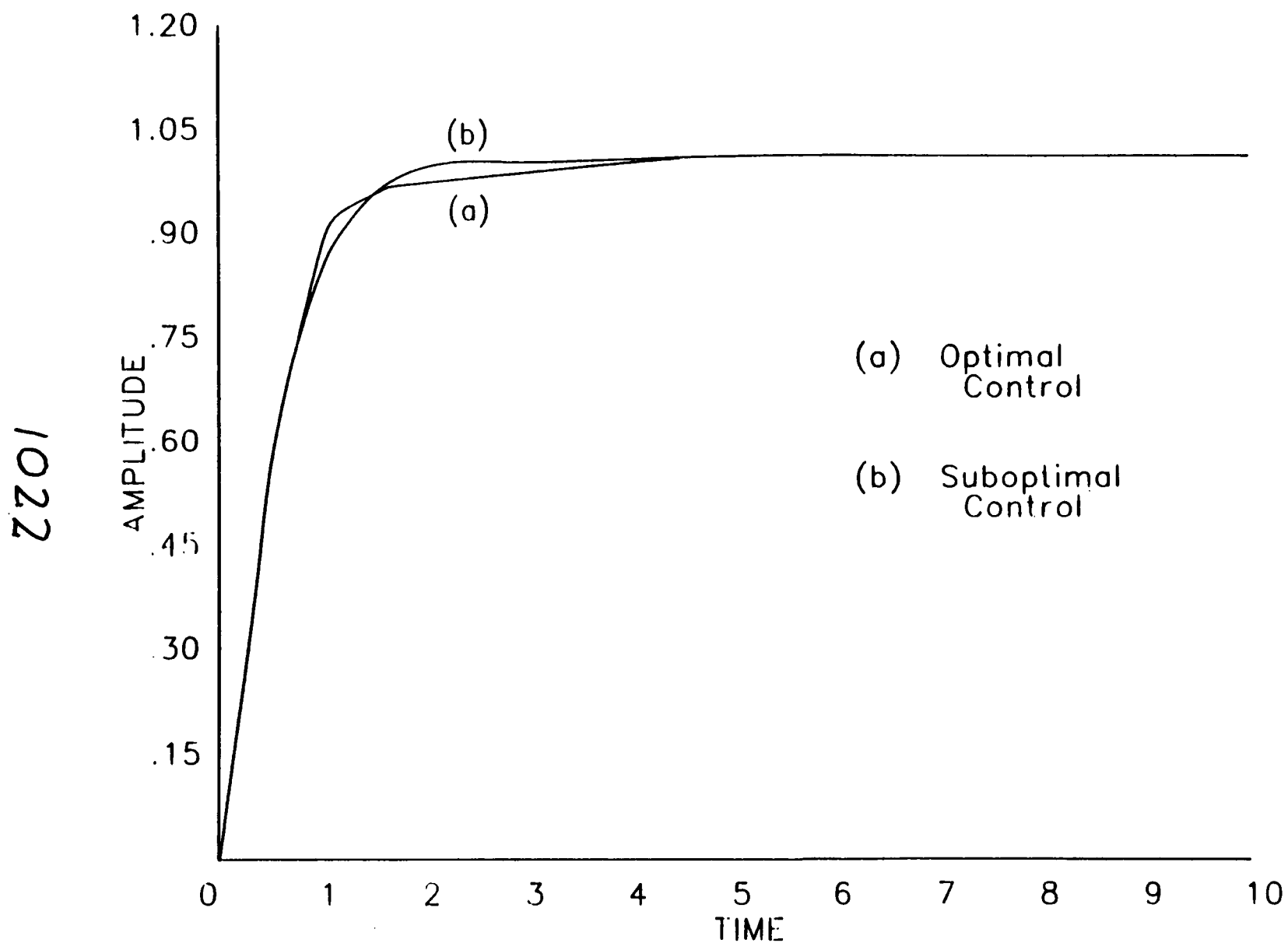
Fig.10.   Third Order System Response Comparison

Summary

Optimal Integral Control Design

Effected by a Combination of

Multivariable Control Analyses

Sensor Failure Accommodation

Accomplished Without Resort to

Supplemental Filter / Estimator Designs

Suboptimal Control Response

Effective for Ill-Behaved,

Third-Order Test Case

1023

Postscript to Computational Aspects...

Lawrence W. Taylor, Jr.
NASA Langley Research Center

What started as an effort to transcend various project and reasearch activities has become an official program..Computational Controls. The following charts describes that program at this early stage in its development. The next meeting on the subjects of the Computational Aspects Workshop will be the 3rd Annual Conference on Aerospace Computational Control. The conference will be held August 28-30, 1989 at Oxnard.

Computational Controls
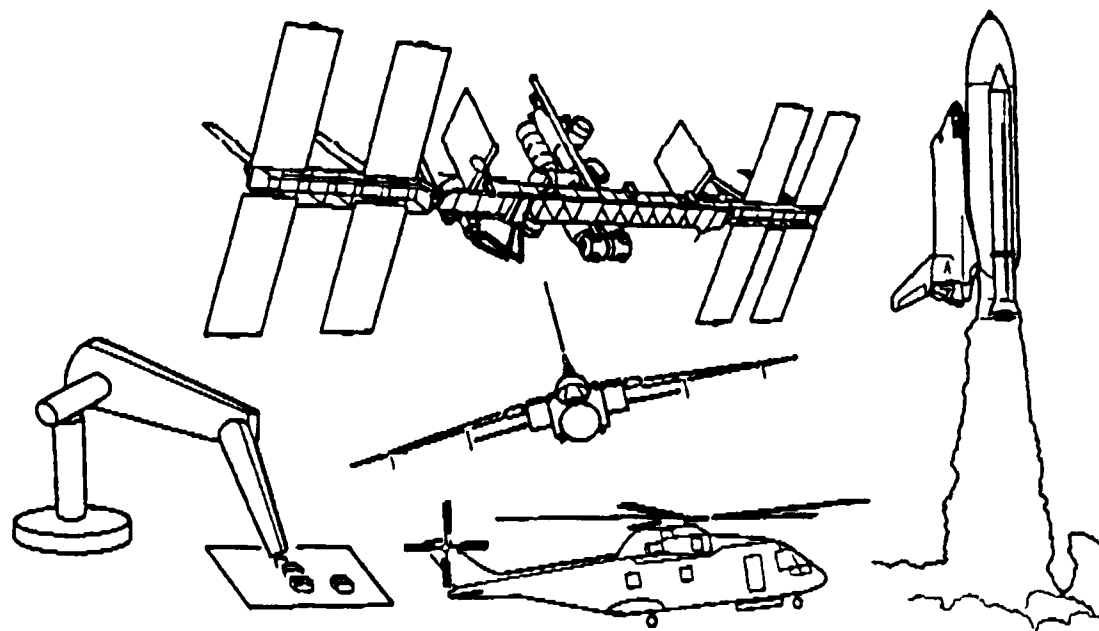
Larry Taylor
NASA Langley Research Center
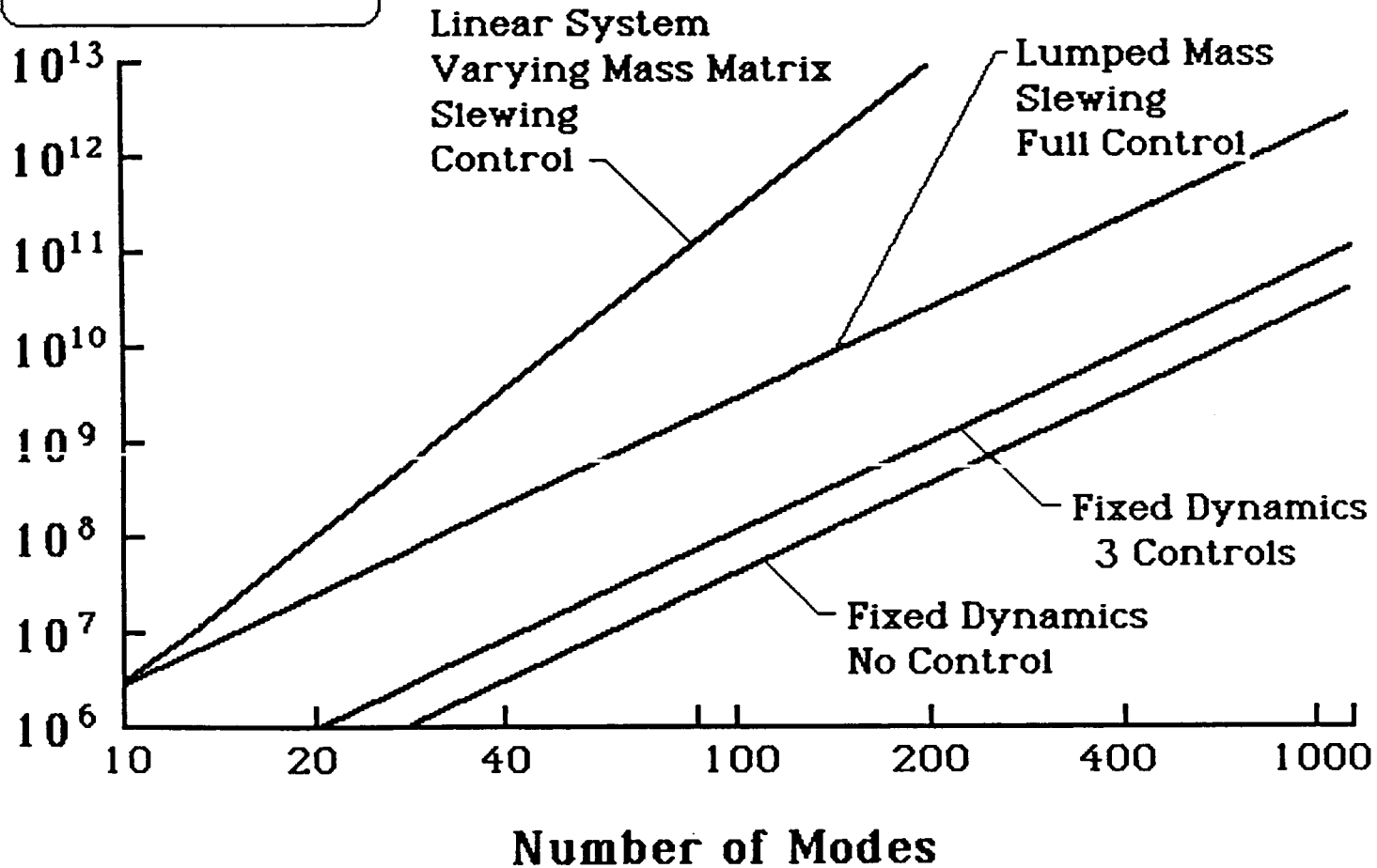
1026

Computational Requirements

Multiplies per P_1

Planar Beam Example

Linear System
Varying Mass Matrix
Slewing
Control

Lumped Mass
Slewing
Full Control

Fixed Dynamics
3 Controls

Fixed Dynamics
No Control

10^{13}

10^{12}

10^{11}

10^{10}

10^9

10^8

10^7

10^6

10   20   40   100   200   400   1000

Number of Modes

1027

OBJECTIVE

"To Develop the NEW GENERATION

HIGH PERFORMANCE Aerospace

Modeling, Control, and Simulation Tools"

1028

A THREE-PART PROGRAM

COMPUTATIONAL CONTROLS

SPACECRAFT

AIRCRAFT

AEROSPACE TRANSPORTATION VEHICLES
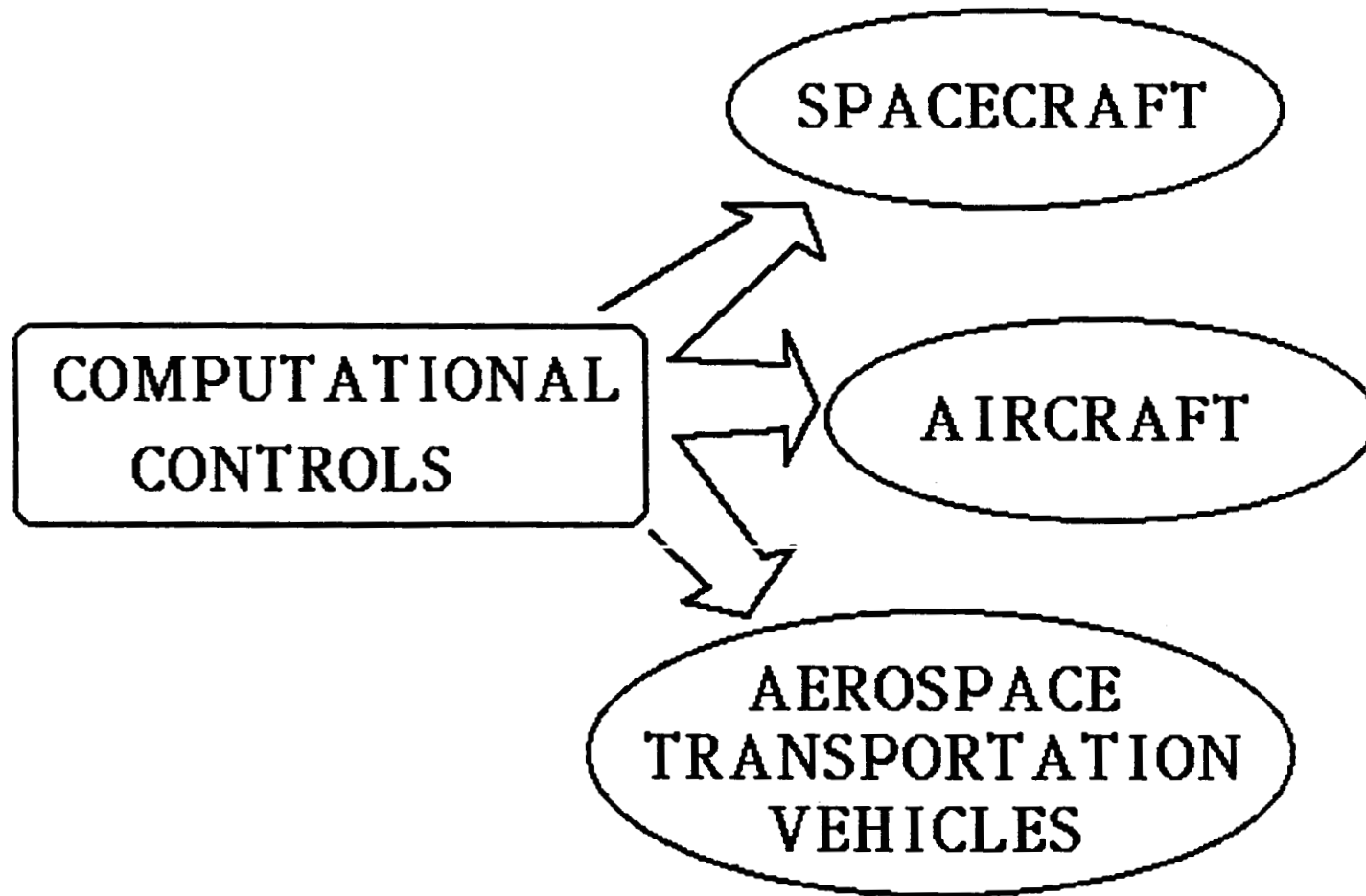
1029

Computational Controls

Contacts:

Lee Holcomb – NASA HQ Code RC

John Dibattista – NASA HQ Code RC

Guy Man – JPL

Larry Taylor – LaRC
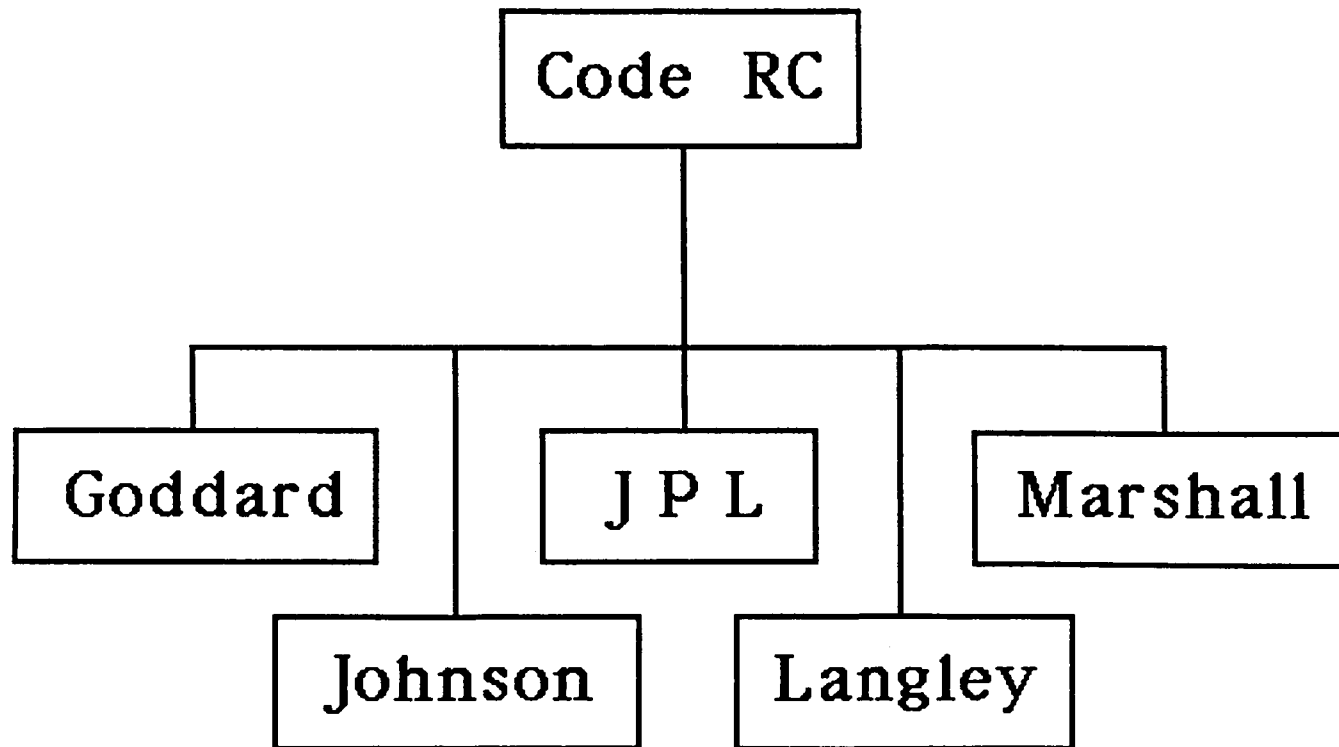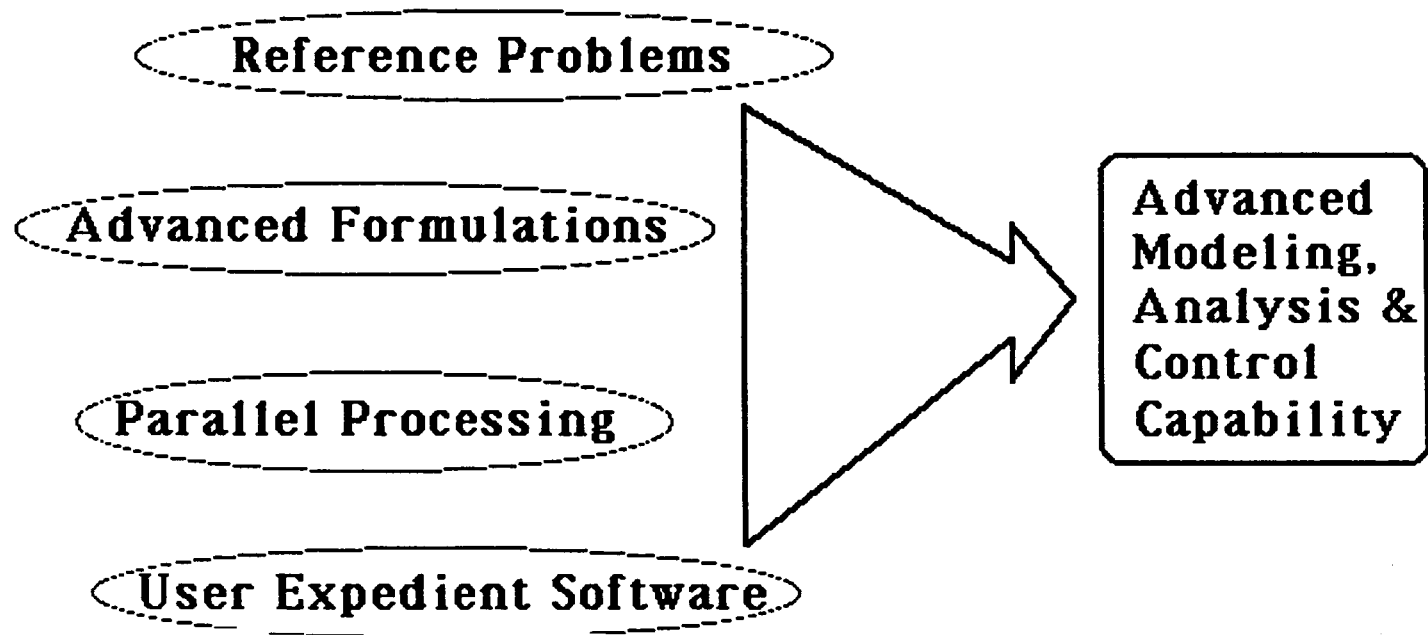
Harry Frisch – GSC

Henry Waites – MSFC

Ken Cox – JSC

1030

JUSTIFICATION

Current Practices in <u>Formulating</u>,
<u>Modeling</u> and <u>Simulating</u> do not
Meet today's needs.

- Hypersonic Cruise Vehicles

- Multi-Component Launch Vehicles

- Aeroassisted Orbital Transfer
  Vehicles

1031

ORGANIZATION

Code RC

Goddard

J P L

Marshall

Johnson

Langley

1032

APPROACH

Reference Problems

Advanced Formulations

Parallel Processing

User Expedient Software

Advanced Modeling, Analysis & Control Capability

1033

Reference Problems

- Shuttle RMS

- Earth Orbiting Satellite

- Mini-MAST

- Pinhole Occulter

- Mariner Mark II

- Optical Interferometer

- Advanced Launch System

- F - 18 Fighter

- Trans-Atmospheric Vehicle

Advanced Formulations

- Order(n) Algorithms   LaRC

- Distributed Parameter Modeling   LaRC

- Mass Referenced Modeling   LaRC

- Composite Modeling   LaRC

1035

Parallel Processing

- Multiple Processors   LaRC

- Array Processors   LaRC

- Benchmarking   LaRC

1036

SOFTWARE

- Macintosh-Like User Environment

- Simultaneous Tasking

- Real-Time and Off-Line

- Modular (Particular Methods)   LaRC

- Data Base Management

- Interactive Graphics

1037

Related Activities

C.S.I.
Integrated Design
Test Data

Focused
Activities
Specific
Applications

R & T Base
Control Techniques
Control Applications

Computational
Controls
Real-Time, Flex. Simulation
Efficient Computations

1038
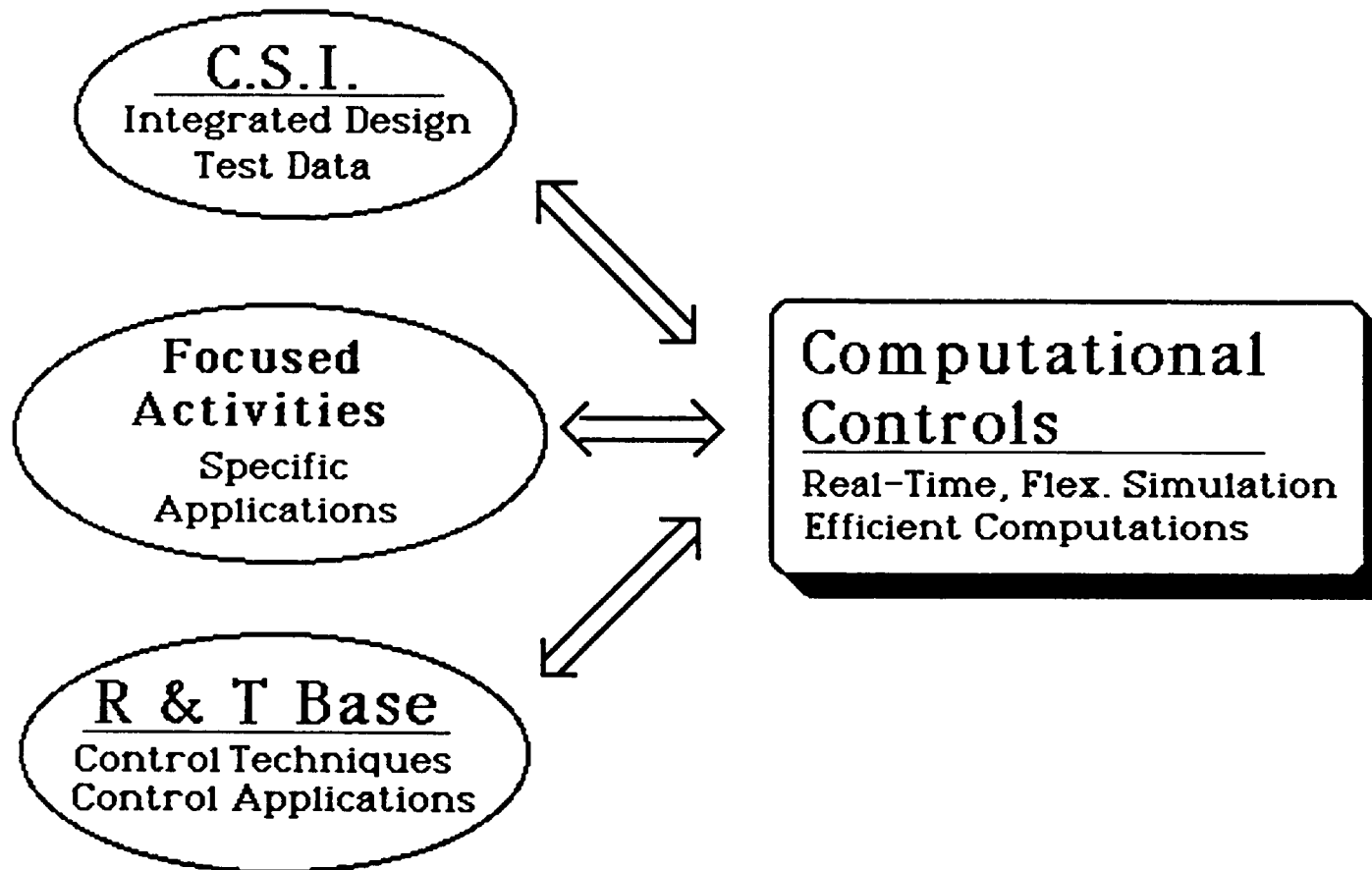
PROPOSED LARC AERO TASKS

1.1

DYNAMICS INTEGRATION AND ADVANCED CONTROL THEORY AND MODELING
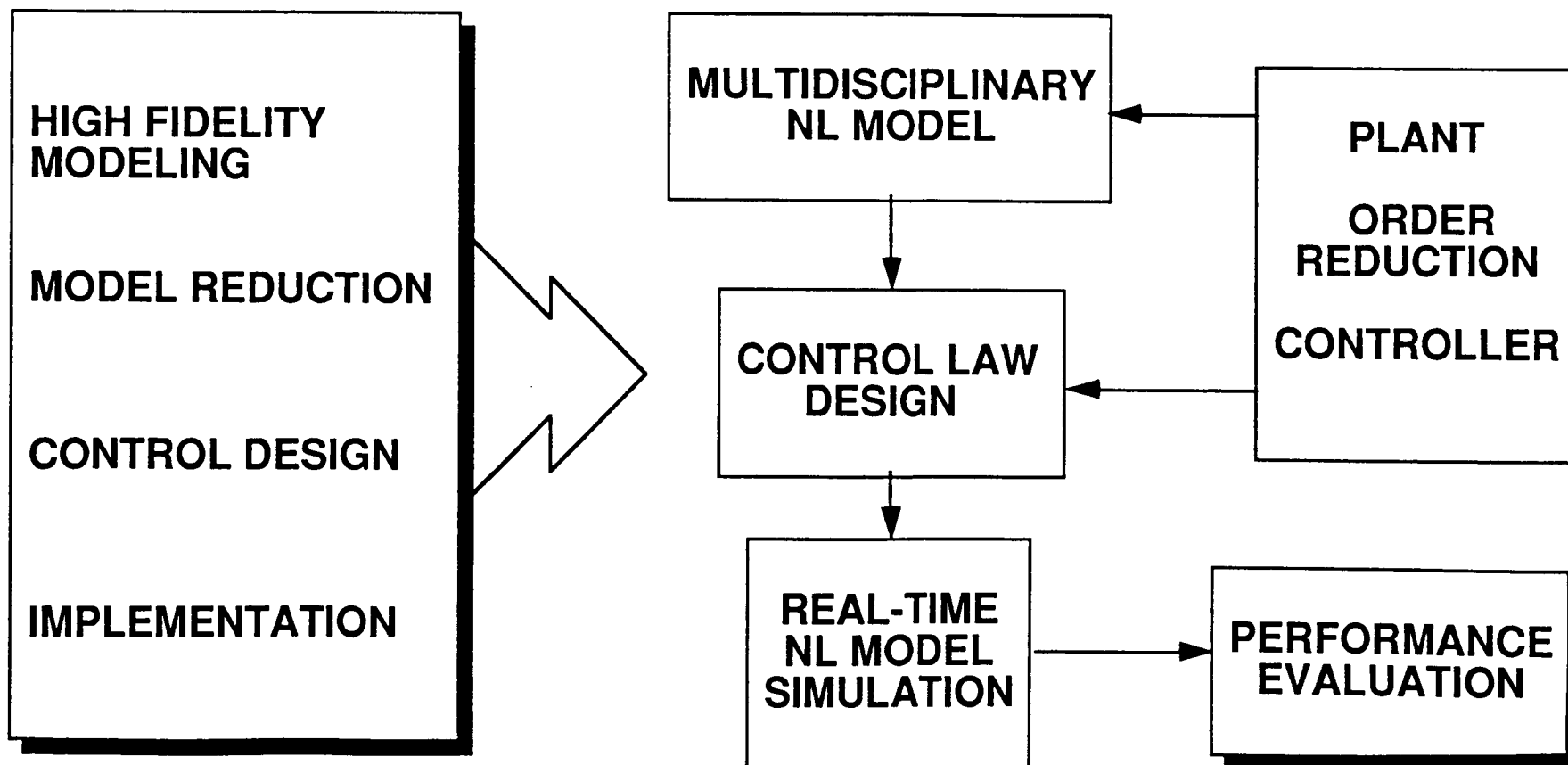
- **F-18 THRUST VECTORED HI- α VERSION**

- **TRANS-ATMOSPHERIC**

1039
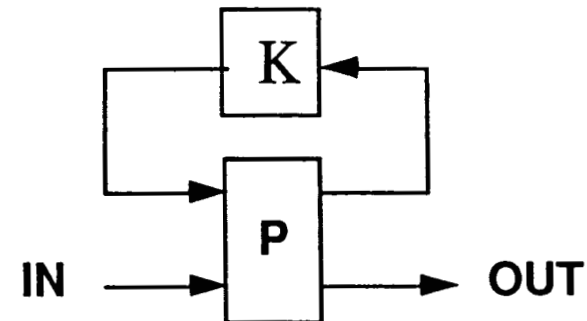
1.4

HIGH-ORDER, HIGH FIDELITY, NONLINEAR MATHEMATICAL MODELS OF HIGH PERFORMANCE AIRCRAFT

ADVANCED MODEL ORDER REDUCTION METHODS
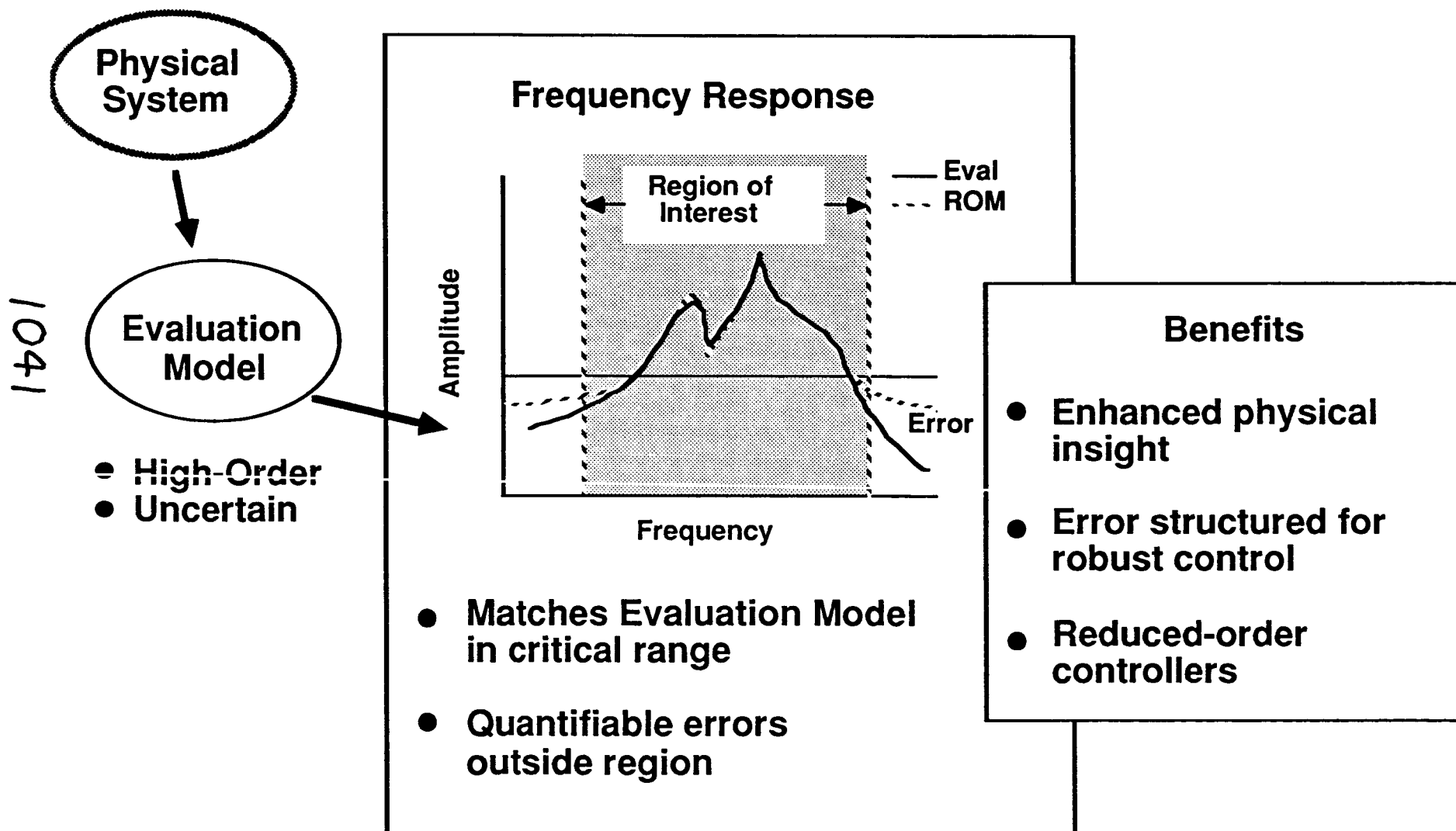
ROBUST INTEGRATED CONTROL DESIGN METHODOLOGIES

1.5

RAPID CONTROLLER IMPLEMENTATION METHODOLOGIES

MASS/INERTIA

AERODYNAMIC

REACTION CONTROL SYSTEM

HEATING

PROPULSION

AEROTHERMO-SERVOELASTIC

ACTUATORS

NASA

1040

HIGH FIDELITY MODELING

MODEL REDUCTION

CONTROL DESIGN

IMPLEMENTATION

MULTIDISCIPLINARY NL MODEL

CONTROL LAW DESIGN

REAL-TIME NL MODEL SIMULATION

PERFORMANCE EVALUATION

PLANT

ORDER REDUCTION
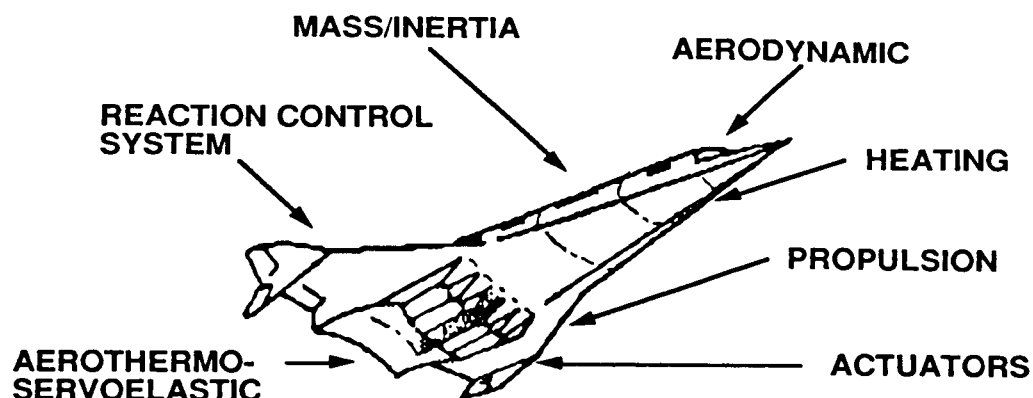
CONTROLLER

Plant Order Reduction for Controller Synthesis

ACTIVITIES

- Advisory Committee   /Quarterly

- Workshops   /Annually

- Programmatic Status Repts   /Quarterly

- Technical Reports   /As Available

1042

ANNOUNCEMENT & CALL FOR PAPERS

3rd Annual Conference on Aerospace
Computational Control

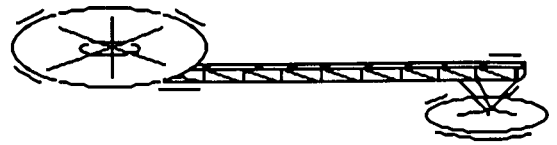Radisson Suite Hotel   August 28-30, 1989   Oxnard, California

1043

NASA

NSF

DoD
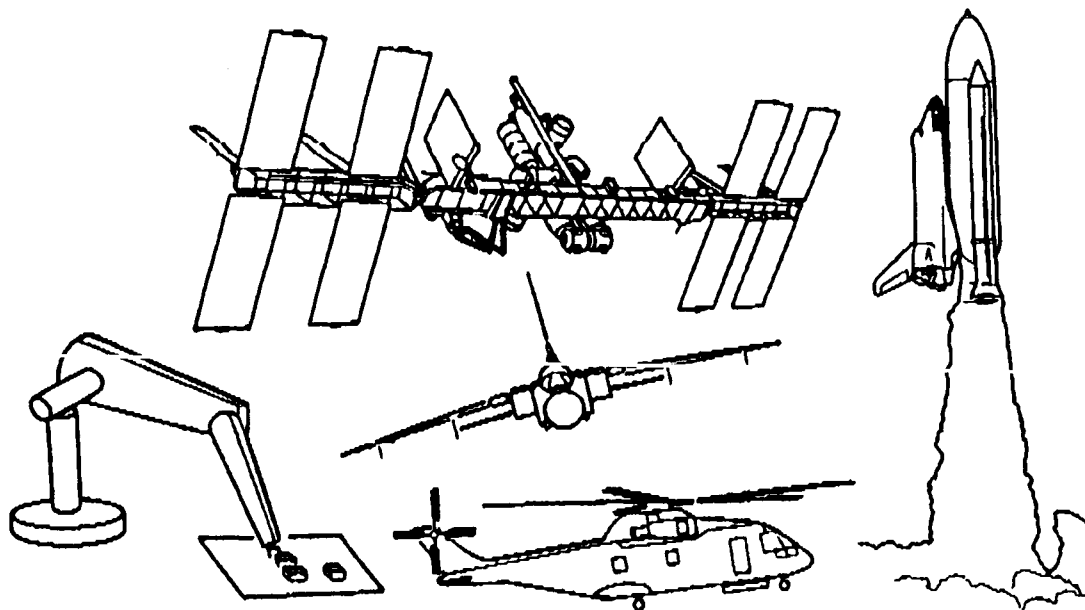
ANNOUNCEMENT of a CLASS on

TREETOPS✦

✦ A Control System Simulation for Flexible and Articulating Structures

---

WHEN: August 31, 1989(After Conference)

WHERE: 3rd Annual Conference on
Aerospace Computational Control
Radisson Suite Hotel, Oxnard, CA

CONTENT:
- Overview
- Example Problems
- Hands-On Experience
- User's Manual

COST: No Charge for Class or Materials
for Registered Conferees

CLASS REGISTRATION: Larry Taylor
NASA Langley
804-864-4040

1044

15. Supplementary Notes

This report is part 2 of two parts published as NASA TM-101578.

16. Abstract

This publication is a collection of papers presented at the Workshop on Computational Aspects in the Control of Flexible Systems held at the Royce Hotel, Williamsburg, Virginia, July 12-14, 1988. The papers address the formulation, modeling, computation, software and control for flexible spacecraft, aircraft and robotic manipulators.

17. Key Words (Suggested by Author(s)) Large Flexible Spacecraft Control, Strucutal Dynamics	18. Distribution Statement Unclassified-Unlimited Subject Category - 18

19. Security Classif. (of this report) Unclassifed	20. Security Classif. (of this page) Unclassified	21. No. of pages 505	22. Price A22